1207

Pavement Design

NOTICE: The Transportation Research Board does not endorse
products or manufacturers. Trade and manufacturers' names
appear in this Record because they are considered essential to its
object.

Transportation Research Record 1207

Contents

Evaluation of 1986 AASHTO Design Guide for Jointed Concrete Pavements

Ming-Jen Liu, Michael I. Darter, and Samuel H. Carpenter

The new *AASHTO Guide for Design of Pavement Structures* (1986) is evaluated using theory and field performance data. Jointed plain (JPCP) and jointed reinforced (JRCP) concrete pavements are considered. The conceptual evaluation considers the assumptions, capabilities, and theoretical limitations of the AASHTO Guide. The analytical field data evaluation includes two approaches: predicted vs. actual ESALs for in-service pavements from NCHRP Project 1-19, and the specific design evaluation. Four broad zones in the United States were used to characterize the performance of the AASHTO designs in different climates. This dual approach to design procedure evaluation provides an overall picture of the capabilities of the new AASHTO Guide. Deficiencies are identified that must be considered by agencies implementing the new AASHTO Guide, and recommendations on how to overcome these deficiencies are provided.

The AASHTO structural slab thickness design model was originally developed using the results from the AASHO road test conducted from 1958 to 1960 near Ottawa, Illinois. The *AASHO Interim Guide for Design of Rigid Pavement Structures (1)* was first developed in 1962 and revised in 1972 (2) and 1981 (3). During 1984–85 the Subcommittee on Pavement Design and a team of consultants revised the existing guide under NCHRP Project 20-7/24 and issued the current version (4). A complete description of the development of the original structural design model is given in the Appendix of the 1981 Interim Guide (3) and in the AASHO Road Test Report (5).

Since the AASHTO Design Guide is widely used for the design of rigid highway pavements, it is important to know its capabilities and limitations and the performance of the AASHTO pavement designs under various conditions. The data base used in this study was developed under NCHRP Project 1-19 (6).

The AASHTO Guide is evaluated conceptually and analytically.

CONCEPTUAL EVALUATION

The conceptual evaluation includes a review of the Guide's fundamental basis for development and a summary of the conceptual weaknesses and limitations of the design procedure.

Department of Civil Engineering, University of Illinois, 208 N. Romine Street, Urbana, Ill. 61801.

Fundamental Basis for Development

Performance data from the AASHO Road Test and regression techniques were used to develop the following empirical model:

$$\log_{10} W = \log r + G/B \qquad (1)$$

where

W = axle load applications, for load magnitude L1 and axle type L2, to a serviceability index of P2,
$\log_{10} r$ = 5.85 + 7.35 log $(D + 1)$ + 4.62 log (L1 + L2) + 3.28 log (L2),
B = 1.0 + [3.63(L1 + L2)$^{5.20}$]/[$(D + 1)^{8.46}$L2$^{3.52}$],
G = log [(P1 – P2)/(P1 – 1.5)],
D = PCC slab thickness (in.),
L1 = load on a single or a tandem axle (kips),
L2 = axle code, 1 for single axles and 2 for tandem axles,
P1 = initial serviceability index, and
P2 = terminal serviceability index.

This empirical model (Eq. 1) is applicable only to the Road Test climate, pavement materials, subgrade, and slab design. To expand its applicability, it was modified by the inclusion of Spangler's corner stress equation, which incorporates slab thickness, load transfer coefficient, material properties such as portland cement concrete (PCC) flexural strength (F), modulus of elasticity (E), and foundation support (k). Basic assumptions made in this extension are:

● There will be no variation in W for different load magnitudes if the level of the ratio of tensile stress/strength of the PCC slab is kept constant and such W will be accounted for by AASHO Road Test Equation 1.
● Any change in the ratio of tensile stress/strength resulting from changes in the values of E, k, and F (modulus of rupture) will have the same effect on W as an equivalent change in slab thickness (calculated by Spangler's equation) will have on W (as per Equation 1).

In the 1986 AASHTO Guide, more empirical factors are included to adjust the designs for various conditions.

1. Design reliability concepts are introduced with the objective of decreasing the risk of premature structural deterioration below acceptable levels of serviceability. The reliability design factor (F_R) accounts for chance variations in both the traffic prediction and the pavement performance prediction for a given W_{18}. This reliability design factor provides a pre-

determined level of reliability (R%) that pavement sections will survive the traffic for which they were designed. It applies only to structural deterioration, however, not to loss of serviceability due to nonload causes (e.g., joint deterioration, swelling soils).

2. The joint load transfer factor, J, is extended to consider different types of shoulders. A value of 3.2 is recommended for the J factor for a jointed plain (JPCP) or jointed reinforced (JRCP) concrete pavement with a mechanical load transfer device (e.g., dowel bars) at joints in pavements with asphalt concrete shoulders, whereas the values ranging from 2.5 to 3.1 are recommended for the same pavement with tied PCC shoulders. Nondoweled pavements have a recommended J ranging from 3.8 to 4.4 for AC shoulders, and from 3.6 to 4.2 for tied PCC shoulders. This method adjusts for different load transfer conditions by varying slab thickness.

3. A drainage coefficient (C_d) multiplier is added to the design equation. Its value represents the quality of drainage and the percent of the time the pavement structure is exposed to moisture levels approaching saturation. It provides a way to approximate the effect of drainage by means of modifying the load transfer coefficient, J. The C_d value for AASHO Road Test subdrainage conditions is 1.0.

4. The potential effect of subgrade swelling and frost heave on the rate of loss in serviceability is considered. The thaw-weakening and seasonal variations in modulus of subgrade reaction are also considered in the new Guide.

5. The subgrade soil-resilient modulus, M_R, is used in the new Guide to estimate the effective modulus of subgrade reaction, k, at the top of the subbase. A loss-of-support factor (LS) included in the design accounts for potential subbase erosion and/or differential vertical soil movement by diminishing the overall effective k value on the basis of the size of the void that may develop beneath the slab. Some suggested ranges of LS, depending on the type of subbase material, are provided. This results in a pavement design for k values as low as 25 pci.

The current structural design model is:

$$W_{18} = W_{18}/F_R = W_{18}/10^{-Z_R So} \qquad (2)$$

where

$$\log W_{18} = 7.35 \log (D + 1) - 0.06$$
$$+ Gt/[1 + 1.624 \times 10^7/(D + 1)^{8.46}]$$
$$+ (4.22 - 0.32 P_t) * \log [(S'_c * C_d(D_{0.75} - 1.132)$$
$$\div (215.63J) * (D_{0.75} - 18.42)/(E_c/k)_{0.25})] \qquad (3)$$

where

Gt = log [$(P_i - P_t)/(4.5 - 1.5)$],
W_{18} = mean predicted total number of 18-kip equivalent single-axle load applications in the design life,
F_R = reliability design factor,
Z_R = standard normal deviate corresponding to selected level of reliability,
So = overall standard deviation for rigid pavement,
D = mean thickness of pavement slab (in.),
P_i = initial serviceability index,
P_t = terminal serviceability index,

S'_c = mean modulus of rupture for PCC used on specific project,
J = load transfer coefficient used to adjust for load transfer characteristics of specific design,
C_d = drainage coefficient,
E_c = mean modulus of elasticity for PCC (psi), and
k = mean modulus of subgrade reaction (pci).

Weaknesses and Probable Limitations

Some major weaknesses and probable limitations of the procedure in designing against important distress types existing in rigid pavement are summarized below.

Accuracy of Structural Design Model

The empirical model of Equation 1 was derived from results from the Road Test data and relates to its specific Road Test conditions. Within these conditions, the ability of Equation 1 to predict the exact number of load applications to any given level of serviceability index for a pavement is shown in Figure 1 (7). The shaded band indicates the range in load applications that includes approximately 90 percent of all the performance data. In the top curve of Figure 1, for example, for slab thicknesses of 8 inches, the resulting number of 30-kip single-axle applications to a terminal serviceability index of 2.0 ranged between 400,000 and 1,910,000 for controlled AASHO Road Test conditions. If Equation 1 is used for conditions other than those for which it was developed, its range of accuracy or associated error of prediction will be greater. This may be particularly true for different climatic conditions. The modified expression, Equation 3, allows for changes in material properties (S_c, E_c, and k), but the accuracy of these adjustments is unknown.

Variability

A serious limitation of the AASHTO design procedure is that the empirical design model (Equation 1 or 3) is based on very short pavement sections where construction and material quality were highly controlled. Typical highway projects, which are normally several miles long, contain much greater construction and material variability and hence show more variability in performance along the project in the form of localized failures. Projects designed using the Guide would, therefore, tend to show significant localized failures before the average project serviceability index (PSI) drops to P_t, unless a level of reliability higher than 50 percent was selected for the design.

Design Period

Design periods under consideration usually range from 20 to 40 years. The number of years and 1.1 million applications, upon which Equation 1 is based, represent only a fraction of the load applications that would be expected on high-volume pavements over the design period (10 million to 100 million
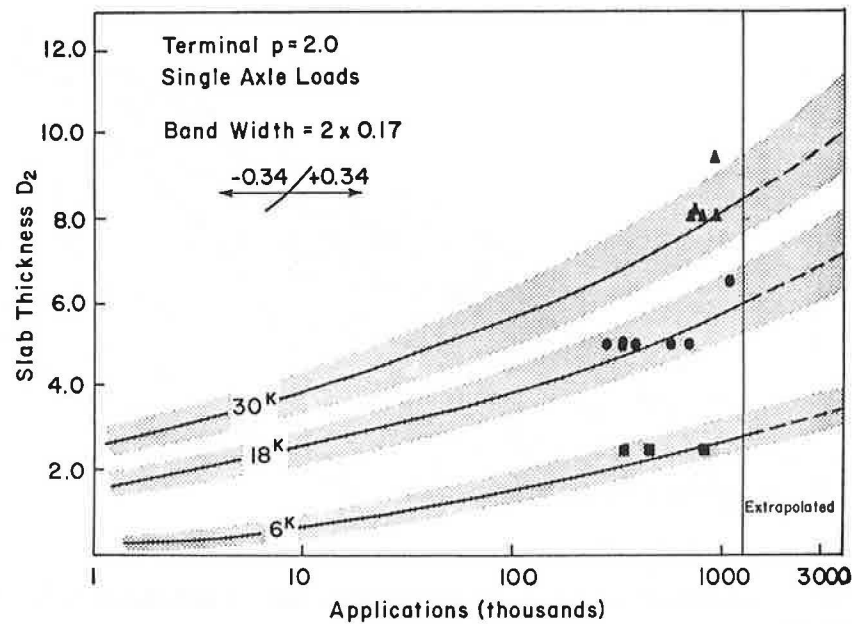
FIGURE 1 Illustration of error of prediction of basic AASHO design model (7). Shaded bands indicate range in load applications that includes approximately 90 percent of all the performance data.

applications). Even if these equations can be extrapolated for the large difference in the number of load applications, there are several climatic effects that occur over time (as represented by age) which cause severe deterioration of the pavements even without heavy load applications (e.g., corrosion of steel, joint freezeup, D-cracking, reactive aggregate, incompressible buildup in joints). Therefore, in similar or more severe climates, the pavements would be expected to endure fewer load applications and fewer years than predicted by Equation 1 or 3. In mild climates, pavements may perform much better than predicted.

Loss of Support

The Road Test used a specific set of pavement materials and one roadbed soil. Many of the Road Test sections showed severe pumping of the subbase with loss of support. Therefore, Equations 1 and 3 are biased toward this high loss-of-support condition.

Joint Design

Only one type of joint design was used in the AASHO Road Test. If other types are used, such as joints without dowels or with some unusual type of load transfer devices, the pavement life would be significantly changed. The type of base would also affect load transfer and, thus, performance. Basic deficiencies in the joint design recommendations include little or no guidance on joint spacing, on rational determination of dowel size and spacing, on when mechanical load transfer devices are required, and on load transfer systems other than dowels.

Drainage Design

In the new Guide, drainage effects are considered in terms of the effect of moisture on subgrade strength and on base erodability. For new rigid pavement design, the effect of drainage is considered by modifying the load transfer coefficient, J, through the C_d factor. It is well known that the subdrainage conditions at the Road Test were very poor because of the huge amount of pumping. Despite this, AASHTO recommendations for C_d show a value of 1.0 to correspond to a quality of drainage of good to fair for subgrade saturation levels of greater than 5 percent, which surely existed at the Road Test. This recommendation cannot be adjusted properly for poor drainage conditions. Another question is whether poor subdrainage can be considered by simply increasing slab thickness. This is not likely since a thickness increase only decreases deflection slightly.

Reinforcement Design

Slab reinforcement is designed using the subgrade drag theory. The mathematical expression for subgrade drag theory used for longitudinal reinforcement design is a major simplification of the actual forces encountered. The most significant limitation arises if the unrestrained slab length (i.e., distance between joints) assumed in reinforcement design is altered through a partial or complete seizing of one or more joints. This phenomenon could cause a significant increase (double or more) in the steel stress, which may result in yielding or rupture of reinforcement at an intermediate crack between joints. Also, the the procedure does not allow for loss of effective reinforcement through corrosion. It is expected, therefore, that long joint spacings in cold climates, accom-
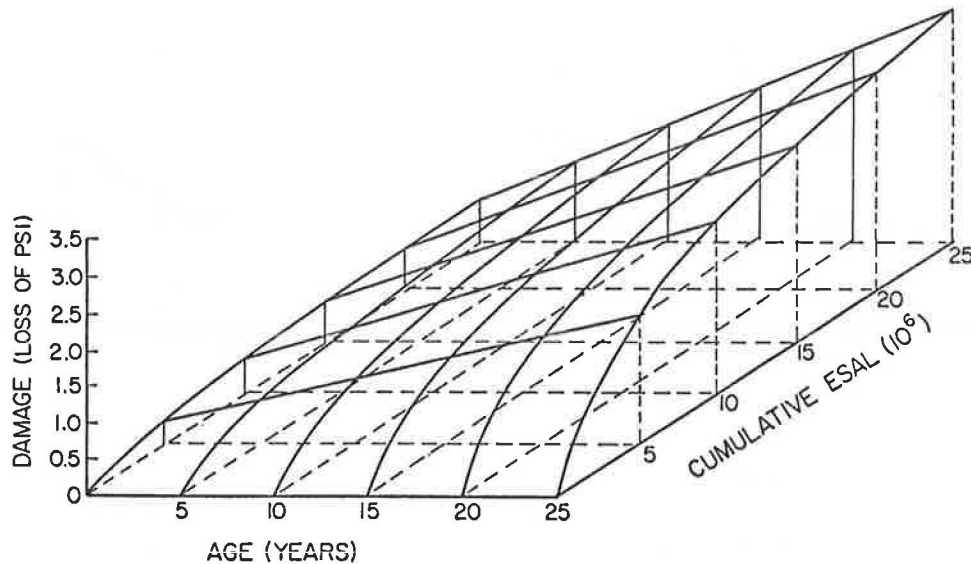
FIGURE 2 Sensitivity of Illinois damage (serviceability) model to cumulative load repetitions and age (6).

panied by joint seizure, would result in rupture of the reinforcement with subsequent faulting and spalling of cracks.

Climate

Concrete pavement performance is highly dependent on the climatic conditions, and evidence exists that climatic conditions could have a significant effect on pavement life (8). Since the AASHO Road Test was conducted over a period of only two years, climatic effects were not as significant as if the same traffic had been applied over a longer period of, say, 20 to 40 years. Steel corrosion requires several years to develop into a serious condition, so joint lockup and subsequent yielding of the steel reinforcement for JRCP pavements would logically not occur for at least several years after initial construction. Figure 2 shows the results of a life prediction model developed from the Illinois data base (6), where age and traffic data were available over short as well as long time periods. An interaction between age and traffic can be observed in that there is much greater pavement damage from heavy traffic over long periods than if the same traffic was applied over a shorter time period.

ANALYTICAL EVALUATION

Predicted Versus Actual ESALs

The actual number of ESALs was compared to the predicted ESAL due to the measured loss in present serviceability index, using the original AASHTO performance equation (i.e., Eq. 3). This comparison was made for each section of JPCP and JRCP in the data base. The actual pavement thicknesses, material properties, serviceability at the time of the study, and actual traffic were input into the equation. The drainage coefficient value for the equation was set at 1.0. The value of the *J* factor was 3.2 for joints with dowels and 4.1 for joints

with aggregate interlock (without dowels). The data retrieval and computations were completed by utilizing the Statistical Package for the Social Sciences (9). The analysis was run at the 50 percent level of reliability.

The pavement sections in the data base were divided into four broad climatic zones and the results were compared by zone. The data base contains jointed pavement sections from the following states: California (wet-freeze JPCP), Georgia (wet-nonfreeze JPCP), Illinois (wet-freeze JPCP and JRCP), Louisiana (wet-nonfreeze JRCP and JPCP), Minnesota (dry-freeze and wet-freeze JRCP), Nebraska (dry-freeze JRCP), and Utah (dry-freeze JPCP). The plots of predicted vs. actual ESALs for each climatic zone for JPCP and JRCP are given in Figure 3 and Figure 4, respectively.

A summary of the results of the predicted vs. actual ESALs for JPCP and JRCP is given in Table 1. The significance and comparison of the results are discussed below.

JPCP

The results are highly dependent on climate. Almost all the sections in the dry-nonfreeze climate performed better than the original AASHO model predicted (52 of 53 sections, or 98 percent acceptable). None of these pavements contained dowels as did the AASHO Road Test sections. The sections in the dry-freeze and wet-nonfreeze climates performed generally as predicted with 60 and 71 percent of the sections acceptable, respectively.

The JPCP sections in the wet-freeze climate (same as AASHO Road Test) performed worse than the AASHO model predicted with only 9 of 36 sections (or 25 percent) acceptable. The average actual ESALs in wet-freeze climate are 7.36 million less than the predicted ESALs (or 92 percent of the average actual ESALs). The JPCP sections performed adequately in the wet-nonfreeze and dry-freeze zones, with the actual ESALs approximately equal to the predicted ESALs.
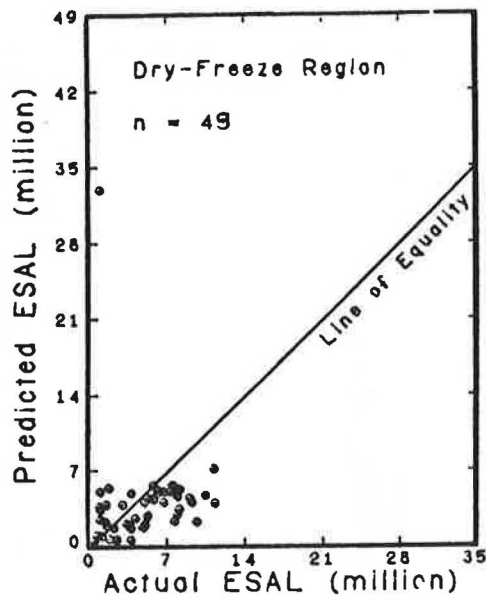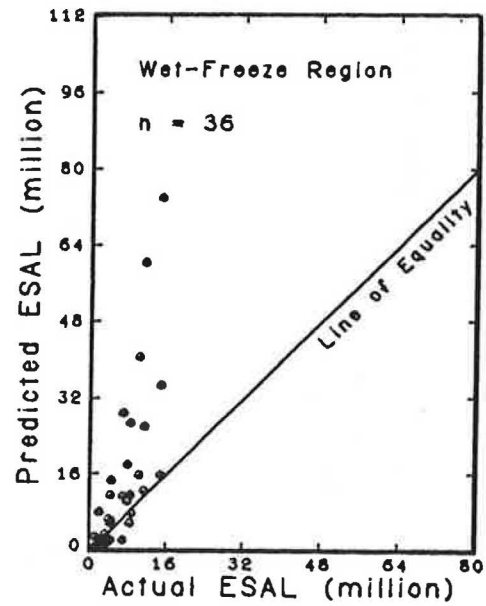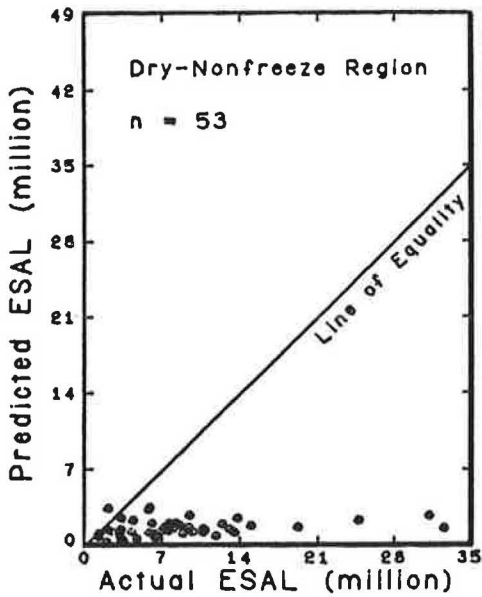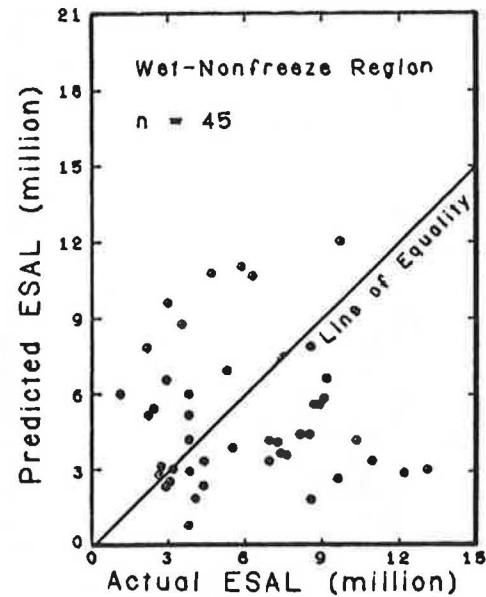
FIGURE 3 Predicted ESALs vs. actual ESALs for JPCP, using original AASHO Road Test PSI prediction model.

Figure 3(d) shows that a higher variation exists in prediction in the wet-nonfreeze zone. The results shown in the dry-freeze zone, that 86.9 percent of the average actual ESALs are less than the predicted ESALs, are somewhat biased because one slight-trafficked 13-in. slab section has an erratically high loss in PSI. See Figure 3(a).

The original AASHO equation seems to provide overly conservative JPCP structural designs in the dry-nonfreeze climate, adequate designs in the dry-freeze and wet-nonfreeze climates, but inadequate designs in the wet-freeze climate, all at the 50 percent reliability level.

JRCP

The results in Table 1 show that the JRCP sections did not perform as well in any climate as the original AASHO model predicted. For all the JRCP sections, only 41 of 374 (or 11 percent) performed better than predicted. The average actual ESALs for all JRCP sections were 10.58 million less than the predicted ESALs (or 193.6 percent of the average actual ESALs). On the basis of these results, the original AASHO equation does not provide adequate JRCP structural designs for any climate at the 50 percent reliability level.

(a)

(b)

(c)
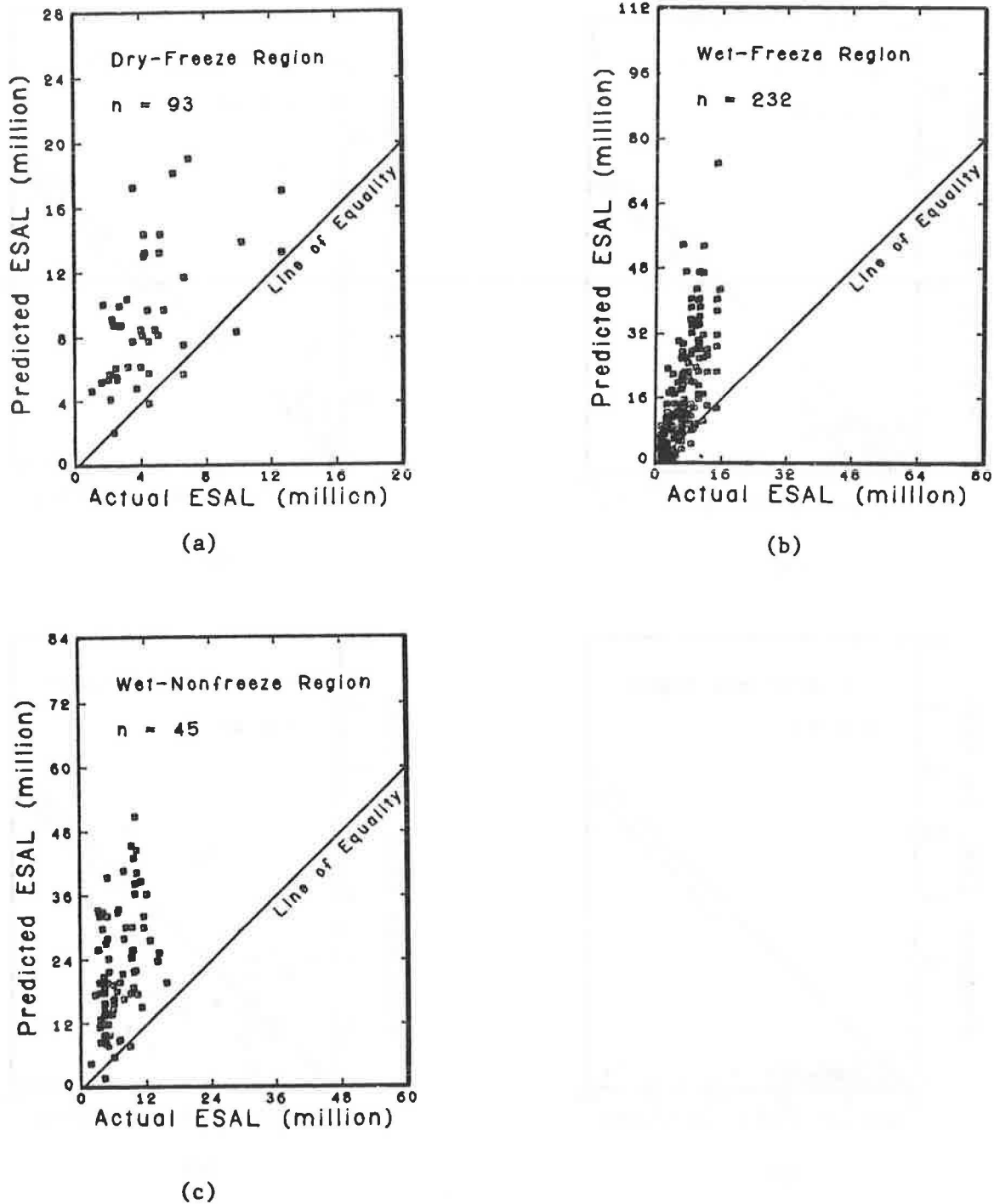
FIGURE 4   Predicted ESALs vs. actual ESALs for JRCP, using original AASHO Road Test PSI prediction model.

Climatic factors affect JRCP more severely than JPCP. Many of the JRCP sections in the NCHRP 1-19 data base have deteriorated because of factors other than traffic loading. Thus, the AASHO model does not provide adequate JRCP designs. The inherent variability in the prediction of pavement section performance indicates that there is a need to increase the reliability level and other design improvements if the equation is to provide adequate designs for JRCP sections.

Specific Design Evaluation

Results obtained from Heinrichs et al. (*10*) showed that a significant difference in pavement performance occurred only between the four major zones: wet-freeze, wet-nonfreeze, dry-freeze, and dry-nonfreeze. The specific design evaluation was then conducted using climatic data from the data base. The classification for the four broad climatic zones is the same

TABLE 1   SUMMARY OF RESULTS FOR ORIGINAL AASHO ROAD TEST PSI PREDICTION MODEL

Climatic Region (1)	# of Cases (2)	# of Section Acceptable* (3)	Percent Acceptable (4)=(3)/(2)	Mean Difference** (5)	Mean Percent Difference*** (6)
JPCP:					
Wet - Nonfreeze	45	27	60%	0.911	-17.1%
Wet - Freeze	36	9	25%	-7.355	-92.0%
Dry - Nonfreeze	53	52	98%	6.405	69.5%
Dry - Freeze	49	35	71%	0.763	-86.9%
Overall	183	123	67%	0.836	-25.4%
JRCP:					
Wet - Nonfreeze	93	3	3%	-15.460	-282.0%
Wet - Freeze	232	34	15%	-9.886	-168.8%
Dry - Nonfreeze	-****	-	-	-	-
Dry - Freeze	49	4	8%	-4.584	-143.0%
Overall	374	41	11%	-10.577	-193.6%

   *   "Acceptable" means the actual number of 18-kip ESALs is equal or greater than the predicted ESALs, i.e. the pavement section performed as good as or better than the AASHO model predicted, otherwise is "unacceptable".

  **   Difference = Actual ESAL - Predicted ESAL, in millions

 ***   Percent Difference = [(Actual ESAL - Predicted ESAL)/Actual ESAL] x 100%

****   No JRCP section is available in dry-nonfreeze region in COPES.

as used in the above predicted vs. actual ESAL evaluation. The prevailing values of the climatic data in each climatic zone as averaged from the data base are shown in Table 2.

A number of pavement design situations were developed for JPCP and JRCP over the four climatic zones. The design factors that were varied included two subgrade soils (fine-grained and coarse-grained), with and without dowels (JPCP only), and shorter and longer joint spacings (JRCP only). The fine-grained subgrade soils were defined as A-7-5 or A-7-6 in the AASHTO soil classification, and the coarse-grained subgrade soils were defined as A-2-6 or A-2-7. The drainage of these two types of subgrade soils was characterized as poor for the fine-grained soils and good for the coarse-grained soils. A resilient modulus of 3,000 psi was assumed for the fine-grained soils and 7,000 psi for the coarse-grained soils. The elastic k values for fine- and coarse-grained soils were assumed to be 100 pci and 190 pci, respectively, when the subgrade degree of saturation was compacted to 70–90 percent. The

1986 AASHTO Guide was used to generate pavement designs for JPCP and JRCP for each of the design situations. The design life was 20 years, and the design traffic was 15 million 18-kip ESALs in the design lane.

Specific soil, subbase, concrete, and other properties for the designs are shown in Table 3. The climatic design inputs for the new AASHTO Guide for each of the four climatic zones are given in Table 4. The values of the drainage coefficient C_d and loss-of-support factor LS were used as recommended in the Guide. The dowel size and the reinforcement (JRCP only) were also designed as recommended. The designs were developed at reliability levels of 50, 80, and 90 percent.

These designs were then evaluated using the deterioration models developed from the NCHRP 1-19 data base for pumping, faulting, cracking, joint deterioration, and PSI using the PREDICT program (written in Microsoft BASIC language for the IBM personal computer by M. I. Darter). These models

TABLE 2   SPECIFIC CLIMATIC DATA IN FOUR CLIMATIC ZONES AVERAGED FROM COPES DATABASE

JPCP:	Climatic Zones	Dry - Freeze	Wet - Freeze
	Annual Precipitation, cms	40	84
	Freezing Index, degree-days	250	625
	Mean Temperature, ^{o}C	11	11
*	Temperature Range, ^{o}C	41	41

	Climatic Zones	Dry - Nonfreeze	Wet - Nonfreeze
	Annual Precipitation, cms	40	120
	Freezing Index, degree-days	0	0
	Mean Temperature, ^{o}C	19	19
	Temperature Range, ^{o}C	25	30

JRCP:	Climatic Zones	Dry - Freeze	Wet - Freeze
	Annual Precipitation, cms	55	78
	Freezing Index, degree-days	1125	1125
	Mean Temperature, ^{o}C	8	8
	Temperature Range, ^{o}C	45	43

	Climatic Zones	Dry - Nonfreeze	Wet - Nonfreeze
	Annual Precipitation, cms	-**	120
	Freezing Index, degree-days	-	0
	Mean Temperature, ^{o}C	-	17
	Temperature Range, ^{o}C	-	34

----

*   Temperature Range = average daily maximum air temperature in July
                        minus average daily minimum air temperature in
                        January, ^{o}C

** No JRCP section is available in dry-nonfreeze climate in COPES.

TABLE 3   DESIGN INPUT PARAMETERS FOR AASHTO PERFORMANCE EQUATION FOR COPES FOUR CLIMATIC ZONES

- -

Parameter	JPCP	JRCP
Reliability level, %	50/80/90	50/80/90
Design period, years	20	20
Traffic, million 18-kip ESAL	15	15
* Subgrade soil type	fine/coarse	fine/coarse
** Subbase type	4" CTB	6" granular
k-value @ top of subbase, pci	300/590	200/420
Initial serviceability	4.5	4.5
Terminal serviceability	2.5	2.5
*** Modulus of rupture, psi	650	650
Concrete E value, psi	4,000,000	4,000,000
Joint spacing, ft	15	27/40
Dowels at joint	yes/no	yes
J factor	3.2/4.1	3.2

- -

* Subgrade M_R = 3,000 psi for fine-grained soil and 7,000 psi for coarse-grained soil.

** Subbase E = 1,000,000 psi for CTB and 30,000 psi for granular material.

*** Third-point loading, at 28 days

TABLE 4 CLIMATIC DESIGN INPUTS FOR AASHTO GUIDE FOR COPES FOUR CLIMATIC ZONES

JPCP Climatic zones	Dry - Freeze				Wet - Freeze			
Subgrade soil type	fine		coarse		fine		coarse	
Dowel bars	no	yes	no	yes	no	yes	no	yes
C_d value	.95	.95	1.13	1.13	.85	.85	1.05	1.05
LS factor	.5	.5	.25	.25	1.0	1.0	.5	.5
* Corrected k-value	175	175	400	400	100	100	290	290
Climatic zones	Dry - Nonfreeze				Wet - Nonfreeze			
Subgrade soil type	fine		coarse		fine		coarse	
Dowel bars	no	yes	no	yes	no	yes	no	yes
C_d value	.95	.95	1.13	1.13	.8	.8	1.0	1.0
LS factor	.5	.5	.25	.25	1.0	1.0	.5	.5
Corrected k-value	175	175	400	400	100	100	290	290

JRCP Climatic zones	Dry - Freeze		Wet - Freeze	
Subgrade soil type	fine	coarse	fine	coarse
Dowel bars	yes	yes	yes	yes
C_d value	.95	1.13	.85	1.05
LS factor	.5	.25	1.0	.5
Corrected k-value	120	300	70	230
Climatic zones	Dry - Nonfreeze		Wet - Nonfreeze	
Subgrade soil type	fine	coarse	fine	coarse
Dowel bars	yes	yes	yes	yes
C_d value	- **	-	.8	1.0
LS factor	-	-	1.0	.5
Corrected k-value	-	-	70	230

* k-value in pci.

** No JRCP section is available in dry-nonfreeze climate in COPES.

represent the data base mathematically. They provide average projections with about one-half the actual showing worse deterioration and the other half showing less deterioration.

The critical level for each kind of deterioration mentioned above that normally generates the need for rehabilitation is as follows:

Deterioration	JPCP	JRCP
Pumping	1 (low severity)	1 (low severity)
Faulting (in.)	0.13	0.26
Cracking (ft/mile)	800 (all severities)	850 (medium and high severity)
Joint deterioration (joints/mile)	55 (mostly medium severity)	27 (mostly high severity)
PSI	3.0	3.0

These are average values that were determined from the NCHRP 1-19 data base for sections that were in need of pavement rehabilitation (6).

JPCP

Tables 5 and 6 show the predicted deterioration for each level of reliability for JPCP designs. Figures 5, 6, and 7 illustrate predicted pumping severity, faulting, and slab cracking, respectively.

● Increasing design reliability from 50 to 90 percent increases the thickness of the slab by about 1.5 in. The deterioration prediction models indicate that JPCP slab cracking decreases greatly with this increase in reliability. Pumping and joint faulting decrease a small amount, and terminal PSI increases

TABLE 5   PREDICTIONS FOR JPCP DESIGNS USING AASHTO GUIDE FOR FOUR CLIMATIC ZONES: 50 PERCENT RELIABILITY LEVEL

Climatic zones	Dry-freeze				Wet-freeze			
Subgrade soil type	fine		coarse		fine		coarse	
Dowel diameter, in	0	1.125	0	1.00	0	1.25	0	1.00
Slab thickness, in	10.6	9.3	9.2	7.9	11.5	10.1	9.8	8.5
Pumping *	.6	1.3	.6	1.7	2	2.6	1.9	2.8
Faulting, in	.1	.05	.11	.07	.12	.05	.13	.09
Cracking, ft/mile	151	368	249	713	115	315	251	853
Joint deter., jts/mile	12	12	12	12	12	12	12	12
PSI	3.7	3.5	3.6	3.4	3.3	3.0	3.1	2.8

Climatic zones	Dry-nonfreeze				Wet-nonfreeze			
Subgrade soil type	fine		coarse		fine		coarse	
Dowel diameter, in	0	1.125	0	1	0	1.25	0	1.125
Slab thickness, in	10.6	9.3	9.2	7.9	11.8	10.4	10	8.7
Pumping	0	.8	0	1.1	.5	1.1	.4	1.3
Faulting, in	.06	0	.07	.03	.06	0	.07	.01
Cracking, ft/mile	51	117	72	144	41	80	70	134
Joint deter., jts/mile	12	12	12	12	12	12	12	12
PSI	4.0	3.8	3.9	3.7	3.6	3.4	3.4	3.2

*   Pumping = 1 for low, 2 for medium and 3 for high severity.

Design traffic: 15 million 18-kip ESAL
Design period: 20 years
Subbase type: 4" CTB
Joint spacing: 15 ft
Level of reliability: 50%

a small amount. Joint deterioration does not change, however. Increasing design reliability is an effective way to reduce slab cracking, but not other types of deterioration.

● The use of dowels in transverse joints results in a decrease of about 1.4 in. of slab thickness. The thinner slab develops more cracking, but joint faulting decreases substantially for designs having dowel bars.

● The required slab thickness is reduced about 1.6 in. when the subgrade soil changes from fine-grained to coarse-grained. Even though a coarse-grained soil improves support and subdrainage, slab thickness is decreased by this extent, which has the overall effect of increasing the amount of slab cracking.

● Pumping is predicted to occur in all climatic regions, but

severe pumping is predicted in the wet-freeze region for these particular designs.

● Transverse joint faulting decreases greatly with the use of dowels. Faulting is greatest in the freeze zones (where without dowels it exceeds the 0.13-in. critical level) and least in the nonfreeze zones. Increased design reliability does not improve faulting very much.

● Slab cracking increases whenever slab thickness is decreased. However, even the maximum predicted cracking is below the critical level for JPCP for all designs.

● Transverse joint deterioration is not affected by design reliability, and joint deterioration for JPCP is minimal.

● Present serviceability ratings at the end of the design life

TABLE 6   PREDICTIONS FOR JPCP DESIGNS USING AASHTO GUIDE FOR FOUR CLIMATIC ZONES:
90 PERCENT RELIABILITY LEVEL

Climatic zones	Dry-freeze				Wet-freeze			
Subgrade soil type	fine		coarse		fine		coarse	
Dowel diameter, in	0	1.375	0	1.125	0	1.375	0	1.25
Slab thickness, in	12.1	10.7	10.6	9.2	13.1	11.5	11.3	9.8
Pumping *	0	.6	0	.6	1.5	2.0	1.2	1.9
Faulting, in	.09	0	.1	.05	.11	.02	.12	.05
Cracking, ft/mile	70	143	109	249	49	115	91	251
Joint deter., jts/mile	12	12	12	12	12	12	12	12
PSI	4.0	3.7	3.8	3.6	3.5	3.3	3.3	3.1

Climatic zones	Dry-nonfreeze				Wet-nonfreeze			
Subgrade soil type	fine		coarse		fine		coarse	
Dowel diameter, in	0	1.375	0	1.125	0	1.5	0	1.25
Slab thickness, in	12.1	10.7	10.6	9.2	13.5	11.9	11.6	10.1
Pumping	0	0	0	0	0	.4	0	.4
Faulting, in	.05	0	.06	0	.05	0	.06	0
Cracking, ft/mile	25	48	37	72	20	39	34	67
Joint deter., jts/mile	12	12	12	12	12	12	12	12
PSI	4.3	4.0	4.1	3.9	3.9	3.6	3.7	3.4

----

*   Pumping = 1 for low, 2 for medium and 3 for high severity.
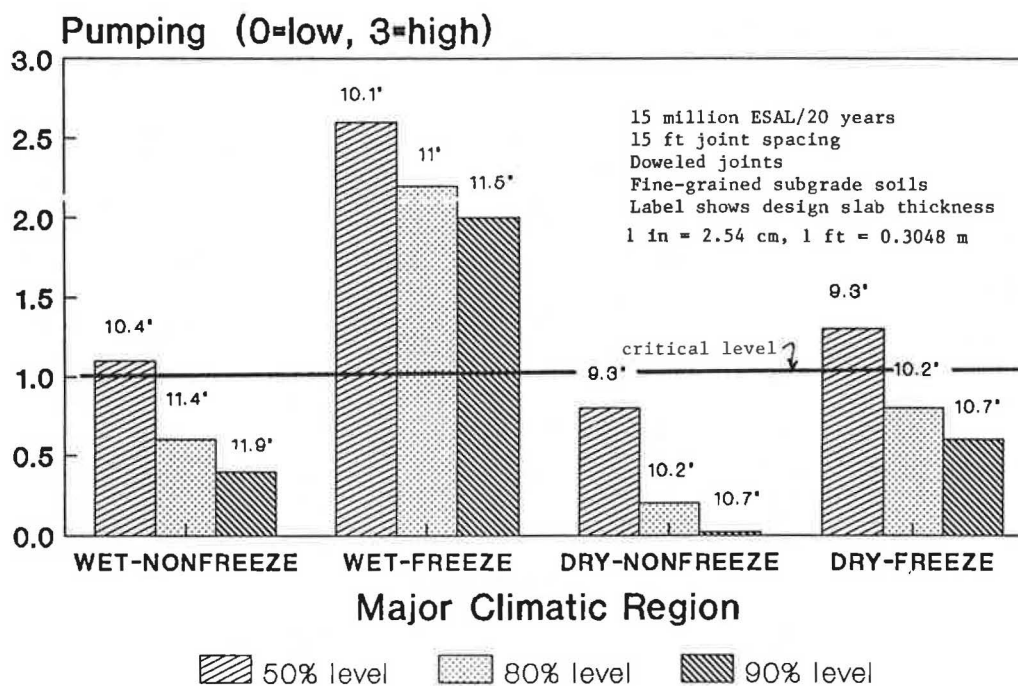
Design traffic: 15 million 18-kip ESAL
Design period: 20 years
Subbase type: 4" CTB
Joint spacing: 15 ft
Level of reliability: 90%

FIGURE 5 Pumping severity by climatic regions at various reliability levels for AASHTO JPCP designs.

are all predicted to be above 3.0 (with one slight exception). Increased design reliability increases terminal serviceability by a small amount.

Overall, deterioration of JPCP generally increases as the climate becomes wetter or colder, even though the design procedure attempts to adjust the design for climate. Deterioration differs significantly among climatic regions. The drainage coefficient, C_d, value had a significant influence on the thickness design.

In general, the results show that the AASHTO Guide provides adequate structural designs for JPCP at the higher design reliability level for this example. JPCP in wet- or dry-freeze regions shows more deterioration (particularly pumping) than other regions. Special design improvements may be necessary in freeze areas.

JRCP

Tables 7 and 8 show the predicted deterioration for each level of reliability for JRCP designs. Figures 8, 9, and 10 illustrate predicted pumping severity, cracking, and joint deterioration, respectively.

- Increasing design reliability from 50 to 90 percent increases the thickness of the slab by about 1.4 in. The deterioration prediction models indicate that JRCP slab cracking, faulting, and pumping decrease substantially with this increase in reliability. Terminal PSI increases somewhat. Joint deterioration does not change, however. Increasing design reliability (and hence slab thickness) is an effective way to reduce slab cracking, but probably not the other types of deterioration.
- All the JRCP sections were designed with dowels. The

presence of dowels replaces approximately 1.4 in. of slab thickness. JRCP with dowels did not show excessive joint faulting.

- At every reliability level, the AASHTO Guide requires thinner slabs for the JRCP on coarse-grained subgrade soil than on fine-grained subgrade soil. For example, at the 50 percent reliability level (Table 8), the required slab thickness for shorter and longer joint spacings varies from 1.3 to 1.7 in. between fine- and coarse-grained subgrade soil designs. Even though a course-grained soil improves support and subdrainage, slab thickness is decreased by this extent, which has the overall effect of increasing the amount of slab cracking.
- Pumping is predicted to occur in all climatic regions, but severe pumping is predicted in both freeze regions.
- Faulting is greatest in the freeze zones; however, predicted faulting for all designs was less than critical for JRCP (0.26 in.). Increased design reliability does not improve faulting very much.
- Transverse joint deterioration is not affected by design reliability. It is greatest in the freezing climatic zones where the 40-ft designs are predicted to exceed the critical level of 27 joints per mile. The shorter 27-ft designs do not exceed this critical level of deterioration.
- Transverse cracks are predicted to become a severe problem for almost all of the design cases. The increased slab thickness for increased reliability helps, but does not solve the problem.
- The PSI at the end of the design life falls below the critical level of 3.0 in several cases at the 50 percent reliability level, but not at the 80 or 90 percent levels. Increased reliability increases terminal serviceability somewhat.

Overall, deterioration of JRCP increases as the climate becomes wetter or colder, even though the procedure attempts

Joint Faulting (in)

15 million ESAL/20 years
15 ft joint spacing
Doweled joints
Fine-grained subgrade soils
Label shows design slab thickness

1 in = 2.54 cm, 1 ft = 0.3048 m

critical →

WET-NONFREEZE   WET-FREEZE   DRY-NONFREEZE   DRY-FREEZE

Major Climatic Region

▨ 50% level   ▤ 80% level   ▨ 90% level

(a)   undoweled

Joint Faulting (in)

15 million ESAL/20 years
15 ft joint spacing
Doweled joints
Fine-grained subgrade soils
Label shows design slab thickness

1 in = 2.54 cm, 1 ft = 0.3048 m

critical →

WET-NONFREEZE   WET-FREEZE   DRY-NONFREEZE   DRY-FREEZE

Major Climatic Region

▨ 50% level   ▤ 80% level   ▨ 90% level

(b)   doweled

FIGURE 6   JPCP faulting predictions by climatic regions for undoweled and doweled pavements at various reliability levels.

Cracking (ft/mile)

15 million ESAL/20 years
15 ft joint spacing
Doweled joints
Fine-grained subgrade soils
Label shows design slab thickness
1 in = 2.54 cm, 1 ft = 0.3048 m

Major Climatic Region

WET-NONFREEZE WET-FREEZE DRY-NONFREEZE DRY-FREEZE

50% level 80% level 90% level

FIGURE 7 Predicted slab cracking by climatic regions at various reliability levels for AASHTO JPCP designs.

to adjust the design for climate. Significant differences in performance exist between climatic regions. The drainage coefficient, C_d, value had a significant influence on the thickness design.

In general, the prediction results show that the new Guide provides only fair structural designs for JRCP for the four climatic regions and worse designs for the wet-freeze region. This is evidenced by excessive crack deterioration, pumping, and joint deterioration. The AASHTO Guide does not provide adequate structural designs for JRCP on coarse-grained subgrade soils. However, a comparison of the results from the predicted vs. actual ESAL evaluation, which simulates the original AASHO Road Test performance model, with these results shows that the adjustment factors provided in the new AASHTO Guide are somewhat effective in improving the JRCP designs.

Some components of the pavement, however, showed serious failure and did not improve at the higher levels of reliability. This included joint deterioration with 40-ft or more joint spacing. For example, the JRCP with 27-ft joint spacing has less faulting than with 40-ft joint spacing. The 40-ft joint spacing also results in serious joint deterioration whereas the 27-ft joint spacing gives much better performance. As many as 61 deteriorated joints per mile were predicted for the 40-ft joint spacing in the freeze climates (Figures 8, 9, and 10). The AASHTO Guide does not provide adequate, coherent guidance on joint design.

CONCLUSIONS

The conceptual evaluation of the 1986 AASHTO Design Guide indicated that, since the AASHTO structural design model

was empirically derived in a single climate, with a single set of materials, and a short traffic loading period, it has many potential inherent weaknesses and limitations. Major ones include subdrainage consideration, climatic extrapolation, long-term climatic effects, joint design, and reinforcement design.
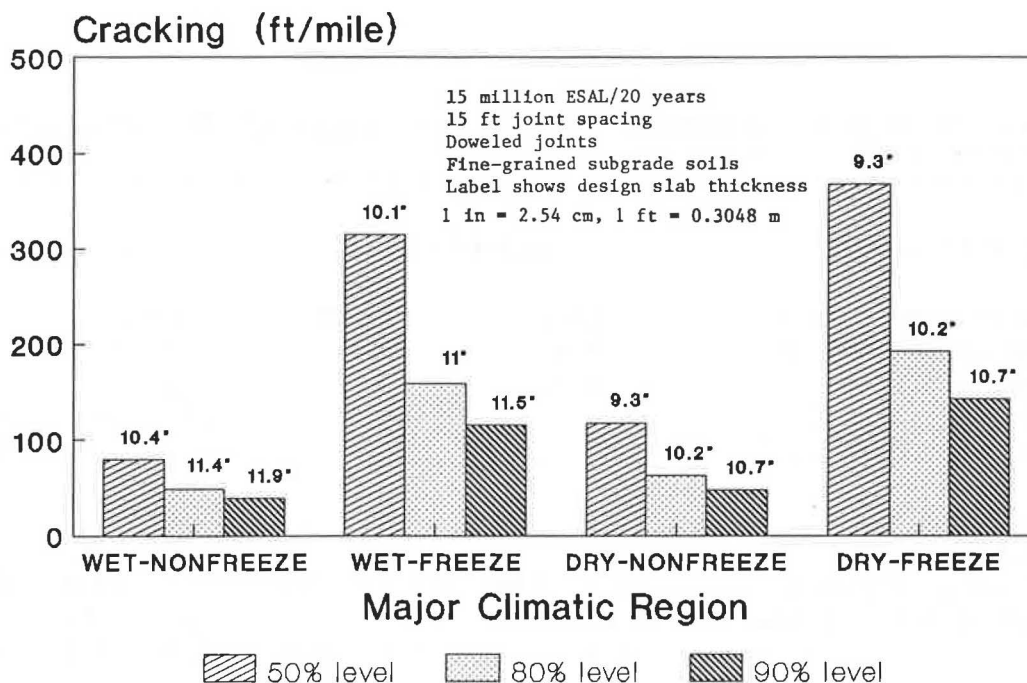
The analytical evaluation generally supports the conceptual evaluation. There is serious prediction error associated with the original AASHO equations when they are used for differing climates and for different pavement designs. The design adjustment factors included in the new AASHTO Guide are beneficial, particularly the design reliability. However, the joint design, loss-of-support, and drainage coefficient recommendations are still particularly deficient. JPCP designs appear to be much more resistant to the long-term damaging effects of time and climate than JRCP designs.

The overall conclusion is that there are several deficiencies in the new Guide. It is recommended that each agency that adopts the guide conduct an evaluation similar to the example reported herein to determine the general deterioration of pavements existing on their highways. Recommendations for joint design must be developed by each agency since none exist in the Guide. Levels of reliability higher than 50 percent must be considered to provide adequate designs. The 90 percent level studied here showed reasonable results for JPCP. Improved reinforcement design is needed for JRCP to control crack deterioration.

ACKNOWLEDGMENT

TABLE 7   PREDICTIONS FOR JRCP DESIGNS USING AASHTO GUIDE FOR FOUR CLIMATIC ZONES:
50 PERCENT RELIABILITY LEVEL

Climatic zones	Dry-freeze				Wet-freeze			
Subgrade soil type	fine		coarse		fine		coarse	
Slab thickness, in	9.4		8.1		10.2		8.6	
Dowel diameter, in	1.125		1		1.25		1.125	
Joint spacing, ft	27	40	27	40	27	40	27	40
Area of steel, sq in/ft	.047	.069	.04	.06	.051	.075	.043	.064
Pumping *	1.6	1.6	3	3	2.2	2.2	3	3
Faulting, in	.07	.12	.16	.17	.06	.11	.09	.14
Cracking, ft/mile	1322	1300	2932	2904	1166	1169	2437	2432
Joint deter., jts/mile	0	61	0	61	0	61	0	61
PSI	3.1	3.0	2.7	2.6	3.3	2.9	3.2	2.8

Climatic zones	Dry-nonfreeze			Wet-nonfreeze			
Subgrade soil type	- **			fine		coarse	
Slab thickness, in	-			10.6		8.9	
Dowel diameter, in	-			1.375		1.125	
Joint spacing, ft	-			27	40	27	40
Area of steel, sq in/ft	-			.053	.078	.044	.066
Pumping	-			1.1	1.1	2.1	2.1
Faulting, in	-			0	.05	.03	.08
Cracking, ft/mile	-			942	944	1636	1639
Joint deter., jts/mile	-			0	35	0	35
PSI	-			3.3	3.2	2.9	2.9

----

*   Pumping = 1 for low, 2 for medium and 3 for high severity.

** No JRCP section is available in dry-nonfreeze climate in COPES.

Design traffic: 15 million 18-kip ESAL
Design period: 20 years
Subbase type: 6" granular
Level of reliability: 50%

TABLE 8 PREDICTIONS FOR JRCP DESIGNS USING AASHTO GUIDE FOR FOUR CLIMATIC ZONES: 90 PERCENT RELIABILITY LEVEL

Climatic zones	Dry-freeze				Wet-freeze			
Subgrade soil type	fine		coarse		fine		coarse	
Slab thickness, in	10.8		9.4		11.7		10	
Dowel diameter, in	1.375		1.125		1.5		1.25	
Joint spacing, ft	27	40	27	40	27	40	27	40
Area of steel, sq in/ft	.054	.08	.047	.069	.058	.086	.05	.074
Pumping *	.5	.5	.9	.9	1.5	1.5	1.6	1.6
Faulting, in	0	.05	0	.05	0	.05	0	.03
Cracking, ft/mile	906	906	1265	1271	822	822	1099	1100
Joint deter., jts/mile	0	61	0	61	0	61	0	61
PSI	3.6	3.5	3.4	3.3	3.5	3.4	3.3	3.2

Climatic zones	Dry-nonfreeze				Wet-nonfreeze			
Subgrade soil type	- **				fine		coarse	
Slab thickness, in	-				12		10.2	
Dowel diameter, in	-				1.5		1.25	
Joint spacing, ft	-				27	40	27	40
Area of steel, sq in/ft	-				.06	.089	.051	.075
Pumping	-				.6	.6	.7	.7
Faulting, in	-				0	.03	0	0
Cracking, ft/mile	-				775	775	1017	1020
Joint deter., jts/mile	-				0	35	0	35
PSI	-				3.6	3.5	3.4	3.3

----

* Pumping = 1 for low, 2 for medium and 3 for high severity.

** No JRCP section is available in dry-nonfreeze climate in COPES.

Design traffic: 15 million 18-kip ESAL
Design period: 20 years
Subbase type: 6" granular
Level of reliability: 90%
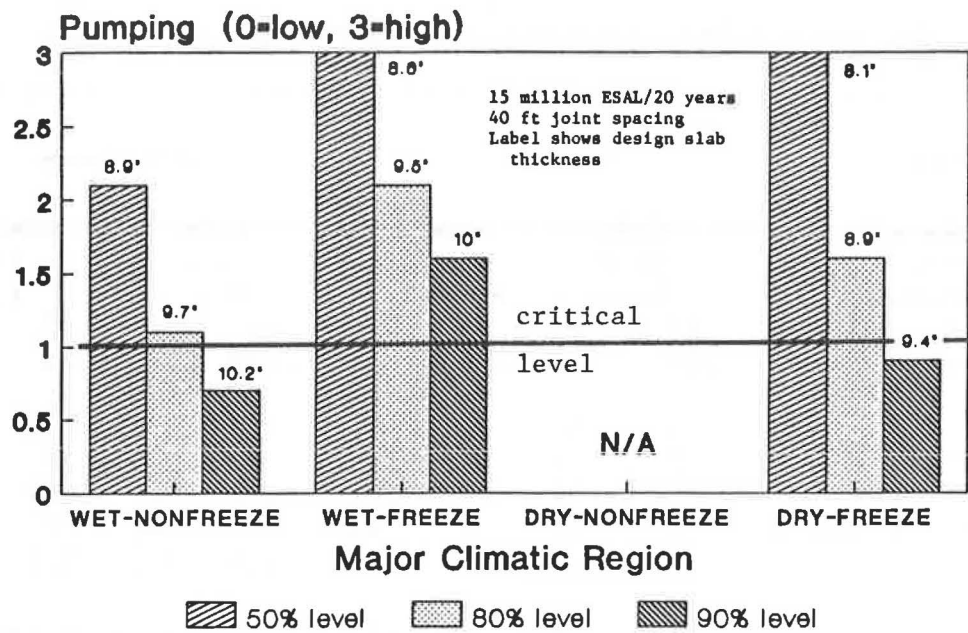
(a) coarse-grained subgrade soil
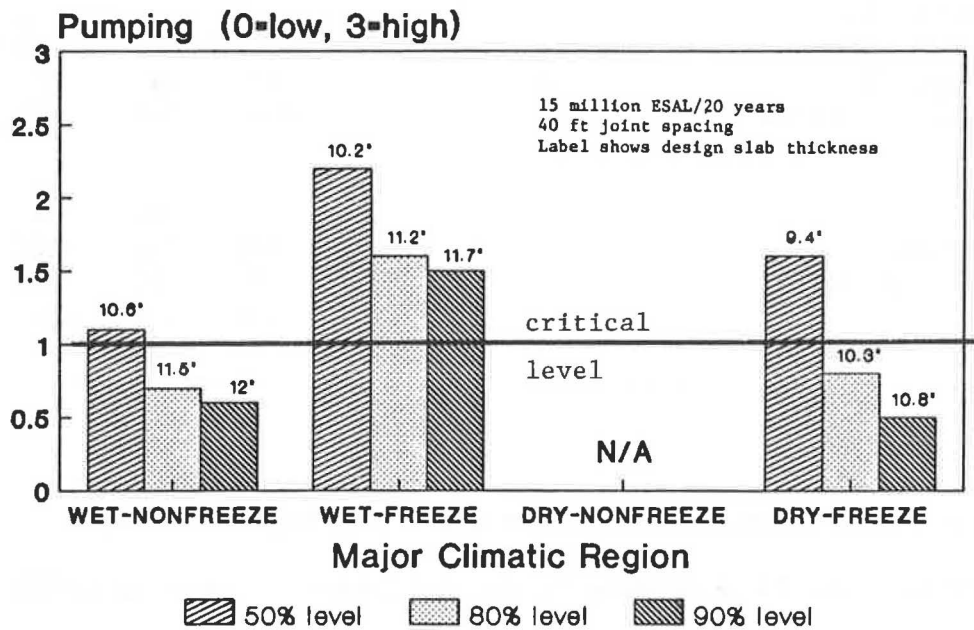
(b) fine-grained subgrade soil

FIGURE 8 Pumping severity by climatic regions at various reliability levels for AASHTO JRCP designs.
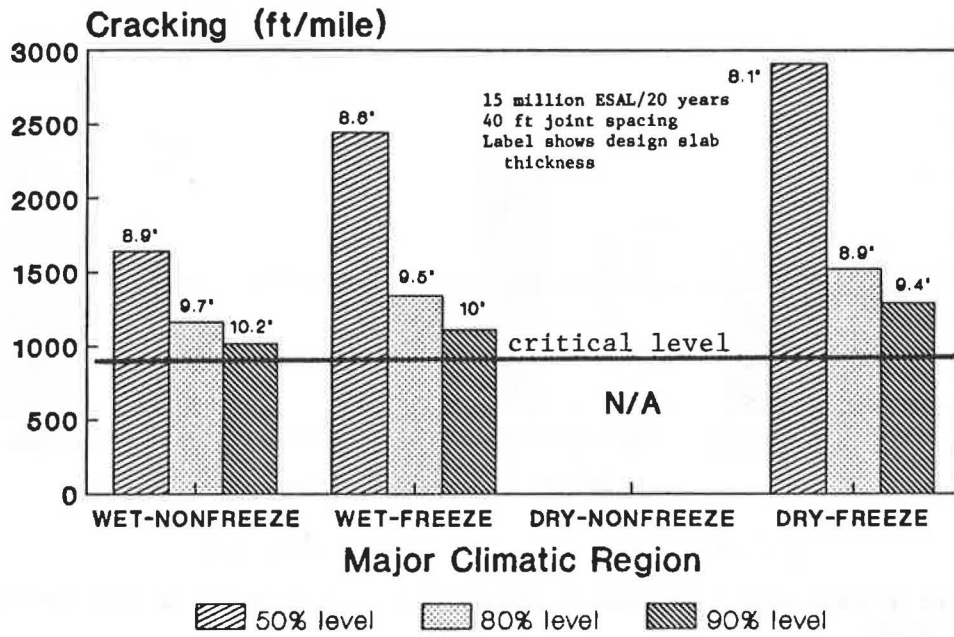
(a)   coarse-grained subgrade soil
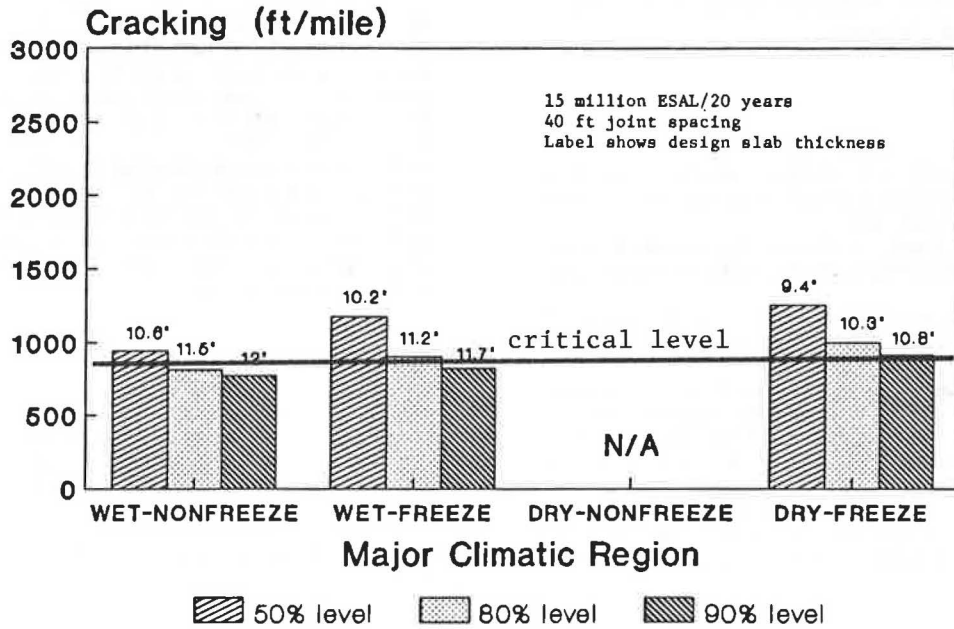
(b)   fine-grained subgrade soil

FIGURE 9 Predicted slab cracking by climatic regions at various reliability levels for AASHTO JRCP designs.
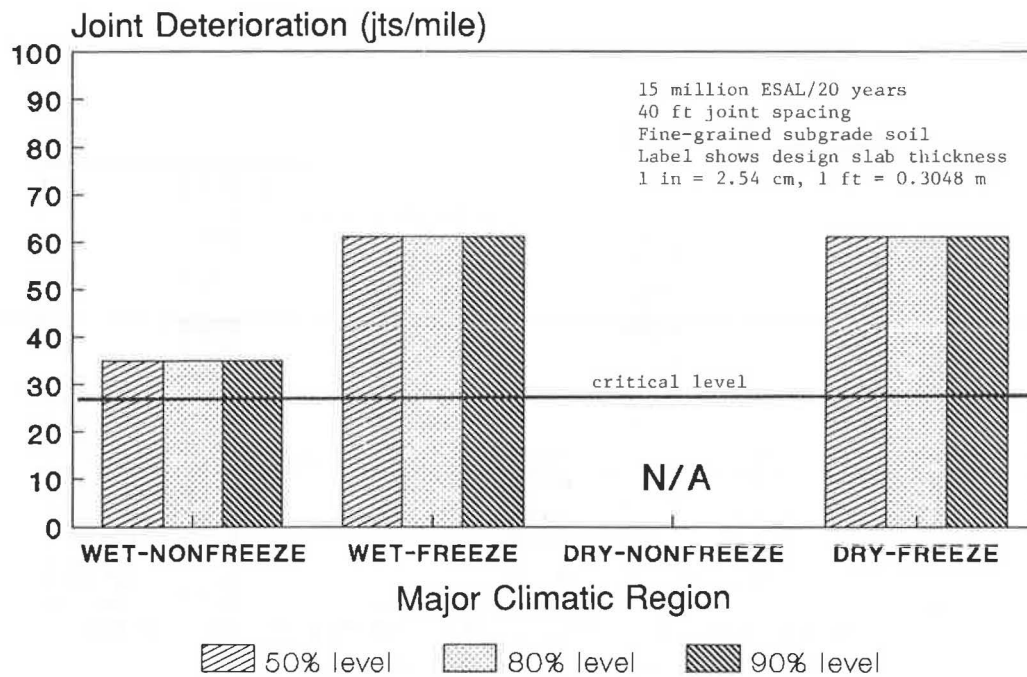
FIGURE 10   Predicted joint deterioration by climatic regions at various reliability levels for AASHTO JRCP designs.

at Urbana-Champaign. The authors express their appreciation to Stephen Forster of the Federal Highway Administration for his assistance and comments.

REFERENCES

1. *AASHO Interim Guide for the Design of Rigid Pavement Structures.* American Association of State Highway Officials, Committee on Design, April 1962.
2. *AASHTO Interim Guide for Design of Pavement Structures.* American Association of State Highway and Transportation Officials, 1972.
3. *AASHTO Interim Guide for Design of Pavement Structures 1972; Chapter III Revised, 1981.* American Association of State Highway and Transportation Officials, 1981.
4. *AASHTO Guide for Design of Pavement Structures.* American Association of State Highway and Transportation Officials, 1986.
5. *Special Report 61E: The AASHO Road Test, Report 5—Pavement Research.* HRB, National Research Council, Washington, D.C., 1962.
6. M. I. Darter, J.M. Becker, M. B. Snyder, and R. E. Smith. *Concrete Pavement Evaluation System (COPES).* NCHRP Report No. 277, TRB, National Research Council, Washington, D.C., 1985.
7. *Special Report 73: The AASHO Road Test—Proceedings of a Conference Held May 16–18, 1962, St. Louis, Mo.* HRB, National Research Council, Washington, D.C., 1962.
8. M. I. Darter and E. J. Barenberg. *Zero-Maintenance Pavement: Results of Field Studies on the Performance Requirements and Capabilities of Conventional Pavement Systems—Interim Report.* Report FHWA-RD-76-105, FHWA, U.S. Department of Transportation, April 1976.
9. N. H. Nie, et al. *Statistical Package for the Social Sciences (SPSS),* 2nd Ed. McGraw-Hill, Inc., New York, 1975.
10. K. W. Heinrichs, M. Liu, M. I. Darter, S. H. Carpenter, and A. Ioannides. *Rigid Pavements Analysis and Design.* Technical Report prepared by the University of Illinois for the Federal Highway Administration, 1987.

Expert System for Concrete Pavement Evaluation and Rehabilitation

KATHLEEN T. HALL, JAMES M. CONNOR, MICHAEL I. DARTER, AND
SAMUEL H. CARPENTER

A prototype knowledge-based system has been developed to
assist state highway engineers in project-level evaluation and
rehabilitation planning and design for high-type (Interstate)
concrete pavements. It uses information provided by the engi-
neer to identify types of deterioration present and determine
their causes, to select rehabilitation techniques that will effec-
tively correct the existing deterioration and prevent its recur-
rence, to combine individual rehabilitation techniques into fea-
sible rehabilitation strategies, and to predict the performance
of alternative rehabilitation strategies. Pavement types addressed
by the system are jointed reinforced concrete, jointed plain
concrete, and continuously reinforced concrete. Predictive
models are incorporated into the system to show future pave-
ment performance with and without rehabilitation. These models
were developed from national data bases of concrete pavement
projects and may be of limited applicability to a specific state's
climatic conditions and materials. Interactive computer pro-
grams for each of the three pavement types will operate on
any IBM-compatible personal computer.

The objective of this research effort was to develop practical
and comprehensive systems to assist practicing engineers in
evaluating concrete highway pavements, in identifying types
of deterioration present and determining their causes, in
selecting rehabilitation techniques that will effectively correct
existing deterioration and prevent its recurrence, in combin-
ing individual rehabilitation techniques into feasible rehabil-
itation strategies, and in predicting the performance of reha-
bilitation strategy alternatives.

The system is intended for use by state highway engineers
in project-level rehabilitation planning and design for high-
type (Interstate) jointed reinforced (JRCP), jointed plain
(JPCP), and continuously reinforced (CRCP) concrete pave-
ments. The system does not perform thickness or joint design;
the engineer must use existing design procedures to determine
these details.

The evaluation/rehabilitation system has been developed
in the form of a knowledge-based expert system, which uses
information about the pavement provided by the engineer to
guide him or her through evaluation of the pavement's present
condition and development of one or more feasible rehabil-
itation strategies. The procedure was developed through
extensive interviewing of and interaction with authorities on
concrete pavement performance. In addition, predictive models
are used to show future pavement performance both with and
without rehabilitation.

Department of Civil Engineering, University of Illinois, 208 N.
Romine Street, Urbana, Ill. 61801.

Evaluation of a pavement and development of feasible
rehabilitation alternatives is performed according to the fol-
lowing steps:

1. Project data collection,
2. Extrapolation of project condition over its entire length,
3. Evaluation of present condition,
4. Prediction of condition without rehabilitation,
5. Physical testing as needed,
6. Selection of main rehabilitation approach,
7. Development of detailed rehabilitation strategy,
8. Prediction of rehabilitation strategy performance,
9. Cost analysis of alternatives, and
10. Selection of preferred rehabilitation strategy alterna-
tive.

The system has been developed in manual as well as com-
puterized form. An interactive computer program has been
developed for each of the three pavement types addressed.
The programs operate on any IBM-compatible personal com-
puter. Use of the computer program is highly recommended
because of the complexity of the manual procedure.

KNOWLEDGE-BASED APPROACH TO CONCRETE
PAVEMENT EVALUATION AND REHABILITATION

Problem Description

Rehabilitation design involves two activities: evaluation of a
pavement's present condition, which includes recognition of
various types of deterioration and identification of the mech-
anisms responsible for them; and development of rehabili-
tation alternatives that will cost-effectively repair the distress
and prevent its recurrence (*1*). Distresses are, to use a medical
analogy, only symptoms of a problem, and treating the symp-
toms does not necessarily treat the problem. Quick-fix repairs,
which correct the existing distress without arresting the mech-
anisms that caused it, have a high probability of premature
failure and thus are ultimately not cost-effective.

Rehabilitation design requires a good understanding of how
pavements perform. However, concrete pavement perform-
ance is a complex phenomenon, which is influenced by a large
number of factors relating to design, construction, materials,
environment, and traffic. These factors interact to influence
performance in ways that are not clearly understood. Thus,
whereas some aspects of concrete pavement performance can

be explained by mechanistic models and well-established principles (e.g., calculation of stresses and fatigue damage), many other aspects cannot.

Engineering Problem Solving with Expert Systems

In many areas of engineering, problem solving relies on two different types of knowledge: *deterministic,* which is the body of information that is widely accepted by and available to engineers in the field; and *heuristic,* which is the subjective knowledge possessed by individual engineers, characterized by beliefs, opinions, and rules of thumb (2). Difficult engineering problems typically cannot be solved with deterministic knowledge alone, for two major reasons. First, the problem may be so complex that available deterministic knowledge is incomplete. Second, many engineering problems do not have clear-cut right and wrong answers. Finding a "good enough" answer or selecting the best option from among a number of alternatives demands that the engineer apply good judgment. This too requires considerable technical skill on the engineer's part, since these decisions must be based on familiarity with the domain and experience in solving similar problems.

Although deterministic knowledge is preservable in references and textbooks, heuristic knowledge definitely is not. Since it is acquired through individual experience, it is not easily communicated to others and, as experienced engineers retire, it is often lost. The challenge of organizing and preserving heuristic problem-solving knowledge is the basis for development of a relatively new type of engineering tool known as knowledge-based systems. These are computer programs in which heuristic knowledge that has been acquired from humans is utilized to solve problems that are intractable with

a purely deterministic approach. A subset of knowledge-based systems are expert systems, which use both the knowledge and the reasoning methods of human experts.

Pavement Evaluation and Rehabilitation with Expert Systems

Pavement evaluation is a *diagnostic* activity, similar to medical diagnosis, in which conclusions about the pavement's condition are drawn from an examination of relevant factual data. Several approaches exist for performing diagnostic activities with knowledge-based expert systems. The approach selected was to develop a decision tree for each major problem area of concrete pavement performance (e.g., roughness, structural adequacy). Decision trees permit factual information as well as reasoning processes to be conceptually expressed and graphically illustrated in a form that is easy to understand, examine, and revise. The paths of the decision trees lead to one or more sentences of text explaining the deficiencies that exist and the factors considered in identifying them. These conclusions are represented by a three-letter code for the major problem area and the number of the specific conclusion reached. The decision tree for structural adequacy of JPCP is shown in Figure 1 as an example.

A pavement evaluation system that can only identify current rehabilitation needs has limited usefulness as a pavement management tool. What about a pavement that does not need rehabilitation now, but will within the next five years? What about a relatively new pavement that does not exhibit much visible distress, but which is inadequately designed or constructed to withstand the traffic loadings and environmental influences that will act upon it over its design life? Deter-
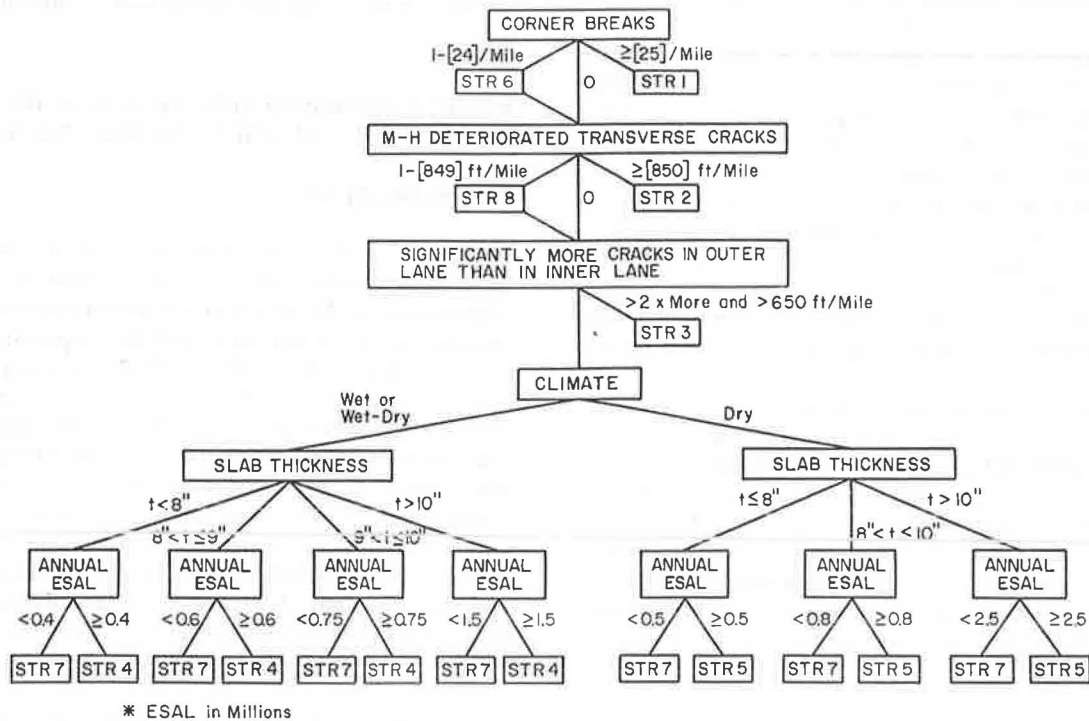

FIGURE 1 Structural deficiency decision tree for JPCP.

ministic knowledge can be applied here, in the form of existing models for predicting concrete pavement performance. A number of predictive models for key concrete pavement distress types are used to project the future condition of the pavement without rehabilitation. The system uses these predicted values to reevaluate the pavement each year for the next 20 years into the future, and identify the years in which deficiencies in the various problem areas will occur. By combining deterministic and heuristic knowledge, the system produces a more comprehensive and useful evaluation than would be possible using either type of knowledge alone.

Unlike evaluation, rehabilitation strategy development is a *design* activity, in which the engineer generates a strategy that satisfies the repair and/or improvement needs identified by the evaluation. Whereas evaluation generally considers a limited set of potential problems, rehabilitation design involves a huge number of combinations of many individual rehabilitation techniques. Generating and evaluating all the possible combinations of techniques would be a formidable task even for a high-speed computer, if done using conventional programming methods. Using an expert system approach, however, rehabilitation strategies can be developed much more quickly and easily by generating *only feasible combinations* of techniques, thus greatly reducing the number of strategies that the engineer must consider. The system does this by applying restrictions on the generation of strategies that reflect heuristic knowledge about the compatibility of various techniques.

After one or more feasible rehabilitation strategies has been developed, the engineer must still choose the best alternative on the basis of life-cycle cost and other selection criteria. However, the engineer cannot perform a life-cycle cost comparison of alternatives without some idea of their expected lives. Deterministic knowledge can be applied here, by using available models for predicting rehabilitation performance in terms of key distress types. Several such models were developed in this study and incorporated in the system. Thus in rehabilitation, as in evaluation, deterministic and heuristic knowledge are combined to improve the quality of the problem solution.

Implementation of the System

One approach to knowledge-based system development is to implement a prototype with a commercially available, off-the-shelf software tool known as a "shell" which provides a suitable development environment (text editor, compiler, and so on), and then to rewrite the system for maximum efficiency when most of the difficult development is finished (*3*). Initially, a shell was used to develop a demonstration prototype for the evaluation portion of the system. The shell used was Insight 2+ (developed by Level V Research, Inc.). Insight 2+ is a production-rule-based system shell, meaning that knowledge is expressed in terms of "if-then" rules. To incorporate the decision trees into the Insight 2+ shell, each path down each tree (a path being composed of a set of nodes and connecting branches terminating at a conclusion) was programmed as a single rule. The decision trees impose a structure on the solution strategy that would not exist in a typical production rule system.

Although the production rule approach using Insight 2+ was helpful in initial prototyping, it soon became too restrictive for continued development of the system. Representing the decision trees with a set of rules was inefficient and unwieldy. Long compilation and execution times slowed the development of the system and detracted from the program's ease of use. It was also very difficult to interface the decision trees with other sections of the system (e.g., data entry and retrieval). To circumvent the limitations of the system as implemented in the shell, the system was rewritten using Turbo Pascal (Borland International, Inc.). This transformation changed the system from a traditional production rule system to a hard-coded system. Hence, some of the transparency of the knowledge was lost, and modifications became more difficult. These problems were more than offset, however, by the increased ease of interfacing the different parts of the system, the ease of programming the predictive models for future performance with and without rehabilitation, and the 10-fold increase in execution speed.

DESCRIPTION OF EVALUATION AND REHABILITATION SYSTEM

The expert system consists of three separate computer programs, one for each of three concrete pavement types (JRCP, JPCP, and CRCP). The steps in evaluation and rehabilitation design are the same in all of the programs.

Project Data Collection

The engineer collects key inventory (office) and monitoring (field) data for the project. Inventory data include design, traffic, materials, soils, and climate. Monitoring data include distress, drainage characteristics, rideability, and other items collected during a field visit to the project. Monitoring data are collected by a sample unit; a sufficient number of sample units distributed throughout the project's length should be surveyed to obtain an accurate representation of the project's condition. The data are entered into a personal computer using a full-screen editor.

Extrapolation of Overall Project Condition

The overall condition of the project is extrapolated by the system from the sample unit monitoring data, and extrapolated distress quantities are summarized.

Evaluation of Present Condition

Evaluation decision trees are used to analyze all data and to develop a specific detailed evaluation in each of the major problem areas identified for that type of pavement. These consist of the following seven areas for all three pavement types: roughness, structural adequacy, drainage, foundation stability, concrete durability, skid resistance, and shoulders. JRCP and JPCP are evaluated in five additional problem areas: transverse and longitudinal joint construction, trans-

verse joint sealant condition, loss of support, load transfer, and joint deterioration. JCRCs are evaluated in two additional problem areas: longitudinal joint construction and construction joints/terminal treatments.

In several of the problem areas, certain distress quantities and present serviceability rating (PSR) levels are considered indicative of deficiencies. Default values for these critical distress levels are incorporated in the system. The engineer may modify these default values if desired to reflect his or her own experience or agency policies.

Prediction of Condition Without Rehabilitation

Current traffic level [annual 18-kip equivalent single axle load (ESAL)] and anticipated ESAL growth rate are used in predictive models to project the condition of the pavement for 20 years into the future, to illustrate the consequences of not performing rehabilitation in the current year. Performance is predicted in terms of serviceability and key distress types: faulting, cracking, joint deterioration, and pumping for JRCP and JPCP, and failures (punchouts, steel ruptures, and full-depth repairs) for CRCP. The predictive models are calibrated to the existing condition of the pavement and cumulative traffic loadings at the time of the survey.

Physical Testing

The initial data collection does not require physical testing. On the basis of the evaluation results, the system recommends specific types of physical testing needed to verify the evaluation recommendations and to provide data needed for rehabilitation design. Types of testing that may be recommended include nondestructive deflection testing, destructive testing (coring and boring), laboratory testing, and roughness and friction measurement. Types of deficiencies that may warrant physical testing include structural inadequacy, poor rideability, poor surface friction, poor subdrainage conditions, poor concrete durability (D-cracking or reactive aggregate distress), foundation movement (due to swelling soil or frost heave), loss of load transfer at joints, loss of slab support, joint deterioration, and evidence of poor joint construction.

Selection of Main Rehabilitation Approach

On the basis of the evaluation results, the engineer then interacts with the system to select the most appropriate main rehabilitation approach for each traffic lane and shoulder. These include all 4R options: reconstruction, recycling, resurfacing (with concrete or asphalt), or restoration. A decision tree has been developed for each pavement type to assist the engineer in selecting the most suitable rehabilitation approach. The decision tree for JPCP is shown in Figure 2.

Development of Detailed Rehabilitation Strategy

Once an approach is selected, the engineer proceeds to develop the detailed rehabilitation alternative by selecting a feasible
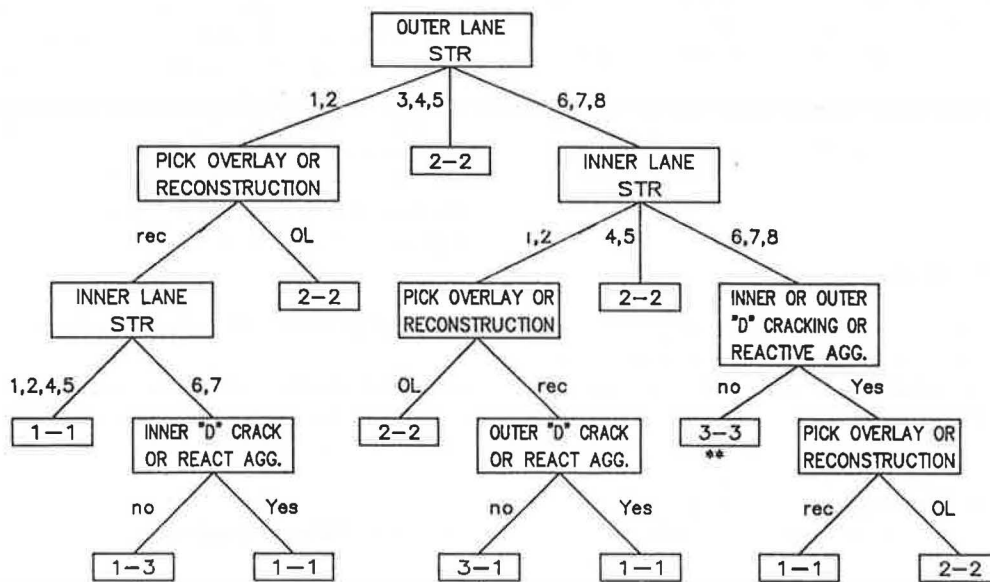
* Option to go to 1–1 provided
** Option to go to 1–1, 1–3, or 2–2 provided

1–1 Reconstruct Both Lanes
1–3 Reconstruct Outer, Restore Inner
3–1 Restore Outer, Reconstruct Inner
2–2 Overlay Both Lanes
3–3 Restore Both Lanes

FIGURE 2 Decision tree for selecting rehabilitation approach for JPCP.

set of individual rehabilitation techniques to correct the deficiencies present. These techniques may include such items as subdrainage, shoulder repair, full-depth repairs, and joint resealing. These are performed for each traffic lane and shoulder by interaction with the system. A set of decision trees has been developed to guide the rehabilitation strategy development process.

Prediction of Rehabilitation Strategy Performance

The future performance of the developed rehabilitation strategy is then predicted in terms of key distress types for 20 years into the future, based upon assumed traffic growth. Faulting, cracking, joint deterioration, and present serviceability rating (and punchouts for CRCP) are projected for concrete restoration, overlays, and reconstruction. Rutting and reflection cracking are projected for asphalt overlays.

Since the system currently addresses only pavements in their first performance period, the strategies developed do not include future maintenance or rehabilitation. The *life* of the strategy is defined as the length of time that the strategy extends the pavement's life, i.e., until a critical level in serviceability or distress is reached. For many strategies the life will be less than the 20 years for which projections are provided. The engineer must evaluate the results and determine whether or not the strategy provides an acceptable life. If so, a cost estimate can be prepared for it. If not, the engineer can develop other rehabilitation strategy alternatives.

It must be noted that most of the predictive models used by the system have significant limitations and should not be used outside the ranges of data from which they were developed. The models should be evaluated for validity with respect to the pavement designs and climatic conditions of the state in which the project under consideration is located.

Cost Analysis of Alternatives

Approximate quantities for each rehabilitation technique included in the alternative strategy are computed from the extrapolated distress quantities for each lane and shoulder. The engineer then must compute the cost for each item and total all costs for the strategy. The engineer then determines the life of the strategy as described above and computes an annual cost for the strategy.

Selection of Preferred Rehabilitation Strategy Alternative

Typically two to four feasible strategies exist for a given project. To select the preferred alternative, the engineer must consider not only life-cycle cost but also constraints that exist for the project, such as traffic control, construction time, and available funding. On the basis of estimated initial and annual costs, expected life and performance, and various constraints, the engineer selects the preferred rehabilitation strategy from among the feasible alternatives available.

APPLICATION OF EVALUATION AND REHABILITATION SYSTEM

Project Description

A 7.5-mile section of Interstate 10 near Tallahassee, Florida, was surveyed on September 30, 1986. The pavement is a 9-inch JPCP over a cement-treated aggregate base and a silty (A-4) subgrade. The joints are undoweled and are spaced uniformly at 20 feet. The shoulders are asphalt concrete. This section of Interstate 10 was constructed in 1974. Its two-way average daily traffic (ADT) at the time of the survey was 12,000 (40 percent trucks). Approximately 5.6 million and 0.8 million ESALs had been accumulated in the outer and inner lanes, respectively, over the life of the pavement.

Evaluation of Present and Future Condition

The project was evaluated in 12 problem areas defined for JRCP. In general, the outer lane was in significantly worse condition than the inner lane. Observed distresses included pumping, joint and crack faulting (0.08 and 0.18 in. in the inner and outer lanes, respectively), longitudinal cracking (26 and 116 ft/mile in the inner and outer lanes, respectively), transverse cracking (948 ft/mile in the outer lane), corner breaks (11/mile in the outer lane), and poor sealant condition noted for both lane/shoulder joints. The predicted future performance of the pavement without rehabilitation is illustrated for PSR and three key distresses in Figure 3 (joint deterioration, which is predicted to be negligible over the next 20 years, is not shown).

Rehabilitation Strategy Development and Performance Prediction

The outer lane of this section of I-10 has a sufficient amount of cracking to warrant a structural improvement. The rehabilitation approaches permitted by the system for this example include bonded and unbonded concrete overlays, asphalt overlay, crack and seat and asphalt overlay, reconstruction of the outer lane only, and reconstruction of both lanes.

For each of these alternatives, rehabilitation techniques for each lane and shoulder were selected by interaction with the program, and the strategy's performance over the next 20 years was predicted. A set of techniques making up an AC overlay alternative is shown below as an example:

Rehabilitation Technique	Quantity
Outer lane	
AC structural overlay	52,941 yd²
Full-depth repair of cracks	15,882 yd²
Stitch longitudinal cracks	874 ft
Subseal at joints and cracks	1,936 ft³ of grout
Install/repair longitudinal subdrains	39,706 ft
Inner lane	
AC structural overlay	52,941 yd²
Outer shoulder	
AC overlay	44,117 yd²
Reseal lane/shoulder joint	39,706 ft
Inner shoulder	
AC overlay	26,470 yd²
Reseal lane/shoulder joint	39,706 ft
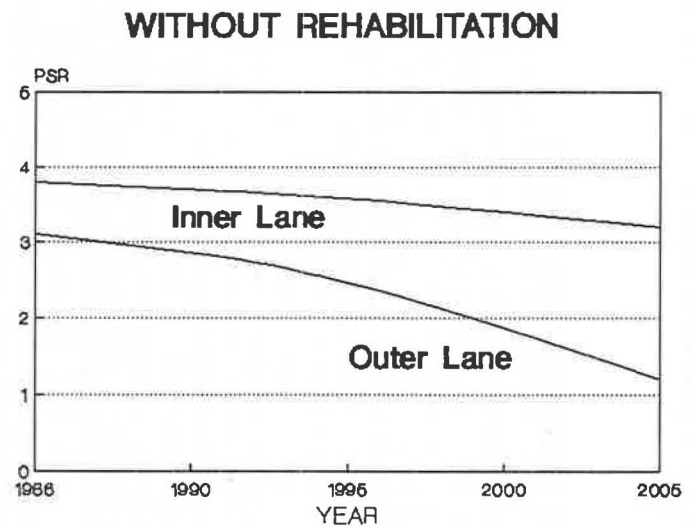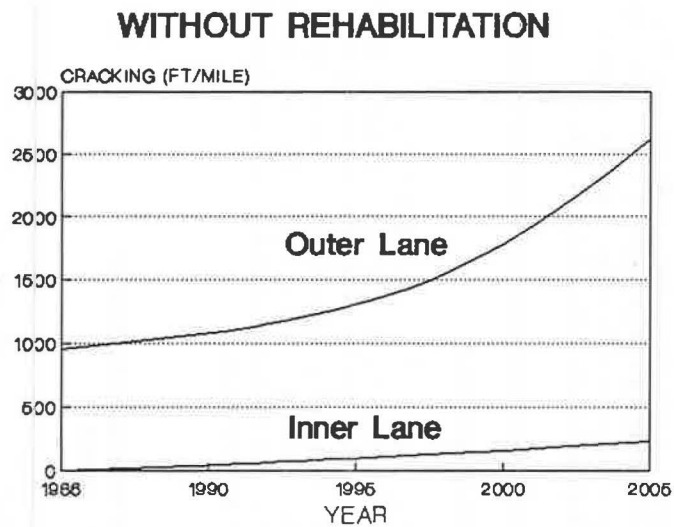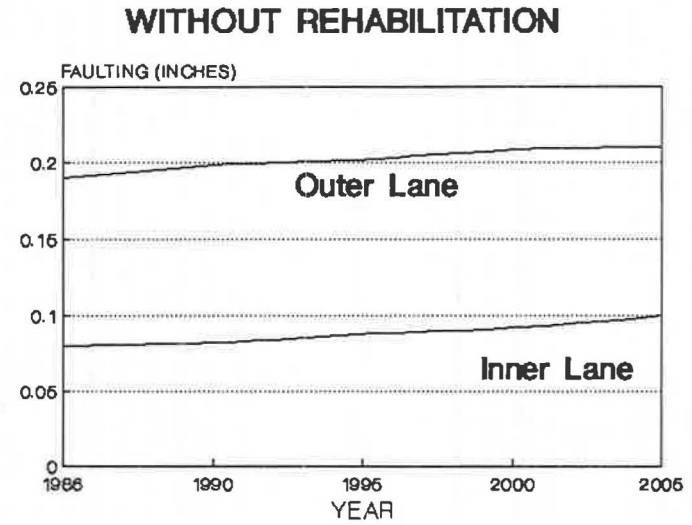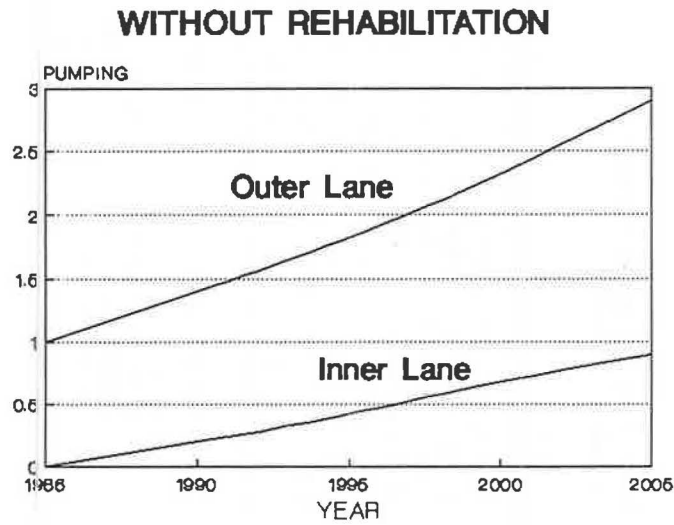
FIGURE 3 Predicted performance of I-10 example without rehabilitation.

UNBONDED PCC OVERLAY

JOINT DETERIORATION (NO/MILE)

Both Lanes

YEAR

UNBONDED PCC OVERLAY

FAULTING (INCHES)

Outer Lane

Inner Lane

YEAR

UNBONDED PCC OVERLAY

CRACKING (FT/MILE)

Outer Lane

Inner Lane

YEAR

FIGURE 4   Predicted performance of unbonded overlay for I-10 example.

For a 4-in. AC overlay, reflective cracking is predicted to reach unacceptable levels (1,000 ft of medium- to high-severity reflective cracks per mile) within seven years, which is understandable, considering the short joint spacing, poor load transfer at undoweled joints, and the large number of full-depth repairs required for preoverlay repair. Greater overlay thicknesses could be investigated to extend the life.
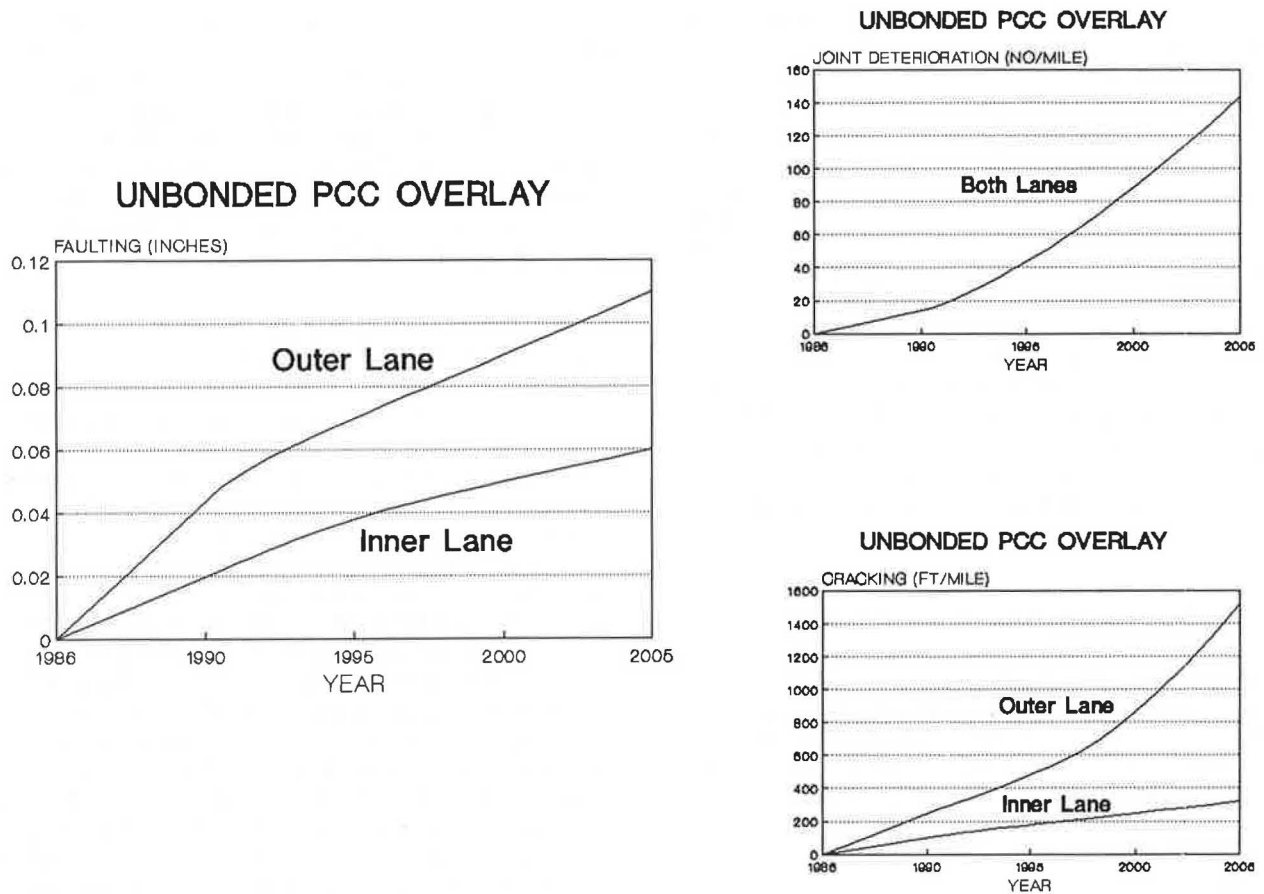
Better performance can be obtained by cracking and seating the pavement prior to AC overlaying. An alternative life of approximately 12 years, constrained by rutting in the outer lane, is predicted for a 4-inch overlay, a seating roller weight of 50 tons, and a cracking pattern of 6 ft by 6 ft. Again, other overlay thicknesses and cracking and seating parameters could be investigated as well.

A 3-in. bonded PCC overlay is predicted to perform even better than the crack and seat. The life of this alternative is constrained by joint deterioration, which is predicted to reach a critical level of 55 joints/mile in the outer lane in approximately 19 years. The unbonded overlay alternative does not perform quite as well, as shown in Figure 4. Even at an overlay thickness of 9 in., with a 1-in. AC separation layer, a 15-ft joint spacing, and 1.25-in. dowels in the overlay, cracking in the outer lane is predicted to reach a critical level of 800 ft/mile in the outer lane within 15 years, although joint deterioration and faulting are not predicted to reach unacceptable levels over the next 20 years. However, it would be premature to assume that a bonded overlay is preferable to an unbonded overlay without performing a life-cycle cost analysis. It may

be that the greater thickness of the unbonded overlay is offset by the savings in preoverlay repair.

The last alternative investigated for this example is a strategy for reconstructing the outer lane and restoring the inner lane. As it happens, there is no restoration work required for the inner lane, since it has no significant distress. The performance of this alternative was predicted using a reconstructed outer lane slab thickness of 12 in., with a 20-ft joint spacing, a stabilized base with a k value of 200 pci, 1.25-in. dowel bars, and a PCC modulus of rupture of 650 psi. This alternative design performs well for the entire prediction period. In the outer lane, PSR is predicted to reach a critical level of 3.0 after 19 years. In the inner lane, however, PSR becomes critical after 15 years (when the pavement in the inner lane is 27 years old). Thus the life of this alternative is 15 years. Since the inner lane requires no rehabilitation and performs acceptably almost as long as the outer lane, it seems unlikely that a strategy for reconstructing both lanes would have any cost advantage over the reconstruct/restore strategy.

Life-Cycle Cost Analysis of Alternatives

Using the rehabilitation quantities and predicted performance periods computed by the program, the five rehabilitation strategy alternatives may be compared on the basis of life-cycle cost. Typical unit costs were obtained from the Illinois Department of Transportation, Florida Department of Trans-

portation, and other sources. A 5 percent discount rate was used in the analysis. The results are summarized below:

Alternative	Initial Cost/Two-Lane Mile	Life (years)	Annual Cost/Two-Lane Mile
AC overlay	$581,000	7	$100,410
Crack and seat	576,900	12	65,090
Bonded overlay	731,000	19	60,490
Unbonded overlay	403,000	15	38,820
Reconstruct/restore	353,300	15	34,040

For this example, the outer lane reconstruction strategy appears to be the most cost-effective. Of course, these costs are estimates for illustrative purposes only and should not be interpreted as indicating any one strategy's superiority over another. A variety of other factors in addition to life-cycle cost must be considered in the final selection of the preferred rehabilitation strategy alternative.

CONCLUSIONS AND RECOMMENDATIONS

A practical and comprehensive system to assist practicing engineers in concrete pavement evaluation and rehabilitation has been developed, using a new and innovative approach that combines human knowledge and analytical techniques into a user-friendly personal computer program.

Conclusions

Concrete pavement evaluation and rehabilitation is a complex engineering problem that defies traditional analytical solutions, because of the large number of interacting factors involved and the lack of adequate analytical models to solve all (or even most) aspects of the problem.

Successful concrete pavement evaluation and rehabilitation currently rely heavily on the knowledge and experience of authorities in the pavement field for diagnosis of the causes of distress and for selection of feasible rehabilitation techniques that cost-effectively correct the deterioration.

Concrete pavement evaluation and rehabilitation is an ideal subject for an expert system application, by which human expertise is compiled, formalized, and applied to evaluation and rehabilitation of specific concrete pavement projects.

An expert system for concrete pavement evaluation and rehabilitation must incorporate not only the rules but also the reasoning processes used by knowledgeable pavement engineers in order to reach solutions in an efficient manner. Decision trees adequately represent factual knowledge and reasoning processes in a way that is easy to understand, examine, and revise.

An evaluation/rehabilitation procedure must be based on identifying and correcting mechanisms of deterioration in order to produce cost-effective rehabilitation strategies.

The inclusion of analytical models to predict the future performance of the pavement with and without rehabilitation was essential for the system to perform as desired. *Combining the human knowledge base with analytical techniques helps to provide feasible solutions for the evaluation and rehabilitation of concrete pavements.*

An expert system for concrete pavement evaluation and rehabilitation has been developed to the stage of a demonstration prototype. The system provided reasonable results in a few example applications but has not been fully tested over a wide range of conditions. More than 30 person-months of effort were expended in the development of the system to this stage. The results achieved thus far demonstrate that the system approach shows great promise in addressing this difficult engineering problem.

Recommendations for Future Work

Extensive field testing, including review by state department of transportation personnel and case studies on concrete pavement projects throughout the United States, is needed to increase the quality, efficiency, speed, and reliability of the system to the level of a research prototype.

Life-cycle cost analysis procedures would greatly increase the usefulness of the system. The analysis should be able to address unequal performance periods of different alternatives, additional rehabilitation needs within the analysis period, and additional costs that cannot now be computed by the system (e.g., bridge clearance, guardrail replacement, side slope improvements, traffic control, user-related costs). A first step toward providing this capability is the computation of rehabilitation quantities currently performed by the system.

The system currently assumes that the rehabilitation work will be performed immediately after the evaluation, which is almost never the case. *Routines need to be added to allow the engineer to specify the year of rehabilitation and have the system design rehabilitation strategies appropriate for the pavement's projected condition in that year.* This may be difficult to implement, since predictive models are lacking for some types of distress (e.g., shoulder deterioration, D-cracking).

Many models are used by the system to predict the future performance of the existing pavement with and without rehabilitation. Most of these models have significant limitations, and are not applicable nationwide over the range of climatic zones. *The development of improved models is a necessity to improve the validity of the system.* These may best be developed for individual states or regions of states (e.g., the southeastern United States). The existing models are most deficient in predicting the effect of retrofit subdrainage on the performance of the rehabilitated pavement.

Other rehabilitation techniques that are not now included in the system could be considered if performance prediction models for them become available. Some techniques that could be added include AC overlays with fabrics, interlayers, or sawed and sealed joints, and CRCP overlays.

The importance of *physical testing* to concrete pavement evaluation and rehabilitation design is addressed to a limited extent in the current system. However, the improvement of the physical testing recommendations and incorporation of physical testing results into the procedures for evaluation and rehabilitation strategy development remain among the most urgently needed improvements to the system.

The system should be extended to existing AC-overlaid concrete pavements. The system currently is restricted to pavements in their first performance period. Many concrete pavements exist that have already been overlaid with AC and are

in need of further rehabilitation. Work on this addition to the system is currently under way.

Adaptation of the system to different pavement geometries (e.g., other than two lanes in each direction) would make the system more applicable to the variety of pavement geometries throughout the United States.

ACKNOWLEDGMENTS

REFERENCES

1. M. I. Darter, E. J. Barenberg, and W. A. Yrjanson. *Joint Repair Methods for Portland Cement Concrete Pavements.* NCHRP Report No. 281, TRB, National Research Council, Washington, D.C., 1986.
2. S. C-Y. Lu. *Knowledge-Based Expert Systems: A New Horizon of Manufacturing Automation,* Knowledge-Based Engineering Systems Research Laboratory, Department of Mechanical and Industrial Engineering, University of Illinois at Urbana-Champaign, 1987.
3. B. Buchanan and E. Shortliffe, *Rule-Based Expert Systems: The Mycin Experiments of the Stanford Heuristic Programming Project,* Addison-Wesley Publishing Co., Inc., Reading, Mass., 1984.

ODE Computer Program: Mechanistic-Empirical Asphalt Concrete Overlay Design

M. R. Tirado-Crovetti, M. I. Darter, P. W. Jayawickrama,
R. E. Smith, and R. L. Lytton

This paper outlines a procedure for the design of asphaltic concrete overlays on existing asphalt concrete and portland cement concrete pavement surfaces. It discusses the type and form of information required by the microcomputer-based design program and all elements necessary for the user to design an overlay. The program provides an estimate of the time and number of traffic loads to failure by reflective cracking. The design equations are based on fracture mechanics and represent the existing pavement as a beam on an elastic foundation. The equations address fracture in the slab due to bending and shear caused by moving wheel loads and due to opening caused by thermal movement of the cracked existing pavements.

This paper is based on a report prepared for the Federal Highway Administration Office of Research (*1*) and outlines design procedures to address reflective cracking in asphalt concrete overlays.

Design equations were developed for six climatic zones using the approach developed in NCHRP Project 20-7, Task 17 (*2*). The equations were developed for flexible overlays of flexible as well as rigid pavements for each climatic zone for which data were available. A complete package of computer programs has been assembled to design overlays capable of resisting reflective cracking in the six geographic/climatic regions of the United States shown in Figure 1. The programs are designed for use on an IBM-compatible microcomputer.

This paper describes the type and form of information required by the program and discusses all elements necessary for the user to design an overlay. It does not cover in detail the theory or logic underlying the procedure.

SUMMARY OF DESIGN METHOD

The basic mechanisms generally believed to lead to reflection cracking are the vertical and horizontal movements of the underlying pavement layers. These damaging movements can be caused by traffic loadings, thermally induced contractions and expansions, or a combination of these mechanisms. Figure 2 illustrates the changes in bending and shear stresses that occur within an overlay as a wheel load passes over a crack

M. R. Tirado-Crovetti and M. I. Darter, ERES Consultants, Inc., P.O. Box 1003, Champaign, Ill. 61820. P. W. Jayawickrama, R. E. Smith, and R. L. Lytton, Texas A&M University, 510 Blocker Building, College Station, Tex. 77840.

in the original, underlying pavement. Cyclic shearing and bending movements cause the crack to propagate into the overlay. In addition, contraction and expansion of the pavement and the underlying layers with changes in temperature also contribute to the growth of reflection cracks with repeated traffic applications.

The overlay design procedure is mechanistic-empirical in concept. Mechanistic equations represent the existing pavement as a beam on an elastic foundation. In-situ deflection testing was used to determine the structural parameters needed to characterize the pavement. Basic asphalt concrete properties are used with fracture mechanics concepts to calculate the rate at which cracks in the existing pavement will propagate through the overlay.

The rate of crack propagation in asphalt concrete was predicted using the empirical power law relation developed by Paris and Erdogan (*3*):

$$(dc/dN) = A(DK)^n$$

where

DK = change in stress intensity factor amplitude,
A, n = fracture parameters of the material,
c = crack length, and
N = number of load applications.

Integrating this equation yields

$$N_f = o^h \{dc/[A(DK)^n]\}$$

where

N_f = number of load applications to failure, and
o^h = thickness of overlay.

The use of the above equations to determine the life of an overlay requires a knowledge of the stress intensity factor, K, and the material constants A and n within the overlay. Detailed procedures to determine these parameters are presented by Jayawickrama et al. (*1*). The stress intensity factor in the overlay for each of the crack growth mechanisms was determined by using a formulation that combines beam-on-elastic foundation theory and the finite-element method. The mechanistic equations were calibrated with in-service data for each of the climatic zones.

To use these equations, the design engineer supplies information on the types and thicknesses of layers in the existing pavement, the deflection data for the pavement, the material properties of the asphalt concrete being considered for use in
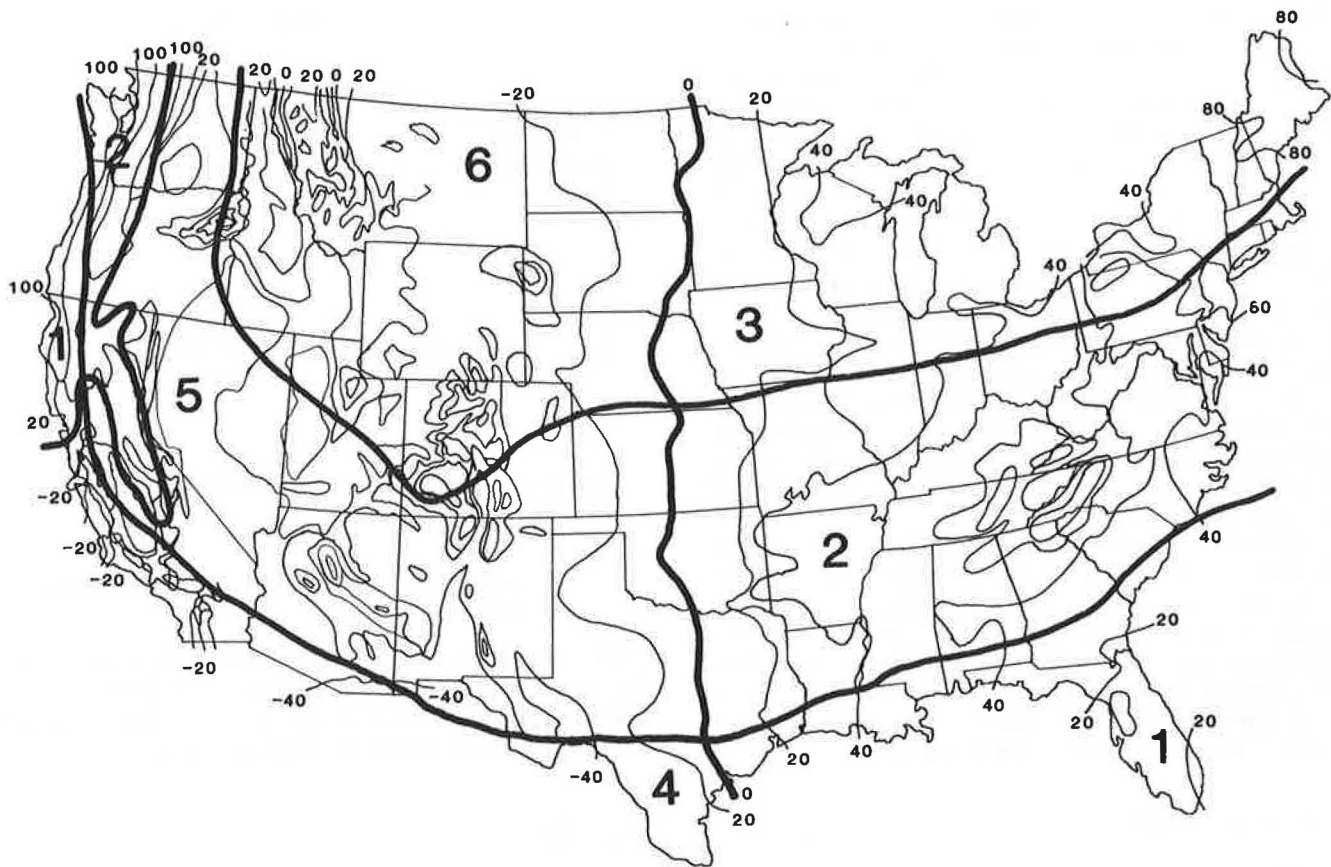
FIGURE 1 The six climatic regions in the United States are characterized as follows: (1) wet, no-freeze; (2) wet, freeze-thaw cycling; (3) wet, hard-freeze, spring thaw; (4) dry, no-freeze; (5) dry, freeze-thaw cycling; (6) dry, hard-freeze, spring thaw.

POSITION OF WHEEL LOAD
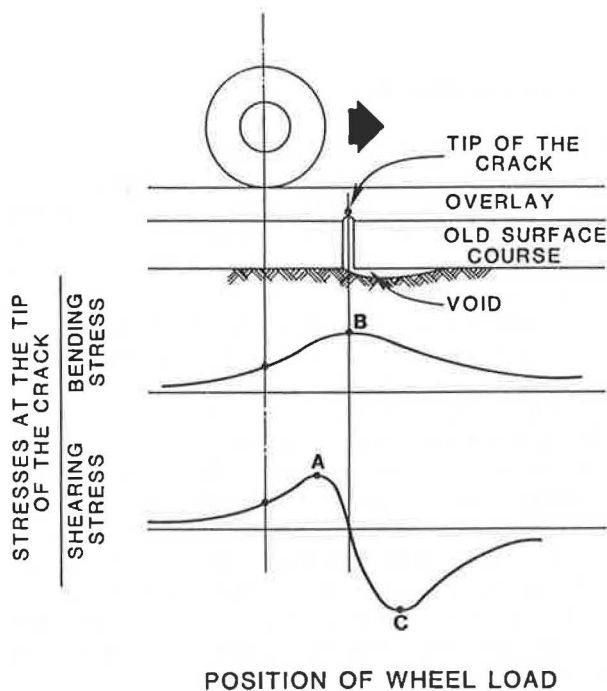
FIGURE 2 Stresses induced at the cracked section by a moving wheel load.

the overlay, thicknesses of overlay being considered, the environmental zone in which the pavement is located, and the traffic to which the overlay is expected to be subjected. The time and number of traffic loads to failure by reflective cracking are predicted by the ODE program. Failure can be set at three different levels of damage. A detailed description of the development is presented by Jayawickrama et al. (*1*).

ODE DESIGN GUIDE

Selection of Input Data

In this design procedure, the following data are required:

1. environmental data,
2. past construction history,
3. traffic data,
4. material characterization,
5. deflection data, and
6. condition evaluation (distress).

Environmental Data

Climatic and geographic factors influence performance. The United States can be divided into the six climatic zones

(Fig. 1) based on moisture availability and freeze-thaw activity (2). The boundary separating the wet zones 1, 2, and 3 from the dry zones 4, 5, and 6 is the major North-South contour on which the Thornthwaite Index is zero. [The Thornthwaite Index is a measure of moisture balance between rainfall and potential evapotranspiration (4, 5).] The boundary separating the nonfreeze zones 1 and 4 from the freeze-thaw cycling zones 2 and 5 is taken from U.S. Weather Bureau data as reported in Highway Research Board Special Report 1 (6). The boundary line represents an extreme frost penetration of 5 in. (13 cm), which corresponds to the typical minimum depth of pavement. The boundary separating the freeze-thaw cycling zones 1 and 5 from the hard-freeze zones 3 and 6 is based on a Corps of Engineers contour representing a 60-day duration of the normal freeze index (7). Any area in which freezing conditions persist for more than two months is considered to be in the hard-freeze zone. (See Figure 1 for a description of the zones.)

Pavements are expected to perform differently and exhibit different types of predominant distress as the climate changes from warm and wet to dry with a hard freeze every winter. In addition to the determination of the climatic region, the 24-hr temperature drop for the pavement location is needed. It is calculated as the monthly maximum temperature minus the monthly minimum temperature. This can be obtained from a National Climate Center publication (8).

Past Construction History

The following construction history data are required:

1. type of overlay: AC/AC (asphaltic concrete overlay on existing asphalt concrete) or AC/PCC (asphaltic concrete overlay on existing portland cement concrete pavement surfaces),
2. thickness of layer or layers of asphalt concrete,
3. thickness of underlying PCC slab, and
4. joint load transfer across PCC joints.

The above data are used in conjunction with nondestructive deflection testing data to back-calculate the in-situ modulus of elasticity of the surface and supporting base layers. For this analysis, the base and subgrade are combined into one homogeneous layer. The in-situ layer thicknesses of the pavement surfaces(s) should be obtained by coring at selected locations where deflection testing was conducted. The use of as-built records to define surface thickness will generally lead to appreciable errors in the back-calculated modulus of the surface and is therefore not recommended.

The existing load transfer across cracks and PCC joints can be determined from deflection testing data, provided that at least one deflection sensor is placed on the unloaded slab during testing while the load plate is positioned near the pavement crack or joint. The existing load transfer can be calculated as follows:

$$\% \, LT = (dU/dL)100$$

where

$\% \, LT$ = percent load transfer,
dU = deflection of the pavement on the unloaded side of the crack or joint, and
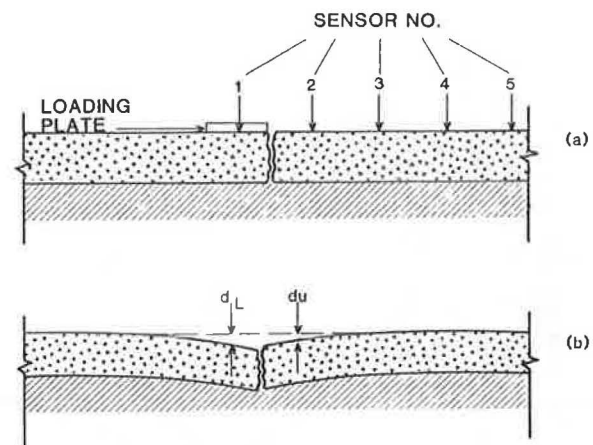
FIGURE 3 Measurement of load transfer with a deflection device.

dL = deflection of the pavement on the loaded side of the crack or joint.

Measured load transfers are grouped into three categories: low, medium, and high, which correspond to 0–40, 40–70, and 70–100 percent, respectively. A method generally used for making this measurement is illustrated in Figure 3.

Traffic Data

The amount of accumulated 18-kip single-axle loads (ESALs) expected to occur in each lane is necessary to determine life of the overlay. This information is typically collected from the traffic bureau, W-4 tables, or traffic maps published by highway agencies. Traffic is expressed in terms of ESALs per day.

Material Characterization

Both the existing materials and the materials in the overlay affect the life of the overlay. The program uses nondestructive deflection testing (NDT) data in conjunction with pavement layer thicknesses in an idealized two-layer pavement system to back-calculate the stiffness of the asphalt concrete and supporting layers.

For sections with rigid pavements (AC/PCC), the modulus of the subgrade reaction, K, is used by the program to determine the modulus of elasticity of the support. Representative values for the modulus of subgrade reaction, K, for the subsoil are shown in Table 1, based on classification.

Programs are supplied to determine the modulus of elasticity of the asphalt overlay. These programs are based on the Van der Poel (9) and McLeod (10) nomographic procedures, which use basic material properties of the bitumen and asphalt concrete to compute the resulting mix stiffness.

The Van der Poel method is based on the results of experimental research by the Shell Oil Company and requires the following properties of the bitumen: penetration at 77°F, ring and ball softening point, asphalt percent by weight of aggregate, time of loading, age of mix or time in service, and volume concentration of minerals.

TABLE 1 MODULUS OF SUBGRADE REACTION *K* FOR DIFFERENT SOIL TYPES

Classification	K(pci)
Plastic clays	75
Silts and silty clays	150
Sands and gravels	300
Cement or asphalt treated base	500

The McLeod method utilizes a different quantitative measure for temperature susceptibility, the pen-vis number, which is based on an asphalt cement's penetration at 77°F (25°C) and viscosity in centistokes at 275°F (135°C). To use McLeod's method, the following properties of the bitumen and mix are required: penetration at 77°F (25°C), penetration index, asphalt percent in the mix, viscosity in centistokes, service temperature, and *CV* (volume concentration of minerals).

Deflection Data

Deflection testing is used to back-calculate the in-situ modulus of elasticity of the existing pavement surface and supporting layers. The design procedure accepts the following types of deflection testing devices: Dynaflect, falling-weight deflectometer, Road Rater 400B, Road Rater 2000, and Road Rater 2008.

The program contains default values for the typical sensor configuration of each of the devices mentioned above (*11*). Data from at least five test locations are required to compute the mean and standard deviation of the pavement and supporting layer stiffnesses for any given section. The distribution of moduli values around the mean is assumed to be normal; therefore, the Student *t*-distribution is used to calculate a design modulus value for the pavement based on the desired confidence level selected by the user. Confidence levels of 50, 80, 90, 95, and 99 percent are allowed.

The deflection data should be carefully screened to ensure that they are relatively uniform within a design section. If the data are dramatically different, the design project may need to be divided into subprojects that exhibit relatively uniform deflection responses.

The deflection data that are to be used for back-calculating material properties should be collected in areas of the pavement that are relatively free from transverse cracking. In general, the load plate should be positioned at least 6 ft from any surface cracks during testing. Additional deflection testing may be obtained across transverse cracks for load transfer measurements, as described earlier; however, these data are *not* used to determine the layer stiffnesses.

Condition Evaluation (Distress)

Because this study is concerned with the potential for reflection cracking of overlays, only this type of distress was used in this analysis. Two forms of reflection cracking were considered: transverse and longitudinal. However, it is suggested that quantitative visual observations of all existing pavement distress be made at the time of testing. This survey will serve as a valuable guide when maintenance alternatives are considered.

The program requires the average transverse crack spacing, in inches, to perform the calculations. For overlays on existing asphalt pavements, a damage level of 1.0 is assumed to equal one crack completely across the lane every 1 ft or the equivalent length of transverse and longitudinal cracks. A damage level of 0.0 is assumed to equal no cracking. A linear relation between damage levels of 0.0 and 1.0 is assumed.

For overlays of portland cement concrete pavements, a damage level of 1.0 is assumed to occur when one crack completely crosses the lane every 10 ft or the equivalent length of transverse and longitudinal cracks. A damage level of 0.0 is assumed to equal no cracking, and a linear relationship between 0.0 and 1.0 is assumed.

Program Description

The program computes either the number of years to reach specific damage levels of reflective cracking for a given AC overlay thickness or the required thickness of an AC overlay when the expected service life is identified. This process is based on the use of the mechanistic model to calculate the material properties of the surface and subgrade support, and the use of finite-element analysis, which determines the magnitudes of stress intensity factors occurring within an actual pavement structure with variable crack length and load transfer values.

The following major steps are used in the design process:

1. selection of input data according to Tirado-Crovetti et al. (*12*) as detailed in chapter 2 of their report;
2. determination of layer properties from measured surface deflections of the existing pavement. The program searches for the elastic moduli that fit the measured basin to the calculated basin with the least average error. This computer program, developed at the Texas Transportation Institute (*13*), uses a pattern-search technique to fit deflection basins with elliptic integral function-shaped curves. These curves are solutions to the differential equations used in elastic-layer theory. The theoretical development of the deflection equation used in the program is discussed by Lytton and Michaleak (*13*). The required data include thickness of AC and granular base layers, force applied and radius of loading plate, and measured deflection values as well as their radial distances from center of loading plate;
3. determination of the mix stiffness of the overlay and the slope *m*. described by Tirado-Crovetti et al. (*12*) in the "Material Characterization" section of chapter 2 of their report, and;
4. calculation of the number of cycles to failure of the overlay using integration of Paris' crack growth law.

Output Description and Data Interpretation

The output format of the ODE program has been designed to best inform the engineer of anticipated reflection cracking problems. Although the required overlay thickness is of ultimate interest to the user, the results of intermediate com-

putations can also be of value when evaluating alternate maintenance strategies other than an overlay. An example design is provided to illustrate the input and output of the program.

Sample Design

The following example illustrates the design of an asphaltic concrete overlay on an existing asphalt concrete pavement surface (AC/AC). The design requirements for this example are described in the same order as they appear during program execution.

Identification Information

Highway Name: USTH 61
Mile Post Start: 0.000
Mile Post End: 2.000
Project Number: 100
County: Carlton

Environmental Information

24-Hour Temperature Drop (°F): 22 (12.2°C)
Climatic Region (1–6): 2

The site of this highway construction project is in a location that can be environmentally classified as U.S. Climatic Region 2, i.e., wet, freeze-thaw cycling (as shown in Figure 1). In addition to the determination of the climatic region, the 24-Hour Temperature Drop for that particular area is needed. This is calculated as:

24-Hour Temperature Drop = Max. Temp. – Min. Temp
24-Hour Temperature Drop = 22°F (12.22°C)

Construction Information for Asphalt Concrete Pavement

AC Thickness (in.): 6.0 in. (15.24 cm)
Degree of Aggregate Outerlock: (L)ow, (M)edium, (H)igh: M

The program requires the thickness of the existing AC pavement and the type of section (AC/AC or AC/PCC). In addition to this information, the program requires the degree of aggregate interlock in order to calculate the bending efficiency factor for the cracked pavement.

Traffic Information

Traffic in 18-kips ESAL per Day: 500

Material Characterization for AC/AC

Base and Subbase Properties
Fixed Modulus of Support (PSI): _____

Surface Properties
Fixed Modulus of the AC (PSI): _____

"Fixed modulus" requires that the user enters his or her own values. If these values are to be calculated based on deflection data, a "0" is entered.

The modulus of elasticity of the asphalt overlay is determined using material properties of the bitumen. Five options are provided based on the available data as described below:

Selection of Asphalt Properties

Select Paths A–E:
Path A–
Viscosity at 275°F in CST
Penetration at 77°F in 0.1 mm
Service temperature
CV
Path B–
Viscosity at 140°F in poises
Penetration at 77°F in 0.1 mm
Service temperature
CV
Path C–
Penetration index
Softening point R & B
Service temperature
CV
Path D–
Penetration at 77°F
Softening point R & B
Service temperature
CV
Path E–
Penetration at 77°F
Pen. w/specified temp
Service temperature
CV

The path used is governed by the available material data. For this example, path A will be used:
  Viscosity at 275°F in CST: 250
  Penetration at 77°F in 0.1 mm: 85
  Service Temperature: 60
  CV: 0.883

Deflection Data

Deflection testing is used to determine the stiffness of the in-service pavement. For this example, the FWD deflection data listed below are used:

FWD Load: 9,226 lbf
Maximum Deflection: 13.54 mils
Deflection at 12 in.: 8.9 mils
Deflection at 24 in.: 7.56 mils
Deflection at 36 in.: 5.2 mils

If five or more deflection sets are used to define deflection basins, confidence levels need to be defined.

TABLE 2   SAMPLE COMPUTER OUTPUT: CALCULATED PROJECT RESULTS
FOR AC/AC

Parameter	Value
Highway name	USTH 61
Mile post start	0.000
Mile post end	2.000
Project number	100
County	CARLTON
24-Hr temperature drop (°F)	22
Climatic region	2
Traffic (18-kip ESALs/day)	500
Thickness of the existing AC layer (in.)	6
Modulus of the existing AC layer (Psi)	457,000
Modulus of the support (Psi)	22,500
Thickness of the overlay (in.)	2.5
Modulus of overlay (mix stiffness) (Psi)	565,000
Slope of LOG mix stiffness vs. LOG time curve	0.653
Life of the overlay (yrs) for low damage	3.9
Life of the overlay (yrs) for medium damage	4.5
Life of the overlay (yrs) for high damage	5.7

Condition Evaluation (Distress)

Average Crack Spacing: 120 in. (304.8 cm)

The program requires the average crack spacing in order to perform calculations.

Table 2 provides a sample output of the program.

Sensitivity Analysis

A sensitivity analysis was conducted to demonstrate the reasonableness of the procedure and to identify the design inputs that influence the overlay thickness calculated. This analysis allows the user to prioritize the importance of design input for a particular overlay design procedure and allocate time and money to each input accordingly. The sensitivity analysis was conducted by individually varying the following major inputs: thickness of the overlay, modulus of the overlay, level of damages, climatic zones, traffic, service temperature, 24-hr temperature drop, and crack spacing.

During the sensitivity analysis, the following pavement parameters were used as the standard section AC/AC:

Existing asphalt concrete: 4 in. (10.16 cm)
Granular base: 7 in. (17.78 cm)
Crack spacing: 120 in. (304.8 cm)
Aggregate interlock: M (medium)
24-Hr temperature drop: 22.5°F (12.5°C)
Modulus-of-support layer: 25,000 psi (172,414 kPa)
Modulus of existing AC: 400,000 psi (2,758,621 kPa)

The pavement section that was selected as the base for the analysis of asphalt concrete overlays of existing portland cement concrete pavement surfaces is as follows:

Subgrade soil type: 3 (sands and gravel)
Existing PCC slab: 9 in. (22.86 cm)
Crack spacing: 360 in. (921.60 cm)
Aggregate interlock: M (Medium)
24-Hr temperature drop: 22.5°F (12.5°C)

Tables 3, 4, and 5 present a representative portion of the results of the sensitivity analysis. As expected, increasing the overlay thickness results in an increase in the life of the overlay for all damage levels in all regions. A dramatic increase in the life of the overlay is seen for the lower modulus value overlays. The climatic region has a large impact on time to failure of the overlay. Using the same parameters for traffic, thickness of overlay, and modulus of the overlay, very different results were obtained when the climatic region was changed.

Changes in service temperature, 24-hr temperature drop, and climatic region also have a major impact on the life of the overlay for all regions.

CONCLUSIONS AND RECOMMENDATIONS

The ODE program offers potential help for highway engineers to determine when reflective cracking will develop in an asphalt overlay on the basis of asphalt cement and mix properties. The equations used in this program were developed for six climatic regions for asphalt overlays of asphalt concrete pavements and for two regions for asphalt for asphalt overlays of portland cement concrete pavements.

The mechanistic-empirical approach provides an excellent means to develop design equations that are soundly based on mechanistically correct concepts with a limited amount of parameters. However, they will only be as good as the data used to calibrate them. Until accurate data are available, the resulting design equations may be less accurate than desired.

ACKNOWLEDGMENTS

TABLE 3   RESULTS OF SENSITIVITY ANALYSIS VARYING THICKNESS AND MODULUS OF OVERLAY
FOR MEDIUM DAMAGE LEVEL (0.40) AC/AC PAVEMENT SECTION

Climatic Region	Damage Level	Traffic (18-kip ESAL/day)	Thickness of Overlay (in.)	Modulus of AC Overlay (Psi)	Time to Reach Medium-Level Reflective Cracking (yr)
1	.40	500	1.0	350,000	2.63
1	.40	500	2.0	350,000	9.23
1	.40	500	3.0	350,000	20.21
1	.40	500	4.0	350,000	19.73
1	.40	500	1.0	700,000	0.75
1	.40	500	2.0	700,000	2.83
1	.40	500	3.0	700,000	3.86
1	.40	500	4.0	700,000	4.02
2	.40	500	1.0	350,000	1.41
2	.40	500	2.0	350,000	4.97
2	.40	500	3.0	350,000	10.88
2	.40	500	4.0	350,000	12.95
2	.40	500	1.0	700,000	0.41
2	.40	500	2.0	700,000	1.52
2	.40	500	3.0	700,000	2.43
2	.40	500	4.0	700,000	3.25
3	.40	500	1.0	350,000	2.24
3	.40	500	2.0	350,000	7.88
3	.40	500	3.0	350,000	17.24
3	.40	500	4.0	350,000	30.48
3	.40	500	1.0	700,000	0.63
3	.40	500	2.0	700,000	2.36
3	.40	500	3.0	700,000	5.35
3	.40	500	4.0	700,000	9.80
4	.40	500	1.0	350,000	1.71
4	.40	500	2.0	350,000	6.00
4	.40	500	3.0	350,000	13.14
4	.40	500	4.0	350,000	11.34
4	.40	500	1.0	700,000	0.48
4	.40	500	2.0	700,000	1.83
4	.40	500	3.0	700,000	2.27
4	.40	500	4.0	700,000	1.92
5	.40	500	1.0	350,000	3.21
5	.40	500	2.0	350,000	11.29
5	.40	500	3.0	350,000	24.72
5	.40	500	4.0	350,000	41.57
5	.40	500	1.0	700,000	0.90
5	.40	500	2.0	700,000	3.40
5	.40	500	3.0	700,000	7.41
5	.40	500	4.0	700,000	13.24
6	.40	500	1.0	350,000	3.08
6	.40	500	2.0	350,000	10.87
6	.40	500	3.0	350,000	23.78
6	.40	500	4.0	350,000	33.16
6	.40	500	1.0	700,000	0.87
6	.40	500	2.0	700,000	3.26
6	.40	500	3.0	700,000	6.01
6	.40	500	4.0	700,000	9.38

NOTE: 1 inch = 2.54 cm, 1 Psi = 6.894 kilopascals, 1 kip = 4.448 kilonewtons

TABLE 4 RESULTS OF SENSITIVITY ANALYSIS VARYING THICKNESS AND MODULUS OF OVERLAY FOR HIGH DAMAGE LEVEL (0.50) IN AC/PCC PAVEMENT SECTIONS

Climatic Region	Damage Level	Traffic (18-kip ESAL/day)	Thickness of Overlay (in.)	Modulus of AC Overlay (Psi)	Time to Reach High-Level Reflective Cracking (yr)
2	0.50	500	1.5	350,000	0.99
2	0.50	500	2.0	350,000	2.08
2	0.50	500	3.0	350,000	5.87
2	0.50	500	4.0	350,000	12.27
2	0.50	500	5.0	350,000	21.74
2	0.50	500	1.5	700,000	0.34
2	0.50	500	2.0	700,000	0.72
2	0.50	500	3.0	700,000	2.09
2	0.50	500	4.0	700,000	4.43
2	0.50	500	5.0	700,000	7.93
3	0.50	500	1.5	50,000	9.52
3	0.50	500	2.0	350,000	19.90
3	0.50	500	3.0	350,000	56.24
3	0.50	500	1.5	700,000	3.30
3	0.50	500	2.0	700,000	7.00
3	0.50	500	3.0	700,000	20.20

NOTE: 1 inch = 2.54 cm, 1 Psi = 6.894 kilopascals, 1 kip = 4.448 kilonewtons

TABLE 5 RESULTS OF SENSITIVITY ANALYSIS VARYING SERVICE TEMPERATURE OF OVERLAY FOR LOW DAMAGE LEVEL (0.33) IN AC/AC PAVEMENT SECTION

Climatic Region	Damage Level	Service Temperature (°F)	Modulus of AC Overlay (Psi)	Time to Reach Low-Level Reflective Cracking (yr)
1	0.33	50	977,298	1.89
1	0.33	60	566,163	5.61
1	0.33	70	273,712	16.97
2	0.33	50	977,298	1.05
2	0.33	60	566,163	2.94
2	0.33	70	273,712	8.86
3	0.33	50	977,298	1.91
3	0.33	60	566,163	4.75
3	0.33	70	273,712	14.62
4	0.33	50	977,298	1.27
4	0.33	60	566,163	3.89
4	0.33	70	273,712	11.77
5	0.33	50	977,298	3.10
5	0.33	60	566,163	7.72
5	0.33	70	273,712	23.49
6	0.33	50	977,298	2.24
6	0.33	60	566,163	5.87
6	0.33	70	273,712	18.09

NOTE: °F = 5/9°C or Kelvins, 1 in. = 2.54 cm, 1 Psi = 6.894 kilopascals, 1 kip = 4.448 kilonewtons

REFERENCES

1. P. W. Jayawickrama, R. E. Smith, R. L. Lytton, and M. R. Tirado-Crovetti. *Development of Asphalt Concrete Overlay Design Equations*. Vol. I. Final Report No. DTFH61-84-C-00053. Washington, D.C., 1987.
2. P. L. Lytton and A. Garcia-Diaz. *Evaluation of AASHO Road Test Satellite and Environmental Studies* Final Report, NCHRP Project 20-7, Task 17, Texas Transportation Institute, Texas A&M University, College Station, 1983.
3. P. C. Paris and F. Erdogan. A Critical Analysis of Crack Propagation Laws. *Transactions of the ASME, Journal of Basic Engineering*, Ser. D, 85, No. 3, 1963.
4. C. W. Thornthwaite. An Approach Toward a Rational Classification of Climate. *Geographical Review*, Vol. 38, No. 1, 1948, pp. 55–94.
5. S. H. Carpenter, R. L. Lytton, and J. A. Epps. *Environmental Factors Relevant to Pavement Cracking in West Texas*. Research Report 18-1, Texas Transportation Institute, Texas A&M University, College Station, January 1974.

6. *Special Report 1: Frost Action in Roads and Airfields.* HRB, National Research Council, Washington, D.C., 1951, p. 123.
7. *Report on Frost Investigation, 1944–1945.* New England Division, U.S. Army Corps of Engineers, U.S. War Department, Boston, Mass., April 1947.
8. *Climatology of the United States No. 81 (by State) Monthly Normals of Temperature, Precipitation, and Heating and Cooling Degree Days 1951–80.* National Climatic Center, Asheville, N.C.
9. C. Van der Poel. A General System Describing the Viscoelastic Properties of Bitumens and Its Relation to Routine Test Data. *Journal of Applied Chemistry,* Vol. 4, May 1954.
10. N. W. McLeod. Asphalt Cements: Pen-Vis Number and Its Application to Moduli Stiffness. *Journal of Testing and Evaluation,* Vol. 4, No. 4, 1976.
11. R. E. Smith and R. L. Lytton. *Synthesis Study of Nondestructive Testing Devices for Use in Overlay Thickness Design of Flexible Pavements.* Report No. DTFH61-82-C-00073. Washington, D.C., 1983.
12. M. R. Tirado-Crovetti, M. T. Darter, R. E. Smith, P. W. Jayawickrama, R. L. Lytton. *Development of Asphalt Concrete Overlay Design Equations,* Vol. II. Final Report No. DTFH61-84-C-00053. Washington, D.C., 1987.
13. R. L. Lytton and C. H. Michaleak. *Flexible Pavement Deflection Using Elastic Moduli and Field Measurements.* Research Report 207-7F, Texas Transportation Institute, Texas A&M University, College Station, August 1979.

Load Transfer in Undoweled Transverse Joints of PCC Pavements

M. Poblete, R. Valenzuela, and R. Salsilli

The results of load transfer evaluations in 21 test sections of the Chilean in-service highway network are presented. Characteristics of transverse joints are described, and procedures to measure the absolute deflections of four points in a slab, plus another one across the transverse joint, are explained. The procedures allow load transfer to be evaluated with good accuracy and repeatability. Measurements conducted over continuous 24-hr cycles in winter and summer show that the load transfer depends upon the thermal conditions of the pavement. Its daily variations are satisfactorily explained by the changes in transverse joint openings. Load transfer on the leave slab is much different from that on the approach slab, unless the joint stiffness is so high that the pavement behaves as a continuous strip. To evaluate internal stresses of pavement slabs, a mechanistic approach is described in which three kinds of joint stiffnesses are proposed to take into account the effects of shear forces and moments developed at joints, as well as compressions built up by the slabs' moisture and temperature.

In undoweled PCC pavements, traffic-induced stresses in the slabs depend highly upon the capacity of structural collaboration of the neighboring slabs, through the interlocking developed at transverse and longitudinal joints. The eventual deterioration of the load transfer implies a progressive increase in internal stresses, and thus slab cracking could be initiated after fewer load repetitions. Consequently, load transfer is usually considered a variable of the pavement condition (1–4), although its value would not be unique because of its dependence on thermal conditions as well as on load position, either upon the approach slab or the leave slab (5).

In view of the general observations of slab upward curlings in the Chilean portland cement concrete (PCC) pavements, varying with the daytime thermal gradients (see another paper in this Record by Poblete et al.), attention was paid to what was simultaneously occurring at transverse joints. In fact, the cycles of variation in mean temperatures across slab thickness produced longitudinal contractions and elongations that caused changes in transverse joint openings; at low temperatures, the pavement behaves as a set of relatively isolated slabs, whereas on very hot days, the pavement behaves as a continuous strip, with complete locking of joints.

The results presented herein are part of extensive research on Chile's concrete pavement network, with the ultimate objective of modeling the structural deterioration of in-service concrete pavements designed and constructed under general AASHTO guides and specifications. Survey and measurement methodologies were periodically performed at 21 loca-

Instituto de Investigaciones y Ensayes de Materiales (IDIEM), Universidad de Chile, Casilla 1420, Santiago, Chile.

tions on the PCC paved highway network where a significant rainfall gradient from north to south and moderate thermal variations are encountered. In each of the 21 test sections, sensors were installed to measure the temperature distribution across the slab thickness, as well as deep reference bases (DRBs) for measuring absolute vertical displacements of slabs (Fig. 1). Furthermore, reference bases were installed at joints to measure horizontal movements and faulting.

To evaluate the load transfer (LT) or, strictly speaking, the efficiency of transverse joints, several expressions have been defined to relate the simultaneous deflections of adjoining edges produced by the traffic loads usually positioned on the approach slab:

$$LT_A = 2\delta_2/(\delta_1 + \delta_2) \tag{1}$$

$$LT_D = \delta_2/\delta_1 \tag{2}$$

$$LT_E = (\delta_1 - \delta_1') + (\delta_2' - \delta_2) \tag{3}$$

where

δ_1, δ_2 = simultaneous deflections at the approach and leave edge, respectively, when the load is on the approach slab, and

δ_1', δ_2' = simultaneous deflections at the approach and leave edges, respectively, when the load is on the leave slab.

Equation 3, developed by the AIPCR Technical Committee (3) to characterize the load transfer in pavements on eroded bases, considers the deflections at transverse edges with both positions of loading, and the present work shows that LT values may differ according to the variation in boundary conditions for the estimation of internal stresses. However, Equation 3 will not be used in the discussions below. Equation 1 from Teller and Sutherland (1) and Equation 2 from Darter (2) are used because they are simpler and better serve the purposes of the paper.

TRANSVERSE JOINT CHARACTERISTICS

Transverse joints of Chilean pavements are spaced 3.5–5.5 m apart, skewed with a slant between 0 and 1/6, and the jointing is accomplished by inserting fiber strips and/or sawing to a depth of about one-fourth of the slab thickness. No dowels or other means of load transfer have been implemented.

The joint efficiency is therefore only the result of interlocking between the irregular faces of joint cracks that are formed with large roughnesses around the high-hardness si-
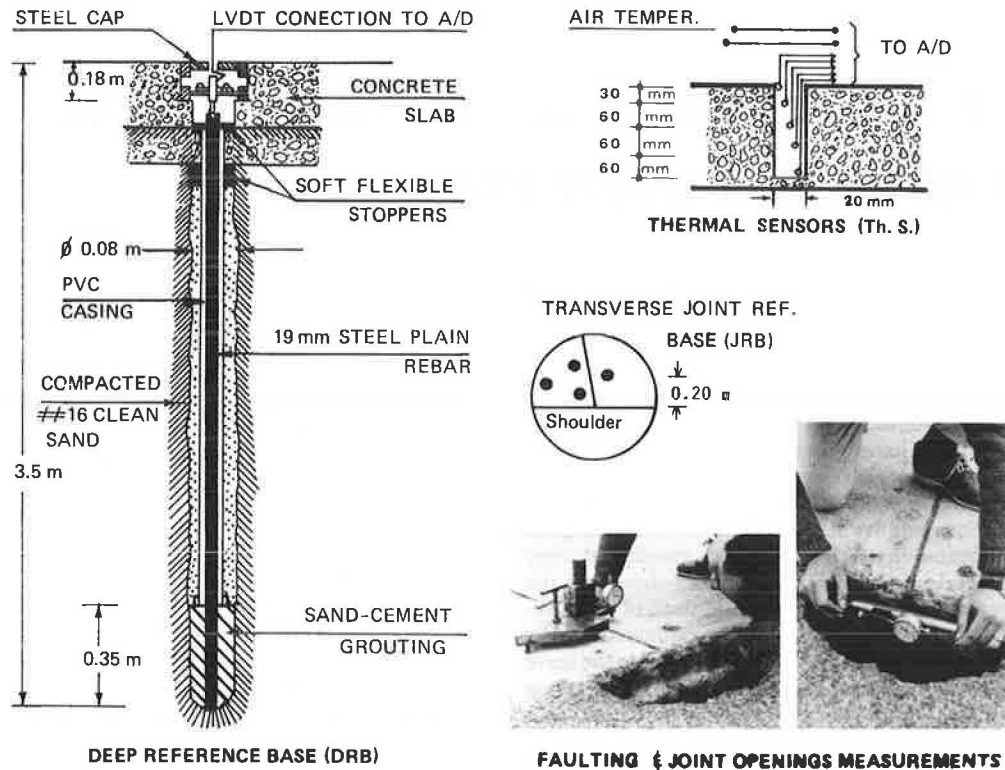
FIGURE 1 Instrumentation devices in the test sections.

liceous aggregates. In general, joint cracks are subvertical with preferential inclination to one side.

Joint materialization is gradual, starting with great spacings on the order of one every three or more nominal slabs during the first hours of concrete age. In Figure 2(a), the variations in openings are shown for 10 consecutive joints measured after 16 days in a test section having reference bases installed in the fresh concrete. At a later age, as shown in Figure 2(b), when all joints are activated, the openings tend to be evenly distributed among the joints. The joints that cracked first, however, can still be identified by openings that are greater, even after several years of service.

For evaluating the joint efficiency, the most open among 10 consecutive joints was selected. Its variation in opening over a daily cycle is representative of the average variation for the whole set of joints.

DEFLECTIONS BY LOAD

In order to measure the slab displacements caused by traffic loads and by the internal temperature variations, four DRBs were installed in the leave slab plus another one in the approach slab at 0.50 m from the outer edge, just to evaluate the joint efficiency, as illustrated in Figure 3. Every base has a steel bar grouted in the subsoil 3.5 m beneath the pavement, and it is isolated from lateral confinement by a PVC casing. Absolute deflections of the loaded slabs are recorded with ±0.01 mm accuracy by means of an analog/digital system. The five simultaneous deflection signals are processed and monitored in the field along with the internal temperature signals, which

are measured continuously at five levels in the slab with ±0.2°C accuracy.

In Figure 4, typical recordings are presented for the simultaneous deflections of DRB border points 1, 2, 5, 3 and DRB center point 4 as the loaded truck moves slowly from the approach to the leave track with respect to the joint. Results correspond to measurements at test section No. 1 for two thermal conditions on a summer day. In the graphs, two maxima represent the deflections of the point upon passage of the front axle and then of the rear axle; also, some rocking of the slabs is detectable from the negative deflections produced by the rear axle pressing the opposite edge of the leave slab. To better illustrate the rocking of slabs with partial support, a similar recording is shown in Figure 5, obtained at test section No. 14 during a cold-winter-day cycle when the joints' efficiency is minimal. From both graphs, it can be deduced that the deflections are always elastic and that for the thermal state of negative gradient (slab surface cooler than bottom), the slabs rock around its supported central zone, whereas DRB points 1, 2, 3, and 5 lift up when the loaded axles press on the slab near the far edge with respect to the DRB point under consideration. For the thermal state of strong positive gradient, the deflections at the same points are minimal and represent the elastic deformation of the supported slab edges by the action of the loaded axle.

On the other hand, comparison of the recordings of representative points DRB 1 and DRB 2 for the negative gradient shows a different behavior between both sets of slabs, which is due to the varying degrees of upward curling as well as to the interlocking at joint faces. In another paper in this Record,
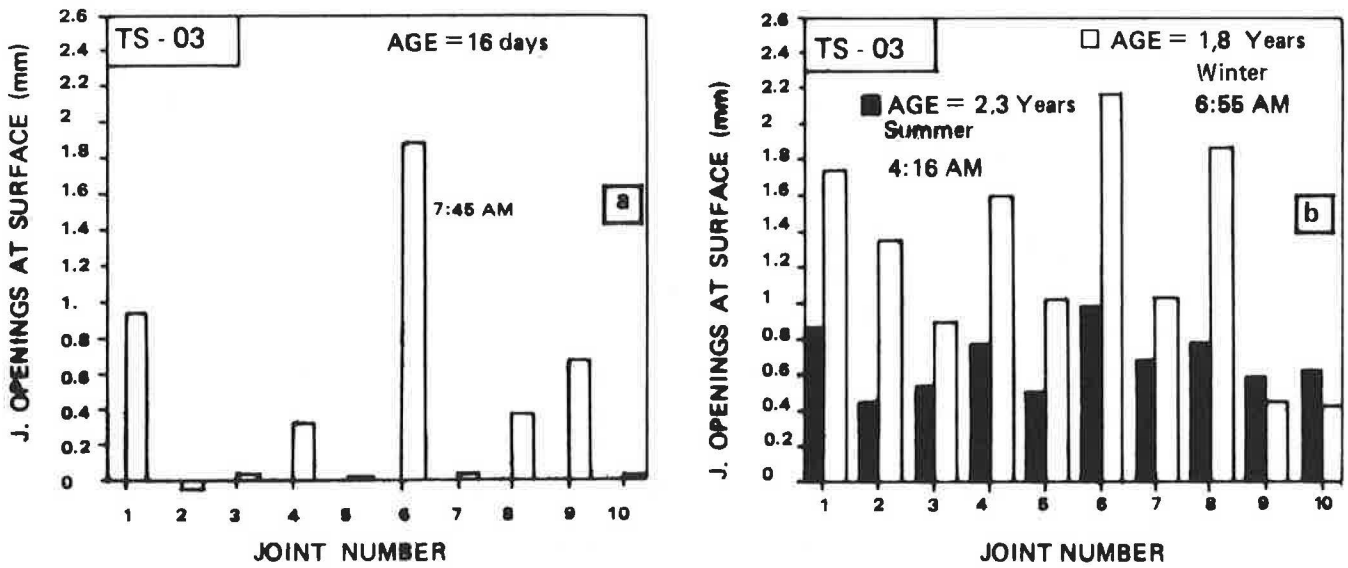
FIGURE 2 Active joints after (a) 16 days and (b) 2 years of age.

Poblete et al. show that the influence of geometrical differences between slabs is of very reduced significance.

In Figure 6, the maximum deflections at points DRB 1 and DRB 2 are plotted against corner uplifts for complete 24-hr thermal cycles during winter and summer days, and are considered representative of the general behavior of all 21 test-section pavements. In winter the deflection is linear with the magnitude of corner uplifting; in summer a similar tendency is recorded, but in a narrow loop. The difference observed between the heating and cooling is related to the joint face interlock due to different compressions of the lower transverse edges. The different loops observed at DRB points 1 and 2

LAY OUT OF INSTRUMENTATION AT EACH TEST SECTION

TRB: Topographical Reference Bases

FLOWCHART OF THE DATA ACQUISITION SYSTEM
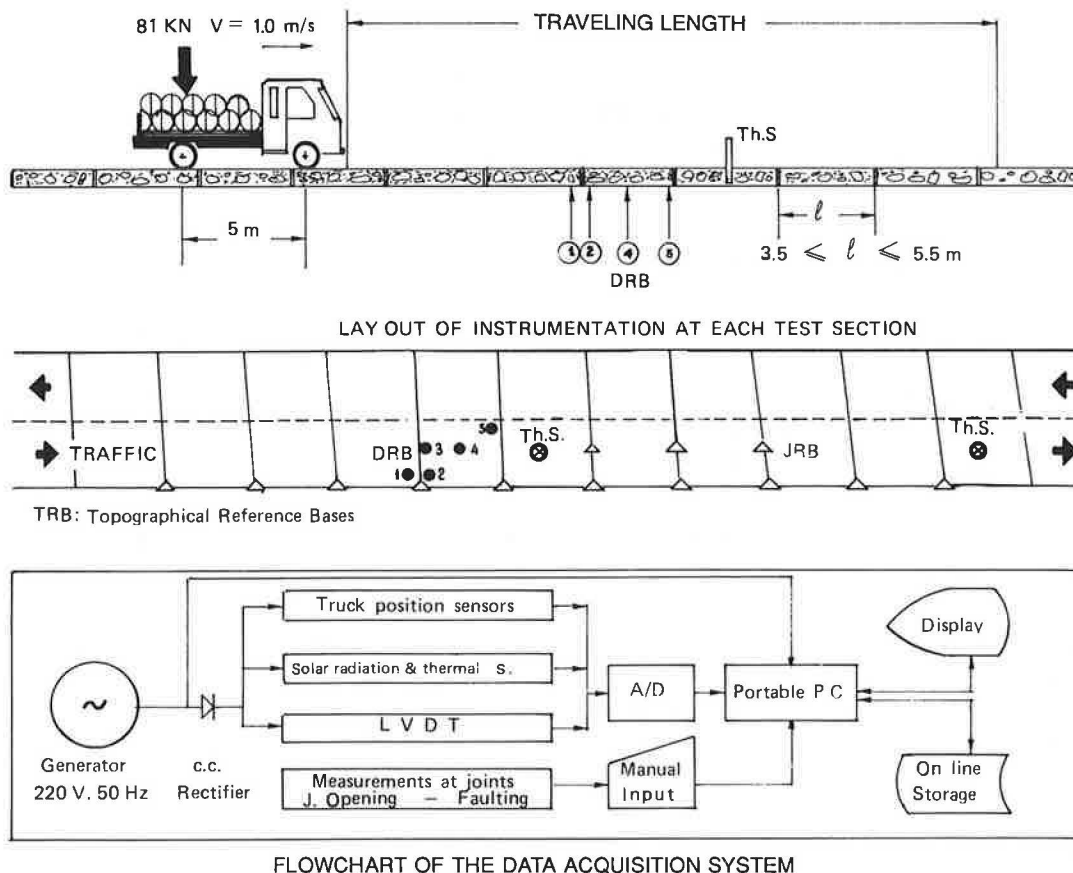
FIGURE 3 Schematic layout of instrumentation.
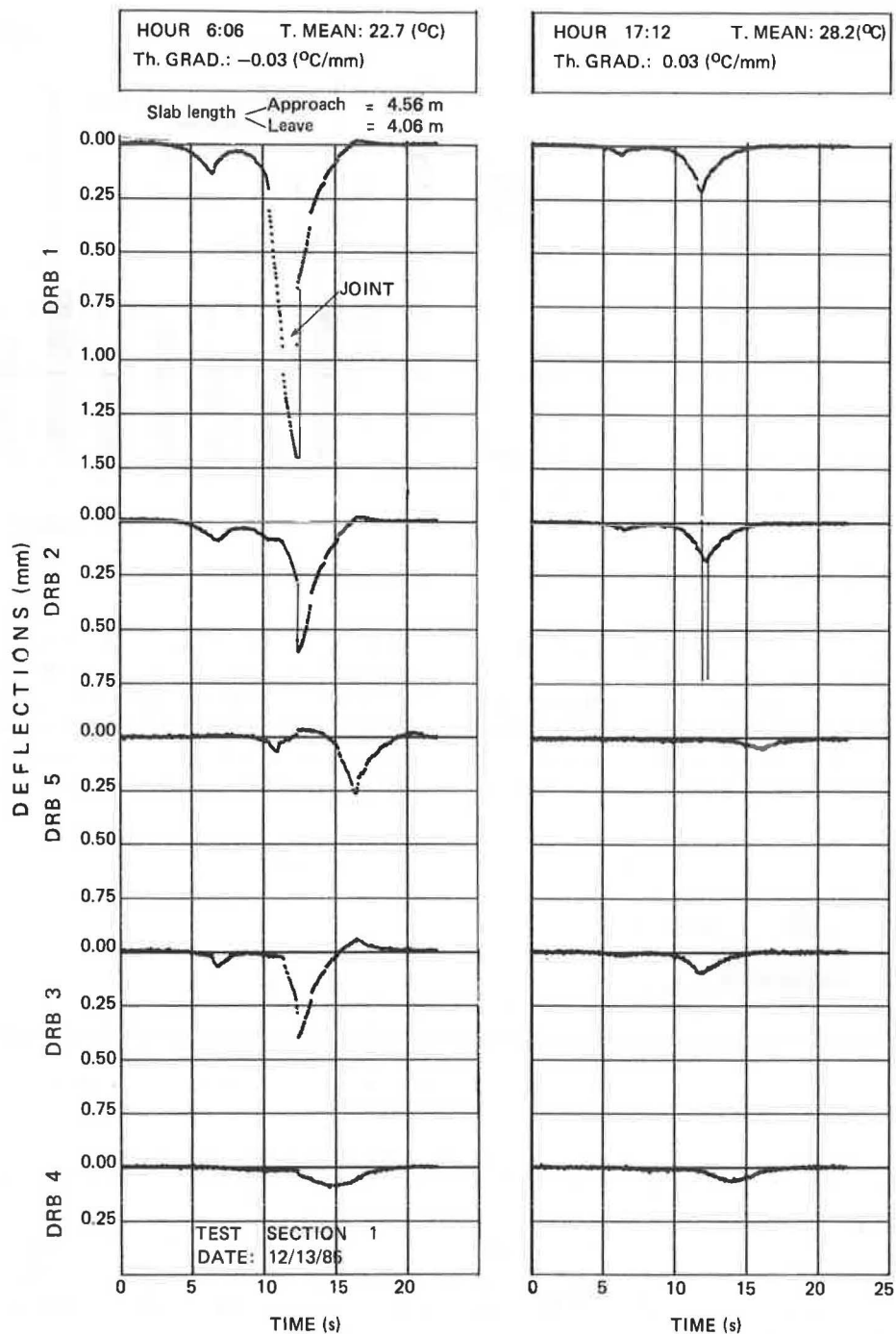
FIGURE 4 Simultaneous deflections under traveling load for two temperature conditions in summer.

suggest that the joint efficiency is different when the load is either on the approach slab or on the leave slab. In any case, the thermal deformations are relative to the minimum day value, so, according to the other work of Poblete et al. in this Record, in summer this reference could be considered as "full support" of slab edges, including some sinking into the base, whereas in winter this condition, which is seldom reached, makes the deflections appear higher.

In all pavement sections included in this study, a generalized prevailing upward curling of the slabs, causing considerable

lack of support at edges, has been verified (Figure 7a). Under high temperatures and associated strong positive gradients, that condition may be reversed, with the slabs expanded and a cylindrical downward curling imposed on the slabs with their longitudinal edges supported (Figure 7c). The condition in which a plain slab is supported under each point occurs only when the slab temperature causes a change from upward to downward curling and vice versa.

Further discussions of this behavior can be found in another paper by Poblete et al. in this Record.
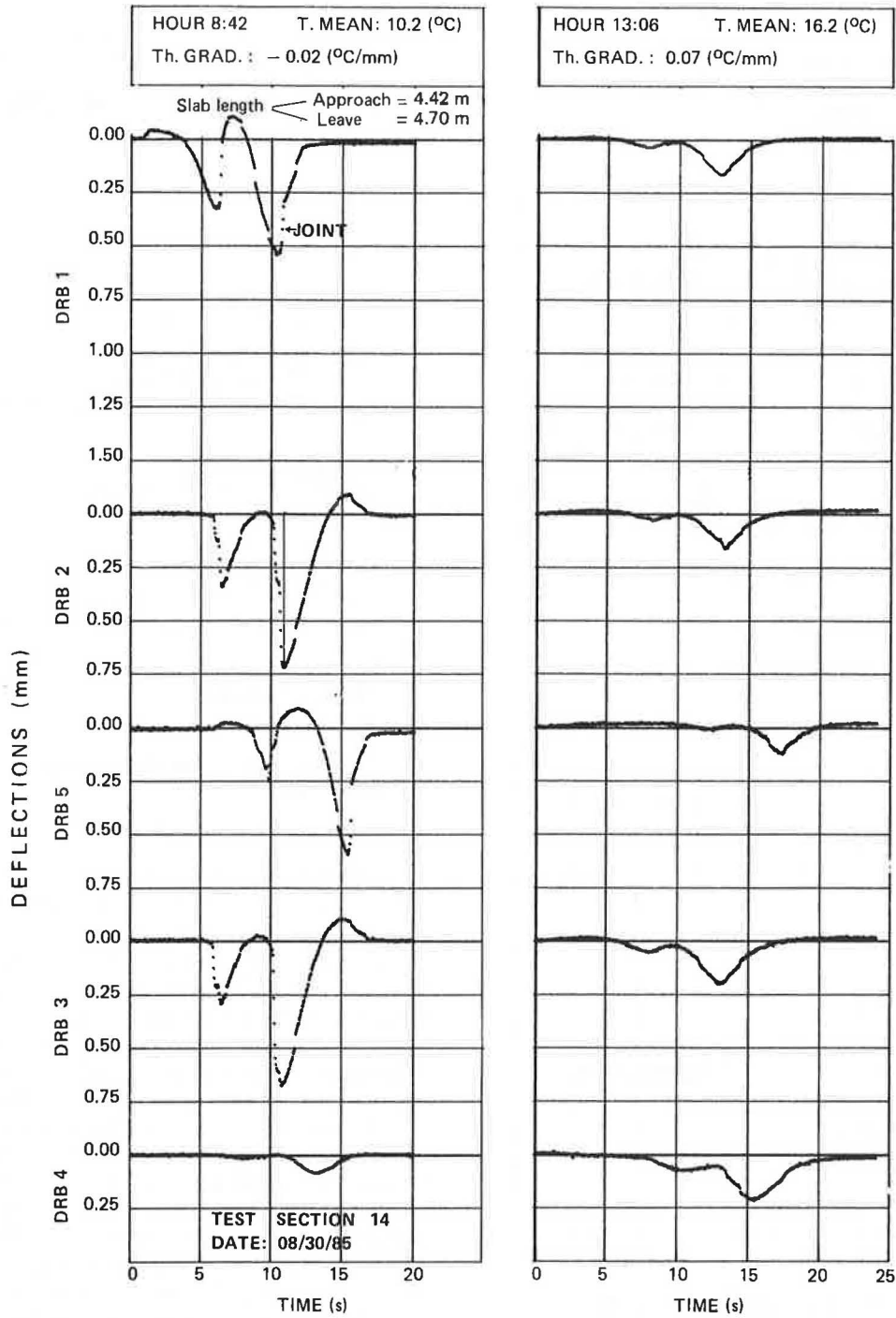
FIGURE 5 Simultaneous deflections under traveling load for two temperature conditions in winter.

LOAD TRANSFER EVALUATIONS

By substituting the simultaneous deflections obtained from the recordings of DRB points 1 and 2 at two representative test sections into Equation 1, load transfer LT_A can be evaluated for different positions of the load. As shown in Figure 8(a) and (b), each of the four curves represents diverse thermal conditions during a 24-hr measurement cycle. As an additional reference, the equivalent LT_D is included on the right ordinate of the graphs. The load transfer is different for each

thermal state and decreases with the distance to the joint. Moreover, the computed LT is different whether the load is on the leave slab (LT_{leave}) or on the approach slab ($LT_{approach}$) with a discontinuity in the joint itself due to differential upliftings of the transverse edges. In such cases, the loaded axle may be intercepting the joint, or the tire treads may be pressing on both edges. In any case, the deflections when the load is too close to the joint are distorted and the corresponding LT values may be erroneous.

All measurements were performed with a truck carrying

UPLIFT OF CORNER DRB 1 (mm)

UPLIFT OF CORNER DRB 2 (mm)

FIGURE 6 Slab corner displacements and maximum deflections during winter and summer day cycles.

FIGURE 7 Shapes of slabs deformed by temperature.

about 80 kN (18 kips) on the rear axle, which is the pavement design load; however, in some cases, measurements at the maximum legal load (110 kN) were also obtained, but no significant differences in the LT values computed from either recording were noted (6). In all case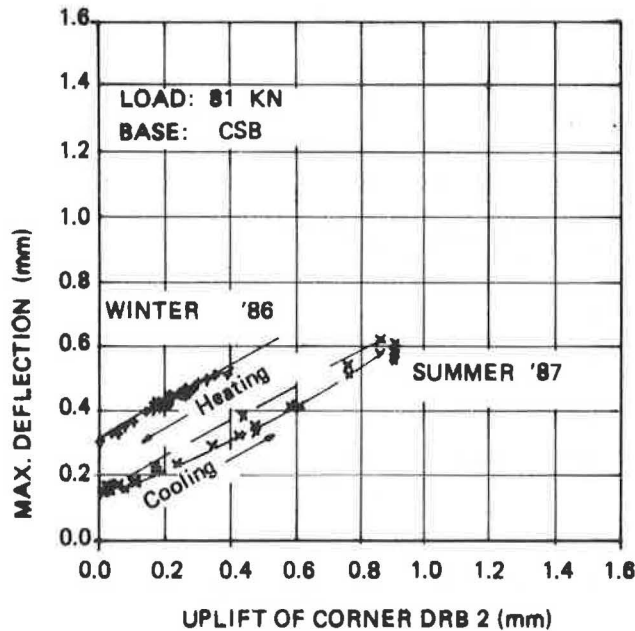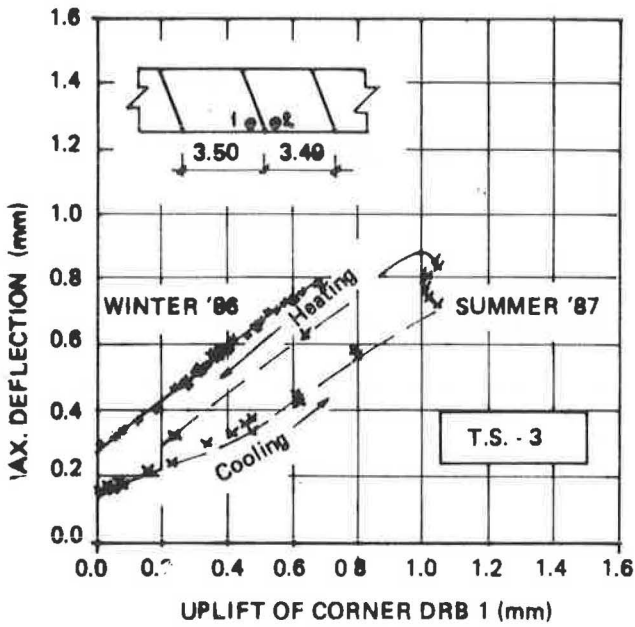s, outer rear wheels pass exactly on point DRB 1 and thereafter on point DRB 2, so that the truck path is somewhat displaced toward the shoulder.

In Figures 9 and 10 the LT computed with the load on DRB points 1 and 2 is presented for two test sections exhibiting typical behavior. The results emphasize the differences between $LT_{approach}$ and LT_{leave} over a daily thermal cycle.

To explain this behavior, a detailed analysis of the influence of slab internal temperatures on the joint interlockings is made. In fact, in the other paper by Poblete et al. in this Record, it was shown that for negative gradients (slab surface cooler than the bottom) the transverse joints may be relatively open if the mean temperature is low and the joint faces are free to rotate due to thermal gradients, so that the contact between slabs is limited to the lower transverse edges. On the other hand, the lower edges may be strongly compressed if the mean temperature is high, resulting in a high mobilization of shear strength at the joint, as illustrated in Figure 11. This effect is maximized when the joint becomes locked by the concurrence of a positive gradient and a high enough mean temperature, where the pavement behaves as a continuous strip.

In the case of the summer cycle shown in Figure 9, there is a moment in the day when the values for $LT_{approach}$ and LT_{leave} converge because of a quick heating of the slab surface without a significant increase in the mean temperature across the slab thickness. This behavior is interpreted as a decompression of the lower transverse edges when the joint faces have a tendency to be mutually parallel. As a consequence, it is not uncommon for the lower edges to break after a number of loading cycles. This has been observed in core samples drilled along the induced joint cracks of medium-aged pavements. Breakage of the lower edges would cause a rapid deterioration of the load transfer; therefore $LT_{approach}$ and LT_{leave} would coincide at last in a residual unique value.

For a better appraisal of these same effects, the influence
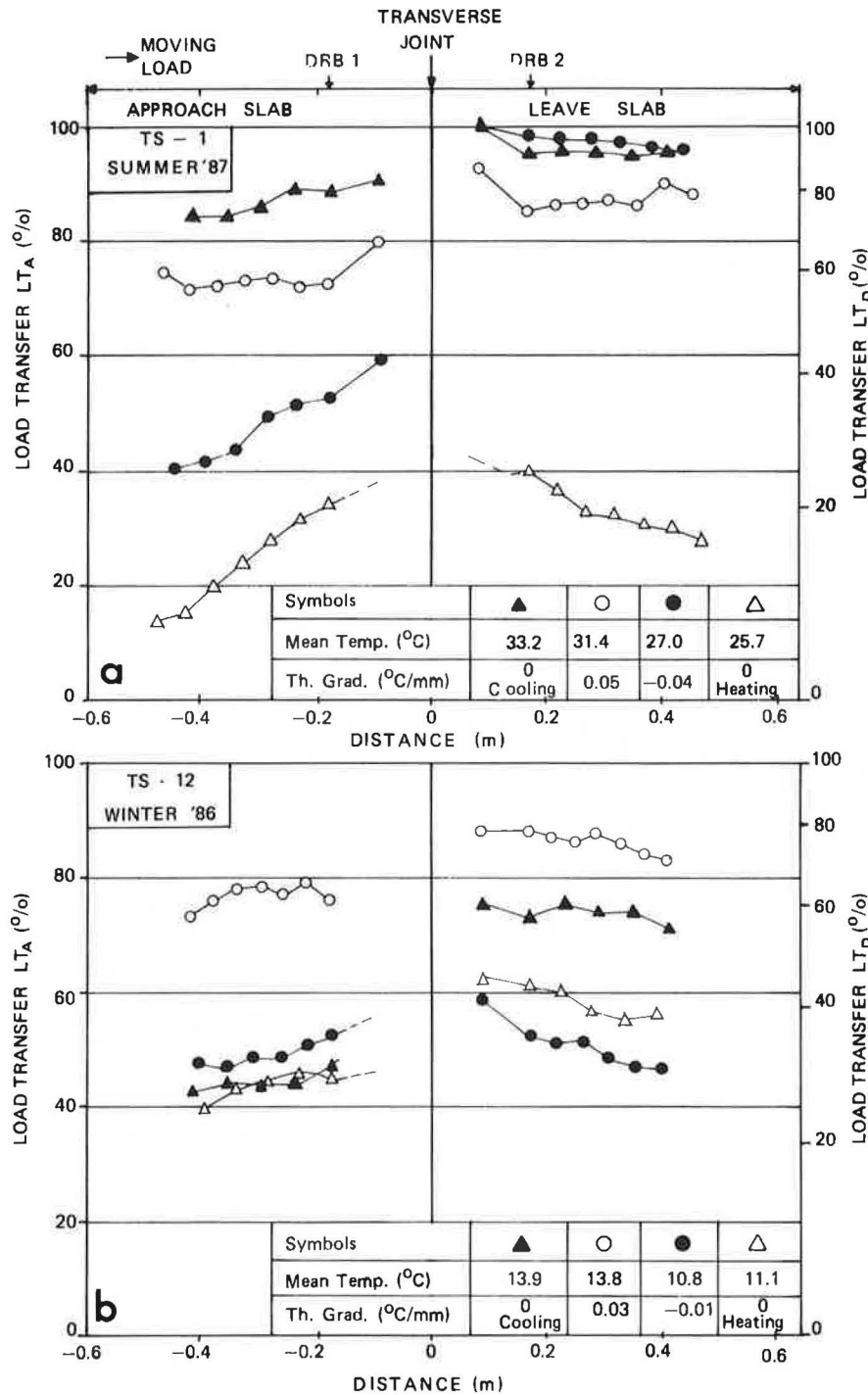
FIGURE 8 Load transfer evaluated for different positions of an 81-kN moving load over a 24-hr measurement period in (a) summer and (b) winter.

of joint openings on $LT_{approach}$ and LT_{leave} is illustrated in Figure 12 for two thermal cycles on a sunny summer day at a representative test section. From the analysis of $LT_{approach}$, different load transfers may be observed whether in the heating or in the cooling curves, and in both, generally a lower load transfer corresponds to a greater opening. Differences at equal openings are explained again by the different compressions at the lower transverse edges.

Some differences between heating and cooling are also pres-

ent in the curves for LT_{leave} and can be explained by similar reasoning. However, comparison with $LT_{approach}$ discloses substantial differences, which may be attributed to a preferent inclination of the induced crack (Figure 13). Every time a loaded slab can rest on the favorably inclined edge of an adjoining slab, a good load transfer will result, independently from the joint opening. If the two consecutive summers of Figure 12 are compared, the different load transfers obtained for similar openings and thermal conditions imply a de-
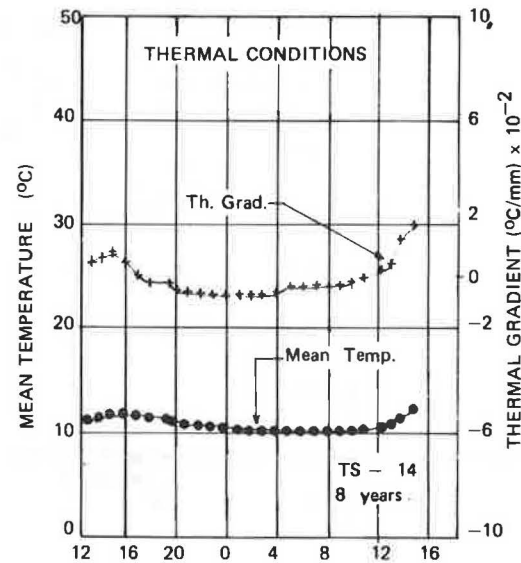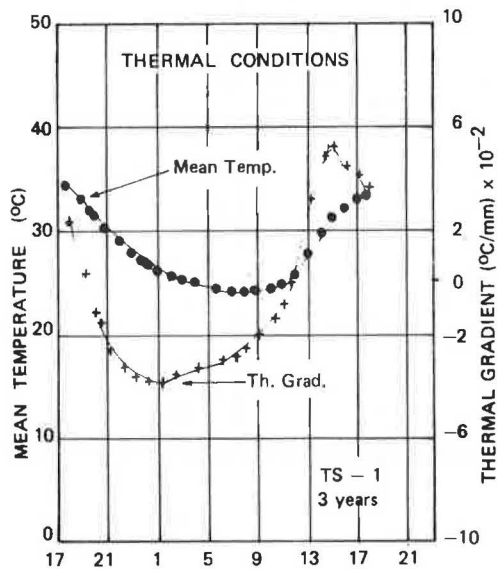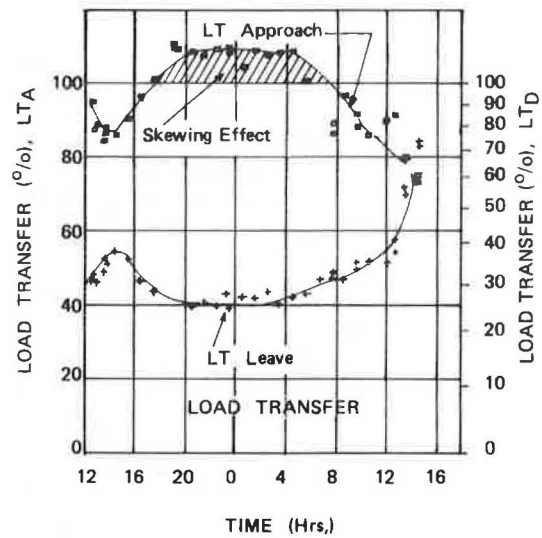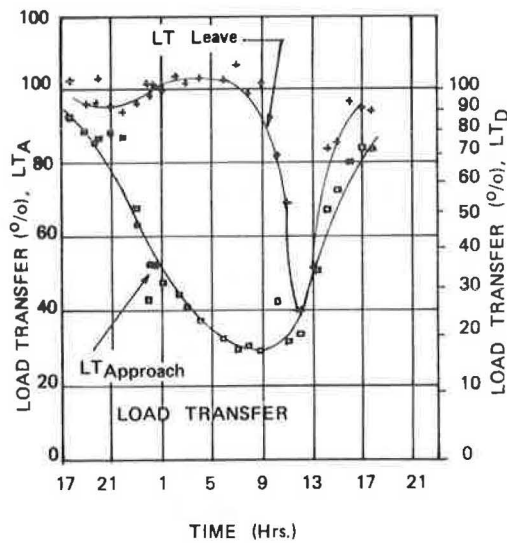
FIGURE 9   Variation of load transfer during a summer day cycle.

FIGURE 10   Variation of load transfer during a winter day cycle.

terioration of the joint interlocking by fracture of some roughnesses.

Table 1 summarizes the $LT_{approach}$ and LT_{leave} pairs estimated for the time at which one of them is lowest on the day of measurement; the duration of that condition is also estimated. In all winter cases the minimum characteristic load transfer is low during most of the day, and particularly during morning hours. In summer the minimum characteristic load transfer is usually much higher, occasionally over 90 percent, and not infrequently lasts the whole day. Such seasonal differences are due to the greater opening of the joints during the lower winter temperatures, except in test sections 11, 15, 19, and 21. In those sections the load transfer seems to remain high throughout the year, in spite of the large temperature differences prevailing between winter and summer days. The high load transfer may be attributable to the low locking

temperature of the joints at these test sections, which were paved under cold and humid ambient conditions, and to the swelling of concrete during winter (7). Finally, the values of Table 1 represent the load transfers of a single joint selected at each test section as the most open among a set of 10 consecutive joints and which is expected to open further over time (Figure 2b). For this reason the actual load transfers at the other joints should be somewhat higher under similar thermal conditions.

CONSIDERATIONS FOR JOINT STIFFNESS MODELING

To model the deterioration of Chilean concrete pavements, a mechanistic approach is taken. To this end, stresses caused by real traffic and environmental loads are evaluated by a
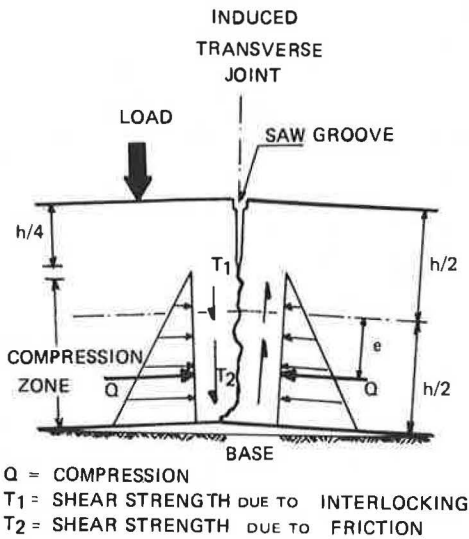
FIGURE 11 Forces acting on an undoweled transverse joint.

Q = COMPRESSION
T_1 = SHEAR STRENGTH DUE TO INTERLOCKING
T_2 = SHEAR STRENGTH DUE TO FRICTION
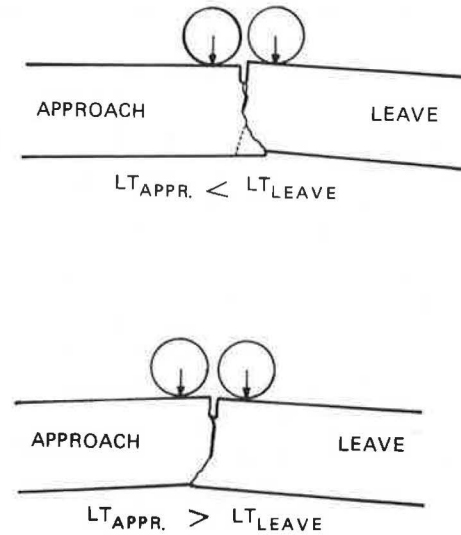
FIGURE 13 Hypothesized crack inclination in induced transverse joints.

finite-element method. The pavement is modeled as a set of three slabs with realistic boundary conditions of partial support, such as discussed in preceding paragraphs in the analysis of deflection results. With regard to the transverse joints and longitudinal borders of the slabs, their actual conditions require that they be discussed separately.

At longitudinal borders, a free edge is evident in the contact with the granular shoulder. In many Chilean pavements, the other border behaves practically as a free edge, up to the relatively high level of deflections necessary to mobilize

the eventual collaboration of the adjacent slabs through the keyed joint (8). In other cases some partial load transfer may be accounted for at this border.

At the transverse edges the restraints can be broken down as illustrated in Figure 11, with an eccentric compression Q depending on the slab temperature, an associated shear strength T_1 of frictional nature, and the aggregate interlocking shear strength T_2. The eccentricity, e, is minimal for the uncurled (plain) slabs and increases with the upward curling caused by rotation of the transverse edges. Both magnitudes Q

Point		a	b	c	d	e	f	a'	b'	c'	d'	e'	f'
Th. Grad.	°C/mm	0.04	0.0	-0.04	-0.03	0.0	0.03	0.02	0.0	-0.04	-0.03	0.0	0.05
M. Temp.	°C	32.2	31.0	26.3	22.7	23.9	26.4	34.6	33.2	26.1	24.1	25.7	30.0
		□ SUMMER 1986						x SUMMER 1987					

FIGURE 12 Influence of joint openings on load transfer.

TABLE 1   LOAD TRANSFER EVALUATED FOR AN 81-kN MOVING LOAD

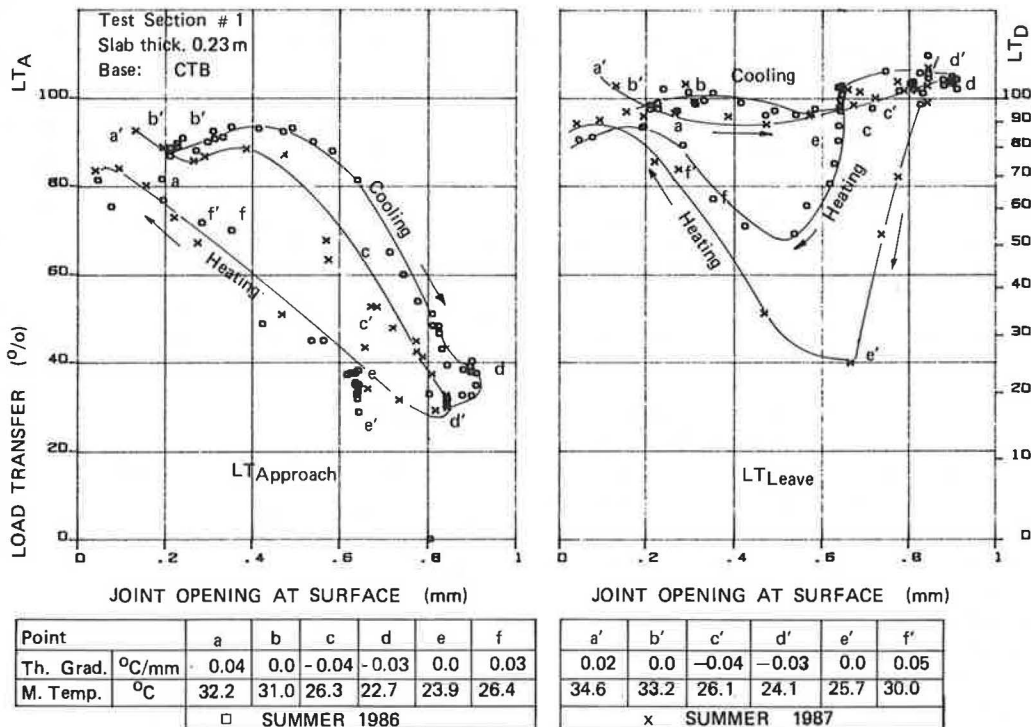| Test Section		Slab thick. (m)	Skew. (m)	Thermal Cond. Mean. Temp. (°C)	Thermal Grad. (°C/mm)	LTΘ (%) Approach	LTΘ (%) Leave	Duration (hrs)	Thermal Cond. Mean. Temp. (°C)	Thermal Grad. (°C/mm)	LTΘ (%) Approach	LTΘ (%) Leave	Duration (hrs)
Longotoma	1	0.23	+0.46	11.5	-0.02	40	40	14	22.5 / 24.5	-0.03 / -0.03	30 / 30	100 / 100	16 / 16
Las Chilcas	2	0.23	+.046	12.0	-0.04	55	80	24	28.5	-0.05	95	100	24
Lampa	3	0.24	+0.74	9.0	-0.02	50	`70	14	26.5	-0.05	60	100	7
Lo Vásquez	4	0.26	+0.46	6.5	-0.03	45	45	14	23.0 / 23.7	-0.05 / -0.05	55 / 40	100 / 85	16 / 12
Talagante	5	0.22	+0.53	12.0	0.00	90	30	--	25.5	-0.06	95	95	24
Paine	6	0.24	+0.66	7.0	-0.03	50	100	17	25.5	-0.04	95	95	24
Graneros	7	0.25	+0.66	8.5	-0.04	35	100	16	23.5 / 25.0	-0.06 / -0.05	95 / 95	95 / 100	24 / 24
San Fernando	8	0.23	-0.55	9.0	-0.01	65	35	16	25.0 / 22.5	-0.04 / -0.05	70 / 90	95 / 80	5 / 7
San Rafael	9	0.23	+0.41	12.5	0.00	50	80	24	25.5 / 23.0	-0.06 / -0.05	95 / 95	100 / 100	24 / 24
Cocharcas	10	0.21	+0.71	11.7	-0.03	70	40	10					
Concepción	11	0.23	0.00	13.0	-0.01	90	90	12	23.5	-0.04	90	95	6
Cabrero	12	0.22	-0.66	11.0	-0.02	50	60	10	28.0	-0.04	100	95	24
Laja	13	0.21	0.00	9.3	-0.02	0 - 30	75	14	26.0	-0.06	95	85	14
C. Esperanza	14	0.21	+0.59	10.0	-0.01	100	45	14	26.5	-0.06	90	90	14
Victoria	15	0.23	+0.75	9.5	-0.01	95	100	24	23.0	-0.03	95	00	24
Temuco	16	0.21	+0.59	11.5	0.00	60	75	14	23.0	-0.03	90	90	24
Gorbea	17	0.22	+0.42	9.0	-0.02	55	80	8	23.0	-0.04	95	95	24
Loncoche	18	0.22	+0.79	4.5	-0.02	45	80	6	17.2	-0.05	95	95	24
Mariquina	19	0.23	+0.84	2.8	-0.03	80	100	14	23.0	-0.04	95	00	24
Mafil	20	0.23	+0.59	5.1	-0.02	70	45	20	23.1	-0.04	70	95	4
Rio Bueno	21	0.22	+0.62	3.2	-0.04	85	100	24	24.0	-0.03	80	85	6

Skewing   + forward   − backward

W I N T E R   1986   S U M M E R   1986   &   1987

and e are functions of the initial joint openings, of the drying shrinkage, and of the thermal expansion of the pavement slabs, going from a maximum value during the afternoon hours of sunny summer days to an uncertain low value on cold nights.

The shear restrictions, $T_1 + T_2$, developed at transverse joints during loading involve the concept of joint stiffness, very similar to that considered in the model proposed by Armaghani et al. (9), with the possible difference that the compression Q should be considered explicitly, since the compressional stress in the slab plane helps to diminish the tensile stresses at the slab surface (8). Hence, three kinds of joint stiffnesses at transverse edges are proposed:

$$K_h = Q/\Delta m \tag{4}$$

$$K_z = (T_1 + T_2)\Delta z = (\tau + \beta Q)/\Delta z \tag{5}$$

$$K_\theta - M/\Delta\theta - Qe/\Delta\theta \tag{6}$$

where

Δm = joint opening variation evaluated at middle plane of joint,
$\Delta\theta$ = relative rotation between adjacent edges,
Δz = relative vertical displacement between adjacent edges $= |\delta_1 - \delta_2|$, and
τ, β = coefficients.

For each specific application, the numerical processes need to be treated in successive iterations, comparing the calculated displacements with those actually measured at the joints and at DRB points 1, 2, 3, 4, and 5 under equivalent loads.

The steps include an initial process of a single slab stressed by a corrected negative thermal gradient that takes into account the existence of a permanent upward curling. The slab is modeled as a thick plate resting on continuous subgrade springs, whose K_s value is back-calculated after adjusting the real compressed area of the support. The next step is to analyze three slabs linked together with joint springs and stressed by the same temperature gradient, whose calculated joint openings and rotations permit, by comparison with those measured, the adjustment of numerical values for K_h, K_z and K_θ. These stiffnesses are to be fed in successive steps, when processing slabs with the axle loads actually used for the deflection measurements. In these final steps some further adjustments of the stiffnesses may be necessary.

The full processing of test-section pavements, with application of the boundary conditions that have been discussed, is under way, and the resulting stresses as well as details of the complete models being used will be presented in future papers.

CONCLUSIONS

The methodology used for the measurement of absolute deflections, whose results are presented herein, allows the evaluation of the load transfer at joints with good accuracy and repeatability, under real traffic and in any thermal condition of the pavement.

The results obtained at 21 test sections confirm the conclusion that load transfer is not constant along a daily cycle but depends on the thermal conditions of the pavement. For each particular case the daily variation is satisfactorily explained in terms of the variations in transverse joint openings; no other variables such as slab thickness and base type were identified as a significant influence.

Load transfer computed from deflections with the load upon the leave slab is much different than with the load on the approach slab, unless the joints stiffness is so high that the pavement behaves as a continuous strip.

The differences between LT_{approach} and LT_{leave} would be the result of a preferent inclination of the induced joint crack (Figure 13). Moreover, the predominant condition of joint faces rotated upward reduces the interlockings to the compressed lower edges; therefore it can be anticipated that LT_{approach} and LT_{leave} will converge to a common residual value after the complete breakage of the compressed edges.

Some pavements constructed under cold and humid ambient conditions present a lower joint blockage temperature, which cause their joints to remain closed, and consequently, they have a high load transfer. Blowups are not common in Chilean pavements.

To evaluate internal stresses of pavement slabs, a mechanistic approach is used in which three kinds of joint stiffnesses are considered to take into account the effects of shear forces and moments developed at joints, as well as compressions built up by the slabs' moisture and temperature.

Followup of the load transfer becomes very complicated in practice because it must always be evaluated at equal thermal and moisture conditions and with load positions far from the joint to avoid the effect of skewing.

ACKNOWLEDGMENTS

REFERENCES

1. L. W. Teller and E. C. Sutherland. The Structural Design of Concrete Pavements, 1936. *Public Roads,* Vol. 17, No. 7, p. 169.
2. M. Darter. *Design of Zero-Maintenance Plain Jointed Concrete Pavements,* Vol. I. *Development of Design Procedures,* University of Illinois, Urbana, 1976.
3. AIPCR Comité Technique des Routes en Bèton. Le Transfer de Charge aux Joints Transversaux. . . . *Bulletin de Liaison LPC,* No. IX, 1979, p. 52.
4. L. Ortega and P. Spratz. Performance Measures on Plain Concrete Pavements Without Dowels. *Proc. International Conference on Roads and Developments,* Paris, 1984, pp. 199–204.
5. P. Foxworthy. *Concepts for the Development of a Nondestructive Testing and Evaluation System for Rigid Airfield Pavements.* Ph.D. thesis. University of Illinois, Urbana-Champaign, 1985.
6. IDIEM, University of Chile, and Highway Division, Chilean Ministry of Public Works. Concrete Pavements Research Project. *Annual Report 1986,* Vol. I. (in Spanish).
7. A. Neville. *Properties of Concrete.* Pittman Publishing Ltd., Aulander, N.C., 1975.
8. IDIEM, University of Chile, and Highway Division, Chilean Ministry of Public Works. Concrete Pavements Research Project. *Annual Report 1987,* Vol. I. (in Spanish), 1987.
9. J. M. Armaghani, J. M. Lybas, M. Tia, and B. E. Ruth. Concrete Pavement Joint Stiffness Evaluation. In *Transportation Research Record 1099,* TRB, National Research Council, Washington, D.C., 1986, pp. 22–36.

Flexible Boundary in Finite-Element Analysis of Pavements

RONALD S. HARICHANDRAN AND MING-SHAN YEH

The finite-element method is finding increasing use in the structural analysis of pavements. In pavement analysis, very deep finite-element meshes need to be used to satisfactorily model the infinitely deep subgrade layer. Programs require large amounts of computer memory and computational time. A scheme is developed in this paper to overcome the computational burden imposed by the requirement of a deep bottom boundary in the finite-element analysis of pavements. A flexible boundary, which accounts for displacements that occur beneath it, is used with finite elements above it. Through case studies it is shown that the method yields accurate solutions. The results are much better than those from a traditional finite-element approach requiring approximately the same amount of computational effort. The proposed method possesses significant advantages over the traditional approach, especially in nonlinear analysis.

The finite-element method is increasingly being used for the structural analysis of pavements (1–3). The method is especially attractive when the nonlinear behavior of the granular and cohesive materials used in pavements is to be considered in mechanistic modeling. Since the depth and width of a typical pavement are large, it is necessary when constructing the finite-element mesh to impose side and bottom boundaries at some reasonable distance from the loaded area. Along the side boundaries it is common to allow vertical displacements but not radial displacements, whereas along the bottom boundary both displacements are usually not allowed. (At interior nodes, vertical as well as radial displacements can occur.) Care must be exercised, especially with the bottom boundary, if acceptable accuracy is to be obtained in the computed displacements and stresses. When a weak subgrade is present, it is imperative that the finite-element mesh be quite deep. Use of a deep mesh, however, increases the computational effort involved, and can become prohibitive, especially for nonlinear problems where iterative or incremental solutions are required.

A technique that overcomes this drawback of the finite-element method is presented in this paper. Finite elements are used to model the soil in the vicinity of the loaded area. The side boundaries are placed, as is usual, at some distance from the loaded area (a distance of 10 to 12 times the radius of the loaded area is recommended). The bottom boundary, however, is placed at a depth below which displacements and stresses are not of interest. (In pavement design, displacements and stresses are of interest only to a depth of about 50 in.) Further, the bottom boundary is assumed to be flexible,

Department of Civil and Environmental Engineering, Michigan State University, East Lansing, Mich. 48824.

and the half-space below the boundary is assumed to be composed of linear elastic layered material. (The boundary will usually be placed at some depth within the subgrade, in which case the half-space below the boundary will be homogeneous. The technique derived herein, however, is general and may be applied to a layered half-space.) Displacements that occur in the soil below the boundary are therefore considered in the analysis.

When dealing with nonlinear soils, the bottom boundary must be placed at a depth below which it is reasonable to neglect nonlinearities. The highly stressed, and therefore significantly nonlinear, soil in the vicinity of the loaded area can be modeled by the finite elements. This technique is computationally efficient and should yield sufficiently accurate results.

The theoretical basis for the technique discussed above is first presented, and the method is then used to analyze homogeneous and layered flexible pavement systems. Results are presented only for linear systems, and comparisons are made with the normal finite-element approach as well as exact solutions from the CHEV51 elastic layer program. The results indicate that the technique is accurate and that it is significantly better than a traditional finite-element approach requiring approximately the same amount of computational effort. The main benefits of the method are realized, however, when it is used in nonlinear analyses. The flexible boundary approach is currently being implemented in a nonlinear finite-element program being developed for the Michigan Department of Transportation. The efficiency achieved by utilizing this technique allows the program to be developed for a personal computer. Results from studies utilizing the flexible boundary with nonlinear materials will be presented at a later date.

MODELING OF FLEXIBLE BOUNDARY

Figure 1 illustrates the modeling of a pavement system. One circular wheel load is assumed, and the problem therefore reduces to an axisymmetric one. The main region of interest under the load is divided into finite elements. The finite-element mesh rests on a half-space consisting of elastic layered strata. The coupling between the finite elements and the half-space occurs at the degrees of freedom (DOF) on the bottom boundary which are shown in the figure.

In order to account for the coupling between the flexible boundary and the finite elements it is necessary to determine the stiffness matrix of the half-space corresponding to the DOF along the boundary. It is illuminating at this point to consider the physical meaning of such a stiffness matrix. Due
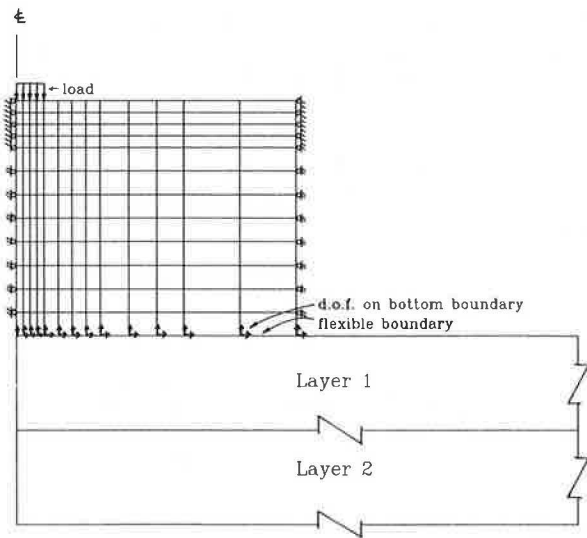
FIGURE 1 Finite-element mesh on flexible boundary.

FIGURE 2 Vertical (*top*) and radial (*bottom*) ring loads.

to the axisymmetric nature of the problem, the DOF along the boundary are really the vertical and radial displacements of the rings shown in Figure 2. At the origin the ring degenerates to a point. If there are n rings as shown in the figure, there will be $(2n - 1)$ DOF, since there is no radial DOF at the origin (the radial displacement at the origin is zero due to symmetry). The stiffness matrix will then have dimensions of $[(2n - 1) \times (2n - 1)]$. The element k_{ij} (i row and j column) of the stiffness matrix $\mathbf{K}$ is the total force required along the ring at DOF i when DOF j is displaced by a unit amount while all other DOF are held fixed. The elements of the stiffness matrix are extremely difficult to compute directly. However, the inverse of the stiffness matrix, commonly known as the flexibility matrix, can be computed. The element f_{ij} of the flexibility matrix $\mathbf{F}$ is the displacement along DOF i due to a unit total uniform ring load along DOF j (vertical and radial uniform ring loads are depicted in Figure 2). This displacement can be obtained from an elastic-layer program such as CHEV51. If the boundary is placed within the subgrade, as will be most common, then the half-space will be homogeneous and analytical results can be used to determine the flexibility coefficients.

There is one problem of incompatibility between finite-element modeling and elastic-layer modeling. If finite elements are used to model the half-space beneath the boundary, concentrated ring loads (load per unit arc length) can be applied at the nodes, and all displacements on the boundary can be computed. When the half-space is modeled by elastic-layer theory, however, concentrated ring loads will produce finite displacements at all points on the boundary except directly under the load. On the ring where the load is placed, the displacements will tend to infinity. This, of course, is the true behavior since it is known that plastic deformation will occur under the concentrated load. In order to link together the finite elements and the elastic half-space, however, some approximation is necessary to compute the diagonal elements of the flexibility matrix (these f_{ij} elements are the displacements directly under the ring loads). One possible approximation is to assume that the load is uniformly distributed over
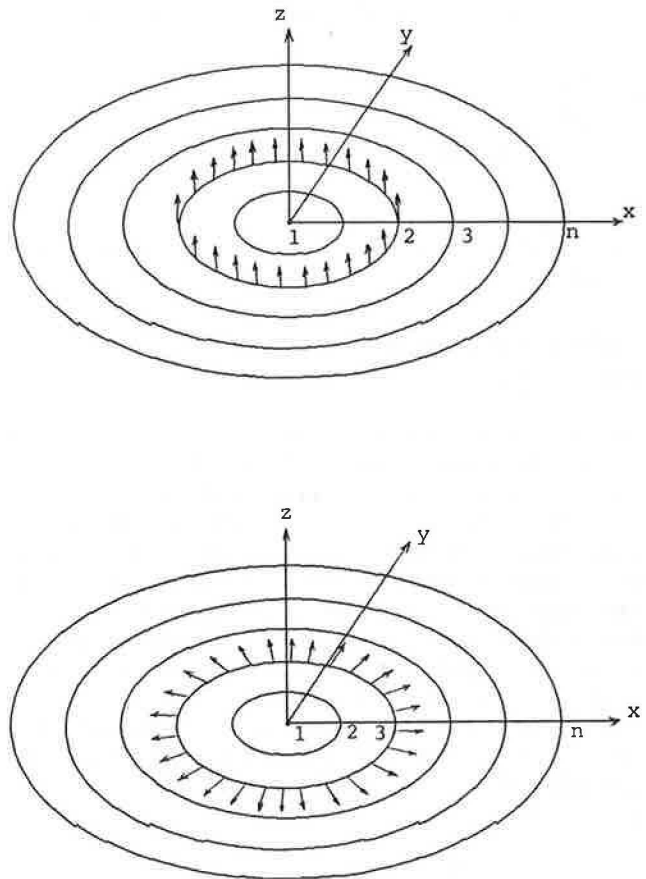
the annular surface halfway from the loaded ring to the two adjacent rings. This concept is further discussed below.

Once the flexibility matrix of the half-space has been estimated, it can be inverted to obtain the corresponding stiffness matrix. The DOF along the bottom boundary are usually about 30, and the inversion of a 30×30 symmetric matrix presents no problem. Further, since the half-space below the boundary is assumed to be elastic, this inversion only needs to be performed once even if finite elements are used to model nonlinear materials above the boundary.

The stiffness matrix of the entire system comprising finite elements and the half-space is assembled from the stiffness matrices of each of the subsystems. The stiffness matrices of the finite elements are computed one by one and assembled as usual. This matrix, denoted by $\mathbf{K}_{FE}$, may be partitioned as follows:

$$\mathbf{K}_{FE} = \begin{bmatrix} \mathbf{K}_{FF} & \mathbf{K}_{FB} \\ \mathbf{K}_{BF} & \mathbf{K}_{BB} \end{bmatrix} \qquad (1)$$

where the $(2n - 1) \times (2n - 1)$ matrix $\mathbf{K}_{BB}$ corresponds to the DOF along the bottom boundary. The stiffness matrix of the half-space is denoted by $\mathbf{K}_{HS}$, also a $[(2n - 1) \times (2n - 1)]$ matrix). $\mathbf{K}_{BB}$ will have many zero elements (since $\mathbf{K}_{FE}$ is usually a banded matrix), but $\mathbf{K}_{HS}$ will be fully populated. The stiffness matrix of the combined system is then

$$\mathbf{K} = \begin{bmatrix} \mathbf{K}_{FF} & \mathbf{K}_{FB} \\ \mathbf{K}_{BF} & \mathbf{K}_{BB} + \mathbf{K}_{HS} \end{bmatrix} \qquad (2)$$

If the nodal displacements $\mathbf{D}$ are partitioned corresponding to $\mathbf{K}$ as

$$\mathbf{D} = \begin{bmatrix} \mathbf{D}_F \\ \mathbf{D}_B \end{bmatrix} \tag{3}$$

then the solution of the stiffness equations

$$\mathbf{KD} = \mathbf{Q} \tag{4}$$

will yield the displacements at all nodes, *including those at the boundary*, $\mathbf{D}_B$.

FLEXIBILITIES FOR HOMOGENEOUS HALF-SPACE

As mentioned earlier, in most cases the bottom boundary will be within the subgrade, and the half-space beneath the boundary will be homogeneous. For this case it is possible to use analytical expressions to evaluate the flexibilities of the half-space. Analytical solutions for vertical and radial ring loads may be derived, but in the absence of simple expressions, it is necessary to resort to numerical integration. Elegant closed-form solutions, however, exist for uniform vertical loads and linearly varying radial loads on a circular area. These can be utilized to estimate the required flexibility coefficients.

According to Poulos and Davis (4), for a uniform vertical upward load p applied to a circular area of radius r_0 the vertical (upward) and radial (outward) surface displacements are, respectively,

$$w_V(r;r_0;p) = \begin{cases} F(0.5, -0.5;1;(r/r_0)^2)\,\dfrac{2(1 - \nu^2)}{E}\,pr_0, \\ \qquad\qquad\qquad\qquad \text{for } r < r_0 \\[2pt] \dfrac{4(1 - \nu^2)}{\pi E}\,pr_0, \\ \qquad\qquad\qquad\qquad \text{for } r = r_0 \\[2pt] F(0.5, 0.5;2;(r_0/r)^2)\,\dfrac{(1 - \nu^2)}{Er}\,pr_0^2, \\ \qquad\qquad\qquad\qquad \text{for } r > r_0 \end{cases} \tag{5}$$

and

$$u_V(r;r_0;p) = \begin{cases} \dfrac{(1 + \nu)(1 - 2\nu)}{2E}\,pr, \\ \qquad\qquad\qquad \text{for } r \le r_0 \\[2pt] \dfrac{(1 + \nu)(1 - 2\nu)}{2Er}\,pr_0^2, \\ \qquad\qquad\qquad \text{for } r > r_0 \end{cases} \tag{6}$$

where

$r = $ horizontal distance from center of load;
$E, \nu = $ elastic modulus and Poisson's ratio of half-space.

$F(\alpha,\beta;\gamma;x)$ is the hypergeometric function with parameters α, β, and γ, the series representation of which is

$$F(\alpha,\beta;\gamma;x) = 1 + \frac{\alpha,\beta}{(1)\gamma}\,x \\ + \frac{\alpha(\alpha + 1)\beta(\beta + 1)}{(1)(2)\gamma(\gamma + 1)}\,x^2 + \ldots \tag{7}$$

For a radial (outward) load varying linearly from zero at the center to p at distance r_0, acting on a circular area of radius r_0, the vertical and radial displacements are, respectively,

$$w_R(r;r_0;p) = \begin{cases} \dfrac{(1 + \nu)(1 - 2\nu)}{2E}\left(1 - \left[\dfrac{r}{r_0}\right]^2\right)pr_0 \\ \qquad\qquad\qquad \text{for } r < r_0 \\[2pt] 0 \qquad\qquad\qquad \text{for } r \ge r_0 \end{cases} \tag{8}$$

and

$$u_R(r;r_0;p) = \begin{cases} F(1.5, -0.5;2;(r/r_0)^2)\,\dfrac{(1 - \nu^2)}{E}\,pr \\ \qquad\qquad\qquad \text{for } r < r_0 \\[2pt] \dfrac{4(1 - \nu^2)}{3\pi E}\,pr_0, \quad \text{for } r = r_0 \\[2pt] F(1.5, 0.5;3;(r_0/r)^2)\,\dfrac{p(1 - \nu^2)}{4E}\left[\dfrac{r_0^3}{r^2}\right] \\ \qquad\qquad\qquad \text{for } r > r_0 \end{cases} \tag{9}$$

Consider now the two boundary nodes shown in Figure 3, with DOF i and j at node A, and DOF k and l at node B. By approximating the vertical ring load at k by a uniform vertical load over a very thin annulus of width 2ε (see Figure 4), the flexibility coefficients f_{ik}, f_{ji}, and f_{lk} can be estimated as follows:

$$f_{ik} = w_V(r_1; r_2 + \varepsilon; p_1) - w_V(r_1; r_2 - \varepsilon; p_1) \tag{10}$$
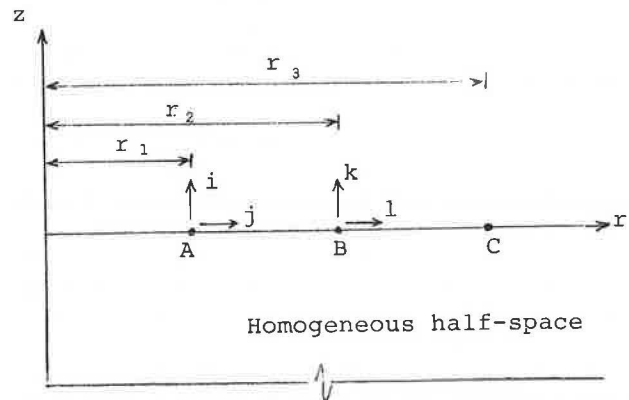
FIGURE 3 Typical nodes and degrees of freedom.
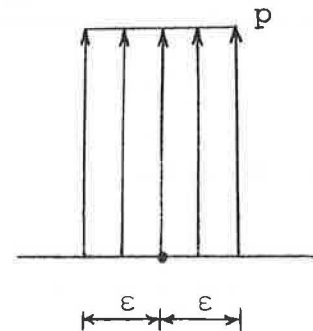
FIGURE 4 Vertical load on thin annulus.
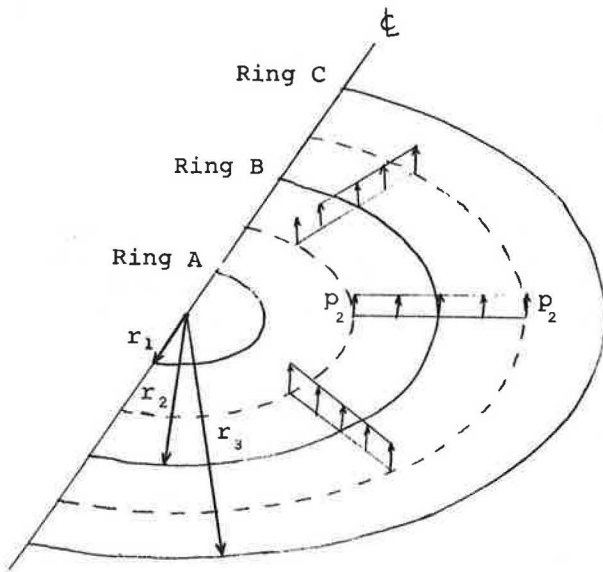
FIGURE 5 Uniform vertical loading to estimate f_{kk}.

FIGURE 6 Linear radial load to estimate f_{ii}.

$$f_{jk} = u_V(r_1; r_2 + \varepsilon; p_1) - u_V(r_1; r_2 - \varepsilon; p_1) \qquad (11)$$

$$f_{lk} = u_V(r_2; r_2 + \varepsilon; p_1) - u_V(r_2; r_2 - \varepsilon; p_1) \qquad (12)$$

where

$$p_1 = 1/4\pi\varepsilon r_0 \qquad (13)$$

With p_1 defined as in Equation 13, the total load on the annulus is unity. As long as ε is small, these coefficients are not sensitive to the exact magnitude of ε. According to the Maxwell-Betti reciprocal theorem, $f_{ki} = f_{ik}$, $f_{kj} = f_{jk}$, and $f_{kl} = f_{lk}$.

This technique cannot, however, be used to estimate f_{kk} or f_{ll}. These flexibilities are very sensitive to the magnitude of ε. In fact, as mentioned before, as $\varepsilon \to 0$, $f_{kk} \to \infty$ and $f_{ll} \to \infty$. To estimate the diagonal flexibilities, therefore, we assume that a uniform load (with unit total load) is applied in an annulus from midway between nodes A and B to midway between nodes B and C in Figure 3. (For the radial load, a linearly varying load is assumed, again because elegant results exists for this case. The difference in f_{ll} from using a uniform or linear load should be small, and since this is an estimate
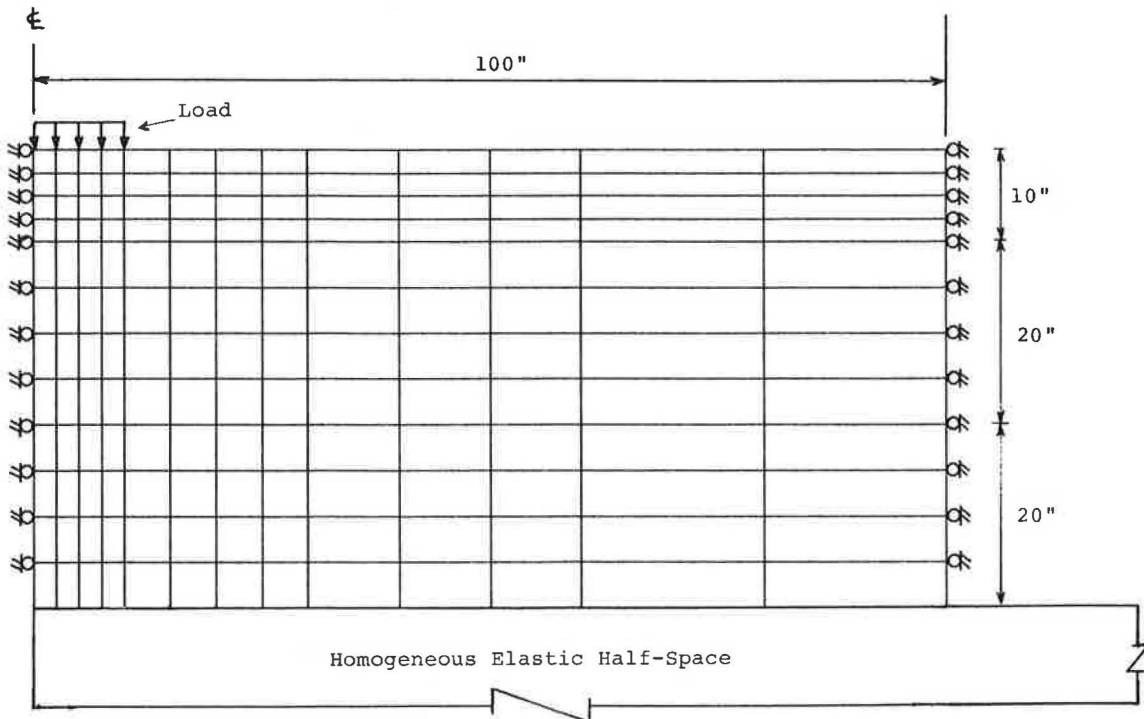
FIGURE 7 Finite-element mesh used with flexible boundary.

anyway, the exact load type is perhaps not too important.) The loading approximations used for the vertical and radial loads are illustrated in Figures 5 and 6. Thus we obtain:

$$f_{kk} \approx w_V(r_2; (r_2 + r_3)/2; p_2) \\ - w_V(r_2; (r_1 + r_2)/2; p_2) \qquad (14)$$

and

$$f_{ll} \approx u_R(r_2; (r_2 + r_3)/2; p_4) - u_R(r_2; (r_1 + r_2)/2; p_3) \qquad (15)$$

where

$$p_2 = \frac{1}{\pi[(r_2 + r_3)^2 - (r_1 + r_2)^2)]} \qquad (16)$$
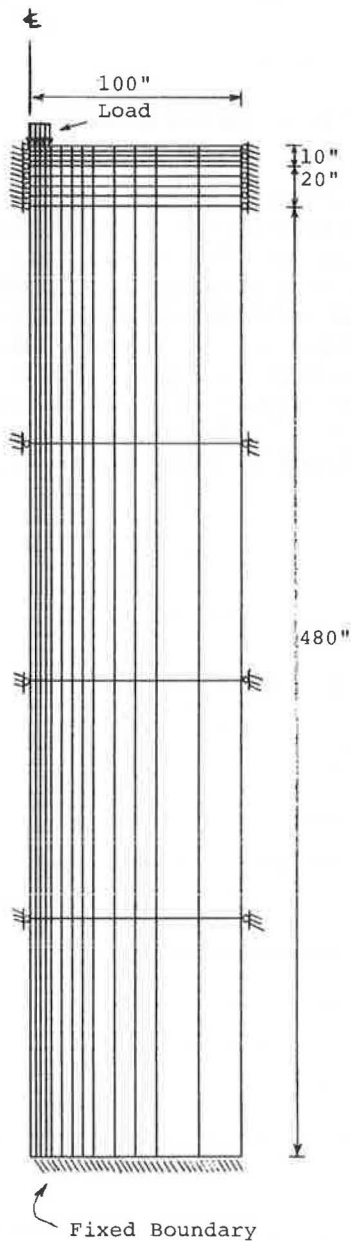
FIGURE 8 Traditional finite-element mesh.

$$p_3 = \frac{6(r_1 + r_2)}{\pi[(r_2 + r_3)^3 - (r_1 + r_2)^3]} \qquad (17)$$

and

$$p_4 = p_3 \frac{(r_2 + r_3)}{(r_1 + r_2)} \qquad (18)$$

The expressions for p_2, p_3, and p_4 given above ensure the load patterns illustrated in Figures 5 and 6 with the total load in each case being unity. All the diagonal terms of the flexibility matrix can be estimated as in Equations 14 and 15.

NUMERICAL RESULTS FOR HOMOGENEOUS AND MULTILAYERED PAVEMENTS

Analyses using the flexible boundary were performed for homogeneous and multilayered (three-layered) half-spaces. In both cases, a load of 100 psi was applied on a circular area of radius 10 in., and the flexible boundary was placed at a depth of 50 in., above which a finite-element mesh was used. The side boundary was placed at 100 in. from the centerline (10 times the radius of the loaded area) for both cases. The material properties were as follows:

Homogeneous: $E = 5,000$ psi; $\nu = 0.45$.
Multilayer: Layer 1 (asphalt) — $E = 200,000$ psi; $\nu = 0.35$; depth $= 10$ in.;
Layer 2 (base) — $E = 15,000$ psi; $\nu = 0.40$; depth $= 20$ in.;
Layer 3 (subgrade) — $E = 5,000$ psi; $\nu = 0.45$; infinite depth.

In order to compare the results with the traditional finite-element approach, a mesh of depth 510 in. was used with a fixed boundary. [As noted by Duncan et al. (*1*), a deep mesh is required in traditional finite-element analysis.] The number of elements was kept the same in both meshes to facilitate a direct comparison, while keeping the computational effort approximately the same. This meant that in the traditional mesh the deeper elements had very large length-to-width ratios. The mesh used with the flexible boundary and the traditional mesh (finite elements only) are shown in Figures 7 and 8, respectively. The same meshes were used for the homogeneous and multilayered cases.

The vertical displacements along the top free surface and the variation of the vertical displacement with depth beneath the center of the loaded area are shown in Figures 9 and 10. The percentage errors in both finite-element approaches, as compared with the exact results, are tabulated in Tables 1 and 2. (The abbreviations "FE + FB" and "FE only" are used to denote "finite elements plus flexible boundary" and "finite elements only," respectively, in the figures and tables.) It is apparent that use of the flexible boundary gives much better results, especially for the multilayered case where displacements within the subgrade contribute significantly toward the total displacements. The flexible boundary approach is more accurate for the homogeneous case than for the multilayered case, but in both cases it is more accurate than the traditional finite-element approach.
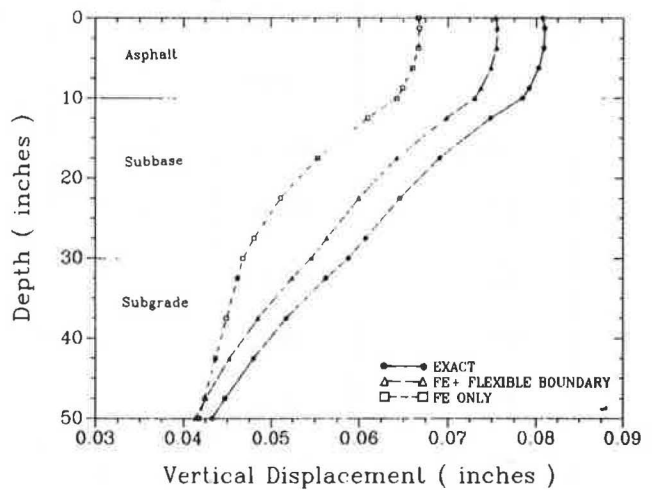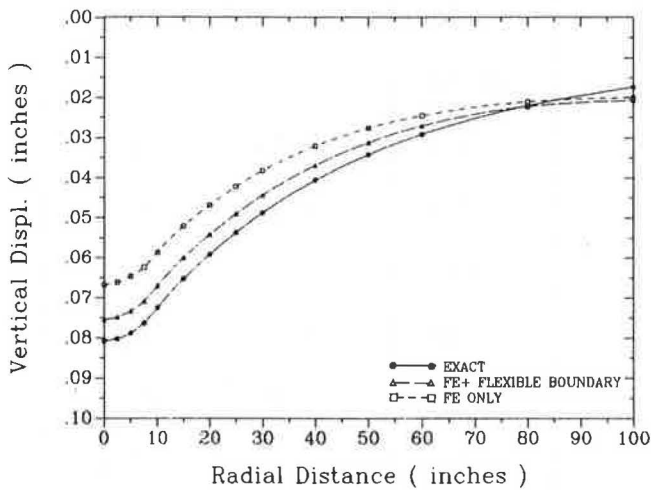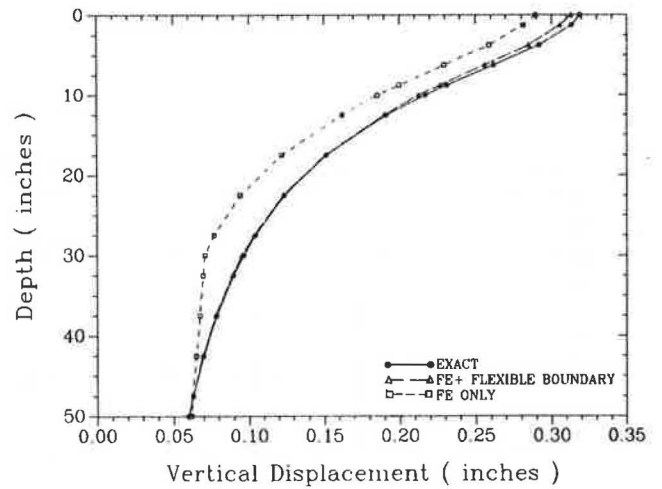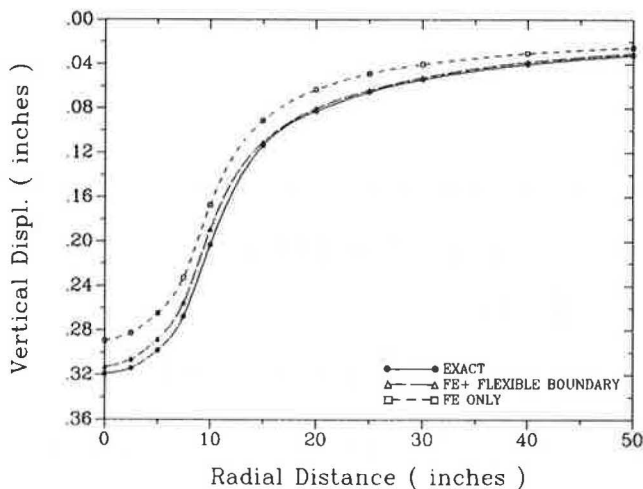
FIGURE 9   Vertical surface displacement: homogeneous (*top*); multilayer (*bottom*).

FIGURE 10   Vertical displacement beneath center of load: homogeneous (*top*); multilayer (*bottom*).

The variation of vertical and radial stresses with depth beneath the center of the loaded area is presented in Figures 11 and 12, respectively. The percentage errors, as compared with exact results, are tabulated in Tables 3 and 4. Again, use of the flexible boundary gives better results than the traditional approach. The differences in the stresses, however, are less significant than those in the displacements. For the homogeneous case, at depths below 30 in., the actual radial stresses are very small. Because of this, a comparison of the percentage errors (which were very large) is somewhat meaningless and has been omitted from Table 4. For the same reason, the percentage errors are very large for the traditional approach at large depths. The percentage errors should be compared with the value of the actual stresses in mind.

One point worth noting is the lack of accuracy of the finite-element method (both with and without the flexible boundary) when stresses are evaluated near the corners of elements (i.e., near nodes). Stresses are most accurate at the middle of the elements and are reasonable at the middle of element edges, but not accurate near element corners. For homogeneous material the stresses from finite-element solutions are not continuous across element boundaries (as they should be). This is the reason for the large errors in the radial stresses at depths of 10 in. and 30 in. (see Table 4). These depths represent the interfaces between layers for the multilayered case. Also, when elements with very large aspect ratios [such as the deeper elements in the traditional mesh (Fig. 8)] are used, the results tend to be poor. A better mesh than the one in Figure 8 would require many more elements and hence would result in a much greater computational effort.

A number of case studies were performed using the flexible boundary approach, varying the moduli and thicknesses of the base and subbase layers. In all cases the results compared favorably with the exact solutions.

TABLE 1   ERRORS IN VERTICAL SURFACE DISPLACEMENTS

Radial Dist. (inches)	Homogeneous			Multilayer		
	Exact Displ. (inch)	Percentage Error		Exact Displ. (inch)	Percentage Error	
		FE + FB	FE only		FE + FB	FE only
0	.3190	-1.9	-9.3	.0807	-6.6	-17.4
2.5	.3140	-2.6	-10.1	.0802	-6.8	-17.6
5	.2980	-3.3	-11.1	.0788	-6.9	-17.9
7.5	.2677	-4.6	-13.1	.0763	-7.1	-18.3
10	.2031	-6.8	-17.7	.0725	-7.5	-19.0
15	.1136	-2.5	-19.8	.0653	-8.0	-20.2
20	.0825	-2.8	-23.6	.0592	-8.4	-20.9
25	.0652	-2.5	-25.4	.0537	-8.7	-21.4
30	.0539	-3.0	-25.1	.0488	-8.9	-21.5
40	.0401	-4.6	-24.4	.0406	-9.1	-21.0
50	.0321	-5.6	-21.9	.0342	-8.9	-19.4
60	.0266	-4.7	-17.8	.0292	-7.3	-16.0
80	.0201	-4.8	-12.0	.0220	0.9	-4.6
100	.0160	6.4	3.1	.0173	19.3	15.2

TABLE 2 ERRORS IN VERTICAL DISPLACEMENTS BENEATH CENTER OF LOAD

| Vert. Dist. (inches) | Homogeneous | | | Multilayer | | |
| | Exact Displ. (inch) | Percentage Error | | Exact Displ. (inch) | Percentage Error | |
		FE + FB	FE only		FE + FB	FE only
0	.3190	-1.9	-9.3	.0807	-6.6	-17.4
1.25	.3134	-2.5	-10.3	.0810	-6.7	-17.5
3.75	.2916	-2.4	-11.1	.0809	-6.6	-17.5
6.25	.2620	-2.3	-12.3	.0803	-6.7	-17.7
8.75	.2314	-1.9	-13.6	.0792	-6.8	-18.0
10	.2171	-2.0	-14.5	.0784	-6.8	-17.2
12.5	.1913	-0.6	-15.2	.0749	-6.7	-18.5
17.5	.1516	-0.4	-19.4	.0691	-7.0	-19.9
22.5	.1239	-0.6	-23.9	.0646	-7.1	-20.9
27.5	.1042	-0.8	-26.1	.0608	-7.2	-20.9
30	.0964	-1.4	-26.4	.0588	-7.1	-20.5
32.5	.0897	-0.9	-22.2	.0563	-6.8	-18.0
37.5	.0785	-0.6	-14.1	.0518	-6.3	-13.3
42.5	.0698	-0.4	-6.7	.0480	-5.8	-9.1
47.5	.0628	-0.0	-0.0	.0447	-4.9	-5.2
50	.0598	-0.0	+2.7	.0433	-4.5	-3.4
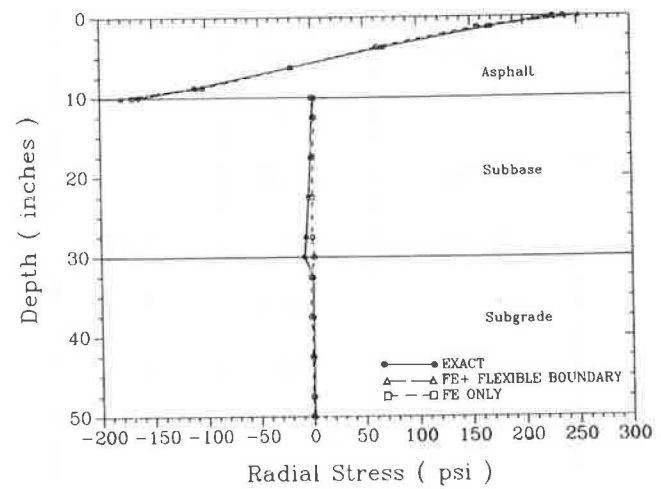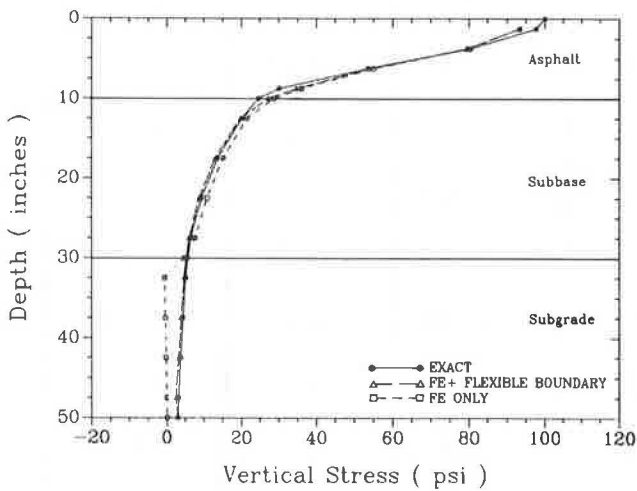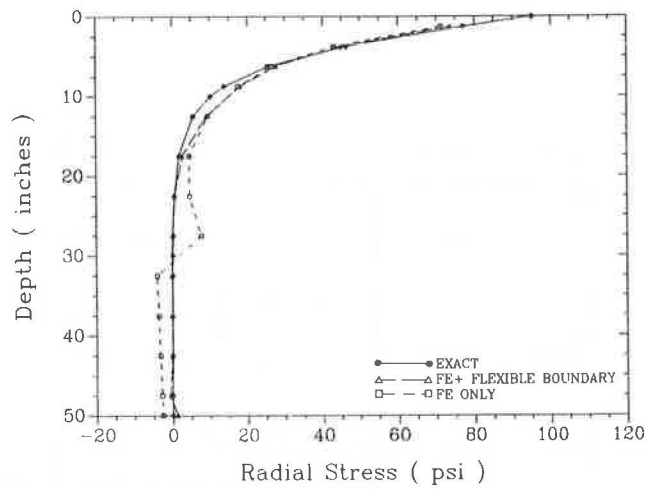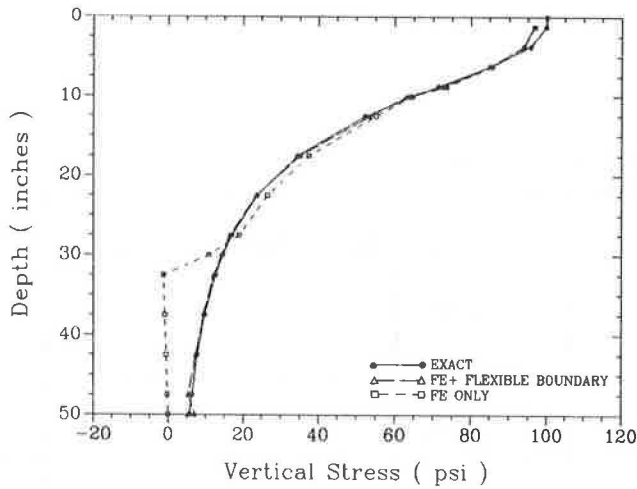
FIGURE 11 Vertical stress beneath center of load: homogeneous (*top*); multilayer (*bottom*).

FIGURE 12 Radial stress beneath center of load: homogeneous (*top*); multilayer (*bottom*).

CONCLUSIONS

A new technique is developed to model the flexibility of the bottom boundary used in static finite-element analyses of pavements. Such modeling enables the bottom boundary to be placed at any depth below which displacements and stresses are not of interest, while accurately representing the displacements occurring in the material below the boundary. Results indicate that the method is accurate. The principal advantage of this new technique is its computational efficiency, especially when used with nonlinear finite-element approaches requiring iterative or incremental solutions. The use of a flexible bound-

ary also yields significantly better results than a traditional finite-element approach requiring approximately the same amount of computational effort.

TABLE 3   ERRORS IN VERTICAL STRESSES BENEATH CENTER OF LOAD

Vert. Dist. (inches)	Homogeneous			Multilayer		
	Exact Stress (psi)	Percentage Error		Exact Stress (psi)	Percentage Error	
		FE + FB	FE only		FE + FB	FE only
1.25	99.81	-3.2	-3.0	97.62	-4.5	-4.4
3.75	95.67	-2.0	-1.8	80.43	-1.3	-0.7
6.25	85.11	-0.0	0.6	53.54	1.1	2.7
8.75	71.45	1.8	2.9	30.11	15.3	19.7
10	64.64	-2.3	-0.5	24.62	10.7	16.9
12.5	52.39	2.3	5.2	20.26	-2.3	6.3
17.5	34.55	1.7	8.6	13.68	-4.6	10.7
22.5	23.69	-0.6	11.8	9.25	-6.2	16.8
27.5	17.00	-2.7	11.7	6.44	-6.8	17.9
30	14.62	-1.6	-25.5	5.65	-6.1	-18.2
32.5	12.69	-3.7	-110.	5.13	-10.3	-112.
37.5	9.79	-3.9	-109.	4.30	-11.3	-109.
42.5	7.76	-4.6	-107.	3.66	-13.0	-106.
47.5	6.30	-14.9	-103.	3.15	-23.6	-100.
50	5.71	22.8	-101.	2.94	1.1	-97.

TABLE 4 ERRORS IN RADIAL STRESSES BENEATH CENTER OF LOAD

Vert. Dist. (inches)	Homogeneous			Multilayer		
	Exact Stress (psi)	Percentage Error		Exact Stress (psi)	Percentage Error	
		FE + FB	FE only		FE + FB	FE only
1.25	77.11	-4.5	-7.6	169.9	-2.2	-7.8
3.75	46.25	-3.3	-7.0	69.39	-3.7	-9.7
6.25	25.59	7.9	3.6	-19.36	3.0	-1.7
8.75	13.79	31.1	27.5	-111.0	-1.8	-7.3
10 (+)	10.15	159.	158.	-163.5	9.9	3.7
10 (-)	10.15	176.	181.	2.05	-217.	-128.
12.5	5.58	62.2	68.8	.54	25.7	352.
17.5	1.83	46.4	145.	-1.63	-9.3	150.
22.5	.65	-9.7	602.	-3.66	-8.9	103.
27.5	.23	-95.3	3197.	-6.27	-9.0	-97.2
30 (+)	.13	-	-	-8.04	-8.6	121.
30 (-)	.13	-	-	3.28	-131.	-165.
32.5	.07	-	-	.28	6.4	-821.
37.5	.00	-	-	.22	25.1	-949.
42.5	-.03	-	-	.17	44.6	-1064.
47.5	-.04	-	-	.14	-106.	-1131.
50	-.04	-	-	.12	403.	-1149.

REFERENCES

1. J. M. Duncan, C. L. Monismith, and E. L. Wilson. Finite Element Analysis of Pavements. In *Highway Research Record 228*, HRB, National Research Council, Washington, D.C., 1968, pp. 18–33.
2. S. F. Brown and J. W. Pappin. Analysis of Pavements with Granular Bases. In *Transportation Research Record 810*, TRB, National Research Council, Washington, D.C., 1981, pp. 17–23.
3. L. Raad and J. L. Figueroa. Load Response of Transportation Support Systems. *Transportation Engineering Journal, ASCE,* Vol. 106, No. TE1, 1980, pp. 111–128.
4. H. G. Poulos and E. H. Davis. *Elastic Solutions for Soil and Rock Mechanics,* Wiley, New York, 1974.

Transition of Critical Fatigue Level from Road Surface to Lower Interface of Asphalt Layer

OLLE ANDERSSON

This paper deals with strains in thin asphalt surfacings on granular pavement layers, the purpose being to find whether highest tensile strains occur in the road surface or at the bottom interface of the asphalt layer. The study was based on an analysis by the BISAR program of an asphalt pavement loaded by a 10-ton axle dual-wheel load. The modulus of the asphalt layer was 1,000–5,000 MPa and of the granular road base 150 and 250 MPa, the thickness of the asphalt layer varying from 20 mm and up. Tensile and shear strains were calculated in the road surface and the asphalt interface at the point of load symmetry and at the center of one of the contact areas. Comparison was made with a crude tire tread pattern model. Thin asphalt surfacings showed the highest tensile strain in the road surface. At increasing thickness there was a transition of highest strain from the surface to the lower interface of the asphalt layer, the transition thickness varying with assumed modulus values. Considering tensile strain, the transition thickness varied between 30 and 40 mm, depending upon assumed modulus values, whereas on the basis of shear strain the transition thickness varied between 30 and 50 mm. The assumed tire tread pattern model showed no significant difference in this strain distribution.

In analytical design of asphalt pavements, the critical stresses or strains are usually allocated to the lower asphalt interface (horizontal tensile strain) or to the subgrade upper interface (vertical compressive strain). The latter will in the long run cause permanent deformation and contribute to rutting of the road surface. The fact that similar permanent deformation occurs in the adjacent granular layers is usually disregarded in pavement design.

Critical strain in the asphalt layer usually occurs in the lower interface and causes cracking after a large number of vehicle passes. Thin asphalt pavements, however, may be under compression in the lower interface, whereas the road surface may at the same time be under tensile strain. When either of the controlling variables attains a certain value, there must be a transition of critical level from one interface to the other (road surface to lower interface or vice versa). In the present paper the conditions for such transitions will be illuminated.

TRAFFIC LOAD

The following wheel load and pavement model was used:

Royal Institute of Technology, S-10044 Stockholm, Sweden.
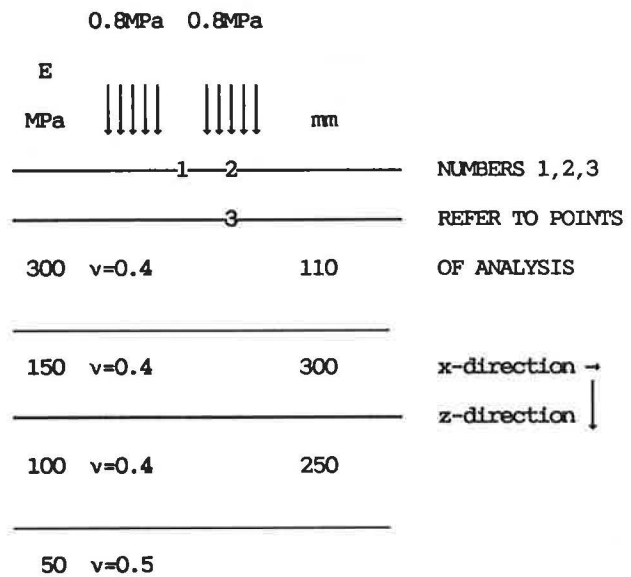
The two circular loading areas have a radius of 100 mm, and the distance between loading centers is 300 mm. This pavement design is typical for rural roads in Sweden and contains a bituminous top layer, whereas the layers below are unbound granular. The thickness and stiffness modulus of the bitumen stabilized layer were varied, the Poisson's ratio being set at 0.35.

Influence of Top Layer Thickness

Strains calculated by the BISAR program are listed in Table 1, the asphalt modulus being set at 3,000 MPa.

Points 1 and 2 are located at the road surface and point 3 at the lower interface of the bitumen stabilized top layer. High thicknesses at the bottom of the table leave the road surface in a compressed state, whereas at lower thicknesses there are tensile strains in the road surface.

In the interval 20–150 mm, the highest tensile strain is vertical and appears under the center of the contact area. At the lower interface the horizontal strains are tensile (vertical is compressed and not shown). At low thickness these horizontal strains increase, thereafter passing a maximum, and then decreasing as the top layer grows in thickness. It may

TABLE 1 TENSILE STRAINS XX, YY, AND ZZ AT POINTS 1, 2, AND 3

XX1	YY1	XX2	YY2	ZZ2	XX3	YY3	THICKN, mm
.359	-.429	-.422	-.525	.345	.156	.149	20
.349	-.464	-.476	-.587	.407	.297	.330	30
.267	-.479	-.459	-.584	.397	.335	.402	40
.176	-.474	-.415	-.551	.355	.327	.419	50
.100	-.456	-.368	-.508	.306	.305	.412	60
.042	-.431	-.326	-.464	.260	.281	.395	70
.001	-.404	-.291	-.423	.219	.259	.373	80
-.046	-.350	-.240	-.355	.155	.221	.327	100
-.065	-.303	-.205	-.303	.108	.190	.285	120
-.068	-.247	-.172	-.246	.060	.154	.231	150

Note: Directions are indicated in the diagram of the model given in the previous section. Values are in units of millistrain (1/1,000).

seem contradictory that vertical tensile strains (ZZ2) exist under the loaded surface. If, however, for simplicity the pavement layer is considered as a beam bent under load, it is obvious that a state of vertical tension exists in the upper surface, which may not be fully neutralized by the compressive action of the bending force.

At some points there is a tensile strain in one direction and compressive strains in other directions. Assessment of the significant state of strain at such a point requires further examination. Significant information will be provided by the strains in the direction of principal stress or the shear in the direction of principal shear stress. The maximum shear strains in these directions are listed by the BISAR program. Thus the highest shear strains are listed in Table 2. At point 1, all maximum shear strains are lower than in points 2 and 3.

The tensile strains are plotted against asphalt thickness in Figure 1 and the shear strains are plotted against asphalt thickness in Figure 2. According to Figure 1, the highest tensile strain is the horizontal tensile strain (XX1), which at an unrealistically low thickness is taken over by the vertical strain under the load center (ZZ2), which at a thickness of 39 mm is taken over by the horizontal tensile strain at point 3 (lower interface under the load center). If the vertical tensile strain is disregarded, the highest tensile strain at low thickness occurs at the point of symmetry between the loads in the road surface, this strain being taken over by the lower interface tensile strain YY3 at 31-mm thickness.

If the shear strains are considered (Fig. 2), it appears that at low thickness the highest strain γ_2 occurs in the road surface under the load center (position 2), but at higher thickness the shear strain γ_3 at the lower interface (position 3) is higher, the transition occurring at a thickness of 47 mm. Since 100 kg/m² of asphalt (40–45 mm) is a common surfacing thickness of rural roads in Sweden, this would mean that, under the

TABLE 2 MAXIMUM SHEAR STRAINS

THICKN	γ_2	γ_3
mm	microradians	
20	435	242
30	497	407
40	491	462
50	453	463
60	407	443
70	362	417
80	322	389
100	255	336
120	206	290
150	153	234

assumptions made, the highest risk of fatigue cracking would exist in the road surface.

Influence of Asphalt Modulus

The relation between strains and moduli of the asphalt-bound layer is demonstrated in Figures 3–6. Figure 3, showing a typical thin 40-mm surfacing, makes the classical horizontal
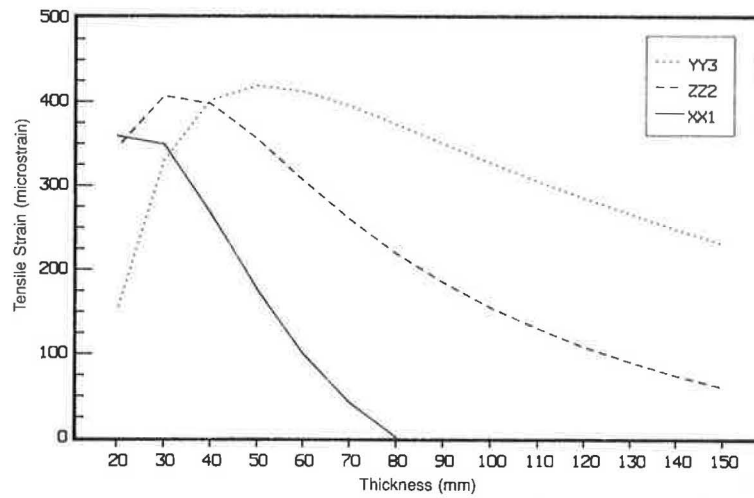
FIGURE 1 Tensile strains XX1, ZZ2, and YY3 as a function of thickness of asphalt-bound layer when asphalt layer modulus is 3,000 MPa (435 ksi).
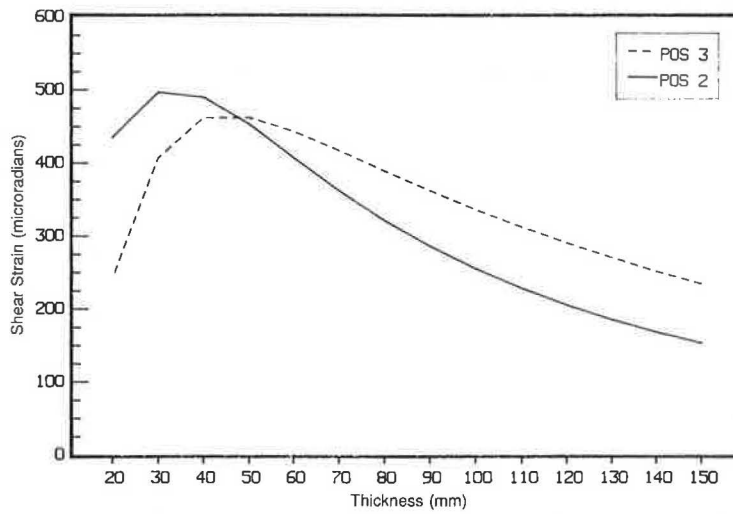
FIGURE 2 Shear strains at positions 2 and 3 when asphalt modulus is 3,000 MPa.

TH = 40 MM

FIGURE 3 Tensile strains XX1, ZZ2, XX3, and YY3 as a function of asphalt-bound layer modulus, thickness 40 mm (1.6 in.).

TH = 35 MM
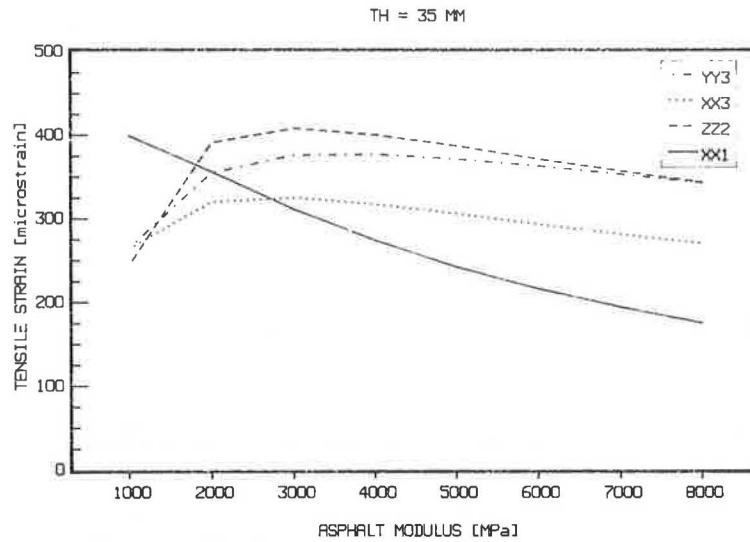
FIGURE 4   Tensile strains XX1, ZZ2, XX3, and YY3 as a function of asphalt-bound layer modulus, thickness 35 mm (1.4 in.).
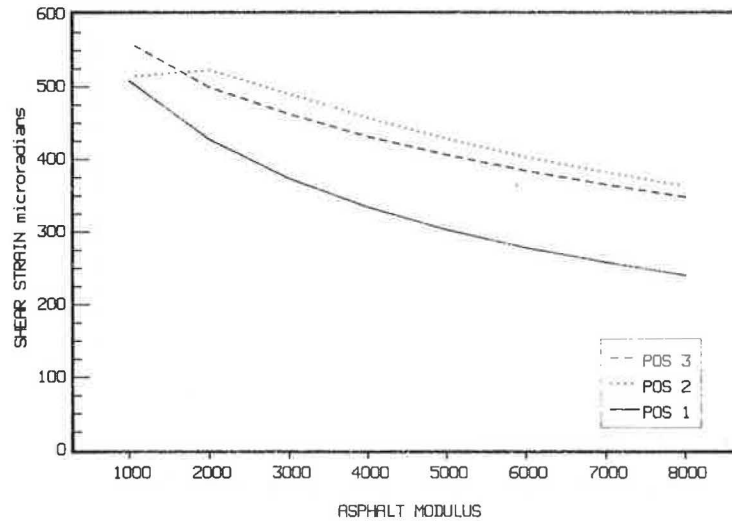
FIGURE 5   Shear strains at positions 1, 2, and 3 as a function of modulus of asphalt-bound layer thickness, 40 mm.

bottom strain critical at any modulus of reasonable value, whereas Figure 4 shows higher values for the vertical tensile strain in the road surface at the center of the contact area (position 2). On the other hand, if shear strains are considered (Figs. 5 and 6), position 2 is critical at both thicknesses at reasonable moduli levels.

Plots of the tensile and shear strains against asphalt thickness at 2,000 and 5,000 MPa asphalt moduli (Figs. 7–10) show a rather unwieldy picture, if tensile strains are considered, whereas the shear diagrams confirm a transition from critical surface to critical interface at an asphalt thickness between 40 and 50 mm.

Influence of Tire Tread Pattern

In a recent study, Roberts et al. (1) demonstrate quite an uneven distribution of contact pressure over the contact area;

further, the contact pressure is considerably higher than expected from consideration of pneumatic pressure and load only. In the present study a contact pressure of 0.8 MPa was assumed, and the tire has so far been treated as giving a rectangular contact pressure distribution.

A simple approach to the influence of tire pattern has been made by considering a contact zone composed of several circular loads, together forming a contact area of approximately the same size as in the simple model used above. The pattern is outlined in Figure 11. For simplicity, the contact zone is assumed to carry a load of 25,000 N equally distributed over 32 circles. The contact pressure will then be 1.1 MPa in the interface between each circle and the road surface and nil between the circles.

Analysis of the strain distribution was made by assuming the pavement shown above, the surfacing having a thickness of 40 mm and an elastic modulus of 3,000 MPa. The result is listed in Table 3.

TH=35 mm
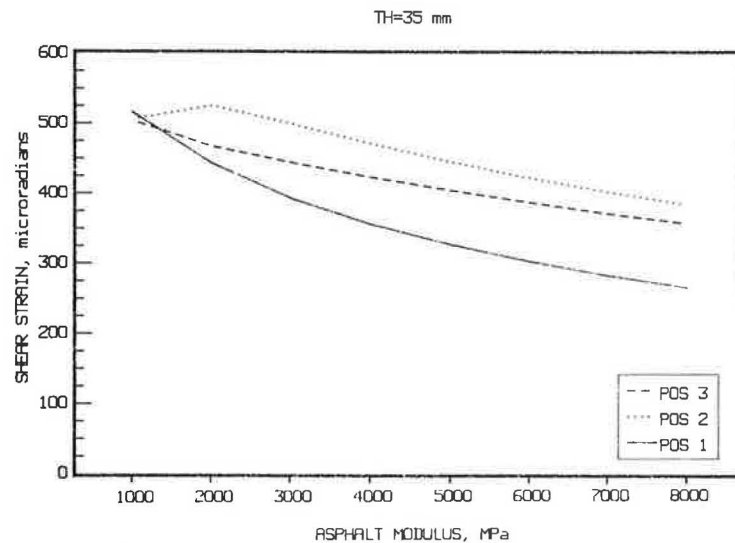
FIGURE 6   Shear strains at positions 1, 2, and 3 as a function of modulus of asphalt-bound layer thickness, 35 mm.
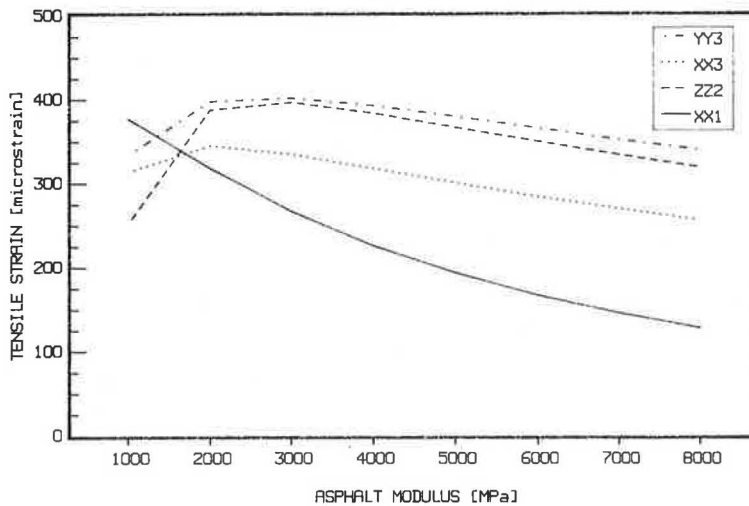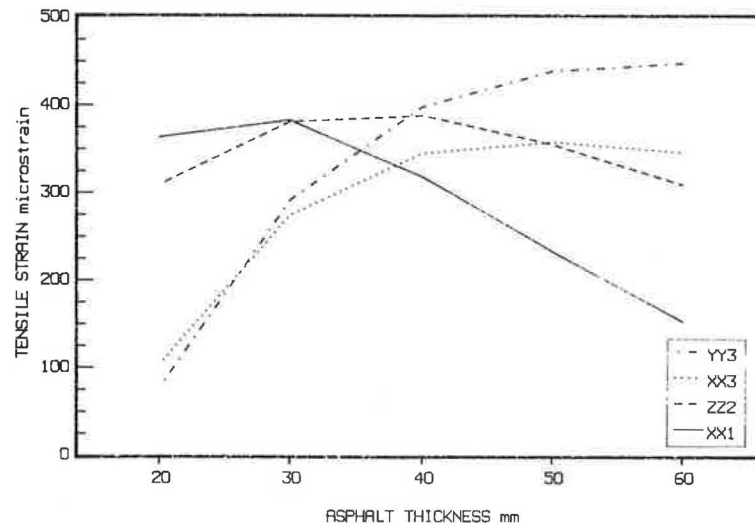

FIGURE 7   Tensile strains XX1, ZZ2, XX3, and YY3 as a function of thickness of asphalt-bound layer, when asphalt layer modulus is 2,000 MPa.

The table shows no dramatic differences between the two tire types. The differences between the subgrade values are negligible. The greatest difference occurs at the asphalt interface, showing horizontal tensile strains 309 and 396, respectively; the higher value appears at the center of the loading circle. This difference may correspond to a displacement of the transition curves found but will not change the general transition picture obtained from the simpler contact area model used.

Influence of Base Course Modulus

The variation with asphalt thickness of the horizontal strain in the direction of motion (YY3) at the asphalt interface at different values of the base course modulus is demonstrated

in Figure 12, the pavement design being the same as in Table 3. The figure demonstrates the neutralizing effect of a thick asphalt layer at different modulus values of the base course.

The combined influence of asphalt modulus and granular base modulus on the transition of highest strain from the surface to the interface is shown in Table 4. The effect of increasing moduli of surfacing as well as granular base is obviously to slightly push the transition point to a greater asphalt thickness, confirming that critical road surface predominantly belongs to comparatively thin surfacings and low stiffness.

CONCLUSIONS

Highest tensile strains have been found to occur at the surface of the road in thin asphalt surfacings; however, the level of
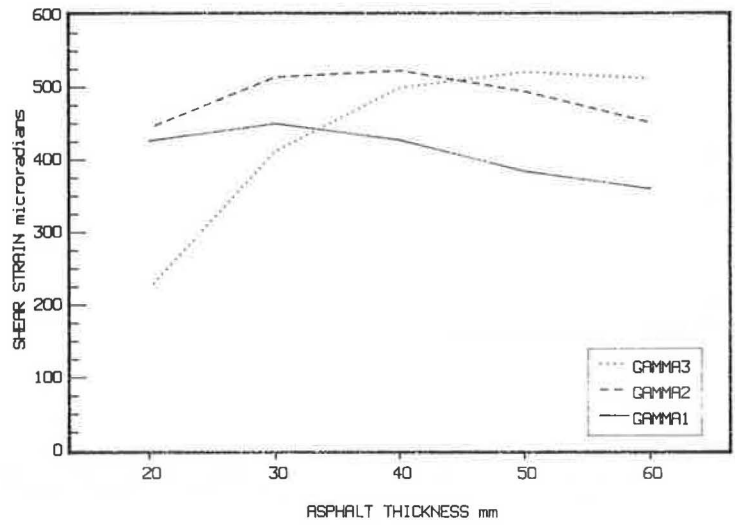
FIGURE 8 Shear strains at positions 1, 2, and 3 as a function of asphalt layer thickness when asphalt layer modulus is 2,000 MPa.
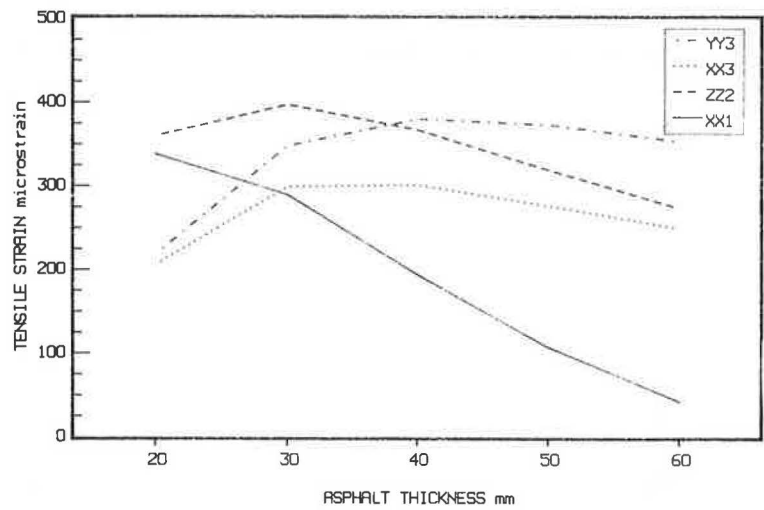
FIGURE 9 Tensile strains XX1, ZZ2, XX3, and YY3 as a function of thickness of asphalt-bound layer when asphalt layer modulus is 5,000 MPa.
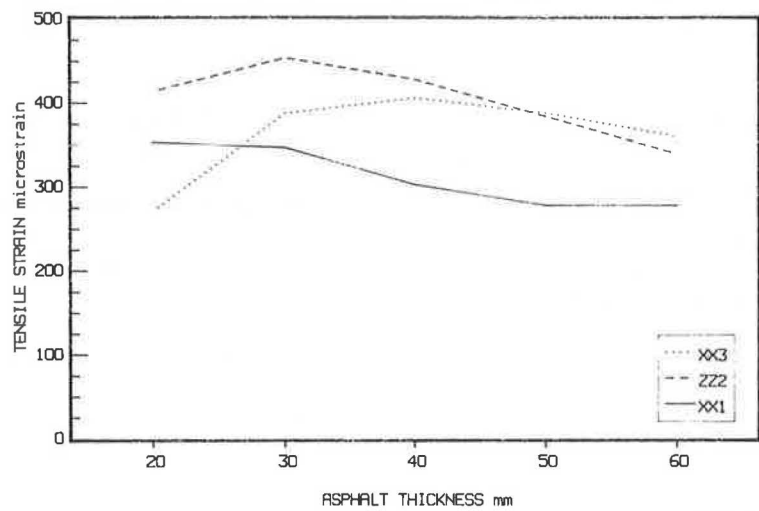
FIGURE 10 Shear strains at positions 1, 2, and 3 as a function of asphalt layer thickness when asphalt layer modulus is 5,000 MPa.
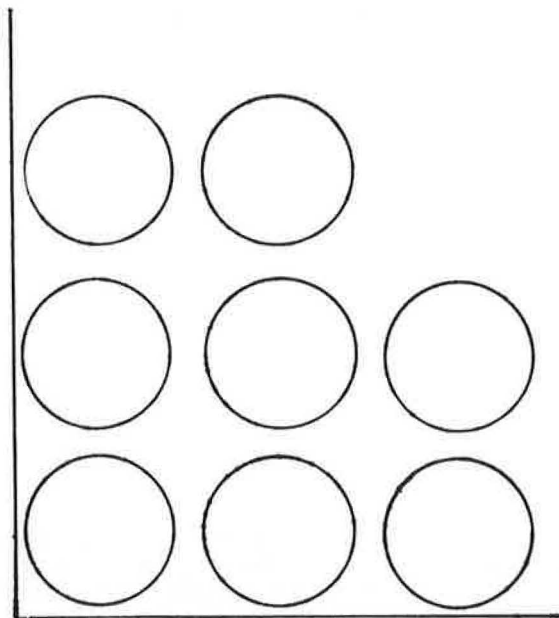
| x | 17.5 | 17.5 | 17.5 | 52.5 | 52.5 | 52.5 | 87.5 | 87.5 |
| y | 17.5 | 52.5 | 87.5 | 17.5 | 52.5 | 87.5 | 17.5 | 52.5 |

FIGURE 11   **Assumed tire contact pattern under the following conditions: number of contact areas, 32; radius of contact areas, 15 mm; contact pressure, 1.11 MPa; total load, 25 kN. Coordinates of contact areas, in millimeters, are given at bottom of figure. One quadrant is shown.**

highest strain is transferred to the lower asphalt interface at increasing thickness of the surfacing. The transition thickness varies moderately with asphalt modulus and with base course modulus. According to the present study, the absence of tread pattern does not influence the findings qualitatively, as long as only contact pressures are considered. The relation between

inflation pressure and contact pressure is a different problem.

The three positions (1, 2, 3) considered above were analyzed only with respect to tensile and shear strains. The strength of the material will also be influenced by the current bulk strain ($\varepsilon_1 + \varepsilon_2 + \varepsilon_3$), i.e., the sum of the tensile strains in the three principal directions of stress. An analysis of the

TABLE 3   INFLUENCE OF MODEL TIRE PATTERN ON PARAMETERS STUDIED

Depth	XX	ZZ	UZ			
mm	microstrain		mm		MPa	mm
0	−387	417	0.61	between	3000	40
40	309	−438	0.61	pattern	300	110
700	122	−244	0.27	circles	150	300
					100	250
0	−387	417	0.61	centre	50	
40	309	−436	0.61	of pat-		
700	122	−244	0.24	tern circle	↑	
					pavement	
0	−515	389	0.64	tire of no	design	
40	396	−594	0.64	tread pat-		
700	123	−246	0.24	tern		
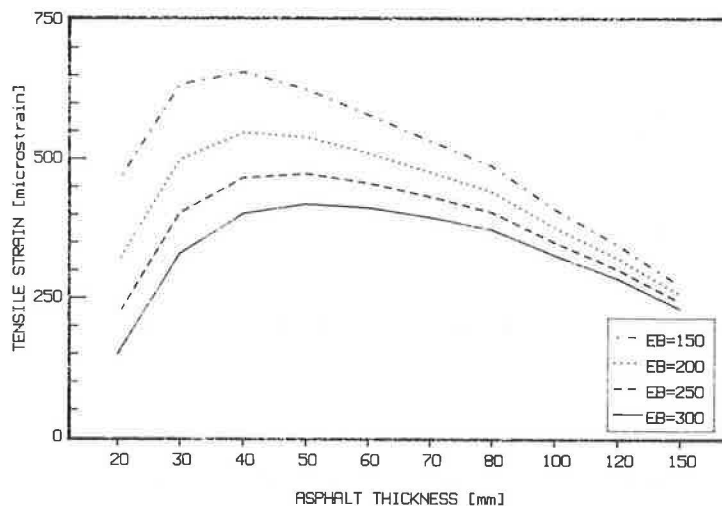
FIGURE 12 **Variation of the horizontal strain at the bottom of the asphalt stabilized layer under one circular load as a function of thickness of the asphalt stabilized layer at different modulus values of the base course.**

TABLE 4   COMBINED EFFECT OF DIFFERENT BASE AND SURFACING MODULI ON TRANSITION OF HIGHEST STRAIN FROM SURFACE TO INTERFACE

Easph	Ebase	Shear crit.		Strain crit.		
MPa	MPa	Z	X	Z	X	change
		mm		mm		of dir.
1000	150	30	0	37	0→150	XX→YY
1000	250	42	150	39	0→150	ZZ→YY
3000	150	37	150	32	150	ZZ→YY
3000	250	47	150	39	150	ZZ→YY
5000	150	35	150	30	150	ZZ→YY
5000	250	53	150	36	150	ZZ→YY

influence of "continuously acting stresses" on the response to fluctuating stresses, given by Monismith et al. (*2*), is an approach to a solution of this very problem.

It is also reasonable that microcracks in the road surface develop into harmful road damage more quickly than similar cracks in the lower interface due to invasion of water and material particles. The transition thicknesses given in this paper may therefore not necessarily reflect transition with respect to fatigue only. These thicknesses probably are greater than those corresponding to transition with respect to highest tensile or shear strain.

The BISAR program used for analysis in the present paper describes a simplified model of real pavements. Therefore, the transition thicknesses reported in the paper cannot be taken as accurate to the millimeter but rather as an indication of the fact that the classical allocation of fatigue crack initiation is not necessarily applicable, especially to pavements with comparatively thin bituminous layers.

Crack initiation in the road surface was the subject of discussion at the recent Ann Arbor Conference, which took place after the present work was finished. However, there is difficulty in establishing by mere observation whether a fully developed crack was initiated at the surface or at the bottom of the pavement layer.

REFERENCES

1. F. L. Roberts, J. T. Tielking, D. Middleton, F. L. Lytton, and K. Tseng. *Effect of Tire Pressures on Flexible Pavements*. Report FHWA/TX-86/60 + 372-1F. Texas Transportation Institute, Texas A&M University, College Station, 1986.
2. C. L. Monismith, D. B. McLean, and R. Yuce. *Design Considerations for Asphalt Pavements*. Report TE 72-4. University of California, Berkeley, 1972.

Application of Equivalent-Layer-Thickness Concept in a Mechanistic Rehabilitation Design Procedure

EMILE HORAK

The South African mechanistic rehabilitation design procedure is well established and has been verified with the help of a fleet of heavy vehicle simulators. Surface deflection basins can be measured with the road surface deflectometer or the National Institute for Transport and Road Research deflectograph. Typical South African pavement structures were analyzed, and various deflection basin parameters were calculated. The equivalent-layer-thickness (ELT) concept was investigated for its applicability to this analysis procedure and was found to be useful in representing the structural capacity of a pavement. The basis for the calculation of the ELT is the effective elastic modulus of the subgrade. Deflection points measured on the extremes of the deflection basin are used to calculate the subgrade effective elastic modulus. Various deflection basin parameters can be used to calculate pavement ELT, which can be related to typical distress determinants or directly to remaining life in a design-curve approach.

Odemark's (1) equivalent-layer-thickness (ELT) concept is often used as a simple method of approximation in pavement structural analysis, since it permits the conversion of a multilayered system into a single layer with equivalent thickness. It is based on the principle that the equivalent layer has the same stiffness as the original layer, so as to give the same pressure distribution beneath the layer. This concept of classifying a pavement by means of one number that represents the approximate bearing capacity of that pavement has been clearly illustrated by Molenaar and Van Gurp (2) and Molenaar (3). In these cases the investigated pavement structures were mainly three-layered structures with different loading conditions.

Typical South African pavement structures found in the TRH4 catalog (4) were analyzed and converted into the ELT. In that catalog, various pavement structures are suggested for various traffic classes and categories of pavement. Pavement types are generally grouped together as bitumen, granular, cemented, or concrete base (Figure 1). Most of the typical flexible pavement structures analyzed, such as the granular- and the cemented-base pavements, have thin asphalt surfacings (30 to 50 mm). The calculated ELT values were then related to various distress determinants and fatigue life in order to evaluate this concept as a possible aid in the mechanistic rehabilitation design procedure (5).

This study is part of an investigation in which various deflec-

National Institute for Transport and Road Research, CSIR, P.O. Box 395, Pretoria 0001, Republic of South Africa.
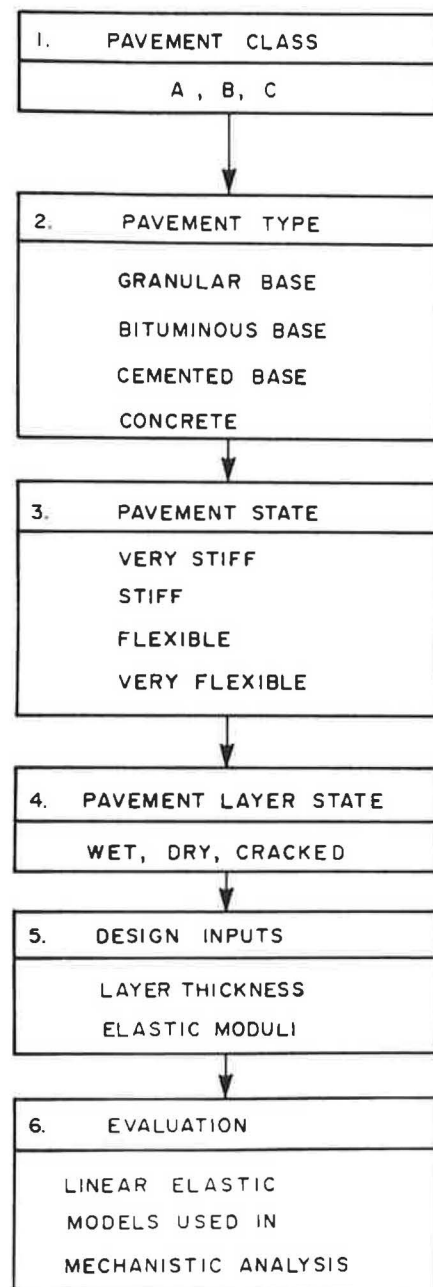
FIGURE 1 Flow diagram of mechanistic pavement rehabilitation design method (5).

TABLE 1   SUMMARY OF DEFLECTION BASIN PARAMETERS

Parameter	Formula		
1. Maximum deflection		δ_0	
2. Radius of curvature	R	$= \dfrac{r^2}{2\delta_0(\delta_0/\delta_r - 1)}$;	$r = 127$ mm
3. Spreadability	S	$= \dfrac{[(\delta_0 + \delta_1 + \delta_2 + \delta_3)/5]100}{\delta_0}$,	$\delta_1 \cdots \delta_3$ space 305 mm
4. Area	A	$= 6[1 + 2(\delta_1/\delta_0) + 2(\delta_2/\delta_0 + \delta_3/\delta_0]$	
5. Shape factors	F	$= (\delta_0 - \delta_2)/\delta_1$; $F_2 = (\delta_1 - \delta_3)/\delta_2$	
6. Surface curvature index	SCI	$= \delta_0 - \delta_r$; $r = 305$ or 500 mm	
7. Base curvature index	BCI	$= \delta_{610} - \delta_{915}$	
8. Base damage index	BDI	$= \delta_{305} - \delta_{610}$	
9. Deflection ratio	Q_r	$= \delta_r/\delta_0$; where $\delta_r \simeq \delta_0/2$	
10. Bending index	BI	$= \delta_0/a$; where $a = $ deflection basin length	
11. Slope of deflection	SD	$= \tan^{-1}(\delta_0 - \delta_r)/r$; where $r = 610$ mm	
12. Tangent slope	ST	$= (\delta_0 - \delta_r)/r$; where $r = $ distance to inflection point	
13. Radius of influence	RI	$= R'/\delta_0$; where R' is the distance from δ_0 to where basin is tangent to horizontal	

TYPICAL   DEFLECTION   BASIN
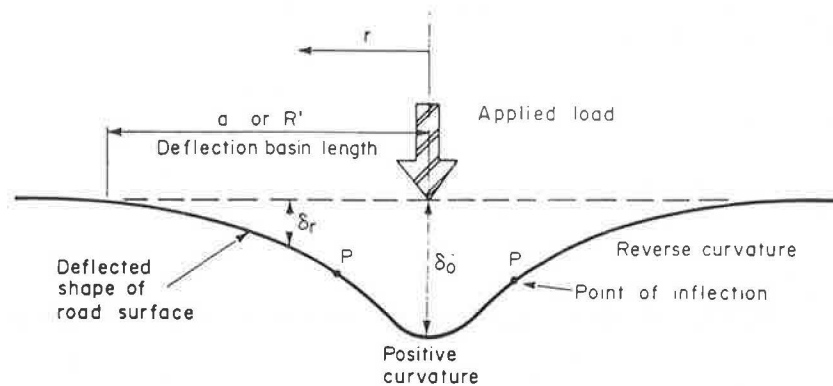
tion basin parameters were calculated for these pavement structures (6) and related to typical distress determinants. In Table 1 the most significant of these deflection basin parameters are listed with their formulas related to the road surface deflectometer (RSD). The RSD is a modernized, automated Benkelman beam (7) which is used with the accelerated testing facilities, i.e., the heavy-vehicle simulators (HVSs). The National Institute for Transport and Road Research (NITRR) deflectograph has also been modernized and can measure the deflections on the deflection basin, thus enabling the calculation of the deflection basin parameters as listed in Table 1.

An attempt is made in this paper to show how the mechanistic design procedure (5, 8) can be enhanced with the aid of these nondestructive deflection measuring devices. These measurements can then also be used to calculate the ELT with a minimum of information. The purpose is to establish typical design curves whereby flexible pavements can be analyzed without the need for detailed calculations typical of

fundamental linear elastic analysis. Such an approach can greatly enhance the South African mechanistic rehabilitation design procedure, which is well established and has been verified with the HVS testing program (8, 9).

MECHANISTIC DESIGN PROCEDURE

The mechanistic pavement rehabilitation design procedure (5) is summarized in the flow diagram of Figure 1. The pavement classes identified as A, B, or C in step 1 can be broadly defined as freeways, major highways, or lightly trafficked roads, respectively (4). Pavement types (step 2) in the present study are restricted to granular, bituminous, and cemented bases, since the focus is on flexible pavements.

Pavement behavior states (step 3) are defined as very stiff, stiff, flexible, and very flexible (5). From data on deflection basins measured under accelerated tests (6), the ranges of

TABLE 2 BEHAVIOR STATES DEFINED BY
DEFLECTION BASIN PARAMETERS

Behaviour state	Deflection basin parameter ranges				
	Max. defl. (mm)	SD (× 10⁻⁶)	SCI (mm)	BDI (mm)	BCI (mm)
Very stiff	< 0,2	< 50	< 0,01	< 0,01	< 0,01
Stiff	0,2 - 0,4	50 - 400	0,01 - 0,2	0,01 - 0,1	0,01 - 0,05
Flexible	0,4 - 0,6	400 - 750	0,2 - 0,4	0,1 - 0,15	0,05 - 0,08
Very flexible	> 0,6	> 750	> 0,4	> 0,15	> 0,08

deflection basin parameters in each behavior state, as shown in Table 2, can be used to define the behavior state accurately. Previously, this distinction of behavior states was based on maximum deflection only, but it is now suggested that at least two of the other deflection basin parameters listed in Table 2 be used for this purpose. Steps 4, 5, and 6 of Figure 1 form part of the normal mechanistic design procedure whereby the design inputs in terms of moisture condition, state of cracking of treated materials, layer thicknesses and elastic moduli are needed before the typical linear elastic models can be used for the analysis.

A design-curve approach is suggested, where with the use of relations established through prior analyses of the typical pavement types in the flexible state, steps 4, 5, and 6, can be greatly simplified. This design-curve approach will also render superfluous detailed knowledge of the design inputs (as shown in step 5) that is required for a fundamental linear elastic analysis. Instead, the evaluation phase follows from the measurement phase of the deflection basins. The purpose is therefore to make use of the ELT to simplify this analysis procedure by determining ELT directly from measured deflection basin parameters.

DETERMINATION OF ELT

The ELT, as developed further by Molenaar and Van Gurp (2), is calculated as follows:

$$\text{ELT} = a \sum_{}^{L-1} \left[h_i \frac{E_i (1 - v_s^2)}{E_s (1 - v_i^2)} \right]^{1/3}$$

where

a = 0.9 for flexible pavements,
h_i = thickness of layer i (m),
E_i = elastic modulus of layer i (N/m²),
E_s = elastic modulus of subgrade (N/m²),
v_i = Poisson ratio of layer i,
v_s = Poisson ratio of subgrade layer with value equal to 0.35, and
L = number of layers.

The general formula for the ELT is related to the effective elastic modulus of the subgrade. This means that the latter has to be determined before the ELT can be determined. Molenaar and Van Gurp (2) established a relationship between deflection measured at 2 m and subgrade elastic moduli as measured under the falling-weight deflectometer (FWD) for
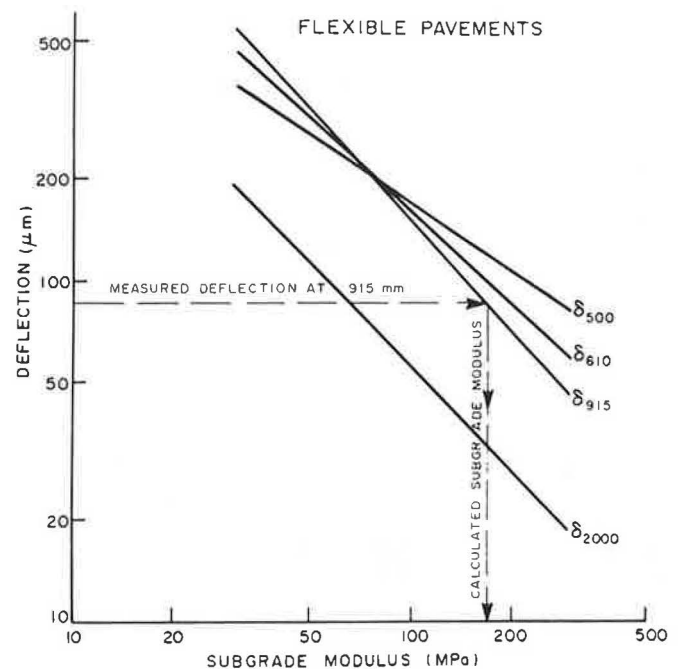
FIGURE 2 Relation of subgrade elastic modulus to deflection in four- and five-layered flexible pavements.

bitumen-base pavements. This same procedure can be used to determine the subgrade effective elastic modulus for the typical South African flexible pavements analyzed (6). Relationships were also established between deflection measured at offsets of 915, 610, and 500 mm and subgrade elastic moduli. In Figure 2, these relations are shown for four- or five-layered flexible pavement structures.

By thus measuring deflections with the RSD or even the NITRR deflectograph at those offsets on the deflection basin, it is possible to determine the subgrade modulus. It is recommended that at least three of these relations (as illustrated in Figure 2) be used to arrive at an average value of subgrade effective elastic modulus.

By measuring deflections with the RSD or even the NITRR deflectograph at those offsets on the deflection basin, it is possible to determine the subgrade modulus. It is recommended that at least three of these relations be used to arrive at an average value of subgrade effective elastic moduli.

Three subgrade effective elastic moduli (50, 70, and 150 MPa), which are typical of the subgrades of South African pavements, were selected as a basis to determine the equivalent thickness for the typical flexible multilayered pavements that were analyzed. In Figure 3, however, it is shown that the deflection basin parameter F_1 (shape factor, see Table 1), if related to ELT, cannot be used to discern such a difference in subgrade effective elastic modulus. In Figure 4, on the other hand, it is shown how the deflection basin parameter SD (slope of deflection, see Table 1) can be used to discern the difference in effective elastic moduli of the subgrade for multilayered flexible pavement structures.

Nevertheless, with the deflection basin parameter SCI (surface curvature index, see Table 1) it was possible to subdivide these flexible pavements into two separate sets of relations. Those with granular bases had a greater sensitivity to ELT than bitumen-base pavements. This is illustrated in Figure 5,
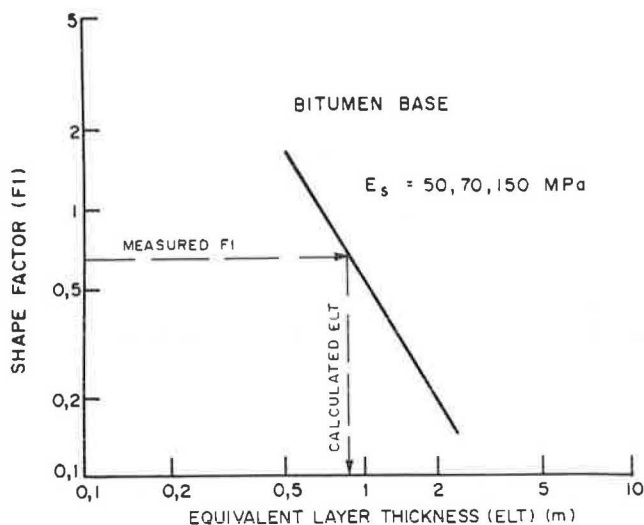
FIGURE 3 Relation of equivalent layer thickness to deflection basin shape factor.
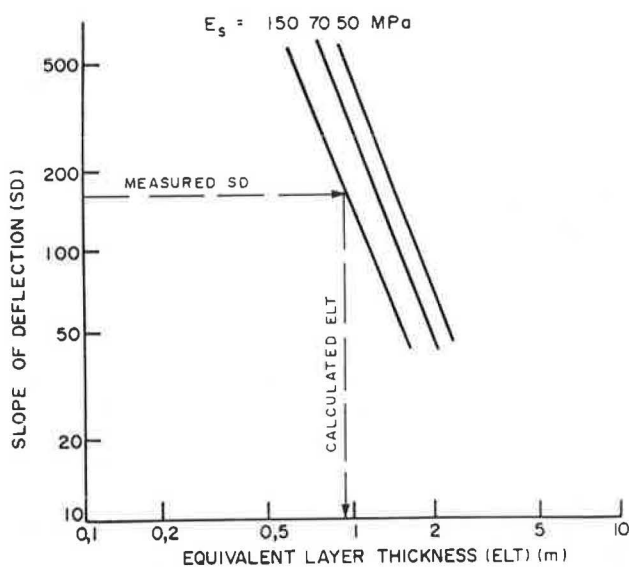
FIGURE 4 Relation of equivalent layer thickness to slope of deflection.

FIGURE 5 Relation of equivalent layer thickness to surface curvature index.

in which the three subgrade effective elastic moduli of the two base types in the flexible behavior state are shown.

The subgrade effective elastic modulus can therefore be determined from Figure 2. Using that subgrade effective elastic modulus, it is thus possible to use the measured deflection basin parameters in Figures 3, 4, or 5 to calculate the ELT.

ANALYTICAL PROCEDURE

In the mechanistic design procedure (5), permanent deformation is related to subgrade vertical strain (ε_{vs}), and fatigue cracking in the bitumen bases is related to the maximum horizontal asphalt strain (ε_{HA}). As stated earlier, the purpose is to use a design-curve approach in order to simplify the analysis procedure. This is achieved by relating the previously determined ELT directly to these strains.

In Figure 6 it is shown how it is possible to relate ELT directly to subgrade vertical strain (ε_{vs}) for the various subgrade support conditions for flexible pavements. When the ELT is related to maximum horizontal asphalt strain (ε_{HA}), it is applicable only to flexible bitumen-base pavements. The relations for the various subgrade support conditions are illustrated in Figure 7. This means that the granular-base pavements, which have relatively thin asphalt surfacings (on average 30–50 mm in the dry regions of South Africa), cannot be analyzed in this fashion. This emphasizes the fact that the ELT concept was developed to calculate compressive strain in the subgrade and does not necessarily give a good indication of horizontal strain in the asphalt layers (10). The ELT determined earlier using Figures 3, 4, or 5 is now used in Figures 6 and 7 to determine the subgrade vertical strain (ε_{vs}) or the maximum horizontal asphalt strain (ε_{HA}).

Remaining life can be determined for subgrade vertical strain (ε_{vs}) by using the typical fatigue life curves of the South African mechanistic design procedure (5, 9). In Figure 8 these curves are shown for the typical road categories according to the NITRR design traffic classes (4). The subgrade vertical strain (ε_{vs}), as determined from Figure 6, can therefore directly be used as input with Figure 8 to calculate the remaining life. All that is needed is to establish the road category. In the calculation of the remaining life of bitumen bases, Figure 9 can be used as in the South African mechanistic design procedure (5, 9). In this case, however, it is necessary to know the stiffness of the base layer.

Stiffness can be determined by using typical tabulated values (5) or by using the typical nomograph approach to deter-
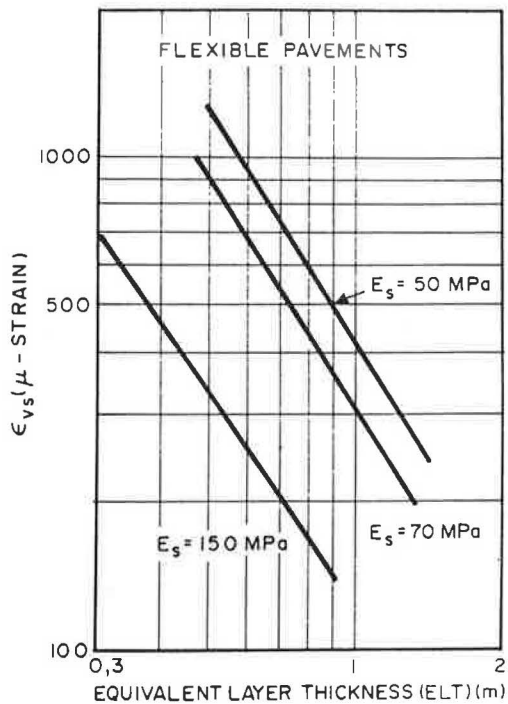
FIGURE 6 Relation of subgrade vertical strain to equivalent layer thickness for flexible pavements.

FIGURE 7 Relation of equivalent layer thickness to maximum horizontal asphalt strain for bitumen-base pavements.

mine stiffness modulus values of bituminous mixes (*2, 11*). By using the previously determined maximum horizontal strain (ϵ_{HA}) as input, the equivalent traffic can be determined for the related bitumen base stiffness. The recommended shift factors shown in Table 3 should be applied to the calculated remaining fatigue life.

ELT can, however, be related directly to fatigue life (*3*) as calculated above. It was shown previously how deflection basin parameters can be used to identify the pavement behavior state accurately. ELT can be used to indicate whether a pavement structure with cemented subbases or bases is in the flexible behavior state. According to the definition given by Freeme (*5*), such flexible pavements with the cemented layers are in the cracked phase, exhibiting equivalent granular behavior. In Figure 10, ELT for the precracked life of pavements with cemented subbases and bases is shown in terms of standard 80-kN axle repetitions. A distinction can be made on the basis of the variance of the elastic modulus of the subgrade. However, an ELT value of at least 1.1 m is required for a subgrade modulus of 70 MPa to have any significant precracked life for the cemented layers. Although the mechanistic rehabilitation procedure (*5*) makes provision for the application of crack growth factors, this does not change the fact that the major portion of the structural life of typical South African pavement structures with cemented layers is in the cracked phase.

In flexible pavement structures, typical fatigue life curves, such as those shown in Figure 11, can be used. In this figure the subgrade support condition applies for a subgrade effective elastic modulus (E_s) of 70 MPa. The relation for subgrade vertical strain (ϵ_{vs}) holds good for all flexible pavements, but the relation for maximum horizontal asphalt strain (ϵ_{HA}) holds only for flexible bitumen-base pavements.
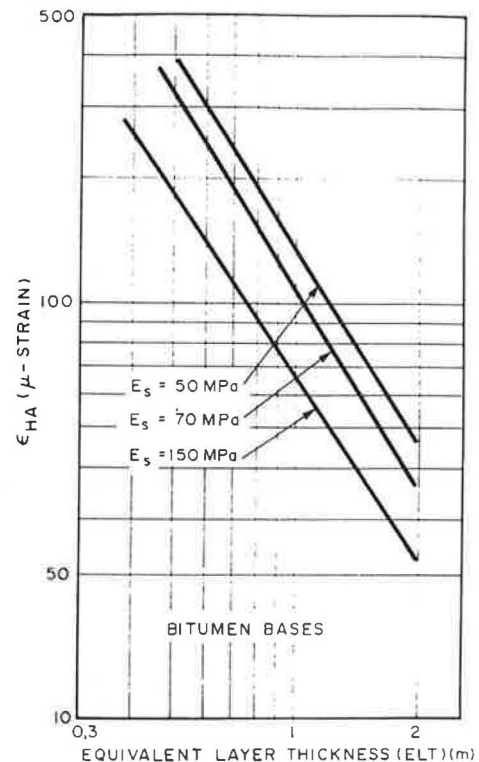
CONCLUSIONS AND RECOMMENDATIONS

Deflection basin parameters, as measured with the RSD or the NITRR deflectograph, can be used to enhance and simplify the South African mechanistic design procedure. The mechanistic design procedure can be simplified by using a design-curve approach, achieved in this instance by using the ELT concept.

The deflections, as measured on the reverse curvature of the deflection basin, correlate well with subgrade effective elastic modulus. The subgrade effective elastic modulus determined using such relations forms the basis for calculation of the ELT. It also has intrinsic significance in terms of identifying statistically uniform sections of subgrade support conditions in a typical initial assessment of a pavement length.

The ELT concept is applicable to the approximation of structural capacity of flexible pavements. Deflection basin parameters correlate well with a value such as ELT in general, as calculated for flexible pavements. For some deflection basin parameters it is even possible to discern between granular- and bitumen-base pavements. Using such measured deflection basin parameters, it is possible to determine ELT for the previously determined subgrade effective elastic moduli.

ELT correlates well with subgrade vertical strain (ϵ_{vs}) for flexible pavement structures and can be used to discern the effect of variance of subgrade elastic moduli. On the other hand, clear relations between maximum horizontal asphalt strain (ϵ_{HA}) and ELT do not exist for granular-base pavements as they do for bitumen-base pavements. This is due to the thin asphalt layer typically used on granular-base pavements
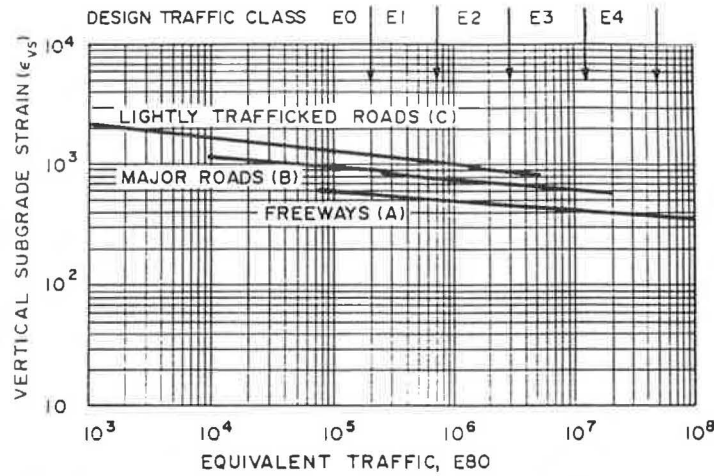
FIGURE 8 Recommended subgrade vertical strain criteria for different road categories.
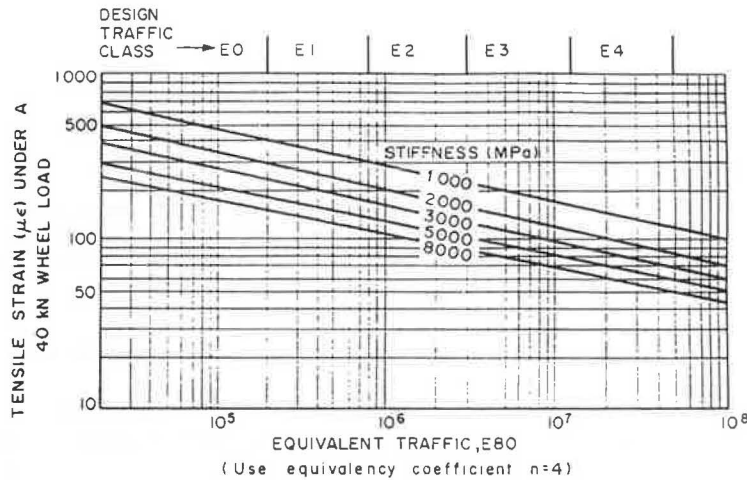
FIGURE 9 Recommended fatigue life criteria for thick bitumen bases.

in South Africa. There are other design curves (6) whereby the maximum horizontal asphalt strain (ε_{HA}) can be calculated by using deflection basin parameters. These distress determinant strains can be calculated from previously determined ELT values.

The value of ELT can be used in a mechanistic design or an analytical procedure to establish the structural life of a flexible pavement with regard to the distress determinants (ε_{vs} and ε_{HA}). Use is made of the typical fatigue-life relations of these two distress determinants.

A design-curve approach can also be followed whereby ELT, as determined from deflection basin measurements, is directly related to remaining life. The precrack life of cemented subbases and bases can also be determined using such a design curve.

Overlays are important rehabilitation options. Although the ELT concept does not allow for the analysis of individual layers, the design-curve approach lends itself ideally to use with overlay-design curves developed for these types of pavements (6). Apart from that, the concept of the ELT can be used in the initial assessment of rehabilitation investigations.

ACKNOWLEDGMENT

TABLE 3 SHIFT FACTORS FOR BITUMINOUS BASES

A (Lightly trafficked roads)	B (Major roads)	C (Freeways)
2	5	10
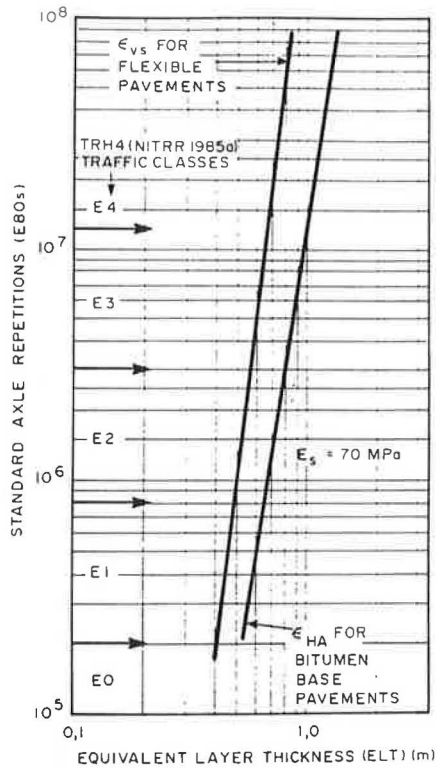
FIGURE 10 Initiation of cracking of cemented bases and subbases in terms of equivalent layer thickness.
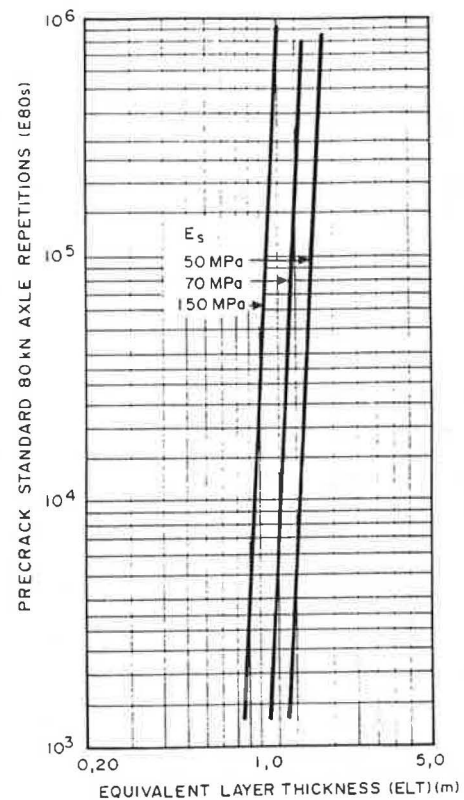
FIGURE 11 Pavement life for maximum horizontal asphalt strain and subgrade vertical strain criteria in terms of equivalent thickness.

REFERENCES

1. N. Odemark. *Investigations on the Elastic Properties of Soils and the Design of Pavements According to the Theory of Elasticity.* Statens Vaeginstitute, Stockholm, Sweden, 1949.
2. A. A. A. Molenaar and Van Gurp. *Optimization of the Thickness Design of Asphalt Concrete.* Proc., 10th Australian Road Research Board Conference, Vol. 10, No. 2, 1980, pp. 31–44.
3. A. A. A. Molenaar. *Structural Performance and Design of Flexible Road Constructions and Asphalt Concrete Overlays.* D. Tech. Sc. thesis, Technische Hogeschool, Delft, The Netherlands, 1983.
4. *Structural Design of Interurban and Rural Road Pavements.* TRH4, National Institute for Transport and Road Research, CSIR, Pretoria, South Africa, 1985.
5. C. R. Freeme. *Evaluation of Pavement Behaviour for Major Rehabilitation of Roads.* NITRR Technical Report RP/19/83, CSIR, Pretoria, Republic of South Africa, 1983.
6. E. Horak. The Use of Surface Deflection Basin Measurements in the Mechanistic Analysis of Flexible Pavements. *Proc., 6th International Conference on the Structural Design of Asphalt Pavements*, Ann Arbor, Mich., Vol. 1, 1987, pp. 990–1001.
7. Horak, E. *Measurement and Data Processing of Deflection Basins.* NITRR Technical Report RP/23, CSIR, Pretoria, Republic of South Africa, 1986.
8. C. R. Freeme, M. De Beere, and A. W. Viljoen. The Behaviour and Mechanistic Design of Asphalt Pavements. *Proc., 6th International Conference on the Structural Design of Asphalt Pavements*, Ann Arbor, Mich., Vol. 1, 1987, pp. 333–343.
9. C. R. Freeme, J. H. Maree, and A. W. Viljoen. Mechanistic Design of Asphalt Pavements and Verification of Designs Using the Heavy Vehicle Simulator. *Proc., 5th International Conference on the Structural Design of Asphalt Pavements*, Pretoria, Republic of South Africa, Vol. 1, CSIR Reprint RR362, 1982, pp. 156–173.
10. G. J. Jordaan. *An Assessment of the Pavement Analytical and Rehabilitation Design Methods: A Method Based on the FWD Measurements and the Equivalent Layer Concept (The Netherlands).* NITRR Technical Note TC/45/85, CSIR, Pretoria, Republic of South Africa, 1985.
11. F. Bonnaure, G. Gest, A. Gravious, and O. Uge. A New Method of Predicting the Stiffness of Asphalt Paving Mixtures. *Proc., Association of Asphalt Paving Technologists*, Dallas, Texas, Vol. 46, 1977, pp. 64–97.

Development of an Improved Overlay Design Procedure for Alaska

MARGOT YAPP, R. G. HICKS, AND BILLY CONNOR

Alaska is currently developing a pavement management system for their road system. An important input to the system is the determination of flexible overlays based on the structural adequacy of the existing pavement. The current overlay procedure (Asphalt Institute method) does not always show a need for overlays, despite the poor surface condition of the pavement and high traffic volumes. Therefore, an improved procedure that considers not only traffic but also surface distress, structural properties of the pavement, and effects of a freezing and thawing of the base, subbase, and subgrade layers is needed. This report recommends two such methods: a simplified mechanistic method using equations developed in Pennsylvania, and a mechanistic procedure using a back-calculation computer program known as ELSDEF. A comparison of these methods showed that the Asphalt Institute procedure was inappropriate and underdesigned the overlay for the road sections. The Pennsylvania equations were slightly more conservative than the mechanistic method using ELSDEF, except for cases where the pavement fatigue life had been utilized completely by past traffic loads. It is recommended that Alaska utilize the mechanistic approach to design overlays and ELSDEF as the back-calculation procedure. The Pennsylvania equations can be used in cases not requiring considerable accuracy.

At present, Alaska uses the falling-weight deflectometer (FWD) to measure pavement deflections and then determines overlay thickness using the Asphalt Institute procedure (*1*). The availability of an FWD for each region enables Alaska to obtain sufficient deflections at the critical time of the year for design. However, this procedure does not consider the remaining life of the pavement or the effects of freezing and thawing on subgrade materials. Therefore, the resulting design thicknesses have been inadequate and, on occasion, the procedure has failed to indicate a need for an overlay.

This paper describes the development of an improved framework for overlay thickness design. Data were collected from selected highway projects to evaluate the proposed methodology. The results are compared with those from the existing design procedure.

The study approach consisted of two phases as shown in Figure 1. Phase I evaluated existing methods of overlay thickness design and developed a framework for a new procedure to be used in Alaska. In Phase II, testing was performed to modify the design procedure as needed. Once tested and evaluated, the overlay design procedures are to be documented in a field manual.

M. Yapp, ARE Inc. Engineering Consultants, Scotts Valley, Calif. 95066. R. G. Hicks, Oregon State University, Corvallis, Ore. 97331. B. Connor, Alaska Department of Transportation and Public Facilities, Fairbanks, Alaska 99709.
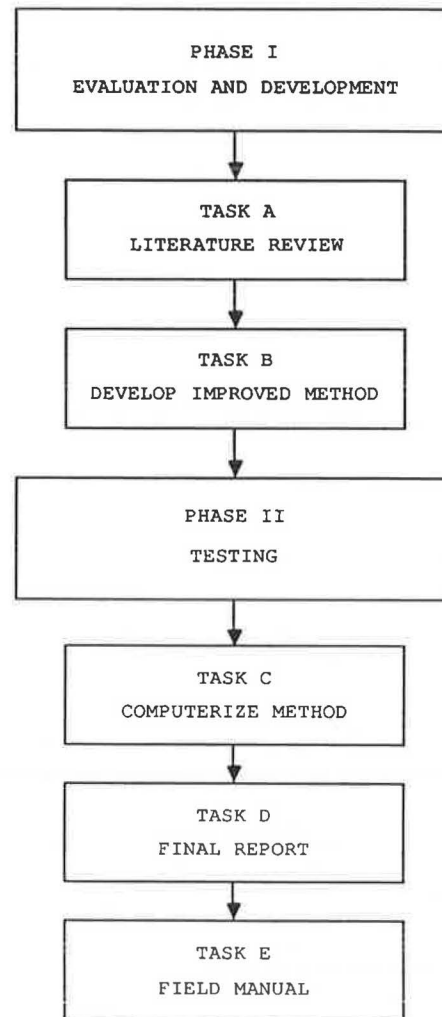
FIGURE 1 Flowchart of study approach.

BACKGROUND

Current Overlay Design Method

The Alaska Department of Transportation and Public Facilities' (ADOT&PF) official flexible overlay design method (*2*) is essentially that contained in the Asphalt Institute's MS-17 (*1*). With this procedure, the representative rebound deflection (RRD) at the center of load is measured with an FWD using an impulse load of 9,000 lb (40 kN). The average of all
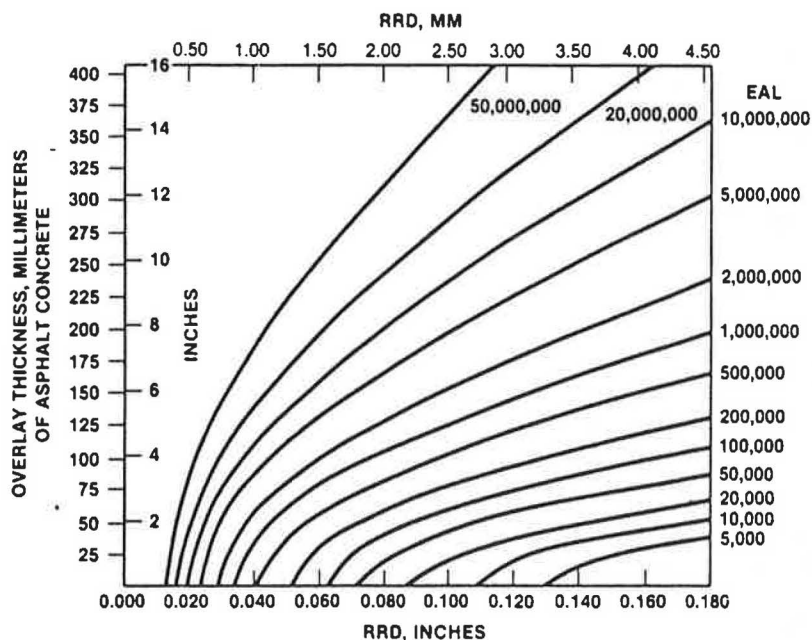
FIGURE 2   Asphalt concrete overlay thickness required to reduce pavement
deflections from a measured to a design deflection value (rebound test) (*1*).

deflection values plus twice the standard deviation, together
with the design traffic, in equivalent 18-kip axle loads (EALs),
is used to obtain the required overlay thickness (Fig. 2).

Although the official overlay design approach is currently
the Asphalt Institute procedure, other methods have been
used by ADOT&PF. For example, in the Central (Anchorage) and Southeastern (Juneau) regions, the Asphalt Institute
procedure indicates that no overlay is required despite the
fact that roadways have high traffic volumes. Therefore,
mechanistic procedures have been used. However, in the Interior region (Fairbanks), only the Asphalt Institute procedure
is used and, interestingly enough, deflections in this region
are higher than in Anchorage despite a colder climate and
lower traffic volumes. One possible explanation could be that
Fairbanks generally uses thinner asphalt concrete pavements
than Anchorage and Juneau.

Problems with Current Overlay Design Methods

The problems associated with the current ADOT&PF overlay
design procedure are as follows:

- Current procedures do not always show a need for overlays despite high traffic volumes.
- Pavement surface condition is not considered, especially
cracking.
- Effects of frozen subgrade and base are not considered.
- Remaining life is not considered.
- Pavement layer dimensions are not used.
- Use of new additives in asphalt concrete is not considered.
- Peak center deflection is not a good indicator of distress.

Typically, higher traffic volumes would require thicker overlays, and a rational design procedure should illustrate this.
Further, although it is known that cracking reduces the

remaining life of the pavement, most existing overlay procedures do not address this issue very well (*3*).

The data collected using current procedures are insufficient
to provide accurate indications of the contributions of each
structural layer, particularly if the pavement structure is partially frozen. When underlying layers are partially frozen, the
surface deflections measured are smaller than when taken
over thawed pavements. However, despite the smaller deflection values for a partially frozen pavement, the stresses and
strains that the pavement endures may be much greater (*4*).
The pavement stresses and strains are actual indicators of the
structural strength, with high value indicating a weaker pavement. Therefore, the center-of-load deflection alone is a poor
indicator of the potential for pavement distress.

The maximum damage potential may occur long before
peak deflection occurs. This is because pavement strains may
be highest when deflections have not yet reached their peak.
This may be remedied if the depth of thaw is known, in which
case an adjustment to the deflection value is made. However,
the thaw depth generally varies greatly from point to point,
depending on factors such as exposure to sunlight, types of
materials present, and water content. Frost tube measurements used to approximate thaw depths may be in error by
several feet (*4*), and the adjusted deflection values may err
by a factor of two or more as well.

Further, the Asphalt Institute method as given in MS-17
(*1*) does not consider the remaining life of the pavement.
Work completed by Kennedy and Lister (*5*) indicates that, in
many pavements, deflections remain relatively constant for
most of the serviceable life of the pavement and only increase
near the end of the pavement life. Therefore, a fatigue relationship that incorporates both past and future traffic should
be used in the analysis. Also, the tolerable deflection used
may not be adequate to properly quantify the desired deflection criteria (*6*). This tolerable deflection is a function of the
materials in the pavement structure, subgrade support, and

the layer thicknesses; however, the deflection method as used does not consider the contributions of the different layers.

In addition, new additives such as rubber and other polymers in asphalt concrete have added new dimensions to the overlay problem which are not addressed in the current method.

DEVELOPMENT OF IMPROVED PROCEDURE

Design Approach

In July 1986, a planning meeting with ADOT&PF was held to discuss existing and future overlay design practices. The advantages and disadvantages of the current overlay procedures were debated, and outlines of an improved procedure were developed. Project sites and data needs were also identified.

A two-tiered concept for overlay design was also determined to be most desirable. The first tier would be a simpler and easier approach than the second. Therefore, it was proposed that the first tier be a simplified mechanistic approach, such as that developed by Fernando et al. (7). This is a simpler and more straightforward approach than the mechanistic approach using back-calculation analysis. However, the range of layer properties used in the study by Fernando et al. is not completely appropriate for Alaska's conditions. Therefore, it may prove necessary to develop strain vs. deflection relationships specifically for Alaskan pavements. This step is outside the scope of the project.

The second tier is a fully mechanistic approach in which layer moduli are back-calculated from surface deflections. A number of automated back-calculation programs with iterative basin-fitting procedures are available for microcomputers (8). Two of these procedures (BISDEF and ELSDEF) were evaluated as a part of this study.

Simplified Mechanistic Procedure

The simplified mechanistic method uses mechanistic principles to arrive at empirical relationships. Linear elastic theory and regression analysis techniques are used to develop equations that describe the relationships between surface deflections and pavement layer properties.

This strain-deflection approach is a simplified mechanistic procedure that was developed by Fernando et al. (7). Essentially, the linear elastic layer theory was used to develop strain vs. deflection relationships for the direct calculation of pavement strains from measured FWD deflections rather than using a deflection-basin-fitting procedure to back-calculate moduli values. The multilayer linear elastic program, BISAR, was used in a large factorial study to develop these relationships. Strain vs. deflection relationships were then developed for the tensile strain (ε_t) at the bottom of the existing asphalt layer and the compressive strain (ε_c) at the top of the subgrade. These are:

$$\log[\varepsilon_t/\log(H_1 + 1)] = -2.261 - 0.944\log(\delta_1 - \delta_2)$$
$$+ 1.947\log[(\delta_1 - \delta_3)/\delta_2]$$
$$+ 0.175(\delta_1 {}^* H_2)$$
$$+ 0.926\log(\delta_1 {}^* \delta_2) \qquad (1)$$

$$\log\varepsilon_c = -0.054 + 1.941\log(\delta_1 - \delta_2)$$
$$- 2.004\log[(\delta_1 - \delta_3)/\delta_2] - 1.465\log(H_1 + H_2)$$
$$- 0.136(H_2)^{0.5} + 0.725\log(\delta_1 {}^* H_2)$$
$$+ 0.285(\delta_1 {}^* H_1)^{0.5} - 0.910\log(\delta_1 {}^* \delta_2) \qquad (2)$$

where

ε_t = tensile strain at bottom of the existing AC layer,
ε_c = compressive strain at top of subgrade,
δ_i = deflection at ith sensor of the FWD (in.),
H_1 = thickness of existing AC layer (in.), and
H_2 = thickness of existing subbase (in.).

Using the calculated strain values, performance prediction estimates are possible. The tensile strains were used with the Austin Research Engineers' fatigue equation (9), and the subgrade strains were used with the performance model developed by Luhr et al. (10) to obtain the equations relating expected life to allowable strain. However, the performance predictions from the deflection-basin-fitting (i.e., back-calculation) procedures match more closely the predictions generated from the theoretical strains than from this simplified strain-deflection procedure. The two performance equations are defined as follows:

$$W_{18} = 9.33 \times 10^{-15}(\varepsilon_t)^{-5.16} \qquad (3)$$

$$\log N_x = 2.15122 - 597.662\varepsilon_x - 1.32967 \log\varepsilon_x$$
$$+ \log[(PSI_i - TSI)/(4.2 - 1.5)]^{0.5} \qquad (4)$$

where

W_{18} = weighted 18-kip applications prior to Class 2 cracking,
ε_t = tensile strain at bottom of the AC layer,
N_x = allowable applications of axle load x,
ε_x = subgrade compressive strain due to axle load x,
PSI_i = initial PSI of pavement, and
TSI = terminal serviceability index.

Once the strains are known, it is possible to input various thicknesses of the overlay and then to recompute the strains. The required overlay thickness would be the one that reduces the strains to a specified tolerable level. The relationships developed for estimating the pavement's tensile and compressive strains are given by the following:

$$\log(\varepsilon_t)_{ov} = -0.689 + 0.793\log\varepsilon_t$$
$$- 0.041(H_{ov} + H_1)^{0.5} - 0.057H_{ov} \qquad (5)$$

$$\log(\varepsilon_c)_{ov} = -0.359 + 0.870\log\varepsilon_c - 0.051H_{ov}$$
$$- 0.109[(H_{ov} + H_1)/H_1]^{0.5} \qquad (6)$$

where

$(\varepsilon_t)_{ov}$ = tensile strain at bottom of original AC layer after overlay
$(\varepsilon_c)_{ov}$ = compressive strain of subgrade after overlay,
ε_t = tensile strain of AC layer before overlay,
ε_c = compressive strain before overlay,
H_{ov} = overlay thickness (in.), and
H_1 = thickness of original AC layer (in.).
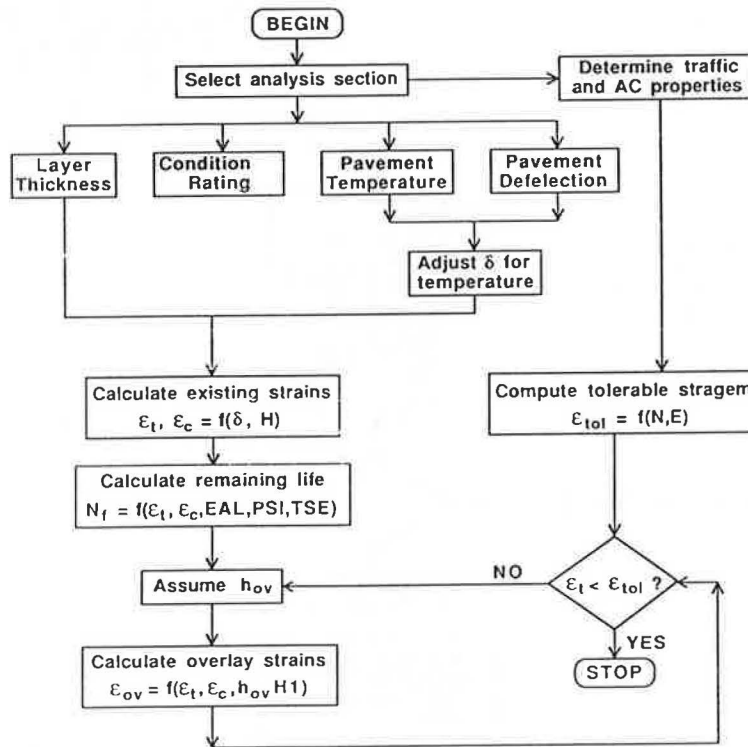
FIGURE 3 Flowchart for the simplified mechanistic procedure.

The relationships and equations were developed for conditions in Pennsylvania; therefore, they may not be valid for Alaska. Some experimentation on the validity of the procedure should be performed. However, it should be possible to derive similar relationships utilizing Alaskan conditions, if needed. Figure 3 provides a flowchart of this procedure.

Mechanistic Procedure

A fully mechanistic design procedure characterizes the response of the pavement to a load in terms of strains and/or stresses in various pavement layers. A fatigue relationship between that response and number of load repetitions to a designated failure criterion is used to determine pavement life. Mechanistic and deflection procedures are not mutually exclusive. Most procedures use a stress or strain level based on deflection testing as the pavement response that is related to performance. The difference between such a system and a deflection approach is that the deflection used to develop the performance relationship is based on a mechanistic model rather than an empirical one.

Figure 4 is a flowchart of a fully mechanistic design procedure (*11*). As in the deflection-based procedures, nondestructive pavement tests, condition surveys, and traffic data are required as inputs. In addition, some knowledge of the stiffness properties and distress characteristics (such as fatigue cracking and plastic deformation) of the various materials constituting the pavement structure are needed. Stiffness characteristics of the various pavement components can either be determined by tests on undisturbed or representative specimens of the pavement components, or back-calculated from NDT measurements.

The FWD, when used to measure the structural response, provides a measure of the surface deflection under an impulse load. Measurements should be obtained at reasonable intervals throughout the project. The condition of the pavement must be carefully ascertained. This is needed to determine the analysis sections and to help establish performance criteria for the observed distress types.

The stiffness characteristics of the various layers can be estimated from surface deflection measurements. The shape of the deflection basin is defined by deflections measured directly under a load and at a number of radii. Computer programs that perform elastic-layer analysis are used to determine a set of modulus values that provides the best fit between the measured and computed deflection basins at the pavement surface. Normally, the procedure involves assuming a set of modulus values and then iterating with the computer until the measured and computed deflections are in "reasonable" agreement. Various programs are available to perform the back-calculation analysis. This paper analyzes two such programs: ELSDEF and BISDEF. With both programs, it is recommended that some laboratory testing be performed to check the back-calculated results (*11*). Figure 5 is a flowchart of the CHEVDEF/BISDEF program (*12*).

As in all design methods, traffic volumes using the facility should be known. The distribution of traffic across lanes and the concentration of truck traffic in the outer lane should be recognized. With the traffic information and layer stiffnesses, critical performance parameters can be determined using elastic-layer analysis. The parameters can be related to "acceptable" and "unacceptable" performances observed in the condition survey as well as to laboratory-defined distress criteria.

Since Alaska has not developed its own design criteria at
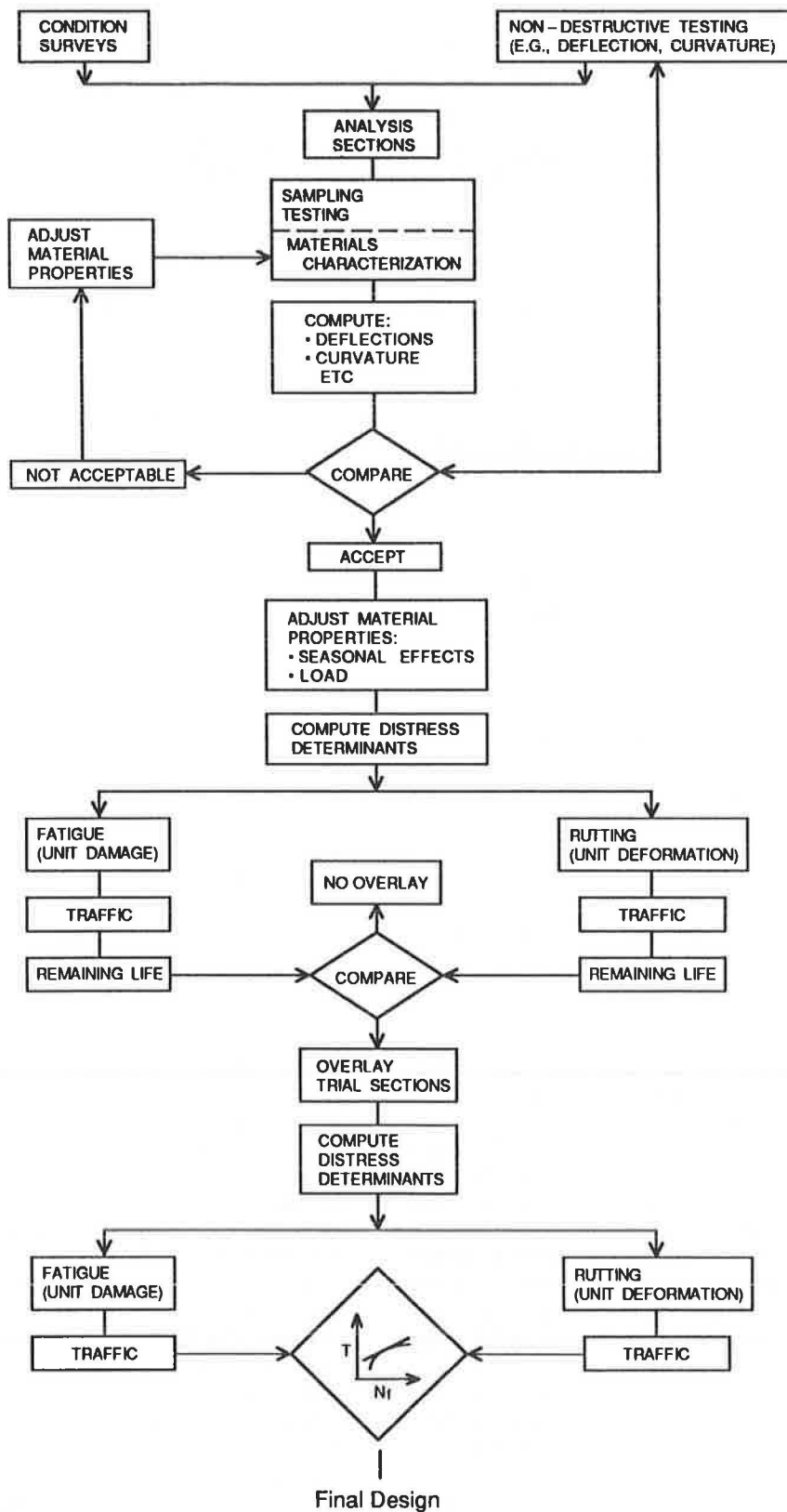
FIGURE 4 Flowchart for the mechanistic procedure (11).
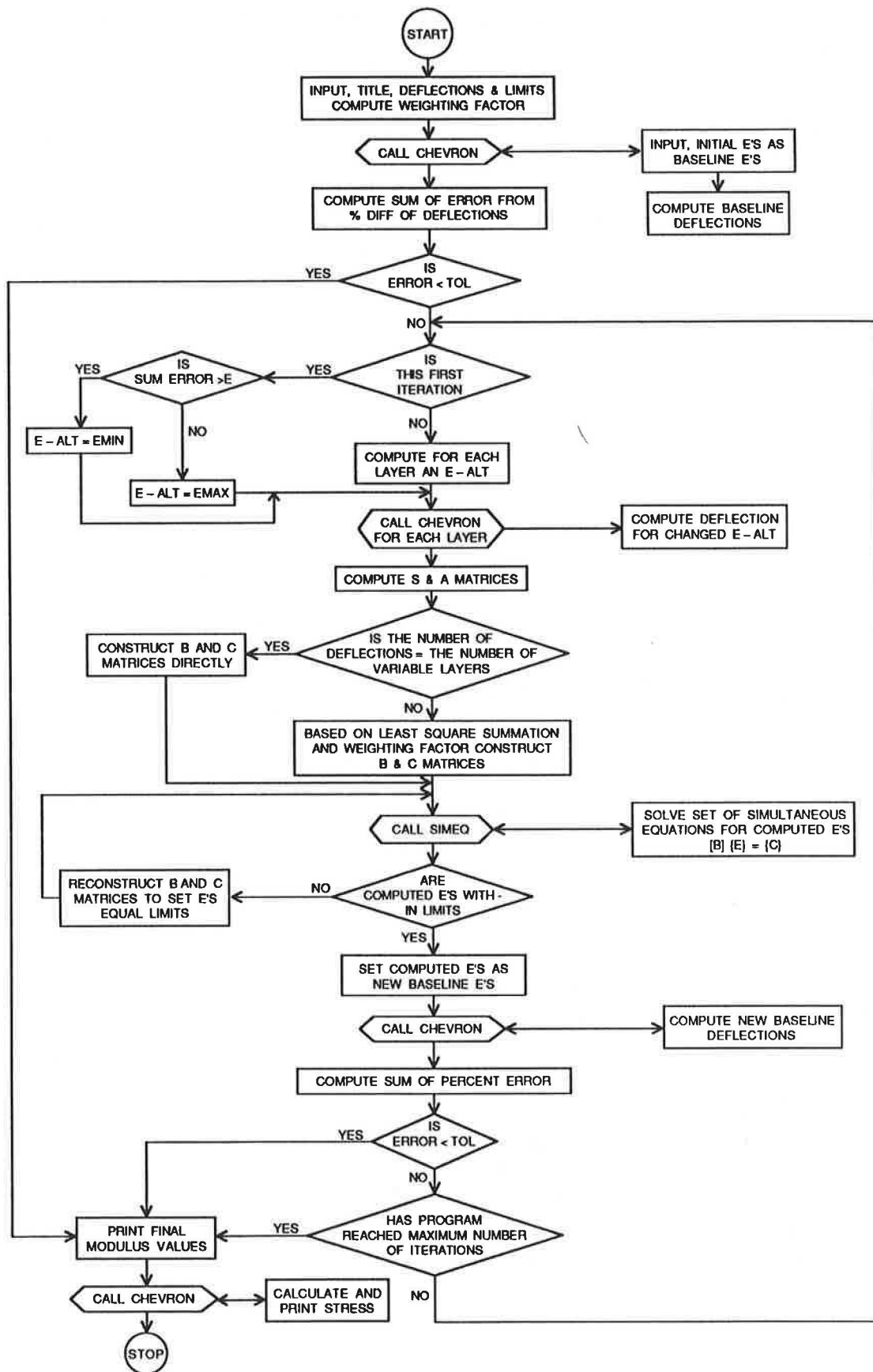
FIGURE 5 CHEVDEF/BISDEF program flowchart (*12*).

present, those developed by the Asphalt Institute (*13*) may be used. For control of fatigue in the asphalt layer, Equation 7 is used:

$$N = 18.4*C*0.004325*\varepsilon_t^{-3.291}*E^{-0.854} \tag{7}$$

where

N = number of 18-kip (80-kN) equivalent single-axle loads,
ε_t = horizontal tensile strain on underside of existing AC layer,
E = modulus of AC layer (psi), and
C = a function of voids and volumes of asphalt in the mix design and can be calculated as

$$C = 10^M \tag{8}$$

and

$$M = 4.84*[V_b/(v_v + V_b) - 0.69] \tag{9}$$

where

V_b = volume of asphalt (%), and
v_v = volume of air voids (%).

Similarly, the vertical compression strain criterion is used to control permanent deformation:

$$N = 1.365 \times 10^{-9}*\varepsilon_c^{-4.477} \tag{10}$$

where

ε_c = vertical compression strain at the subgrade surface.

If the future anticipated traffic for the life of the overlay is known, it is possible to rearrange Equations 7 and 10 to obtain the tolerable strains.

The remaining life of the pavement can be determined using Miner's Hypothesis. A simple form of the expression is:

$$N_r/N_{D1} = 1 - N_{A1}/N_{D1} \tag{11}$$

where

N_r/N_{D1} = remaining life,
N_{A1} = number of applications of EALs to date,
N_{D1} = allowable number of applications of EALs according to fatigue relationships, and
N_r = additional number of applications of EALs that can be applied to the existing pavement.

If an overlay is needed, it must be designed to resist fatigue and rutting. For a specific thickness of overlay to minimize fatigue, the tensile strain on the underside of the existing layer must be determined. The allowable number of applications can be estimated using some form of fatigue relationship modified by the remaining life ratio. It is possible to define the relationship between overlay thickness and additional load applications. Similarly, relationships exist between the compressive subgrade strain and the pavement life to preclude rutting. At present, the Asphalt Institute criteria (*13*) are recommended for use in Alaska.

If other distress modes are considered, similar relationships between thickness and load applications can be developed. The design overlay is the maximum thickness value required to satisfy fatigue and rutting criteria (*11*).

EVALUATION OF IMPROVED PROCEDURE

Project Sites

Three sites were evaluated, two in Anchorage and one in Fairbanks. Figure 6 shows the location of the three project sites. Sterling and Seward Highways are located in the Anchorage region, and Parks Highway is located near Fairbanks. Parameters of all three projects are summarized in Table 1. Generally, Sterling and Parks Highways are rural highways, with low traffic volumes and thin AC layers ranging from 1.5 to 2 in. (3.8 to 5 cm). The Seward Highway project site, however, is located in downtown Anchorage with thicker AC layers ranging from 2.25 to 5 in. (5.7 to 12.7 cm). All projects, therefore, consist of an asphalt concrete surface over untreated aggregate base and subbase.

Results of Analysis

Four overlay design procedures are evaluated in this section. The first is the current Asphalt Institute MS-17 (*1*) procedure. The second design procedure was developed by Newcomb (*14*) for the state of Washington. The procedure utilizes regression equations to calculate the layer moduli and was added only for comparison. These values were used in the mechanistic design procedure to calculate overlay thickness. The last two are the simplified mechanistic procedure developed by Fernando et al. (*7*) and the fully mechanistic procedure that uses the back-calculation programs ELSDEF and BISDEF to determine the layer moduli of the pavements. Comparisons of layer moduli are given in Table 2, and the overlay thicknesses resulting from the four procedures are summarized in Table 3.
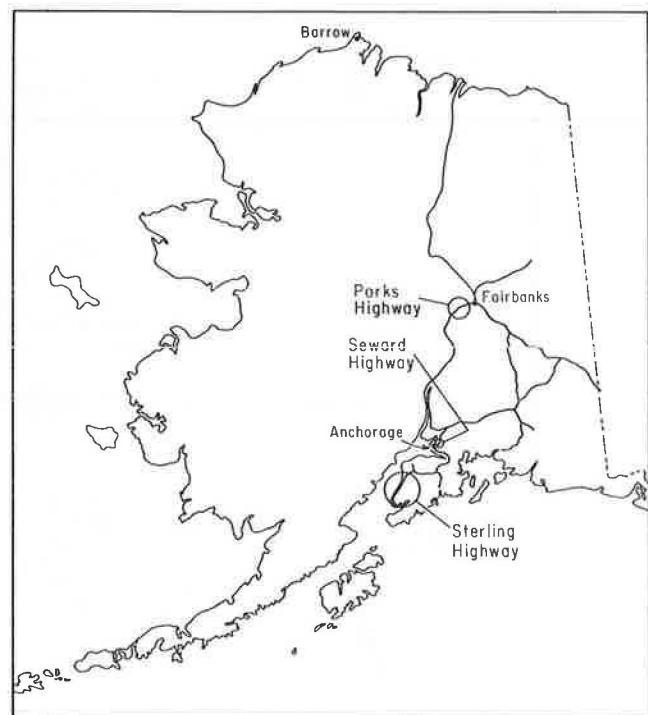
FIGURE 6   Location of project sites in Alaska.

TABLE 1 SUMMARY OF PARAMETERS FOR PROJECT SITES

Project Location	Pavement Structure[1]	Traffic To Date	20 yr. EAL	Pavement Condition
STERLING HIGHWAY				
MP 117-130	AC - 1.5 in. Base - 4.0 Subbase - 6.0 Borrow - 24.0	130,000[2]	1,800,000	Good
MP 130-157	Same as above	130,000[2]	1,800,000	Extensive alligator cracking and rutting.
MP 157-162	AC - 1.5 Base - 6.0 Borrow - 0 to 36.0	130,000[2]	1,800,000	No fatigue cracking.
MP 162-166	Same as above	unknown	2,770,000	5-26% cracking.
MP 166-171	Same as above	unknown	7,980,000	100% cracked.
SEWARD HIGHWAY				
36th to 4th Ave	AC - 2 to 5.25 Base - 6.0 Subbase - 18.0	4,400,000	5,083,000 (10 years)	Extensive cracking and rutting.
PARKS HIGHWAY				
North Section	AC - 2.0 Base - 4.0 to 6.0 Subbase - 6.0 to 12.0 Borrow - 24.0 to 36.0	78,723[2]	390,521	Severe rutting and alligator cracking.
South Section	Same as above	76,069[2]	345,526	Severe rutting and alligator cracking.

[1]For Parks Highway, these are assumed dimensions.
[2]Traffic data are assumed.
 1 in. = 2.54 cm

Sample layer moduli that were obtained from BISDEF, ELSDEF, and Newcomb's equations for the three sites are summarized in Table 2. Because of the presence of frozen subsurface layers and thin surface layers, it was difficult to close in on the layer moduli with BISDEF. It is apparent that the layer moduli obtained are at the limits of the input ranges. Final moduli values were also output despite the fact that error messages indicating that computations had been suspended were present. This occurred in more than half of the deflection basins that were analyzed.

The layer moduli calculated with ELSDEF appear more reasonable when these results are compared with those obtained from laboratory tests. In approximately half of the pavements analyzed, the subgrade values show substantial stiffnesses of 150 to 650 ksi (1,030 to 4,480 kPa) indicating that this layer is frozen or partially frozen. Also, about half of the sections show asphalt concrete moduli in the 400–1200 ksi range (2,750–8,270 kPa), which would be in accordance with pavements tested during March when pavement temperatures were 37°F (2.8°C). For the remaining sections, temperatures averaged 60°F (15.6°C), and the moduli are correspondingly lower. The base moduli average from 30 to 40 ksi (206 to 275 kPa).

The layer moduli from Newcomb's equations are significantly different from those obtained using ELSDEF. As Table 2 indicates, the surface moduli are much lower whereas the base and subgrade moduli are higher than expected. It should be emphasized that these equations were not developed for frozen soil applications. These equations were included in the study only because initially it was thought that the thawed pavement would be the critical case. Also, the models were built with the assumption that the underlying moduli are smaller than the overlying layers, and this is not true for our sites. For the Parks Highway, the surface moduli were so low that adding an overlay did not decrease the tensile strains as expected. Instead, there was an *increase* in strains. This is apparently due to the weak AC layer moduli computed. The equations of Fernando et al. (*7*) and the Asphalt Institute procedure (*1*) do not yield layer moduli results and are therefore not included in Table 2.

Table 3 summarizes the overlay thicknesses for the projects. Two reliability levels as defined by AASHTO (*15*), 50 percent and 90 percent, are included in the analysis. The reliability level concept is further discussed in the technical appendices of the Asphalt Institute's MS-17 (*1*). Briefly, a 50 percent

TABLE 2   COMPARISON OF LAYER MODULI

Location	BISDEF[2]			ELSDEF			NEWCOMB[3]		
	E1	E2	E3	E1	E2	E3	E1	E2	E3
Sterling Highway									
MP 117.5	1688	93	125	399	71	120	289	136	148
118.0	1719	36	103	919	33	76	112	119	146
118.5	657	51	93	304	37	91	97	115	144
119.0	2000	34	346	971	41	165	-	-	-[4]
119.5	398	42	189	274	37	161	98	115	143
Seward Highway									
TH 1	2000	46	29	1038	52	24	247	88	78
TH 2	2000	52	16	634	62	9	307	76	54
TH 3	2000	16	47	1892	21	12	198	79	74
TH 4	1488	37	14	438	39	10	252	58	40
TH 45	570	26	12	485	21	11	131	46	34
TH 34	2000	32	14	1269	40	6	359	64	44
TH 35	1522	42	24	620	44	15	169	75	65
Parks Highway									
CDS 206	2000	18	1000	422	24	17	18	22	240
206.2	286	25	1000	383	24	45	5	37	684
206.4	1035	24	171	381	26	32	15	21	225
206.6	1194	21	552	352	23	31	14	21	233
206.8	554	25	89	243	20	203	23	21	225

All moduli values are in ksi (1 ksi = 6.89 MPa)
[2]BISDEF values did not converge. The results included here are not reliable, and are only for general comparison purposes. Most of the moduli are at the extremes of the ranges specified.
[3]Newcomb's regression equations specifically do not consider the effects of a frozen base and subbase, whereas these sections are partially frozen.
[4]Moduli values were not calculated due to a zero deflection reading.

level would imply a probability of .5 that a pavement will perform well over the design period. Therefore, different levels may be used to underscore the relative importance of a road structure's failure. For example, it would be desirable for a high-volume highway to have a high probability of achieving its design life and performance, and so a higher reliability level would be selected.

As shown in Table 3, the mechanistic procedure indicates that overlays ranging from 0 to 7 in. (0 to 17 cm) are needed for 50 percent reliability. For Seward Highway, reconstruction is recommended because of the high traffic volumes. The increase in the reliability level from 50 to 90 percent generally increases overlays by 2 in. (5 cm). The current procedure does not directly incorporate reliability levels.

The equations of Fernando et al. (7) tend to be more conservative and produce overlays that are approximately 2 in. (5 cm) thicker than the mechanistic procedure. However, for the Seward Highway project, they recommend a 2 to 6 in. (5 to 15 cm) overlay rather than reconstruction.

The results of the analyses using the layer moduli from Newcomb's regression equations indicate that no overlays are required. However, they agree with the mechanistic procedure for Seward Highway and recommend reconstruction. The Asphalt Institute procedure (1) is confirmed as producing the thinnest pavement sections. Overlay thicknesses range from 0 to 3 in. (0 to 7.5 cm) and are typically lower than those

determined with the mechanistic method, by 2 to 3 in. (5 to 7.5 cm) or more.

Discussion of Results

From the preceding sections, some clear trends or conclusions can be drawn. Overall, use of the program BISDEF was not very successful. This may be due to the presence of frozen layers, the presence of thin surface layers, or a combination of both. ELSDEF gives more reasonable values. Still, there are some anomalies. In the case of Seward Highway, more sections should have been analyzed to obtain a better sample of the population. The base moduli seem to be on the low side, but the program seems to handle the presence of a frozen layer well. To ensure that the back-calculated moduli are accurate, particularly for thin surface layers (< 2 in.), cores should be obtained from the project sites and tested in the laboratory.

Newcomb's equations for layer moduli are not recommended for Alaskan conditions. They were specifically developed for nonfrozen pavements and probably should not have been included in this paper. Also, the presence of a frozen layer and a very thick base and subbase result in shallower deflection basins, and the outermost sensors should probably be extended farther than 48 in. (122 cm). Figure 7 shows an

TABLE 3   COMPARISON OF OVERLAY THICKNESSES

Location	The Asphalt Institute	Newcomb	Fernando	Mechanistic* 50%	90%
Sterling Highway					
MP 117.5	The overlay	0	2.5	0.0	0.0
118.0	thickness	0	5.0	4.0	6.5
118.5	required	0	5.5	5.0	8.0
119.0	is 2.0 in.	**	5.5	**	**
119.5		0	5.5	5.5	8.0
Seward Highway					
TH 1	RRD = 26	0	3.5	Reconstruction is	
TH 2	Overlay is	6	2.0	recommended for	
TH 3	2 in. (50%)	Recon.	4.0	this section.	
TH 4	& 3 in. (90%)	Recon.	5.0		
TH 45		Recon.	6.0		
TH 34		Recon.	4.5		
TH 35		6	4.0		
Parks Highway					
CDS 206	RRD = 26	**	6.5	4.0	6.5
206.2	Overlay	**	6.5	4.5	6.5
206.4	is 0.	**	6.5	3.5	6.5
206.6		**	7.0	4.5	7.0
206.8		**	5.0	7.0	>8.0

NB: The minimum overlay thickness is 1 inch, and values are rounded
    up to the nearest 0.5 inch. (1 inch = 2.54 cm)
 *These are the 50% and 90% reliability levels as defined by AASHTO.
 **Overlay thicknesses could not be computed.

example of a deflection basin. If equations were to be developed for deflections beyond this point, the layer moduli might be more reasonable.

The method of Fernando et al. (7) did not always yield reasonable results. For example, it was determined that an overlay is sufficient for Seward Highway even though the pavement fatigue life is used up. Generally, this procedure produces overlay thicknesses at least equal to or greater than those determined by the mechanistic method in the majority of cases. The presence of the frozen layers generally does not
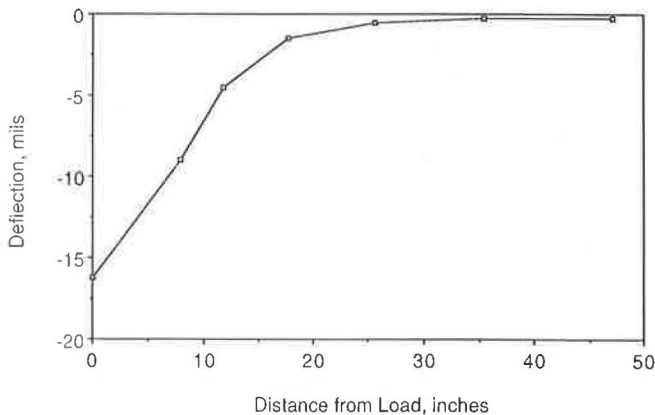
FIGURE 7   Typical deflection basin for Alaska.

appear to distort the results from the regression equations. However, the conservative tone of the overlay designs should prove sufficient for Alaskans to develop their own equations.

The results from the Asphalt Institute procedure confirm that this procedure may not always be appropriate for use in Alaska. The lack of consideration of surface distress or of the presence of frozen layers is obvious in the results. The overlay thicknesses obtained are either significantly lower than those obtained by the other procedures or no need for an overlay is indicated.

A final comment is necessary on the present procedure of using center deflections to determine the critical section for analysis. Figure 8 illustrates both the overlay thicknesses (for the 50 percent reliability level) and center deflections at the same location for Sterling Highway. They show little, if any, coherent relationship between the center deflection (corrected to 70°F and normalized to a 9,000-lb load) and the overlay thickness (from the mechanistic method). On the other hand, Figure 9 indicates a clearer relationship between the overlays and the tensile strains. This again emphasizes the point that center deflections should not be used as a criterion for selection of an analysis section.

As a final note, the lack of accurate data on the historical traffic EALs and the pavement layer thicknesses can be a major obstacle in the analyses. Efforts are needed to improve the quality of traffic and thickness data. It cannot be emphasized strongly enough that an accurate knowledge of the traffic
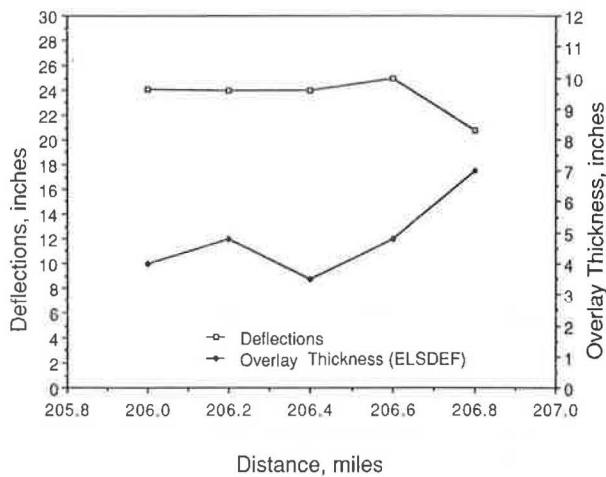
FIGURE 8 Comparison between overlay thickness and center deflections for Sterling Highway.
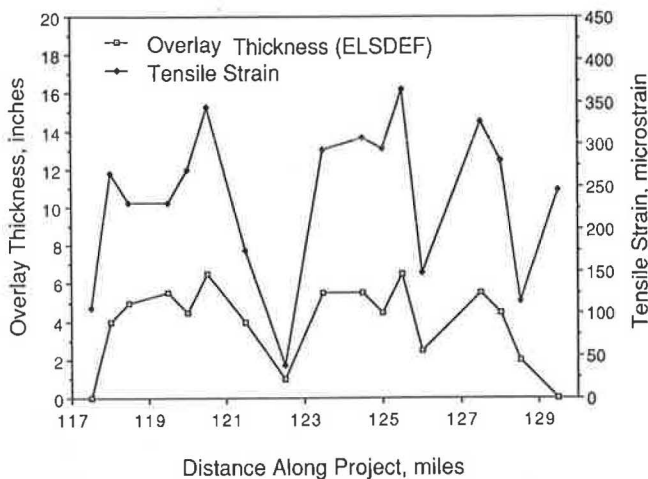
FIGURE 9 Relationship between overlay thickness and tensile strain for Sterling Highway.

and layer thicknesses is very important. The thickness of the asphalt concrete layer, in particular, markedly affects the back-calculated results (8), and inaccurate traffic counts disguise the actual remaining life of the pavement.

CONCLUSIONS

The present overlay design procedure used by the state of Alaska does not acknowledge the special problems that the climate presents in that region. It also does not utilize the concept of remaining life and tends to underdesign the pavement by specifying a thinner overlay than needed.

Four methods of overlay design were analyzed in this report. They include the Asphalt Institute procedure, the strain-deflection relationships developed in Pennsylvania by Fernando et al., and a mechanistic method using the back-calculation programs BISDEF and ELSDEF and one set of regression equations developed in Washington State.

The tensile strain at the base of the asphalt concrete layer was the criterion used in determining the remaining life, as fatigue appeared to be the predominant failure mode. The fatigue equation developed by the Asphalt Institute was also used. However, other criteria such as the compressive subgrade strain and corresponding equations are available.

There were insufficient traffic and pavement structural data for the projects. This led to assumptions used in the analysis that may be inaccurate and, as a result, the overlay thicknesses could be misleading. However, the data are representative of what is actually available for most design situations. Often, more accurate data are simply not available.

The BISDEF program did not always close; therefore, it was determined that the back-calculated moduli were not always reliable. The ELSDEF program resulted in layer moduli that compared favorably with prior laboratory tests. However, additional work is needed to verify these back-calculated values. The Asphalt Institute procedure appears inappropriate for use in Alaska in that the resulting overlay thicknesses are very thin. This method indicates that overlays are not required for several sections despite contrary results from the other methods.

The equations of Fernando et al. perform reasonably well compared with the mechanistic method; if anything, they are more conservative. However, when a pavement is badly fatigued, the procedure can give misleading results. On the other hand, there probably should be more sections analyzed where the remaining life is close to zero before a definitive conclusion can be reached.

The basis for selection of the critical section should not be the center deflection alone because the overlay thicknesses obtained are not related to the magnitude of these deflections. Instead, tensile strain is a better indicator, and the procedure discussed in this report is recommended.

For the projects evaluated, an increase in the AASHTO reliability levels from 50 to 90 percent generally increases the overlay thickness by approximately 2 in.

RECOMMENDATIONS

The Asphalt Institute procedure should not be used for overlay design in Alaska. The proposed mechanistic procedure using ELSDEF should be considered as a replacement for the Asphalt Institute procedure in the design of flexible overlays. For thin asphalt layers (< 2 in.), it is recommended that asphalt cores and aggregate samples be obtained and tested to determine how well the mechanistic method back-calculates the layer properties.

The tensile strain criterion and the Asphalt Institute fatigue relationships appear adequate at present. For a simpler overlay design procedure, the equations of Fernando et al. may be used. However, the results are more conservative than those using the mechanistic procedure.

More accurate traffic data (EALs) are needed, particularly historical data. Efforts should also be concentrated on collecting traffic data for future use and making growth projections. It is recommended that weigh-in-motion and automatic vehicle classification units be left in the field for several weeks at different times of the year to obtain a better representation of the traffic profile. Similarly, accurate layer thicknesses are needed, since this strongly influences the back-calculated

moduli. If construction records have not been kept, then cores should be taken, approximately at the rate of five per mile.

The 50 percent reliability level is recommended for design on roads with low volumes. However, for roads with significant traffic volumes or those that may expect a substantial increase in traffic, a 90 percent level may be more appropriate.

REFERENCES

1. *Asphalt Overlays and Pavement Rehabilitation, Manual Series No. 17 (MS-17).* The Asphalt Institute, College Park, Md., 1983.
2. R. L. McHattie. *Deflection Testing and Its Application to Pavement Rehabilitation in Alaska.* Report No. FHWA-AK-RD-85-15. Alaska Department of Transportation and Public Facilities, Fairbanks, 1985.
3. N. F. Coetzee, H. Harrington, and V. Venkatesh. *Life Estimation of Pavement Rehabilitation Alternatives.* E84.16, Alaska Department of Transportation and Public Facilities Research Section, Fairbanks, 1986.
4. R. N. Stubstad and B. Connor. *Prediction of Damage Potential on Alaskan Highways during Spring Thaw Using the Falling Weight Deflectometer.* Report No. AK-RD-83-11. Alaska Department of Transportation and Public Facilities, Division of Planning and Programming, Research Section, 1982.
5. C. K. Kennedy and N. M. Lister. *Prediction of Pavement Performance and the Design Of Overlays.* TRRL Report 833. Transport and Road Research Laboratory, Crowthorne, Berkshire, England, 1978.
6. R. E. Smith, R. P. Palmieri, M. I. Darter, and R. L. Lytton. *Pavement Overlay Design Procedures and Assumptions—Vol. I: Analysis of Existing Procedures,* Report RD-85/006, FWHA, U.S. Department of Transportation, 1986.
7. E. Fernando, D. Luhr, and O. Anderson. Development of a Simplified Mechanistic Pavement Evaluation for Flexible Pavements. Presented at the 65th Annual Meeting of the Transportation Research Board, 1986.
8. T. Rwebangira, R. G. Hicks, and M. Truebe. Sensitivity Analysis of Selected Back-calculation Procedures. In *Transportation Research Record 1117*, TRB, National Research Council, Washington, D.C., 1987, pp. 25–37.
9. Austin Research Engineers. *Asphalt Concrete Overlays of Flexible Pavements: Vol. I—Development of New Design Criteria.* Report No. FHWA-RD-75-75, Federal Highway Administration, Washington, D.C., 1975.
10. D. R. Luhr, B. F. McCullough, and A. Pelzner. Simplified Rational Pavement Design Procedure for Low-Volume Roads. In *Transportation Research Record 898*, TRB, National Research Council, Washington, D.C., 1983, pp. 202–206.
11. F. N. Finn and C. L. Monismith. *Asphalt Overlay Design Procedures.* Synthesis No. 116, National Cooperative Highway Research Program, Washington, D.C., 1984.
12. A. J. Bush, III. *Nondestructive Testing for Light Aircraft Pavements, Phase II—Development of the Nondestructive Evaluation Methodology.* FAA-RD-80-9-II. Federal Aviation Administration, Washington, D.C., 1980.
13. *Research and Development of the Asphalt Institute's Thickness Design Manual (MS-1),* 9th ed. Research Report 82-2, The Asphalt Institute, College Park, Md., 1982.
14. D. E. Newcomb. *Development and Evaluation of a Regression Method to Interpret Dynamic Pavement Deflections.* Ph.D. Thesis. University of Washington, Seattle, 1986.
15. *AASHTO Guide for Design of Pavement Structures.* American Association of State and Highway Transportation Officials, Washington, D.C., 1986.

Performance Prediction and Cost-Effectiveness of Asphalt-Rubber Concrete in Airport Pavements

Denise M. Hoyt, Robert L. Lytton, and Freddy L. Roberts

An asphalt-rubber concrete and an asphalt concrete were tested in the laboratory and materials characterizations and properties were generated. The characterization parameters and a runway model for a municipal airport were input into the modified ILLIPAVE computer program for predictions of rutting and cracking damage and relative lives of the materials as airfield pavement surfaces in each of four climatic zones. An economic evaluation was performed comparing the expected service lives and costs of each material in each zone. An equivalent uniform annual cost per square yard over the life of the pavement for the construction cost of each pavement was determined. The material with the least equivalent uniform annual cost was selected as the most cost-effective. In every zone but the dry no-freeze zone, the asphalt-rubber concrete was calculated to be the most cost-effective material.

A research study was conducted to investigate the feasibility of using asphalt-rubber concrete, which contains ground and recycled tire rubber, as a surface material for airfield pavements at municipal airports. This research indicated that asphalt-rubber concrete, when properly designed and compacted, could provide a temperature-resistant and long-wearing pavement surface course for the large aircraft typically using a municipal airport. The asphalt-rubber concrete was predicted to be particularly advantageous over asphalt concrete in cases of wide seasonal temperature variation.

The study was performed in two parts. The first phase included development of the laboratory procedure for preparing asphalt-rubber for mix design and an evaluation and modification of the Marshall mix design procedure for designing an asphalt-rubber concrete mix (*1*, *2*). The second phase involved designing and testing an asphalt-rubber concrete mix and an asphalt concrete mix and, using a computerized pavement analysis program, evaluating and comparing the two mixes as airfield pavement surface materials (*3*). This paper describes the testing, analysis and results generated by this second phase of the study.

MATERIALS

Aggregate

The aggregate used in both mixes (asphalt concrete and asphalt-rubber concrete) was made up of crushed limestone and field

D. M. Hoyt and R. L. Lytton, Texas Transportation Institute, Texas A&M University, College Station, Tex. 77843. F. L. Roberts, National Center for Asphalt Technology, Auburn University, Auburn, Ala. 36849.

sand and was blended to meet the 1977 Federal Aviation Administration (FAA) aggregate grading specification for pavements with a bituminous surface course that will accommodate aircraft with gross weights of 60,000 lb or more or with tire pressures of 100 psi or more (*4*). The maximum particle size was ½ in. (100% passing the ½-in. sieve and some retained on the ⅜-in. sieve).

Asphalt Concrete Control Mix

The asphalt concrete control mix was prepared with an AC-10 lab standard binder (American Petrofina). A Marshall mix design was performed according to the Asphalt Institute's MS-2 (*5*) with results as follows:

Property	Design Criterion	% Binder
Unit weight	maximum	5.30
Marshall stability	maximum	4.82
Air voids (%)	median of 3–5	4.41
Optimum	numerical average	4.84

For a binder content of 4.8 percent, the properties of the asphalt concrete mix as determined from the mix design curves were as follows:

Property	Value of the Mix	Value Specified in Design Procedures
Unit weight (lb/ft³)	151	—
Marshall stability (lb)	2,300	minimum = 1,500
Air voids (%)	3.0	3 to 5
Voids in mineral aggregate (%)	13	minimum = 15
Flow (0.01 in.)	8.8	8 to 16

It can be seen that the voids in mineral aggregate (VMA) of the asphalt concrete mix are below the design specification. However, the mix meets the other mix design criteria (*5*). The mix was accepted with a low VMA because the limestone aggregate had previously been used in many successful mixes.

Asphalt-Rubber Concrete

The name *asphalt rubber* has been given to a blend of asphalt paving cement and ground tire rubber which is formulated at an elevated temperature to promote chemical as well as physical bonding of the two component materials. Rubber content

of the blend is between 18 and 25 percent by total weight of the blend (6).

The asphalt-rubber binder used for this study was obtained from a Texas State Department of Highways and Public Transportation road project. The binder was produced by the Arizona Refining Company and was a mixture of 77 percent AC-10 asphalt cement, 20 percent rubber, and 3 percent extender oil. The rubber was a blend of several types of ambient temperature grind, vulcanized whole tire rubber: 40 percent Baker CR40, 20 percent Baker C107, 30 percent Genstar C106, and 10 percent Genstar C112. The rubber gradation included particle sizes between the No. 16 and No. 200 sieves, with 37.5 percent of the rubber particles being retained on the No. 30 sieve. As discussed in an earlier report on this research (1), the aggregate blend used in the asphalt-rubber concrete mix should be adjusted to account for the rubber particles. However, in this case, the change in the aggregate blend due to this correction was smaller than the anticipated variation in the aggregate gradation itself. Therefore no adjustment was made and the same aggregate blend was used for both mixes.

A Marshall method mix design, modified for asphalt-rubber binder as described in an earlier report on this study (1), was performed on the asphalt-rubber concrete. However, the air void contents in the Marshall samples of the asphalt-rubber concrete were too high to meet the Marshall design criterion for air voids. This occurrence is consistent with difficulties experienced by earlier researchers in compacting asphalt-rubber materials in the laboratory (1). Therefore, the air void content requirement for the asphalt-rubber concrete was relaxed to 6 to 8 percent to allow the study to continue. At this time, it is not known whether the higher air void content will adversely affect the oxidation and aging rates of an asphalt-rubber concrete as it does with asphalt concretes with high air void contents. Also, it is possible that a lower air void content can be attained during field compaction with higher laydown temperatures and/or greater compaction efforts than those used for asphalt concrete.

The optimum binder content for the asphalt-rubber concrete is:

Property	Design Criterion	% Binder
Unit weight	maximum	4.88
Marshall stability	maximum	4.05
Air voids (%)	median of 3–5	5.27
Optimum	numerical average	4.73

Thus, the binder contents for the two mixes were close enough to each other to be considered the same. This does not usually occur, and separate mix designs need to be performed for the two materials.

For a binder content of 4.7 percent, the properties of the asphalt-rubber concrete mix as determined from the mix design curves were as follows:

Property	Value of the Mix	Value Specified in Design Procedures
Unit weight (lb/ft³)	145	—
Marshall stability (lb)	2,200	minimum = 1,500
Air voids (%)	7.5	6 to 8 (see above)
Voids in mineral aggregate (%)	16	minimum = 15
Flow (0.01 in.)	7.3	8 to 16

The density of the asphalt-rubber concrete mix is seen to be about 6 lb/ft³ less than that of the asphalt concrete mix. This is largely due to the relaxed air void content requirement for the asphalt-rubber concrete.

LABORATORY TESTS

Laboratory tests were performed on the asphalt concrete control material at optimum binder content (AC) and on the asphalt-rubber concrete at optimum binder content and at +0.5 percent binder content (ARC-low, ARC-medium, and ARC-high).

Marshall Stability

Marshall stabilities were measured on the two materials as part of the mix design process. The maximum Marshall stabilities for both mixes were almost the same (about 2,300 lb), but the maximum for the asphalt concrete control mix occurred at a higher binder content (about 4.8 percent) than that of the asphalt-rubber concrete (about 4.1 percent). The shapes of the stability vs. binder content plots were similar, indicating that the materials were about equally sensitive in stability to changes in the binder content.

Resilient Modulus

Resilient modulus was measured on each material, and curves of resilient modulus vs. temperature were plotted. The modulus of the asphalt concrete control was slightly more sensitive to temperature change than that of the asphalt-rubber concrete.

Fatigue

To study the fatigue characteristics of the materials, a third-point bending test was used on beam specimens. Plots of strain vs. cycles to failure were generated. Regression lines were fitted and fatigue parameters were calculated according to the familiar fatigue equation:

$$N_f = K_1(1/\varepsilon_t)^{K_2} \tag{1}$$

where

N_f = number of load applications to failure,
ε_t = tensile strain induced, and
K_1, K_2 = regression constants.

Two sets of regression equations, as shown in Table 1, were generated to describe the variation of the fatigue parameters with temperature for each material. These equations predict longer laboratory fatigue lives for the asphalt-rubber concrete than for the asphalt concrete.

It has been shown that the fatigue life of a material during laboratory testing is less than that experienced by the same material in the field (7). The difference between laboratory and field fatigue lives can be accounted for by applying a multiplier to the laboratory value of K_1. Finn et al. (8) suggested a multiplier of 13 after looking at data for asphalt

TABLE 1 REGRESSION EQUATIONS TO PREDICT
FATIGUE PARAMETERS FOR ANY TEMPERATURE
(°F) FOR MATERIALS AT OPTIMUM BINDER
CONTENTS

$\lfloor\log K_1\rfloor$ vs. log T (°F)	
Material	Regression Equation
AC	$\lfloor\log K_1\rfloor = 14.630 - 4.558 \log T$
ARC-Medium	$\lfloor\log K_1\rfloor = 20.483 - 7.879 \log T$
K_2 vs. log K_1	
Material	Regression Equation
AC	$K_2 = 1.512 - 0.280 (\log K_1)$
ARC-Medium	$K_2 = 1.900 - 0.243 (\log K_1)$

Note: Generated from laboratory data.

TABLE 2 AVERAGE VALUE OF CRACK SPEED INDEX
FOR EACH MATERIAL AT EACH TEST TEMPERATURE

Material	Temperature (°F)	Crack Speed Index
AC	34	-1.223
	77	-5.054
ARC-Low	34	2.474
	77	-4.476
ARC-Medium	34	-2.288
	77	-0.740
ARC-High	34	-1.408
	77	---

concrete from the AASHO road test. The multiplier of 13
was used to estimate field fatigue for all materials in this
project, but it may not be accurate for all types of materials.
A means has been developed at Texas A&M University to
derive the K_1 multiplier from laboratory data (9), but tests
on healing would have been necessary to perform this analysis
on the materials in this study.

Fracture

The Texas Transportation Institute overlay tester was used
to investigate the fracture properties of the materials. The
overlay tester opens a crack of controlled width at the bottom
of a beam specimen. Repeated cycles drive the crack pro-
gressively upward through the beam. The load, P, and the
length of the crack up into the beam, c, are measured.

The fracture of asphaltic concrete obeys a law of fracture
mechanics known as Paris's law (10). Although it originally
was an empirically derived relation, it has subsequently been
derived from first principles of mechanics by Schapery (11).
The fracture constants A and n, which can be calculated from
the results of the overlay test, appear in Paris's law:

$$dc/dN = A(\Delta K)^n \tag{2}$$

where

c = crack length,
N = number of load cycles,
dc/dN = crack speed, or rate of growth of the crack,
ΔK = change of stress intensity factor during load
application,
A = fracture coefficient, and
n = fracture exponent.

Empirically, it has been found that the sum of $\log_{10} A$ and
n, called the crack speed index, is an indicator of the relative
effectiveness of materials in resisting cracking. A lower crack
speed index indicates greater effectiveness at reducing crack-
ing. The average values of crack speed index for each material
are shown in Table 2. On this basis, the ranking of the mate-

rials for fracture resistance at low temperature (34°F) from
best to worst is: ARC-medium, ARC-high, AC, ARC-low.
At moderate temperature (77°F), one of the two high-binder-
content asphalt-rubber concrete samples proved defective and
therefore this material was not evaluated. Of the other mate-
rials, their order from best to worst fracture resistance was
as follows: AC, ARC-low, ARC-medium. The results indicate
that, with respect to the fracture resistance, the asphalt-rubber
concrete with medium (optimum) binder content performed
best at low temperature (34°F) but the asphalt concrete per-
formed best at moderate temperature (77°F).

Creep

Creep tests were performed on cylindrical samples, and creep
compliances were calculated. Averages of the compliances at
each test temperature were fitted with a curve of the form:

$$D(t) = D_1 t^m \tag{3}$$

The degree to which the resulting constants change with tem-
perature is an indicator of the relative temperature suscep-
tibility of the material. In order to numerically compare the
temperature susceptibilities, a time-temperature shift prop-
erty was calculated for each material. A "master" creep curve
was created by shifting the average creep compliance curves
horizontally parallel to the time axis until each one lined up
with the curve for 70°F, the reference temperature. The amount
of the time shift for each temperature was expressed as a
ratio, a_T, as follows:

$$a_T = t/(t_{T_0}) \tag{4}$$

where

t_{T_0} = time at which a given compliance is reached when
the material is at the reference temperature, and
t = time at which the same compliance is reached when
the material is at some other temperature.

TABLE 3   TIME-TEMPERATURE SHIFT CONSTANTS FOR EACH
MATERIAL AT EACH TEST TEMPERATURE

Material	Temperature (°F)	$\log_{10} a_T$	Time-Temperature Shift Constants C_1	C_2
AC	40	2.25	6.75	120
	70	0.0		
	100	-1.35		
ARC-Low	40	2.65	3.76	72.6
	70	0.0		
	100	-1.10		
ARC-Medium	40	2.70	2.70	60.0
	70	0.0		
	100	-0.9		
ARC-High	40	2.4	2.40	60.0
	70	0.0		
	100	-0.80		

One commonly used function that can be fitted to the curves of $\log_{10} a_T$ vs. temperature is the "WLF equation" (*12*):

$$\log_{10} a_T = \frac{-C_1(T - T_0)}{(C_2 + T - T_0)} \qquad (5)$$

where

C_1, C_2 = materials constants; the constant C_1 is the temperature susceptibility constant.
T_0 = the master curve temperature; 70°F, in this case.
T = any other temperature.

The values of the temperature shift constants for the materials in this study are shown in Table 3. On the basis of the WLF equation and the constant c_1, the materials in this study can be ranked in order of increasing temperature susceptibility in creep behavior: ARC-high, ARC-medium, ARC-low, AC. Thus, the results of the creep testing indicate that the rubber helps the material to maintain a more stable compliance (or modulus) during temperature changes.

Permanent Deformation

Repeated load tests as described in the VESYS manual (*13*) were performed on cylindrical samples in order to obtain permanent deformation parameters for the prediction of rutting behavior. A three-parameter equation was generated to describe the shape of the permanent strain vs. cycles curves:

$$\varepsilon_a = \varepsilon_o \, e^{-(\rho/N)^\beta} \qquad (6)$$

where

ε_a = permanent (accumulated) strain,
N = loading cycle, and
ε_o, ρ, and β = calculated parameters.

This equation describes an S-shaped curve.

The permanent deformation parameters were sensitive to several factors, including stress level and temperature, during testing. Therefore, an adjustment had to be applied to the permanent deformation parameters from the laboratory results before they were used to predict field behavior. The adjustment procedure is described in an earlier project report (*3*). The adjusted values of permanent deformation parameters were plotted vs. temperature.

The permanent deformation parameters calculated from the laboratory tests for the mixes at optimum binder contents are shown in Table 4. If the values generated from the laboratory results are used in Equation 6, then the equation predicts that at low temperature (40°F) and at high temperature (100°F) the asphalt-rubber concrete would experience less strain under a given number of loadings than would the asphalt concrete. Thus, it appears as though the addition of rubber causes the material to become more resistant to permanent deformation at low and at high temperatures. At moderate temperature (70°F), however, the asphalt concrete is predicted to be less susceptible to permanent deformation at high numbers of cycles.

TABLE 4 PERMANENT DEFORMATION PARAMETERS FROM LABORATORY
TESTS FOR MATERIALS AT OPTIMUM BINDER CONTENTS

Material	T(°F)	ϵ_o	ρ	β	ϵ_o/ϵ_r	Regression
AC	40	0.0187E+0	1.1539E16	0.0637	1,662	Nonlinear
	70	0.8232E-3	0.9817E04	0.2070	27.44	Linear
	100	0.9355E+0	6.3750E16	0.0591	31,509	Nonlinear
ARC-Medium	40	0.0181E+0	3.4514E16	0.0645	1,445	Nonlinear
	70	0.0238E+0	2.8904E16	0.0524	544	Nonlinear
	100	0.0588E+0	2.5023E16	0.0560	1,680	Nonlinear

DESIGN DATA

A comparative analysis of the materials was performed by selecting a structural model and environmental and loading conditions and by putting this information along with material parameters obtained from the laboratory tests into the modified ILLIPAVE pavement analysis program (*14*).

Airport Type and Traffic

Asphaltic materials are typically used as surface layer materials at medium to small civil airports. Therefore, the Robert Mueller Municipal Airport in Austin, Texas, was selected as an appropriate airport model for this study.

Total numbers of aircraft using the Austin airport between 1969 and 1981 were known, and projections were available for 1985 and 1990 (*15*). Five air carriers were included in the traffic: DC-9, DC-10, B-727, B-737, and B-757. The total yearly traffic for each aircraft, as summarized in Table 5, was divided by 365 to obtain an estimate of daily traffic. This was then multiplied by a wander factor to account for lateral wan-

der of the aircraft. The wander factors used in this study were computed by Brent Rauhut Engineering, Inc. (*15*), generally following a procedure by Ho-Sang (*16*) which assumes that the lateral movement of each aircraft type over the width of the runway is normally distributed. The wander factors are shown in Table 6.

Previous research has shown that the contact pressures against a pavement can be much higher than the tire inflation pressure (*14*). This can greatly increase the pavement damage caused by heavy vehicles, thus greatly reducing pavement life. Therefore, an attempt was made to estimate the contact pressures of the aircraft. A previously calculated pressure distribution (*17*) for a 32 × 8.8 Type VII aircraft tire was used as a model, and similar pressure distributions along the width centerline of the tire were calculated for each aircraft in the traffic pattern.

Pavement Structure

A typical pavement section was chosen from the main runway at the Austin municipal airport, and material properties were

TABLE 5 SUMMARY OF AIRCRAFT TRAFFIC DATA FROM
THE AVIATION DEPARTMENT, AUSTIN, TEXAS

	Aircraft Type				
Year	DC-9	DC-10	B-727	B-737	B-757
1969	32,660				
1971	17,410		2,176	2,176	
1974	2,570		15,430	7,710	
1976	1,870		11,230	5,610	
1981	5,200		31,200	15,600	
1985	2,910	580	36,670	17,460	580
1990	3,100	3,100	37,200	15,500	3,100

TABLE 6 SUMMARY OF AIRCRAFT TRAFFIC WANDER FACTORS FOR EACH AIRCRAFT CONSIDERED IN PAVEMENT EVALUATION

Aircraft	Wander Factor[a]
B-727	0.77
B-737	0.57
B-757	0.61
DC-9	0.68
DC-10	0.72

[a] Wander Factor is the inverse of the Pass-to-Coverage Ratio
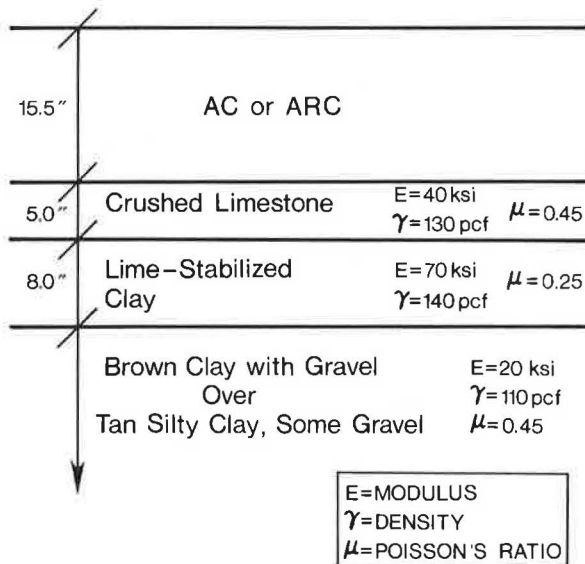
FIGURE 1 Schematic of pavement structure used for the modified ILLIPAVE performance analysis.

estimated for the underlying layers. Material characterizations obtained from the laboratory testing were used for the top bituminous layer. Figure 1 shows the typical section.

Seasonal Temperatures

Because asphaltic materials are temperature sensitive, the analysis was performed using four climatic zones of four seasons each. Seasonal average temperatures were used and are shown in Table 7.

COMPUTER ANALYSIS

Modified ILLIPAVE Computer Program

The computer program used in this analysis was the third in a series of programs developed to analyze the stresses, strains,

TABLE 7 AVERAGE SEASONAL TEMPERATURE FOR EACH OF FOUR SEASONS FOR EACH CLIMATIC ZONE

Zone	Temperature, °F			
	Winter	Spring	Summer	Fall
Wet-Freeze	35	65	95	60
Wet-No Freeze	75	95	105	95
Dry-Freeze	35	60	90	50
Dry-No Freeze	55	75	95	75

and displacements in a pavement under repeated loads. The original program was developed by Duncan et al. (*18*). The program was revised at the University of Illinois (19) and was renamed ILLIPAVE. The program was then obtained and revised by Texas A&M University (*14*) and provides for multiple tires on one or two axles, nonuniform vertical and horizontal contact pressure distributions on circular loaded areas, and all of the nonlinear stress-strain curve capabilities available in the two previous programs. This program predicts rut depth and fatigue cracking.

Mixed-Traffic Damage Evaluation: Comparison of Mixes

Computer runs were made for every combination of aircraft, climatic zone, and material using the modified ILLIPAVE computer program. For any particular computer run, one aircraft was considered as making up the entire traffic count. Then calculations were performed on the totals for each of the damage criteria (cracking and rutting) to produce damage totals for the mixed-traffic condition (*3*). A 20-year period was analyzed.

Rutting was chosen as the critical failure mode because the cracking indices that predict field cracking behavior never got very large. A rut depth of 0.7 in. was chosen as the comparative level. This is a large rut depth for an airport runway,

but it allowed a better comparison between materials in the climates with large temperature ranges than a smaller rut depth would have.

A cracking index of 0.2 (adjusted to the field fatigue condition) was chosen as a comparison level, but not as a failure index. A pavement with this level of cracking index would exhibit low-severity fatigue cracking with few of the cracks being interconnected and none of them being spalled.

In every combination of type of damage and climatic zone, the modified ILLIPAVE program predicted that the asphalt-rubber concrete would experience less damage and therefore would perform better than the asphalt concrete control material.

Predicted Cracking

For all four climatic zones, the predicted field cracking index was highest for the asphalt concrete control and lowest for the asphalt-rubber concrete with medium (optimum) binder content. This means that the asphalt concrete pavement would be expected to crack earlier than the asphalt-rubber concrete pavement. Of the four environmental zones, the wet non-freeze zone displayed the greatest difference between the predicted cracking performances of the control vs. the rubberized materials. Also, the predicted field cracking indices for all

materials were the highest in this zone, which had three hot seasons (> 90°F). This indicates that the predicted cracking behavior of all four mixes was most susceptible to hot temperatures, with the asphalt concrete mix being the worst case. Table 8 is a tabulation of the calculated 20-year field damage indices that illustrate these observations. Figure 2 shows plots of calculated field cracking index vs. time (years) for all four materials in two of the climatic zones.

Predicted Rutting

The modified ILLIPAVE program predicted that all four of the materials considered would reach a rut depth of at least 0.5 in. during the 20-year analysis period. The years in which each material reached 0.5-in. predicted rut depth and the comparison level of 0.7-in. predicted rut depth are shown in Table 9. Figure 3 shows plots of calculated rut depth vs. time (years) for all four materials in two of the climatic zones.

For all four climatic zones, the modified ILLIPAVE program predicted that the asphalt concrete would experience the largest rut depths and the asphalt-rubber concrete, optimum (medium) binder content, would experience the smallest rut depths. The difference between the predicted rut depths of the control and the rubber material was greatest in the wet

TABLE 8 FIELD CRACKING INDICES FOR COMBINED TRAFFIC AT 20 YEARS

Zone (Temperatures, °F)	Material	Cracking Index (Field, 20 Years)
Wet-Freeze	AC	0.21
(35-65-95-60)	ARC-Low	0.07
	ARC-Medium	0.04
	ARC-High	0.05
Dry-Freeze	AC	0.16
(35-60-90-50)	ARC-Low	0.06
	ARC-Medium	0.03
	ARC-High	0.04
Wet-No Freeze	AC	0.83
(75-95-105-95)	ARC-Low	0.15
	ARC-Medium	0.10
	ARC-High	0.11
Dry-No Freeze	AC	0.35
(55-75-95-75)	ARC-Low	0.13
	ARC-Medium	0.06
	ARC-High	0.07

DRY-FREEZE
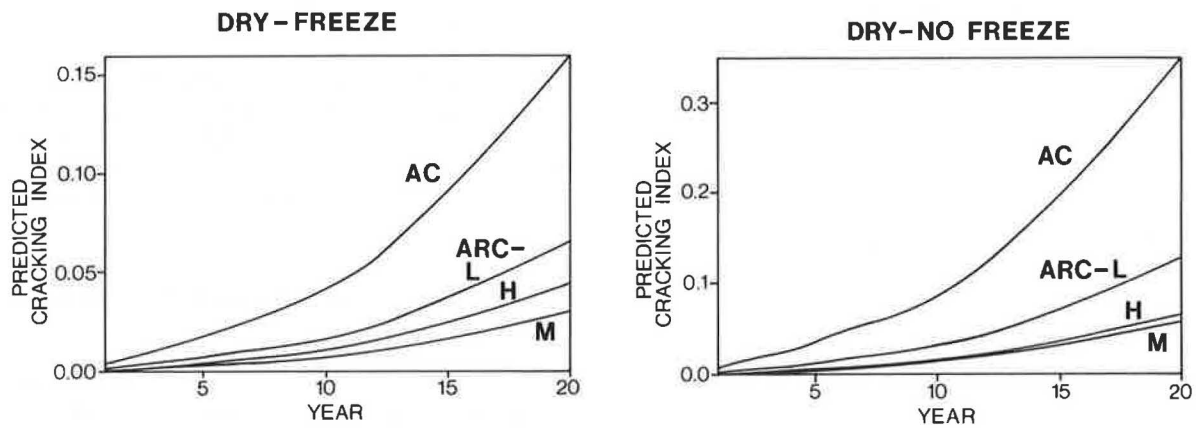
DRY-NO FREEZE

FIGURE 2 Plots of predicted field cracking index for combined traffic vs. year, for all four mixes, in two climatic zones.

nonfreeze zone, and the difference was very small and probably would be considered insignificant for the dry nonfreeze zone. Therefore, it could be concluded that the asphalt concrete or the asphalt-rubber concrete would perform equally well as pavement materials in moderate temperatures, but that at hot or cold temperatures the asphalt-rubber concrete would be considerably more resistant to permanent deformation than the asphalt concrete.

TABLE 9   TIMES TO RUT DEPTHS OF 0.5 IN. AND 0.7 IN. FOR COMBINED TRAFFIC AND FOR VARIOUS MATERIALS AND CLIMATIC ZONES

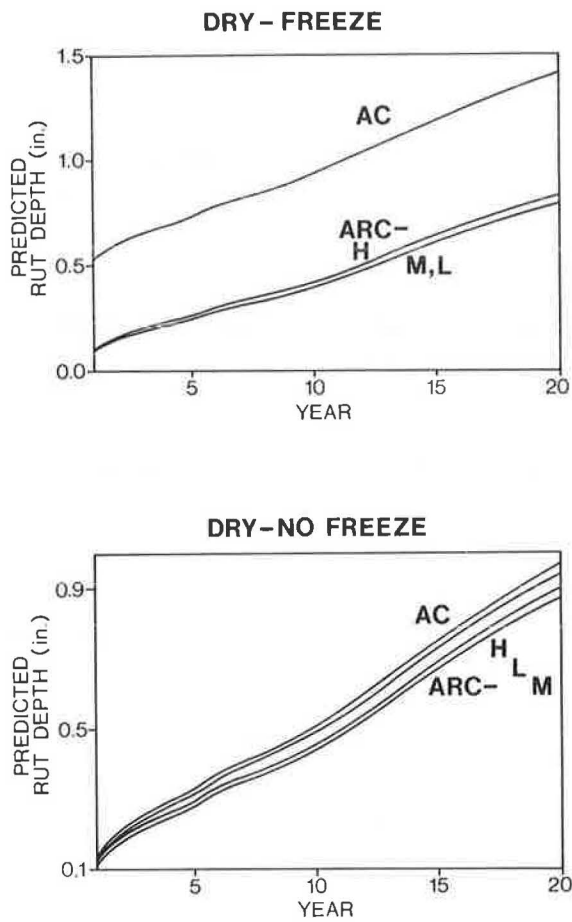| ZONE (Seasonal Temperatures, °F)	MATERIAL	YEAR (First Rut Depth ≥ 0.50 in.)	FIELD CRACKING INDEX	YEAR (First Rut Depth ≥ 0.70 in.)	FIELD CRACKING INDEX
Wet/Freeze	AC	01	0.006	04	0.020
(35-65-95-60)	ARC-Low	12	0.024	17	0.050
	ARC-Med.	13	0.016	17	0.027
	ARC-High	12	0.018	17	0.038
Dry/Freeze	AC	01	0.004	05	0.017
(35-60-90-50)	ARC-Low	13	0.028	18	0.054
	ARC-Med.	13	0.013	18	0.025
	ARC-High	12	0.016	17	0.033
Wet/No Freeze	AC	01	0.019	01	0.019
(75-95-105-95)	ARC-Low	09	0.031	13	0.062
	ARC-Med.	11	0.031	15	0.060
	ARC-High	08	0.020	13	0.045
Dry/No Freeze	AC	10	0.086	15	0.201
(55-75-95-75)	ARC-Low	11	0.034	16	0.083
	ARC-Med.	12	0.020	16	0.038
	ARC-High	11	0.020	15	0.038

DRY – FREEZE

DRY – NO FREEZE

FIGURE 3   Plots of predicted rut depth for combined traffic vs. year, for all four mixes, in two climatic zones.

COST-EFFECTIVENESS COMPARISON

Approximate costs for asphalt concrete and for asphalt-rubber concrete were estimated for the materials compacted in place. A cost-effectiveness analysis was then performed for each of the mixes. Because the material used in the surface layer was the only difference between the pavements analyzed, the cost-effectiveness of that layer was analyzed.

Cost Data

Cost estimates for asphalt-rubber concrete were based on (1) the cost of producing the asphalt-rubber binder and (2) substitution of the cost of the asphalt-rubber binder for the cost of the asphalt cement in asphalt concrete unit prices. An additional 10 percent was added to the cost of haul, laydown, and compaction for the asphalt-rubber concrete over that cost for the asphalt concrete to account for higher temperatures or greater compactive effort possibly required for compaction of the asphalt-rubber concrete. An industry-supplied price of $100 per ton, delivered to the batch plant, was used for the asphalt cement. A price of $370 per ton was used for the asphalt-rubber binder; this was based on a binder containing 18 percent rubber, 82 percent asphalt

cement, and no cutback, for a job using 1,000 tons or more of the binder material.

Approximate in-place component costs for hot mixes made with asphalt cement binder and asphalt-rubber binder are given in Table 10. Using an asphalt-rubber binder increased the cost of the concrete by 50 percent. Most of this cost increase was related to production of the asphalt-rubber binder.

Cost-Effectiveness Analysis Based on Projected Lives of Pavements

Rutting was chosen as the type of pavement distress that controls the useful lives of the pavement surface layers. As discussed above, a limiting rut depth of 0.7 in. was set, and predicted pavement lives were determined.

The steps in the cost comparison were as follows:

1. Determine the construction cost of each paving material in place per square yard.
2. Determine the equivalent uniform annual cost per square yard of each pavement over its predicted life.
3. Select the most cost-effective material in each climatic zone as the one that provides the least equivalent uniform annual cost per square yard for the life of the pavement.

The equivalent uniform annual cost per square yard is the annual cost per square yard that, if paid annually over the life of the pavement, has a present value equal to the in-place cost per square yard of construction of the asphaltic surface layer. It includes only the cost of construction distributed uniformly over the expected life of the pavement. It does not include the cost of maintenance or rehabilitation of the pavement or the costs to the user while these activities are being carried out. Because these are largely unknown for asphalt-rubber concrete pavements, it was assumed for the purposes of this cost-effectiveness analysis that they are roughly proportional to the equivalent uniform annual cost of construction and that a comparison of these would provide a rational means of selecting the preferable material in each climatic zone.

The interest rate that was used in calculating the equivalent uniform annual cost was 4.0 percent. This was considered to be a reasonable estimate of the difference between actual interest and actual inflation rates as applied to construction.

Construction Cost per Square Yard

The following steps were followed for the determination of the in-place construction cost per square yard for the asphaltic surface layer:

1. Using the compaction curves from the Marshall mix designs, determine the in-place density of each of the four materials.
2. Determine the tons per square yard of each material.
3. Determine the cost per square yard of each material in place.

The results of these determinations are shown in Table 11.

TABLE 10 UNIT COST PER TON OF MATERIAL IN PLACE FOR ASPHALT
CONCRETE AND ASPHALT-RUBBER CONCRETE

| | Asphalt Cement | | Asphalt-Rubber Cement Binder | | | | | |
| | Binder | | Low Binder | | Medium Binder | | High Binder | |
Component	$/Ton	%	$/Ton	%	$/Ton	%	$/Ton	%
Binder[a]	4.80	16.3	15.65	36.5	17.50	38.8	19.35	41.0
Aggregate	8.85	30.1	8.85	20.6	8.85	19.7	8.85	18.7
Energy Costs	1.28	4.4	1.28	3.0	1.28	2.8	1.28	2.7
Mixing	3.51	11.9	3.51	8.2	3.51	7.8	3.51	7.4
Haul, Laydown and Compaction[b]	5.92	20.1	6.51	15.2	6.51	14.4	6.51	13.8
Miscellaneous	0.66	2.2	0.66	1.5	0.66	1.5	0.66	1.4
Mark-Up (15%)	4.42	15.0	6.43	15.0	6.76	15.0	7.09	15.0
TOTALS	29.44	100.0	42.89	100.0	45.07	100.0	47.25	100.0

[a] 4.8% - Asphalt Cement Binder; 4.23% - Low Asphalt-Rubber Cement Binder;
4.73% - Medium Asphalt-Rubber Cement Binder; 5.23% - High Asphalt-Rubber
Cement Binder. Asphalt Cement at $100 per ton, and Asphalt-Rubber Cement
at $370 per ton, at the batch plant.

[b] 10% added to cost for compaction of Asphalt-Rubber Concrete due to
anticipated increase in compaction temperature and/or compactive effort
over that required for Asphalt Concrete.

TABLE 11 IN-PLACE COSTS FOR ASPHALT CONCRETE AND ASPHALT-RUBBER
CONCRETE

	Percent Binder	In-Place Costs per ton, $/Ton	Density, lb/ft	Tons per Square Yard, T/S.Y.	In-Place Costs per Square Yd., $/S.Y.
Asphalt Concrete	4.80	29.44	151.2	0.851	25.04
Asphalt-Rubber Concrete					
Low Binder	4.23	42.89	144.8	0.815	34.93
Medium Binder	4.73	45.07	145.3	0.817	36.84
High Binder	5.23	47.25	144.9	0.815	38.51

TABLE 12 EQUIVALENT UNIFORM ANNUAL CONSTRUCTION COSTS FOR ASPHALT
CONCRETE AND ASPHALT-RUBBER CONCRETE

| | | 0.5 in. Rutting | | 0.7 in. Rutting | |
Material	Climatic Zone (Temperature, °F)	Age, Years	Cost[a] per Square Yard per Year	Age, Years	Cost[a] per Square Yard per Year
AC	Wet-Freeze	1	25.04	4	6.63
ARC-Low	(35-65-95-60)	12	3.58	17	_2.76_
ARC-Medium		13	_3.55_	17	2.91
ARC-High		12	3.95	17	3.04
AC	Dry-Freeze	1	25.04	5	5.41
ARC-Low	(35-60-90-50)	13	_3.36_	18	2.65
ARC-Medium		13	3.55	18	2.80
ARC-High		12	3.95	17	3.04
AC	Wet-No Freeze	1	25.04	1	25.04
ARC-Low	(75-95-105-95)	9	4.52	13	3.36
ARC-Medium		11	_4.04_	15	_3.19_
ARC-High		8	5.50	13	3.71
AC	Dry-No Freeze	10	_2.97_	15	_2.17_
ARC-Low	(55-75-95-75)	11	3.83	16	2.88
ARC-Medium		12	3.77	16	3.04
ARC-High		11	4.23	15	3.33

[a] Most cost effective choices in each climatic zone are underlined.

Equivalent Uniform Annual Cost per Square Yard of Materials in Place

The formula for the equivalent uniform annual cost per square yard is

$$\frac{EUAC}{SY} = \frac{(PV/SY)(i)}{(1 + i)\,[1 - (1 + i)^{-n}]} \qquad (7)$$

where

$EUAC/SY$ = equivalent uniform annual cost per square yard;

PV/SY = the "present value" or construction cost per square yard;

i = effective interest rate, which is assumed to be the difference between the actual interest and the actual inflation rates, in percent divided by 100; and

n = useful pavement life in years.

Two comparisons are shown in Table 12, one for a critical rut depth of 0.5 in. and one for a critical rut depth of 0.7 in. The most cost-effective material to use depends, not surprisingly, on the climatic zone and the level of the critical rut depth. The low or medium (optimum) binder content asphalt-rubber concretes are predicted to be more cost-effective than the asphalt concrete in every climatic zone except the dry nonfreeze zone.

CONCLUSION

The use of asphalt-rubber concrete for municipal airport pavements appears to be justified on the basis of its expected cost-effectiveness in three of the four unique climatic zones in the United States that were included in this study, excluding only the dry-no freeze zone. Production and construction practices may need to be altered to account for higher temperatures

or increased compaction effort which may be required to properly mix and place ARC.

ACKNOWLEDGMENTS

REFERENCES

1. F. L. Roberts, R. L. Lytton, and D. M. Hoyt. *Criteria for Asphalt-Rubber Concrete in Civil Airport Pavements: Mixture Design.* Final Report DOT/FAA/PM-86/39, Federal Aviation Administration, Washington, D.C., July 1986.
2. F. L. Roberts and R. L. Lytton. FAA Mixture Design Procedure for Asphalt-Rubber Concrete. Presented at 66th Annual Meeting of the Transportation Research Board, Washington, D.C., 1987.
3. D. M. Hoyt, R. L. Lytton, and F. L. Roberts. *Criteria for Asphalt-Rubber Concrete in Civil Airport Pavements: Evaluation of Asphalt-Rubber Concrete.* Final Report DOT/FAA/PM-86/39, II, Federal Aviation Administration, Washington, D.C., 1987.
4. Bituminous Surface Course. In *Standards for Specifying Construction of Airports — New Standard for Plant Mix Bituminous Material.* Advisory Circular No. 150/5370-10, Item P-401. Federal Aviation Administration, Washington, D.C., 1977.
5. *Mix Design Methods for Asphalt Concrete and Other Hot-Mix Types. Manual Series No. 2 (MS-2).* The Asphalt Institute, College Park, Md., 1984.
6. T. S. Shuler, R. D. Pavlovich, and J. A. Epps. Field Performance of Rubber Modified Asphalt Paving Materials. Presented at 64th Annual Meeting of the Transportation Research Board, Washington, D.C., 1985.
7. D. N. Little, A. H. Al-Balbissi, C. Gregory, and B. Richey. *Design and Characterization of Paving Mixtures Based on Plasticized Sulfur Binders—Engineering Characterization.* Final Report RF 4247. Texas Transportation Institute, Texas A&M University, College Station, 1984.
8. F. Finn, C. Saraf, R. Kulkarni, K. Nair, W. Smith, and A. Abdullah. The Use of Distress Prediction Subsystems for the Design of Pavement Structures. In *Proc., 4th International Conference on the Structural Design of Asphalt Pavements,* Vol. 1. University of Michigan, Ann Arbor, 1977, pp. 3–38.
9. A. H. Al-Balbissi. *A Comparative Analysis of the Fracture and Fatigue Properties of Asphalt Concrete and Sulflex.* Ph.D. dissertation. Texas A&M University, College Station, 1983.
10. P. C. Paris and F. Erdogan. A Critical Analysis of Crack Propagation Laws. In *Transactions of the ASME. Journal of Basic Engineering,* Ser. D., Vol. 85, No. 3, 1963.
11. R. A. Schapery. *A Theory of Crack Growth in Viscoelastic Media.* Technical Report No. MM 2764-73-1. Mechanics and Materials Research Center, Texas A&M University, College Station, 1973.
12. M. L. Williams, R. F. Landel, and J. D. Ferry. Visco-Elastic Properties of Polymers. In *Journal of the American Chemical Society,* Vol. 77, 1955, p. 3701.
13. W. J. Kenis. *Predictive Design Procedures, VESYS Users' Manual—An Interim Design Method for Flexible Pavement Using the VESYS Structural Subsystem.* Final Report No. FHWA-RD-77-154. Federal Highway Administration, Washington, D.C., 1978.
14. F. L. Roberts, J. T. Tielking, D. Middleton, R. L. Lytton, and K. Tseng. *Effects of Tire Pressures on Flexible Pavements.* Research Report No. 372-1F. Texas Transportation Institute, Texas A&M University, College Station, 1985.
15. Brent Rauhut Engineering, Inc. *Runway and Taxiway Pavement Evaluations: Robert Mueller Municipal Airport, Austin, Texas.* Final Report for the City of Austin Aviation Department, 1982.
16. V. Ho-Sang. *Field Survey and Analysis of Aircraft Distribution on Airport Pavements.* Final Report. Federal Aviation Administration, Washington, D.C., 1975.
17. J. T. Tielking. A Tire Contact Solution Technique. In *Tire Modeling,* NASA Conference Publication 2264. Proceedings of a Workshop Held at Langley Research Center, Hampton, Va., September 1982, pp. 95–121.
18. J. M. Duncan, C. L. Monismith, and E. L. Wilson. Finite Element Analysis of Pavements. In *Highway Research Record 228.* HRB, Washington, D.C., 1968, pp. 18–33.
19. *ILLIPAVE User's Manual.* Transportation Facilities Group. Department of Civil Engineering, University of Illinois at Urbana-Champaign, 1982.

Measurement and Analysis of Truck Tire Pressures in Oregon

OK-KEE KIM AND CHRIS A. BELL

As axle loads have increased, the use of higher tire pressures has become more popular in the truck market. To collect data on tire pressures and types of tires in use, a survey was carried out at a weigh station located near Woodburn, Oregon, on Interstate 5 during the summer of 1986. The data show that 87 percent of the tires surveyed are of radial construction. The average measured pressures of radial and bias tires are 102 psi and 82 psi, respectively. The survey results show that the difference between the manufacturer's maximum recommended tire pressure and the measured tire pressure is very small, particularly for radial tires. Therefore, if government agencies wish to control tire pressures, it would be expedient to control the manufacturer's maximum recommended pressure rather than the inflation pressure used by truckers. This would ensure reasonable control, since the data collected in this study show that measured and recommended tire pressures are nearly equal. The survey results show that most tires are 11 in. wide with a rim diameter of 24.5 in. (i.e., 11/80 R 24.5 or 11-24.5) and the average tread depth of radial tires is slightly greater than that of bias tires.

The economics of truck transportation have contributed to an increase in the average gross weight of trucks such that the majority of trucks are operating close to the legal gross loads or axle loads (*1*). Many states, including Oregon (*2*), also issue permits for trucks to operate above normal legal load limits. As axle loads have increased, the use of radial tires with higher pressures has become more popular in the truck market to support the increased axle loads.

Higher tire inflation pressures decrease the contact area, resulting in reduced tire friction or reduced skid resistance and increased potential for pavement damage under the high stress. The higher tire pressures contribute to greater deformation in flexible pavements, manifested as high-severity wheel track rutting. Rutting results in hazardous pavements, since ruts create an uneven pavement where water and ice can accumulate in harsh weather. The higher tire pressures also tend to be accompanied by higher loads, and these will tend to increase the severity of fatigue cracking.

In order to determine the levels of tire pressures in use, a survey was carried out at a weigh station located on Interstate 5 during the summer of 1986 by the Oregon Department of Transportation (ODOT) and Oregon State University (OSU). This paper presents a part of the study on procedures for controlling the effect of increased tire pressure of trucks on asphalt pavement damage (*3*) performed by the ODOT and OSU. It describes existing operating characteristics of Ore-

gon's trucks, particularly levels of tire pressures and tire sizes, and analyzes the survey data.

BACKGROUND

Economic incentives that often exceed the expected costs of overweighting to the trucker are a major reason for increasing the cargo weight of trucks. The benefit to a trucker from increasing the load capacity of a truck is increased financial returns.

Table 1 indicates that the cash incentive to load 80,000 lb rather than 73,000 lb is $180, and the incentive increases as cargo weight increases (*4*). This results from decreasing costs per ton-mile as cargo weight increases. Figure 1 shows how costs per ton-mile decrease dramatically and costs per mile increase only slightly as the weight of the load increases. As the weight increases from 10 to 25 tons, the cost per ton-mile decreases 60 percent, whereas the cost per mile increases only 1.5 percent. Since fuel cost per mile traveled does not vary proportionately with the weights of trucks, as shown in the Mississippi and Oregon studies (*1*), the more a truck is loaded the greater the financial benefit.

Consequently, the economics of long-haul truck transportation have contributed to the increase in the average gross weight of trucks such that the majority of trucks are operating close to or above the legal gross loads or axle loads. In 1982, the federal government permitted 80,000 lb gross vehicle weight, 20,000 lb single-axle weights, and 34,000 lb tandem-axle weights on Interstate highways.

As axle loads have increased, so have tire pressures, due in part to attempts to decrease the contact area between the tire and the pavement, resulting in reduced rolling resistance of vehicles and, therefore, reduced fuel consumption. A recent study in Texas (*5*) indicates that trucks typically operate with tire pressures of about 100 psi in that state. A study by Roberts and Rosson (*6*) indicated that the contact pressure between the tire and pavement for a bias tire with an inflation pressure of 125 psi could be as high as 200 psi. That study showed that for legal axle loads, increasing the tire pressures from 75 to 125 psi for a bias-ply tire (10.00-20) can cut the life of the typical thin asphalt concrete pavements of Texas by 30 to 80 percent.

Thus, increased tire inflation pressures and axle load configuration are important factors to be considered in asphalt pavement design and rehabilitation strategies (particularly overlay design). Consideration of these factors could result in the refinement of paving mix design and pavement structure design methods, as well as in the

Department of Civil Engineering, Oregon State University, Corvallis, Oreg. 97331-2302.

TABLE 1 INCREMENTAL INCENTIVES TO OVERWEIGHT (4)

Vehicle Weight (lb)	Cargo Weight (lb)	Rate per Pound* ($)	Resulting Rate ($)	Incentive ($)
73,000	45,000	0.056	2520	0
75,000	47,000	0.054	2540	20
80,000	52,000	0.052	2700	180
90,000	62,000	0.050	3100	580
100,000	72,000	0.048	3460	940

*A typical rate $0.056; the decreases in rate per pound are given in an attempt to account for the rate reduction that might be offered by a trucker planning to overweight.
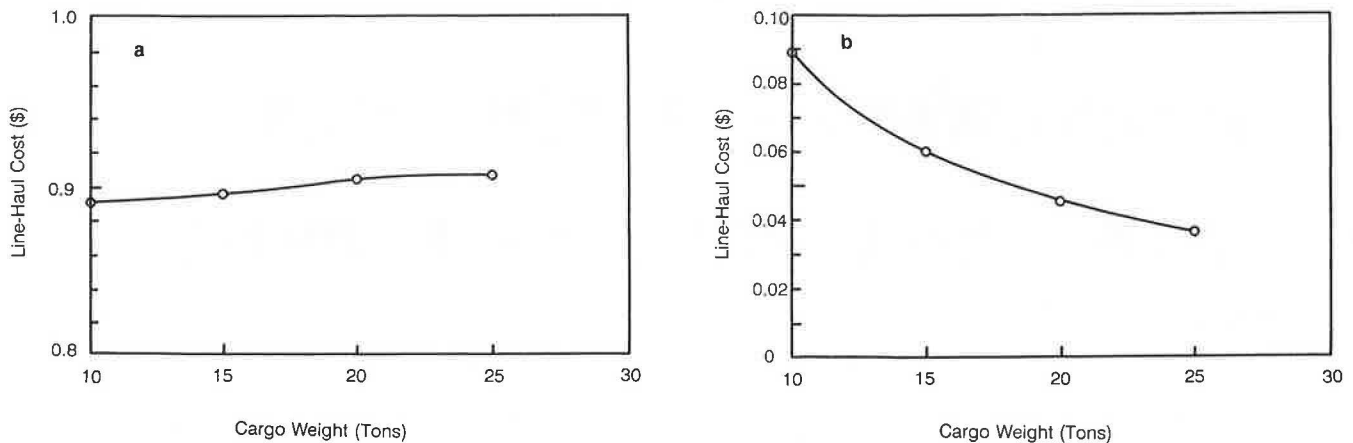

FIGURE 1 Cargo weight vs. line haul cost (4): (a) per mile; (b) per ton-mile.

adjustment of highway user costs. Also, highway maintenance schedules should be reviewed and the remaining life of the existing pavements constructed on the basis of truck tire pressures of about 80 psi.

RESULTS

A survey to evaluate tire inflation pressures and types of tires in use was carried out at a weigh station located near Woodburn, Oregon, on Interstate 5 from July 28 to July 30 and from August 25 to August 31, 1986. The data for each truck took about 15 to 30 min for two or three inspectors to collect, depending on the truck type. The survey was performed day and night for the above-mentioned period.

A tire pressure data collection sheet is shown in Figure 2. One data collection form represents one truck, and the form consists of four parts, as follows:

1. Basic data: date, time (start time and finish time), Public Utility Commission (PUC) safety inspection number, inspector, PUC plate number, and commodity;

2. Weather information, including air temperature and pavement temperature;

3. Truck classification used in Oregon's Weigh-in-Motion study;

4. Tire data: axle number, dual/single tire, tire manufacturer, tire construction (radial/bias), tire size, tread depth, and tire pressure [recommended maximum pressure (cold) by manufacturer, first and second measured tire pressure].

The tire manufacturer, tire construction, and tire size were read from the tire. As Middleton et al. (5) did in Texas, tire pressure was measured twice. The first measured pressure was the inflation pressure measured after the truck was stopped. The second pressure measurement was the last step of collecting the data. Therefore, a time interval between the first and the second measurement was 15 to 30 min. The reason for the second measurement was to determine whether or not a change in pressure occurred as the tires cooled down.

TIRE PRESSURE DATA COLLECTION SHEET

BASIC DATA: Test No. (no entry required): _____ Date: 08/26/86 Start Time: 9-10A

PUC Safety Inspection No.: 068579 Place of Inspection: Woodburn POE Inspector: _____

PUC Plate No.: AAX 678 Commodity: Forklift parts Comments: _____

WEATHER: (tick one)

a) Hot & Sunny ___; b) Cool & Sunny X; c) Hot & Cloudy ___; d) Cool & Cloudy ___; e) Intermittent Showers ___; f) Frequent Showers ___; g) Persistent Rain ___

*Air Temperature ___ °F   *Pavement Temperature 70 °F   *Record immediately after start time

TRUCK CLASSIFICATION: (tick one)

A. Single Units:

___ a) SU-2   ___ b) SU-3   ___ c) SU-4
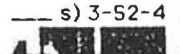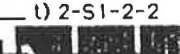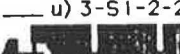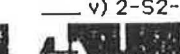
B. Trucks & Trailers:

___ d) 2-2   ___ e) 2-3   ___ f) 3-2   ___ g) 2-2-2   ___ h) 2-2-3   ___ i) 3-2-2

C. Tractors & Semitrailers:

___ j) 2-S1   ___ k) 3-S1   ___ l) 2-S2   X m) 3-S2

D. Tractors, Semitrailers & Trailers:

___ n) 2-S1-2   ___ o) 3-S1-2   ___ p) 2-S1-3   ___ q) 3-S2-2   ___ r) 3-S2-3

___ s) 3-S2-4   ___ t) 2-S1-2-2   ___ u) 3-S1-2-2   ___ v) 2-S2-3-2   ___ w) 3-S1-2-3

TIRE DATA:

A. Left Side - Outer Tires

Axle #	Twin/ Single Tire	Mfr. Name	Rec/Max Pressure (psi)	Rad/ Bias (R/B)	Size	Pressure (psi) 1st*/2nd**	Tread Depth†
(1) (strg)	S	1	120	R	A	102/100	13
(2)	D	2	100	R	A	102/102	11
(3)	D	3	120	R	A	92/90	10
(4)	D	4	100	B	B	80/76	8
(5)	D	5	100	B	B	94/94	8
(6)							
(7)							
(8)							
(9)							

B. Right Side - Outer Tires

Axle #	Twin/ Single Tire	Mfr. Name	Rec/Max Pressure (psi)	Rad/ Bias (R/B)	Size	Pressure (psi) 1st*/2nd**	Tread Depth†
(1) (strg)	S	1	120	R	A	110/110	10
(2)	D	2	100	R	A	90/90	9
(3)	D	3	120	R	A	94/92	7
(4)	D	6	85	B	B	92/90	2
(5)	D	7	85	B	B	96/94	7
(6)							
(7)							
(8)							
(9)							

*measured at beginning of inspection; ** measured at end of inspection; †1/32nd in.

Finish time: 9-35 A

1 Remington
2 Michelin
3 Aurora
4 Dunlop
5 Toyo
6 Firestone
7 Goodrich

A 11R225
B 10.00-20

FIGURE 2 Tire pressure data collection sheet.

TABLE 2   NUMBER OF TRUCKS BY TYPE IN THE SAMPLE

	Truck Type	Frequency	%
Single Units	SU-2	11	4.1
	SU-3	9	3.3
Trucks and Trailers	2-3	2	0.7
	3-2	16	5.9
	3-3	4	1.5
	3-4	3	1.1
	4-4	1	0.4
Tractors and Semi-Trailers	2-S1	12	4.4
	3-S1	3	1.1
	2-S2	11	4.1
	3-S2	151	55.9
	4-S2	1	0.4
	2-S3	1	0.4
	3-S3	1	0.4
Tractors, Semi-Trailers and Trailers	2-S1-2	10	3.7
	3-S1-2	11	4.1
	3-S2-2	3	1.1
	3-S2-3	3	1.1
	3-S2-4	1	0.4
	2-S1-2-2	4	1.5
	3-S1-2-2	2	0.7
	2-S1-2-1	1	0.4
Unknown		9	3.3
TOTAL		270	100

Truck Types

Trucks were classified as shown in Figure 2. As presented in Table 2, of the 270 trucks surveyed, 55.9 percent were 3-S2 (18-wheelers), 7.4 percent were single-unit trucks, and 13 percent were trucks with tractors, semitrailers, and trailers.

Tire Construction

The tires surveyed were divided into three groups:

1. Single tires used for steering axles,
2. Single tires for nonsteering axles, and
3. Dual tires for nonsteering axles.

As presented in Table 3 the data collected show that the majority of tires are radials, i.e., 87 percent of total tires (total is 2,704 tires). Radial tires constitute 91 percent of tires used for steering axles, which is the greatest percentage among the three groups.

Recommended Maximum Tire Pressure

Figure 3 shows the distribution of the recommended maximum tire pressure (cold) by manufacturers for three groups of radial and bias tires, and Table 3 presents the mean value and one standard deviation. The averages of recommended maximum pressure for dual radial and bias tires are 101 psi and 81 psi, respectively.

Measured Tire Pressure

Figure 4 shows the distribution of the first measured tire pressure for three groups of radial and bias tires. Table 3 presents the mean value and one standard deviation of the first measured tire pressure and the difference between the first and the second measured tire pressures. The averages of the first measured pressure of dual radial and bias tires are 102 and 82 psi, respectively. The first measured tire pressures are slightly higher by 1.2 to 2.4 psi than the second measured pressures.

TABLE 3   RESULTS OF TIRE SURVEY

	Single Tire for Steering Axle		Single Tire for Non-Steering Axle		Dual Tire for Non-Steering Axle	
	Radial	Bias	Radial	Bias	Radial	Bias
A. Tire Construction						
Sample Number	499	46	91	11	1755	292
Sample Frequency, %	91.5	8.5	89.2	10.8	85.7	14.3
B. Recommended Tire Pressure						
Mean	106	84	108	84	101	81
One Standard Deviation (psi)	7	9	14	4	8	8
Sample Number	495	46	89	11	1735	285
C. 1st Measured Tire Pressure						
Mean (psi)	106	86	107	93	102	82
One Standard Deviation (psi)	10	17	15	10	12	15
Sample Number	498	46	91	11	1755	292
D. (1st Measurement)-(2nd Measurement)						
Mean (psi)	1.5	2.4	1.6	1.5	1.2	1.6
One Standard Deviation (psi)	2.3	2	1.9	0.7	3	2.7
Sample Number	316	18	66	2	1064	202
E. Tread Depth (1/32-in.)						
Mean	13	11	12	12	11	9
One Standard Deviation	3.4	3.7	4.3	3.7	4.9	3.4
Sample Number	496	46	88	11	746	287

a. Single Tire, Steering Axle

b. Single Tire, Non-Steering Axle

c. Dual Tires, Non-Steering Axle

d. Total Tires
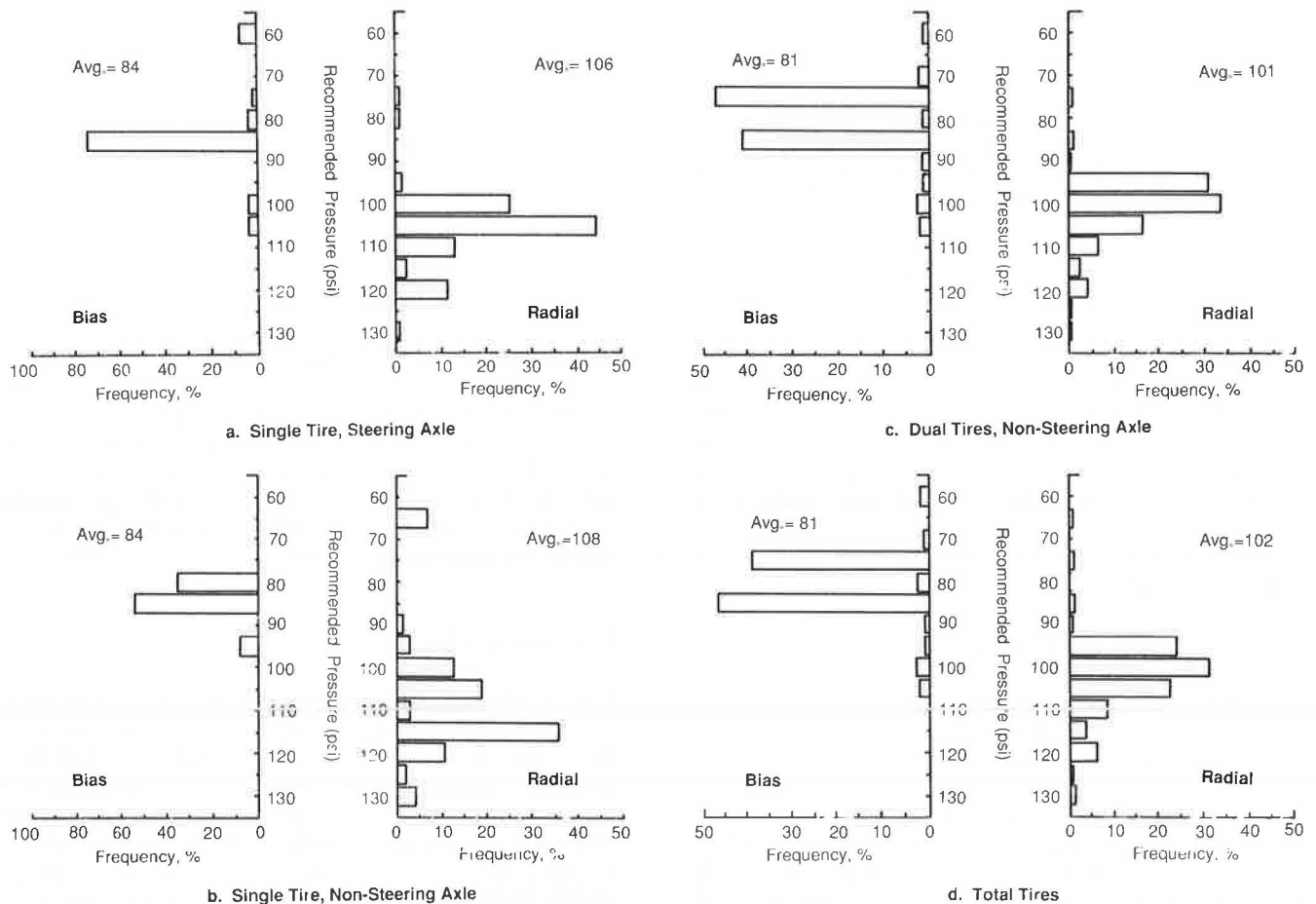
FIGURE 3   Distribution of the recommended tire pressure.

a. Single Tire, Steering Axle

c. Dual Tires, Non-Steering Axle

b. Single Tire, Non-Steering Axle

d. Total Tires
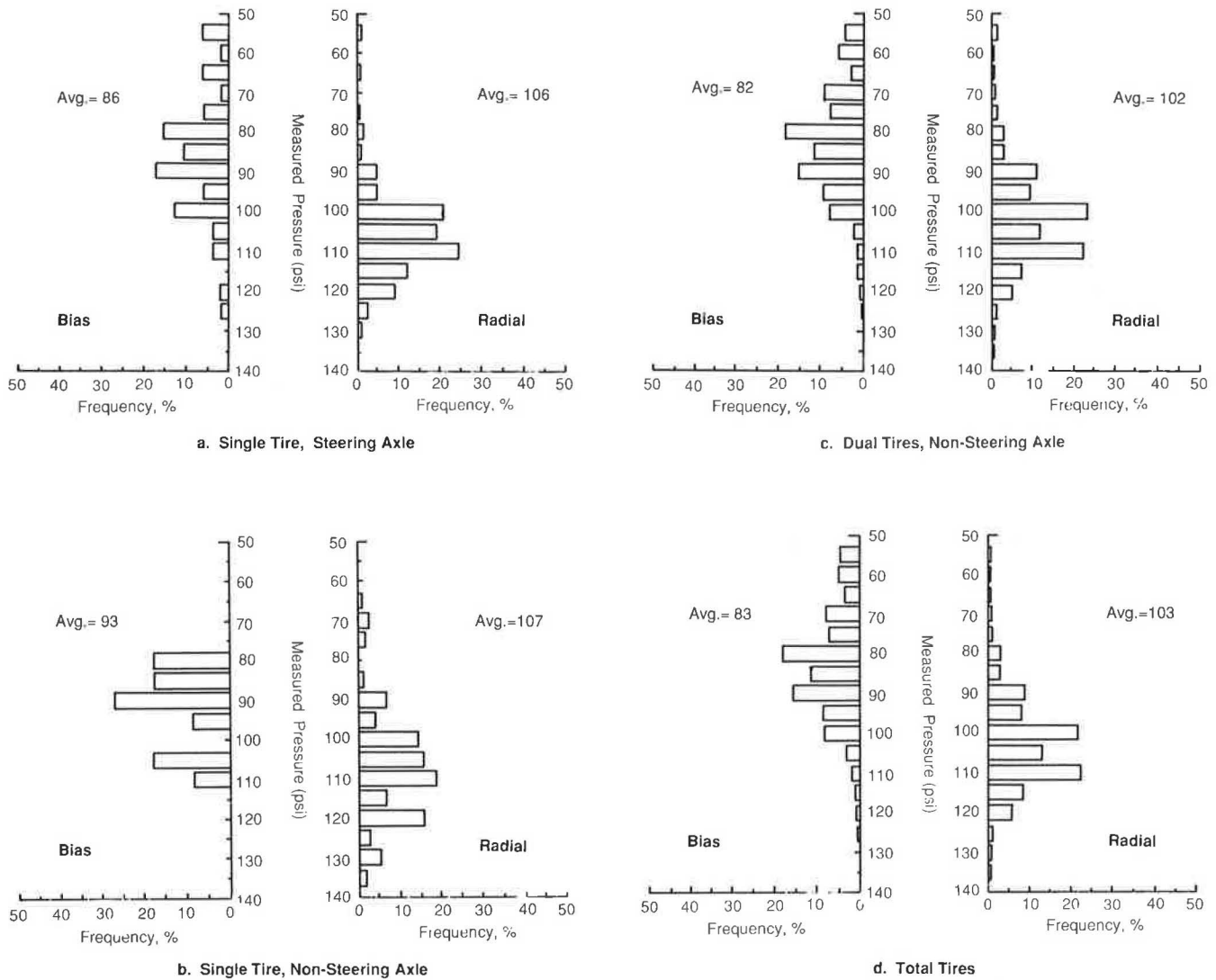
FIGURE 4   Distribution of the measured tire pressure.

Tread Depth

Figure 5 and Table 3 present the results of the tread depth survey. The average tread depth for radial tires used for steering axles is $^{13}/_{32}$ in. This is the highest tread depth among the groups. The average tread depth for bias dual tires used for nonsteering axles is $^{9}/_{32}$ in. This is the lowest measured tread depth.

Tire Size

Table 4 presents the distribution of tire size for radial and bias tires. The major tire size for radials is 11/80 R 24.5. However, for the single tire for nonsteering axles, the major tire size is 12 R 22.5, which is slightly wider than 11/80 R 24.5. The major tires sizes for bias are 11-24.5 and 10.00-20 as presented in Table 4b. It should be noted that 13.2 percent of single radial tires used for nonsteering axles are 15 R 22.5,

i.e., 15-in.-wide tires, which are wider than the major tire sizes.

Figure 6 (7) shows the description of tire dimensional information used in truck tire sizing nomenclature. For example, 11/80 R 24.5 means that the size of the tire is 11 in. wide, has an aspect ratio of 0.8 (section height/section width, see Figure 7), radial, and rim diameter of 24.5 in. Bias ply tires are designated with a hyphen in place of the R.

More detailed data on tire size are presented by Kim et al. (3).

Manufacturer

Table 5 presents the distribution of the eight manufacturers surveyed for radial and bias tires. One company, which supplies 28 percent of the radial tires, did not produce any bias tires. More detailed data on tire manufacturers are presented by Kim et al. (3).

a. Single Tire, Steering Axle

c. Dual Tires, Non-Steering Axle

b. Single Tire, Non-Steering Axle

d. Total Tires

FIGURE 5 Distribution of tread depth.

DISCUSSION OF RESULTS

As expected, the majority of tires were of radial construction. As presented in Table 5, one company which supplies 28 percent of the radial tires did not produce any bias tires. There may be several reasons that bias tires have been replaced with radial tires, as outlined below.

From the 1970s, the trucking industry increased their use of radial truck tires as tire service demands on medium and heavy trucks increased. Testing done on bias and radial tires with similar tread designs from the same manufacturer confirmed that the radial tire generally offered improvements over the bias, as presented in Table 6 (8).

As mentioned earlier, the federal government permitted 80,000 lb gross vehicle weight and 34,000 lb tandem-axle weights on Interstate highways in 1982. This allowed 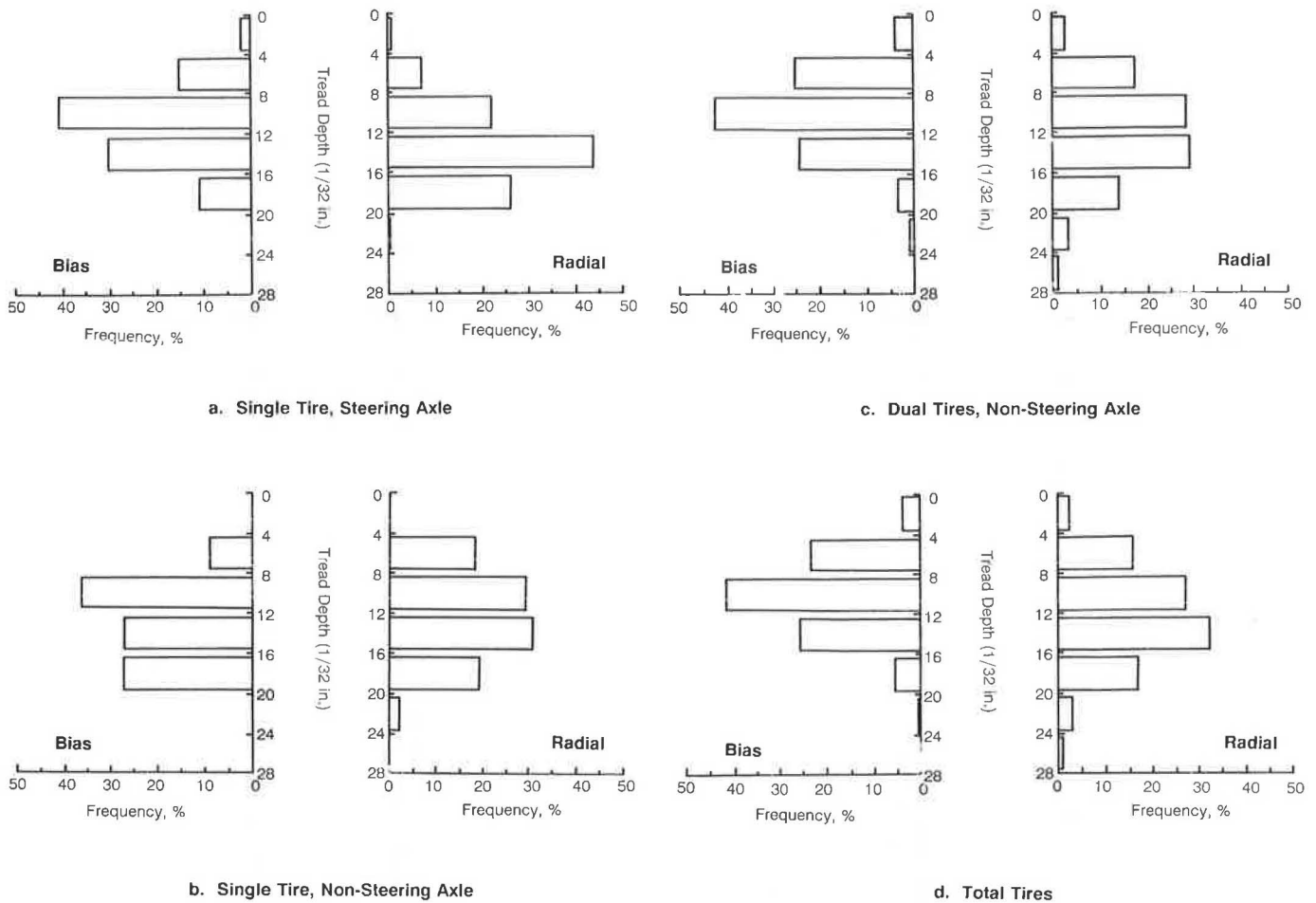a potential 12,000-lb load on the steering axle. Most states invoke a restriction on the load per inch width of tire of 600 lb, i.e., two 10-in.-wide tires could legally support a 12,000-lb axle load. According to Cooper (8), two bias tires in the commonly used sizes and standard 12-ply rating do not have 12,000-lb capacity, but two standard 14-ply-rating radial tires which allow the higher inflation pressure necessary for a higher capacity rating do carry over 12,000 lb. The improved loading capacity and the advantages presented in Table 6 are some of the reasons that

have led to an increase in radial truck tire usage. Wong (9) indicated that for a radial ply tire on a hard surface, there is a relatively uniform ground pressure over the whole contact area. In contrast, the ground pressure for a bias ply tire varies greatly from point to point as tread elements passing through the contact area undergo a complex localized wiping motion. However, the effect of different tire construction on asphalt pavements is still not well known.

As shown in Table 3, the average of the recommended tire pressure of single tires (for steering axles and nonsteering axles) is higher than that of dual tires. The same trend is apparent in the first measured tire pressure distribution in Table 3. Therefore, the data show that truckers tend to use higher tire pressure (i.e., higher rated tires) for a single tire for steering axles as well as nonsteering axles than for dual tires for nonsteering axles.

As indicated in Table 3, the first measured tire pressure is slightly higher than the second measured one. For radial tires, the difference between the first measurement and the second measurement is smaller than that for bias tires except in the case of single tires for nonsteering axles.

For radial tires, Table 3 and Figures 4 and 5 show that truckers tend to use the manufacturer's maximum recommended tire pressure. This is due to operation safety and efficiency. For bias single tires with nonsteering axle, the

TABLE 4   TIRE SIZE DISTRIBUTION (%)

(a)   Radial Tire

Tire Size	Single Tire on Steering Axle	Single Tire on Non-Steering Axle	Dual Tire on Non-Steering Axle
11/80 R 24.5	46.5	15.4	49.1
11 R 22.5	22.2	19.8	21.1
285/75 R 24.5	9.6	1.1	7.1
275/80 R 24.5	6.1	3.3	3.9
275/80 R 22.5	3.9	-	4.1
12 R 22.5	2.0	33.0	2.2
10.00 R 22	2.0	-	3.9
15 R 22.5	-	13.2	-
Others	7.7	14.2	8.6
Number in Sample	490	91	1737

(b)   Bias Tire

Tire Size	Single Tire on Steering Axle	Single Tire on Non-Steering Axle	Dual Tire on Non-Steering Axle
11-24.5	30.8	-	30.8
10.00-20	15.4	36.4	29.8
10.00-22	11.5	18.1	21.2
11-22.5	17.3	-	9.9
9.00-20	3.8	45.5	2.6
Others	21.2	0.0	5.8
Number in Sample	52	11	302

average of the measured pressure is higher by about 10 psi than that of the recommended maximum pressure, but the sample size of 11 tires is very small.

As shown in Table 7, the difference between recommended pressure and measured pressure for radial tires is almost zero. However, for bias tires, the inflated pressure is greater than the recommended pressure. As presented in Table 3, radial tire pressure is higher by 20 psi than bias tire pressure. The study performed by Middleton et al. (5) indicated that radial tires on the average showed 12 to 21 psi higher pressure than did bias tires.

If government agencies wish to control tire pressures, it would be expedient to control the manufacturer's maximum recommended pressure rather than the inflation pressure used by truckers. This would ensure reasonable control, since the data collected in this study show that measured and recommended tire pressures are nearly equal.

In general, higher-inflation-pressure tires have deeper tread depth as presented in Table 3. This implies that operators may use higher pressures with newer tires.

Recently, the trucking and tire industries have started to promote super single radials and new low-profile (or low-aspect-ratio) tubeless tires. The concept of replacing dual tires with a wide single is not new but has gained popularity recently in the long-haul market. As mentioned in the earlier section, 13.2 percent of single tires used for nonsteering axles are 15 R 22.5 (Table 4a). According to the restriction of 600 lb per in. width of tire, two tires 15 in. wide can support 18,000 lb, that is, the equivalent standard single-axle load used in pavement design by many states.

New super single radial tires are claimed to have 10 percent or better tread mileage and 8 to 10 percent better fuel economy than conventional dual radials (10). Also, the lighter weight of the wide-base single tire assembly permits higher payloads. The reduced tire aspect ratio decreases tire deflection, thereby improving vehicle handling and stability while increasing tread life and fuel economy. However, the effect of the super single tire on the performance of asphalt pavement needs more study. The pressure data collected indicate that the mean pressure of the whole sample is similar to that found in the Texas study (5) and is considerably higher than that traditionally used in pavement design (i.e., 80 psi). Since
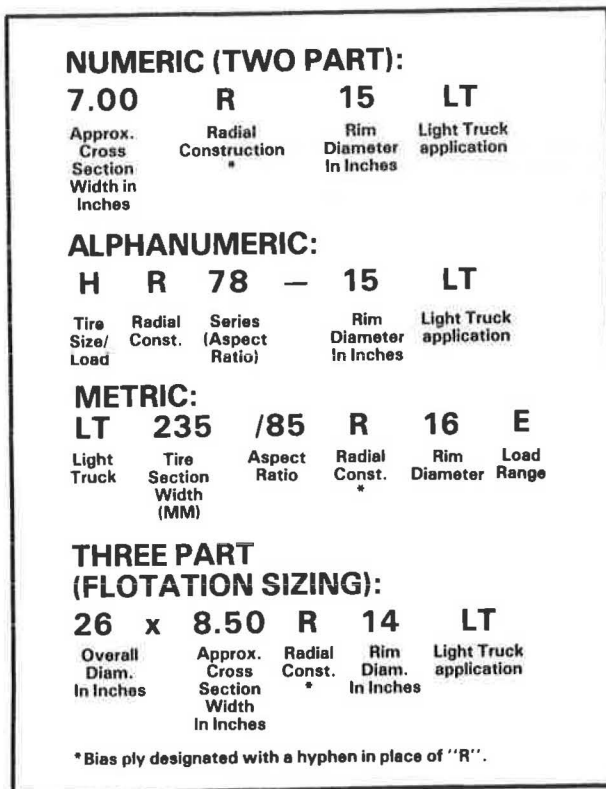
NUMERIC (TWO PART):

7.00   R   15   LT

Approx. Cross Section Width in Inches   Radial Construction *   Rim Diameter In Inches   Light Truck application

ALPHANUMERIC:

H   R   78   —   15   LT

Tire Size/ Load   Radial Const.   Series (Aspect Ratio)   Rim Diameter In Inches   Light Truck application

METRIC:

LT   235   /85   R   16   E

Light Truck   Tire Section Width (MM)   Aspect Ratio   Radial Const. *   Rim Diameter   Load Range

THREE PART (FLOTATION SIZING):

26   x   8.50   R   14   LT

Overall Diam. In Inches   Approx. Cross Section Width In Inches   Radial Const. *   Rim Diam. In Inches   Light Truck application

* Bias ply designated with a hyphen in place of "R".

FIGURE 6   Tire sizing designation (7).

the study described herein and other studies have confirmed that a wide variety of tires and pressures are used, it is necessary to refine paving mix design and pavement structure design methods to account for the prevailing levels of tire pressure. Also, the remaining life of existing asphalt pavements or maintenance schedules on the section having high
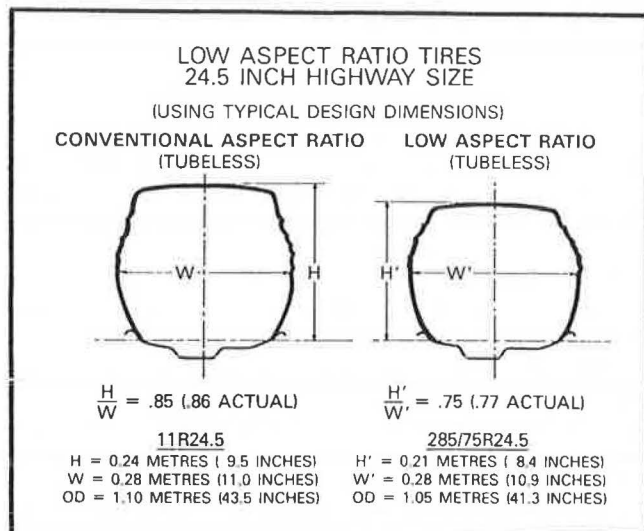

LOW ASPECT RATIO TIRES
24.5 INCH HIGHWAY SIZE

(USING TYPICAL DESIGN DIMENSIONS)

CONVENTIONAL ASPECT RATIO (TUBELESS)   LOW ASPECT RATIO (TUBELESS)

$\frac{H}{W}$ = .85 (.86 ACTUAL) $\frac{H'}{W'}$ = .75 (.77 ACTUAL)

11R24.5   285/75R24.5
H = 0.24 METRES (9.5 INCHES)   H' = 0.21 METRES (8.4 INCHES)
W = 0.28 METRES (11.0 INCHES)   W' = 0.28 METRES (10.9 INCHES)
OD = 1.10 METRES (43.5 INCHES)   OD = 1.05 METRES (41.3 INCHES)

FIGURE 7   Comparison of conventional and low-aspect-ratio tires (8).

truck traffic may need adjustment because the increased truck tire pressure may result in severe damage.

The factor of truck tire pressure, as well as axle loads, could be a consideration in setting registration fees and fine schedules.

However, caution is advised when considering the effects of tire pressures on asphalt pavements for, say, 80 psi (a typical tire pressure in the 1960s) with 100 psi (a typical tire pressure in the 1980s) because the former were almost exclusively bias tires and the latter are predominantly radial tires.

CONCLUSIONS AND RECOMMENDATIONS

The existing operating characteristics of Oregon's trucks, including levels of tire pressures, were surveyed and analyzed. The major findings and conclusions of this study are:

1. As expected, the use of radial tires is dominant. Eighty-seven percent of the tires surveyed were of radial construction. The bias tires used may be replaced with radial tires in the future.
2. The average measured pressures of radial and bias tires are 102 and 82 psi, respectively. Therefore, adequate consideration of current levels of tire pressure should be reflected in paving mix design, pavement structure design methods including overlay design, and maintenance schedules.
3. Since the difference between the recommended maximum tire pressure by manufacturer and the measured tire pressure is very small, it can be said that truckers tend to use the recommended maximum pressure (cold) for reasons of operating safety and efficiency.
4. The sizes of most radial tires are 11/80 R 24.5 and 11-24.5, respectively.
5. The average tread depth of radial tires is slightly greater than that of bias tires.

In order to control the effect of increased tire pressure on asphalt concrete pavement, the following recommendations are made:

1. If government agencies wish to control tire pressures, it would be expedient to control the manufacturer's maximum recommended tire pressure (cold) rather than the inflation pressures used by truckers, since the data collected in this study show that measured and recommended tire pressures are nearly equal.
2. For overload permits, fees, and fine schedules, the levels of tire pressure might be included in assigning appropriate cost responsibility after an investigation into the effect of higher tire pressures on the asphalt pavements is performed.

ACKNOWLEDGMENTS

TABLE 5 DISTRIBUTION OF RADIAL AND BIAS TIRES BY TIRE MANUFACTURER

(a) Radial Tire

		Single Tire on Steering Axle	Single Tire on Non-Steering Axle	Dual Tire on Non-Steering Axle
1.	Michelin	25.0	36.3	28.4
2.	Goodyear	22.0	11.0	22.7
3.	Bridgestone	15.5	24.2	15.0
4.	Toyo	9.7	15.4	9.6
5.	Kelly	3.6	2.2	4.0
6.	Yokohama	3.8	1.1	3.0
7.	Firestone	2.2	1.1	2.8
8.	OHTSU	3.6	1.1	1.7
	Others	14.6	7.6	12.8
	Number in Sample	496	91	1755

(b) Bias Tire

		Single Tire on Steering Axle	Single Tire on Non-Steering Axle	Dual Tire on Non-Steering Axle
1.	Goodyear	10.9	30.0	23.2
2.	Firestone	6.5	-	9.5
3.	Goodrich	10.9	20.0	6.7
4.	Bridgestone	-	-	7.7
5.	General	-	10.0	7.0
6.	Multimile	8.7	-	3.5
7.	Dunlop	4.3	0	3.9
8.	OHTSU	8.7	20.0	2.1
	Others	50.0	20.0	36.4
	Number in Sample	46	10	284

TABLE 6 COMPARISON OF BIAS AND RADIAL TIRE PERFORMANCE (8)

Property	Type Test	Bias Tire	Radial Tire
Wear Rate	Proving Grounds	Par	Better
Wear Regularity	Proving Grounds	Par	More Sensitive
Running Temperature	Laboratory	Par	Better (Lower)
Fuel Economy	Proving Grounds	Par	Better (6% Savings)
Tire Noise	SAE J57A	Par	Better (3 dBA Less)
Puncture Resistance	Commercial Fleet	Par	Better (40% Fewer)

TABLE 7 MEAN VALUES OF DIFFERENCE BETWEEN RECOMMENDED TIRE
PRESSURE AND FIRST MEASURED PRESSURE

	Single Tire on Steering Axle		Single Tire on Non-Steering Axle		Dual Tire on Non-Steering Axle	
	Radial	Bias	Radial	Bias	Radial	Bias
Mean (%)	0.3	2.5	-0.2	10.0	1.3	2.2
Standard Deviation (%)	10.7	14.6	8.0	9.6	12.9	19.9
Number of Tires	495	44	89	11	1734	285

$$\frac{\text{Measured Pressure} - \text{Recommended Pressure}}{\text{Recommended Pressure}} \times 100\%$$

REFERENCES

1. W. T. Druhan. Federal Weight-Distance Tax: An Old Tax as Modern as Today. *AASHTO Quarterly,* Vol. 63, No. 3, July 1984.
2. *Rolling Thru Oregon.* Oregon Department of Transportation, Salem, 1985.
3. O-K. Kim, C. A. Bell, and J. E. Wilson. *Procedures for Controlling the Effect of Increased Tire Pressure on Asphalt Concrete Pavement Damage.* Final Report OR-RD-88-1. FHWA, U.S. Department of Transportation; Oregon Department of Transportation, 1988.
4. D. S. Paxon and J. P. Glickert. Values of Overweighting to Intercity Truckers. In *Transportation Research Record 889,* TRB, National Research Council, Washington, D.C., 1982, pp. 33–37.
5. D. R. Middleton, F. L. Roberts, and T. Chira-Chavala. Measurement and Analysis of Truck Tire Pressures on Texas Highways. In *Transportation Research Record 1070,* TRB, National Research Council, Washington, D.C., 1986, pp. 1–8.
6. F. L. Roberts and B. T. Rosson. Effects of Higher Tire Pressures on Strain in Thin ACP. In *Transportation Research Record 1043,* TRB, National Research Council, Washington, D.C., 1985, pp. 68–77.
7. *Firestone Light Truck Tire Sales Handbook.*
8. L. C. Cooper. Radial Truck Tire Trends. *SAE Technical Paper Series 851463,* 1985.
9. J. Y. Wong. *Theory of Ground Vehicles.* John Wiley and Sons, Inc., New York, 1978, p. 5.
10. A. Chbugil, R. Ridout, and D. Ross. Recent Development in Truck Technology: Potential for Improved Energy Efficiency in Long-Haul Trucking. *Transportation Forum,* Vol. 2, No. 3, 1985. pp. 53–61.

Evaluation of Flexible Pavement Performance from Pavement Structural Response

EMMANUEL G. FERNANDO, DAVID R. LUHR, CHARLES E. ANTLE, AND DAVID A. ANDERSON

A model for predicting flexible pavement performance was developed from AASHO Road Test data. The pavement condition indicator selected for quantifying performance is pavement surface roughness, which correlated highly with pavement serviceability as perceived by the road user. In the development of the model, pavement performance was initially defined as the history of a pavement condition indicator(s) over time or with increasing axle load applications. Consequently, the performance model developed predicts the trend in pavement surface roughness with cumulative axle load applications. Since strain basins provide more information on the pavement response under load than just the maximum pavement response, indices determined from an evaluation of subgrade compressive and asphalt tensile strain basins were evaluated for their utility as performance predictors. The results obtained strongly indicate that strain basin indices are important predictors of the performance of AASHO flexible pavement sections.

A wide range of analytical procedures are used to determine the structural response of flexible pavements, including linear-elastic, viscoelastic, and finite-element methodologies. The specific performance-related pavement response variables (e.g., asphalt tensile strain, subgrade compressive strain) determined by these methodologies are used to design new pavement construction or pavement rehabilitation.

The task of designing pavements for transporting people and commodities is logically related to what pavement performance is perceived to be. One commonly accepted definition states that performance is the amount of service rendered by a pavement before reaching a failure condition (1). This definition is attractive in its simplicity, but has certain shortcomings for the same reason. Figure 1 illustrates what these shortcomings are.

Consider two pavement structures, A and B, and assume that the trend in each pavement's present serviceability index (PSI) with increasing load applications is as shown in Figure 1. From the definition given previously, the two pavements would be characterized as having the same performance, using terminal serviceability level PSI_1, since both pavements reached this terminal level of PSI after the same number of load applications. However, it is apparent that these two pavements

E. G. Fernando, Texas Transportation Institute, Texas A&M University, College Station, Tex. 77843. D. R. Luhr, Keystone Management Systems, Inc., State College, Pa. 16801. C. E. Antle and D. A. Anderson, Pennsylvania State University, University Park, Pa. 16802.
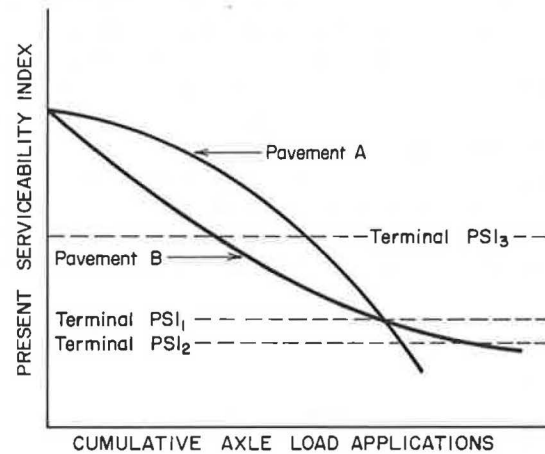

FIGURE 1 Conceptual serviceability histories for pavements A and B.

provided different levels of service. Significantly different user and maintenance costs may be associated with pavements A and B. In addition, if PSI_2 is used as the terminal level of serviceability, pavement B would be considered to have the better performance, whereas if PSI_3 is used, then pavement A would be considered to have the better performance.

In view of the above shortcomings, a different definition of pavement performance was used in this research. Specifically, it was defined as the history of a pavement condition indicator(s) over time or with increasing axle load applications. This is believed to be a better definition than the one given previously for the following reasons:

1. A performance history is needed to consider the difference between two pavements that fail at the same time.
2. A performance history allows the comparison of two pavements that have not failed, rather than considering them as equally satisfactory.
3. A performance history is required for determining user and maintenance costs in a life-cycle cost analysis.

This definition was subsequently used to develop a performance model through an evaluation of the relationships between pavement performance and theoretical pavement response.
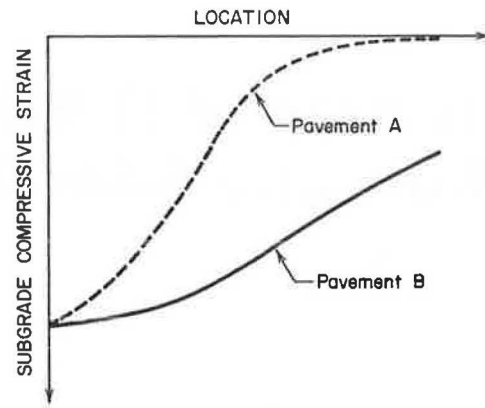
RESEARCH SCOPE

The objective of this research was the evaluation of the relationships between pavement performance and structural response. Pavement failure was assumed to be a function of the response to vehicle loadings, and it was hypothesized that the variation in pavement performance can be explained from the corresponding variation in the theoretical structural response.

Although maximum asphalt tensile strain and maximum subgrade compressive strain are the most frequently used variables for predicting pavement performance, strain basin indices, developed from an evaluation of theoretical strain basins, were also examined for their usefulness as performance prediction variables. These quantities are analogous to deflection basin indices such as surface curvature index (SCI), base curvature index (BCI), or base damage index (BDI) (defined in Figure 2), which are used as indicators of pavement structural integrity. Strain basin indices are therefore related to theoretical strains at different locations within a pavement structure. Figure 3 shows a subgrade compressive strain basin for an 18,000-lb single-axle load.
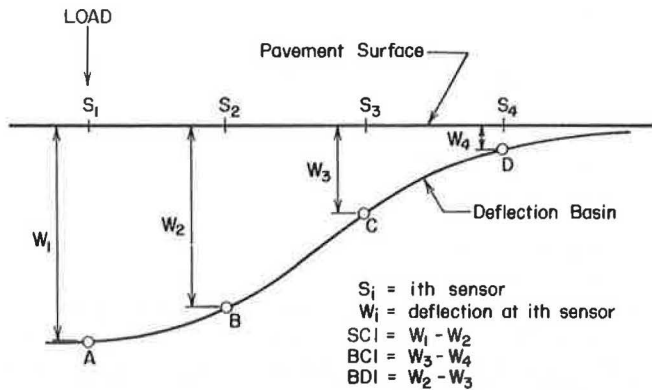
The importance of strain basins in the evaluation of pavement performance is illustrated conceptually in Figure 4, which shows plots of the longitudinal distribution of subgrade compressive strains for two different pavements. If only the max-

FIGURE 2   Example of surface deflection basin.

FIGURE 3   Subgrade compressive strain basin for an 18-kip single-axle load.

FIGURE 4   Conceptual subgrade compressive strain basins for pavements A and B.

imum subgrade compressive strain is considered, then the two pavements would be characterized as having the same pavement response under load. However, it is apparent from an examination of the strain basins in Figure 4 that this is not the case. The load distribution across the subgrade for pavement A is different from the load distribution for pavement B. Inasmuch as pavement performance is logically related to how the pavement responds under load, indices developed from an evaluation of strain basins may provide a better explanation of the variation in performance for different pavement structures.

Performance data from flexible pavement sections at the AASHO Road Test (2) were used in the development of the performance model presented herein. Pavement surface roughness, as measured by slope variance (SV), was the pavement condition indicator selected for modeling pavement performance. This pavement condition indicator is strongly correlated with riding quality as perceived by the road user. This is evident in Figure 5, which shows a plot of present service-

FIGURE 5   Present serviceability rating vs. $\log_{10}(1 + SV)$.

ability ratings vs. $\log_{10}(1 + SV)$, an indicator of pavement roughness. The present serviceability ratings were made by a panel of highway users who rated, on a scale of 0 to 5, the riding quality of 74 selected flexible pavement sections at the time of the AASHO Road Test (2).

For this research therefore, roughness was used in modeling pavement performance. It was beyond the scope of the research to develop performance models using other pavement condition indicators such as cracking and rutting. In addition, the evaluation of pavement structural response was made using linear elastic-layer theory, which is widely used for the analysis of pavement structures. The stress dependency of the moduli of unbound pavement materials was considered in the computation of pavement strains. Subgrade compressive and asphalt tensile strain basins were evaluated in the study, and statistical regression techniques were used to evaluate relationships between pavement performance and pavement response.

LOGISTIC REGRESSION ANALYSIS OF AASHO ROAD TEST DATA

Performance data from the AASHO Road Test (2) were analyzed to develop an equation for identifying pavement designs that would likely lead to premature pavement failure. Examination of AASHO Road Test data revealed that certain flexible pavement sections experienced early failure. These sections did not last beyond the first spring season, after traffic operations began in October 1958, and sustained less than 100,000 18-kip ESALs prior to reaching a terminal serviceability level of 1.5.

Figure 6 shows a comparison of the performance history of a section that failed prematurely with the performance history of a section that lasted the duration of the AASHO Road Test. For most of the sections that failed early, the PSI values were adequate until a sharp decrease in serviceability was observed at the onset of the spring season. This sudden loss in serviceability was most likely due to the adverse subsurface conditions that existed during this period. Because of the thawing that occurred at this time of the year, subgrade support conditions were poor, leading to the development of pavement distress, primarily cracking and rutting.
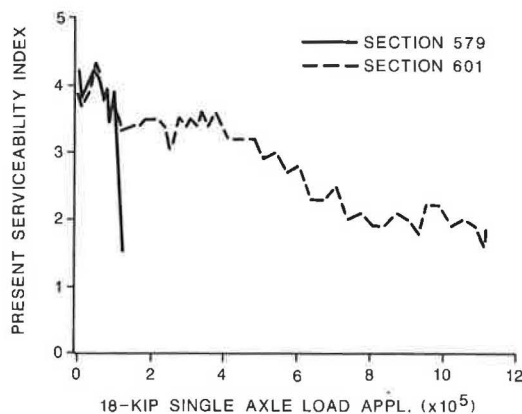

FIGURE 6   Comparison of PSI histories of sections 579 and 601.

In this particular study, AASHO Road Test pavements that experienced premature failure (i.e., sustained less than 100,000 18-kip ESALs) were categorized as Class 1 sections, and those that lasted longer were categorized as Class 2. Since this research was concerned with evaluating the performance of flexible pavements designed for high-volume traffic conditions, the procedure developed for discriminating between Class 1 and Class 2 pavements was used to sort the AASHO flexible pavement sections into the aforementioned categories. Only the performance of Class 2 sections was subsequently evaluated.

A statistical technique, known as logistic regression, was used to develop an equation for discriminating between Class 1 and Class 2 pavement sections. The logistic model for the case where the dependent variable is binary (0 or 1) is given by the following equation:

$$\Pr[Y = 1] = 1/[1 + \exp(-\mathbf{X'\beta})] \tag{1}$$

where

$$\Pr[Y = 1] = \text{probability of premature failure,}$$
$$\mathbf{X'} = \text{transpose of the vector of independent variables, and}$$
$$\boldsymbol{\beta} = \text{vector of model parameters.}$$

In the development of the logistic regression equation from AASHO Road Test data, the binary dependent variable Y_i was set to 1 for flexible pavement sections that failed early. Sections that failed early were defined as those that did not last beyond the first spring season and sustained less than 100,000 18-kip ESALs. For all other sections, Y_i was set equal to 0. The independent variables included in the analysis were the surface, base, and subbase layer thicknesses, and the theoretical values of subgrade compressive strain, calculated using multilayer linear elastic theory. Subgrade compressive strain was calculated using the applied axle load for a given test section. The subgrade strain directly beneath one tire was calculated.

Table 1 summarizes the material properties assumed for the various layers of the AASHO flexible pavement sections. The material properties are representative of average yearly conditions at the AASHO test site. The modulus of the asphalt concrete mix was obtained at a test temperature of 70°F (3).

A computer program called NEL1 was used to calculate the compressive strain at the top of the subgrade for each of the 284 AASHO flexible pavement sections included in the experiment. This program was developed by Luhr and McCullough (4) and is a modification of the BISAR program (5). NEL1 considers the stress dependency of the resilient modulus of unbound pavement materials in the calculation of stresses, strains, and displacements within the pavement structure. This is accomplished through an iterative application of linear elastic-layer theory to get stress-compatible moduli.

The theoretical values of subgrade compressive strain and the layer thicknesses of the flexible pavement sections were used as independent variables in a logistic regression analysis. A stepwise nonlinear regression procedure (6) was used to determine the coefficients of the logistic model given by Equation 1. Table 2 summarizes the results of the regression analysis, showing the independent variables that entered at each

TABLE 1 MATERIAL PROPERTIES OF AASHO FLEXIBLE
PAVEMENT SECTIONS

	Material	Modulus (psi)
1.	Asphalt concrete	450,000
2.	Crushed limestone base	$4000\,\theta^{0.6}$
3.	Sand-gravel subbase	$5400\,\theta^{0.6}$
4.	Subgrade	$27,000\,\sigma_d^{-1.06}$

step of the procedure, and the fraction of concordant pairs. The final logistic regression equation is:

$$Pr[Y = 1] = 1/\Big(1 + \exp\{-[16.586 - 0.300\,H_1$$
$$- 0.722\,H_2 - 0.353\,H_3$$
$$+ 3.824\,\log_{10}(\varepsilon_{sg})]\}\Big) \qquad (2)$$

where

$Pr[Y = 1]$ = probability of premature failure,
H_1 = asphalt concrete thickness (in.),
H_2 = base thickness (in.),
H_3 = subbase thickness (in.), and
ε_{sg} = subgrade compressive strain.

The fraction of concordant pairs is a statistic that measures the predictive ability of the model. This statistic can have a maximum value of 1.0 indicating a model with excellent ability to classify observations into the different levels of the dependent variable. For the logistic regression equation developed, the fraction of concordant pairs is equal to 0.93, indicating that a model with good predictive ability has been obtained.

The results of the analysis summarized in Table 2 reveal that, for the independent variables considered, the base and subbase layer thicknesses initially provided the largest contribution to the predictive ability of the model. As can be seen in the table, the fraction of concordant pairs increased from 0.500 to 0.805 with the addition of base thickness as an independent variable, and attained a value close to 0.90 with just the base and subbase thicknesses in the logistic regression equation. The significant ability of these two variables to discriminate between Class 1 and Class 2 pavements reflects the fact that of the 84 flexible pavement sections that failed early during the Road Test, 56 had either no base and/or subbase. This is indicated in Figures 7 and 8, which show the distributions of base and subbase layer thicknesses drawn according to the level of the pavement class variable.

Most of the Class 1 pavements failed during the initial spring season at the AASHO Road Test. Considering the adverse subgrade support conditions that existed during this time period, the absence of base and/or subbase layers would further accelerate pavement distress and lead to premature failure.

The results of the analysis shown in Table 2 also indicate that the contribution of asphalt concrete thickness to the fraction of concordant pairs is small relative to those for the base and subbase layer thicknesses. However, this observation does not imply that asphalt concrete thickness has little effect on

TABLE 2 RESULTS OF STEPWISE LOGISTIC REGRESSION ANALYSIS

Step	Variable entered	Variable removed	Fraction of concordant pairs
0	intercept	-	0.500
1	base thickness	-	0.805
2	subbase thickness	-	0.896
3	$\log_{10}(\varepsilon_{sg})$	-	0.926
4	surface thickness	-	0.930

ε_{sg} = compressive strain at the top of the subgrade
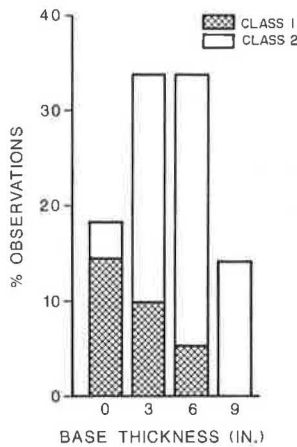
FIGURE 7 Distribution of
base thicknesses of AASHO
flexible pavement sections.
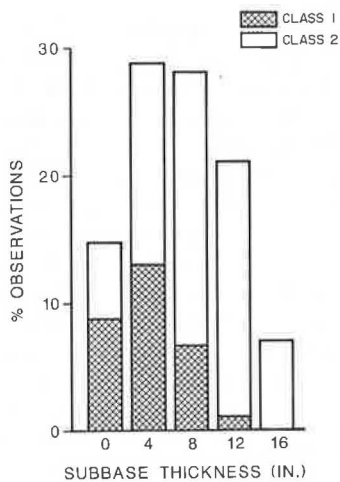
FIGURE 8 Distribution of
subbase thicknesses of AASHO
flexible pavement sections.

pavement performance. Rather, the results presented should be viewed relative to the purpose for conducting the analysis, which was to develop an equation for discriminating between two different classes of pavement sections. For this purpose, the base and subbase thicknesses are variables that better discriminate between Class 1 and Class 2 sections. A plausible explanation for this was given previously, i.e., that most of the premature failures were associated with sections that were built without base and/or subbase layers. It is expected that in the evaluation of the performance of sections categorized as Class 2, the thickness of the asphalt concrete layer would have a significant effect on pavement performance.

DEVELOPMENT OF PERFORMANCE MODEL

The logistic regression equation presented above was used to select the AASHO flexible pavement sections to include in the performance modeling phase of the research effort. As part of the development of the performance model, an eval-

uation was made to identify trends in pavement performance with increasing axle load applications. In the evaluation, the variation in roughness with increasing axle load applications was examined for each of the AASHO flexible pavement sections categorized as Class 2 from the logistic regression analysis. From this examination, the performance trends illustrated in Figure 9 were identified.

Efforts were made to identify a model that would define the five trends shown in Figure 9. Three different models were evaluated: The Weibull (Eq. 3); the logistic (Eq. 4); and the cubic, i.e., third-degree polynomials (Eq. 5).

$$y = \beta_3 \left(1 - \exp\{- [(N - \beta_0)/\beta_1]^{\beta_2}\} \right) \tag{3}$$

$$y = \beta_0/[1 + \beta_1 \exp(- \beta_2 N)] \tag{4}$$

$$y = \beta_0 + \beta_1 N + \beta_2 N^2 + \beta_3 N^3 \tag{5}$$

where

$y = \log_{10}(1 + SV)$,
N = cumulative number of axle load applications, and
β_i = model parameters determined from regression analysis.

Using linear as well as nonlinear regression techniques, efforts were made to determine whether any of the models given in the above equations fit all of the five trends identified in Figure 9. It was found that the cubic model could fit the five performance trends shown. Consequently, in the development of the performance model, the form of the model was taken to be a cubic or third-degree polynomial.

The next step in the development of the performance model was the evaluation of the parameters of the cubic model. Pavement performance can be predicted if, for any given design, the parameters of this model can be specified. Consequently, it was essential to develop prediction equations for the parameters of the cubic model. In connection with this, it was reasonable to assume that the model parameters are functions of certain attributes of the pavement design. Consistent with the hypothesis for this research, an evaluation of the relationships between the model parameters and pavement structural response variables (strains and strain basin indices) was conducted.

For each of the AASHO flexible pavement sections included in the analysis, the cubic model was fitted to the observed performance data to estimate the model parameters for each test section. Inasmuch as there were 202 sections to analyze, a program was written to accomplish this task on a personal computer.

An evaluation of the relationships between the fitted model parameters and pavement structural response variables was then conducted. Each model parameter (i.e., β_1, β_2, β_3) was plotted vs. pavement structural response variables such as compressive strain at the top of the subgrade, tensile strain at the bottom of the asphalt layer, and strain basin indices. Compressive strain basins at the top of the subgrade, and tensile strain basins at the bottom of the asphalt layer were determined using computer program NEL1 with the material properties shown in Table 3.

In the development of the performance model, the evaluation of seasonal effects was considered important. However, after a careful examination of AASHO Road Test data, it
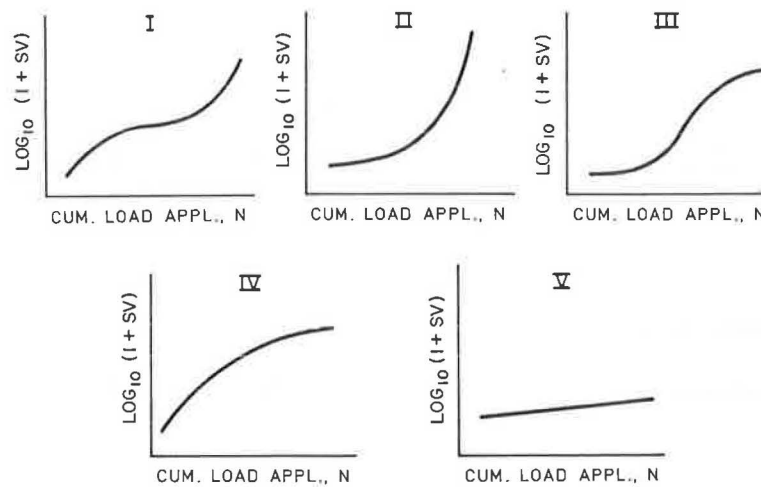
FIGURE 9 Observed performance trends of AASHO flexible pavement sections.

was found that an analysis of seasonal effects cannot be made since the rate of loading was not systematically varied during the Road Test. Consequently, it was not possible to separate the effects of load and season on the observed trends in pavement performance. The decision was therefore made to use material properties representative of average yearly conditions at the AASHO Road Test site, and to model the entire performance history exhibited by each Class 2 section during the duration of the Road Test.

From the strain basins determined, the indices shown in Table 3 were evaluated. As noted previously, strain basin indices are analogous to deflection basin indices, which are currently used by many highway agencies as indicators of pavement structural integrity. These indices are related to strains at different locations within the pavement structure. Inasmuch as the strain basin provides more information on the response of the pavement under load than just the maximum pavement response, strain basin indices were evaluated for their utility as performance prediction variables.

Figures 10 and 11 show conceptual illustrations of compressive strain basins at the top of the subgrade for single and tandem axles, respectively. These were the axle configurations that were considered at the AASHO Road Test. For each axle configuration, the elements of the strain basin used for calculating the subgrade strain basin indices presented in Table 3 are shown. Similar illustrations can be drawn for tensile strain basins at the bottom of the asphalt layer.

Through regression analysis, prediction equations for β_1, β_2, and β_3 of the cubic model were developed. Table 4 shows the prediction equations for the cubic model parameters. It was found that the subgrade strain basin index V_2 provided equations with the highest coefficients of determination.

No prediction equation was developed for β_0. Physically, this parameter represents the initial surface roughness after construction, and is an input to the pavement design process that is provided by the highway engineer. Alternatively, β_0 may be one of the specifications established for the construction of flexible pavement structures.

The prediction equations shown in Table 4 were subsequently evaluated by comparing predicted performance trends with the observed performance trends at the AASHO Road

Test. As may be discerned from Figure 12, the results obtained were not very encouraging. It was found that the predicted performance trend usually diverged from the observed performance trend. The divergence is very significant. Observed values of pavement roughness $[\log_{10}(1 + SV)]$ for bituminous sections ranged from 0.18 to 2.4 at the AASHO Road Test. However, because of the significant disparity between the predicted and observed values for pavement roughness, the observed performance trend appears to be just a horizontal line passing through the zero point of the y axis.

The predictions for pavement roughness were so unrealistic that the possibility of arithmetic or programming errors in the analysis was initially investigated. However, a careful review showed that no such errors were committed. The predicted parameters of the cubic model were simply giving unacceptable results. Consequently, efforts were made to improve the accuracy of the prediction equations for the cubic model parameters (Table 4), and new equations were subsequently developed. However, the results obtained were again very discouraging; many predicted performance trends still diverged unreasonably from the observed trends.

The difficulties encountered may be attributable to the extreme sensitivity of the predictions from the cubic model to deviations in the model parameters, primarily those that are multipliers of the X^2 and X^3 terms (i.e., β_2 and β_3). Even though the cubic model adequately fitted the observed performance histories, the model coefficients, particularly those that are multipliers of the x^2 and x^3 terms, have to be predicted very accurately in order to come up with performance predictions comparable with the observed data. Deviations between the predicted and fitted coefficients were significantly magnified by the higher order terms leading to unrealistic predictions of pavement performance.

In view of the difficulties encountered with the cubic model, it was decided that further modeling involving the cubic polynomial would not be productive, and that working with another model would be the best direction to follow. Consequently, efforts were made to identify another mathematical equation for modeling the observed AASHO performance trends. Previously, plots showing the variation in pavement surface roughness, as quantified by $\log_{10}(1 + SV)$, with cumulative

TABLE 3 EVALUATION OF STRAIN BASIN INDICES

Strain Basin Index		Definition
1.	V_1	$\varepsilon_{sg_1} - \varepsilon_{sg_{max}}$
2.	V_2	$\varepsilon_{sg_2} - \varepsilon_{sg_{max}}$
3.	V_3	$\varepsilon_{sg_3} - \varepsilon_{sg_{max}}$
4.	V_4	$\varepsilon_{sg_4} - \varepsilon_{sg_{max}}$
5.	V_5	$\varepsilon_{sg_2} - \varepsilon_{sg_1}$
6.	V_6	$\varepsilon_{sg_3} - \varepsilon_{sg_2}$
7.	V_7	$\varepsilon_{sg_4} - \varepsilon_{sg_3}$
8.	V_8	$\varepsilon_{sg_3} - \varepsilon_{sg_1}$
9.	V_9	$\varepsilon_{sg_4} - \varepsilon_{sg_2}$
10.	V_{10}	$\varepsilon_{sg_4} - \varepsilon_{sg_1}$
11.	T_1	$\varepsilon_{ac_{max}} - \varepsilon_{ac_1}$
12.	T_2	$\varepsilon_{ac_{max}} - \varepsilon_{ac_2}$
13.	T_3	$\varepsilon_{ac_{max}} - \varepsilon_{ac_3}$
14.	T_4	$\varepsilon_{ac_{max}} - \varepsilon_{ac_4}$
15.	T_5	$\varepsilon_{ac_1} - \varepsilon_{ac_2}$
16.	T_6	$\varepsilon_{ac_2} - \varepsilon_{ac_3}$
17.	T_7	$\varepsilon_{ac_3} - \varepsilon_{ac_4}$
18.	T_8	$\varepsilon_{ac_1} - \varepsilon_{ac_3}$
19.	T_9	$\varepsilon_{ac_2} - \varepsilon_{ac_4}$
20.	T_{10}	$\varepsilon_{ac_1} - \varepsilon_{ac_4}$

$(\varepsilon_{sg})_{max}$ = maximum subgrade compressive strain directly underneath the tire load

$(\varepsilon_{sg})_i$ = subgrade compressive strain located along the longitudinal direction and at a distance of 'i' feet from the maximum

$(\varepsilon_{ac})_{max}$ = maximum asphalt tensile strain directly underneath the tire load

$(\varepsilon_{ac})_i$ = asphalt tensile strain at a distance of 'i' feet from the maximum

number of load applications, were examined to identify a mathematical equation for modeling the performance of AASHO flexible pavement sections. In the reevaluation of observed performance trends, new plots showing the variation in pavement roughness with the logarithm (base 10) of the cumulative number of load applications were examined. It was realized that the trends observed would be affected by transformations to the variables being plotted. Consequently, a logarithmic transformation of the cumulative number of load applications was applied to see if a different set of performance trends would be obtained. It was found that with this transformation, the new trends observed could be modeled by the hyperbolic equation

$$y = (\beta_0 + \beta_1 x)/(1 + \beta_2 x) \qquad (6)$$

where

y = pavement surface roughness, $\log_{10}(1 + SV)$,
x = logarithm (base 10) of cumulative number of load applications, and
β_i = parameters of the hyperbolic model.
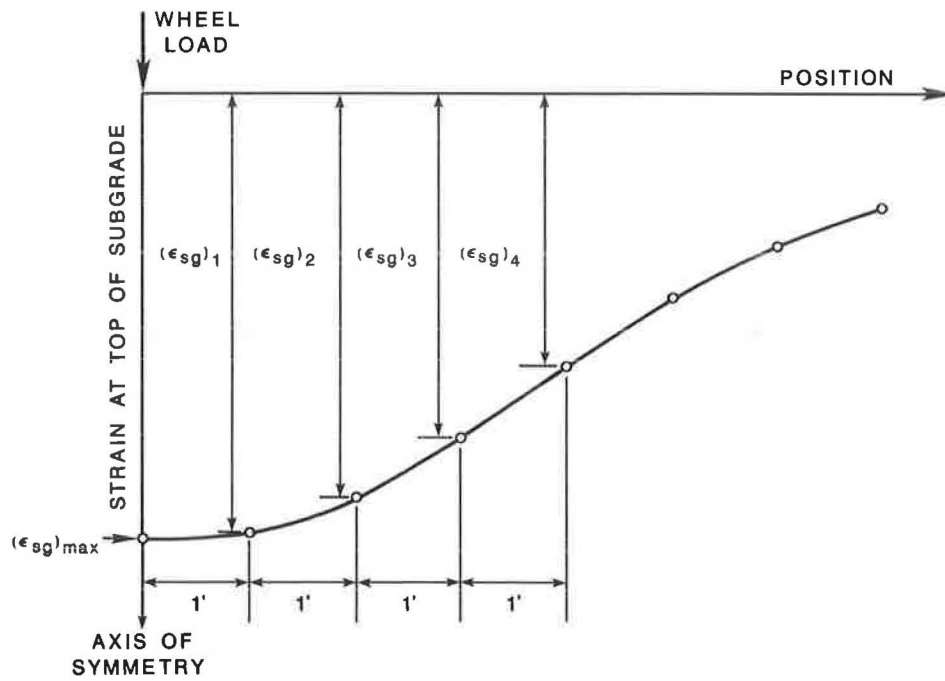
FIGURE 10 Conceptual illustration of subgrade compressive strain basin for single-axle configuration.

Using nonlinear regression, the parameters of the hyperbolic model were estimated by fitting the model to the observed performance data for each AASHO flexible pavement section included in the modeling phase of the research effort. Prediction equations for the fitted model parameters (β_1 and β_2) were subsequently developed using stepwise multiple linear regression. No prediction equation was established for β_0 for reasons mentioned previously. The prediction equations are as follows:

$$\beta_1 = -0.035 - 0.220\,\beta_0 - 0.035\,\log_{10}V_3$$
$$- 0.050\,\log_{10}(1 + H_1)$$
$$R^2 = 0.56 \qquad N = 202 \text{ obs.} \quad (7)$$
$$\beta_2 = -0.354 + 1.232\,\beta_1 + 0.269\,\sqrt{\beta_0} - 31.958\,V_5$$
$$- 0.026\,\log_{10}T_2 + 0.007\,\log_{10}(1 + H_2)$$
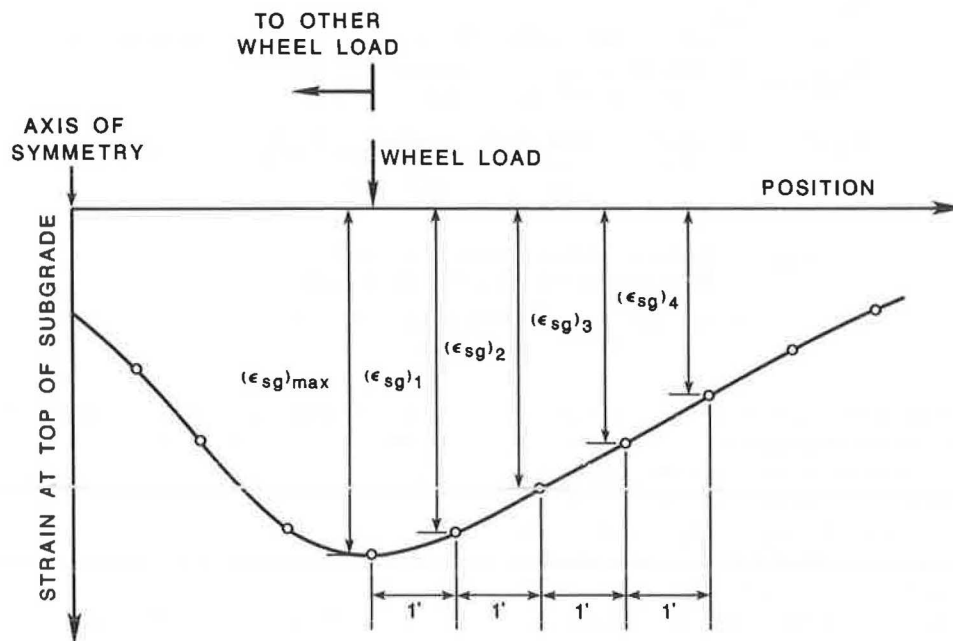$$R^2 = 0.93 \quad N = 202 \text{ obs.} \quad (8)$$

FIGURE 11 Conceptual illustration of subgrade compressive strain basin for tandem-axle configuration.

TABLE 4 PREDICTION EQUATIONS FOR CUBIC MODEL PARAMETERS

$$\beta_1 = -0.109 + 0.959\ V_2 \qquad\qquad\qquad \text{for } V_2 < 0.700$$

$$= -0.109 + 0.959\ V_2 + 9.143\ (V_2 - 0.700)$$
$$-4.143\ (V_2 - 0.700)^2 \qquad\qquad \text{for } V_2 \geq 0.700$$

$$R^2 = 0.56 \qquad\qquad N = 202\ \text{obs.}$$

$$\beta_2 = 0.500 - 2.146\ V_2 \qquad\qquad\qquad \text{for } V_2 < 0.700$$

$$= 0.500 - 2.146 V_2 - 35.771(V_2 - 0.700)$$
$$+ 13.895\ (V_2 - 0.700)^2 \qquad\qquad \text{for } V_2 \geq 0.700$$

$$R^2 = 0.59 \qquad\qquad N = 202\ \text{obs.}$$

$$\beta_3 = -0.616 + 2.253\ V_2 \qquad\qquad\qquad \text{for } V_2 < 0.700$$

$$= -0.616 + 2.253\ V_2 + 31.474\ (V_2 - 0.700)$$
$$- 9.956\ (V_2 - 0.700)^2 \qquad\qquad \text{for } V_2 \geq 0.700$$

$$R^2 = 0.62 \qquad\qquad N = 202\ \text{obs.}$$

$$V_2 = \epsilon_{sg2} - \epsilon_{sgmax} \quad (\ \times\ 10^{-3})$$

ϵ_{sgmax} = maximum subgrade compressive strain directly underneath the tire load

ϵ_{sg2} = compressive strain at the top of the subgrade located along the longitudinal direction and at a distance of 2 feet from the maximum

where

β_i = the ith parameter of the hyperbolic model;
V_3, V_5, T_2 = strain basin indices defined in Table 3;
H_1 = thickness of asphalt concrete layer (in.); and
H_2 = thickness of base layer (in.).

To evaluate the accuracy of the performance predictions from these equations, observed vs. predicted trends were compared. It was found that the predicted performance trends were much more reasonable than those obtained with the prediction equations for the cubic model parameters. In addition, a root-mean-square (RMS) statistic, indicating the accuracy of the predictions, was calculated from the following equation:

$$RMS = \left[\sum_{i=1}^{n} (y - y')^2 / n \right]^{1/2} \qquad (9)$$

where

y = observed $\log_{10}(1 + SV)$,
y' = predicted $\log_{10}(1 + SV)$, and
n = total number of observations.

The RMS statistic for the performance predictions was 0.24 on the basis of 5,895 observations. A similar statistic calculated from the observed performance data for the replicate sections at the AASHO Road Test was 0.19 for 767 observations. (Replicate sections were identical pavement sections constructed at the AASHO Road Test.) Thus the RMS statistic for the performance model compares favorably with the RMS statistic for the replicates, which gives a measure of the pure error in observed pavement performance.

Figure 13 illustrates how the predictions from the model compare with the observed values for pavement roughness. The predictions generally compare favorably with the observed roughness data as reflected by the dark region around the line of equality. The correlation coefficient between the predicted and observed $\log_{10}(1 + SV)$ was determined to be 0.59. In contrast, the correlation coefficient for the observed $\log_{10}(1 + SV)$ between replicates was found to equal 0.44. The fact that a higher correlation coefficient was obtained from the model predictions reflects the smoothing effect of the curve-fitting conducted as part of the model development. In addition, it further indicates that a performance model with reasonable predictive ability has been developed.
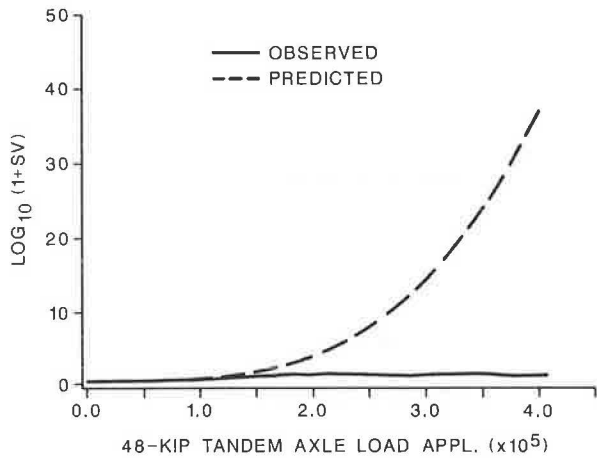
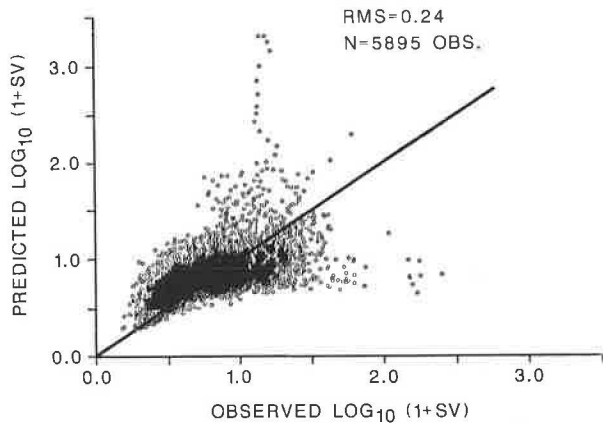**FIGURE 12 Comparison of observed and predicted performance trends for section 262 using the cubic model.**

FIGURE 13 Comparison of predicted $\log_{10} (1 + SV)$ from the hyperbolic model with the observed $\log_{10} (1 + SV)$.

SUMMARY

A performance model was developed in this paper for predicting the trend in pavement surface roughness with cumulative number of load applications. In view of the difficulties encountered with the cubic model, a reevaluation of observed AASHO performance trends was conducted in order to identify another mathematical function for modeling the performance of AASHO flexible pavement sections. It was found that the predictions from the cubic model were extremely sensitive to deviations in the model coefficients, primarily those that are multipliers of the X^2 and X^3 terms. Consequently, the model coefficients have to be predicted very accurately in order to come up with performance predictions comparable with the observed performance. The reevaluation of observed AASHO performance histories resulted in the selection of the hyperbolic equation for modeling the performance of AASHO flexible pavement sections.

Prediction equations for the parameters of the hyperbolic model were subsequently developed. It was found that the hyperbolic equation adequately modeled the observed performance of AASHO flexible pavement sections. However, it should be realized that the performance model was developed using pavement surface roughness as the condition indicator, and that other mathematical functions may be more appropriate for other condition indicators.

Consistent with the hypothesis for this research, an evaluation of the relationships between the hyperbolic model parameters and pavement structural response variables (strains and strain basin indices) was conducted. Through stepwise multiple linear regression, prediction equations were developed that included subgrade and asphalt strain basin indices as independent variables. In the stepwise regression analysis, both the maximum asphalt tensile strain and maximum subgrade compressive strain were allowed to enter into the prediction equations in addition to strain basin indices. The fact that strain basin indices were selected as independent variables reflects the importance of the strain basin for evaluating pavement performance, and provides a strong indication of the utility of strain basin indices as performance predictors.

ACKNOWLEDGMENT

REFERENCES

1. P. E. Irick. Elements of a Framework for the Development of Performance-Related Materials and Construction Specifications. Presented at the 66th Annual Meeting of the Transportation Research Board, Washington, D.C., 1987.
2. *Special Report 61E: The AASHO Road Test: Report 5—Pavement Research.* HRB, National Research Council, Washington, D.C., 1962.
3. F. Finn, C. L. Saraf, R. Kulkarni, K. Nair, W. Smith, and A. Abdullah. *Development of Pavement Structural Subsystems, Vol. 1.* Final Report NCHRP Project 1.10B, 1977.
4. D. R. Luhr and B. F. McCullough. Structural Analysis of AASHO Road Test Flexible Pavements for Performance Evaluation. In *Transportation Research Record 888,* TRB, National Research Council, Washington, D.C., 1982, pp. 63–69.
5. D. L. De Jong, M. G. F. Peutz, and A. R. Korswagen. *Computer Program BISAR.* External Report. Koninklijke/Shell—Laboratorium, The Netherlands, 1973.
6. F. E. Harrell, Jr. *The LOGIST Procedure.* SAS Technical Report S-131, SAS Institute Inc., Cary, N.C., 1985, pp. 15–20.

Rigorous Application of Linear Damage Concepts in Development of Improved Flexible Pavement Performance Models

STEPHEN B. SEEDS AND LUIS M. MEDUS

This paper describes the development of improved flexible pavement performance prediction models in which Miner's linear damage hypothesis was rigorously applied in evaluating original data from the AASHO Road Test. Effects of seasonal variation of soil and pavement properties were considered along with the actual steering and trailing axle loads within the linear damage framework of Miner's hypothesis. Separate models to predict the number of single- and tandem-axle loads sustained were developed using five mechanistic response criteria: asphalt concrete (AC) tensile strain, AC tensile stress, AC shear strain, AC shear stress, and roadbed soil vertical strain. The single- and tandem-axle models based on AC tensile strain had the highest overall precision, i.e., coefficients of determination (r^2) of 0.83 and 0.68, respectively. The models correlate highly with Road Test data, but they do not compare well with other performance models or even the basic AASHO Road Test performance equation. The implication is that the improved models require their own set of standard 18-kip equivalency factors for use in projecting the number of load applications that would be used in designing a flexible pavement structure.

A study for the Arizona Department of Transportation (DOT) was recently completed to evaluate increased pavement loading. In it, new procedures were developed for accurately considering the effects of load magnitude, load configuration, and tire pressure on pavement design and performance. One major task in that study was the development of improved mechanistic-empirical models to simulate the performance of flexible pavement sections at the AASHO Road Test. The models, which are based on a rigorous application of elastic-layer theory and Miner's linear damage hypothesis, were used to develop an improved set of load equivalence factors and a new mechanistic pavement design (McPAD) procedure. The focus of this paper, however, is on model development.

BACKGROUND

A damage-based pavement performance prediction model (or damage model as it will sometimes be referred to) is an equation that can be used to predict the number of load applications that can be sustained by a given pavement structure in a given environment before it reaches a certain failure criterion. (In this context, a damage model does not have to be one that is based on fatigue cracking; it only has to be one that considers cumulative load applications.) The primary and

ARE Inc., 2600 Dellana Lane, Austin, Tex. 78746.

most obvious application of a damage model is in the pavement structural design process where it provides a means for the determination of pavement layer thicknesses. Depending on the nature of the model, it also provides a basis for determining the relative effects of different wheel loads, tire pressures, and load configurations on a pavement's load-carrying capacity. The latter provision translates further into a means for converting mixed-axle-load traffic into an equivalent *design* number of axle load repetitions of a uniform magnitude.

Existing damage models vary from empirical (relying on experience or observation alone) to mechanistic (relying on engineering mechanics). Historically, pavement performance models have been empirically derived; however, there is now a trend toward developing mechanistic-empirical models. These models are based on mechanistic response factors (i.e., stress, strain, and deformation) but are statistically calibrated to observed performance.

Existing pavement damage models have one of two general criteria for failure: one is pavement condition (i.e., extent and severity of distress); the other is pavement roughness (i.e., ride quality or serviceability). The AASHTO flexible pavement performance algorithm (1) is an example of an empirical damage model having terminal serviceability as its failure criterion. Fatigue damage equations developed under NCHRP Project 1-10B (2) are examples of mechanistic-empirical models having an allowable level of cracking as their failure criterion. In general, empirical models are adequate for predicting future performance under conditions similar to those under which observations are made; however, they are not necessarily reliable for predicting performance under conditions outside those inherent in their development. Mechanistic (or mechanistic-empirical) models are better suited for prediction outside the range of the data from which they were developed, since they rely on pavement responses generated by proven theoretical models for their extrapolation. Because of the need to consider loads and tire pressures significantly higher than those considered in the past, a mechanistic approach was selected for developing the damage-based prediction models in this study.

CRITERIA FOR DAMAGE MODEL DEVELOPMENT

In addition to the use of a mechanistic-empirical approach, the following criteria were selected for the development of damage-based pavement performance prediction models for Arizona DOT:

1. AASHO Road Test data. Although 25 years old, the data base from the original AASHO Road Test experiment is still the best organized, most extensive and accurately collected set of roadway performance data.

2. Seasonal variation of roadbed soil support. To develop a mechanistic damage model with a potentially higher degree of accuracy than that of previous research efforts, it was considered essential that the seasonal variation of roadbed soil support at the Road Test be evaluated. To accomplish this, it was necessary to translate seasonal deflections and laboratory test results into pavement material properties so that the resulting variation of critical pavement stresses and strains could be considered. Miner's linear damage hypothesis (3) was assumed to be valid, thus allowing the individual seasonal damages for each AASHO Road Test section to be accumulated and used in the analysis process.

3. Consideration of the effects of steering axles independently from load axles. Since steering axle loads ranged as high as 12,000 lb at the Road Test, it was decided that their effects should be considered separately from the trailing load axles. This was accomplished within the same linear damage framework used for considering seasonal effects.

4. Serviceability as performance criterion. Traffic repetitions corresponding to a serviceability index of 2.5 were used in developing the damage models. Traditionally, pavement damage has been associated with the development of cracking; however, there was no reason not to associate it with loss of serviceability.

5. Separate damage models for single- and tandem-axle loads. This was included in the criteria for model development in order to maximize precision and to provide a better basis for evaluating the relative difference between single- and tandem-axle loads.

ANALYTICAL PROCEDURE

Several steps were accomplished in the process of developing the damage models. These steps are discussed in a logical sequence below.

Step 1: Section Selection

All of the primary AASHO Road Test flexible pavement sections consisted of cross sections having three pavement layers: asphalt concrete surface, granular base, and granular subbase. In choosing sections for detailed analysis, only those meeting the following layer thickness constraints were included: asphalt concrete surface thickness ($D_1 \geq 2$ in.), base thickness ($D_2 \geq 6$ in.), and subbase thickness ($D_3 \geq 8$ in.). These layer thickness constraints were selected in order to confine the analysis to sections having significant load-carrying capacity. Since several of these sections did not reach a terminal serviceability of 2.5 during the two-year traffic loading period, only 33 single-axle and 27 tandem-axle sections were considered.

Step 2: Season Delineation

Primary seasonal divisions were established on the basis of a detailed examination of seasonal deflections and on the find-
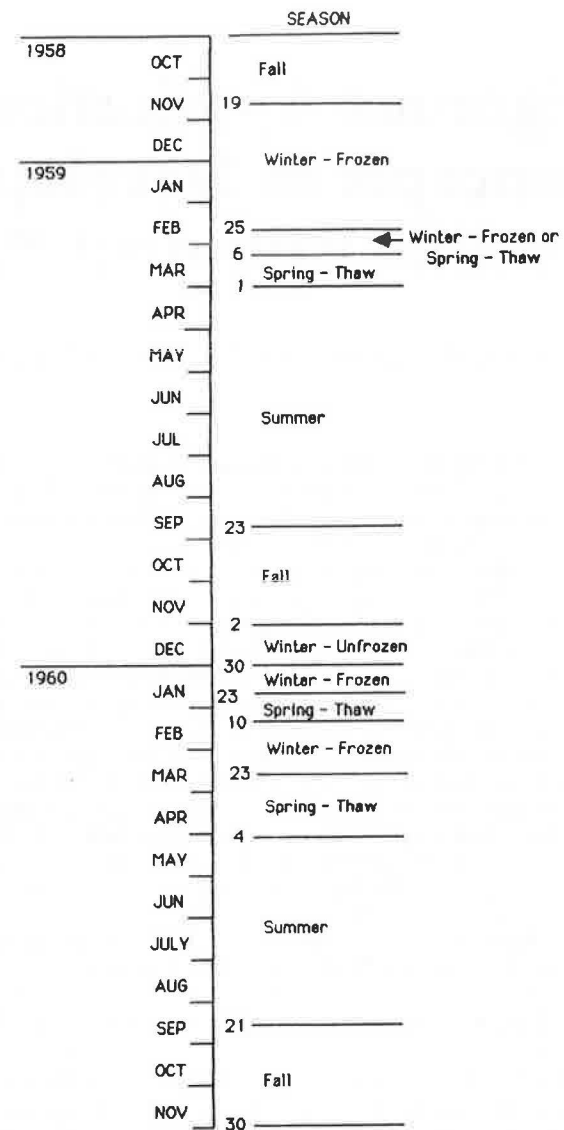
FIGURE 1 Seasonal divisions established for AASHO Road Test experiment.

ings of NCHRP Project 1-10B (2). These are depicted in Figure 1. Note that because of the different rates of thawing associated with section thickness, there is a variable division between the first hard-freeze winter and the first spring thaw. This variation was handled on a section-by-section basis. The asphalt concrete elastic modulus values for each of the seasons were based on laboratory test results and recommendations from NCHRP 1-10B (2): summer (230 ksi), fall (450 ksi), winter (1,700 ksi) and spring (710 ksi).

Step 3: Determine Cumulative Load Applications

Appendix A of AASHO Road Test Special Report 61E (4) was used to determine the cumulative number of wheel load applications sustained by each section (single and tandem) until it reached a serviceability of 2.5.

Step 4: Determine Seasonal Deflections

The graph in Figure 2 provides an example of deflection vs. time for Section 253. That plot represents the pavement surface deflection under a 30-kip single-axle load measured using a Benkelman beam. The plot indicates the critical deflection values that were selected for each season. Note that in one case (summer 1959), deflections were divided into two subseasons because of a significant difference in deflection at the beginning and end of the season. This subdivision was considered necessary because of the potential impact on materials characterization and was applied on several other sections.

Seasonal deflection estimates were made for all sections under the different deflection loads. Table 1 identifies the single-axle loads that were used to measure deflection on each of the sections. Recall that Lane 1 was loaded solely with single-axle load groups whereas Lane 2 was loaded primarily with tandem-axle load groups. (The tandem-axle trucks did have single-axle steering axles.)

Step 5: Characterize Seasonal Material Properties Under Deflection Loads

To characterize the seasonal material properties of each section, a computer program, MODEST-1, was developed which basically uses an elastic-layer-theory model, ELSYM5 (5), to identify a unique set of pavement layer moduli that will match the specified critical seasonal deflections and satisfy the bulk stress relationships established in NCHRP Project 1-10B (2) for base and subbase materials at the Road Test. Figure 3 provides a flow diagram of the basic iterative deflection matching process used by the MODEST-1 program. The tolerances selected for satisfying the bulk stress and deflection criteria were 5 and 3 percent, respectively.

Step 6: Solve for Seasonal Material Properties for Each Lane 1 Section

Unfortunately, because of stress (or load) sensitivity of the materials and the fact that the deflection loads were not always

TABLE 1   AXLE LOADS USED IN AASHO ROAD TEST DEFLECTION STUDIES (4)

Loop	Lane	Single Axle Load (kips)
2	1	-
	2	6
3	1	6, 12
	2	6, 12
4	1	12, 18
	2	12
5	1	12, 22.4
	2	12
6	1	12, 30
	2	12

equivalent to the actual wheel loads (compare Table 2 with Table 1), it was necessary to include this additional task as part of the materials characterization process. To predict seasonal material properties under the actual applied wheel loads, two additional computer programs were developed: STAX-1 and TANDAX-1.

Since the loads used to measure deflection matched the actual single-axle wheel loads in Lane 1, STAX-1 was designed only to estimate the material properties under the Lane 1 steering-axle loads. The diagram in Figure 4 shows roadbed soil resilient modulus vs. deviator stress, which illustrates this process for a given section during a given season. The solid line is established by plotting the modulus–deviator stress values generated in Step 5 for the two deflection loads. (The slope of the line that connects these two points is indicative of the roadbed soil's sensitivity to load.) The theoretical steering-axle relationship was generated by solving for the deviator stress values corresponding to the two previous roadbed soil modulus values. In solving for these deviator stress values, it was still necessary to satisfy the bulk stress criteria for the base and subbase materials. The intersection of the two lines defines the point at which roadbed soil stress conditions under the steering axle are consistent with the in-situ behavior of the soil. Thus, the roadbed soil resilient modulus and corresponding base and subbase modulus values at this point represent the material properties required for steering-axle load conditions.

The actual stresses and strains for each season of each segment are a by-product of the MODEST-1 and STAX-1 solutions. The results for this and the previous five steps [as they pertain to all single-axle (Lane 1) sections] are included within the draft final report to the Arizona DOT (6), but are too lengthy to include in this paper.

Step 7: Solve for Seasonal Material Properties for Each Lane 2 Section

Unlike the single-axle sections, neither the steering- nor the tandem-axle loads in Lane 2 matched the loads used to measure deflection. Consequently, it was necessary to incorporate a slightly different approach into the TANDAX-1 program to solve for the material properties required for the Lane 2 sections. As can be seen in Table 1, most of the deflections in the Lane 2 sections were measured using only a 12-kip single axle. Thus, to solve for the material properties under the steering- and tandem-axle loads, the single resilient modulus vs. deviator stress point (derived from the MODEST-1 program for the 12-kip single-axle load) had to be combined with an estimate of the roadbed soil's stress sensitivity.

The single resilient modulus vs. deviator stress point from the MODEST-1 deflection analysis is plotted, and a straight line corresponding to the estimated stress sensitivity (slope) is drawn through the point. This line represents the in-situ resilient modulus vs. deviator stress relationship for that section during that season. Since the stress sensitivity for most of the Lane 2 sections was unknown, individual estimates were based on the calculated stress sensitivity of the adjacent Lane 1 sections. For the cases where Lane 1 information was unavailable, stress sensitivity estimates were based on trends observed in other Lane 1 sections.

Once the in-situ relationship for the roadbed soil was estab-
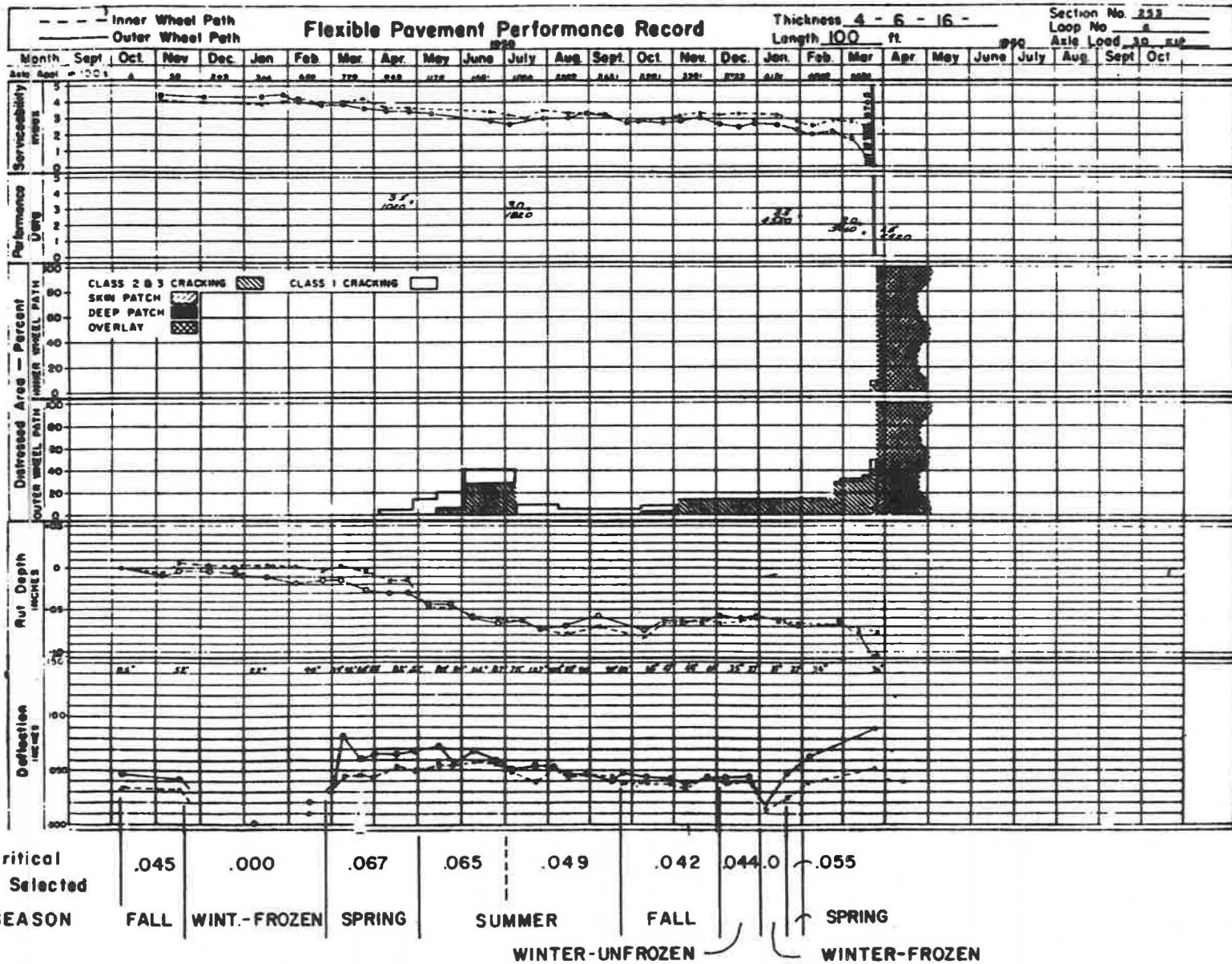
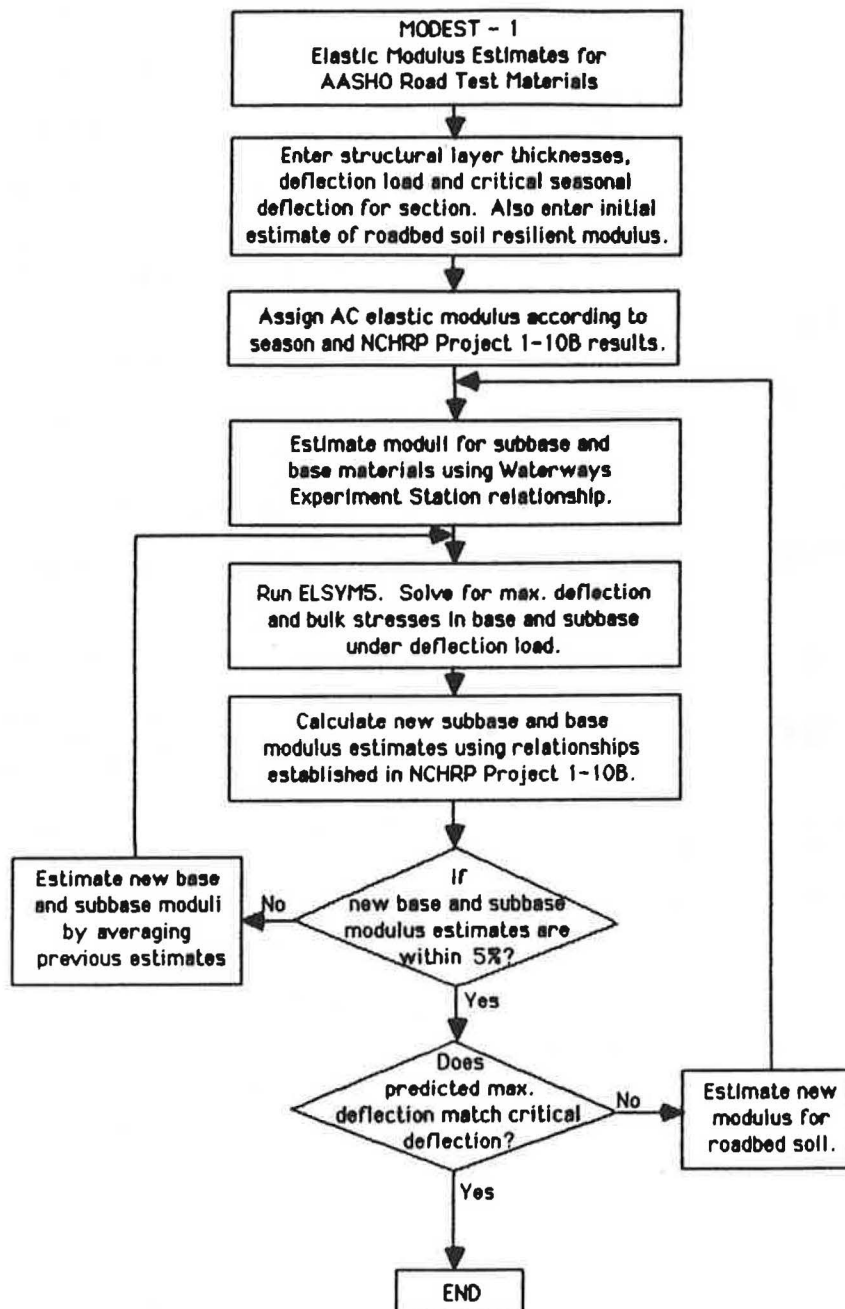FIGURE 2 Example of average critical deflection values by season.

```
┌─────────────────────────────────┐
│          MODEST - 1             │
│   Elastic Modulus Estimates for │
│   AASHO Road Test Materials     │
└─────────────────────────────────┘
                 │
                 ▼
┌─────────────────────────────────┐
│  Enter structural layer thicknesses, │
│  deflection load and critical seasonal │
│  deflection for section. Also enter initial │
│  estimate of roadbed soil resilient modulus. │
└─────────────────────────────────┘
                 │
                 ▼
┌─────────────────────────────────┐
│  Assign AC elastic modulus according to │
│  season and NCHRP Project 1-10B results. │
└─────────────────────────────────┘
                 │
                 ▼
┌─────────────────────────────────┐
│  Estimate moduli for subbase and │
│  base materials using Waterways │
│  Experiment Station relationship. │
└─────────────────────────────────┘
                 │
                 ▼
┌─────────────────────────────────┐
│  Run ELSYM5. Solve for max. deflection │
│  and bulk stresses in base and subbase │
│  under deflection load. │
└─────────────────────────────────┘
                 │
                 ▼
┌─────────────────────────────────┐
│  Calculate new subbase and base │
│  modulus estimates using relationships │
│  established in NCHRP Project 1-10B. │
└─────────────────────────────────┘
```


FIGURE 3 Flow diagram of MODEST-1 program.

lished, the theoretical steering- and tandem-axle relationships were generated and plotted in the same way that the steering-axle relationship was produced for the Lane 1 sections. Similarly, the intersections of the two theoretical relationships with that established for the in-situ soil represent the points at which the roadbed soil stress conditions under the given steering and tandem-axle loads are consistent with the in-situ behavior of the soil. Thus, the roadbed soil modulus values and their corresponding base and subbase moduli at these two points are the material properties required for the two particular loading conditions.

The actual stresses and strains for each season of each section are, in this step, a by-product of the TANDAX-1 solu-

tions (6). Like the single-axle results, however, they are too lengthy to include in this paper.

Step 8: Develop Single-Axle Damage Models

Separate damage models were developed for single- and tandem-axle loads. The reason for this was the desire to independently examine the effects of single and tandem axles. A combined model would have required some assumption as to the relative impact on pavement performance of positioning two single-axle loads of a given magnitude in a tandem configuration. This assumption would have introduced an addi-

TABLE 2 TEST VEHICLE LOADINGS AT AASHO ROAD TEST (4)

LOOP	LANE		WEIGHT IN KIPS		
------	------	--	FRONT AXLE	LOAD AXLE	GROSS WEIGHT
②	① LOAD LOAD		2	2	4
	② FRONT LOAD		2	6	8
③	① FRONT LOAD LOAD		4	12	28
	② FRONT LOAD LOAD		6	24	54
④	①		6	18	42
	②		9	32	73
⑤	①		6	22.4	51
	②		9	40	89
⑥	①		9	30	69
	②		12	48	108

tional source of error into the analysis and also made it impossible to use the model to examine the effects of axle configuration.

To apply a mechanistic analysis approach using elastic-layer theory and Miner's linear damage hypothesis, it was first necessary to assume a form for the damage model. Previous research efforts, including NCHRP Project 1-10B (2), suggested a form which was adopted for this study:

$$\log (N_f) = a_0 + a_1 * \log (R) + a_2 * \log(E_{AC}) \tag{1}$$

where, in this case,

N_f = estimated number of load repetitions to serviceability of 2.5,
R = selected mechanistic response (i.e., stress or strain),
E_{AC} = estimated elastic modulus of the asphalt concrete, and
a_0, a_1, and a_2 = coefficients to be determined through statistical analysis of the data.

The mechanistic responses that were considered in developing damage models (for both the single- and tandem-axle loads) include: (1) maximum asphalt concrete (AC) tensile strain, ε_{AC}; (2) maximum AC tensile stress, σ_{AC} (psi); (3) maximum AC shear strain, γ_{AC}; (4) maximum AC shear stress, τ_{AC} (psi); and (5) maximum vertical strain on roadbed

soil, λ_{RS}. The first four of these mechanistic responses were calculated at the bottom of the surface (asphalt concrete) layer and were considered in order to determine if any one in particular is a better predictor of pavement performance than the other. The last response, vertical strain at the top of the roadbed soil, was considered because of its applicability in predicting the performance of thin-surfaced pavements.

As discussed in Step 6, seasonal values for all the mechanistic responses were generated using the ELSYM5 program (5), based on elastic-layer theory. Actual values for each load and season of each section are contained within the single-axle data base presented in Appendix B of the report to ADOT (6).

The machinery for producing the a_0, a_1, and a_2 coefficients for the damage models was incorporated into a program called DAMOD-4. Figure 5 is a flow diagram of the major operations of this interactive program.

First, the desired mechanical response is identified and, for a specified trial a_2 value, initial values for both a_0 and a_1 are provided (operation 1). The program then goes through every season for a given section and calculates the allowable load repetitions for both the steering- and the single-axle loads (operations 2 and 3). The next two operations (4 and 5) require an explanation of a technique derived by Taute et al. (7) which uses Miner's linear damage hypothesis (3) to consider multiple seasons and nonuniform axle loads in developing a new damage model.

The linear damage hypothesis basically implies that one repetition of a given stress or strain produces the same amount of damage to a pavement whether it is applied at the beginning, middle, or end of the pavement's life. It can be expressed mathematically as follows:

$$D = \sum_{j=1}^{m} \frac{n_j}{(N_f)_j} \tag{2}$$

where, in this case,

D = total damage to the ith section,
n_j = actual number of stress or strain repetitions of a given load during a given season,
$(N_f)_j$ = allowable number of stress or strain repetitions of a given load during a given season, and
m = product of the number of different axle loads times the number of different seasons (on the ith section).

The allowable number of repetitions, $(N_f)_j$, is determined by solving the damage model (Eq. 1) for the stress or strain level corresponding to a given axle load and season. The key to estimating the a_0, a_1, and a_2 coefficients in the damage model, then, is to find an effective stress or strain level that would produce the same amount of damage to the section as the combination of all the axle load repetitions during the different seasons. This means that the total damage (to the ith section) can also be expressed as:

$$D = \frac{\sum_{j=1}^{m} n_j}{(N_f)_{eff}} \tag{3}$$

where $(N_f)_{eff}$ is the allowable number of load repetitions corresponding to the "effective" stress or strain level.
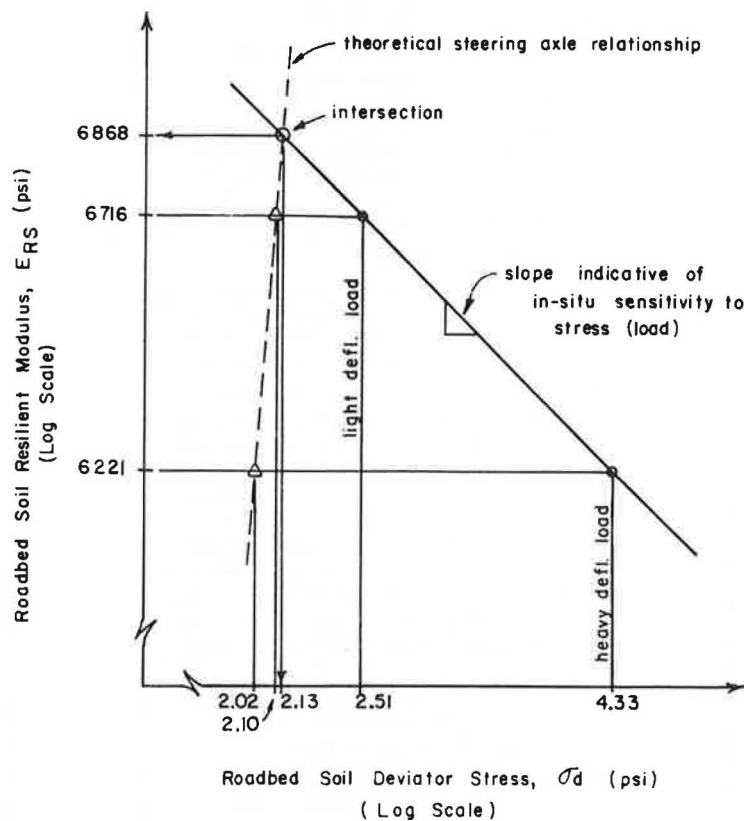
FIGURE 4 Graph of roadbed soil resilient modulus vs. deviator stress, illustrating technique used to solve for material properties under steering-axle loads in Lane 1 sections.

Rearranging the terms to solve for $(N_f)_{eff}$ and recognizing that the total damage is calculated using Equation 2 gives:

$$(N_f)_{eff} = \frac{D}{\sum_{j=1}^{m} n_j} \quad (4)$$

Substituting the form of the damage model for N_f in Equation 1 and solving for the effective stress or strain, R_{eff}, results in:

$$R_{eff} = \left[\frac{D}{10^{a_0} * (E_{AC})^{a_2} * \sum_{j=1}^{m} n_j} \right]^{1/a_1} \quad (5)$$

Note that because asphalt concrete elastic modulus, E_{AC}, is in the equation, it is necessary to calculate the effective stress or strain, R_{eff}, for a modulus value corresponding to a particular season. Since it occurs between the extreme seasons, fall (autumn) was selected as the season for R_{eff} calculations. Thus, the asphalt concrete elastic modulus value used was 450,000 psi. It should be recognized that the selection of fall as the season for R_{eff} calculations theoretically has no effect on the ultimate predictive accuracy of the damage model.

Operations 2, 3, 4, and 5 of the flow diagram in Figure 5 are performed for one Road Test section at a time. Consequently, operations 6 and 7 are included to provide a means for incrementing through each section.

Once effective stress or strain values are calculated for each section, a regression analysis (operation 8) is performed on N_f (in this case, the actual number of load repetitions experienced by the section before it "failed") vs. R_{eff} to generate new a_0 and a_1 coefficients for the damage model. A measure of the "fit" of the model to the data, known as the coefficient of determination (or r^2), is also generated as part of this regression analysis.

Operation 9 provides a test of whether the new a_0 and a_1 values are significantly different from the assumed initial values. If they are, then the process must be reexecuted using the new a_0 and a_1 values as initial estimates (operation 10). When the a_0 and a_1 values are essentially equivalent to the assumed initial values (operation 11), they represent the "best" solution for the trial a_2 value.

Table 3 is an example of output from the DAMOD-4 program for one of the initial asphalt concrete tensile strain models. For the trial a_2 value of -3.97, eight iterations were required before the final a_0 and a_1 values matched the initial specified values. These values, then, represent the best combination of a_0 and a_1 for the selected trial value of a_2. To get the best combination of a_0, a_1, and a_2, it was necessary to try different a_2 values with the objective of finding the combination that provides the highest coefficient of determination (r^2). Table 4 illustrates how the a_2 value of -3.97 and the corresponding a_0 and a_1 values of 6.89 and -6.21 (respectively) provided the maximum r^2. Therefore, they represent the best set of single-axle coefficients.
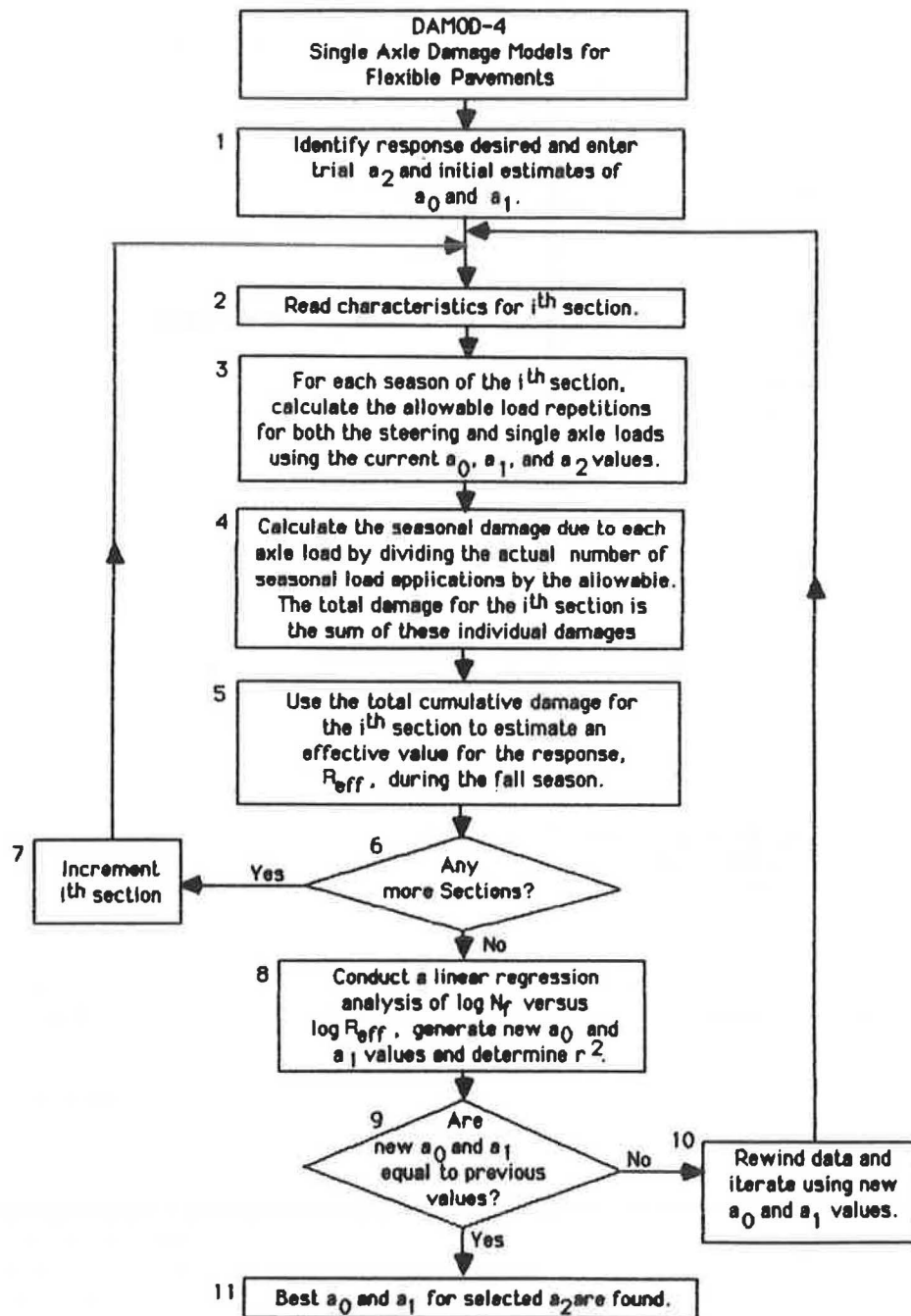
FIGURE 5   Flow diagram of DAMOD-4 program.

The DAMOD-4 analysis for single-axle loads was performed considering five different mechanistic responses (including asphalt concrete tensile strain). The results are summarized in Table 5. Figure 6 illustrates how well the tensile strain model fits the Road Test data. However, this and the other relationships were all considered *initial* or preliminary single-axle damage models. Although they are certainly valid and could be used for design or pavement performance prediction, additional equations (described next) were developed which may be more suitable.

In the process of trying to develop a single-axle damage

model based on vertical strain at the top of the roadbed soil, the analysis indicated an impractical and undue correlation with vertical strains sustained during the winter. This was probably due to the fact that the underlying materials were assigned modulus values based on engineering judgment of the properties during the winter rather than on the deflection-based materials characterization technique used for the other seasons. Whatever the explanation, it was reasoned that if pavement damage during the winter was indeed insignificant, then a suitable damage model could be developed by not considering the frozen-winter seasons in the DAMOD-4 anal-

TABLE 3   SAMPLE DAMOD-4 OUTPUT FOR PRELIMINARY SINGLE-AXLE
LOAD MODEL

CRITICAL RESPONSE FOR DAMAGE MODEL: AC TENSILE STRAIN
TRIAL NO.   8

```
AO    6.890
A1   -6.210
A2   -3.970
```

SEASONAL EFFECTS:
```
SPRING -23.2295000
SUMMER -21.2860600
FALL   -22.4432500
WINTER -24.7348800
```

NSEC	D1	D2	D3	TRSUM	DAMSUM	TRPRIM	STREF	X	Y	YPRIM
111	2.	6.	8.	.9315E+06	.3528E+01	264037.	.000419	-3.37760	28.41244	5.96918
155	3.	6.	8.	.9555E+06	.1587E+01	602083.	.000367	-3.43525	28.42348	5.98023
623	3.	6.	8.	.1245E+06	.4273E+00	291340.	.000413	-3.38449	27.53842	5.09517
601	3.	6.	12.	.9315E+06	.1739E+01	535789.	.000374	-3.42709	28.41244	5.96918
577	4.	6.	8.	.1140E+07	.1891E+01	602813.	.000367	-3.43534	28.50016	6.05690
625	4.	6.	12.	.1019E+07	.9352E+00	1089033.	.000334	-3.47670	28.45122	6.00796
419	3.	6.	8.	.1095E+06	.3208E+00	341288.	.000402	-3.39555	27.48267	5.03941
487	3.	6.	12.	.1155E+06	.2264E+00	510210.	.000377	-3.42367	27.50584	5.06258
471	3.	9.	8.	.1185E+06	.7254E+00	163350.	.000453	-3.34402	27.51697	5.07372
455	4.	6.	8.	.1449E+06	.9820E+00	147563.	.000460	-3.33691	27.60432	5.16107
453	4.	6.	8.	.1359E+06	.4430E+00	306764.	.000409	-3.38809	27.57647	5.13322
425	4.	6.	12.	.7575E+06	.1042E+01	726904.	.000356	-3.44843	28.32264	5.87938
417	4.	9.	8.	.2520E+06	.8012E+00	314520.	.000408	-3.38984	27.84465	5.40140
477	4.	9.	12.	.1649E+07	.1429E+01	1153994.	.000331	-3.48075	28.66034	6.21709
469	5.	6.	8.	.8400E+06	.7164E+00	1172530.	.000330	-3.48186	28.36753	5.92428
445	5.	6.	12.	.1052E+07	.6511E+00	1615064.	.000313	-3.50426	28.46506	6.02181
303	4.	6.	8.	.1200E+06	.7707E+00	155697.	.000456	-3.34067	27.52244	5.07918
323	4.	6.	12.	.1200E+06	.1071E+01	112036.	.000481	-3.31765	27.52244	5.07918
253	4.	6.	16.	.6765E+06	.1950E+01	346877.	.000401	-3.39669	28.27352	5.83027
321	4.	9.	8.	.1200E+06	.1248E+01	96156.	.000493	-3.30696	27.52244	5.07918
267	4.	9.	12.	.1620E+06	.1538E+01	105324.	.000486	-3.31333	27.65277	5.20952
309	4.	9.	16.	.1535E+07	.4167E+01	368219.	.000397	-3.40086	28.62922	6.18597
259	5.	6.	8.	.1365E+06	.6848E+00	199322.	.000439	-3.35794	27.57839	5.13513
307	5.	6.	12.	.8775E+06	.1576E+01	556653.	.000372	-3.42976	28.38650	5.94325
305	5.	6.	12.	.1890E+06	.6615E+00	285720.	.000414	-3.38312	27.71972	5.27646
327	5.	6.	16.	.1014E+07	.1700E+01	596383.	.000368	-3.43459	28.44929	6.00604
313	5.	9.	8.	.6615E+06	.1551E+01	426449.	.000388	-3.41113	28.26378	5.82053
331	5.	9.	12.	.8355E+06	.8997E+00	928599.	.000342	-3.46555	28.36520	5.92195
325	6.	6.	8.	.1530E+06	.4016E+00	380967.	.000395	-3.40324	27.62795	5.18469
257	6.	6.	12.	.1070E+07	.1150E+01	929806.	.000342	-3.46564	28.47243	6.02918
263	6.	9.	8.	.7680E+06	.8489E+00	904675.	.000344	-3.46373	28.32862	5.88536
271	6.	9.	8.	.1058E+07	.1384E+01	764358.	.000353	-3.45194	28.46754	6.02428
311	6.	9.	12.	.1005E+07	.8740E+00	1149881.	.000331	-3.48050	28.44542	6.00217

REGRESSION LINE IS:
```
AO       6.883
A1      -6.212
R-SQUARE     .599
```

Notes: NSEC = AASHTO section number; D_1, D_2, D_3 = layer thickness (in.) for surface, base, and subbase; DAMSUM = total damage for section computed using a_0, a_1, and a_2; STREF = effective fall stress or strain for section; TRPRIM = allowable load applications corresponding to effective fall stress or strain; $X = \log_{10}$ of STREF (independent variable in the regression analysis); YPRIM = $\log_{10}$ of TRSUM (dependent variable in the regression analysis); Y = YPRIM minus the fall seasonal effect.

ysis. When this analysis was performed, the results for the vertical strain model were so remarkable that similar analyses were carried out to develop models for the other four mechanistic response variables. The results are summarized in Table 6 and a graph illustrating the relative precision for the asphalt concrete tensile strain model is presented in Figure 7.

A test of these models was made to determine if the increase in damage that results in each section when the frozen winters are included was indeed insignificant. This test basically consisted of an examination of the differences between the damage calculated with the frozen-winter effects and those calculated without the frozen-winter effects. The results indicated that there was no significant difference for all 33 Road Test sections. Thus, it was concluded that the increase in damage

TABLE 4   SAMPLE OF OPTIMUM COMBINATIONS OF a_0, a_1, AND a_2 FOR SINGLE-AXLE DAMAGE MODEL

Coefficients			Coefficient of Determination
a_2	a_1	a_0	(r^2)
-3.50	-6.46	3.33	0.588
-3.70	-6.35	4.85	0.597
-3.90	-6.23	6.40	0.597
-3.95	-6.21	6.78	0.597
-3.97	-6.21	6.89	0.599 (Optimum)
-4.00	-6.19	7.13	0.597
-4.10	-6.15	7.85	0.596
-4.30	-6.06	9.34	0.587

TABLE 5   INITIAL SINGLE-AXLE DAMAGE MODELS RESULTING FROM DAMOD-4 COMPUTER ANALYSIS

Mechanistic Response Considered	Symbol (R)	Optimum Coefficients			Coefficient of Determination (r^2)
		a_0	a_1	a_2	
Asphalt Concrete Tensile Strain	ε_{AC}	6.89	-6.21	-3.97	0.599
Asphalt Concrete Tensile Stress	σ_{AC}	4.68	-6.40	2.80	0.615
Asphalt Concrete Shear Strain	γ_{AC}	8.96	-6.43	-4.20	0.584
Asphalt Concrete Shear Stress	τ_{AC}	6.69	-6.28	2.10	0.562
Vertical Strain on Roadbed Soil	ε_{RS}	(Model not possible)			

Form of Damage Model

$$\log(N_f) = a_0 + a_1 * \log(R) + a_2 * \log(E_{AC})$$
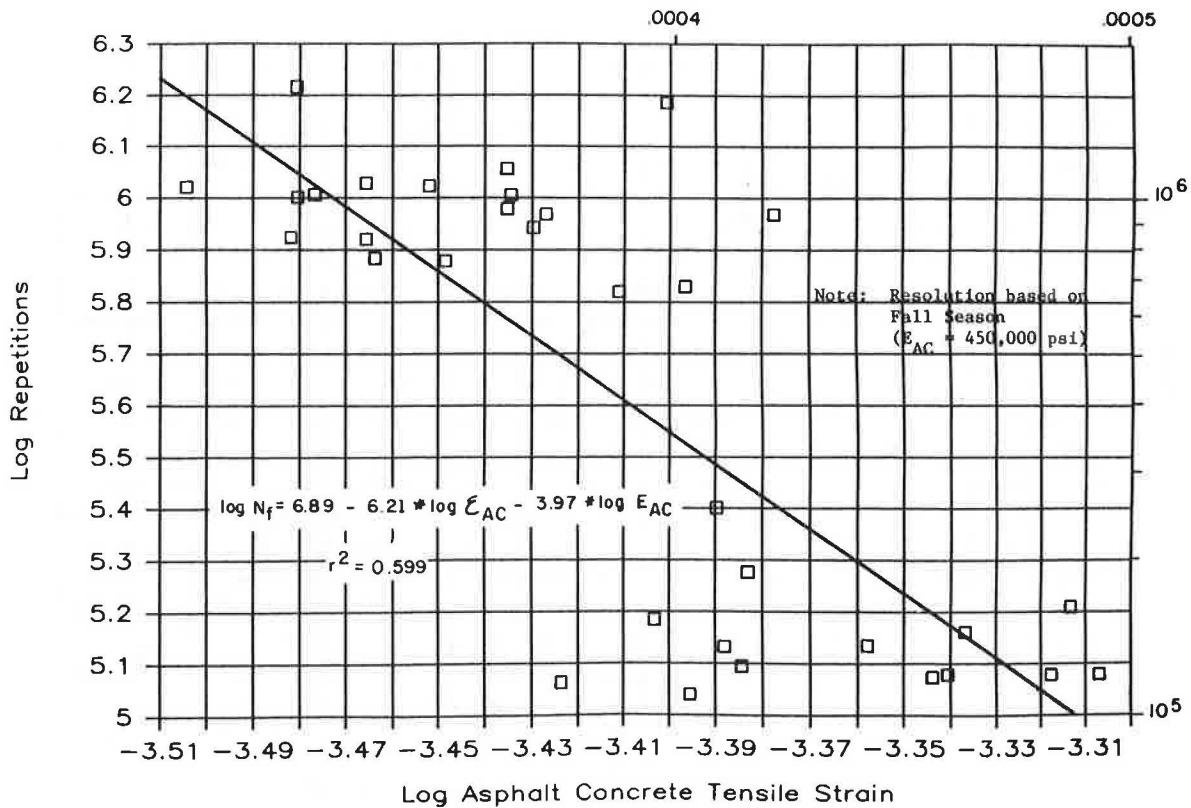
FIGURE 6 Single-axle damage model based on asphalt concrete tensile strain.

TABLE 6   SINGLE-AXLE DAMAGE MODELS RESULTING FROM DAMOD-4
COMPUTER ANALYSIS ON DATA WITHOUT FROZEN-WINTER EFFECTS

Mechanistic Response Considered	Symbol (R)	Optimum Coefficients			Coefficient of Determination (r^2)
		a_0	a_1	a_2	
Asphalt Concrete Tensile Strain	ε_{AC}	3.25	-7.50	-4.10	0.834
Asphalt Concrete Tensile Stress	σ_{AC}	2.69	-7.47	3.60	0.841
Asphalt Concrete Shear Strain	γ_{AC}	6.61	-7.72	-4.50	0.829
Asphalt Concrete Shear Stress	τ_{AC}	3.85	-7.62	3.10	0.819
Vertical Strain on Roadbed Soil	ε_{RS}	-7.75	-4.28	-	0.723

Form of Damage Model

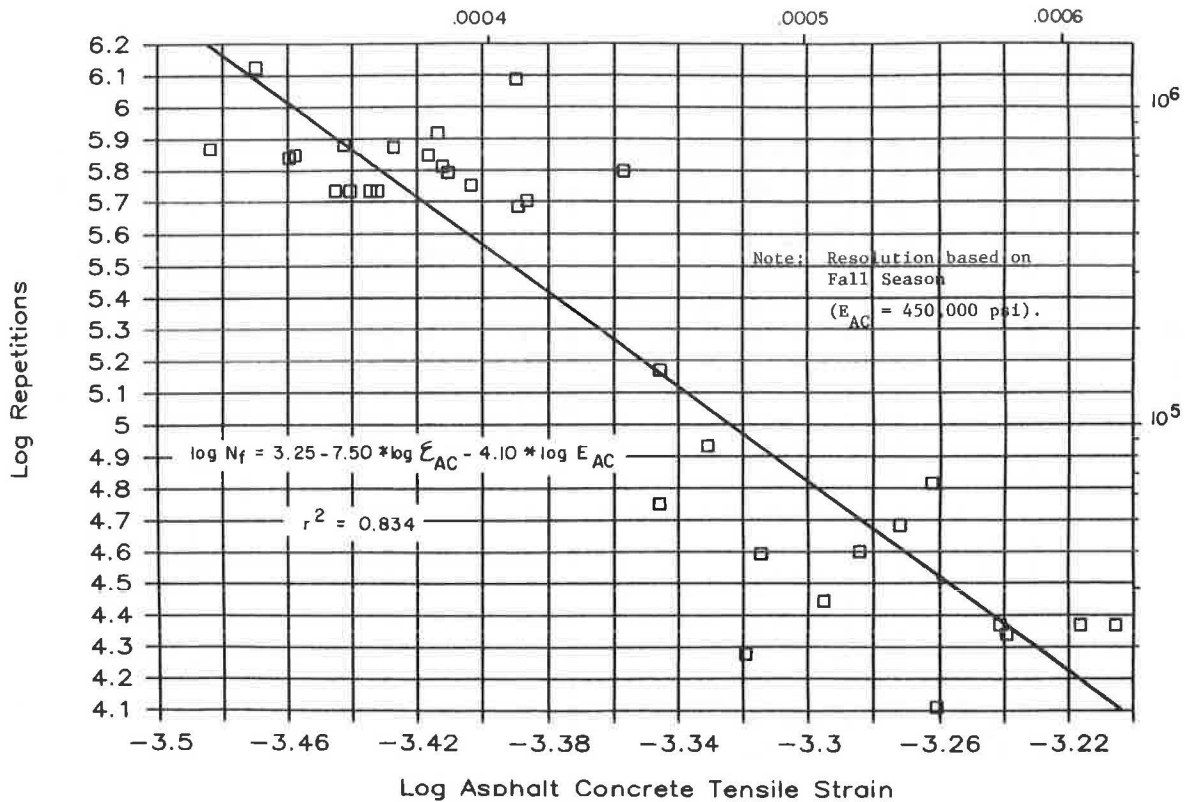$$\log(N_f) = a_0 + a_1 * \log(R) + a_2 * \log(E_{AC})$$

FIGURE 7   Single-axle damage model based on asphalt concrete tensile strain (frozen-winter effects not included).

due to load applications during the frozen-winter season is indeed negligible.

Step 9: Develop Tandem-Axle Damage Models

The approach to developing the tandem-axle damage models was almost identical to that for the single-axle models in Step 8. The form of the model was the same, the same five mechanistic response variables were considered, and, for consistency, load applications during the frozen-winter season were not considered. The principal difference in the analysis was in the recognition that damage due to the steering axles had to be assessed using the appropriate single-axle damage model. The necessary changes were incorporated into the DAMOD-4 program to produce DAMOD-5. The differences are in operations 1, 3, 4, and 5 (see Figure 5).

In operation 1, fixed a_0, a_1, and a_2 values from the single-axle model are entered along with the trial a_2 value and initial estimates of a_0 and a_1 for the tandem-axle model. In operation 3, the allowable load repetitions for the steering and tandem-axle loads are calculated using the appropriate a_0, a_1, and a_2 values. In operation 4, total damage is calculated with particular attention to the load configuration (steering or tandem). In operation 5, the effective stress or strain is calculated with a formula derived using the same basic approach as that used to derive Equation 5 for single-axle loads.

The final results of this step for all five mechanistic response variables are presented in Table 7.

RECOMMENDED MODELS

Based on the results of the analyses, it was recommended that the single- and tandem-axle damage models that are based on asphalt concrete tensile strain without frozen-winter effects be used both for asphalt concrete pavement design and for examining the relative effects of different loads, load configurations, and tire pressures on pavements with asphalt concrete thicknesses greater than 2 in. The predictive accuracy of all the models based on a mechanistic response in the surface layer was very high; however, the single- and tandem-axle tensile strain models had the highest combined precision. The fact that most of the experience to date with asphalt concrete damage models has been with tensile strain was another reason for recommending these particular models.

The roadbed soil vertical strain models were only recommended for the case where surface treatments or thin asphalt-concrete-surfaced pavements are being designed or evaluated. Although these models have a somewhat lower level of precision, they still explain a high percentage of the variability observed in the AASHO Road Test data.

CONCLUSION

In order to minimize the effects of extreme seasonal variations observed at the AASHO Road Test and to provide a better basis for extrapolation to heavier loads, higher tire pressures, and more repetitions, a rigorous mechanistic approach was

TABLE 7 TANDEM-AXLE DAMAGE MODELS RESULTING FROM DAMOD-5
COMPUTER ANALYSIS ON DATA WITHOUT FROZEN-WINTER EFFECTS

Mechanistic Response Considered	Symbol (R)	Optimum Coefficients			Coefficient of Determination (r^2)
		a_0	a_1	a_2	
Asphalt Concrete Tensile Strain	ε_{AC}	0.82	-6.18	-3.0	0.676
Asphalt Concrete Tensile Stress	σ_{AC}	0.91	-5.51	3.0	0.654
Asphalt Concrete Shear Strain	γ_{AC}	5.19	-5.30	-3.0	0.580
Asphalt Concrete Shear Stress	τ_{AC}	4.75	-5.05	1.9	0.578
Vertical Strain on Roadbed Soil	ε_{RS}	-5.27	-3.42	-	0.649

Form of Damage Model

$$\log(N_f) = a_0 + a_1*\log(R) + a_2*\log(E_{AC})$$

used to develop improved flexible pavement performance prediction models. This has resulted in a methodology that should be better suited for use over loads, tire pressures, and environments that are well outside those of the Road Test.

As part of the Arizona DOT study, revised load equivalency factors and a computerized flexible pavement design procedure (McPAD) were developed based on the new damage models. Although the damage model coefficients (i.e., the a_1 values) are higher than those generated in past research studies, comparisons with designs derived from the Road Test performance equations indicate an excellent correspondence for Road Test conditions. The differences occur when comparisons are made for loading and environmental conditions outside the Road Test, where heavier loads, higher tire pressures, and stronger soils result in significantly different pavement structural requirements. Obviously, this means that the final results of the study will need further investigation before the models and procedures can be implemented.

ACKNOWLEDGMENTS

REFERENCES

1. *AASHTO Interim Guide for Design of Pavement Structures, 1972* (Chapter III Revised, 1981), American Association of State Highway and Transportation Officials, Washington, D.C., 1981.
2. F. Finn, C. L. Saraf, R. Kulkarni, K. Nair, W. Smith, and A. Abdullah. *Development of Pavement Structural Subsystems.* Vol. I. Final Report, NCHRP Project 1-10B. TRB, National Research Council, Washington, D.C., 1977.
3. M. A. Miner. Cumulative Damage in Fatigue. *Journal of Applied Mechanics,* September 1945.
4. *Special Report 61E: The AASHO Road Test, Report 5, Pavement Research,* HRB, National Research Council, Washington, D.C., 1962.
5. G. Ahlborn. *Elastic Layered System with Normal Loads.* Institute of Transportation Studies, University of California at Berkeley, 1972.
6. S. W. Hudson, S. B. Seeds, F. N. Finn, and R. F. Carmichael III. *Evaluation of Increased Pavement Loading.* Draft Final Report by ARE Inc. for Arizona Department of Transportation, 1986.
7. A. Taute, B. F. McCullough, and W. R. Hudson. *Improvements to Materials Characterization and Fatigue Life Prediction Methods for the Texas Rigid Pavement Overlay Design Procedure.* Research Report 249-1. Center for Transportation Research, University of Texas at Austin, 1981.

Comparison of AASHTO Structural Evaluation Techniques Using Nondestructive Deflection Testing

G. R. Rada, M. W. Witczak, and S. D. Rabinow

Two approaches for evaluating the structural capacity of asphalt concrete pavements from nondestructive deflection data are presented in the newly revised AASHTO Guide. Both procedures should ideally yield similar results, but studies to confirm this have not been performed. This paper describes a study undertaken by the authors to compare the two techniques. Deflection data from 1,049 tests performed on 55 homogeneous pavement sections were used. Structural capacities were calculated according to both AASHTO techniques in terms of the structural number (SN) value. On the basis of comparisons of the resulting SN values, it was concluded that both AASHTO techniques predict similar capacities. However, the computational time, required effort, and amount of information generated by each method are significantly different. Therefore, selection of the particular evaluation technique for use in a given project should be based on a clear understanding of the type of information required.

Since its introduction several decades ago, nondestructive deflection testing (NDT) has been an integral part of the structural evaluation of pavements. In the earliest years, this evaluation was based upon the analysis of a single deflection measurement resulting from a static or slow-moving load. However, as experience with deflection testing grew and technical advances were made, predictive capabilities greatly improved. Currently, the most accurate assessment of pavement structural capacity is achieved through the measurement and subsequent analysis of deflections at various radial distances (i.e., deflection basin) resulting from a dynamically applied load.

In the newly revised AASHTO Guide (1) for the design of pavement structures, two procedures for evaluating the effective structural capacity of an asphalt concrete pavement from nondestructive deflection data are presented: the Pavement Layer Moduli and the Direct Structural Capacity prediction techniques. Both approaches are based on the use of dynamic loads and the subsequent measurement of the deflection basin.

The first NDT approach utilizes the entire measured deflection basin to assess the in-situ modulus of each layer. The resulting moduli are then used, along with established AASHTO correlations between modulus and structural layer coefficient, to calculate the effective structural capacity of the pavement in terms of an effective structural number.

The second NDT approach is based on theoretical deflection equations that allow for prediction of the effective structural number (SN) directly from the maximum NDT deflection and knowledge of the subgrade modulus as interpreted from the outer geophone deflection measurements.

Both procedures should theoretically yield similar results, but, until now, verification studies have not been performed. This study is one of the first attempted direct comparisons in the United States and has been conducted primarily because of its importance to the long-range verification and modification of the NDT methodology suggested in the AASHTO Guide.

Three major research tasks were performed:

1. deflection and pavement data collection,
2. analysis of deflection data, and
3. comparison of results.

In Task 1, deflection basin data and other pertinent pavement information were collected for direct use in this study. Those data were analyzed using both AASHTO evaluation techniques in Task 2. And, in Task 3, a comparison of the effective structural capacity results generated was undertaken to verify the AASHTO NDT methodology.

A more detailed discussion of the study is presented in this paper. In the ensuing section, a brief description of the nondestructive testing equipment and a summary of the deflection data and pavement information collected are provided. A later section presents the analysis of deflection data according to the two AASHTO evaluation techniques. The results of the analysis are summarized and compared later. Finally, the major findings and conclusions of the study are discussed.

DEFLECTION AND PAVEMENT DATA COLLECTION

Nondestructive Testing Equipment

All nondestructive field data used in this comparison study were collected with a Phonix model ML10000 falling-weight deflectometer (FWD). This Phonix FWD model is a trailer-mounted pavement loading device capable of applying impulse loads ranging from approximately 2,500 lb to 24,000 lb. This impulse load range facilitates deflection studies on pavement structures ranging from low-volume roads to heavy-load airfield pavements.

G. R. Rada and S. D. Rabinow, Pavement Consultancy Services, 4700 Berwyn House Road, #202, College Park, Md. 20740. M. W. Witczak, Department of Civil Engineering, University of Maryland, College Park, Md. 20740.

The standard electronic package consists of six deflection sensors that can be positioned at various radial offset distances from the load plate center so that an accurate measurement of the complete deflection basin can be made under a given dynamic load. Additional standard features include a pavement surface and air temperature recording system and a trailer-mounted distance measuring instrument.

The complete FWD operation—data collection and subsequent data reduction and analysis—is accomplished using IBM-PC or compatible microcomputers and software systems developed by the authors. The FWD is operated by a single person from within the tow vehicle using a data collection program (COLLECT) that monitors the test mode condition and stores all pertinent field data such as load, deflections, and temperature.

Data reduction tasks are accomplished using the program REDUCE, which converts the raw field data from sequential test files to random-access binary files; allows for the correction of bad data elements and the creation of subset files and/or normalized deflection files; and provides tabular and graphical printouts of the deflection data along with statistical summaries. On completion, the resulting deflection data are analyzed using programs EMOD or SNEFF which back-calculate the in-situ layer moduli and/or structural capacity of the pavements tested.

Nondestructive Field Data

A total of 1,049 nondestructive deflection tests conducted between October 1985 and December 1986 were used in this study. These tests were performed on 55 unique pavement sections located in five different states: Virginia, Maryland, Colorado, Connecticut, and Texas.

In Virginia and Maryland, 593 tests on 23 pavement sections were conducted to assess the condition and structural capacity of the pavements under investigation and, on the basis of the results of the evaluation, to make rehabilitation recommendations. In Colorado, 253 tests results on 18 different pavement sections were used, along with other pertinent information, in the development of a data base for implementation of a pavement management system. And, in Connecticut and Texas, deflection tests were performed to demonstrate the operation and capabilities of the Phonix ML10000 FWD.

Table 1 is a summary of the pavement sections, indicating the section identification number, route number or name, location, pavement cross section, pavement temperature, and the number of tests conducted.

ANALYSIS OF NONDESTRUCTIVE DATA

In order to compare the approaches recommended in the AASHTO Guide detailing the uses of NDT within structural evaluation and rehabilitation studies, the deflection results for the pavements under investigation were analyzed using the EMOD and SNEFF programs. EMOD is a computerized solution to the Pavement Layer Moduli procedure recommended in the AASHTO Guide. SNEFF is the computerized solution to the AASHTO Direct Structural Capacity technique. Both programs and the methodology used in each are described below.

Subgrade Moduli Predictions

Regardless of the pavement structural evaluation technique selected, the first step in the overall analysis is to determine the in-situ subgrade modulus from the measured deflection basin. The fundamental concept used in either approach to establish this value is best illustrated in Figure 1, which shows a pavement structure being deflected under a dynamic NDT load. As the test is conducted, the load applied to the surface is distributed through the depth of the pavement system. The distribution of stresses, represented in this figure by the "Zone of Stress," is obviously dependent upon the stiffness or modulus of the material within each layer. As the stiffness of the material increases, the stress is spread over a much larger area.

More important, Figure 1 shows a radial distance ($r = a_{3e}$) in which the stress zone intersects the interface of the subbase and subgrade layers. When the deflection basin is measured, any surface deflections obtained at or beyond the a_{3e} value are due only to stresses, and hence deformations, within the subgrade itself. Thus, the outer readings of the deflection basin primarily reflect the in-situ modulus of the subgrade soil.

Using this concept, the in-situ subgrade modulus is determined in both EMOD and SNEFF programs from the composite moduli predicted for radial distances greater than the effective radius, a_{3e}, of the stress bulb at the pavement-subgrade interface, as indicated by the horizontal dashed line in Figure 2 for linear elastic subgrades or by the upward trend for nonlinear (stress dependent) subgrades. The composite modulus is a single-value representation of the overall pavement stiffness, at a given radial distance, that combines the modulus of elasticity of all layers present in the pavement.

The specific evaluation technique used by both programs involves the generation of pavement composite moduli plots from measured radial NDT deflections. Computer-generated plots of the composite moduli vs. radial distance are calculated by means of the following equations:

$$E_c = [2(1 - u_{sg}^2)p_c a_c]/\delta; \text{ if } r \leq 0.25*a_c \qquad (1a)$$

or

$$E_c = \{[(1 - u_{sg}^2)p_c a_c]/\delta\}(C); \text{ if } r > 0.25*a_c \qquad (1b)$$

where

$\quad E_c$ = composite modulus,
$\quad r$ = radial distance,
$\quad p_c$ = contact pressure applied by NDT device,
$\quad a_c$ = radius of contact of NDT device,
$\quad u_{sg}$ = Poisson's ratio of the subgrade,
$\quad \delta$ = measured or predicted (from curve-fitting analysis) deflection, and
$\quad C$ = $[1.1*\log(r/a_c) + 1.15]$ or $[0.5*u_{sg} + 0.875]$ (lowest of the two values).

A more detailed discussion of the theories contained in this section is presented in the 1985 AASHTO Guide (2).

Pavement Layer Moduli Analysis

The AASHTO Pavement Layer Moduli analysis technique is based on the supposition that a unique set of layer moduli

TABLE 1 PAVEMENT TEST SECTIONS

SECTION ID NUMBER	ROUTE / LOCATION	PAVEMENT STRUCTURE			PAVEMENT TEMP.	NUMBER OF NDT POINTS
		LAYER 1	LAYER 2	LAYER 3		
VADT5-2	Route 17 SBL, Stafford Co., Virginia	7.5" AC	6.0" GB	SG	73	9
VADT5-3	Route 3 EBL, Spotsylvania Co., Virginia	4.4" AC	6.0" GB	SG	76	19
VADT5-4	Route 301 NBL, King George Co., Virginia	9.0" AC	3.0" GB	SG	59	10
VADT5-5	Route 17 NBL, Caroline Co., Virginia	8.2" AC	7.0" GB	SG	54	46
VADT5-6	Route 17 NBL, Caroline Co., Virginia	5.8" AC	7.0" GB	SG	56	28
VADT5-9	Route 360 EBL, Richmond Co., Virginia	5.9" AC	6.0" GB	SG	52	46
VADT5-10	Route 203 SBL, Westmoreland Co., Virginia	3.1" AC	10.0" GB	SG	52	20
VADT5-11	Route 3 NBL, Lancaster Co., Virginia	5.3" AC	10.0" GB	SG	54	28
VADT5-12	Route 3 NBL, Lancaster Co., Virginia	4.4" AC	10.0" GB	SG	55	20
VADT5-13	Route 201Y NBL, Lancaster Co., Virginia	1.9" AC	6.0" GB	SG	60	8
VADT5-14	Route 200 NBL, Northumberland Co., Virginia	2.5" AC	10.0" GB	SG	58	25
VADT5-18	Route 14 EBL, King & Queen Co., Virginia	2.7" AC	8.0" GB	SG	80	11
VADT5-20	Route 360 WBL, King & Queen Co., Virginia	4.5" AC	6.0" CTB	SG	80	45
VADT5-21	Route 207 SBL, Caroline Co., Virginia	3.9" AC	6.0" CTB	SG	60	10
PAFB	Paine Street, Peterson AFB, Colorado	3.0" AC	6.0" GB	SG	65	15
PAFB-1	Hamilton Street, Peterson AFB, Colorado	2.5" AC	5.0" GB	SG	75	20
PAFB-2	Kincheloe Loop, Peterson AFB, Colorado	2.5" AC	5.0" GB	SG	80	10
PAFB-3	Thule Loop, Peterson AFB, Colorado	2.5" AC	5.0" GB	SG	90	13
PAFB-4	Suffolk Street, Peterson AFB, Colorado	2.5" AC	5.0" GB	SG	80	11
PAFB-5	Otis Street, Peterson AFB, Colorado	3.0" AC	5.0" GB	SG	90	19
PAFB-6	Mitchell Street, Peterson AFB, Colorado	2.0" AC	6.0" GB	SG	90	12
PAFB-7	Glasgow Street, Peterson AFB, Colorado	2.5" AC	5.0" GB	SG	90	9
PAFB-8	Loring Street, Peterson AFB, Colorado	2.5" AC	6.0" GB	SG	90	9
PAFB-9	Dover Ave., Peterson AFB, Colorado	2.5" AC	6.0" GB	SG	90	8
PAFB-10	Vincent Street, Peterson AFB, Colorado	2.5" AC	5.0" GB	SG	90	17
PAFB-11	ENT Ave., Peterson AFB, Colorado	2.5" AC	3.0" GB	SG	90	18
PAFB-12	Peterson Blvd., Peterson AFB, Colorado	4.5" AC	5.0" GB	SG	50	28
PAFB-13	Stewart Ave., Peterson AFB, Colorado	3.0" AC	5.0" GB	SG	65	31
PAFB-14	Truax Street, Peterson AFB, Colorado	3.0" AC	1.0" GB	SG	75	12
PAFB-15	Tinker Street, Peterson AFB, Colorado	2.5" AC	5.0" GB	SG	75	4
PAFB-16	Goodfellow Rd., Peterson AFB, Colorado	2.5" AC	6.0" GB	SG	75	10
PAFB-17	Duluth Street, Peterson AFB, Colorado	2.5" AC	5.0" GB	SG	80	7
VADT6-3	Route 29 NBL, Culpeper Co., Virginia	9.7" AC	6.0" GB	SG	88	34
VADT6-4	Route 55 WBL, Fauquier Co., Virginia	3.1" AC	12.0" GB	SG	79	13
VADT6-5	Route 29 SBL, Fauquier Co., Virginia	8.4" AC	6.0" GB	SG	74	25
VADT6-7	Route 17 SBL, Fauquier Co., Virginia	8.0" AC	3.0" GB	SG	87	53
CTDT-A6	Route 77 NBL, Guilford, Connecticut	4.0" AC	2.0" GB	SG	59	20
CTDT-B1	Route 218 EBL, Bloomfield, Connecticut	4.0" AC	29.0" GB	SG	54	20
CTDT-C8A	Route 80 EBL, Guilford, Connecticut	4.0" AC	3.0" GB	SG	55	11
CTDT-E4	Route 68 EBL, Wallingford, Conneticut	9.0" AC	10.0" GB	SG	44	14
CTDT-E7	Route 187 NBL, Bloomfield, Conneticut	9.0" AC	20.0" GB	SG	46	18
CTDT-F4	Route 202 NBL, New Hartford, Conneticut	4.3" AC	13.0" GB	SG	56	19
CTDT-F9	Route 140 EBL, Windsor Locks, Connecticut	3.3" AC	9.0" GB	SG	58	20
ARE-9A	Route 71 EBL, Lagrange, Texas	10.5" AC	12.0" GB	SG	91	12
ARE-10	Route 71 EBL, Lagrange, Texas	10.5" AC	12.0" GB	SG	93	12
ARE-11	Route 71 EBL, Lagrange, Texas	10.5" AC	12.0" GB	SG	96	12
ARE-12	Loop 360 SBL, Austin, Texas	3.0" AC	15.0" GB	SG	100	12
ARE-12A	Loop 360 SBL, Austin, Texas	3.0" AC	15.0" GB	SG	91	12
ARE-14	Route 183 NBL, Austin, Texas	2.5" AC	17.0" GB	SG	86	12
ARE-14B	Route 183 NBL, Austin, Texas	2.5" AC	17.0" GB	SG	103	9
ALF-F4Z	FHWA Turner-Fairbanks Research Lab, Virginia	5.0" AC	5.0" GB	SG	72	7
ALF-S10L1	FHWA Turner-Fairbanks Research Lab, Virginia	5.0" AC	5.0" GB	SG	58	18
ALF-F3Z	FHWA Turner-Fairbanks Research Lab, Virginia	7.0" AC	12.0" GB	SG	65	26
ALF-S10L2	FHWA Turner-Fairbanks Research Lab, Virginia	7.0" AC	12.0" GB	SG	59	32
CTI-GP	Grosvenor Pk. Loop Rd., Montgomery Co., MD	4.0" AC	6.0" GB	SG	60	60

Total Number of Sections = 55
Total Number of Test Points = 1049

AC = Asphalt Concrete Layer
CTB = Cement Treated Base Layer
GB = Granular Base Layer

exists such that the theoretically predicted deflection basin is equivalent to the measured deflection basin. This NDT approach utilizes the entire measured deflection basin to assess the in-situ (E_i) modulus of each layer. By using AASHTO correlations between the modulus and structural layer coefficient (a_i) values, the effective structural number of the pavement can be computed, assuming that the thicknesses of each layer (h_i) have been accurately determined.

The EMOD program has been developed to estimate in-situ pavement layer moduli from measured NDT deflection basin data. The analysis technique is based on the concepts of linear multilayer elastic theory and uses the Chevron N-Layer computer code (3) as a subroutine within the back-calculation procedure. In general, layer moduli are estimated from the combination of E_i values that result in the minimum cumulative residual error at all deflection (geo-
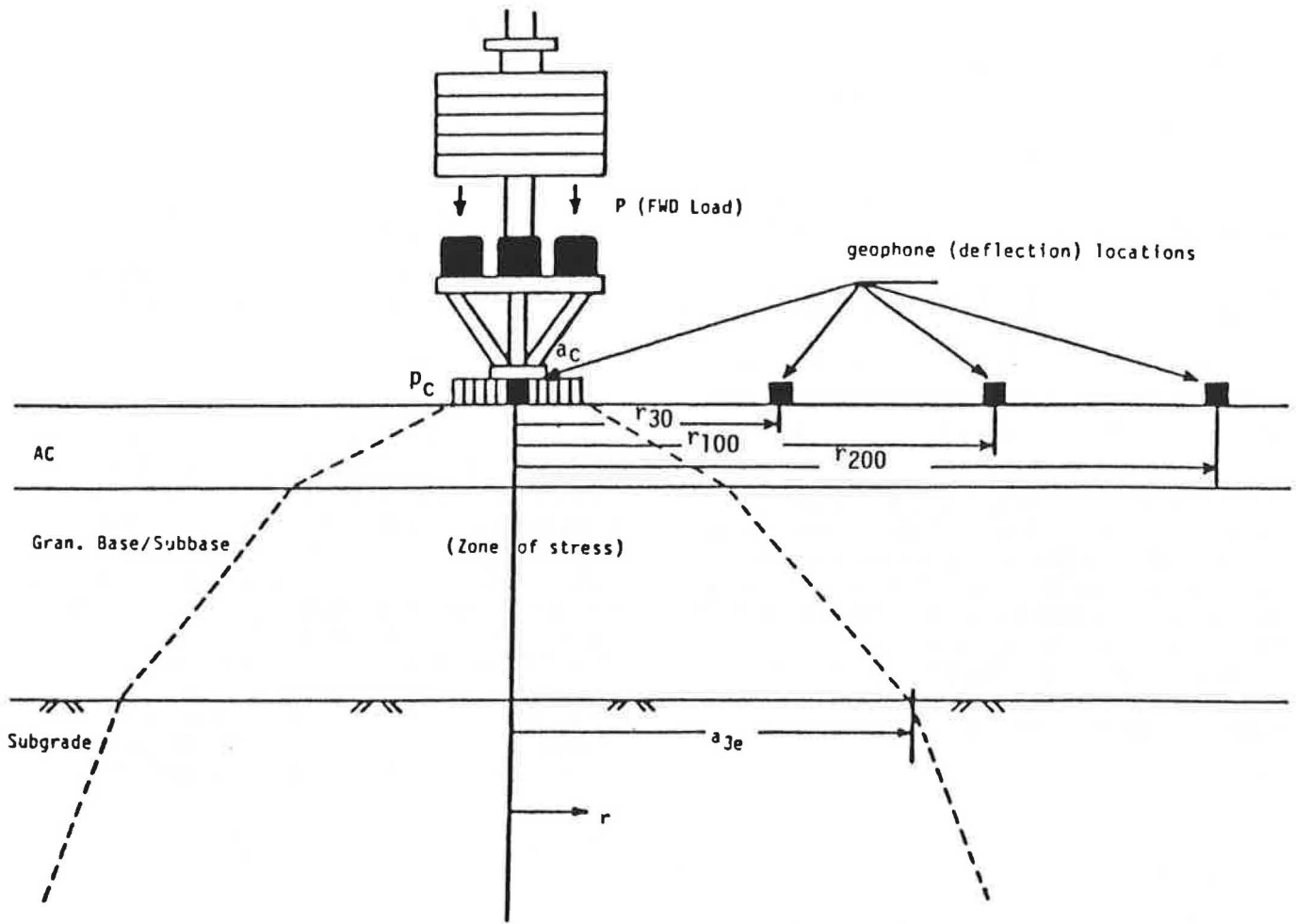
FIGURE 1 Schematic of stress zone within pavement structure under FWD load (*1*).

phone) readings. In order to utilize this program, the layer thicknesses and Poisson's ratio of each layer must be known or assumed.

Once the layer moduli have been calculated, the predicted asphalt concrete modulus must be corrected to a standard temperature of 68° to 78°F. The same temperature correction correlation recommended in the AASHTO Guide is contained in EMOD:

$$E(70) = \frac{E(T)}{10^{3.245} \times 10^{-4*(2079.446 - T_p{}^{1.798})}} \qquad (2)$$
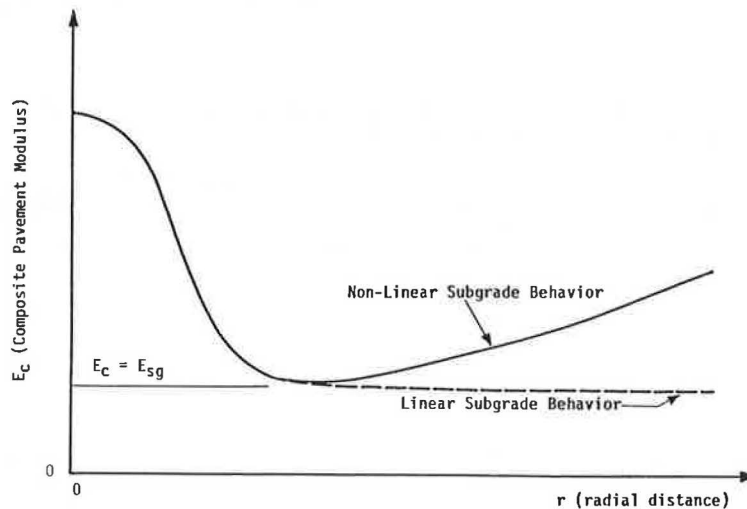

FIGURE 2 Composite modulus vs. radial distance plot.

where

$E(70)$ = temperature-corrected modulus,
$E(T)$ = modulus back-calculated from deflection basin (in EMOD), and
T_p = pavement temperature at time of NDT test.

After temperature correction, the estimated layer moduli are correlated with the empirical AASHTO structural layer coefficients through the use of nomographs or layer coefficient-modulus relations found in the AASHTO Guide. The predicted layer coefficients are then used, along with the known layer thicknesses, to estimate the effective structural capacity of the pavement system by means of the following expression:

$$SN = a_i h_i + a_2 h_2 + \ldots a_{n-1} h_{n-1} = \sum_{i=1}^{n-1} a_i h_i \qquad (3)$$

However, instead of the nomographs or layer coefficient relations found in the AASHTO Guide, an alternate analytical form of layer coefficients to elastic modulus was used in this study. The theoretical bases behind the development of this alternate correlation are detailed in the 1985 AASHTO Guide (2) and are summarized below.

Assuming that the individual pavement layers (h_i, a_i) can be represented by equivalent thicknesses ($h_{s,i}$) of a standard material (a_s) having the same structural number, then

$$a_i h_i = a_s h_{s,i} \qquad (4a)$$

or

$$a_i = a_s (h_{s,i}/h_i) \qquad (4b)$$

Also, if the structural number of the equivalent layers is the same as that of the in-situ layers, then the "stiffness" of the two must be the same:

$$\frac{E_i h_i^3}{12 (1 - u_1^2)} = \frac{E_s h_{si}^3}{12 (1 - u_s^2)} \qquad (5a)$$

or

$$\frac{h_{si}}{h_i} = \left[\frac{E_i (1 - u_s^2)}{E_s (1 - u_i^2)} \right]^{1/3} \qquad (5b)$$

where

a_i = layer coefficient of ith layer material,
a_s = layer coefficient of standard (arbitrarily selected) material,
E_i = elastic modulus of ith layer materials,
E_s = elastic modulus of standard material,
u_i = Poisson's ratio of ith layer material, and
u_s = Poisson's ratio of standard material.

Substituting Equation 5 into Equation 4 yields the alternate modulus-layer coefficient relation used in the study:

$$a_i = a_s \left[\frac{E_i (1 - u_s^2)}{E_s (1 - u_i^2)} \right]^{1/3} \qquad (6)$$

This alternate relation fits with every material-layer-type correlation in the AASHTO Guide except for the asphalt surface course. To illustrate this fact numerically, if one arbitrarily selects (as was done in this study) a crushed stone base course as the standard material—$a_s = 0.14$, $E_s = 30,000$ psi, and $u_s = 0.35$—the computed a_i values shown in Table 2 are obtained for commonly accepted moduli values. As can be seen from this table, the predicted layer coefficients fit the AASHTO correlations very well except for the asphalt surface material.

Furthermore, if crushed stone is assumed to be the standard material, substitution of Equation 6 into Equation 3 yields the SN predictive equation contained in the EMOD program:

$$SN = \sum_{i=1}^{n-1} a_i h_i = \sum_{i=1}^{n-1} a_s \left[\frac{E_i (1 - u_s^2)}{E_s (1 - u_i^2)} \right]^{1/3} h_i$$

$$SN = 0.0043 \sum_{i=1}^{n-1} h_i \left(\frac{E_i}{1 - u_i^2} \right)^{1/3} \qquad (7)$$

In addition to the above theoretical considerations, a much longer computational time is associated with the Pavement Layer Moduli technique because layer elastic solutions (e.g., Chevron) are required to iteratively back-calculate the layer moduli. However, since individual layer strengths are predicted, the results of the analysis can be used in the identification of problem layers/materials or as input into the more rational mechanistic approaches presently available.

TABLE 2   COMPARISON OF STRUCTURAL LAYER COEFFICIENTS FROM AASHTO AND ALTERNATE APPROACH

Material Type	Modulus (ksi)	Layer Coefficients	
		AASHTO	Alternate Approach
A.C. Surface	930	>.45	.44
	450	.44	.35
A.C. Base	340	.30	.31
Granular Base	30	.14	.14
Granular Subbase	15	.11	.11
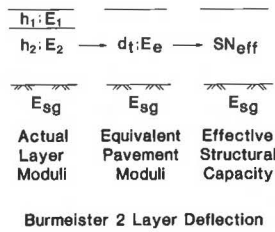
FIGURE 3 Basis for
Direct Structural Capacity
technique.

Direct Structural Capacity Analysis

The approach used in the AASHTO Direct Structural Capacity analysis technique is based on the premise that the overall pavement structural capacity is the result of the combined stiffness influence of each layer. Consequently, the maximum NDT deflection may be viewed as comprising two separate components: (1) pavement structural capacity and (2) subgrade support.

Using these concepts, a computerized solution (SNEFF) to the AASHTO Direct Structural Capacity analysis technique was developed. The procedure uses outer deflection basin data to estimate the subgrade modulus and then uses this parameter, along with the maximum NDT deflection, to directly estimate the effective structural capacity of the pavement system.

More specifically, the effective structural capacity of the pavement is determined in the program SNEFF through an iterative process. Assuming that the pavement structure can be represented by a one-layer system resting on the subgrade (see Figure 3) and that crushed stone ($a_s = 0.14$, $E_s = 30,000$ psi, and $u_s = 0.35$) is the standard material, the equivalent modulus (E_e) of the one-layer system (for a given iteration of the SN value) can be calculated by rearranging Equation 7 as follows:

$$E_e = (SN/0.0043*h_t)^3(1 - u_{te}^2) \tag{8}$$

where h_t is the total pavement thickness (i.e., $h_t = \Sigma h_i$).

In turn, the theoretical maximum deflection (δ_o) of the one-layer system with modulus E_e can be derived from the following expression contained in the 1985 AASHTO Guide (2):

$$\delta_o = \frac{2p_c a_c (1 - u_{sg}^2)}{E_{sg}} F_w$$

$$F_w = \frac{E_{sg}(1 - u_e^2)}{E_e(1 - u_{sg}^2)} + F_b \left(1 - \frac{E_{sg}}{E_e}\right)$$

$$F_b = [(1 + A^2)^{1/2} - A]$$

$$\times \left[1 + \frac{A}{2(1 - u_{sg})(1 + A^2)^{1/2}}\right]$$

$$A = h_e/a_c$$

$$h_e = 0.9 \, h_t \left[\frac{E_e(1 - u_{sg}^2)}{E_{sg}(1 - u_e)}\right]^{1/3} \tag{9}$$

where

F_w = Burmeister's two-layer deflection factor,
F_b = Boussinesq's one-layer deflection factor,
h_e = transformed thickness of pavement in terms of the subgrade modulus,
A = depth radii of the transformed section,
E_{sg} = subgrade modulus, and
u_e = Poisson's ratio of transformed section.

Therefore, by iterating on the SN value, the structural number that results in a predicted maximum deflection equal to, or within 1 percent of, the measured value is determined in the SNEFF program.

It should also be noted that the maximum measured NDT deflection must be adjusted to the standard temperature of 70°F before the effective structural number, SN, is calculated. The adjustment correlation used in SNEFF is that developed by the U.S. Army Corps of Engineers (4):

$$d_c = d_m/(1 + t_{ac}*m)$$

$$m = -8.491 \times 10^{-2} + (1.213 \times 10^{-3})*T_{air} \tag{10}$$

where

d_c = corrected maximum deflection (to 70° F),
d_m = measured maximum NDT deflection,
t_{ac} = total thickness of asphalt layers, and
T_{air} = air temperature at time of NDT test.

Because a simpler, two-layer solution is used in the Direct Structural Capacity technique, the computational time associated with this procedure is much faster. However, it cannot be used to isolate problem layers nor can the results be used as input into a mechanistic analysis.

Analysis Results

As previously described, calculations were performed analyzing the structural response of more than 1,000 sets of deflection measurements by means of Pavement Layer Moduli (EMOD program) and Direct Structural Capacity (SNEFF program) techniques. It should be emphasized that the calculations were performed for each set of deflection measurements individually, and that statistical analyses were performed on the results for each homogeneous pavement section investigated.

Table 3 presents the results of these analyses. Under the heading "EMOD ANALYSIS," reported results are based on the Pavement Layer Moduli techniques. Since all pavements were modeled as three-layer systems, results consist of mean layer moduli for the surface and base courses, as well as for the subgrade. The fourth column of this group represents the mean calculated effective SN value represented by the layer moduli.

Under the heading "SNEFF ANALYSIS," reported results are based on the Direct Structural Capacity techniques. The results include the mean subgrade modulus, thickness of pavement modeled, mean equivalent modulus of that thickness of pavement, and the mean calculated effective SN of that combination of modulus and thickness.

TABLE 3   STATISTICAL SUMMARY OF LAYER MODULI AND SN VALUES

SECTION ID NUMBER	MEAN LAYER MODULI (ksi)			MEAN EFFECTIVE SN	MEAN SUBGRADE MODULUS (ksi)	PAVEMENT THICK. (in)	EQUIVALENT MODULUS (ksi)	MEAN EFFECTIVE SN
	SURFACE	BASE	SUBGRADE					
VADT5-2	445.8	42.2	20.0	3.52	20.0	13.5	192.3	3.50
VADT5-3	416.5	49.2	26.0	2.47	26.0	10.4	135.6	2.40
VADT5-4	305.9	36.0	23.6	3.18	23.6	12.0	209.3	3.20
VADT5-5	167.5	19.7	21.6	2.89	21.6	15.2	89.2	3.05
VADT5-6	214.5	28.6	15.3	2.53	15.3	12.8	87.3	2.55
VADT5-9	118.1	18.2	12.5	2.02	12.5	11.9	56.4	2.05
VADT5-10	179.9	33.8	18.5	2.25	18.5	13.1	55.9	2.25
VADT5-11	233.3	24.1	17.8	2.77	17.8	15.3	71.3	2.85
VADT5-12	323.9	32.4	23.6	2.80	23.6	14.4	85.6	2.85
VADT5-13	162.4	27.1	10.2	1.28	10.2	7.9	43.7	1.25
VADT5-14	856.6	21.8	16.8	2.33	16.8	12.5	56.2	2.15
VADT5-18	495.3	22.6	20.0	1.98	20.0	10.7	57.0	1.85
VADT5-20	490.7	93.3	21.1	2.83	21.1	10.5	198.2	2.75
VADT5-21	269.3	580.0	40.8	3.39	40.8	9.9	390.5	3.25
PAFB	585.5	51.0	17.5	2.13	17.5	9.0	121.1	2.00
PAFB-1	1080.4	61.5	21.4	2.05	21.4	7.5	165.6	1.85
PAFB-2	1138.7	65.0	18.9	2.08	18.9	7.5	165.6	1.85
PAFB-3	953.8	70.4	22.7	2.04	22.7	7.5	165.6	1.85
PAFB-4	469.1	52.3	15.2	1.72	15.2	7.5	107.2	1.60
PAFB-5	772.8	46.1	16.8	2.05	16.8	8.0	136.5	1.85
PAFB-6	929.5	63.3	17.8	1.96	17.8	8.0	125.7	1.80
PAFB-7	620.5	65.6	16.1	1.87	16.1	7.5	140.2	1.75
PAFB-8	1155.7	50.6	17.7	2.18	17.7	8.5	133.3	1.95
PAFB-9	739.1	61.9	17.2	2.09	17.2	8.5	133.3	1.95
PAFB-10	613.0	48.8	17.0	1.78	17.0	7.5	117.5	1.65
PAFB-11	1573.4	74.7	19.3	1.88	19.3	5.5	271.7	1.60
PAFB-12	348.2	62.5	21.0	2.32	21.0	9.5	146.6	2.25
PAFB-13	545.8	52.1	16.6	1.95	16.6	8.0	104.8	1.80
PAFB-14	1667.0	43.0	19.2	1.76	19.2	4.0	642.2	1.55
PAFB-15	153.7	20.0	10.3	1.22	10.3	7.5	39.8	1.15
PAFB-16	380.3	43.0	21.7	1.76	21.7	8.5	88.3	1.70
PAFB-17	1271.9	45.9	18.8	2.03	18.8	7.5	140.2	1.75
VADT6-3	327.8	16.8	21.4	3.71	21.4	15.7	156.5	3.80
VADT6-4	527.3	39.8	29.4	2.98	29.4	15.1	82.3	2.95
VADT6-5	971.0	46.2	37.5	4.72	37.5	14.4	383.7	4.70
VADT6-7	405.4	18.2	19.4	3.02	19.4	11.0	213.9	2.95
CTDT-A6	305.7	32.3	12.7	1.50	12.7	6.0	140.2	1.40
CTDT-B1	512.9	30.8	21.2	5.54	21.2	33.0	69.7	6.10
CTDT-C8A	578.6	50.0	21.0	2.00	21.0	7.0	203.7	1.85
CTDT-E4	516.6	29.6	34.3	4.65	34.3	19.0	195.2	4.95
CTDT-E7	475.1	39.7	23.8	6.24	23.8	29.0	162.0	7.10
CTDT-F4	591.3	24.2	45.9	3.32	45.9	17.3	83.8	3.40
CTDT-F9	769.8	34.3	14.8	2.68	14.8	12.3	98.3	2.55
ARE-9A	571.5	30.0	36.1	5.61	36.1	22.5	225.4	6.15
ARE-10	471.2	18.3	31.5	5.11	31.5	22.5	174.8	5.65
ARE-11	427.5	15.8	22.2	4.92	22.2	22.5	152.6	5.40
ARE-12	1559.0	107.1	125.7	4.78	125.7	18.0	209.3	4.80
ARE-12A	1516.9	103.8	122.7	4.73	122.7	18.0	202.8	4.75
ARE-14	653.3	42.1	18.9	3.64	18.9	19.5	72.4	3.65
ARE-14B	1236.4	44.4	17.9	3.92	17.9	19.5	88.3	3.90
ALF-F4Z	204.7	7.4	7.2	1.77	7.2	10.0	49.6	1.65
ALF-S10L1	338.9	11.8	8.3	2.08	8.3	10.0	81.8	1.95
ALF-F3Z	325.1	22.6	19.0	3.70	19.0	19.0	99.2	3.95
ALF-S10L2	398.5	33.9	18.8	4.07	18.8	19.0	127.9	4.30
CTI-GP	375.9	24.1	13.0	2.08	13.0	10.0	81.8	1.95

COMPARISON OF STRUCTURAL EVALUATION TECHNIQUES

The analysis results generated by the EMOD and SNEFF programs allowed for a direct comparison of the NDT structural evaluation techniques presented in the newly revised AASHTO Manual. As noted earlier, this study was conducted primarily because of its potential importance to the long-range verification and modification of the NDT methodology suggested in the AASHTO guide for asphalt concrete pavements.

The effective structural number for all 55 pavement sections under investigation has already been presented for the Pavement Layer Moduli approach (EMOD based) and the Direct Structural Capacity approach (SNEFF based) in Table 3. EMOD vs. SNEFF plots of the predicted effective SN values for *all* test points (1,049) and the *section means* are presented in Figures 4 and 5, respectively.

On the basis of these results, it is apparent that the effective structural capacities predicted by both AASHTO procedures are generally in excellent agreement with each other. The R-squared value (R = correlation coefficient) for both the point-by-point and section-by-section comparison is 0.98, and the
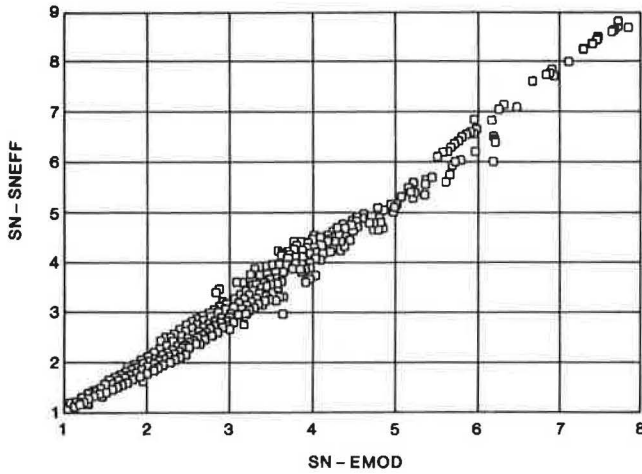
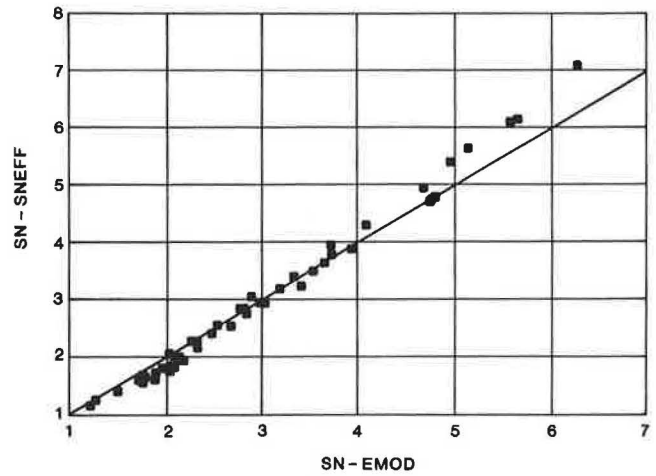**FIGURE 4   EMOD vs. SNEFF-predicted SN values for all test points.**

FIGURE 5   EMOD vs. SNEFF-predicted SN values for section means.

slope is approximately equal to one when the correlations are forced through a y-intercept of zero.

Figures 4 and 5 also show that for SN values approximately equal to or greater than 5, a more systematic error away from the line of equality occurs; the SNEFF program predicts larger SN values. However, because this systematic error is limited to 5 of the 55 pavement sections or 78 of the 1,049 test points investigated, further research is needed to compare the two AASHTO techniques for pavements with high SN values.

To further verify the agreement shown in Figures 4 and 5, a statistical comparison of the predicted SN values was undertaken. The acceptance criteria used to determine whether or not the hypothesis that the mean SN values generated by both AASHTO techniques are equal for the various pavement sec-

tions is shown in Table 4. The statistical test assumes that the SN values are normally distributed and that the true standard deviations are known.

Using the equations shown in Table 4, the test statistic (U) was calculated. The resulting values are summarized in Table 5. Next, assuming α values of 5 and 1 percent (or confidence levels of 95 and 99 percent) and using a two-sided confidence test yields $K_{\alpha/2}$ values of 1.96 and 2.57, respectively.

On the basis of the results presented in Table 5, acceptance of the hypothesis is dependent on the level of confidence selected. For an α value of 5.0 percent, 45 (or 81.8 percent) of the 55 pavement sections have equal means. On the other hand, for an α value of 1.0 percent, 50 (or 90.1 percent) of the pavement sections have statistically equal mean SN values.

TABLE 4   EQUATIONS FOR HYPOTHESIS TEST FOR EQUALITY OF SN MEANS ($H: u_x = u_y$)

Test Description:

    Mean, two populations, known standard deviation

Test Statistic:

$$U = \frac{(\bar{x} - \bar{y})}{[(\sigma_x^2/n_x) + (\sigma_y^2/n_y)]^{\frac{1}{2}}}$$

where:

U	= test statistic (normal distribution)
$\bar{x}, \bar{y}$	= mean of population x and y;
σ_x, σ_y	= standard deviation associated with population x and y; and
n_x, n_y	= number of units in population x and y.

Acceptance Criteria:

    $- K_{\alpha/2} \leq U \leq + K_{\alpha/2}$

where: $K_{\alpha/2}$ = values of the standard normal variate with cumulative probability levels ($\alpha/2$) and ($1 - \alpha/2$).

<u>Note</u>: in this study, σ_x^2 and σ_y^2 represent the pooled variance of SN derived from the layer moduli and direct capacity approaches, respectively.

TABLE 5   RESULTS OF HYPOTHESIS TEST FOR EQUALITY OF SN MEANS

SECTION ID NUMBER	NUMBER OF NDT POINTS	EFFECTIVE SN				PERCENT DIFFERENCE	U	STATISTICAL COMP. ACCEPTANCE	
		METHOD 1		METHOD 2					
		SN	STD DEV	SN	STD DEV			ALPHA=5%	ALPHA=1%
VADT5-2	9	3.52	0.61	3.50	0.59	0.7%	0.12	YES	YES
VADT5-3	19	2.47	0.35	2.40	0.32	2.9%	0.59	YES	YES
VADT5-4	10	3.18	0.77	3.20	0.72	-0.6%	-0.12	YES	YES
VADT5-5	46	2.89	0.64	3.05	0.60	-5.6%	-2.09	NO	YES
VADT5-6	28	2.53	0.53	2.55	0.51	-0.8%	-0.20	YES	YES
VADT5-9	46	2.02	0.43	2.05	0.38	-1.7%	-0.39	YES	YES
VADT5-10	20	2.25	0.34	2.25	0.18	-0.2%	0.00	YES	YES
VADT5-11	28	2.77	0.43	2.85	0.42	-2.8%	-0.81	YES	YES
VADT5-12	20	2.80	0.50	2.85	0.50	-1.8%	-0.43	YES	YES
VADT5-13	8	1.28	0.23	1.25	0.18	2.3%	0.16	YES	YES
VADT5-14	25	2.33	0.20	2.15	0.20	7.7%	1.73	YES	YES
VADT5-18	11	1.98	0.12	1.85	0.13	6.7%	0.83	YES	YES
VADT5-20	45	2.83	0.32	2.75	0.31	2.7%	1.03	YES	YES
VADT5-21	10	3.39	0.45	3.25	0.32	4.2%	0.85	YES	YES
PAFB	15	2.13	0.29	2.00	0.24	6.3%	0.97	YES	YES
PAFB-1	20	2.05	0.30	1.85	0.18	9.6%	1.72	YES	YES
PAFB-2	10	2.08	0.24	1.85	0.14	11.2%	1.40	YES	YES
PAFB-3	13	2.04	0.11	1.85	0.09	9.3%	1.32	YES	YES
PAFB-4	11	1.72	0.13	1.60	0.14	6.9%	0.77	YES	YES
PAFB-5	19	2.05	0.18	1.85	0.18	9.7%	1.68	YES	YES
PAFB-6	12	1.96	0.13	1.80	0.10	8.1%	1.07	YES	YES
PAFB-7	9	1.87	0.11	1.75	0.09	6.4%	0.69	YES	YES
PAFB-8	9	2.18	0.21	1.95	0.15	10.7%	1.33	YES	YES
PAFB-9	8	2.09	0.15	1.95	0.15	6.6%	0.76	YES	YES
PAFB-10	17	1.78	0.16	1.65	0.17	7.4%	1.03	YES	YES
PAFB-11	18	1.88	0.22	1.60	0.15	14.9%	2.29	NO	YES
PAFB-12	28	2.32	0.40	2.25	0.32	3.1%	0.71	YES	YES
PAFB-13	31	1.95	0.24	1.80	0.19	7.6%	1.61	YES	YES
PAFB-14	12	1.76	0.12	1.55	0.10	12.0%	1.40	YES	YES
PAFB-15	4	1.22	0.06	1.15	0.05	5.4%	0.27	YES	YES
PAFB-16	10	1.76	0.21	1.70	0.22	3.6%	0.37	YES	YES
PAFB-17	7	2.03	0.27	1.75	0.18	13.7%	1.43	YES	YES
VADT6-3	34	3.71	0.37	3.80	0.37	-2.5%	-1.01	YES	YES
VADT6-4	13	2.98	0.24	2.95	0.25	0.9%	0.21	YES	YES
VADT6-5	25	4.72	0.91	4.70	0.91	0.4%	0.19	YES	YES
VADT6-7	53	3.02	0.35	2.95	0.34	2.5%	0.98	YES	YES
CTDT-A6	20	1.50	0.26	1.40	0.21	6.8%	0.86	YES	YES
CTDT-B1	20	5.54	0.24	6.10	0.27	-10.1%	-4.82	NO	NO
CTDT-C8A	11	2.00	0.24	1.85	0.17	7.5%	0.96	YES	YES
CTDT-E4	14	4.65	0.50	4.95	0.48	-6.5%	-2.16	NO	YES
CTDT-E7	18	6.24	0.53	7.10	0.58	-13.8%	-7.02	NO	NO
CTDT-F4	19	3.32	0.36	3.40	0.34	-2.4%	-0.67	YES	YES
CTDT-F9	20	2.68	0.21	2.55	0.17	4.9%	1.12	YES	YES
ARE-9A	12	5.61	0.20	6.15	0.16	-9.7%	-3.60	NO	NO
ARE-10	12	5.11	0.13	5.65	0.15	-10.6%	-3.60	NO	NO
ARE-11	12	4.92	0.19	5.40	0.22	-9.7%	-3.20	NO	NO
ARE-12	12	4.78	0.13	4.80	0.12	-0.4%	-0.13	YES	YES
ARE-12A	12	4.73	0.18	4.75	0.18	-0.4%	-0.13	YES	YES
ARE-14	12	3.64	0.13	3.65	0.09	-0.2%	-0.07	YES	YES
ARE-14B	9	3.92	0.11	3.90	0.07	0.6%	0.12	YES	YES
ALF-F4Z	7	1.77	0.08	1.65	0.06	6.7%	0.61	YES	YES
ALF-S10L1	18	2.08	0.17	1.95	0.14	6.5%	1.06	YES	YES
ALF-F3Z	26	3.70	0.32	3.95	0.35	-6.8%	-2.45	NO	YES
ALF-S10L2	32	4.07	0.50	4.30	0.25	-5.6%	-2.50	NO	YES
CTI-GP	60	2.08	0.42	1.95	0.40	6.4%	1.94	YES	YES

In either case, the results show that from a statistical point of view the SN values predicted by both AASHTO methods are in excellent agreement. This is particularly true for pavements with SN values less than 5.

Finally, a comparison of NDT-derived vs. typical SN values was performed. Typical SN values were calculated using Equation 4. The layer thicknesses for input into this equation have been summarized in Table 1. Typical structural layer coefficients were assumed for the various materials as follows:

a_i = 0.42 for asphalt concrete surfaces up to a maximum thickness of 3 in. For thicknesses greater than 3 in., a value of a_i = 0.28 (typical of asphalt concrete base materials) was assumed.

a_i = 0.24 for cement-treated bases.

a_i = 0.14 for granular base materials.

The resulting NDT-derived (average of values shown in Table 3) and typical SN values are presented in Table 6 and plotted in Figure 6. On the basis of these results, a very good correlation (R-squared = 0.86) between the NDT-derived and typical SN values exists. Also, the NDT-derived SN values appear to be quite reasonable.

TABLE 6 NDT-DERIVED VS. TYPICAL SN VALUES

SECTION ID NUMBER	NUMBER OF NDT POINT	AVG NDT SN VALUE	TYPICAL SN VALUE	% DIFF
VADT5-2	9	3.5	3.3	6.0%
VADT5-3	19	2.4	2.4	1.4%
VADT5-4	10	3.2	3.3	-3.4%
VADT5-5	46	3.0	3.6	-21.2%
VADT5-6	28	2.5	3.0	-18.1%
VADT5-9	46	2.0	2.9	-42.5%
VADT5-10	20	2.3	2.6	-15.6%
VADT5-11	28	2.8	3.2	-13.9%
VADT5-12	20	2.8	3.0	-6.2%
VADT5-13	8	1.3	1.6	-26.5%
VADT5-14	25	2.2	2.4	-7.1%
VADT5-18	11	1.9	2.2	-14.9%
VADT5-20	45	2.8	2.5	10.4%
VADT5-21	10	3.3	2.3	30.7%
PAFB	15	2.1	2.0	3.1%
PAFB-1	20	2.0	1.7	12.8%
PAFB-2	10	2.0	1.7	13.5%
PAFB-3	13	1.9	1.7	12.6%
PAFB-4	11	1.7	1.7	-2.4%
PAFB-5	19	2.0	1.9	2.6%
PAFB-6	12	1.9	1.6	14.9%
PAFB-7	9	1.8	1.7	6.1%
PAFB-8	9	2.1	1.8	12.8%
PAFB-9	8	2.0	1.8	10.9%
PAFB-10	17	1.7	1.7	0.9%
PAFB-11	18	1.7	1.4	19.5%
PAFB-12	28	2.3	2.3	-0.7%
PAFB-13	31	1.9	1.9	-1.3%
PAFB-14	12	1.7	1.4	15.4%
PAFB-15	4	1.2	1.7	-43.5%
PAFB-16	10	1.7	1.8	-4.0%
PAFB-17	7	1.9	1.7	10.1%
VADT6-3	34	3.8	3.9	-3.9%
VADT6-4	13	3.0	2.8	5.6%
VADT6-5	25	4.7	3.6	23.6%
VADT6-7	53	3.0	3.1	-3.9%
CTDT-A6	20	1.5	1.8	-24.1%
CTDT-B1	20	5.8	5.3	8.9%
CTDT-C8A	11	1.9	1.9	1.3%
CTDT-E4	14	4.8	4.2	12.5%
CTDT-E7	18	6.7	5.5	17.5%
CTDT-F4	19	3.4	3.3	1.8%
CTDT-F9	20	2.6	2.5	4.4%
ARE-9A	12	5.9	4.9	16.7%
ARE-10	12	5.4	4.9	8.9%
ARE-11	12	5.2	4.9	5.0%
ARE-12	12	4.8	3.2	33.2%
ARE-12A	12	4.7	3.2	32.5%
ARE-14	12	3.6	3.3	9.5%
ARE-14B	9	3.9	3.3	15.6%
ALF-F4Z	7	1.7	2.5	-46.2%
ALF-S10L1	18	2.0	2.5	-24.1%
ALF-F3Z	26	3.8	3.9	-2.0%
ALF-S10L2	32	4.2	3.9	6.8%
CTI-GP	60	2.0	2.3	-14.1%

SUMMARY AND CONCLUSIONS

The ultimate goal of this study was to compare the NDT structural evaluation techniques presented in the newly revised AASHTO Guide. In order to accomplish this objective, three major tasks were undertaken: (1) deflection and pavement data collection, (2) analysis of deflection data, and (3) comparison of analysis results.

In Task 1, a total of 1,049 deflection test results, along with other pertinent pavement information, performed on 55 unique pavement sections in five different states were collected. This information was analyzed in Task 2 using computerized solutions of the AASHTO NDT techniques. In Task 3, a detailed comparison of the analysis results was performed to verify the NDT methodologies contained in the new AASHTO Guide.

Based upon the results of this study, it was concluded that both AASHTO evaluation procedures predict similar structural capacities. This is particularly true for pavements with SN values of 5 or less. However, the computational time, required effort, and amount of information generated by each method are significantly different.

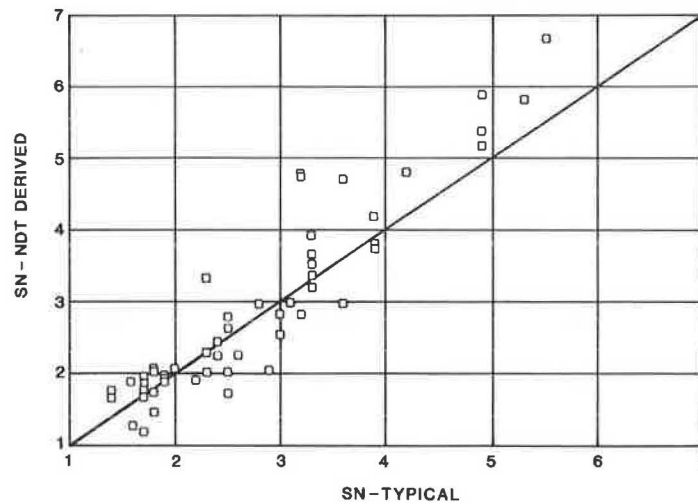The Pavement Layer Moduli procedure is a slower solution,

FIGURE 6   NDT-derived vs. typical SN values.

but the results of the analysis can be used in the identification of problem layers/materials or as input into the more rational mechanistic approaches presently available. The Direct Structural Capacity procedure, on the other hand, is a much faster computational solution but cannot be used to isolate problem layers, nor can the results be used as input into a mechanistic analysis. Therefore, although both procedures yield similar results, the selection of the particular AASHTO NDT evaluation technique for use in a given project should be based on a clear understanding of the type of information required.

REFERENCES

1. *AASHTO Guide for Design of Pavement Structure.* American Association of State Highway and Transportation Officials, Washington, D.C., 1986.

2. *Proposed AASHTO Guide for Design of Pavement Structures.* NCHRP Project 20-7/24. American Association of State Highway and Transportation Officials, Washington, D.C., 1985.
3. J. Michelow. *Analysis of Stresses and Displacement in an N-Layered Elastic System Under a Load Uniformly Distributed Over a Circular Area.* California Research Corporation, 1963.
4. A. J. Bush. *Nondestructive Testing for Light Aircraft Pavements.* Technical Report GL-80-1. U.S. Army Engineer Waterways Experiment Station, Vicksburg, Miss., 1980.

Effects of Dynamic Loads on Performance of Asphalt Concrete Pavements

Jorge B. Sousa, John Lysmer, Shi-Shuenn Chen, and C. L. Monismith

To determine the influence of dynamic loading on pavement response, an analytical and a laboratory study were undertaken. In the analytical study, temporal and spatial variation of stresses and deformations in a pavement system, resulting from dynamic loading conditions, were estimated using the computer program SAPSI. To compute these stresses and deformations, elastic and damping characteristics of various materials constituting pavement sections were defined by a laboratory investigation that provided such data for an asphalt concrete (AC) and a fine-grained soil (silty clay) for a limited range in service conditions. With the SAPSI program, a representative pavement system consisting of an AC layer resting directly on silty clay subgrade was analyzed to determine the pavement life that might result using actual load histories for three tandem-axle suspensions as compared to that obtained for the same axle with a uniform static load. Results of the dynamic analyses suggest that pavement life is reduced when dynamic effects are considered, and the magnitude of reduction is dependent on the tandem-axle suspension. The largest reduction in pavement life was obtained for the axle with the walking beam suspension. Comparable smaller reductions, as compared to the static case, were obtained for the torsion bar and four-leaf spring suspensions.

Assessment of pavement response to dynamic loads requires the following information:

1. Time history and spatial distribution of loads that specific vehicles apply to the pavement as a function of vehicle speed and pavement profile.
2. Solutions for stresses, strains, and deformations of representative pavement structures subjected to loads that duplicate those applied in-situ both in magnitude and as functions of time.
3. Measures of the dynamic response of the materials constituting pavement systems over the range in loading times, stress states, and material states that might be anticipated.

Many studies have been conducted on the effects of dynamic loads of trucks on pavements. Recent investigations have included: evaluation of theoretical vehicle models; in-situ measurements of dynamic loads resulting from special trucks or from truck loads passing over bumps, or other predefined obstacles; and the measurement of dynamic loads by special instrumentation mounted on the trucks themselves. This paper provides a brief summary of some of those investigations to provide the background for the methodology described herein

Department of Civil Engineering, Institute of Transportation Studies, University of California, Berkeley, Calif. 94720.

for estimating the influence of dynamic loads on pavement response.

BACKGROUND

Truck Studies

Results of instrumented truck studies indicate that dynamic response of these vehicles is influenced by:

1. Suspension type (Figure 1 illustrates some examples of suspension systems);
2. Vehicle type; and
3. Load (the magnitude of the load on the vehicle as well as its center of gravity influence dynamic response).
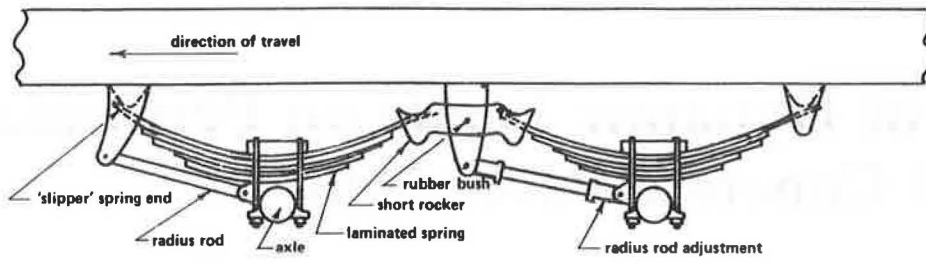
Vehicle speed and pavement roughness also have significant influences on dynamic response. Figure 2 illustrates results obtained by Sweatman (1) which demonstrate the influence of suspension type as well as pavement roughness and speed on dynamic load coefficients.

The results reported by Sweatman (1) indicate that different suspensions exhibit different levels of dynamic response. For tandem axles the "walking-beam" type produced the greatest dynamic loads, and torsion-bar suspensions, with hydraulic absorbers, produced the least (e.g., Fig. 2). Other factors such as tire pressure and tire "out-of-roundness" also have some influence, but it appears that the primary factors affecting the response of dynamic wheel loads are suspension type, vehicle type, truck loading and its spatial distribution on the truck, pavement roughness, and vehicle speed.
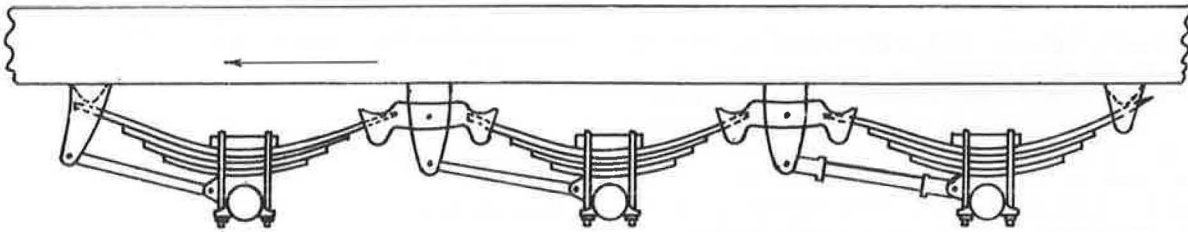
Analysis of Truck-Pavement Interactions

It is possible to estimate the dynamic load caused by a particular truck if certain characteristics of the truck are known and the surface profile of the pavement on which it is operated has been defined. One such representation for the truck system is illustrated in Figure 3 and has been proposed by Lee (2). The experimental setup for the scale location is shown in Figure 4. Figure 5 illustrates the computed responses for the left dual wheels of the loaded truck of Figure 3 as it moved at 30 mph. Figure 5 also shows loads measured at specific points by weigh-in-motion (WIM) scales.
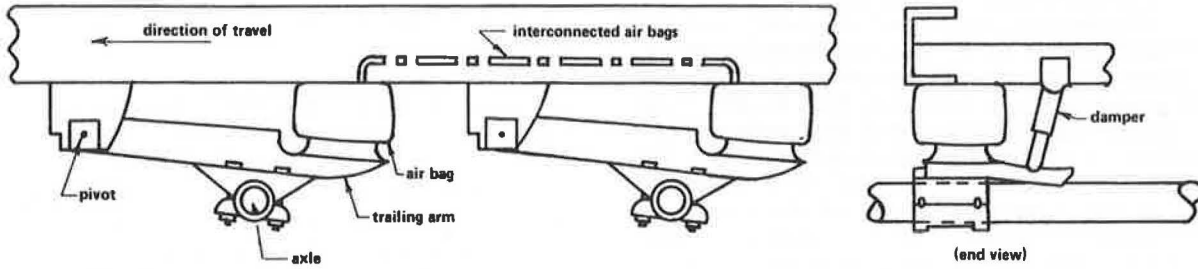
These results illustrate that it is possible to model dynamic response; however, model parameters such as those identified in Figure 3 must be available. The results in Figure 5 indicate
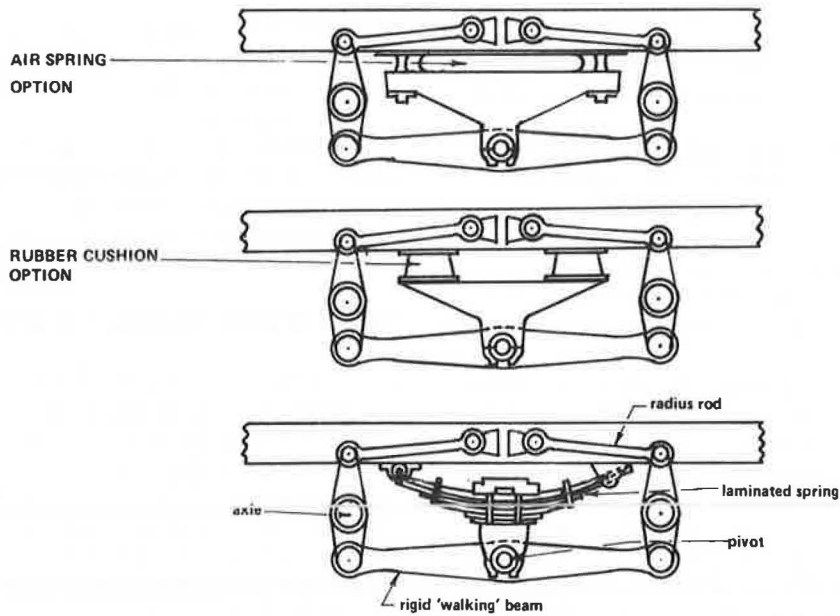
direction of travel

'slipper' spring end
rubber bush
short rocker
radius rod
axle
laminated spring
radius rod adjustment

·Current four-spring tandem (short rockers) suspension

Current six-spring triaxle (short rockers) suspension

direction of travel
interconnected air bags
damper
pivot
air bag
axle
trailing arm
(end view)

- Trailing arm tandem air suspension

AIR SPRING
OPTION

RUBBER CUSHION
OPTION

radius rod
laminated spring
axle
pivot
rigid 'walking' beam

- Walking beam (rigid beam) tandem drive axle suspension

FIGURE 1   Commonly used truck suspensions (1).

— Single point tandem drive axle suspension

·Torsion bar tandem drive axle suspension
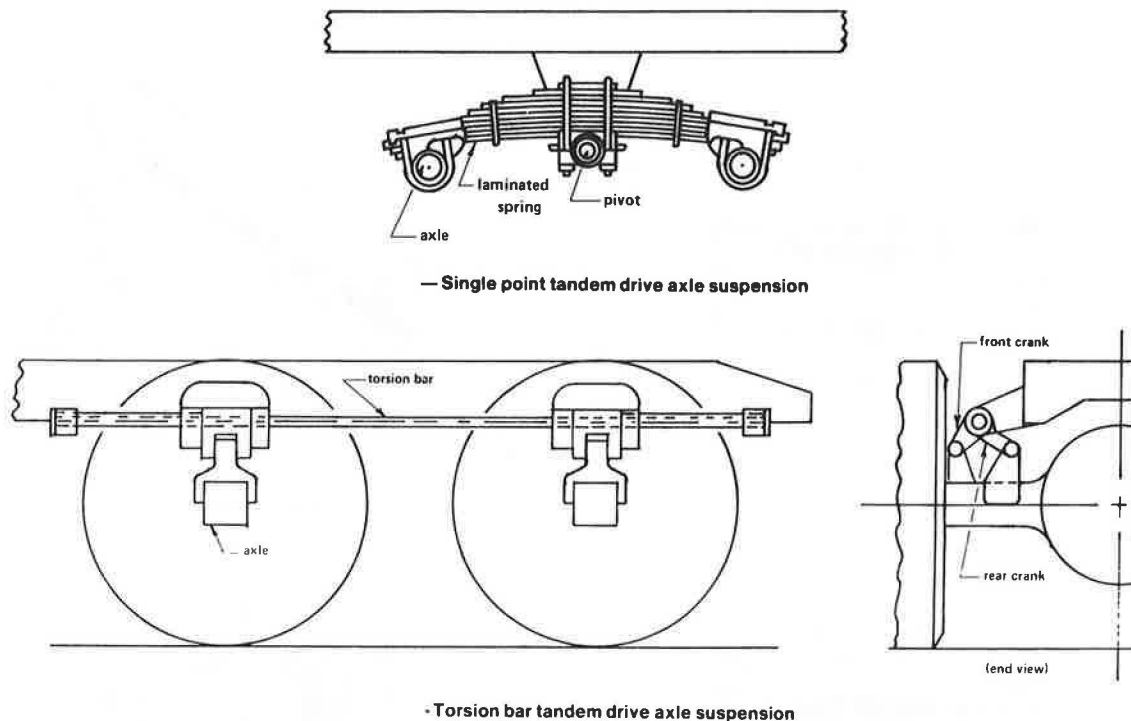
FIGURE 1 *continued.*

that WIM systems may provide a check on any computational procedures used to define dynamic loads. However, since WIM devices provide measurements of dynamic loads only at specific points, WIM results do not provide a complete check on the loading that a particular vehicle exerts on a pavement.

Several researchers have provided estimates for the complete spectrum of dynamic loading (3, 4). Although loading frequencies can be developed from data such as those shown in Figure 5, it is possible to directly ascertain specific frequency ranges associated with different types of suspensions and vehicles (5). Figure 6 illustrates the results of such determinations; note that the frequencies are less than 20 Hz.

ANALYTICAL DEVELOPMENTS

Current capabilities to perform dynamic analyses are highly developed. However, the computational effort required to solve a completely general three-dimensional dynamic problem representative of a pavement system subjected to a moving load is very large—too large, in fact, to be acceptable for practical pavement analyses. This effort can be reduced through simplifying assumptions regarding material properties, the type and distribution of the dynamic loads, and the geometry of the problem. This section briefly discusses these efforts and the resulting computer solution termed SAPSI.

Material Properties

For this analysis, the materials constituting the pavement section have been assumed to be linear viscoelastic in response to loads. With this assumption, the laws of superposition are valid and, in turn, provide considerable computational advantages. Unfortunately, by choosing these material properties, it is not possible to directly obtain permanent displacements. It may, however, be possible to estimate them from the computed stress time histories.

An additional advantage of using viscoelastic materials in the computational models is that it leads to stable algorithms and computer codes. Furthermore, the description of the material properties is simple and unambiguous, and can directly utilize the data described subsequently.

Dynamic Loads

A major challenge to the development of an efficient method of dynamic analysis is the fact that actual traffic loads move over the surface of the pavement. Thus, one of the first theoretical tasks undertaken in this study was to investigate the effects of vehicle velocity on the stresses in a typical pavement. More specifically, an attempt was made to answer the question: "How different is the stress field developed under a moving load from the stress field developed under the same load acting at a stationary location?"

This problem has been investigated by Cole and Huth (6) for the special case of a vertical line load moving at constant velocity over the surface of a uniform elastic half space. They found that the major effect of the nonstationarity of the load is an increase of the maximum stresses that occur in the pavement. This increase can be closely approximated by the ratio:

$$\text{Amplification ratio} = \frac{\text{maximum dynamic stress}}{\text{static stress}}$$

$$= \frac{1}{1 - (V/V_s)^2} \qquad (1)$$
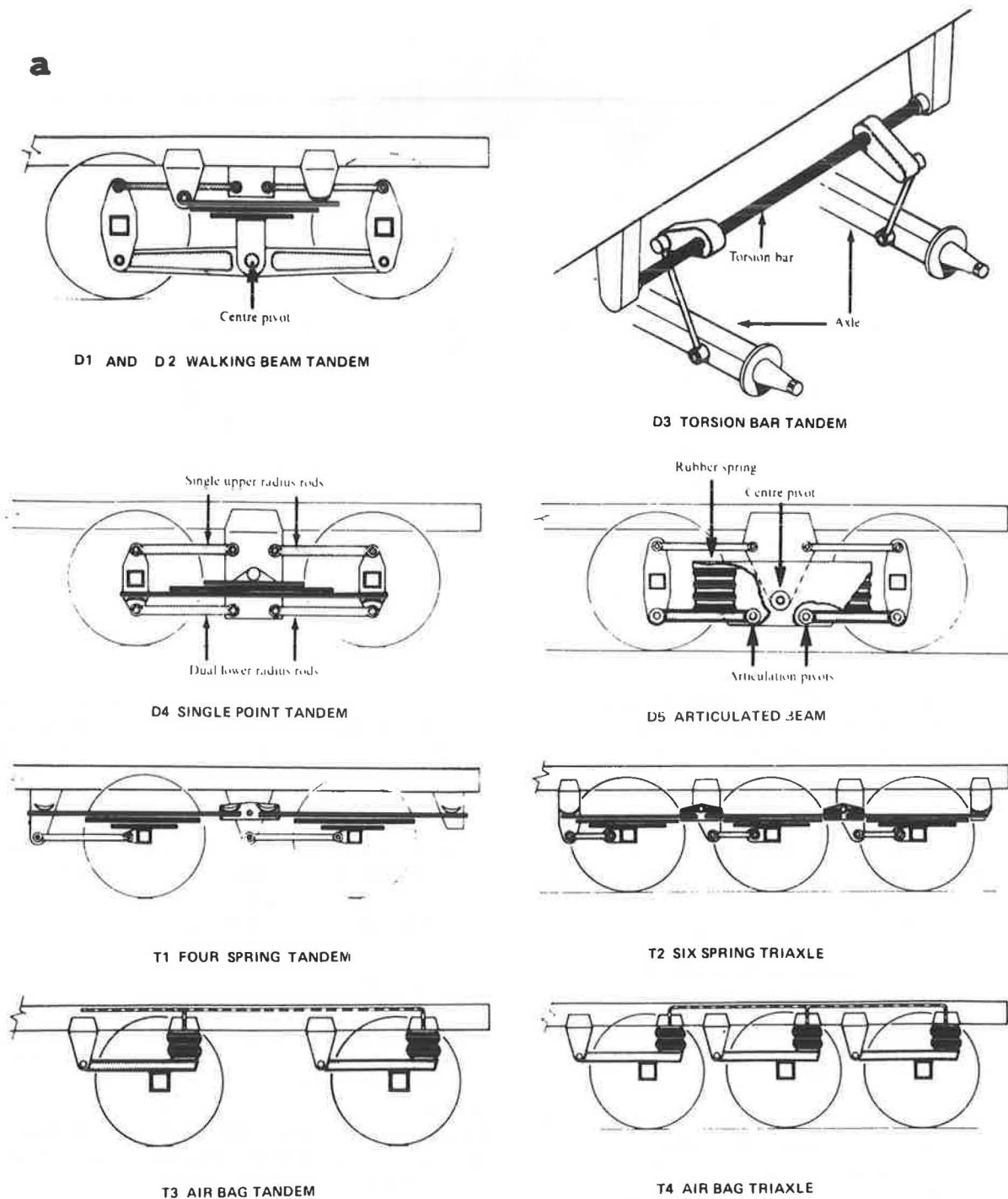
FIGURE 2 Factors influencing dynamic response: (a) suspension types tested for dynamic loading (1).

where

V = velocity of the moving load, and
V_s = shear wave velocity in the half space.

Unfortunately, the above result is not directly applicable to pavement structures, which behave like layered systems, and no solutions for such systems are available. It was, therefore, necessary to develop a new theory and an associated computer program, MOVE (7), for dynamic analysis of the

layered system shown in Figure 7. The computational model consists of a number of viscoelastic layers resting on a rigid base, and the loading is a vertical line load that moves with a constant velocity, V, over the free surface of the system. A lower half-space can be simulated by placing the rigid boundary at a large depth.

The computer program was verified by comparing it with a static solution by Poulos and Davis (8), and also with the Cole and Huth (6) solution (where P_0 = 2,000 lb/ft, V_s =

b
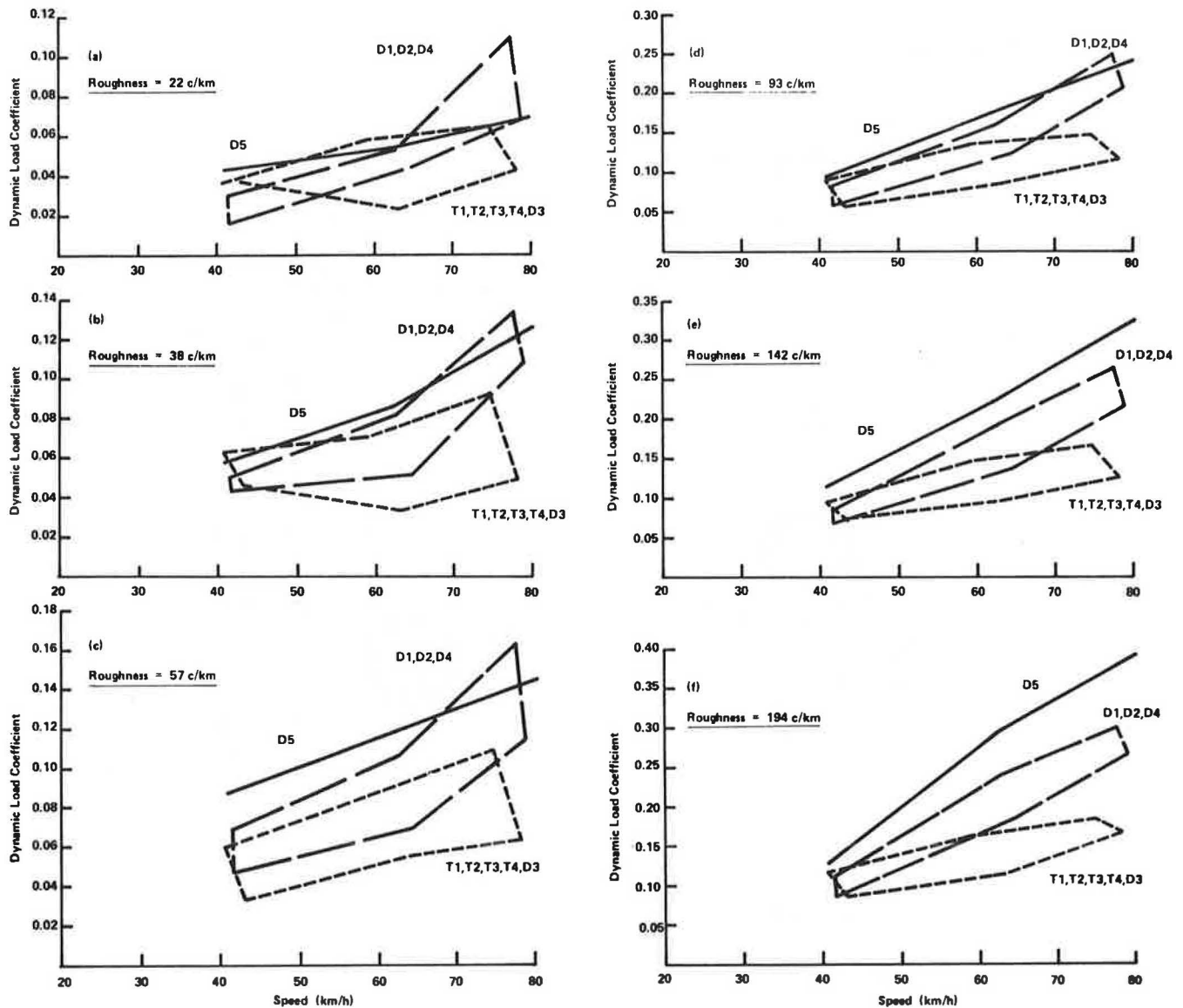
FIGURE 2   Factors influencing dynamic response: (b) effects of speed and pavement roughness on dynamic load coefficient for three groups of suspensions (*1*).

500 ft/sec, Poisson's ratio = 0.4, *H* = 30.0 ft). In both cases, excellent agreement was obtained (Tables 1 and 2). Following verification, several pavement structures were analyzed. The two-layer structure shown in Figure 8 is an example; it consists of an asphalt concrete layer 20-in. thick resting on a half-space subgrade. This model was analyzed for line loads moving with three different velocities: *V* = 0, 60, and 90 mph. For each case, the maximum shear stresses developed at different depths were computed. The values so obtained were compared to those resulting from a stationary load. Results of this analysis are shown in Figure 8 in the form of a plot of amplification ratio vs. depth. Also shown is the amplification ratio predicted by Equation 1, using the properties of the subgrade for the half space.

The results indicate that the Cole-Huth solution overestimates the importance of vehicle velocity. At a velocity of 60 mph, the amplification in the actual pavement is only 7 percent; and within depths that are of interest for analyses of subgrade stresses, it is less than 10 percent. These increases are relatively small so that a major computational effort does not seem appropriate for an accurate determination. Accordingly, the assumption has been made that the dynamic stresses in a pavement can be computed using stationary loads. It is also recommended that a small dynamic amplification factor thus neglected be included in the design by multiplying the stresses by approximate stress amplification factors obtained using the program MOVE. The savings in computation effort thus achieved can be significant.
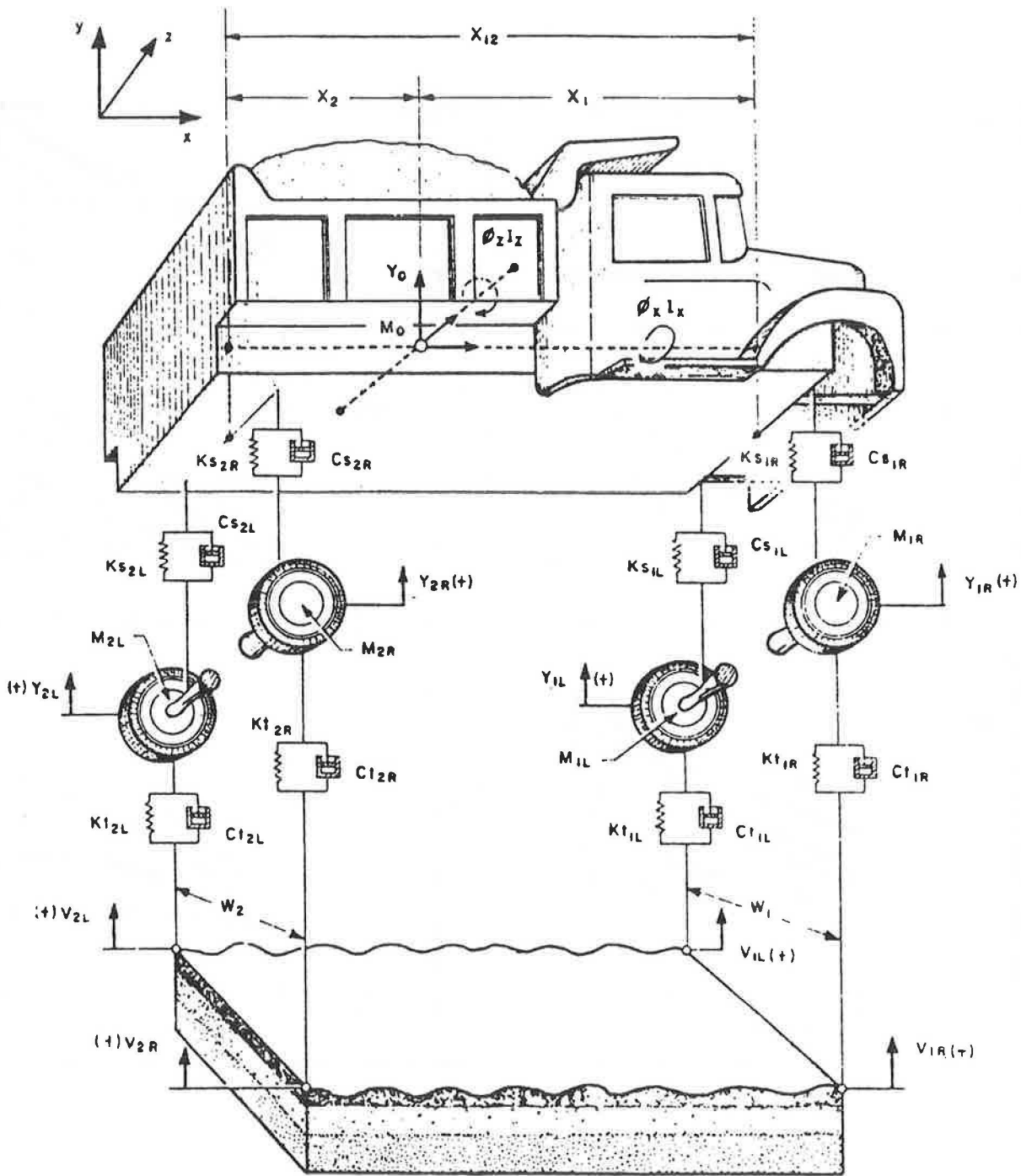
FIGURE 3 Truck elements used to estimate dynamic response (2).

The above conclusions and simplifying assumption should not be construed to mean that dynamic effects can be neglected or that the stresses in a pavement will be independent of the velocity of the traffic moving on the pavement. It can be assumed that wheel loads are stationary as to their location on the pavement, but the magnitude and time variations of these loads are strongly dependent on the type and velocity of the traffic and the stiffness and roughness of the pavement. Also, dynamic effects are likely to be significant for the man-

ner in which stresses from different wheel loads superimpose in a pavement. That is, in computing the stress field caused by a group of wheels, dynamic effects may have to be considered.

The finding that all loads can be considered stationary is significant. It means that, provided the magnitude and time variation of typical wheel loads can be determined, relatively simple computer programs can be used for stress and distress analysis of pavements.
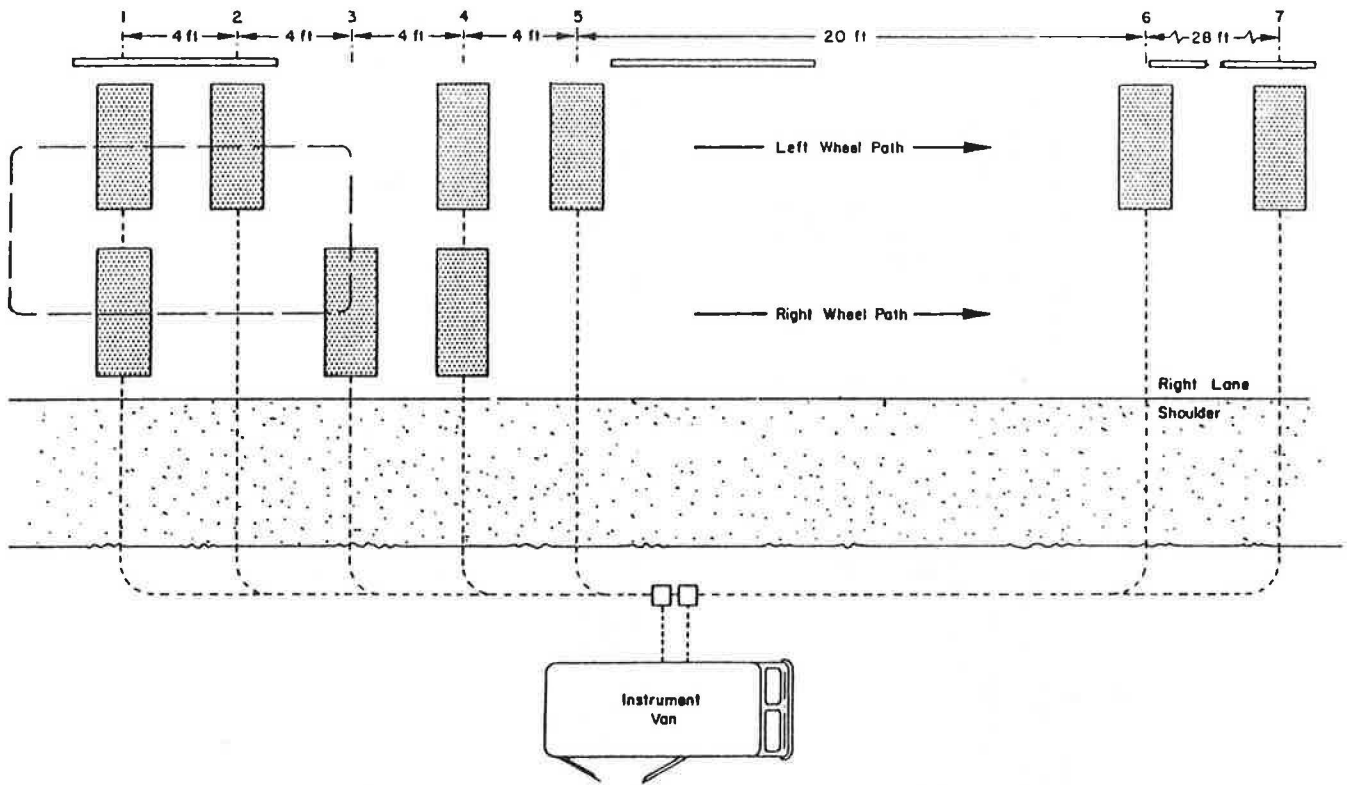
FIGURE 4   Weigh-in-motion installations to assess dynamic response (2).
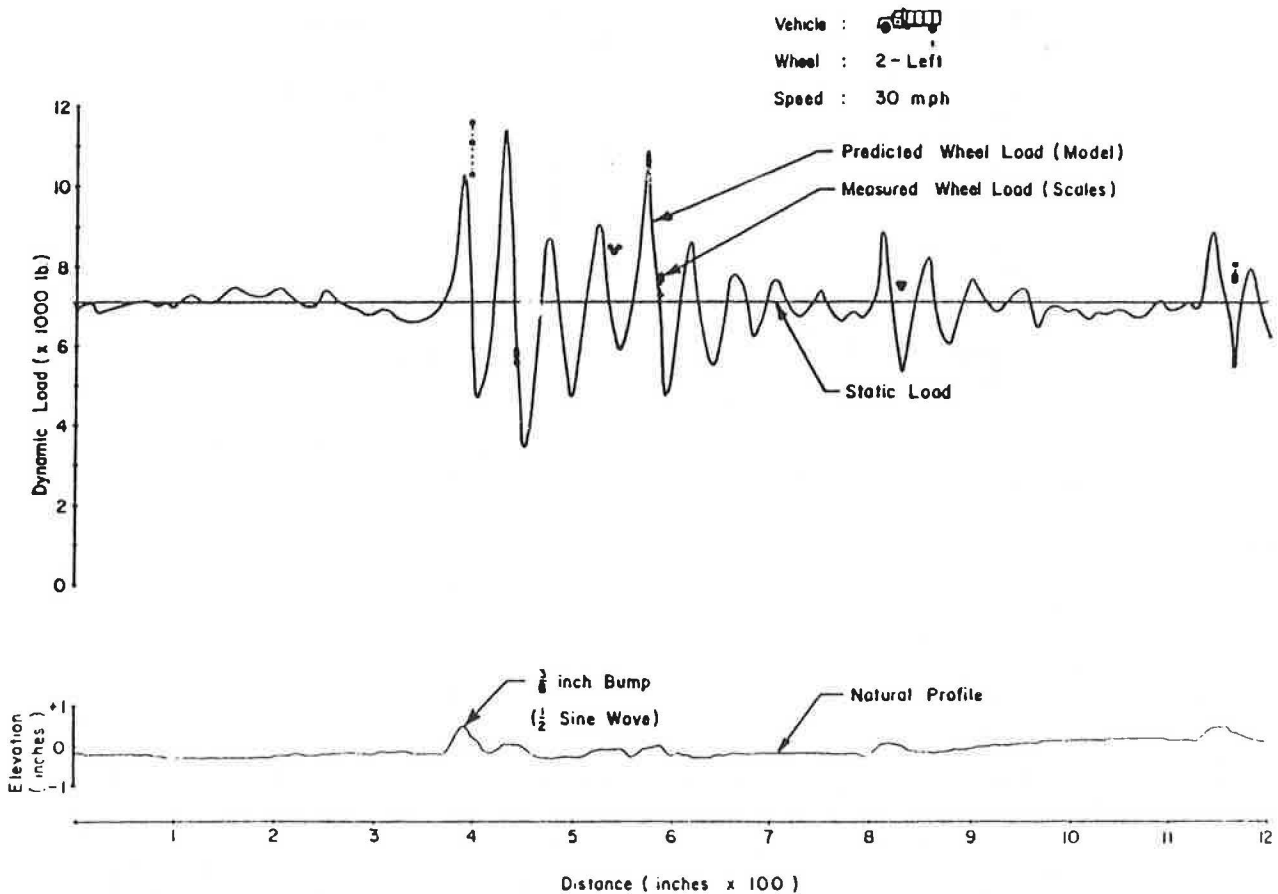
FIGURE 5   Comparison of measured and computed dynamic loads of a fully loaded truck moving at 30 mph (4).
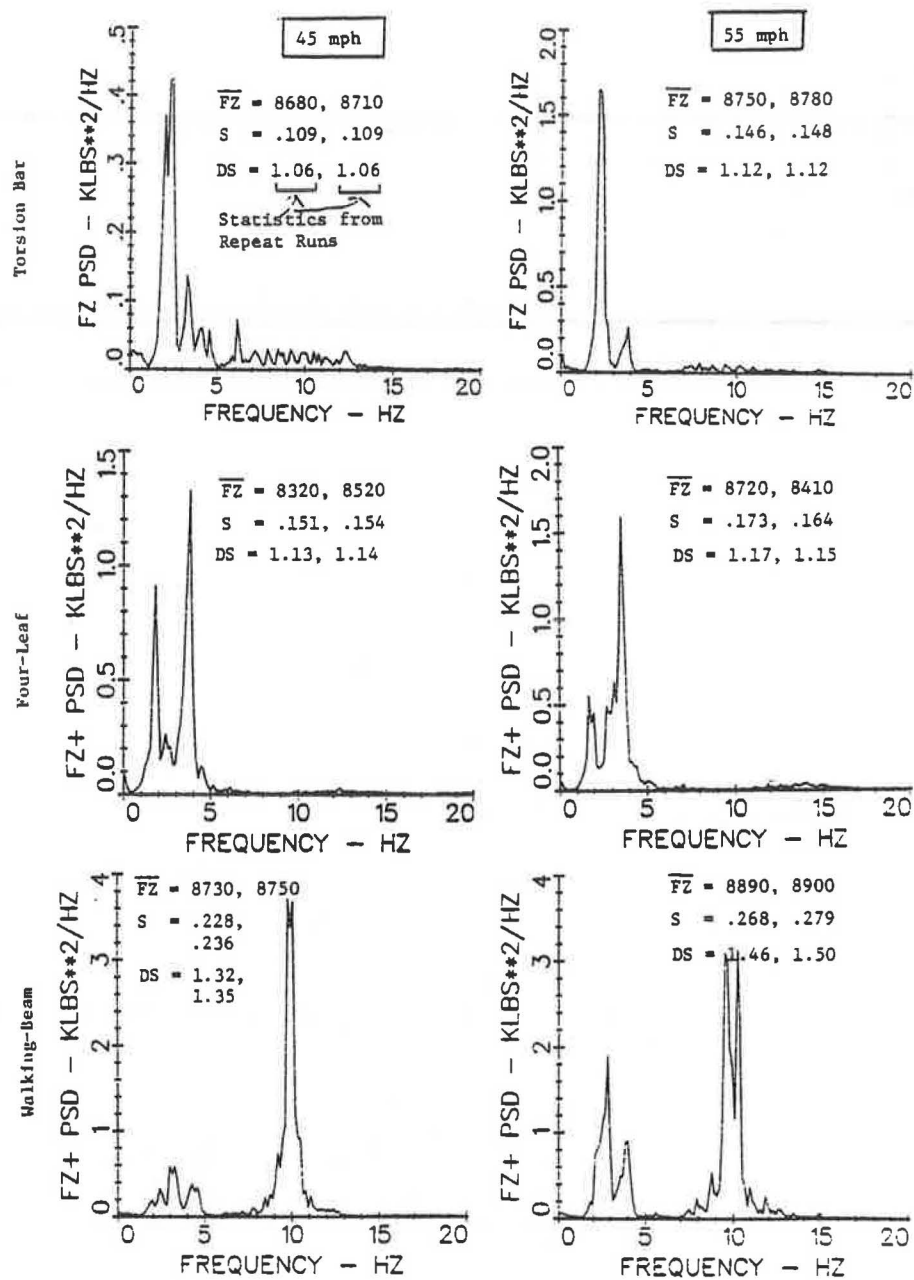
FIGURE 6   Response of vehicles, by suspension type and speed, on aged portland cement concrete roadway with considerable faulting, cracking, and patching (5).

Geometry

Complex geometry will inevitably lead to complicated computer programs which are expensive to run. This is especially true if the geometry is three-dimensional and the loading is dynamic. Significant simplifications can be achieved by imposing restrictions on the generality of the geometry and load distribution.

For pavement analyses, the single most effective restriction is that of allowing only semifinite horizontally layered models. This will effectively reduce the dimensionality of the problem from three to two dimensions, since with viscoelastic materials, the problem reduces to a superposition of similar axisymmetric solutions. Unfortunately, this restriction precludes

the analysis of joint and edge problems. Nevertheless, in the interest of progress and economy, this restriction has been adapted for the solutions used herein.

SAPSI Program

A computer code was developed which takes advantage of the above-mentioned simplifications and involves many of the concepts embodied in the SASSI code (a computer program developed for the solution of soil-structure interaction problems). This new code, SAPSI, is a menu-driven program written in FORTRAN and can be utilized on an IBM-PC/AT (7).

SAPSI can be used to calculate the response of a viscoelastic
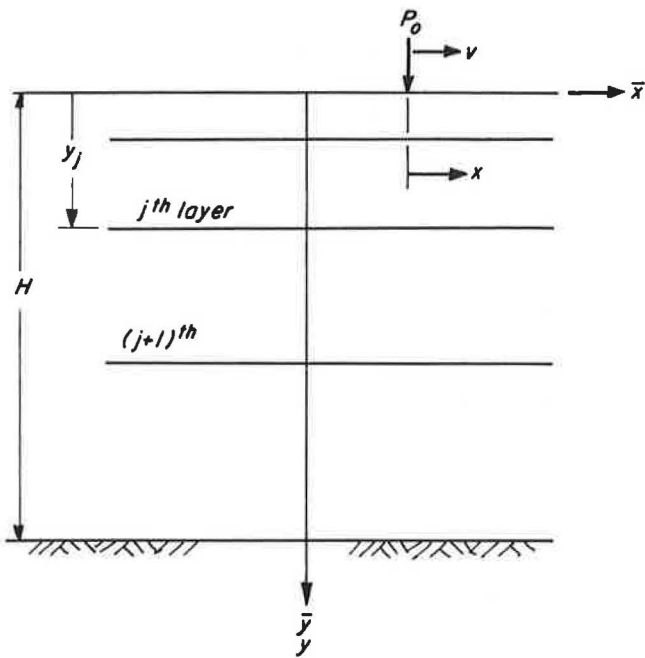
FIGURE 7 Model for pavement-subgrade system subjected to moving loads.

layered system subjected to surface circular loads. It can be assumed that the layered system is resting on a half space. This is simulated by vertically extended layers and by a series of dashpots attached to the bottom of the extended layers. The layer properties, which include the shear modulus, the damping ratio, and Poisson's ratio, can be varied with the excitation frequencies of the loads. Multiple loads (up to 40) are acceptable for harmonic and transient motions. The loads may have different radii and time histories. Static loads can be simulated by specifying a harmonic motion with zero excitation frequency.

The program uses special techniques in the frequency domain to interpolate results obtained at only a few frequencies (up to 20 frequencies can be analyzed). Thus, computation time can be significantly reduced. Furthermore, to facilitate modifications and adaptability to different computer memory sizes, the program also uses the dynamic allocation technique. This allows the dimensions of the program to be easily increased, if so desired, without much effort.

With respect to output for time histories, the program can calculate displacement, stress, or strain at any point in the middle of any layer (in global coordinates) up to 108 points. The output can be as follows:

- displacements at layer interfaces,
- stresses at center of layers,
- strains at center of layers.

The general output or the printout contains control information, input layer profile and properties, eigen values and vectors, and maximum responses for displacements, stresses, and strains.

LABORATORY EVALUATION OF DYNAMIC PROPERTIES OF PAVING MATERIALS

To determine the dynamic response of representative pavement materials, a testing system was devised which can test specimens as hollow cylinders at frequencies up to 30 Hz. The specimens can be subjected to axial, torsional, or combined axial and torsional loads in this frequency range to attempt to simulate the three-dimensional stress states that occur in pavement materials in situ when subjected to moving loads. This equipment has been described in detail by Sousa and Monismith (9).

Although they reported the results of tests on an asphalt concrete (California Type B mixture, ⅜-in. maximum size aggregate consisting of Watsonville granite, AR-4000 asphalt cement supplied by Chevron) and Vicksburg silty clay (LL

TABLE 1 COMPARISON OF MOVE PROGRAM AND STATIC SOLUTION (8) FOR HORIZONTAL AND VERTICAL DISPLACEMENTS IN MULTILAYERED SYSTEMS

Coordinate x (ft)	Horizontal Displacement 10^{-3} (ft)		Vertical Displacement 10^{-3} (ft)	
	MOVE	Poulos and Davis	MOVE	Poulos and Davis
3	0.07713	0.07716	0.6721	0.6425
6	0.05226	0.05296	0.3930	0.3802
12	0.00990	0.01024	0.1459	0.1423
18	-0.02689	-0.02367	-0.03586	-0.03539
24	-0.05051	-0.04734	-0.01404	-0.01391
30	-0.06255	-0.05852	-0.03281	-0.03293

TABLE 2 COMPARISON OF MOVE PROGRAM AND STATIC SOLUTION (8) FOR NORMAL AND SHEAR STRESSES IN MULTILAYERED SYSTEMS

Coordinates (x, y) ft.	Normal Stress σ_{yy}, psf		Shear Stress τ_{yy}, psf	
	MOVE	Poulos and Davis	MOVE	Poulos and Davis
(3, 6)	137.10	126.41	66.70	61.29
(3, 12)	95.50	97.30	18.40	21.40
(3, 18)	78.96	74.23	8.76	9.25
(3, 24)	62.26	61.96	5.26	5.14
(3, 30)	52.57	52.40	5.57	5.65
(6, 18)	63.44	63.45	15.62	15.39
(6, 24)	56.03	56.07	9.45	9.32
(6, 30)	48.54	48.62	10.72	10.53
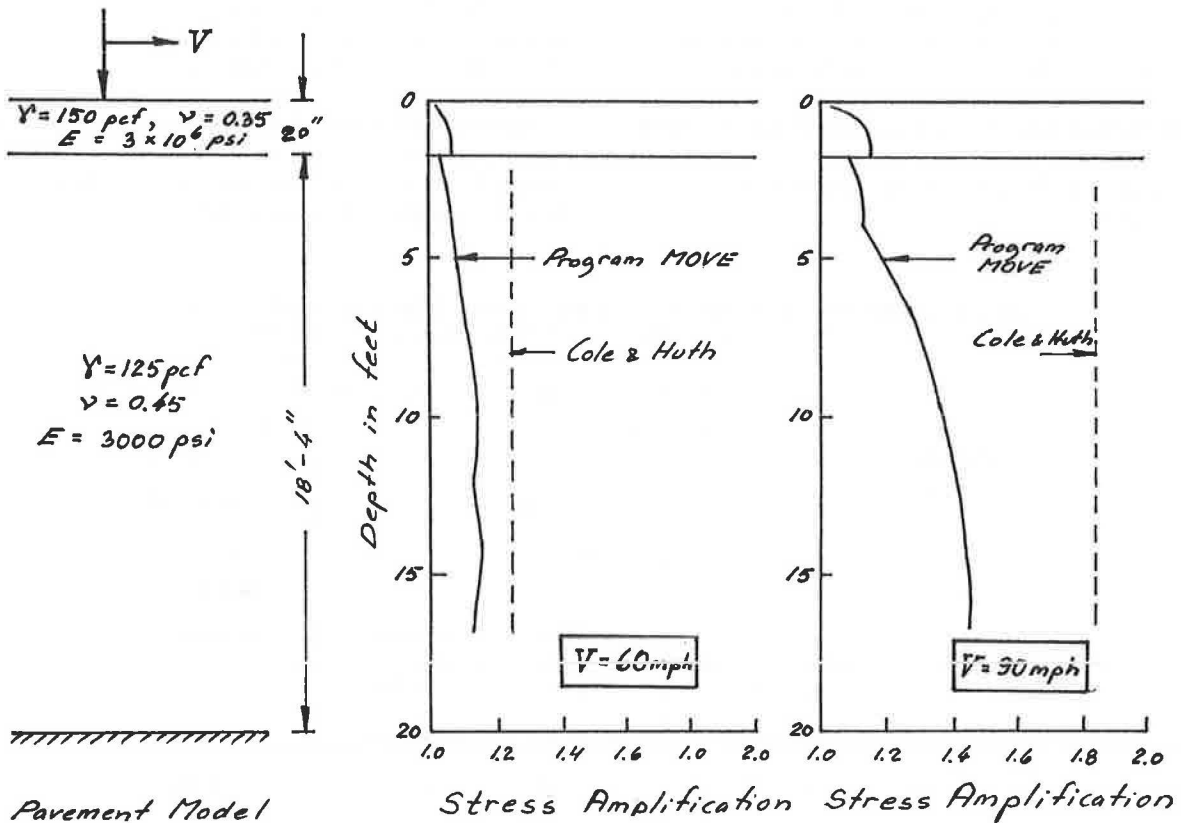
FIGURE 8 Load moving at 0, 60, and 90 mph on an asphalt concrete layer 20-in. thick resting on a half-space subgrade.

35, PI 13), some of the test data are presented herein since they are germane to the analyses described below. Both materials were tested as hollow cylindrical specimens 18-in. high, 9-in. outside diameter, and with a 1-in. wall thickness.

Asphalt Concrete

The properties of the asphalt concrete were measured by the application of several vertical and torsional sinusoidal loads to the hollow cylindrical specimens at three different temperatures (11°C, 25°C, and 40°C). At 11°C the vertical sinusoidal compression pressure had a mean value of 40 psi and an amplitude of 70 psi, and the torsional sinusoidal loads produced shear stresses with a mean value of 12 psi and amplitudes of 20 psi. At 25°C and 40°C, the axial values were 25 psi and 40 psi and shear stresses of 4 psi and 6 psi, respectively. At each temperature level the frequency of the sinusoidal loads varied between 0.5 and 20 Hz (0.5, 1.0, 5.0, 10, 15, and 20 Hz). A total of 200 loading cycles was applied at each frequency (at 0.5 Hz only 60 cycles were applied, and at 1.0 Hz only 100 cycles were applied). All tests were performed under stress control (feedback from the load cells) with LVDTs placed 2.5 in. from the ends of the specimen. Each specimen was initially tested at 11°C, then at 25°C, and at 40°C. This sequence was repeated three times. A specimen was maintained at each temperature level for at least 3 hr prior to testing. Vertical vibratory loads (20 to 0.5 Hz) were applied first, then torsional vibrations (20 to 0.5 Hz). This sequence was repeated twice at each temperature.

The effect of temperature and frequency on the variation of the dynamic modulus $|E^*|$ and the dynamic shear modulus $|G^*|$ is illustrated in Figure 9. Repeatability of the results after various tests had been performed indicates that the dynamic properties of the specimen are not influenced by previous testing frequencies and temperatures. Thus, several different tests can be performed on the same specimen using various frequencies, temperatures, load applications, and levels of stress without changing the data significantly. However, the stiffness moduli exhibit strong dependence on frequency and temperature.

From stress-strain hysteresis loops (Fig. 10), the internal damping can be determined. The effects of temperature and frequency on the values of internal damping, measured under vertical loading and torsional loading, are plotted in Figure 11. Note that the differences in damping increase with temperature. Temperature and frequency effects are particularly noticeable on the values of the dynamic Poisson's ratio $[v^* = E^*/(2\ G^*) - 1]$, as shown in Figure 12. The high values obtained at 40°C and at 25°C under low frequencies are probably due to volume change during the shear loading cycles. Under those conditions the contribution of the bitumen for the resistance of the mix is reduced, and this results in a behavior more like that of an aggregate. Similar results have been reported by Hills and Heukelom (*10*).

Silty Clay

Specimens of silty clay were tested at three strain levels (0.01, 0.1, and 1.0 percent), four frequency levels (0.5, 1.0, 5.0, and 10 Hz), and four levels of confining pressure (29, 20, 11, and again at 29 in. Hg). During testing, approximately 30 sinusoidal load cycles were applied at each level.
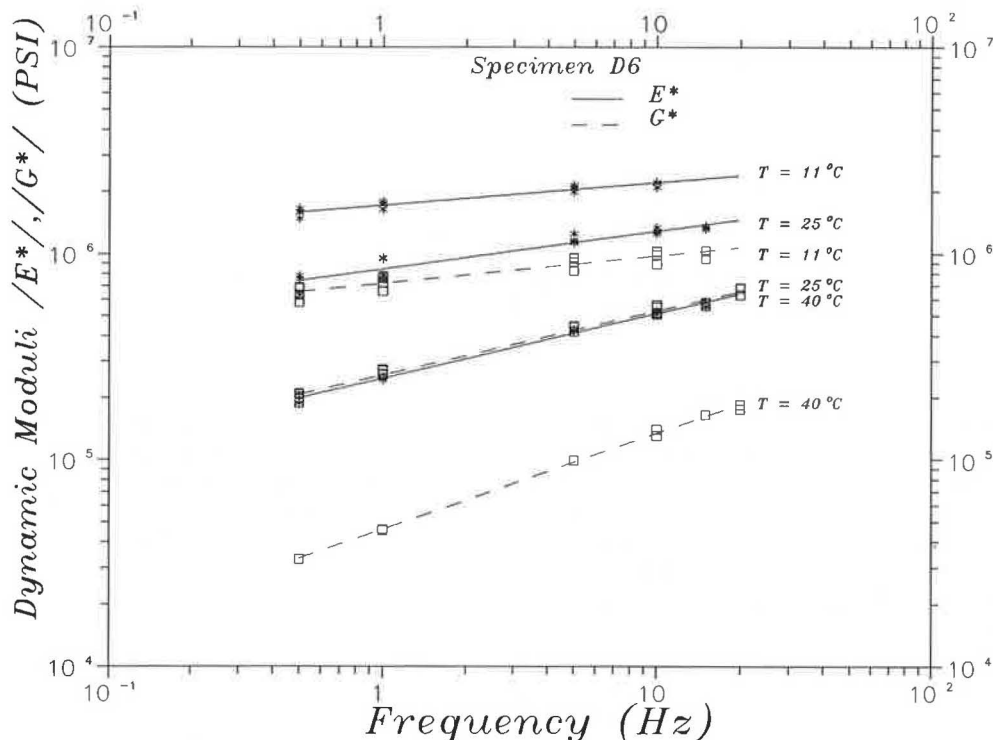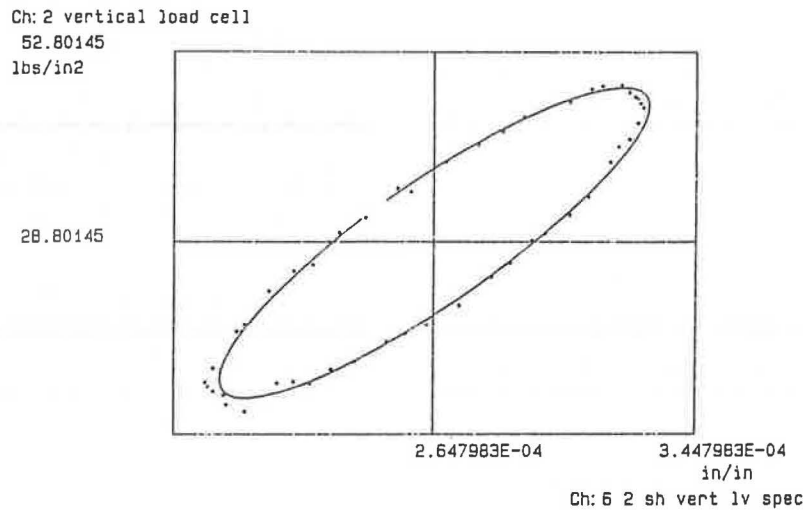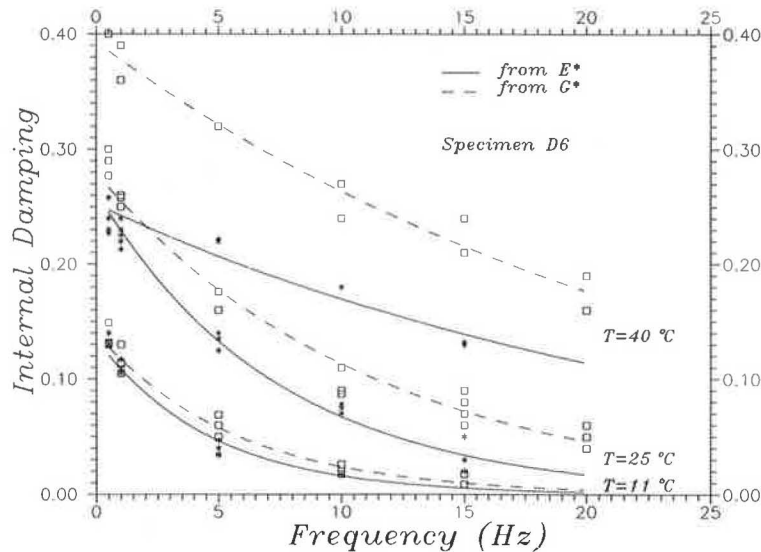

FIGURE 9 Influence of frequency and temperature on dynamic moduli of an asphalt concrete in compression and shear.

Ch: 2 vertical load cell
52.80145
lbs/in2

28.80145

2.647983E-04   3.447983E-04
in/in

Ch: 6 2 sh vert lv spec

FIGURE 10   Hysteresis loop for an asphalt concrete mixture where frequency = 1 Hz, T = 40°C.

FIGURE 11   Influence of temperature and frequency on damping characteristics of an asphalt concrete.

Figure 13 illustrates the effects of shear strain amplitude and confining stress on the dynamic shear modulus $|G^*|$. To obtain these values, confining pressure was changed at each strain level; this was done to mitigate the effects of damage that might occur at higher strain levels on the test results. The repeatability of results at 29 in. Hg after several cycles were applied at 20 and 11 in. Hg indicates that the number of load applications (even if applied at lower confining pressures and different frequencies) does not significantly alter the dynamic shear modulus. Furthermore, it can be inferred from the data (Fig. 14) that frequency of loading does not affect the dynamic shear modulus.

The effects of confining stress, frequency, and strain amplitude on damping were also evaluated. The data presented in

Figure 15 suggest that internal damping increases with increase in shear strain amplitude but is little affected by confining pressure. Furthermore, the effects of loading frequency on internal damping are also evident. Note also that the frequency effect is similar at each level since all of the lines plotted are essentially parallel.

ANALYSIS OF A PAVEMENT DESIGN

This section presents a methodology used to assess the relative damage caused by tandem axles with three different suspension systems: a torsion bar, a four-leaf spring, and a walking beam.
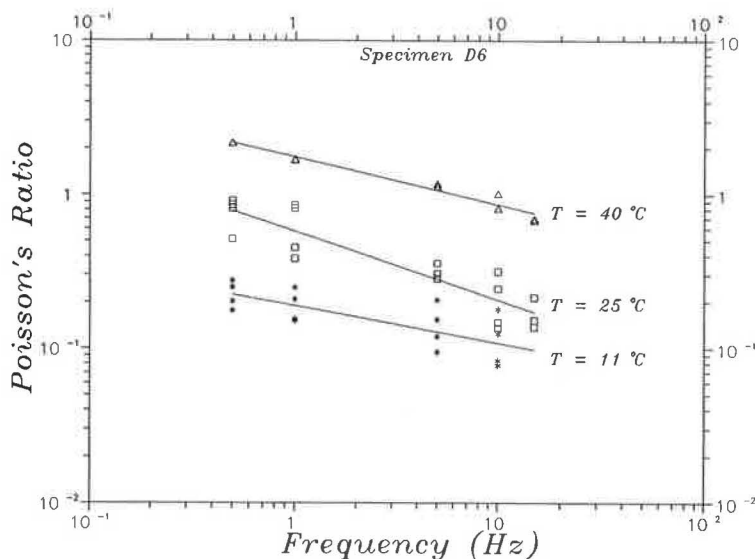
FIGURE 12 Influence of temperature and frequency on Poisson's ratio for an asphalt concrete.
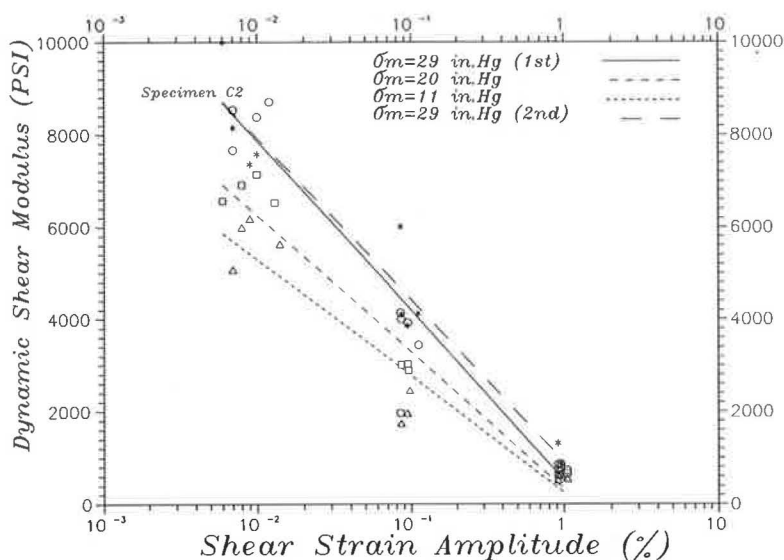
FIGURE 13 Influence of shear strain amplitude on the dynamic shear modulus of a silty clay specimen at three different confining pressures.

To properly solve this problem requires data defining the time histories of the loads applied to a pavement structure with trucks equally loaded but equipped with different suspension systems.

Gillespie et al. (5) have presented data from measurements of the time variations of loads applied to the same pavement section and nearly conforming to these requirements. Their data, illustrated in Figure 16, represent the loads measured at the wheel hub and do not include the inertia forces caused by vibrations of the mass of the wheel. This implies that the actual variation in magnitude of the dynamic loads on the pavement was only slightly higher than that recorded and that the data can therefore be considered representative.

Another requirement is to decide on the mode or modes

of distress to be analyzed, that is, modes that will lead to a reduction in pavement serviceability. In the example that follows, the fatigue mode of distress was selected. The relative damage effects of the three types of suspensions were determined in three steps:

1. *Determination of time histories of the tensile strain at the bottom of a representative pavement structure using dynamic material properties determined in this investigation.* The strains were computed using the SAPSI program (7). This program, as noted above, simulates the dynamic response of layered systems to dynamic surface loads and incorporates the variation of the material properties with loading frequency.

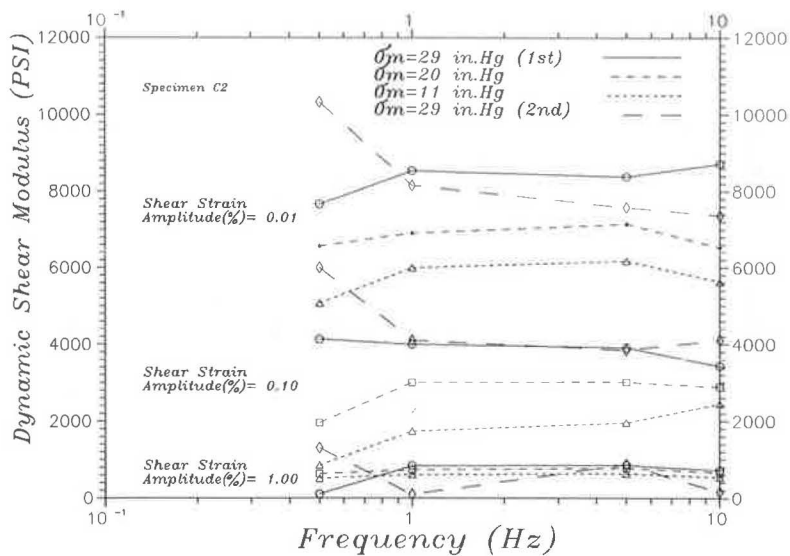2. *Determination of pavement life expectancy using gener-*

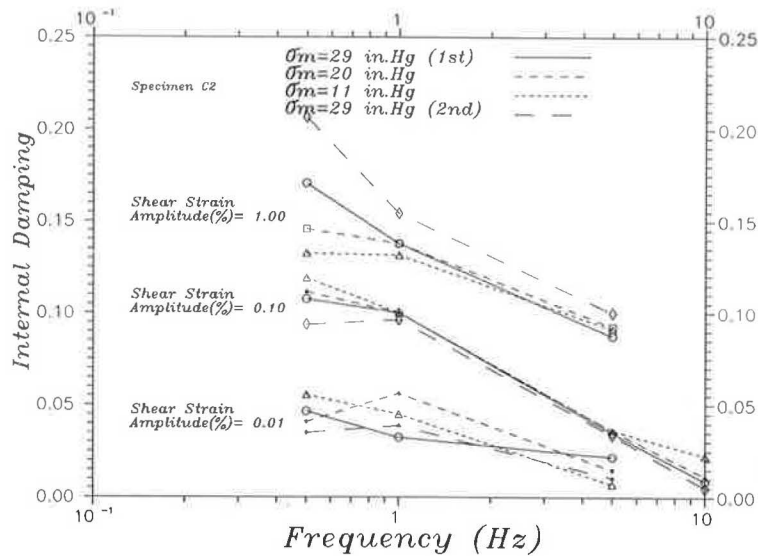**FIGURE 14 Influence of frequency loading on the dynamic shear modulus.**

FIGURE 15 Influence of load frequency on internal damping at different strain levels for Vicksburg silty clay.

ally accepted fatigue criteria. For each of the suspension types the number of load applications to failure was computed. The Linear Summation of Cycle Ratio Cumulative Damage Hypothesis was used to assess the relative damage imposed at each level of strain.

3. *For comparison, a reduction of pavement life (RPL) index was developed for each suspension type.* Each RPL value represents the percentage of pavement life consumed solely by the dynamic effects incurred by one type of suspension. The definition of the RPL index is as follows:

$$RPL = 1 - N_F(\text{suspension})/N_F(\text{static}) \qquad (2)$$

where

N_F (static) = number of load applications to failure computed by current quasi-static methods.

N_F (suspension) = number of load repetitions to failure (taking into consideration the dynamic effects of the suspension).

During this analysis it was assumed that the dynamic loads produced by a moving truck on a rough surface were a random phenomenon. Consequently, any particular point on the pavement may be subjected to the full spectrum of loads that a given truck might apply. In essence, any single point in the wheel path is likely to sustain the same level of loading as any other point might sustain. In addition, based on the analysis presented earlier, velocity effects of a moving load (velocity > 0) on a layered structure are negligible for velocities below 70 mph.
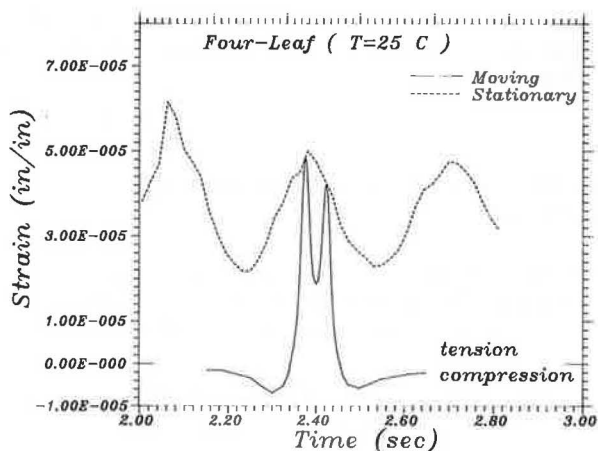
These two considerations enable the conversion of the spatial and temporal problem of determining the maximum strain variation under a moving truck to that of determining the

FIGURE 16   Comparison of three vehicle responses to the same road input, by type of suspension (note that signals are not accurately synchronized) (5).
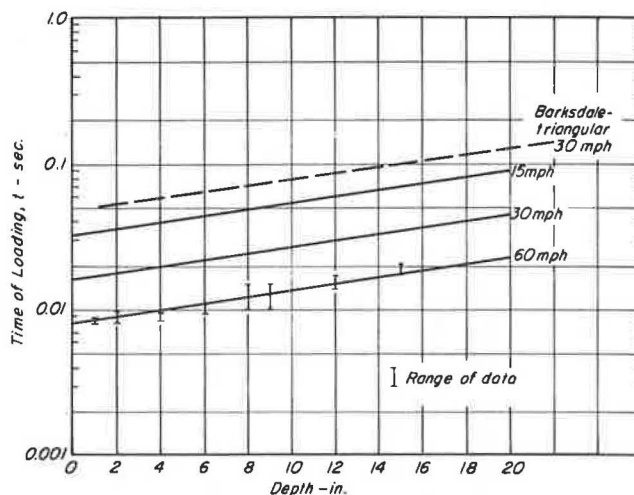
on the layered structure) under a nonmoving random load represents the maximum variation of the strain (on equivalent points of the layered system) over a section of pavement 0.073 mile long excited by the same load (or truck) moving at 55 mph [0.073 mile = 4.8 (sec) 55 (mph)/3,600 (sec/hr).]

Figure 17 illustrates this assumption. The solid line represents the time variation of the tensile strain at the bottom of the asphalt concrete layer. The two peaks are due to the passage of a moving (velocity = 55 mph) tandem wheel suspension (the difference in the values is due to the time variation of the loads on each of the wheels). The dashed line represents the time variation of the tensile strain for the nonmoving (velocity = 0) case but subjected to the same time load history.

Pavement Life Determination for Quasi-Static Case

To determine the pavement life for the quasi-static or constant-load case (i.e., no dynamic load variation with time), the pavement system was assumed to respond to the load as a layered elastic system. For an asphalt concrete pavement system, the stiffness modulus of the asphalt-bound layer is dependent on the velocity of the moving vehicle (time of loading) and the temperature of the material at the time of loading. In this type of analysis, equally loaded trucks equipped with different suspension types and traveling at the same speed are expected to produce the same pavement response and, hence, the same damage.

To determine the time of loading to be used to estimate the stiffness modulus of the asphalt-bound layer, use can be made of an approach recommended by McLean (*11*) and shown in Figure 18. In this figure the solid curves are those computed by McLean assuming square vertical compressive stress pulses; as shown in the figure, the time of loading depends on the layer thickness as well as the velocity of the vehicle. As an example, this figure suggests that asphalt properties obtained from a testing sequence using square waves with a loading time of 0.024 sec are representative of the asphalt concrete behavior in a 10-in.-thick pavement structure excited by a truck traveling at 30 mph. Barksdale's (*12*) analysis for

time history of the tensile strain (at any chosen point on the pavement structure) for a nonmoving (velocity = 0) randomly applied load. According to this assumption, one can state (for instance) that 4.8 sec of time strain history (for a single point

FIGURE 17   Time variation of tensile strain at a point on the underside of the asphalt concrete layer.

FIGURE 18   Relationship between equivalent time of loading and depth for vertical compressive stress (*11*).

TABLE 3 STIFFNESS CHARACTERISTICS OF ASPHALT CONCRETE FOR QUASI-STATIC ANALYSIS
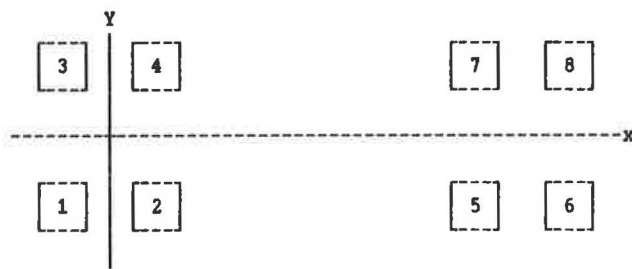
Temperature $^\circ$C	Shear Modulus[1] $\lvert G* \rvert$ psi	Poisson's[2] Ratio ν	S_{mix}[3] $\lvert E* \rvert$ psi
25	4.24×10^5	0.28	1.09×10^6
11	8.92×10^5	0.13	2.01×10^6

1. From line of best fit, Fig. 20, assuming 5 Hz loading frequency.

2. From line of best fit, Fig. 22, assuming 5 Hz loading frequency.

3. Computed from $\lvert E* \rvert = \lvert G* \rvert / 2(1 + \nu)$.

the same conditions (also shown in Figure 18) suggested a testing sequence based on triangular pulses with loading times of 0.075 sec. If sinusoidal loading is chosen instead of triangular or square loading waves, it is reasonable to expect (from interpolation) that a loading time of 0.03 sec would be representative of a truck traveling at 55 mph on the same 10-in.-thick pavement (Figure 18). In this analysis it was assumed that this loading time corresponds to asphalt concrete properties tested under a 5-Hz sinusoidal loading frequency [5 Hz = $1/(2\pi \times 0.03 \text{ sec})$].

For these loading frequencies, estimates of the stiffness properties of the asphalt concrete to be used for the quasi-static analyses are shown in Table 3.

Figure 19 illustrates the dimensions of the tandem axle used in the analysis. A 5,000-lb static load was applied to each circular surface location with a radius of 4.2 in. (tire pressure = 90 psi). The pavement system consisted of 12 in. of asphalt concrete resting on the silty clay subgrade.

The maximum tensile strain at the bottom of the asphalt layers was computed by the SAPSI program. This program is also capable of performing static analyses. However, for increased accuracy, the subdivision of each layer into idealized sublayers of the same material is necessary. Table 4 shows the thicknesses of the various layers used in the calculation. However, the program can only compute the stresses, strains, or displacements at the center of each layer. Thus, to determine the tensile strains of an element at a distance sufficiently close to the bottom of the asphalt concrete layer, an idealized thin sublayer had to be created. The stresses were computed 0.06 in. from the bottom of the asphalt layer.

Estimates of the fatigue life were made using the relationship for asphalt concrete developed by Finn et al. (13) for less than 10 percent cracking in the wheel path:

$$\log N_F = 15.947 - 3.291 \log (\varepsilon_t / 10^{-6}) \\ - 0.854 \log (S_{mix}/10^3) \quad (3)$$

where

N_F = number of load repetitions to failure,
ε_t = tensile strain in asphalt layer (in./in.), and
S_{mix} = asphalt mixture stiffness modulus (dynamic modulus in psi).

For the two temperatures the computed strains and the corresponding fatigue lives according to Equation 3 are shown in Table 5.

LOAD NUMBER	X COORDINATE (FEET)	Y COORDINATE (FEET)
1	-0.5265	2.0
2	0.5265	2.0
3	-0.5265	-2.0
4	0.5265	-2.0
5	6.465	2.0
6	7.526	2.0
7	6.465	-2.0
8	7.526	-2.0

FIGURE 19 Spatial distribution of tandem-axle loads.

Dynamic Load Considerations in Pavement Life Determination

To establish the influence of the load applied dynamically, as compared to the previous solution for the quasi-static case, at least three major aspects must be considered:

1. time variation of the load applied to the pavement,
2. pavement model capable of simulating dynamic response, and
3. variation of material properties as a result of different loading frequencies.

TABLE 4   IDEALIZATION OF PAVEMENT SYSTEM FOR STRAIN
DETERMINATION

Layer Number	Thickness (in.)	Material
1	6.00	
2	4.80	
3	2.40	Asphalt
4	1.20	Concrete
5	0.48	
6	0.12	
7	0.48	
8	1.20	
9	2.40	
10	4.80	Subgrade
11	12.00	(silty clay)
12	36.00	
13	60.00	
14	84.00	
15	120.00	

The spatial loading pattern for the dynamic loads was the same as for the quasi-static solution (Fig. 19). The time history for each suspension type (Fig. 16), was applied simultaneously to each of the eight load locations.

The SAPSI program is capable of simulating the dynamic response of layered structures excited by loads on the surface. The layered structure is assumed to consist of a number of layers over a half space. Viscoelastic materials are assumed in both the layers and the half space. To simulate the half space, the program automatically generates 10 additional layers with thicknesses varying depending on the frequency of excitation. Table 6 lists the thicknesses of the sublayers used to simulate the pavement structure.

The program is capable of incorporating frequency-dependent material properties. Careful consideration of the properties was necessary in order that the speed effect of the moving trucks might also be included. The current design criteria, used to convert velocity of moving trucks into appropriate loading frequencies for determination of material properties, has been described previously. Such criteria assume that the response of a pavement, $R(t)$, can generally be given by:

$$R(t) = LA_1 e^{i(\omega_1)t} \qquad (4)$$

where

t = time,
L = constant load applied by the truck,
A_1 = function of pavement structure, and
ω_1 = constant (function of the pavement structure and velocity).

With the incorporation of dynamic loads, L is no longer a constant. Furthermore, the variation of the rate of loading affects frequency-dependent material properties. Therefore, the combined effect of truck speed and the variation of the rate of loading must be incorporated into the model. If L is a function of time, it can be assumed that:

$$L(t) = S + De^{i(\omega_2)t} \qquad (5)$$

where

S = static component of the load,
$De^{i(\omega_2)t}$ = dynamic component of the load, and
ω_2 = predominant frequency of the dynamic load.

Therefore, a dynamic analysis must consider a pavement response function, $R_D(t)$, such that:

$$R_D(t) = [S + De^{i(\omega_2)t}]A_2 e^{i(\omega_1)t} \qquad (6)$$

TABLE 5   FATIGUE LIFE CRITERIA FOR STATIC ANALYSIS

	Temperature, ^{o}C	
	25	11
Strain, ϵ_t in. per in. $\times 10^{-6}$	35.2	24.2
Predominant Frequency	V = 55 mph (5 Hz)	
S_{mix} psi $\times 10^6$	1.09	1.17
$N_F{}^1$	183×10^6	373×10^6

$$^1\log N_F = 15.947 - 3.291 \times \log\left(\frac{\epsilon_t}{10^{-6}}\right) - 0.854 \times \log\left(\frac{S_{mix}}{10^{-3}}\right)$$

TABLE 6   PAVEMENT SYSTEM FOR DYNAMIC ANALYSIS

Pavement Structure

Layer Number	Thickness (in.)	Material
1	6.00	
2	4.80	
3	2.40	Asphalt
4	1.20	Concrete
5	0.48	
6	0.12	
7	0.48	Subgrade
8	1.20	(silty clay)
9	2.40	
10	4.80	

10 additional layers simulate half space

or

$$R_D(t) = A_2 Se^{i(\omega_1)t} + A_2 De^{i[(\omega_1) + (\omega_2)]t}$$

where

A_2 = constant dependent of pavement structure.

Essentially, this indicates that the dynamic response to a moving truck can be given by the sum of the following two components:

$$A_2 Se^{i(\omega_1)t}$$

which represents the effect of the static component of the load and can be determined by current quasi-static analyses with material properties depending only on truck speed and pavement structures; and
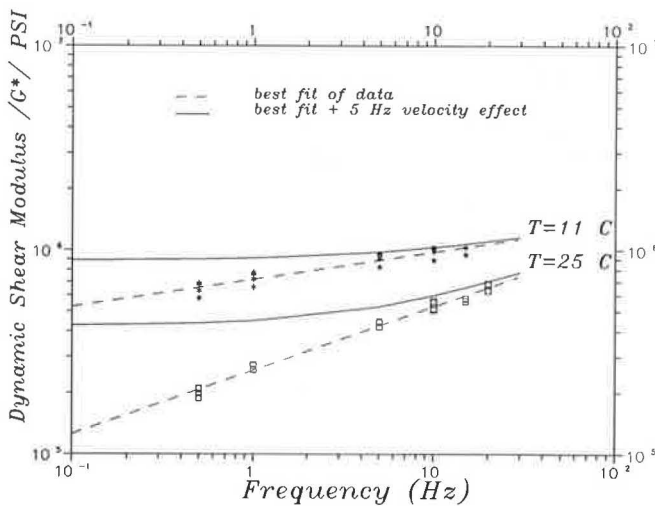
$$A_2 De^{i[(\omega_1) + (\omega_2)]t}$$

which represents the response of the pavement due to dynamic effects. The material properties used in this analysis should be determined at a frequency level $(\omega_L) = (\omega_1) + (\omega_2)$.

To determine the actual material properties of the pavement, taking into account the dynamic components of pavement response, a frequency shift $(\omega_1 = 5$ Hz$)$ is necessary to simulate the adopted truck speed of 55 mph. To accomplish this, material properties at each frequency level were replaced by those obtained at a frequency level 5 Hz higher (see Figures 20, 21, and 22). The resulting properties are summarized in Tables 7, 8, and 9. Material properties at intermediate frequencies can be interpolated within the program.

Time histories of the tensile strain obtained with these properties using SAPSI are plotted in Figures 23, 24, and 25. The general shape of each of these time histories is similar to that of the corresponding load (see Figure 16).

SAPSI is capable of determining the time variation of the strain, at any particular point, caused by a moving load (assuming no velocity effects as discussed earlier). The output of such calculations obtained with the four-leaf suspension traveling at 55 mph at the bottom of the asphalt concrete layer $(X = 0, Y = 2$ ft$)$ is shown in Figure 26. Note the difference

FIGURE 21 Variation of internal damping with frequency for an asphalt concrete mixture at 11°C and at 25°C; adopted properties simulate a 5-Hz velocity effect.
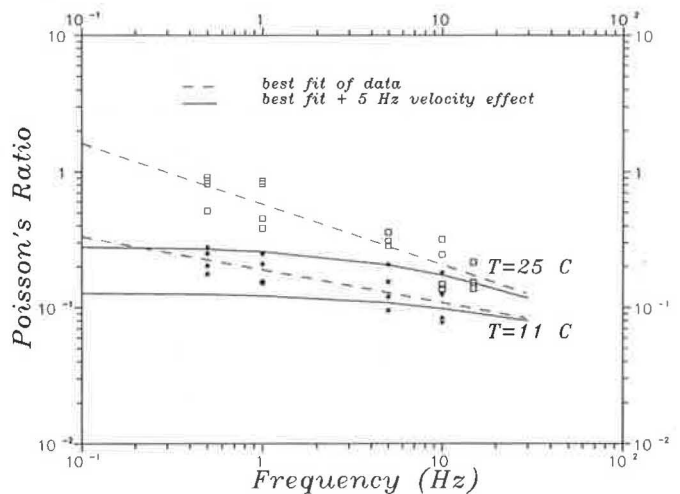
FIGURE 22 Variation of Poisson's ratio with frequency for an asphalt concrete mixture at 11°C and at 25°C; adopted properties simulate a 5-Hz velocity effect.

in the high of the two peaks due to the time variation of the loads. The first peak is caused by the passage of loads 1 and 2 (see Figure 19) and the second due to loads 3 and 4. Figure 27 shows, on a different time scale, the same graph superimposed on the time variation of the maximum tensile strain obtained with the four-leaf suspension (Fig. 24). The graph in Figure 17 is an enlargement of this plot in the time span 2 to 3 sec.

To determine the fatigue life of the pavement, assuming it is subjected to only one type of suspension loading, the Linear Summation of Cycle Ratios Cumulative Damage Hypothesis was used. The time history of the tensile strain caused by each type of suspension was digitized into 256 equal parts. For each part (i), the fatigue life (N_i) corresponding to that level of strain was computed using the fatigue criteria shown in Equa-

FIGURE 20 Variation of dynamic shear modulus with frequency for an asphalt concrete mixture at 11°C and 25°C; adopted properties simulate a 5-Hz velocity effect.

TABLE 7 MATERIAL PROPERTIES FOR ASPHALT CONCRETE CONSIDERING 5-Hz
FREQUENCY SHIFT TO SIMULATE TRUCK VELOCITY AT 11°C

Frequency (Hz)	Adjusted Frequency	Shear Moduli $\lvert G*\rvert$ (psi)	Internal Damping	Poisson's Ratio
0.1	(5.1)	892000	.056	0.127
0.5	(5.5)	901000	.053	0.125
1.0	(6.0)	911000	.048	0.122
5.0	(10.0)	976000	.024	0.108
10.0	(15.0)	1030000	.010	0.098
15.0	(20.0)	1071000	.004	0.091
30.0	(35.0)	1154000	.0003	0.080

TABLE 8 MATERIAL PROPERTIES FOR ASPHALT CONCRETE CONSIDERING 5-Hz
FREQUENCY SHIFT TO SIMULATE TRUCK VELOCITY AT 25°C

Frequency (Hz)	Adjusted Frequency	Shear Moduli $\lvert G*\rvert$ (psi)	Internal Damping	Poisson's Ratio
0.1	(5.1)	427000	.1761	0.278
0.5	(5.5)	437000	.1698	0.269
1.0	(6.0)	449000	.1623	0.258
5.0	(10.0)	527000	.1132	0.206
10.0	(15.0)	598000	.0721	0.172
15.0	(20.0)	654000	.0459	0.151
30.0	(35.0)	778000	.0118	0.117

TABLE 9 MATERIAL PROPERTIES OF SUBGRADE (SILTY CLAY)

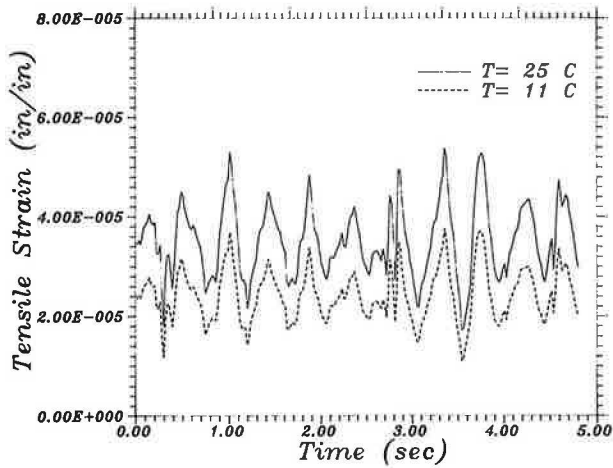| Frequency (Hz)	Shear Moduli $\lvert G*\rvert$ (psi)	Internal Damping	Poisson's Ratio
0.1	3,000	0.06	0.30
0.5	3,000	0.05	0.30
1.0	3,000	0.04	0.30
5.0	3,000	0.02	0.30
10.0	3,000	0.01	0.30
15.0	3,000	0.005	0.30
30.0	3,000	0.002	0.30

FIGURE 23 Time variation of tensile strain for torsion-bar suspension at 11°C and 25°C.

FIGURE 24 Time variation of tensile strain for four-leaf spring suspension at 11°C and 25°C.
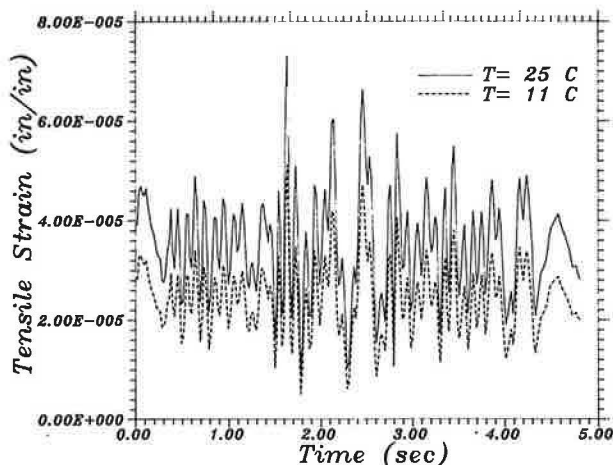
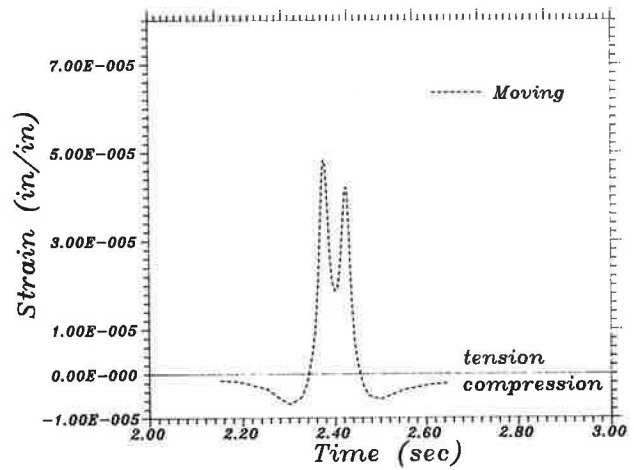**FIGURE 25** Time variation of tensile strain for walking-beam suspension at 11°C and 25°C.

FIGURE 26 Time variation of tensile strain for four-leaf spring suspension with tandem configuration of Figure 19 at 25°C.
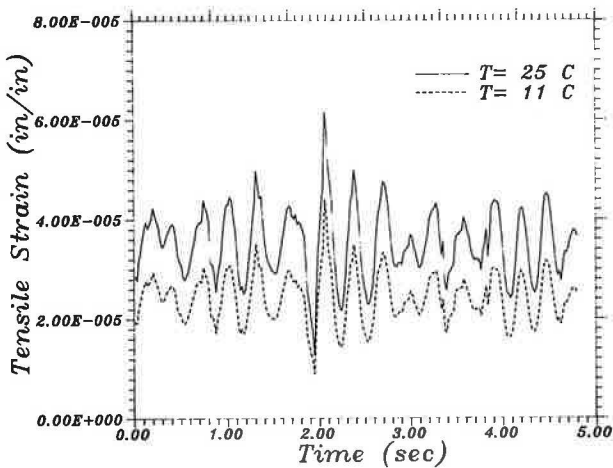
tion 3. The total number of load applications to failure for each suspension type was then calculated by:

$$1/N_F \text{ (suspension)} = \sum_{i=1}^{256} [1/(256 \cdot N_i)] \tag{7}$$

This analysis required consideration of the variation of the stiffness modulus of the mix with the predominant loading frequency of the suspension (see Figure 7) and the 5-Hz frequency shift. For the torsion bar, this value is 2 Hz; for the four-leaf, it is approximately 4 Hz; and for the walking beam, it is about 8 Hz. Tables 10 and 11 summarize the results.

The N_F values for each of the suspension types differ significantly from the values predicted by the quasi-static model. The lowest N_F value was obtained from the truck equipped with a walking-beam suspension ($N_F = 115E + 06$). If this value is compared with that predicted by the quasi-static model ($N_F = 183E + 06$), it can be inferred that the dynamic effects
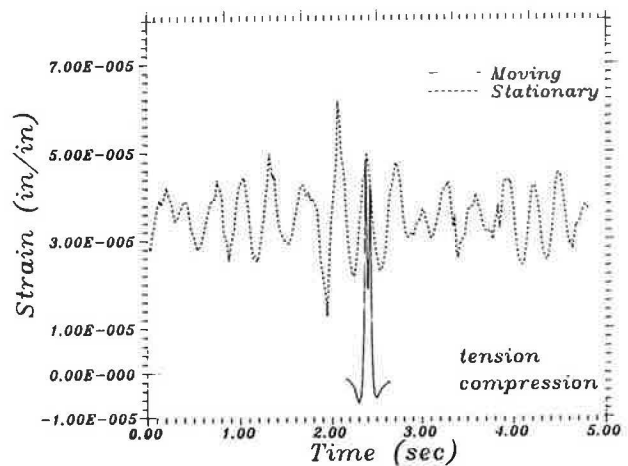

FIGURE 27 Time variation of tensile strain for four-leaf spring suspension with tandem configuration at 25°C superimposed on time variation of maximum tensile strain obtained with four-leaf suspension.

TABLE 10   ESTIMATED FATIGUE LIFE FOR THREE SUSPENSION TYPES AT 25°C

Temperature 25°C	Loading/Suspension Type			
	Q/Static	Torsion	Four Leaf	Walking
Strain (ϵ_t) (E-04)	.352	See Fig. 23	See Fig. 24	See Fig. 25
Predominant Frequency	V = 55 mph (5 Hz)	5 + 2 = 7 Hz	5 + 4 = 9 Hz	5 + 8 = 13 Hz
S_{mix} psi (E + 06)	1.087	1.171	1.240	1.353
N_F * (E + 06)	183	148	143	115
RPL Percent	0	19	22	37

TABLE 11   ESTIMATED FATIGUE LIFE FOR THREE SUSPENSION TYPES AT 11°C

Temperature 11°C	Loading/Suspension Type			
	Q/Static	Torsion	Four Leaf	Walking
Strain (ϵ_t) (E-04)	.242	See Fig. 23	See Fig. 24	See Fig. 25
Predominant Frequency	V = 55 mph (5 Hz)	5 + 2 = 7 Hz	5 + 4 = 9 Hz	5 + 8 = 13 Hz
S_{mix} psi (E + 06)	2.008	2.081	2.139	2.228
N_F * (E + 06)	373	306	304	252
RPL Percent	0	18	19	33

produced by walking-beam suspensions consume more than one-third of the expected pavement life.

The introduction of the RPL index facilitates the evaluation of the dynamic effects caused by different suspension types. An ideal suspension would have RPL = 0. Values for the torsion bar (RPL = 19) and for the four-leaf suspension (RPL = 22) at 25°C are quite close. This indicates that both suspension types produce similar levels of damage. However, the walking-beam suspension with an RPL of 37 is clearly the most damaging.

The RPL of a suspension depends on the roughness level of the pavement surface. The results obtained in this research are representative of a rough pavement surface; smaller RPL values may be expected for smoother pavements.

SUMMARY

A methodology has been developed to determine the effects of dynamic vehicle loads on pavements. It involves use of the SAPSI computer program, which can be used on an IBM-PC/AT. To estimate the influence of dynamic loads requires a knowledge of the load time history at a point in the pavement. If this is not available, it is possible to prepare an estimate provided the pavement profile and the dynamic response characteristics of representative trucks using the pavement are available.

In addition, a knowledge of the dynamic response of paving materials is required. For the SAPSI program, this requires a measure of the elastic and damping characteristics of the materials. For this investigation these properties were determined using the dynamic loading system described by Sousa and Monismith (9). The ability to control the values of three principal axes of stress or strain over a representative range of frequencies provides a valuable tool for determining material properties.

Results of the test program for the asphalt concrete illustrate the dependence of the stiffness and damping characteristics of the mixture on frequency, temperature, and mode of loading. Some nonlinearities are apparent in the response characteristics of this asphalt concrete. This is evidenced, for example, by changes in values for internal damping computed from the stiffness moduli $|E^*|$ and $|G^*|$. As the differences in damping determined in the axial and shear modes of loading increase, computed Poisson's ratios exceed 0.5, indicating some volume increase—most likely in the shear mode of loading.

This investigation also considered the effect of frequency, confining pressure, and strain level on the dynamic shear modulus and the internal damping characteristics of a silty clay. The data clearly indicate that frequency has no influence on the dynamic shear modulus of clay specimens (within the range tested). At the same time, frequency has a marked effect on the internal damping.

A representative pavement system consisting of an asphalt concrete layer resting directly on silty clay subgrade was analyzed by the SAPSI program to determine the pavement life that might result using actual load histories for three tandem-axle suspensions (on the same pavement traveling at the same speed) as compared to that obtained for the same axle with a uniform static load.

Results of the dynamic analysis suggest, at least for the load histories used herein, that pavement life is reduced when considering dynamic effects and that the magnitude of reduction is dependent on the tandem suspension. For this investigation, the largest reduction in pavement life was obtained for the axle with the walking-beam suspension. Comparable smaller reductions, as compared to the static case, were also obtained for the torsion-bar and four-leaf spring suspensions.

These determinations were based on load histories obtained from measurements of truck response on rough pavements. Less damage would result from operations on smoother pavements. Nevertheless, the study indicates that different damage will result from different suspension types for the same total static load. It would seem important to pursue this issue with further research since the RTAC study (14, 15) indicates similar findings. The trailer suspension producing the highest dynamic loading in the RTAC study was the walking beam, the same as obtained in this investigation.

The natural frequencies of the truck-suspension assembly play an important role on the amplitude of the dynamic components of the loads. As the predominant frequencies of the excitation caused by the pavement roughness approach the natural frequencies of the truck-suspension assembly, higher dynamic load components will occur.

ACKNOWLEDGMENTS

REFERENCES

1. P. F. Sweatman. *A Study of Dynamic Wheel Forces in Axle Group Suspensions of Heavy Vehicles.* Special Report No. 27. Australian Road Research Board, 1983, 56 pp.
2. C. E. Lee. Concepts of Weigh-in-Motion. Presented at National Weigh-in-Motion Conference, Denver, Colo., July 1983.
3. D. R. Leonard, J. W. Grainger, and R. Eyre. *Loads and Vibrations Caused by Eight Commercial Vehicles with Gross Weights Exceeding 30 Tons (32.5 Mg).* TRRL Report 582. Transportation and Road Research Laboratory, Great Britain, 1974.
4. A. T. Bergan and A. T. Papagianakis. Axle and Suspension Systems of Heavy Trucks for Minimizing Pavement Distress. *Proc., 4th Conference on Asphalt Pavements for Southern Africa,* Vol. 1, 1984, pp. 177–200.
5. T. D. Gillespie, et al. *Influence of Size and Weight Variables on the Stability and Control Properties of Heavy Trucks.* Report No. UMTRI-83-10/2. University of Michigan, Ann Arbor, 1983.
6. J. Cole and J. Huth. Stresses Produced in a Half Plane by Moving Loads. *Journal of Applied Mechanics,* December 1958, p. 433.
7. S. S. Chen. *The Response of Multilayered Systems to Dynamic Surface Loads.* Ph.D. dissertation. University of California, Berkeley, 1987.
8. H. G. Poulos and E. H. Davis. *Elastic Solutions for Soil and Rock Mechanics.* John Wiley and Sons, New York, 1973.
9. J. B. Sousa and C. L. Monismith. Dynamic Properties of Paving Materials. Presented at 66th Annual Meeting of the Transportation Research Board, Washington, D.C., 1987.
10. J. F. Hills and W. Heukelom. The Modulus and Poisson's Ratio of Asphalt Mixes. *Journal of the Institute of Petroleum,* Vol. 55, No. 541, 1969.
11. D. B. McLean. *Permanent Deformation Characteristics of Asphalt Concrete.* Ph.D. dissertation. University of California, 1974.
12. R. D. Barksdale. Compressive Stress Pulse Times in Flexible

Pavements for Use in Dynamic Testing. In *Highway Research Record 345,* HRB, National Research Council, Washington, D.C., 1971.

13. F. N. Finn, C. Saraf, R. Kulkarni, K. Nair, W. Smith, and A. Abdullah. The Use of Distress Prediction Subsystems for the Design of Pavement Structures. *Proc., 4th International Conference on the Structural Design of Asphalt Pavements.* University of Michigan, Ann Arbor, Vol. 1, 1977, pp. 3–38.

14. J. R. Pearson. *The Canadian Vehicle Weights and Dimensions Study—Research Program Overview.* Canroad Transportation Research Corporation, Ottawa, Canada, 1985.

15. *Vehicle Weights and Dimensions Study,* Vols. 8, 9 119. Roads and Transportation Association of Canada, Ottawa, Canada, 1986.

Incremental Design of Flexible Pavement

RAYMOND A. FORSYTH, JOSEPH B. HANNON, AND WILLIAM A. NOKES

Deficiencies and problems inherent in existing empirical and mechanistic design procedures have prompted an incremental design approach based primarily on the response of in-situ pavement to nondestructive tests. The first increment is designed with a structural section sufficient to preclude excessive subgrade deformation using conventional pavement design procedures. The second, if necessary, is placed in sufficient thickness to avoid excessive tensile strain of the asphalt concrete surfacing and, thus, premature fatigue cracking. A field evaluation was conducted on incremental sections with and without fabric reinforcement, and on control sections designed using the standard California (empirical) procedure. On the basis of laboratory tests characterizing all elements of the structural section, pavement designs for the site were developed using two empirical and one mechanistic-empirical procedure. These designs were compared to that designed by the incremental procedure. The results revealed that substantial savings in initial structural section costs are possible by incremental pavement design.

As defined by C. K. Kennedy, "Pavement design is essentially a structural engineering problem in which it is necessary to define the load conditions and to ensure that, for the range of environmental conditions to which the pavement is subjected, the materials can absorb the stresses and strains imposed without suffering unacceptable deterioration" (1). More specific to the semiarid environment representative of most of California, flexible pavement design has, as its primary objectives, avoidance of two conditions that will result in premature distress. As shown by Figure 1, one of these is permanent subgrade deformation, ultimately resulting in pavement rutting. The second is excessive tensile strain, which induces fatigue cracking within the design life of an asphalt concrete (AC) surfacing.

EMPIRICAL DESIGN

Empirical flexible pavement design procedures, including the California (R-value) and AASHTO methods, are primarily aimed at avoiding excessive subgrade deformation. All are based on standard soil strength tests, accelerated test track data, and/or long-term performance of in-service pavements.

California procedure is based, in part, on a triaxial-type soil strength test (R-value) and the results of the Brighton test track in California conducted in the early 1940s. In 1957, the traffic factor was modified so that the California procedure would conform to the results of the WASHO Road Test (2). As a result, structural section thickness increased an average of 3 in.

Office of Transportation Laboratory, Division of Construction, California Department of Transportation, 5900 Folsom Blvd., Sacramento, Calif. 95819
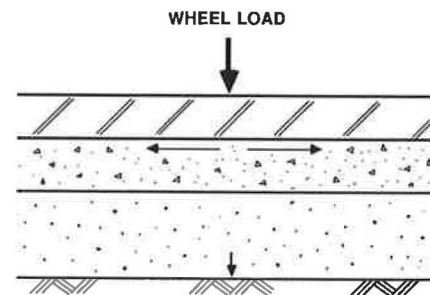
FIGURE 1 Subgrade deformation and AC tensile strain criteria used for flexible pavement design.

In 1959, the procedure was adjusted further based on the assumption of a greater degree of base, subbase, and subgrade saturation than was previously utilized (3). This modification resulted in a significant decrease in R-value, particularly on subgrade soils with a high silt content. In 1963, additional adjustments were implemented using the results of the AASHO Road Test (4). The R-value, and gravel equivalence for asphalt concrete, and the method of calculating the traffic factor for the design equation were all modified so that required pavement thickness was increased. As a result of these modifications, evidence of permanent subgrade deformation (rutting) is extremely rare in California, even on badly cracked asphalt concrete pavements.

In 1982, a further modification of the flexible pavement design policy in California was made to ensure rapid positive drainage of water entering the pavement surface. The Caltrans design manual was modified in 1987 (5), based upon the experience of the previous four years, to simplify the procedure. Except in areas of extremely low rainfall (<5 in./yr), or where a relatively permeable subgrade is available (≥100 ft/day), new structural section designs incorporate a drainage element with collectors and outlets. Rapid drainage is normally accomplished by an asphalt-treated permeable base with a permeability of ± 15,000 ft/day. Positive rapid drainage of the pavement structural section should extend pavement life significantly and/or permit reductions in pavement thickness, the extent of which has not, as yet, been determined. The quantification of the benefits of positive rapid pavement structural section drainage should be given a high priority in future flexible pavement research.

The empirical pavement design procedure utilized by California, in common with those used by other entities with which the writers are familiar, share the following deficiencies:

1. They are usually based on a worst-case subgrade strength
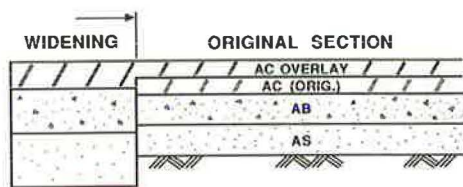
FIGURE 2 Overlay design for a thin structural section (AC = asphalt concrete, AB = aggregate base, and AS = aggregate subbase).

condition both in terms of material properties and degree of saturation.

2. They have been developed from accelerated test track data which do not adequately incorporate the critically important performance variable of asphalt concrete—resistance to fatigue cracking.

3. They do not allow for the effects of positive rapid pavement drainage.

4. They are based on a relatively limited range of traffic loading conditions.

The innate conservatism of California's present empirical design procedure has also been demonstrated repeatedly upon application of the overlay design procedure in connection with widenings. As shown by Figure 2, almost without exception, overlay design requirements of an existing relatively thin structural section, as determined by nondestructive tests (pavement deflection measurements), are such that the existing structural section, plus required overlay, is usually substantially thinner than that required by the conventional R-value design procedure. This phenomenon was graphically illustrated by an investigation in March 1980 by the Transportation Laboratory (6). That study required recommending a structural section design for a widened portion of Bottle Rock Road in Lake County and an overlay design for the existing pavement. In the past, that road had performed remarkably well in spite of its thin structural section (in some cases, as little as 0.1 ft of asphalt concrete over existing soil). On the basis of conventional design procedure, the following structural section was found to be necessary for the widened portion of Bottle Rock Road: 0.4 ft asphalt concrete, 0.5 ft aggregate base, and 1.15 ft aggregate subbase. On the basis of the results of the nondestructive test conducted on existing structural section, the design of the widened portion was modified to 0.35 ft of asphalt concrete over 0.5 ft of aggregate base. The use of nondestructive tests on the existing facility as the basis of the widening design resulted in a 43 percent savings in structural section construction costs.

MECHANISTIC DESIGN

In recent years there has been a concerted effort on the part of many in the pavement design community to move from empirical to mechanistic design, a system by which elements of the structural section are modeled by elastic-layer theory or by finite-element analysis. Design criteria require sufficient layer thickness to ensure that asphalt concrete tensile strain and subgrade deformation do not exceed tolerable limits.

Practical application of mechanistic procedures to routine pavement design presents real difficulties including the use of simplifying theoretical assumptions and material characterization procedures. Thus, it has been necessary to calibrate mechanistic designs with observed pavement behavior, utilizing "shift factors." Other problems associated with mechanistic design are appropriate characterization of typically stress-dependent and moisture-sensitive subgrade materials, extent and effects of seasonal changes in the moisture regime, and changing properties of the asphalt concrete due to aging.

For current use, and in the near future, mechanistic procedures show more promise in analysis than in routine design. Mechanistic procedures have already been used by Caltrans and others as an analytical tool to evaluate new materials, unique structural sections, and loading conditions.

Although mechanistic design has a much sounder basis in structural theory than does conventional empirical design, its reliance on uncertain pavement loading and materials properties data makes it, at best, a *mechanistic-empirical* procedure. Future research may eventually overcome the problems in the mechanistic approach, but this does not provide today's pavement design engineer with a cost-effective and efficient design tool for routine use.

INCREMENTAL DESIGN

Another approach to flexible pavement design which is currently being evaluated by Caltrans has been identified as "incremental design." This approach, not to be confused with stage construction, requires design of the pavement in two separate increments. The first addresses excessive subgrade deformation. It can be developed by the use of a mechanistic procedure or an empirical design based on a 3- to 5-year traffic loading.

The second increment is developed during construction on the basis of nondestructive tests conducted on the first increment. From the resulting data, an overlay of sufficient thickness to preclude premature fatigue cracking completes the pavement. The basis of the design of the second increment is the Caltrans Overlay Design Procedure, the development of which began in 1938 with the installation of permanent linear variable differential transformer gages in pavements throughout California. In 1955, critical levels of pavement deflection were determined for average traffic loading conditions, which, if exceeded, would result in premature fatigue cracking (7). An overlay design procedure based on these critical deflection levels was adopted in 1965 along with a means of varying critical levels for traffic conditions. The critical deflection–ESAL–thickness curves were adjusted slightly as a result of a 14-year study of 27 test pavements completed in 1978 (8).

In 1980, further follow-up studies (9) on 40 selected pavements designed by the overlay procedure indicated an average life of 11 years (see Figure 3). The overlay design procedure has stood the test of time and is deemed an appropriate and reasonable procedure to develop designs sufficient to preclude fatigue cracking of an asphalt concrete pavement under average conditions in California.

The basic rationale for incremental pavement design was aptly stated by C. R. Foster in his discussion of the AASHO
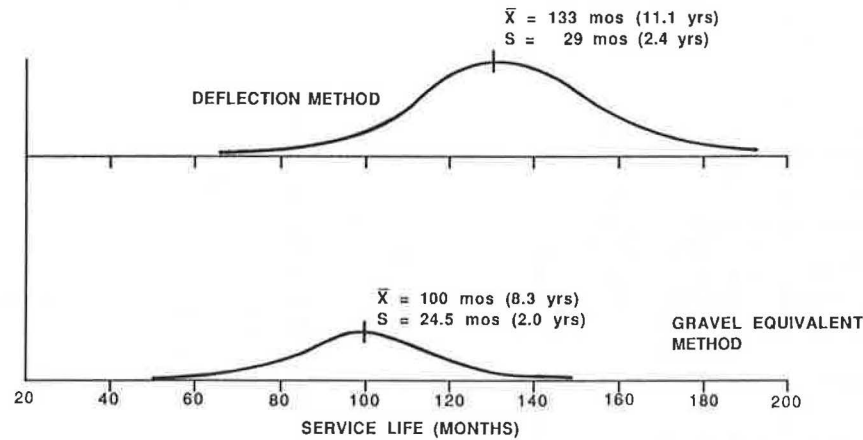
FIGURE 3 Service life of structural overlays.

Road Test at the 1962 International Conference on the Structural Design of Pavements (*10*):

> [P]erformance of a pavement under traffic is related only to the in-place strength of the materials in the pavement cross section. It is not related to the strengths predicted by a laboratory design test (although the laboratory test for predicting strength is a necessary part of any design system), it is not related to the as-constructed strengths; nor is it related to the strengths measured in loop 1 which received no traffic. Performance is related only to the in-place strengths in the section being trafficked.

Put another way, using proven nondestructive testing techniques, incremental design offers the possibility of utilizing the most cost-effective and efficient design tool available, the response of the prototype to load.

The potential economics in an incremental approach to flexible pavement design suggested by over 20 years of pavement deflection studies in California prompted the development of the field evaluation that is reported herein. An integral part of that evaluation also involves a comparison of the incremental-design section with designs developed for the same site by conventional empirical and mechanistic procedures.

Test Project Description

The first project selected for field evaluation of the incremental procedure is on a section of Route 99 between Sacramento and Marysville/Yuba City. This facility was recently widened to provide additional capacity and safety for significant increases in truck and automobile traffic. The previous alignment consisted of two-lane roadway traversing farmland that is subject to rice farming and irrigation. The existing basement soils in the area are silty clays and claying silts of low strength when saturated.

This project consisted of widening the existing roadway and constructing a separate two-lane southbound roadbed. The existing two-lane roadway now serves as the northbound lanes. The final grade is 3 to 4 ft above adjacent irrigated farmland.

Construction began during the spring of 1986. The limits of this contract were from 0.5 mile north of Route 5 to 0.8 mile north of Elverta Road, about 10 miles north of Sacramento.

Experiment Design

Because of the generally uniform, and relatively weak, subgrade conditions (*R*-value = 5) the site also provided an excellent opportunity to evaluate the use of high-strength geotextiles for subgrade enhancement.

The experimental and control structural sections were developed based on the California (*R*-value) design procedure and are shown in Figure 4. In addition to the incremental design, a high-strength woven fabric for subgrade enhancement was also included. The test section from Stations 175 to 180 is designed with an "effective" *R* value of 40 based on subgrade support provided by the fabric, as shown by recent research of the Transportation Laboratory (*11, 12*). A second test section from Station 180 to 185 is basically the incremental design underlain with the same fabric. The test sections between Stations 170 and 175 and between 195 and 200 are control sections designed on the basis of 5 *R*-value basement soil and a traffic index (TI) of 12.5 over a 20-year design period. The incremental sections are designed for the same basement soil conditions and a TI of 10.0 for a 5-year design period.

The conventional section for the remainder of the project was also designed for 20 years and was placed over imported material with minimum *R*-value of 15. The upper 1.0 ft of the imported material was treated with lime. The field experiment was extended from Station 200 to 210 to include a 1,000-ft test section (see Figure 4).

During the field-testing period, it was proposed that the constructability and performance of the various experimental test sections be evaluated by materials sampling and by the following tests:

1. Sampling basement soil, aggregate subbase (AS), aggregate base (AB), asphalt-treated permeable base (ATPB), and AC surfacing and performing applicable laboratory tests for grading, *R*-value, sand equivalent (SE), density, stability, and resilient modulus (M_r).
2. Obtaining samples of proposed geotextile fabric and testing for grab tensile strength and elongation.
3. Obtaining deflection measurements with the Dynaflect during construction, on the subgrade and on each subsequent layer of structural section.
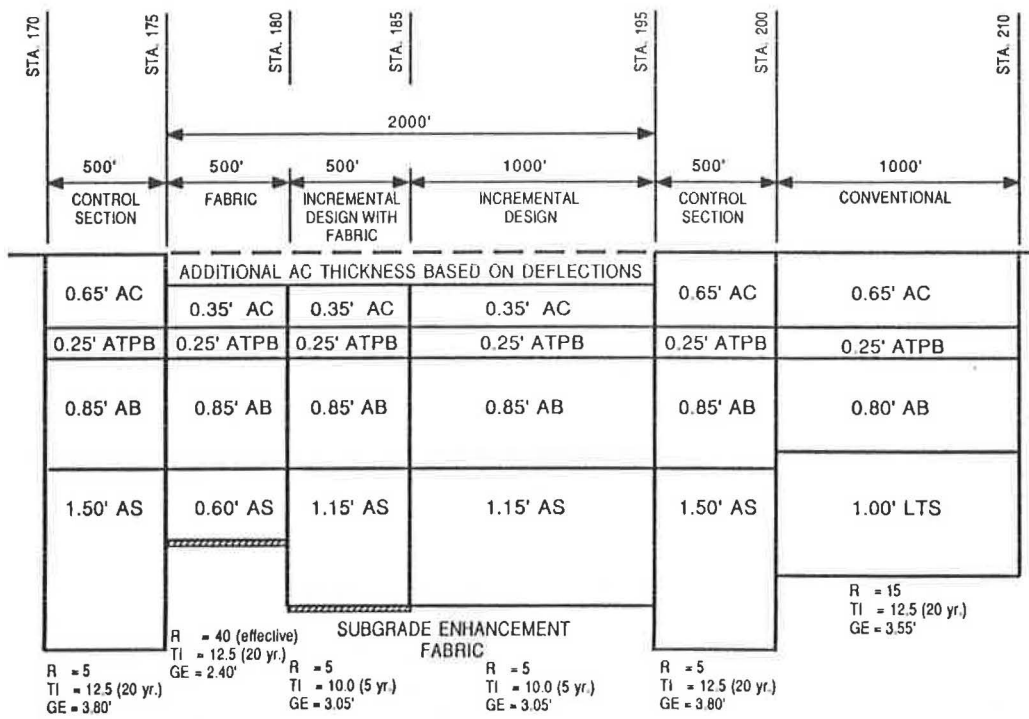
FIGURE 4 Experimental test section: 3-Sac-99-P.M.32.6/36.2.

4. Observing structural section construction progress and noting any difficulties or advantages of using subgrade enhancement fabrics.

5. Using deflection measurements on AC surface course to determine need for additional AC to satisfy structural requirements of the structural section for each of the proposed test sections.

Ultimately, the performance of the incremental sections would be evaluated in terms of what would have been required under test site subgrade and loading conditions using conventional empirical and mechanistic design procedures.

In the construction phase, contract contingency funds provided for an additional 0.15-ft AC thickness, if needed. In remote areas where significant amounts of aggregate processing are required, separate bid items may be needed for this procedure. Pavement deflection measurements on the incremental sections would determine if any additional AC thickness is required to satisfy the tolerable deflection requirements for the conventional 10- or 20-year design period. Figures 5 and 6 from California Test 356 provide the criteria for this procedure. Figure 5 presents the relationships between pavement thickness, loading, and deflection level at or below which premature fatigue cracking will be precluded. Figure 6 is utilized to determine the amount of additional material (AC) needed to reduce the measured deflection to a tolerable level.

Sampling and Testing

The initial field study was conducted by the Transportation Laboratory during construction in October 1986. The purpose of the field study was to evaluate the incremental procedure by comparing deflection measurements on all structural layers at several test sites. The field study consisted of (1) measuring surface deflections on the asphalt concrete pavement; (2) determining in-situ density and moisture content of the base, subbase, and basement soil; and (3) collecting samples of these materials for laboratory testing. Surface deflections were measured using the Dynaflect at 0.01-mile intervals on each layer of the structural section except the ATPB. Deflection measurements were obtained over all test sections shown in Figure 4.

After AC surface deflections were measured, one site was chosen in each test and control section to measure in-situ conditions and to collect material samples including "undisturbed" subgrade samples. Sampling sites were judged to be representative of each control and test section based on deflection measurements. All laboratory and field tests were performed following standardized test procedures (13, 14).

In-situ material density and moisture content were measured at each sampling site. Density of each layer was measured using a nuclear gage. AC density was measured by backscatter whereas direct transmission was used to determine density of base, subbase, and basement soil. Moisture content was determined by oven drying. Test data for each layer are shown in Table 1. Density shown for AC is the mean of five or more measurements at and near each sampling site.

Material samples were collected at all sites for classification and evaluation of material properties. Extensive laboratory testing of samples was performed to fully characterize the behavior of materials in each test section. In this way, differences in deflection measurements from one section to another could be evaluated in terms of material characteristics as well as structural section variations. Subgrade soils were classified by sieve and hydrometer analysis as well as plasticity index (PI). Typical subgrade material is classified as a sandy silty

TRAFFIC INDEX
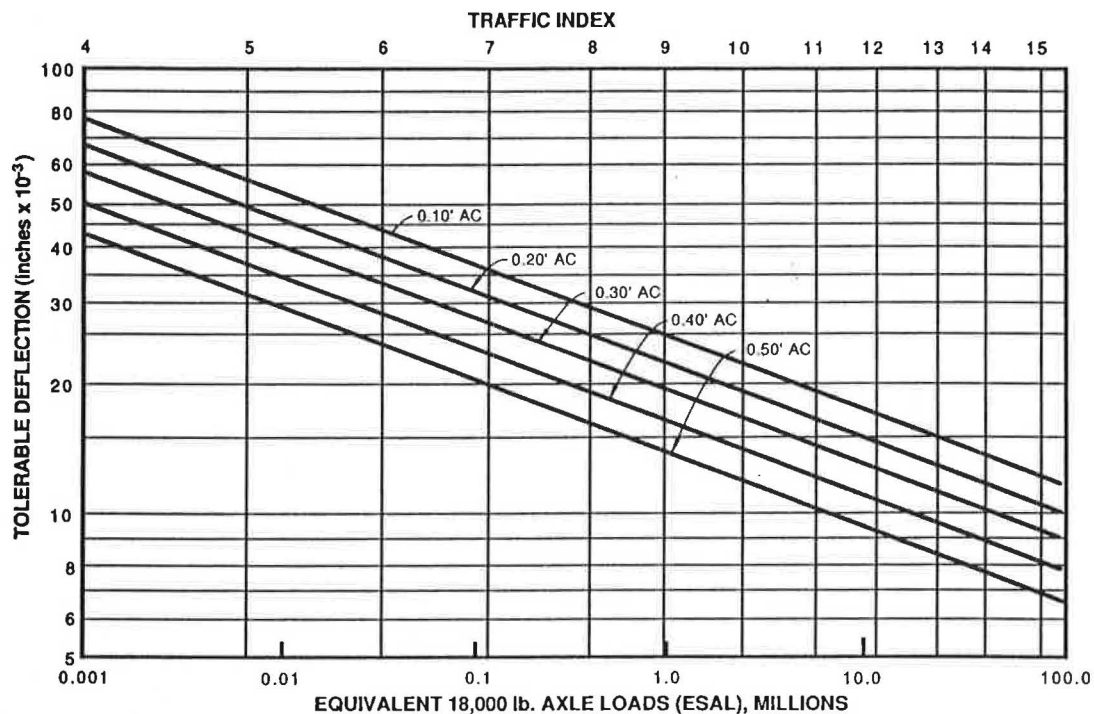
FIGURE 5 Relationships between pavement thickness, loading, and deflection level at or below which premature fatigue cracking will be precluded.

clay (CL, AASHO A-6) with low to medium plasticity, medium to high dry strength, firm and damp in place. An exception to this is the subgrade sample for Station 198, in the northern control test section. Subgrade soil at that site is a silty clay (AASHO A-7-6) characterized by higher compressibility and greater volume change than other samples. This classification is based on a PI of 23, liquid limit of 42, and more than 89 percent passing a No. 200 sieve. Higher-than-normal deflections, which were measured in the incremental and northern control sections during December 1986, are probably attributable to this more moisture-sensitive clay subgrade.

Grading analysis was performed on all base and subbase material samples. Base material samples conform to Class 2 aggregate described in Caltrans Standard Specifications (*15*). Subbase material grading met specifications for Class 2 aggregate subbase.

Basement soil properties were evaluated by triaxial compression and resilient modulus (M_r) tests. Triaxial tests were performed on at least one subgrade sample from each sampling site. Unconsolidated-undrained (UU) triaxial tests were used to determine in-situ shear strength of the subgrade soil. Subgrade cohesion was typically 14–18 psi, and the angle of internal friction varied from 16° to 24°. The strength properties of the subgrade soil at Station 198 exhibited lower strength compared to typical values at the other sampling sites. These differences correspond to the damper and more moisture-sensitive clay at the northern control section.

Resilient modulus testing was performed by the Transportation Laboratory on material from each structural layer. Subgrade cores measuring 4 in. by 8 in. were extracted from the southern control section (Station 172 + 50) and the subgrade enhancement test section (Station 177). Several base, sub-

base, and subgrade samples were also tested at the University of California, Berkeley (UCB), for interlaboratory comparison of test procedures, equipment, and results. M_r was determined according to AASHTO T274-82 (*14*). This test is usually performed on granular and cohesive soils. ATPB samples were also tested using the AASHTO procedure to determine M_r. Modulus of the AC was determined using the diametral test (*14*).

Results for base and subbase materials show moduli that are dependent on bulk stress (sum of principal stresses, θ) similar to research reported by Hicks (*16*). This dependence is represented by a log-linear relationship shown as $M_r = 6{,}000\ \theta^{0.5}$. Test results from UCB compared favorably with those determined at the Transportation Laboratory. Subgrade soil from the sampling sites did not exhibit typical deviator stress sensitivity as documented in the literature (*17–19*). On the basis of test results, a fixed resilient modulus of 20,000 psi was determined to be reasonable.

The subgrade M_r is much higher than the modulus used for design. The higher measured values probably reflect the lower subgrade moisture content during October, when samples were collected. Test results for the ATPB showed erratic M_r/bulk stress relationships similar to behavior described by Monismith and McLean (*20*). The variability of the ATPB moduli can be attributed to temperature sensitivity of the material. A fixed modulus of 120,000 was determined to be representative for the ATPB. On the basis of diametral modulus tests of pavement cores, a dynamic modulus of 250,000 is reasonable for the AC. The relatively low M_r for the AC is most likely attributable to the short interval between placement and compaction of the AC course and subsequent coring.
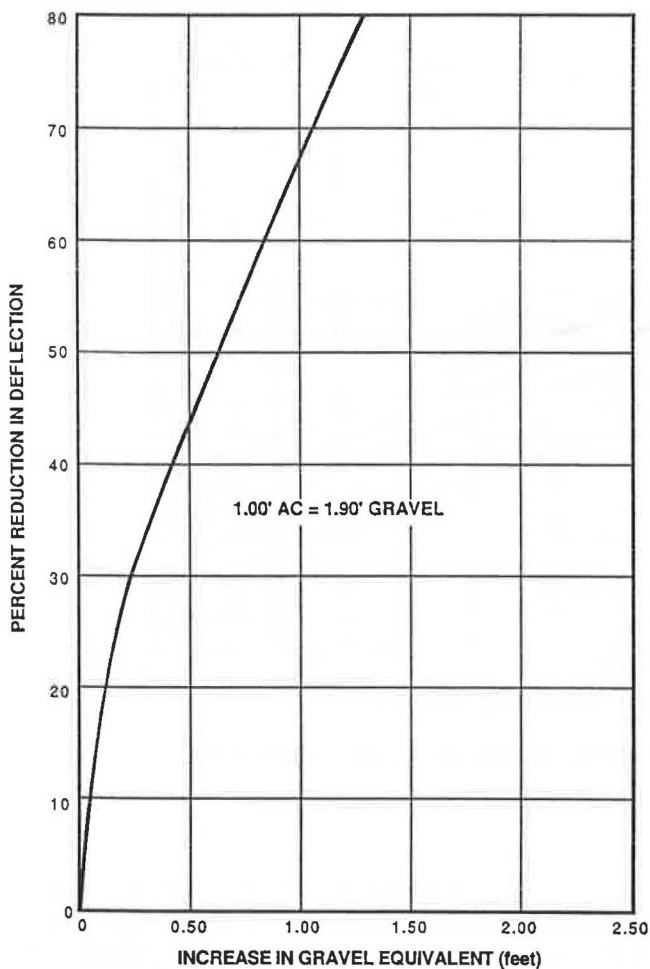
1.00' AC = 1.90' GRAVEL

FIGURE 6 Reduction in deflection resulting from pavement overlays.

AASHTO Procedure

Structural section layer thicknesses for the test project were determined using an AASHTOWARE Software Program DNP

s86/PC, v2.0 (© AASHTO 1986). The AASHTO design assumptions are shown in Table 2 (*21*). Results are shown for comparison in Table 3. An effective subgrade modulus of 6,000 psi was assumed to reflect seasonal variations in subgrade moisture at the site.

The resulting structural section thicknesses for the 10- and 20-year AASHTO design levels are considerably less than those required by the California *R*-value procedure and slightly thicker than the incremental design (see Figure 4). This is undoubtedly the result of the drainage coefficients recently adopted by AASHTO, which permit significant reduction in structural section thickness for positively drained pavement structural sections.

Mechanistic Procedure

Two methods were used to design structural sections for a 10-year and 20-year design life. The first is the Asphalt Institute procedure, which is a simplified user-friendly approach to design (*22*). Fatigue curves, granular material properties, and critical strains are implicit in this method (*23*). The other mechanistic procedure relies on the same fatigue curves as in the Asphalt Institute method. However, strains were predicted using a primary response model, PSAD, to determine layer thicknesses.

Both methods allow the engineer to determine layer thicknesses based on critical strains. The design thicknesses must satisfy two separate strain criteria, which are the horizontal tensile strain at the bottom of the AC pavement and the vertical compressive strain at the top of the subgrade. Both procedures require the number of equivalent 18-kip single-axle loads (ESALs) and material properties

The Asphalt Institute procedure requires three inputs: ESALs, subgrade resilient modulus, and types of base and surfacing. For the 3-Sac-99 project, structural elements of the design section are AC over untreated aggregate base (including subbase) supported by a weak subgrade. Design M_r for the subgrade was 4,000 psi, which is based on the relationship between M_r and *R*-value described in the Asphalt Institute Design Manual (*22*). This subgrade modulus is lower than the

TABLE 1 MATERIAL DENSITY AND MOISTURE CONTENT AT SAMPLING SITES

Structural Layer	Control Section Sta. 172+50	Fabric Section Sta. 177	Incremental & Fabric Section Sta. 182+50	Incremental Design Section Sta. 188	Control Section Sta. 198
Asphalt Concrete	2.19 gm/cc	2.26 gm/cc	2.16 gm/cc	2.25 gm/cc	2.29 gm/cc
Aggregate Base	2.21 gm/cc	2.21 gm/cc	2.19 gm/cc	2.21 gm/cc	2.27 gm/cc
	2.9%	3.6%	3.4%	2.9%	3.1%
Aggregate Base	2.31 gm/cc	2.23 gm/cc	2.25 gm/cc	2.22 gm/cc	2.24 gm/cc
	5.2%	4.8%	4.4%	3.5%	4.0%
Subgrade	2.05 gm/cc	1.97 gm/cc	2.05 gm/cc	1.95 gm/cc	1.97 gm/cc
	14.9%	14.4%	13.9%	14.3%	19%

TABLE 2   AASHTO DESIGN ASSUMPTIONS *(21)*

Structural Section Layer	Layer Coefficient (a_i)	Modulus (psi)	Drainage Coefficient (m_i)	Design Level/Traffic	
				10-Year TI = 11.5 *W_{18}=8x10^6$	20-Year TI = 12.5 $W_{18}=16x10^6$
AC	0.44	4.5×10^5	---	**SN=1.83	SN=2.06
ATPB	0.14	1.2×10^5	1.4	SN=0.59	SN=0.59
AB	0.13	---	1.1	SN=1.46	SN=1.46
AS	0.09	---	1.1	SN=1.67	SN=1.99
Basement Soil***	---	6×10^3	---	---	---
			Total (SN) =	5.55	6.10

Other Assumptions

Design Reliability = 95%

Overall Standard Deviation = 0.35

Terminal Serviceability Level = 2.5

 *W_{18} = ESAL's

 ** SN = Structural Number

*** M_{re} = Effective Modulus

value used in the AASHTO design because converting *R*-value to M_r in the Asphalt Institute method does not consider drainage and seasonal adjustments, which are included in the AASHTO procedure *(21)*. Table 3 shows designs using the Asphalt Institute method. Sections for both design periods require relatively thick AC layers over a relatively thin base, which is characteristic of the Asphalt Institute procedure *(23)*.

The designs from the Asphalt Institute method cannot be compared directly to the sections designed using the other procedures since this method does not consider an ATPB layer. To compensate for this, a primary response model was used that included a structural element of ATPB. Use of a primary response model also allowed direct computation of strains based on M_r values from laboratory materials tests. Primary response was determined using the PSAD model developed at the UCB. The model computes strains by iteration solving M_r/stress level using tested materials properties and the CHEV5L elastic-layer algorithms *(24)*. Critical strains were determined from the fatigue curves that are used implicitly in the Asphalt Institute method. A balanced design for each design life was determined by maximizing both strain criteria without exceeding the limits. Table 3 presents designs using this approach. The AC layers are noticeably thinner and the base layers are thicker than those resulting from the Asphalt Institute method. It is reasonable to conclude that an acceptable mechanistic design lies between the values shown in Table 3.

FIELD PERFORMANCE

Plots showing the results of Dynaflect deflection testing are presented in Figures 7 and 8. Figure 7 illustrates maximum deflections (Sensor No. 1) obtained at 50-ft intervals in the outer wheel track of lane 1 over individual layers of the structural section during construction. No deflection measurements were obtained directly on the ATPB. Figure 8 illustrates three sets of measurements obtained on the AC surfacing in the outer wheel track of the southbound number 2 lane (outer lane). All deflection measurements on the AC surfacing in Figures 7 and 8 have been adjusted for temperature by normalizing data to 70°F based on the Asphalt Institute procedure *(25)*.

The October 1986 deflections on the 0.35-ft AC surfacing were utilized as the initial decision tool to evaluate the incremental procedure during construction, i.e., to determine if the deflection levels were at or below the tolerable level. In order to determine tolerable deflections it was first necessary to convert Dynaflect deflections to equivalent Deflectometer deflections using Figure 9. The resulting adjusted mean $(\bar{x})$ and evaluated (80th percentile) deflections along with tolerable deflection levels are presented for each test section in Table 4. These data revealed deflection levels somewhat higher than the tolerable level, suggesting the need for an additional increment of AC to satisfy the 10-year design criteria. However, a decision was made to accept the design as constructed, without any additional AC placement, anticipating a further

TABLE 3 STRUCTURAL SECTION DESIGNS

10-Year Design Layer Thickness (feet)

	Incremental	Empirical		Mechanistic	
		R-value	AASHTO	A.I.	PSAD
Asphalt Concrete	0.35	0.60	0.35	1.15	0.58
Asphalt-Treated Permeable Base	0.25	0.25	0.25	---	0.25
Aggregate Base	0.85	0.85	0.85	1.5	2.08
Aggregate Subbase	1.15	1.25	1.41		
Total SN	5.27	6.71	5.55	6.80	6.67

20-Year Design Layer Thickness (feet)

	Empirical		Mechanistic	
	R-value	AASHTO	A.I.	PSAD
Asphalt Concrete	0.65	0.39	1.29	0.83
Asphalt-Treated Permeable Base	0.25	0.25	---	0.25
Aggregate Base	0.85	0.85	1.5	1.75
Aggregate Subbase	1.50	1.67		
Total SN	7.26	6.10	7.54	7.51

SN = Structural Number

reduction in deflection level due to age stiffening of the asphalt concrete, with provision for monitoring pavement performance by subsequent deflection surveys. Also, the final surface layer of 0.06-ft open graded AC would still be placed. The control sections would also receive an additional 0.30 ft of dense graded AC, plus 0.06 ft open graded AC, as scheduled, after the December 1986 deflection survey. The deflection levels of the various sections were found to be quite uniform at the time of the October 1986 survey. Results of surveys in December 1986 and June 1987 reflect additional densification due to traffic compaction, age stiffening of the AC, changes in subgrade moisture, and deflection attenuation of the control sections due to placement of additional AC.

The temperature-adjusted June 1987 deflections are all below the tolerable level (Table 5). Note that the incremental and control sections were designed using a 5-R-value basement soil. In actuality, samples taken from the subgrade at two locations produced R-value test results of 14 at Station 186 and 40 at Station 200. This probably indicates that the imported material was carried into the experimental area and was of higher quality than 15 R-value. This also suggests conservatism in the original R-value design. Future deflection measurements will provide a better overall evaluation of seasonal variations as the different sections reach equilibrium.

DISCUSSION OF RESULTS

The June 1987 deflection measurements were surprisingly low on all test sections, considering that they were made in the late spring on a relatively soft subgrade.

The basis for this comment is an earlier research study on this portion of Route 99 which was carried out between 1959 and 1969. The goal of that study was to establish the deflection attenuation properties of asphalt concrete, cement-treated base, and aggregate base (26). The original structural section consisted of 0.08-ft armor coat and 0.50-ft aggregate base over 0.75-ft aggregate subbase.

Three test sections were overlain with 0.05-ft open-graded asphalt concrete, 0.25-ft asphalt concrete, 0.25-ft asphalt concrete base and 0.50-ft aggregate base. The total gravel equivalence of the original structural section plus the overlay was 2.99 ft, which is close to 3.11 ft for the incremental sections. Spring deflection measurements over the completed roadway averaged 0.029 in. in contrast to 0.014 in. for the incremental sections.

Similarly, four test sections were overlain with 1.00-ft aggregate base, 0.25-ft asphalt concrete, and 0.05-ft open-graded asphalt concrete. These, plus the original structural section, were almost identical in gravel equivalence to the incremental

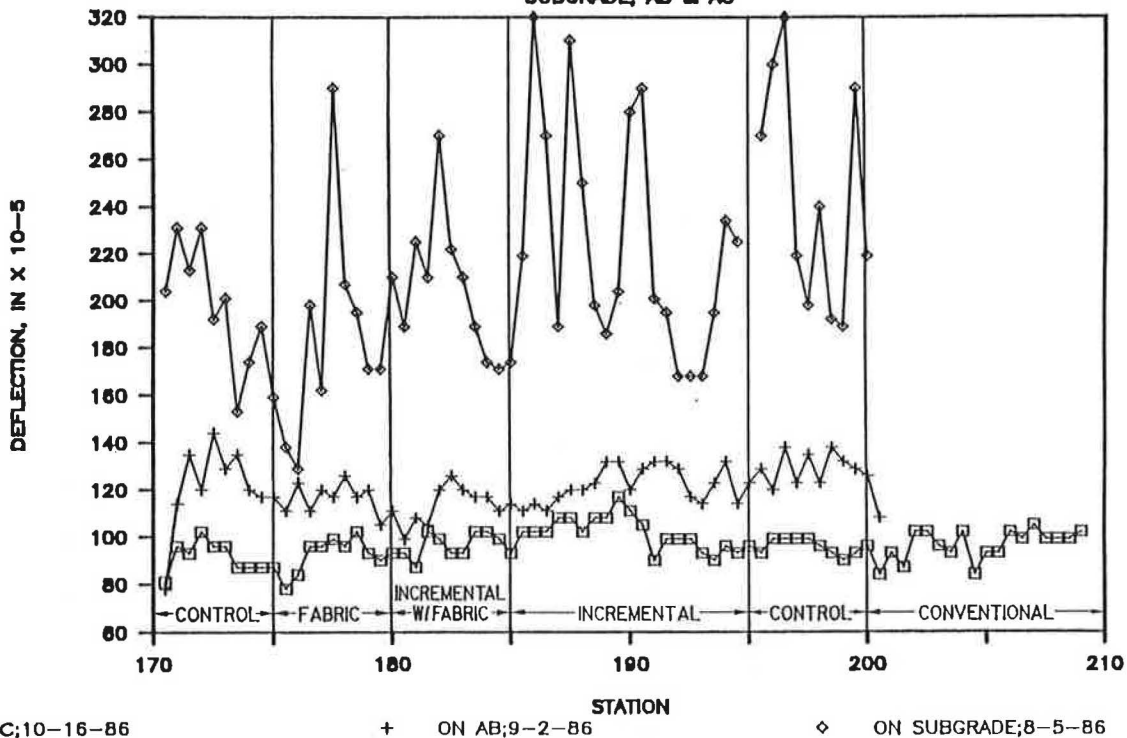## 3-SAC-99-32.6/36.2 #1 LANE
SUBGRADE, AB & AC

□ AC;10-16-86   + ON AB;9-2-86   ◇ ON SUBGRADE;8-5-86

FIGURE 7 Dynaflect deflections on subgrade, base, and AC.

3-SAC-99-32.6/36.2-#2 LANE
ON AC-ADJUSTED FOR TEMPERATURE
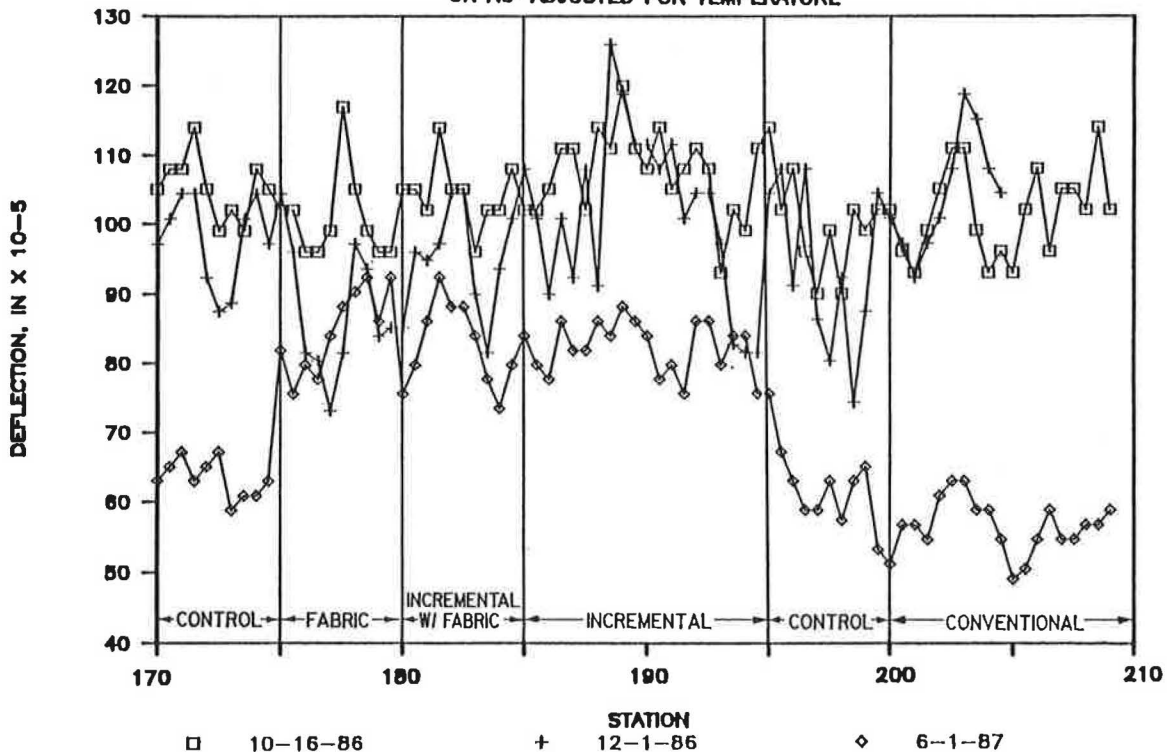

□   10-16-86   +   12-1-86   ◇   6-1-87

FIGURE 8 Dynaflect deflections on AC adjusted for temperature.
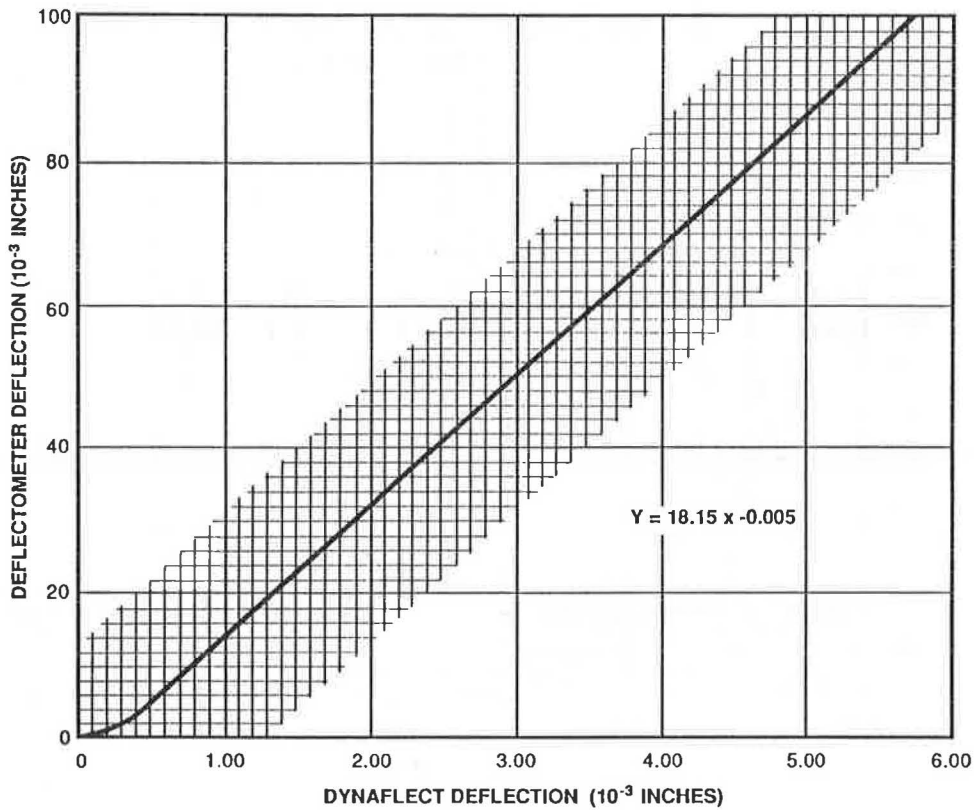
FIGURE 9 Comparison of Dynaflect and deflectometer deflections.

TABLE 4 DEFLECTION MEASUREMENTS TO EVALUATE INCREMENTAL DESIGN

| | Deflection Measurements (10^{-3} Inches) | | | | Tolerable Deflectometer** Deflection (10^{-3} Inches) Design Level/Traffic Index | | |
| | Dynaflect | | Equivalent Deflectometer | | | | |
Test Section	$\overline{x}$*	80%tile	$\overline{x}$	80%tile	5 yrs/10	10 yrs/11.5	20 yrs/12.5
Control Section	1.05	1.09	14	15	15	12	11
Subgrade Enhancement Fabric Section	1.01	1.07	13	14	"	"	"
Incremental Design with Subgrade Enhancement Fabric	1.04	1.08	14	15	"	"	"
Incremental Design	1.07	1.12	14	15	15	12	11
Control Section (Sta. 195 to 200)	1.01	1.08	13	15	"	"	"
Conventional Section with Lime-Treated Subgrade (LTS)	1.02	1.07	14	14	"	"	"

* $\overline{x}$ = mean deflection.

** Deflections tolerable for 0.35 foot of AC surfacing.

TABLE 5   MEAN AND TOLERABLE DEFLECTION MEASUREMENTS ON AC SURFACING

| | Mean Deflection Level (10^{-3} Inches)* | | | | | | Tolerable Deflectometer** Deflection (10^{-3} Inches) | | |
| | Dynaflect | | | Equivalent Deflectometer | | | Design Level/Traffic Index | | |
Test Section	10/16/86	12/1/86	6/1/87	10/16/86	12/1/86	6/1/87	5 yrs/10	10 yrs/11.5	20 yrs/12.5
Control Section (Sta. 170 to 175 0.65 foot AC)	1.05	0.98	0.62	14	13	6	10	9	8
Subgrade Enhancement Fabric Section (0.35 foot AC)	1.01	0.88	0.84	13	11	10	15	12	11
Incremental Design with Subgrade Enhancement Fabric (0.35 foot AC)	1.04	0.95	0.81	14	12	10	15	12	11
Incremental Design (0.35 foot AC)	1.07	1.02	0.81	14	14	10	15	12	11
Control Section (Sta. 195 to 200 0.65 foot AC)	1.01	0.94	0.64	13	12	7	10	9	8
Conventional Section with Lime-Treated Subgrade (LTS) (0.65 foot AC)	1.02	1.04	0.61	14	14	6	10	9	8

*   Corrected for temperature

**   Deflection tolerable for AC thickness shown in parentheses for each test section.

sections (3.07 ft). Spring deflection measurements over the completed roadway averaged 0.026 in., which is almost double those on the incremental sections. Because of the uniform nature of the subgrade and the fact that the area is subject to irrigation, one would not expect to find this degree of variation in the response of nearly equivalent structural sections.

The surprisingly low level of deflection on the incremental sections is very possibly the result of the positive rapid drainage feature common to all test sections, including the controls. Although, as would be expected, control section deflection levels were substantially lower than those of the incremental sections, the relatively high strength of all test sections masked the effect of lime stabilization or subgrade enhancement with geotextiles even though an earlier limited study (*11*) on the same subgrade revealed that the use of geotextiles was equivalent to 0.58 ft of aggregate base in terms of deflection attenuation. In retrospect, construction of equivalent but undrained test sections in the experiment would have proven extremely informative.

The decrease in deflection level on all sections between October and June represents the frequently observed effect of traffic compaction and age stiffening of the asphalt concrete pavement. All sections, however, exhibited deflection levels that would preclude premature fatigue cracking for average asphalt concrete pavements in California.

CONCLUSIONS

The results of laboratory and field measurements and tests on the six test sections on Route 03-Sac-99 justify the following conclusions:

1. For the assumed traffic, subgrade conditions, and pavement section material characteristics at the test site, the mechanistic-empirical and one empirical (California) procedure indicate the need for a thicker structural section than was found to be necessary using the incremental procedure.

2. The structural section indicated by the recently modified

AASHTO (empirical) procedure for the 10-year design was relatively consistent with that resulting from the incremental procedure. This is probably due to drainage coefficients, which apparently are reasonable for this site.

3. The deflection measurements on all test sections were uniformly low although they are consistent with structural section strength and thickness characteristics. This is attributed to the positive rapid drainage features used on all test sections.

4. The late spring deflection measurements reflected the normal effects of traffic compaction and age stiffening of the asphalt concrete surfacing. For the incremental sections, they confirmed that the second increment of asphalt concrete surfacing was not required to avoid premature fatigue cracking of the surfacing.

5. The incremental procedure can reduce thickness requirements by providing a way to quantify the effects of favorable subgrade materials variations and rapid positive drainage of the pavement structural section. At this particular site, a structural section cost savings of 18 percent for a 10-year design would have been realized with comparable fatigue performance of the AC surfacing.

ACKNOWLEDGMENT

REFERENCES

1. C. K. Kennedy. Analytical Flexible Pavement Design: A Critical State of the Art Review 1984. *Proc., Institution of Civil Engineers,* Vol. 78, Part 1, 1985, pp. 897–917.
2. G. B. Sherman. *Recent Changes in the California Design Method for Structural Sections of Flexible Pavement.* California Division of Highways, Materials and Research Department, Sacramento, 1958.
3. E. Zube, C. G. Gates, and D. R. Howe. *A Report on an Investigation Concerning the Effect of Lowering the Exudation Pressure Interpolation Point in the R-Value Test.* California Division of Highways, Materials and Research Department, Sacramento, 1959.
4. F. N. Hveem. *Thickness of Flexible Pavements by the California Formula Compared to AASHO Road Test Data.* California Division of Highways, Materials and Research Department, Sacramento, 1963.
5. Drainage of the Structural Section. *Highway Design Manual,* Topic 606. California Division of Transportation, 1987.
6. R. L. Moore. *Comparison of AC Pavement Structural Deficiencies Calculated Using Deflection Measurements and the R-Value Procedure.* Transportation Laboratory, California Department of Transportation, Sacramento, 1981.
7. F. N. Hveem. Pavement Deflections and Fatigue Failures. *Bulletin 114,* HRB, National Research Council, Washington, D.C., 1955.
8. D. V. Roberts, J. B. Skog, J. A. Matthews, W. Mann. *Statewide Flexible Pavement Performance and Deflection Study.* Report No. FHWA-CA-TL-78-28. Transportation Laboratory, California Department of Transportation, Sacramento, 1978.
9. W. Mann, J. A. Matthews, and J. T. Webster. *An Evaluation of the Current California Method to Determine AC Overlay Thickness.* Report No. FHWA-CA-TL-80-28. Transportation Laboratory, California Department of Transportation, Sacramento, 1980.
10. C. R. Foster. *Proc., 2nd International Conference on the Structural Design of Asphalt Pavements.* University of Michigan, Ann Arbor, 1962, p. 13.
11. R. L. Moore. *Evaluating the Use of Reinforcing Fabric to Support the Pavement Structural Section.* Memo Report 641139. Transportation Laboratory, California Department of Transportation, Sacramento, 1983.
12. R. L. Moore. *Geotextiles as Pavement Structural Section Elements.* Memo Report 643380. Transportation Laboratory, California Department of Transportation, Sacramento, 1985.
13. *Manual of Test,* 3rd Ed., Vols. I, II, and III. Transportation Laboratory, California Department of Transportation, Sacramento, 1978.
14. *Standard Specifications for Transportation Materials and Methods of Sampling and Testing,* Part II, 14th Ed. AASHTO, 1986.
15. *Standard Specifications.* California Department of Transportation, Sacramento, 1984.
16. R. G. Hicks. *Factors Influencing the Resilient Properties of Granular Materials.* Ph.D. dissertation. University of California, Berkeley, 1970.
17. R. D. Barksdale and R. G. Hicks. Material Characterization and Layered Theory for Use in Fatigue Analyses. In *Special Report 140.* HRB, National Research Council, Washington, D.C., 1973.
18. D. E. Newcomb. *A Review of Pavement Analysis Computer Programs—Interim Report No. 1.* University of Washington, Seattle, 1984.
19. R. G. Hicks. *Use of Layered Theory in the Design and Evaluation of Pavement Systems.* Alaska Department of Transportation and Public Facilities, Fairbanks, 1982.
20. C. L. Monismith and D. B. McLean. *Design Considerations for Asphalt Pavements.* Report No. TE 71-8. Institute of Transportation and Traffic Engineering, University of California, Berkeley, 1971.
21. *AASHTO Guide for Design of Pavement Structures.* American Association of State Highway and Transportation Officials, Washington, D.C., Chap. 2, 1986.
22. *Thickness Design—Asphalt Pavements for Highways and Streets.* Manual Series No. 1 (MS-1). The Asphalt Institute, College Park, Md., 1981.
23. *Research and Development of the Asphalt Institute's Thickness Design Manual (MS-1),* 9th Ed. Research Report No. 82-2 (RR-82-2). The Asphalt Institute, College Park, Md., 1982.
24. H. Warren and W. L. Dieckmann. *Numerical Computation of Stresses and Strains in a Multiple-Layer Asphalt Pavement System.* Chevron Research Corp., 1963.
25. *Asphalt Overlays for Highway and Street Rehabilitation.* Manual Series No. 17. The Asphalt Institute, 1983, p. 39, Fig. IV-2.
26. G. G. Sherman, C. G. Gates, M. M. Hatano, and D. L. Durr. *Deflection Studies Performed on El Centro Road (03-Sac-99) Ten-Year Report.* California Division of Highways, Materials and Research Department, 1970.

Stability of Multilayer Systems Under Repeated Loads

LUTFI RAAD, DIETER WEICHERT, AND WAJIH NAJM

Multilayer systems such as pavements and railroads are subjected to repeated traffic loads of varying magnitude and number of repetitions. The accumulation of plastic strains in a given system may increase under repeated load applications, leading to a state of incremental collapse, or plastic strain may cease to increase with time, resulting in a stable response or shakedown condition. An improved numerical method for the application of shakedown theory to multilayer systems is presented. The proposed method is used to analyze two-layer pavements with varying geometry and material properties. Fatigue and shakedown analyses are also performed for two-layer systems consisting of a cement-treated layer and an asphalt concrete layer overlying a subgrade. Results of analyses are compared and discussed in relation to the design of such systems.

Multilayer systems such as pavements and railroads are subjected to repeated traffic loads of varying magnitude and number of repetitions. A major form of distress is the accumulation of plastic or permanent deformations associated with long-term repeated loading effects. The accumulation of plastic strains in a given system may increase under an additional number of load repetitions thereby leading to a state of incremental collapse or may cease to increase with time resulting in a stable response or a shakedown condition, as illustrated in Figure 1.

The shakedown theory was first presented by Melan (1). According to this theory, a system will shake down under repeated cyclic loads if a self-equilibrated residual stress field could be found such that equilibrium conditions, boundary conditions, and yield conditions are pointwise satisfied. It is assumed in this case that the material is elastic–perfectly plastic with convex yield surface and applicable normality condition and that viscous and inertial effects are negligible. The theory has been applied to discrete structures and plates (2–5). Although attempts have been made to apply the theory to general continua using various numerical algorithms (6–9), these methods fall short of satisfying all constraints associated with the shakedown theory, specifically, equilibrium conditions, boundary conditions, and yield criteria by an arbitrary chosen residual stress field in the system under consideration.

In this paper an improved numerical method for the application of shakedown theory to multilayer systems is presented. The proposed method is used to analyze two-layer

L. Raad, Department of Civil Engineering, American University of Beirut, 850 Third Avenue, New York, N.Y. 10022. Current affiliation: Department of Civil Engineering, University of Alaska, 306 Tanana Dr., Fairbanks, Alaska 99775. D. Weichert, Institute of Mechanics, Ruhr University, Bochum, West Germany. W. Najm, American University of Beirut.
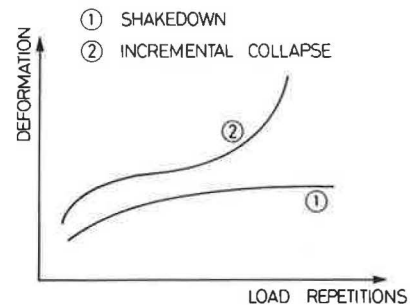

FIGURE 1 Shakedown and incremental collapse with load repetitions.

pavements with varying geometry and material properties. Fatigue and shakedown performance for typical cement-treated layers and asphalt concrete layers overlying a clay subgrade is discussed.

PROPOSED NUMERICAL FORMULATION

The proposed numerical approach involves analysis of the discrete elements of the system using the finite-element method. Rectangular elements with four external primary nodes are used in this case. The displacement functions are complete to the second degree and satisfy compatibility conditions. A quasi-static analysis is implemented whereby inertial and viscous effects are assumed negligible. If stress states σ_o, σ_s, and σ_a correspond respectively to body forces P_o, statically applied load f_s, and repeated loads f_a, then according to shakedown theory the system will not collapse provided a stress increment $\Delta\sigma$ can be found such that equilibrium conditions, boundary conditions, and yield conditions are satisfied. In this respect, the following terms could be defined for a two-dimensional plane stress or plane strain analysis:

$(\sigma_{ij})_o$ = stresses due to body forces P_o at the center of a given element,

$(\sigma_{ij})_s$ = stresses due to statically applied forces f_s at the center of a given element,

$(\sigma_{ij})_a$ = stresses due to repeated loads f_a at the center of a given element,

$\Delta\sigma_{ij}$ = arbitrary stress increment applied at the center of each element,

S_{xi}, S_{yi} = result of forces in the x and y directions at a nodal point due to $\Delta\sigma_{ij}$ with respect to a global set of coordinates x-y,

α = load multiplier associated with repeated loads f_a, and

f = yield function with yield occurring when $f \geq 0$.

In the analysis of a multilayer transportation support system, a Mohr-Coulomb failure criterion is proposed. The yield function (f) in this case will be given by

$$f = \sigma_1 - \sigma_3 \tan^2(45 + \phi/2) \tag{1}$$
$$- 2C \tan(45 + \phi/2)$$

where

σ_1, σ_3 = major and minor principal stresses, respectively (compressive stresses are positive, tensile stresses are negative),

C = cohesion,

ϕ = angle of friction.

Determination of the shakedown load reduces mathematically to a minimizing function (Q) subject to a series of constraints stated as follows:

$$\text{Minimize } Q = -\alpha + \sum_{i=1}^{NP} (S_{xi})^2 + \sum_{i=1}^{NP} (S_{yi})^2 \tag{2}$$

Subject to the following constraints:

$$\alpha > 0 \tag{3}$$

$$f[(\sigma_{ij})_o + (\sigma_{ij})_s + \alpha(\sigma_{ij})_a + \Delta\sigma_{ij}] \leq 0 \tag{4}$$

$$\sigma_3 \geq -2C \tan(45 - \phi/2) \tag{5}$$

where NP is the number of nodal points in the discretized system.

Minimizing Q, subject to the above constraints, would yield a maximum value of the load multiplier α which, when multiplied by f_a, would give the shakedown load for the system under consideration. It should be emphasized, however, that in this case, equilibrium conditions, boundary conditions, and yield criteria are satisfied in the "weak sense." This is a direct consequence of the numerical approach adopted.

Minimizing Q is based on a pattern search approach originally developed by Hooke and Jeeves (10). The minimization algorithm assumes a unimodal function. Therefore, if more than one minimum exists, several sets of starting solutions are recommended. However, in order to avoid this problem, the search is shifted to the vicinity of the region of interest by using a starting value of the load multiplier α_{st} such that the most critically stressed element in the system is on the verge of yielding. The search starts by determining Q for α_{st} and a set of $\Delta\sigma_{ij}$ that satisfy constraint conditions 4 and 5. During a given exploratory sequence, the α variable is allowed one disturbance in the direction of decreasing Q. Each of the stress variables is allowed as many disturbances, each equal to its step size and in the same direction, as long as the objective function Q decreases and the imposed constraints are satisfied. Otherwise, the exploratory sequence is rated a failure, and a new search is initiated about the last base point using smaller step sizes. The algorithm terminates when the values of the step sizes have been reduced to a certain preassigned value.
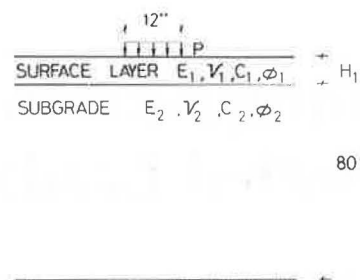
Where :

E_1 = Modulus of surface layer
E_2 = Modulus of subgrade layer
V_1 = Poisson's ratio of surface layer
V_2 = Poisson's ratio of subgrade
C_1 = Cohesion of surface layer
C_2 = Cohesion of subgrade layer
ϕ_1 = Angle of friction of surface layer
ϕ_2 = Angle of friction of subgrade layer
H_1 = Thickness of surface layer
P = Applied surface pressure

FIGURE 2 Representation of two-layer system consisting of a surface layer overlying a clay subgrade.

APPLICATIONS

The proposed numerical approach was applied to investigate the shakedown behavior of a two-layer system consisting of a surface layer overlying a clay subgrade (Fig. 2). The influence of layer stiffness, shear strength, and geometry on long-term stability under repeated loads was considered (Table 1). Fatigue and shakedown performance for cement-treated and asphalt concrete surface layers are compared in Table 2. Results of analyses are summarized below.

1. In the case where the surface layer overlies a soft subgrade, the shakedown load P_s increases with increasing surface layer modulus E_1 but decreases for higher values of E_1, as illustrated in Figure 3 (Cases 1A, 2A) and Figure 4 (Cases 5A, 6A). For lower values of E_1 the subgrade seems to be carrying a large proportion of the applied load. As E_1 increases, the subgrade will carry less, thereby resulting in a larger shakedown load. However, with further increase in E_1 the surface layer will carry most of the applied load in flexure, and the shakedown load will decrease for a given top-layer shear strength. For a stiff subgrade condition, no increase in P_s is observed with increasing E_1 for the range of values considered, which indicates that most of the load is carried through flexure of the surface layer as shown in Figure 3 (Cases 3A, 4A) and Figure 4 (Cases 7A, 8A).

2. The shakedown load increases with increase in surface layer thickness and shear strength, and subgrade stiffness and shear strength (Figs. 3 and 4).

3. Results of analyses indicate that shakedown of a system would still occur although a number of elements in the system exhibit plastic yield. In this case the plastic zone is "contained" and would not propagate further under repeated loads to induce incremental collapse. The influence of material properties on failure zones that develop when the shakedown load is applied is illustrated in Figure 5. The failure zone seems

TABLE 1 MATERIAL PROPERTIES USED IN TWO-LAYER SYSTEMS

		Surface Layer				Subgrade			
	E_1 (psi)	H_1 in	v_1	C_1 (psi)	ϕ_1	E_2 (psi)	v_2	C_2 (psi)	ϕ_2
Case 1A	0.5×10^6 1.0×10^6 1.5×10^6 3.0×10^6	9	0.25	100	35°	3000	0.47	3	0°
Case 2A	0.5×10^6 1.0×10^6 1.5×10^6 3.0×10^6	9	0.25	500	35°	3000	0.47	3	0°
Case 3A	0.5×10^6 1.0×10^6 1.5×10^6 3.0×10^6	9	0.25	100	35°	20000	0.47	20	0°
Case 4A	0.5×10^6 1.0×10^6 1.5×10^6 3.0×10^6	9	0.25	500	35°	20000	0.47	20	0°
Case 5A	0.5×10^6 1.0×10^6 1.5×10^6 3.0×10^6	15	0.25	100	35°	3000	0.47	3	0°
Case 6A	0.5×10^6 1.0×10^6 1.5×10^6 3.0×10^6	15	0.25	500	35°	3000	0.47	3	0°
Case 7A	0.5×10^6 1.0×10^6 1.5×10^6 3.0×10^6	15	0.25	100	35°	20000	0.47	20	0°
Case 8A	0.5×10^6 1.0×10^6 1.5×10^6 3.0×10^6	15	0.45	500	35°	20000	0.27	20	0°

to extend more into the subgrade with increasing cohesion of the top layer (Fig. 5a and b). This could be a result of increasing tensile strength of the top layer, resulting in a larger shakedown load and hence larger stresses in the subgrade layer. An increase in the number of failed elements is also obtained when the thickness of the top layer is reduced. In this case, a system with a 4-in.-thick top layer (Fig. 5c) would exhibit a much larger failure zone under applied shakedown load than a system with a 15-in.-thick top layer whose failure zone is similar to that shown in Figure 5a.

4. In a cement-treated surface layer (Cases 1B, 2B) or an asphalt concrete surface layer (Cases 3B, 4B), the variation

of shakedown load with layer thickness is shown in Figure 6. An increase in layer thickness and subgrade stiffness would yield a larger shakedown load. The variation represented in Figure 6 reflects similar trends for all the cases considered. Specifically, an inflection point appears in all such representations. This would probably indicate more subgrade contribution to the shakedown load for systems with smaller surface-layer thickness.

5. A comparison between fatigue and shakedown performance for a cement-treated layer overlying a soft subgrade (Case 1B) is shown in Figure 7. The variation of the load required to initiate cracking on the underside of the stabilized

TABLE 2   MATERIAL PROPERTIES FOR SYSTEMS WITH CEMENT-TREATED AND
ASPHALT CONCRETE LAYERS

	Surface Layer					Subgrade			
	E_1 (psi)	υ_1	H_1 (in)	C_1 (psi)	$\emptyset_1$	E_2 (psi)	υ_2	C_2 (psi)	$\emptyset_2$
Case 1B	1.5×10^6	0.25	4,6,9 15	200	$35°$	3000	0.47	3	$0°$
Case 2B	1.5×10^6	0.25	4,6,9 15	200	$35°$	20000	0.47	20	$0°$
Case 3B	1.5×10^6	0.25	4,6,9 15	500	$35°$	3000	0.47	3	$0°$
Case 4B	1.5×10^6	0.25	4,6,9 15	500	$35°$	20000	0.47	20	$0°$

layer with layer thickness for a given number of load repetitions is illustrated. Similar plots are shown for crack propagation to the surface of the cement-treated layer. The fatigue failure criterion used is presented elsewhere (*11*). Results indicate that for a given thickness of surface layer, crack initiation always occurs at a smaller load than the shakedown load. However, the load associated with fatigue crack prop-

agation to the surface of the cement-treated layer could be greater or smaller than the shakedown load depending essentially on the thickness of the surface layer, interface conditions, and number of load repetitions under consideration. A similar illustration of fatigue failure for an asphalt concrete layer overlying a soft subgrade (Case 3B) is shown in Figure 8. The variation of applied load with layer thickness for a
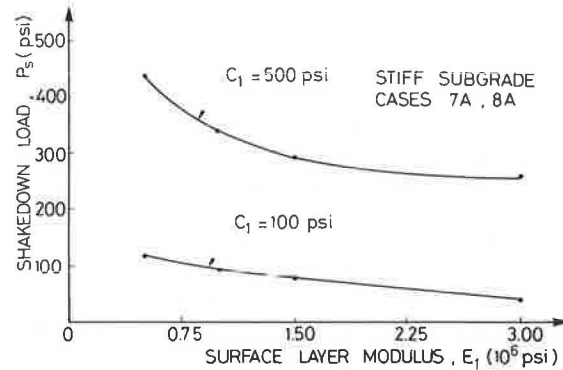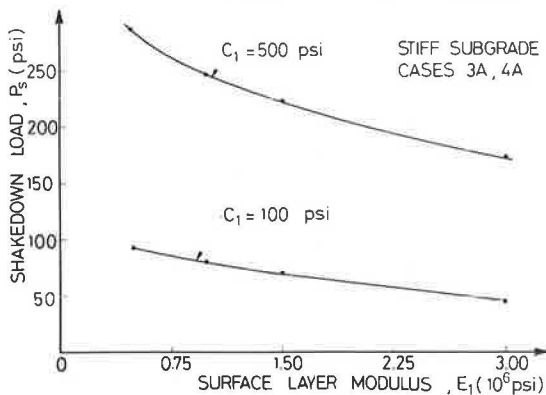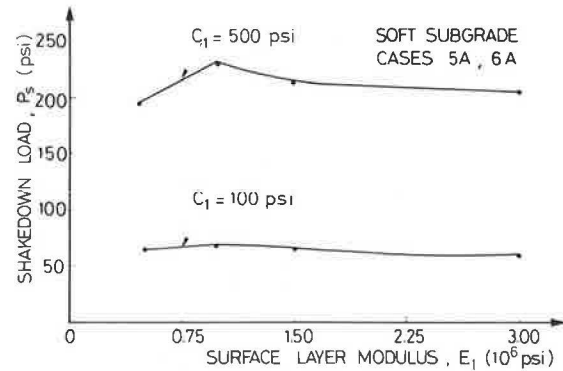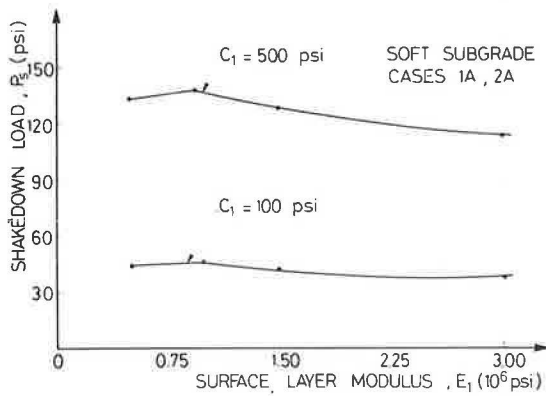

FIGURE 3   Influence of material properties on
shakedown load for a 9-in. surface layer.

FIGURE 4   Influence of material properties on
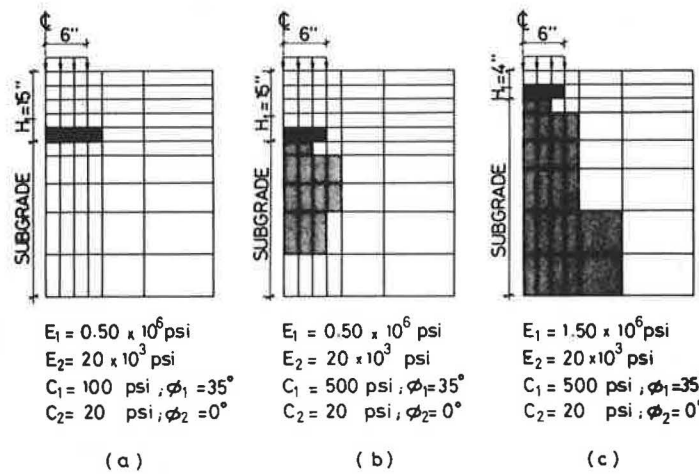shakedown load for a 15-in. surface layer.

FIGURE 5 Failure zones under applied shakedown loads (scale 1:10).

given number of load repetitions required to cause fatigue in the asphalt concrete is determined using a fatigue failure criterion proposed by Brown and Pell (12). In this case the load required to induce fatigue in the asphalt concrete could be smaller or greater than the shakedown load, depending on layer thickness and number of load repetitions. It should be emphasized that in the case of the cement-treated layer and the asphalt concrete layer, thickness design represented by points above the shakedown curve could result in accelerated distress modes of fatigue and accumulated plastic deformations, whereas for points below the shakedown curve the system is relatively stable and could adapt to a longer service life after maintenance measures are implemented following signs of fatigue failure.

SUMMARY AND CONCLUSIONS

An improved numerical method for the application of shakedown theory was proposed and applied in the analysis of two-layer systems. Results indicate that the shakedown load increases with increase in surface layer thickness and shear strength, and subgrade stiffness and shear strength. Shakedown and fatigue analyses were also conducted on two-layer systems consisting of a cement-treated layer and an asphalt concrete layer over a soft subgrade. Fatigue and shakedown behavior were compared, and results show that for a given thickness of stabilized layer the load associated with fatigue failure could be greater or smaller than the shakedown load, depending essentially on the number of load repetitions under consideration. It is concluded that design loads smaller than
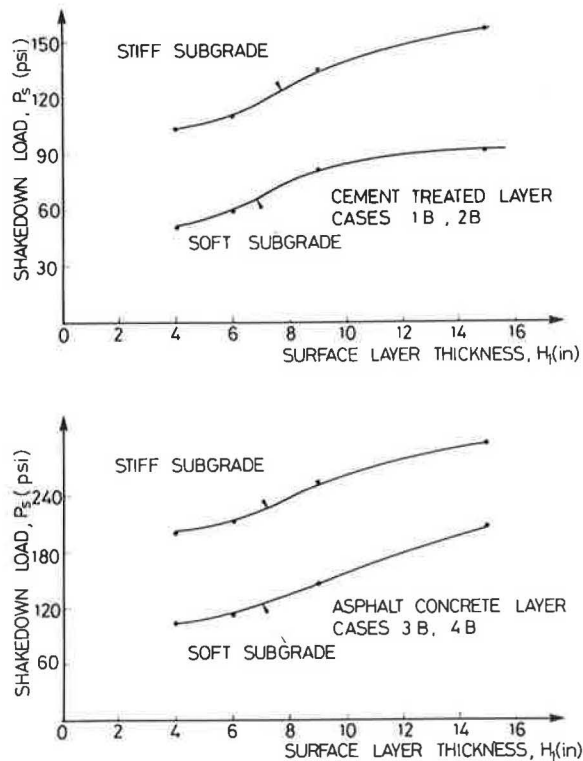

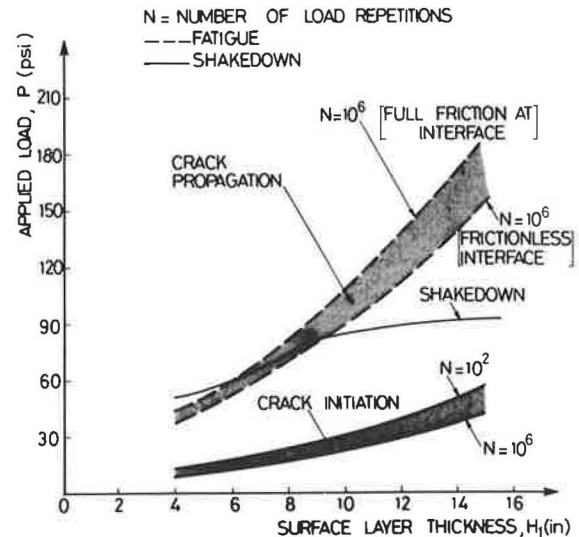FIGURE 6 Influence of surface layer thickness on shakedown load.

FIGURE 7 Fatigue and shakedown behavior for the cement-treated surface layer.
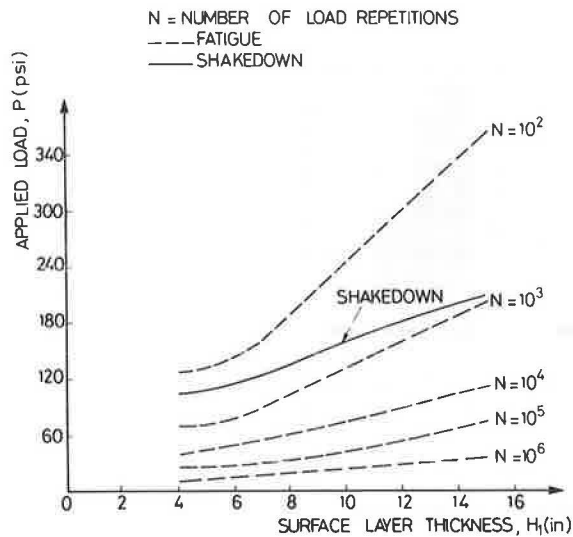
FIGURE 8   Fatigue and shakedown behavior for the asphalt concrete surface layer.

the shakedown load would result in a relatively stable response and a longer service life provided the system is periodically maintained following signs of fatigue in the surface layer.

Although the proposed numerical formulation is simple and yields a reasonable degree of convergence in the analysis of two-dimensional plane stress or plane strain multilayer systems, further research using higher order finite-element modeling and advanced optimization procedures is needed to improve shakedown predictions of pavement structures.

REFERENCES

1. E. Melan. *Theorie Statisch unbestimmter Systeme aus ideal-plastischen Baustoff.* Sitzungsberichte der Akademie der Wiissenschaften in Wien, Vol. IIa, 1936, pp. 145–195.

2. W. A. M. Alwis and P. Grundy. Shakedown of Plates under Moving Loads. *Proc., 7th Australian Conference on Mechanics of Structures and Materials.* 1980, pp. 191–196.
3. T. Belytschko. Plane Stress Shakedown Analysis by Finite Elements. *International Journal of Mechanical Sciences,* Vol. 14, 1972, pp. 619–625.
4. J. A. Konig. Shakedown Theory of Plates. *Archiwum Mechaniki Stosowanej,* Vol. 21, No. 5, 1969, pp. 623–637.
5. G. Maier and L. Corradi. Upper Bounds on Dynamic Deformations of Elastoplastic Continua. *Meccanica,* Vol. IX, March 1974, pp. 30–35.
6. B. L. Aboustit and D. V. Reddy. Finite Element Linear Programming Approach to Foundation Shakedown. *Proc., International Symposium on Soils Under Cyclic and Transient Loading.* Swansea, Wales, U.K., 1980, pp. 727–738.
7. G. N. Pande, W. S. Abdullah, and E. H. Davis. Shakedown of Elasto-Plastic Continua with Special Reference to Soil-Rock Structures. *Proc., International Symposium on Soils Under Cyclic and Transient Loading.* Swansea, Wales, U.K., 1980, pp. 739–746.
8. R. W. Sharp and J. R. Booker. Shakedown of Pavements Under Moving Surface Loads. *Journal of the Transportation Engineering Division, ASCE,* Vol. 110, No. TE1, 1984, pp. 1–14.
9. R. W. Sharp. Pavement Design Based on Shakedown Analysis. In *Transportation Research Record 1022,* TRB, National Research Council, Washington, D.C., 1985, pp. 99–107.
10. R. Hooke and T. A. Jeeves. Direct Search Solution of Numerical and Statistical Problems. *Journal of the Association for Computing Machinery,* Vol. 8, 1961, pp. 212–229.
11. L. Raad, C. L. Monismith, and J. K. Mitchell. Crack Propagation in Soil-Cement Bases Subjected to Repeated Wheel Loads. In *Transportation Research Record 690,* TRB, National Research Council, Washington, D.C., 1978, pp. 1–5.
12. S. F. Brown and P. S. Pell. A Fundamental Structural Design Procedure for Flexible Pavements. *Proc., 3rd International Conference on the Structural Design of Asphalt Pavements.* London, England, 1972, pp. 369–381.

Effects of Dynamic Loads on Flexible Pavements

T. Papagiannakis, R. C. G. Haas, J. H. F. Woodrooffe, and P. A. Leblanc

Dynamic axle loads were measured with an instrumented vehicle, and pavement performance was modeled using a modified version of VESYS-III-A. The experiment involved five levels of pavement roughness, three levels of vehicle speed, and two suspension types—air and rubber. A method was proposed for modeling the impact of the repetitive in-space dynamic loads experienced by AASHO Road Test sections. It consisted of dividing the load frequency distribution experienced by each section into segments and assigning segment combinations from the axles of a vehicle to pavement subsections. The method yielded a considerable improvement in performance prediction accuracy. Another part of the study examined the impact of suspension type on pavement performance by assuming that dynamic loads are random in space. The load frequency distributions obtained for the highest vehicle speed tested were used for this purpose. Comparisons were based on the area contained between the performance curve and a minimum PSI value. For the roughest section, the rubber suspension caused 17 to 22 percent more damage than the static load, depending on the terminal PSI value assumed. Similar values calculated for the air suspension ranged between 4 and 8 percent. Results were sensitive to the way the tire inflation pressure was handled in modeling dynamic load.

The AASHO Road Test was one of the earliest efforts to evaluate the impact of axle loads on pavement performance (1). Special studies conducted during the Road Test provided measurements of dynamic axle loads for a variety of vehicle speeds, suspension types, and levels of pavement roughness (2). A tire pressure transducer was used for the dynamic load measurements, and it was calibrated using a Weigh-in-Motion (WIM) scale. The general trend observed was that higher levels of pavement roughness and/or vehicle speed result in an increase in the dynamic load variation. There were no further efforts, however, to account for the effect of the dynamic axle loads on pavement performance.

Whittemore et al. (3) presented an NCHRP-sponsored study dealing with a variety of experimental and analytical methods for determining dynamic axle loads on pavements. The study evaluated three different methods for measuring dynamic axle loads: a tire pressure transducer, a combination of strain gauges and accelerometers on the axles, and a wheel-force transducer mounted on the hub of one of the tires. The latter was developed by General Motors for the study. It was concluded that

the tire inflation pressure is not in phase with the dynamic load, and therefore the tire inflation pressure transducer was considered unsuitable for dynamic load measurements. The other two systems yielded comparable results in measuring dynamic loads. Efforts to model dynamic axle loads were limited to an analog model of a quarter-car which yielded estimates of dynamic load within 15 percent of the measured values.

Recently, there has been a renewed interest in the area of dynamic axle loads and their impact on pavements. Sweatman (4), Woodrooffe et al. (5), and Woodrooffe and Leblanc (6) examined the vehicle parameters affecting dynamic axle loads. Sweatman used the General Motors wheel-force transducer, whereas Woodrooffe and co-workers used a combination of strain gauges and accelerometers. Both studies considered factors such as axle configuration, suspension type, tire pressure, vehicle speed, and pavement roughness. The primary objective of those studies was to optimize vehicle design rather than to evaluate the pavement damage aspect of dynamic axle loading. Those studies established that pavement roughness can induce substantial variations in axle load. They also showed that the suspension type significantly affects the magnitude of dynamic axle load variation. Furthermore, they found that vehicle speed causes an increase in the magnitude of dynamic load variation for all suspension types tested.

Gorge (7) and Addis et al. (8) examined the relationship between dynamic axle load and pavement response parameters. Gorge used a number of different methods for measuring dynamic loads, such as an accelerometer arrangement, a combination of strain gauges and accelerometers, and a wheel-force transducer. Addis et al. used an optical tire deflection device calibrated to yield tire load from tire deflection. In both studies, strain gauges embedded in the pavement layers were used to measure pavement response. Although these efforts established a good relationship between dynamic load and pavement response parameters, they stopped short of relating dynamic load to pavement performance.

A joint study has been undertaken by the University of Waterloo and the National Research Council of Canada to fill this gap. The objective was to examine the impact of roughness-induced dynamic axle load on pavement performance. Dynamic axle loads were measured using the instrumented vehicle developed by the Research Council in the context of the Roads and Transportation Association of Canada (RTAC) Vehicle Weights and Dimensions Study (5, 6). Pavement performance was modeled using a modified version of VESYS-III-A (9). Predictions of pavement performance were compared to observations from a number of AASHO Road Test sections. The basic hypothesis tested was that proper

T. Papagiannakis, College of Engineering, Memorial University of Newfoundland, St. John's, A1B 3X5, Canada. R. C. G. Haas, Department of Civil Engineering, University of Waterloo, Waterloo, Ontario N2L 3G1, Canada. J. H. F. Woodrooffe and P. A. Leblanc, Vehicle Dynamics Laboratory, National Research Council of Canada, Ottawa, Ontario K1A 0R6, Canada.

consideration of dynamic axle loads improves the accuracy of pavement performance predictions.

This paper reports on some of the findings of the study documented by Papagiannakis (10). Three major parts of the study are presented. The first describes the experimental program and summarizes its findings. The second deals with the methodology followed for simulating the performance of the AASHO Road Test sections. The third studies the impact of suspension type on pavement performance.

EXPERIMENTAL PROGRAM

The dynamic load testing was conducted in two phases. First, exploratory tests were carried out in May 1986 as part of the RTAC Vehicle Weights and Dimensions Study. The emphasis in this phase of the testing was on the dynamic behavior of a leaf spring suspension, which was the type of suspension used in the AASHO Road Test. Second, an experiment was conducted in June 1987 to explore the dynamic properties of the two suspension types that were shown to exhibit extreme dynamic behavior—an air and a rubber suspension (5, 6). The following sections briefly describe the two experimental phases of the study and present some of the findings.

Experimental Phase One, May 1986

The vehicle runs for the RTAC Vehicle Weights and Dimensions Study were conducted on three pavement sections in Ottawa, Ontario. Two local streets and a freeway section were selected, representing a range of pavement roughnesses. Pavement roughness was measured on all three sections with a Mays Ride Meter (MRM) expressed in in./mi. In addition, roughness profile data were obtained for the two local streets using the rod-and-level technique. Elevation was measured in both wheelpaths at 0.5-m intervals. The profile data were intended for calculating slope variance (SV), which was the roughness statistic used in the AASHO Road Test.

Study of the dynamic load waveforms of the leaf spring suspension revealed two important findings. First, the load

waveforms of the lead and the trailing axles of a tandem assembly are approximately in phase and have roughly equal amplitudes as shown in Figure 1. As a result, load sharing between tandem axles is not important in evaluating their impact on pavements, and therefore the sum of the load of a pair of tandem axles can be treated as a single load. Second, the predominant oscillation frequency is on the order of 3 Hz and remains constant with changes in pavement roughness and/or vehicle speed as shown in Figures 2 and 3. These observations are important in modeling the spatial arrangement of dynamic load waveforms for pavement roughness levels increasing over time.

A number of problems were experienced during the first phase of the experiment. First, the calculated variance in the measured pavement elevation slope was not comparable to the SV calculated from the CHLOE Profilometer. This is probably because the actual dynamics of the device were not taken into account. Indeed, estimates of SV made from measured profiles were not equivalent to the outputs of the old instruments (11). The problem was resolved by using the dynamic load data obtained in the special AASHO Road Test study mentioned earlier. A regression equation was fitted to the coefficient of variation of the dynamic load for a vehicle speed of 48 kph (CV) and the pavement roughness (SV) as shown by Equation 1. The general form of the relationship proposed by Sweatman (4) was used for this purpose.

$$CV = 3.974 \ SV^{0.5} \tag{1}$$

Another problem was realized in relating the load waveform to locations along the length of the pavement. To alleviate this problem, an axle detector was developed for the second phase of the experiment. Finally, it was decided to abandon the rod-and-level technique for profile measurements in favor of a profilometric roughness device. For this purpose, a Surface Dynamics Profilometer was used (12).

Experimental Phase Two, June 1987

The second phase of the experiment involved five levels of pavement roughness and three levels of vehicle speed. Five
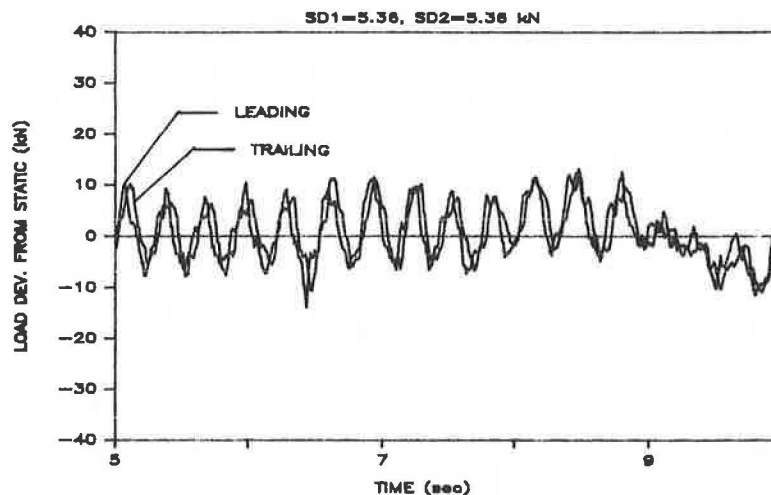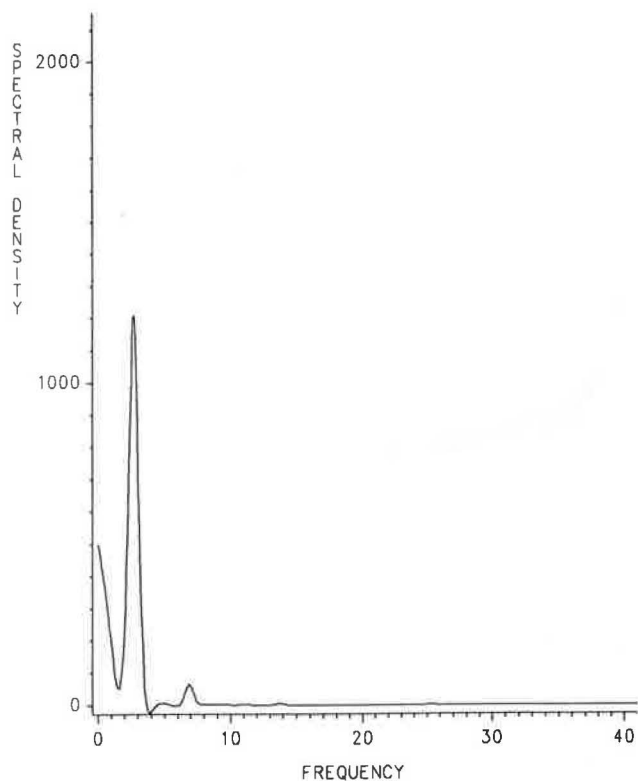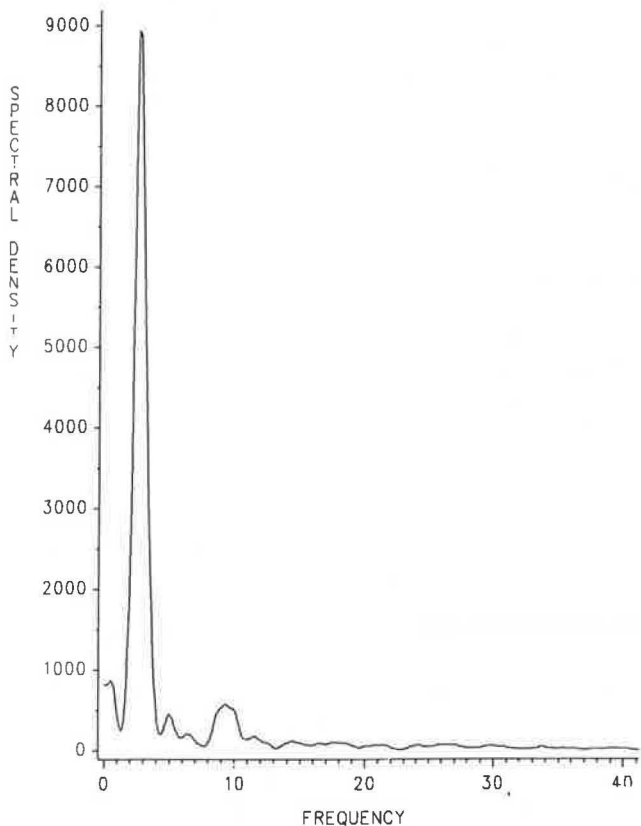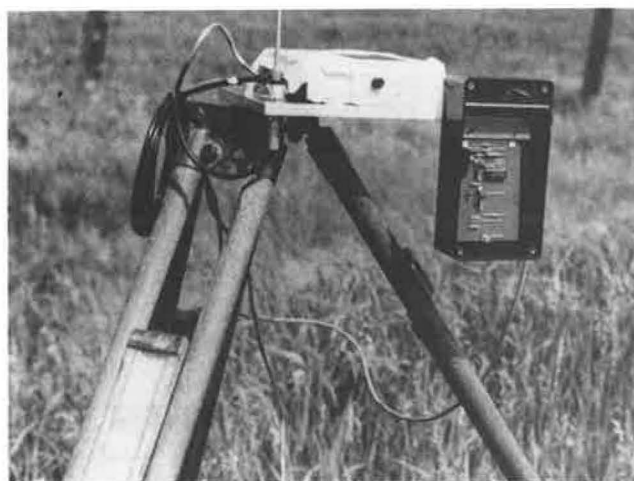

FIGURE 1　Dynamic load waveform of a leaf spring suspension, $V = 40$ kph, $R = 73$ in./mi.

FIGURE 2 Spectral density of the leaf spring suspension, V = 80 kph, R = 73 in./mi.

FIGURE 4 Axle detector and transmitter assembly.

pavement sections were selected in the vicinity of Ottawa, Ontario, representing a wide range of pavement roughnesses. A laser-based axle detector coupled with a transmitter-receiver assembly was built (Fig. 4). Its function was to transmit signals to the instrumented vehicle every time the laser beam was interrupted by an axle. A typical output of this device is shown in Figure 5. The laser beam was set across the road at the beginning of each section, and a fifth wheel on the vehicle provided exact distance measurements. In addition to the 15 runs mentioned above, a number of replicate runs were conducted to study the spatial arrangement of successive dynamic load waveforms.

The results of the second phase of the experiment are summarized in Table 1 in the form of the standard deviation (SD) of the dynamic load generated by each suspension type. The profile data were used to produce simulated MRM indices at 50-m intervals according to the procedure described by McQuirt et al. (*13*). For each section, the MRM indices were averaged to produce a representative value which is shown in Table 1. The observed range in SD was between 8 and 42 kN depending on suspension type, pavement roughness, and vehicle speed. Curves were fitted to the experimental data obtained for the air and the rubber suspensions (Equations 2 and 3, respectively).

$$SD = 0.087V^{0.398} R^{0.725}, (r^2 = 0.797) \qquad (2)$$

$$SD = 0.005V^{1.265} R^{0.671}, (r^2 = 0.903) \qquad (3)$$

The dynamic behavior of the two suspensions is quite different, mainly their response to vehicle speed, as indicated by the magnitudes of the exponents of speed in equations 2 and 3. The effect of vehicle speed is further demonstrated by plotting SD vs. speed for the roughest section, as shown in Figure 6. For vehicle speeds higher than 40 kph, the rubber suspension yields significantly higher load variation than the air suspension.

The replicate runs revealed an important finding. Dynamic load waveforms from replicate runs are repeatable in space as shown in Figure 7. A similar observation was made by Addis et al. (*8*). Although this loading condition is clearly not the case for pavements under normal traffic, it was typical of the loading experienced by AASHO Road Test sections. In
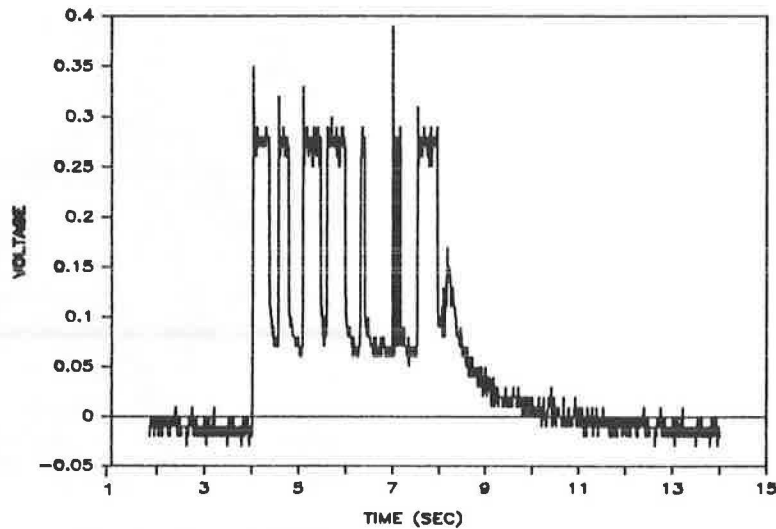

FIGURE 3 Spectral density of the leaf spring suspension, V = 80 kph, R = 217 in./mi.

FIGURE 5 Output of the axle detector.

the latter, a particular vehicle type carrying a given payload and traveling at a constant speed was assigned to each loop or lane. Thus, a loading condition resulted where certain points on the pavement experienced loads consistently higher than the static whereas others experienced loads consistently lower than the static. This localized application of the dynamic load

is taken into account in simulating the performance of AASHO Road Test sections as subsequently described.

ANALYTICAL PROGRAM

The analytical program of the study had two main objectives. The first was to demonstrate that consideration of dynamic axle loads can improve the accuracy of pavement performance predictions. For this purpose, the performance of a number of AASHO Road Test sections was analyzed by simulating the dynamic axle loads experienced over their service lives. The second objective was to study the impact of suspension type on pavement performance. For this purpose, the experimental dynamic load data obtained for the air and the rubber suspensions were input into VESYS, and comparisons of pavement performance predictions were made.

Simulation of AASHO Road Test Sections

Ten AASHO Road Test sections were selected for the performance simulations. The selected sections included six that developed severe roughness (i.e., SV higher than 10×10^{-6}) and four that remained relatively smooth through their service lives (i.e., SV lower than 10×10^{-6}). The material properties documented by Rauhut et al. (14) were used throughout. The temporal variation in material properties was accommodated by distinguishing five "seasons." For each season, the spatial variation in material properties was described by their coefficients of variation.

The analysis of the sections that remained smooth was intended for calibration of the VESYS simulations with respect to material properties. These sections were analyzed by assuming that axle loads are static. Since a number of the sections analyzed carried 5-axle vehicles, it was decided to modify VESYS-III-A to accommodate the overlapping influence of tandem axles. For this purpose, the "rainflow" method described in ASTM E1049-85 was followed (15).

Another modification considered necessary was the addition of a model describing the component of pavement rough-
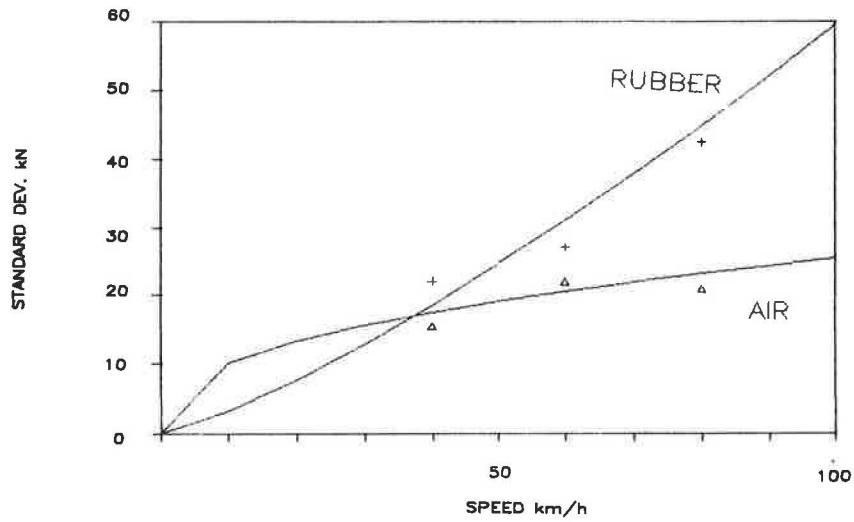
TABLE 1 RESULTS OF PHASE TWO OF THE EXPERIMENT

RUN	SITE	ROUGH. (Mays)	SPEED (km/h)	OBSERV.	LENGTH (m)	S.D.(kN) RUBBER	S.D.(kN) AIR
29			40	7069		8.04	8.07
30	1	56	60	4440	746.17	10.87	6.94
31			80	3400		14.28	7.40
21			40	7207		11.06	9.44
22	2	87	60	4527	760.74	18.76	8.66
24			80	3467		28.17	11.01
13			40	7286		10.86	10.40
14	3	96	60	4576	769.08	14.49	11.30
12			80	3505		30.11	13.67
3			40	4913		14.76	12.60
4	4	115	60	3085	518.59	16.81	19.07
40			80	2363		33.57	19.46
16			40	6423		22.15	15.65
17	5	201	60	4034	677.98	27.06	22.11
20			80	3090		42.55	21.08

Note 1: Static loads on the tandem groups are 205.52 and 204.54 kN for the drive and trailer axles, resp.

Note 2: 100 observations correspond to 1 sec

FIGURE 6 Impact of vehicle speed on axle load variation.

ness caused by fatigue cracking. Two relationships were used, the first relating the damage index (DI) to the area cracked (A_c) and the second relating the area cracked to pavement roughness, SV. Equation 4 describes the first relationship as proposed by Rauhut et al. (*14*), and Equation 5 describes the

other relationship, which was developed through regression from the data on the 10 sections analyzed.

$$A_c = 1.91e^{3.958DI} \tag{4}$$
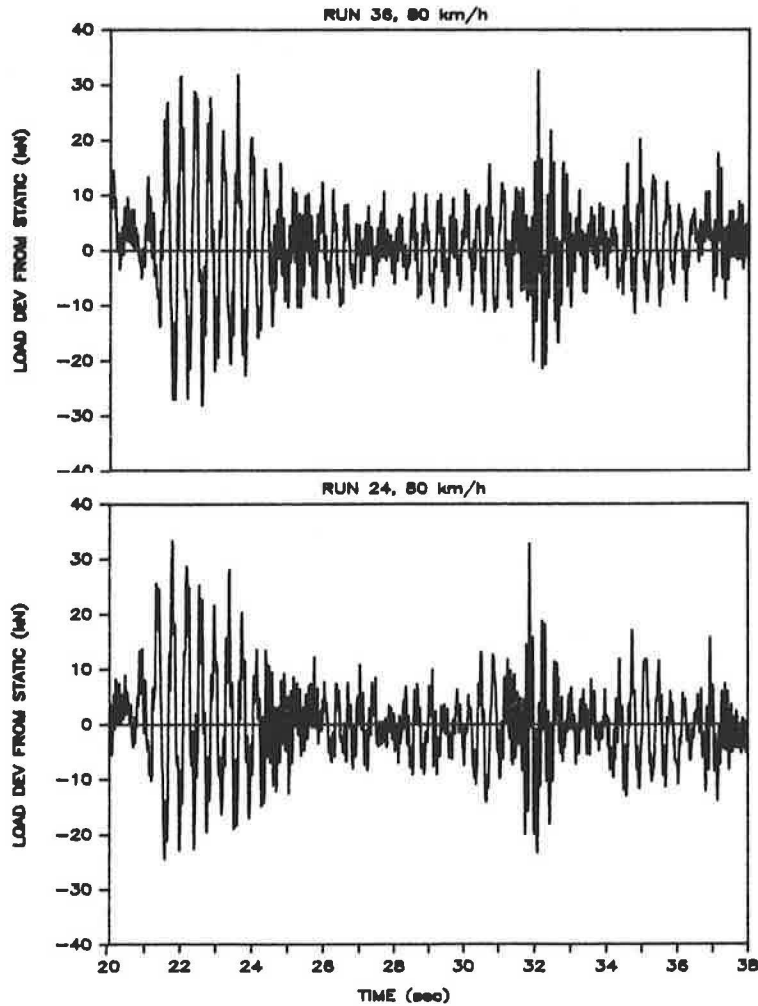
$$SV = A_c^{0.556} \tag{5}$$

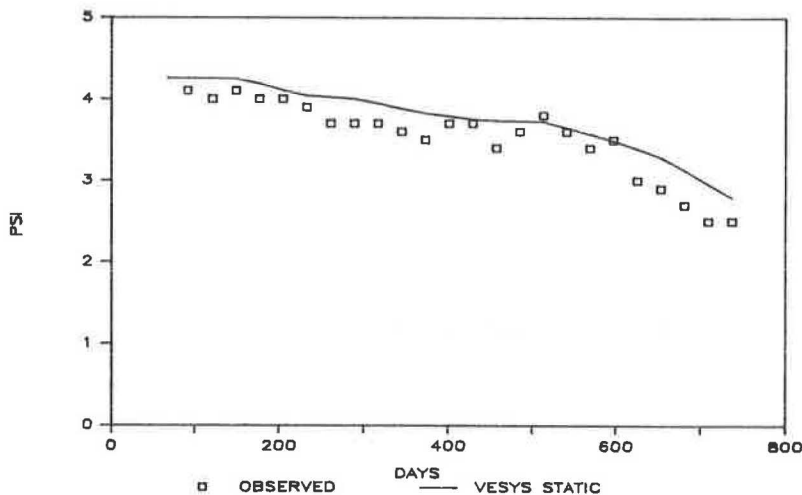**FIGURE 7 Spatial repetitiveness of dynamic load.**

FIGURE 8   Predicted vs. observed performance, section 312.

The results of the analysis demonstrated that VESYS can provide fairly accurate predictions of distress and performance for sections that remained relatively smooth through their service lives. An example of observed vs. predicted PSI values for one of the smooth sections is shown in Figure 8.

The analysis of the sections that developed severe roughness was carried out by taking into account the spatial repetitiveness of dynamic load from replicate vehicle passes. The analysis concentrated on the pavement length over which an axle completes a load cycle. Given a frequency of load variation of 3 Hz and a vehicle speed of 58 kph (35 mph), this length was calculated as 5.2 m. The methodology followed consists of dividing the 5.2-m length into six subsections and assigning load segments from the axles of the passing vehicle to each subsection. The procedure involved the following steps:

1. Coefficients of Variation (CV) of dynamic axle load were estimated on the basis of the observed pavement roughness, using Equation 1. For each section, three time intervals were distinguished over which the CV of the load was considered constant.

2. For each time interval, a frequency distribution of dynamic load was assumed. A normal distribution was assumed for CV values below 15 percent and a trapezoid distribution for CV values higher than 15 percent.

3. Each load frequency distribution was divided into six load segments of equal probability, and the average value of load in each segment was calculated by numerical integration as shown in Figure 9. A combination of load segments from the axles of a vehicle was assigned to each subsection on the basis of axle spacing as shown in Figure 10.

4. VESYS simulations were performed for each subsection to yield estimates of pavement distress and performance (i.e., DI, SV, rut depth, and PSI vs. time).

5. The distress predictions of the subsections were combined into distress and performance predictions for the entire section. This was done by averaging the rut depth of subsections, while assuming that the subsection with the highest DI
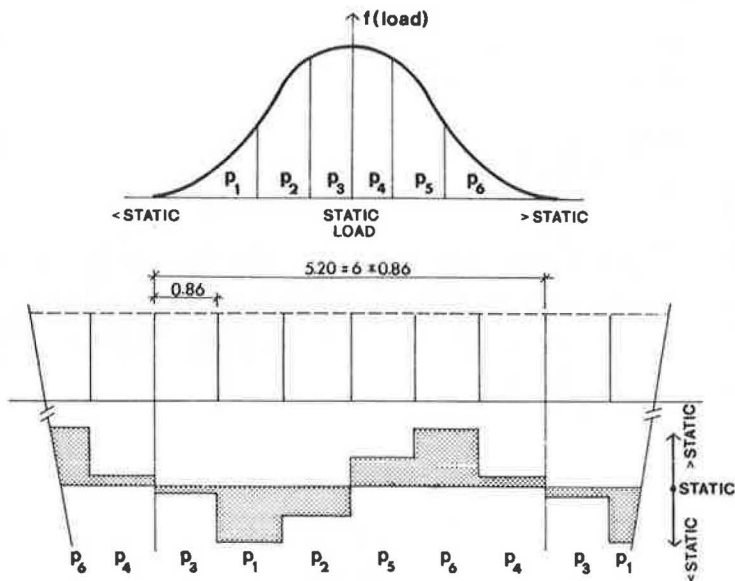

FIGURE 9   Dividing a load frequency distribution into six segments.
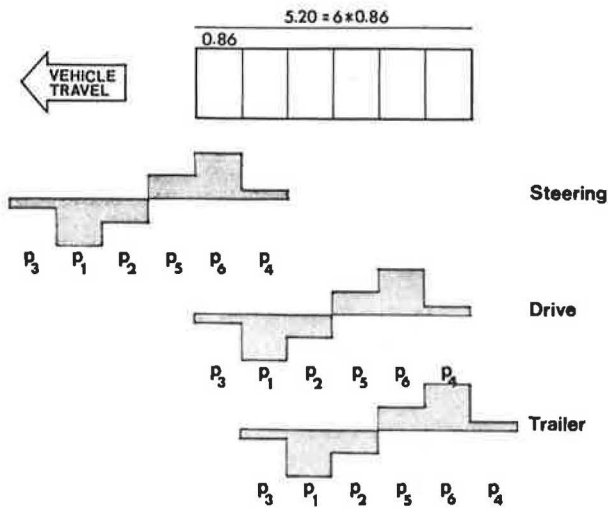
FIGURE 10 Assigning load segments to subsections.

determines the amount of cracking and therefore the pavement roughness on the entire section.

Another modification to VESYS-III-A accommodated the increasing in-time axle load variation. An algorithm was used where three independent sets of pavement distress parameters were calculated and subsequently superimposed to produce overall distress and performance predictions. Examples of the results of the analysis are shown in Figures 11, 12, and 13. Overall, the described methodology considerably improved the performance predictions for four of the six rough sections analyzed, whereas only a marginal improvement was realized for the other two sections.

Impact of Suspension Type on Pavement Performance

The objective of this part of the study was to evaluate the impact of suspension type on pavement performance under normal traffic. As pointed out earlier, vehicles under normal
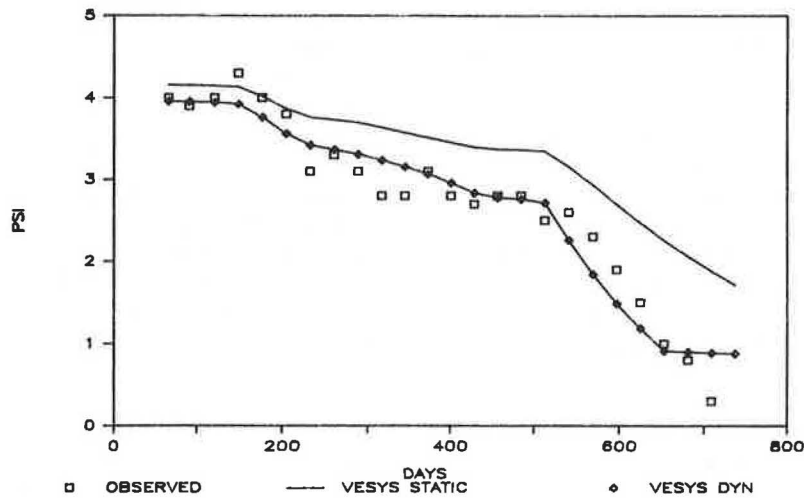

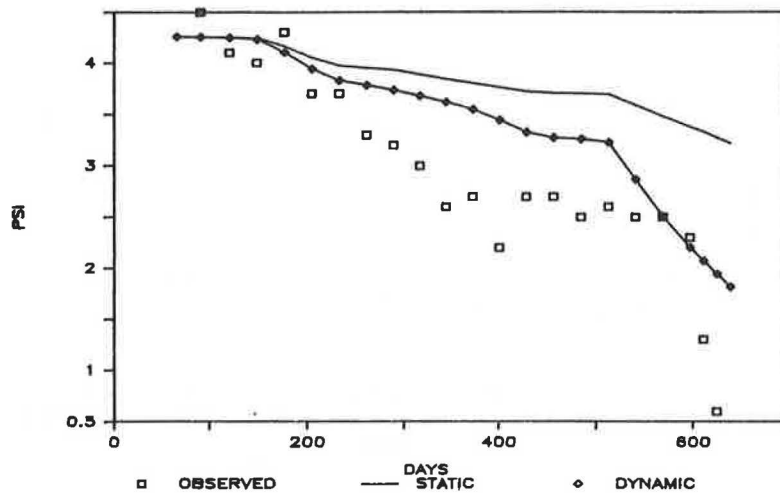FIGURE 11 Predicted vs. observed performance, section 331.

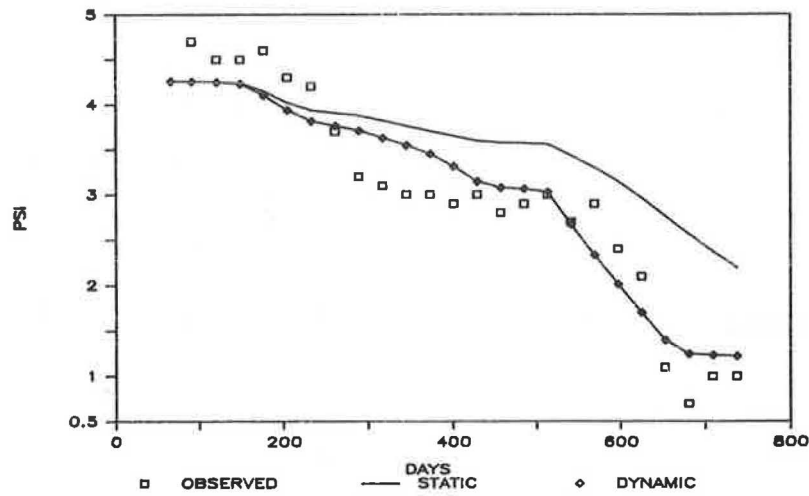FIGURE 12 Predicted vs. observed performance, section 469.

FIGURE 13 Predicted vs. observed performance, section 479.

traffic apply dynamic axle loads randomly in space. Under these conditions, dynamic axle loads can be input into VESYS as their frequency distributions. The analysis focused on the experimental data of the air and the rubber suspensions obtained for the highest vehicle speed tested (80 kph). Two modifications to VESYS-III-A were considered necessary. The first was the previously described algorithm that accounts for the pavement roughness caused by fatigue cracking. The second consisted of increasing the dimension of a number of arrays to allow input of a combination of 12 load intervals and 5 seasons (i.e., a dimension of 60 replaced the original dimension of 25). Each load interval was input as a circular tire imprint of uniform pressure which was assumed to be equal to the tire inflation pressure. Under dynamic conditions, the tire inflation pressure was assumed to vary with the load within 20 percent of the pressure under static conditions. However, VESYS is sensitive to the tire inflation pressure specified rather than to the tire imprint radius, as suggested by other studies (*16*). As a result, the performance predictions depended

to a large extend on the assumption used for the tire inflation pressure variation under dynamic conditions.

The pavement performance predictions for the air and rubber suspensions were compared to the performance predictions obtained under static load. The comparisons were based on the calculated "areas" under the performance curves. These were obtained by summing the ordinate segments contained between a performance curve and a selected terminal present serviceability index (PSI). Minimum PSI values of 2.0 and 2.5 were considered. The sums obtained for each suspension type and level of pavement roughness were divided by the sum obtained under static load. The results were plotted in the form of additional pavement damage vs. pavement roughness (Figures 14 and 15 corresponding to terminal PSI values of 2.0 and 2.5, respectively). The analysis of the load data for the roughest section, for example, revealed that the rubber suspension caused 17 to 22 percent more damage than the static load, depending on the assumed value of terminal PSI. Similar values calculated for the air suspension ranged between
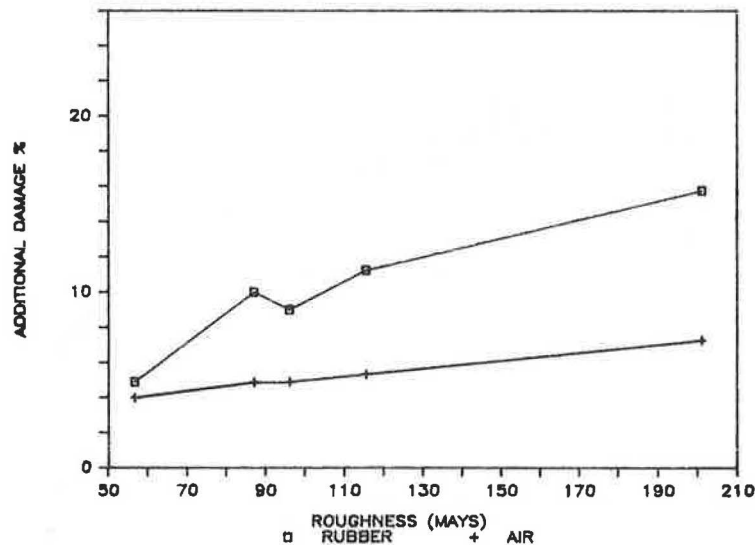

FIGURE 14 Impact of suspension type on pavement performance: terminal PSI = 2.0.
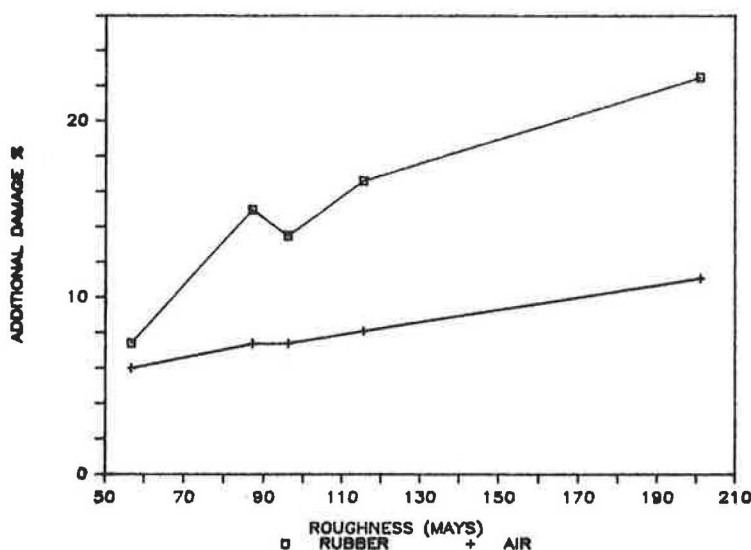
FIGURE 15 Impact of suspension type on pavement performance: terminal PSI = 2.5.

4 and 8 percent. These results depended on the assumption used for the variation in tire inflation pressures, as pointed out earlier.

SUMMARY

The major findings of the experimental part of the study are:

1. For the leaf spring suspension tested, the dominant frequency of the load variation was 3 Hz. This frequency remained constant with changes in vehicle speed and pavement roughness.
2. Axle load variation depends on suspension type, pavement roughness, and vehicle speed. The range of the observed standard deviations of dynamic load was between 8 and 42 kN.
3. The load variation of the air suspension is less sensitive to vehicle speed than the load variation of the rubber suspension.
4. Replicate runs generate load waveforms repetitive in space.

The last observation suggests that for replicate runs, certain points on the pavement experience loads consistently higher than the static whereas others experience loads consistently lower than the static. It was pointed out that although this loading condition is not the case for pavements under normal traffic, it was typical of the loading experienced by AASHO Road Test sections.

The analytical part of the study had two main objectives: first to demonstrate that consideration of dynamic axle loads can improve the accuracy of pavement performance predictions, and second to study the impact of suspension type on pavement performance. The first objective was addressed by modeling the performance of a number of AASHO Road Test sections and by treating dynamic load as being repetitive in space. This method yielded significant improvements in performance prediction accuracy for four of the six rough sections analyzed.

The second objective was addressed by modeling pavement performance under the experimental dynamic load data

obtained for the air and the rubber suspensions. That part of the study considered dynamic axle loads as being random in space. The load frequency distributions obtained for the highest vehicle speed tested were input into a modified version of VESYS-III-A. Pavement performance predictions were compared on the basis of the areas contained between the performance curve and a terminal PSI value. The results of the analysis indicated that the rubber suspension caused substantially higher pavement damage than the air suspension. This trend became more pronounced at higher levels of pavement roughness.

It was suggested that the pavement performance predictions obtained by VESYS-III-A depend to a large extent on the inflation pressure of the tires. Since little is known about the variation of the tire inflation pressure under dynamic conditions, it is recommended that similar future experiments include measurements of tire inflation pressures.

ACKNOWLEDGMENTS

REFERENCES

1. *Special Report 61E: The AASHO Road Test—Report 5, Pavement Research*, HRB, National Research Council, Washington, D.C., 1962.
2. *Special Report 61F: The AASHO Road Test—Report 6, Special Studies*, HRB, National Research Council, Washington, D.C., 1962, pp. 45–47.
3. A. P. Whittemore, J. R. Wiley, P. C. Schultz, and D. K. Pollock. *NCHRP Report 105: Dynamic Pavement Loads of Heavy Highway Vehicles*. HRB, National Research Council, Washington, D.C., 1970.
4. P. F. Sweatman. *A Study of Dynamic Wheel Forces in Axle Group Suspensions of Heavy Vehicles*. Special Report SR No. 27. Australian Road Research Board, 1983.

5. J. H. F. Woodrooffe, P. A. Leblanc, and K. R. LePiane. *Effect of Suspension Variations on the Dynamic Wheel Loads of a Heavy Articulated Vehicle*. Vehicle Weights and Dimensions Study, Technical Report, Vol. 11, Road and Transportation Association of Canada, 1986.

6. J. H. F. Woodrooffe and P. A. Leblanc. *The Influence of Suspension Variations on Dynamic Wheel Loads of Heavy Vehicles*. Paper 861973. Society of Automotive Engineers, 1986.

7. W. Gorge. *Evaluation of Research Efforts Concerning the Influence of Commercial Vehicle Development on the Road Fatigue*. German Automotive Technical Research Association. Summary and Evaluation of the Reports 900, 938, and 992 of the Testing Bureau for Road Engineering, Technical University of Munich, 1984.

8. R. R. Addis, A. R. Halliday, and C. G. B. Mitchell. Dynamic Loading of Road Pavements. Presented at International Symposium on Heavy Vehicle Weights and Dimensions, Kelowna, British Columbia, June 8–13, 1986.

9. Predictive Design Procedures. *VESYS User's Manual*. FHWA Report RD-77-154, 1977.

10. A. T. Papagiannakis. *Impact of Roughness-Induced Dynamic Load on Flexible Pavement Performance*. Ph.D. dissertation. Department of Civil Engineering, University of Waterloo, 1988.

11. M. W. Sayers, T. D. Gillespie, and C. A. V. Queiroz. *The International Road Roughness Experiment; Establishing a Correlation and a Calibration Standard for Measurements*. World Bank Technical Paper No. 45, 1986.

12. E. B. Spangler and W. J. Kelly. Road Profilometer—A Method for Measuring Road Profile. In *Highway Research Record 121*, HRB, National Research Council, 1965, pp. 27–54.

13. J. E. McQuirt, E. B. Spangler, and W. J. Kelly. *Use of the Inertial Profilometer in the Ohio DOT Pavement Management System*. Special Technical Publication 929, American Society for Testing of Materials, 1986.

14. J. B. Rauhut, R. L. Lytton, and M. I. Darter. *Pavement Damage Functions for Cost Allocation*, Vols. 1, 2, and 3. Report No. FHWA/RD-84/018, /019, and /020, 1984.

15. *Cycle Counting in Fatigue Analysis*. ASTM E1049-85, pp.836–848, 1985.

16. J. B. Rauhut, J. C. O'Quin, and W. R. Hudson. *Sensitivity Analysis of FHWA Structural Model VESYS-II-M, Preparatory and Related Studies*, Vol. 1. Report FHWA-RD-76-23, 1976.

Evaluation of Increased Pavement Loading and Tire Pressures

STUART W. HUDSON AND STEPHEN B. SEEDS

This research was directed toward developing a system for estimating changes in the flexible pavement design process as a result of trends noted in truck traffic. Maximum use was made of existing Arizona traffic and weight data, with field studies made only where data were not available. Case studies were used to verify the accuracy and sensitivity of the procedures. The work involved (1) a search of available data on file within the Arizona DOT and from the AASHO Road Test, (2) collection of pertinent field data, and (3) analysis of these data to develop a computer simulation procedure for predicting the effects of current truck loading conditions. The output from this research is a computer model for estimating pavement design loadings (18-kip equivalent single-axle loads) using the old and "new" estimation techniques.

Research on evaluation of increased pavement loading (1, 2) has been directed toward developing a system for estimating changes in the flexible pavement design process as a result of trends noted in truck traffic. Data collected as part of the Arizona investigation, and supported by information from the AASHTO Road Test (3) and Middleton et al. (4), confirm that actual truck tire pressures under operating conditions are likely to be in the range of 90–130 psi. Legal axle load limits may increase in the near future in order to take advantage of developments in truck and tire manufacturing capabilities. The Transportation Research Board's proposed Turner Truck Study (5) will help decide this issue.

In order to extend the findings from the AASHO Road Test, a mechanistic approach was used to evaluate changing tire pressures, increased loads, and steering axle damage; to isolate single-axle and tandem-axle effects; and to evaluate the effects of tridem axles.

Early in the project, an effort was made to collect existing data in several important areas, including

• data from tire manufacturers and researchers concerning current design tire pressures, loads, and the shape, size, and pressure distribution of tires in contact with a pavement surface—to assist in modeling the tire/pavement interface;
• vehicle weight data from the 14 port-of-entry weigh stations in Arizona, as well as weigh-in-motion data—to be used for comparisons and program verification, but not for model development;
• Arizona Department of Transportation (ADOT) traffic volume and classification data from throughout Arizona—to be used for program development and verification;
• ADOT overlay design and traffic analysis programs—to evaluate design procedures; and

ARE Inc., 2600 Dellana Lane, Austin, Tex. 78746.

• data on typical Arizona pavement cross sections—for modeling purposes.

The data were used for different purposes, some of which are described in the following sections.

TIRE DATA

A number of sources were examined for information on truck tire footprint size and shape, and the distribution of pressures over the footprint area. Data were obtained from the AASHO Road Test, research performed at Texas A&M University and the University of Texas (4, 6–12), tire manufacturing companies, The Tire and Rim Association (13), and tire researchers.

Table 1 summarizes the relevant data found in the AASHO Road Test report (14). This table illustrates tire pressure levels that were used for the AASHO Road Test. These data also show the observed differences in the tire pressure and the unit ground pressure, assuming a uniform pressure distribution.

Information on tire construction, tire pressures, footprint shape, and tire pressure distribution was provided by several of the major truck tire manufacturers. Figures 1 and 2 graphically illustrate the pressure data provided by Tire Company A. Figure 1 indicates that the area of highest pressure occurs at the edge of a static tire (295/75 R 22.5) footprint whereas for a rolling tire (11 R 22.5), the highest pressure occurs at the center (Figure 2). These are the only data available from Company A and unfortunately do not compare the same type of tire.

Company B provided footprint pressure data for a 10.00 R 20 (radial) rolling truck tire, including normal, lateral, and circumferential pressures. Figures 3 and 4 show the circumferential footprint load distribution for a 10.00 R 20 tire. These figures are comparable to Figures 1 and 2 from the Company A data in that they illustrate the pressure distribution along the length of the tire at four transverse positions. Figures 3 and 4, however, seem to contradict the data from Company A (Fig. 2), which predicted the maximum normal stress occurring at the midpoint of the footprint centerline on a rolling tire. These data indicate that the pressure distribution of the tire/pavement contact area is not uniform. They also show wide variations between the results of investigators who have attempted to quantify the distributions. Because of this and the difficulty in modeling a nonuniform pressure distribution with available models, uniform pressure distributions were used in the modeling efforts for this investigation.

An independent tire research firm (Smithers Scientific Ser-

TABLE 1   SUMMARY OF LOADS, TIRE TYPE, TIRE PRESSURE, AND
CONTACT AREA USED IN TRUCKS IN AASHO ROAD TEST

Tire Load(lbs)	Tire Size & Ply Rating	Tire Pressure[1](psi)	Gross Contact Area(in^2)	Unit Ground[2] Pressure(psi)
1,000	6.70 x 15/4[3]	24	36.6	29.1
1,500	7.00 x 16/6	45	37.4	42.3
3,000	7.50 x 20/10	75	45.4	65.7
3,000	7.50 x 20/10	75	45.4	65.7
4,500	10.00 x 20/12	75	67.8	67.5
4,000	9.00 x 20/10	75[4]	59.3	69.5
5,600	11.00 x 20/12	75	77.7	66.4
5,000	11.00 x 20/12	75	77.7	66.4
7,500	12.00 x 24/14	80	97.3	69.7
6,000	12.00 x 20/14	80	86.4	69.8

[1] Taken with tires at approximately the prevailing atmospheric temperatures and do not include any inflation build-up due to vehicle operation as per Tire and Rim Association standard.

[2] Calculated with assumption of uniform pressure.

[3] Tubeless tire; Tire and Rim Association standard inflation pressure is 28 psi for 1,065-lb load.

[4] Tire and Rim Association standard inflation pressure is 70 psi for a recomended maximum load of 3,960 lb. This tire was operated at 75 psi inflation pressure and the data given for this pressure are at a load of 4,120 lb. A measured value of the gross contact area was not available for these conditions, but was assumed to be the same as that for 3,960-lb load at 70 psi.

vices), cooperating with ARE Inc., provided performance specifications for five different brands of radial truck tires. The relevant data are summarized in Table 2. It can be seen from these data that the inflation pressure is approximately equal to the load divided by the *net* contact area. This is the assumption that is normally used in layer theory analysis. All of the tires compared are type 11 R 24.5.

TRUCK TIRE PRESSURE MEASUREMENTS

Truck tire pressures were inventoried at three Arizona port-of-entry weigh stations. Pressure data from 350 trucks were recorded over 4 days of measurements.

The field crew checked tire pressures on trucks as they were stopped on the weigh-station scales. The trucks had just come off the highway, so the tires were at operating temperature and pressure. The test procedure was to check the pressures of three tires on each truck: one front steering tire, one drive tire on the tractor, and one of the rear tires on the trailer or trailers. Information noted on each truck was: configuration, tire size and type, tire pressure, and ambient temperature in both the sun and shade at intervals throughout the day.

The tire pressure data were reduced and analyzed. Table 3 summarizes the radial tire pressure information collected at all three truck stations. The tire pressures are subdivided by their location on the truck: front (steering axle), middle (drive axle), and rear (trailer axle).
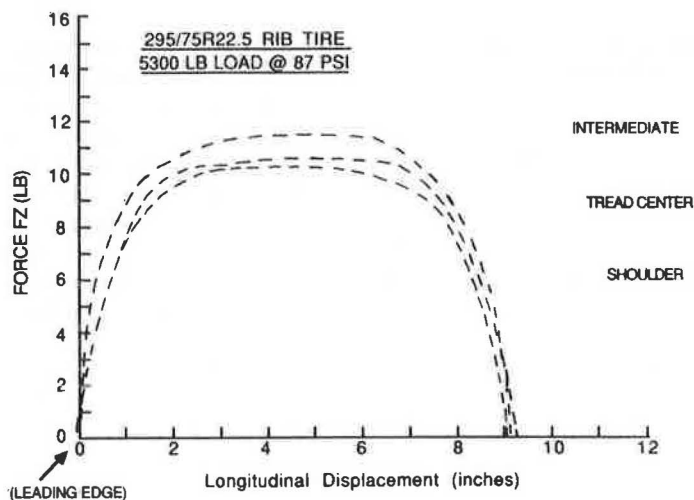

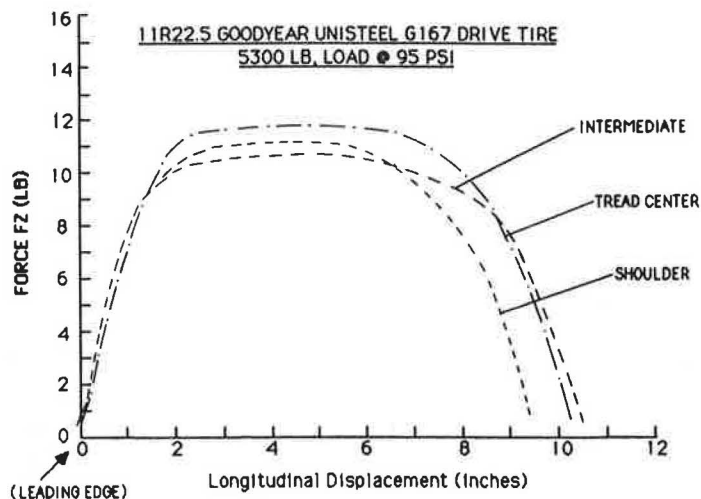FIGURE 1   Static footprint load distribution (Company A).

FIGURE 2 Rolling footprint load distribution (Company A).

The most common tire size observed was the 11 R 24.5, constituting over 50 percent of all the front-tire measurements. Three other tire sizes (11 R 22.5, 275/80 R 24.5, and 285/75 R 24.5) in conjunction with the 11 R 24.5s constituted almost 90 percent of the front tire observations. As might be expected, the measured standard deviation is lowest for front tires because truckers check front tire pressure more often to ensure optimum ride and handling of the truck. Many of the truckers do not own the trailer they haul; consequently, trailer tire pressures vary (higher standard deviation) more than tractor tire pressures.

Table 4 includes all types of tires measured but separates bias ply from radials. For three truck axle locations (front, middle, and rear), the number of observations, the mean tire pressure, and the standard deviation are calculated. In addition, intervals are calculated that indicate a range of tire pressures between which 99, 95, and 90 percent of the tire population should statistically fall.

The following conclusions can be drawn from the analysis of the pressure data collected on this project:

1. The number of bias ply tires as compared to the number of radial tires (tractor = 5.1 percent, trailer = 17.2 percent) is small enough that only radials could be considered in the equivalence factor analysis.

2. Tire pressures on the steering axle exhibit a lower standard deviation than do tires on the middle or rear (trailer) axles. This indicates that the front axle may be more representative of the tire pressure favored by truckers.

3. Average radial tire pressure for the front, middle, and rear axles is 105.9, 102.4, and 101.8 psi, respectively.

4. These data cannot prove or disprove that tire pressures are significantly higher when temperatures in the sun are greater than 100°F. On the days when tire pressure measurements were recorded, the temperature fluctuated because of partly cloudy conditions. The sun was never out long
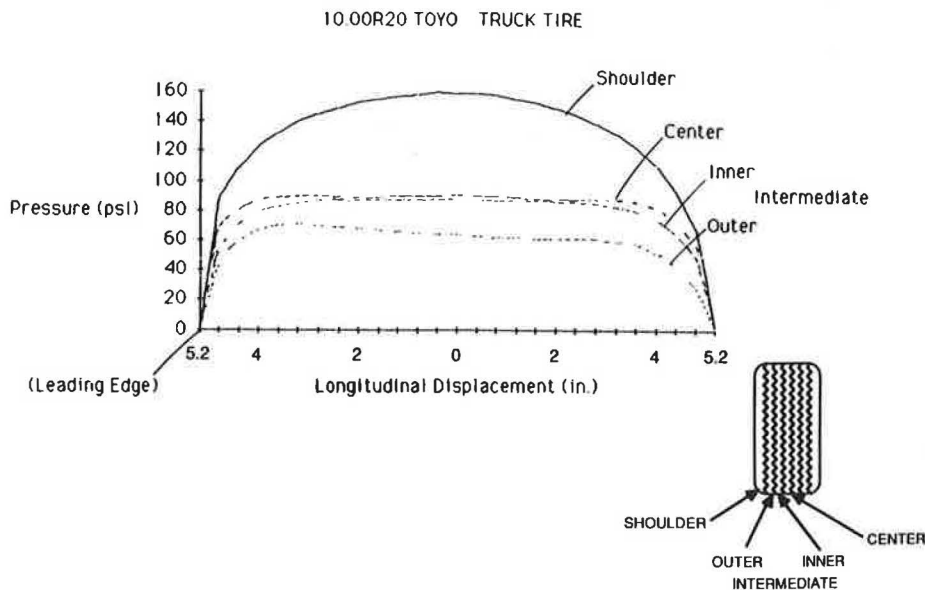

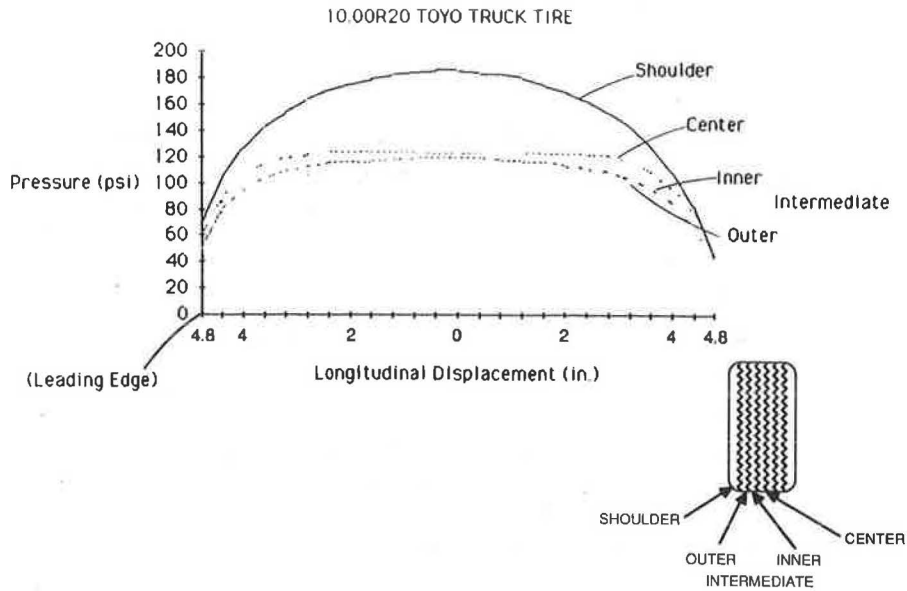**FIGURE 3** Rolling footprint pressure distribution (65 psi).

10.00R20 TOYO TRUCK TIRE

FIGURE 4 Rolling footprint pressure distribution (105 psi).

TABLE 2   SUMMARY OF INFORMATION PROVIDED BY COMPANY A

Brand	Total Footprint Area(in^2)	Net Contact Area(in^2)	Load on Tire(lb)	Infl. Pressure (psi)
Bridgestone	78.04	59.56	5640	95
Goodyear	72.62	53.37	5640	95
Michelin	79.15	57.95	5790	100
Firestone	81.52	61.65	5640	95
General	73.39	57.06	5640	95

TABLE 3   TIRE PRESSURE BREAKDOWN BY TIRE TYPE

Front Radials Tire Type	Obs.	Mean	St.Dev.	Middle Radials Tire Type	Obs.	Mean	St.Dev.	Rear Radials Tire Type	Obs.	Mean	St.Dev.
10.00R20	3	100.0	6.9	10.00R20	3	98.3	12.6	10.00R17.5HC	1	116.0	0.0
10.00R22	4	98.3	9.5	10.00R22	4	102.0	15.6	10.00R20	3	97.3	15.5
10.00R24.5	1	122.0	0.0	10.00R24.5	1	122.0	0.0	10.00R22	5	95.8	12.2
11/80R22.5	2	106.0	5.7	11/80R22.5	2	106.0	2.8	10.00R22.5	2	97.5	3.5
11R22.5	33	104.4	8.3	11R22.5	33	100.5	7.2	10.00R24.5	1	118.0	0.0
11R24.5	189	106.5	9.9	11R24.5	180	103.5	11.2	10/70R22.5	1	102.0	0.0
275/80R22.5	9	107.4	5.2	275/80R22.5	9	103.1	8.4	10R22.5	2	96.0	8.5
275/80R24.5	35	107.3	9.2	275/80R24.5	33	102.4	10.0	11/80R22.5	2	105.0	1.4
275/85R22.5	1	86.0	0.0	275/85R22.5	1	98.0	0.0	11/80R24.5	3	107.7	0.6
275/85R24.5	1	112.0	0.0	274/85R24.5	1	102.0	0.0	11R17.5	1	112.0	0.0
275/95R24.5	1	108.0	0.0	275/95R24.5	1	88.0	0.0	11R22.5	40	102.1	11.2
280/75R24.5	1	108.0	0.0	280/75R24.5	1	92.0	0.0	11R24.5	137	102.2	11.6
285/75R24.5	37	103.9	10.8	285/75R24.2	1	102.0	0.0	255/70R22.5	4	105.5	4.9
285/80R22.5	1	100.0	0.0	285/75R24.5	36	99.1	10.9	275/80R22.5	7	100.1	8.8
285/80R24.5	1	110.0	0.0	285/80R22.5	1	102.0	0.0	275/80R24.5	24	102.5	11.7
295/75R22.5	9	106.0	4.0	285/80R24.5	1	110.0	0.0	280/75R24.5	1	66.0	0.0
9R22.5	1	95.0	0.0	295/75R22.5	9	103.8	4.9	285/75R24.2	1	100.0	0.0
				9R22.5	1	75.0	0.0	285/75R24.5	32	99.8	11.8
								285/80R22.5	1	103.0	0.0
								295/75R22.5	5	97.6	12.0
								8.25R20	1	98.0	0.0
								9.00R20	1	110.0	0.0
								9R17.5	1	114.0	0.0
								9R22.5	3	103.3	10.8

TABLE 4 STATISTICAL BREAKDOWN OF ARIZONA TIRE PRESSURE DATA

Tire Type	Truck Axle	% * Used	Obs.	Sample Mean	Stand. Dev.	99% Obs. Low	99% Obs. High	95% Obs. Low	95% Obs. High	90% Obs. Low	90% Obs. High
Bias Ply	Front	100%	18	90.6	7.9	70.2	111.0	75.1	106.1	77.6	103.6
		95%	17	89.8	7.2	71.3	108.3	75.8	103.9	78.0	101.6
	Middle	100%	17	86.4	7.7	66.5	106.2	71.3	101.4	73.7	99.0
		95%	16	85.5	6.8	67.9	103.1	72.1	98.9	74.3	96.7
	Rear	100%	58	88.1	12.5	55.8	120.4	63.5	112.6	67.5	108.7
		95%	55	87.4	10.9	59.4	115.4	66.2	108.7	69.6	105.3
Radial	Front	100%	329	105.9	9.5	81.2	130.5	87.2	124.6	90.2	121.6
		95%	313	105.8	7.8	85.7	126.0	90.5	121.2	93.0	118.7
	Middle	100%	318	102.4	10.6	75.1	129.7	81.6	123.2	85.0	119.8
		95%	302	102.7	8.6	80.5	125.0	85.8	119.6	88.5	116.9
	Rear	100%	279	101.8	11.4	72.4	131.1	79.5	124.0	83.1	120.5
		95%	265	102.6	9.5	78.2	127.1	84.1	121.2	87.0	118.2

* Indicates the percentage of observations in the analysis.
  100% - all observations were included.
  95% - 5% of the observations furthest from the mean were dropped as
        outliers for this analysis.

enough to substantially heat the pavement for a prolonged period of time.

The apparent increase in truck tire pressures since the AASHO Road Test led to investigation of the effects on pavement stresses and strains and on pavement life. These investigations are discussed in detail in following section.

TIRE PRESSURE EFFECTS STUDY

In this portion of the project, the effects of tire pressure on pavements were examined using a mechanistic approach. An elastic-layer-theory program, ELSYM5 (*15*), which assumes a uniform pressure distribution, was used to model an average

pavement structure. The following pavement cross section was considered in the analysis:

Layer	Elastic Modulus (psi)	Poisson's Ratio	Thickness (in.)
1	300,000	0.30	3
2	20,000	0.35	6
3	12,000	0.40	8
4	3,000	0.45	

Runs were made simulating axle loads of 18 and 28 kips. Each set of runs consisted of tire pressures ranging from 70 to 160 psi, varying at 10-psi increments.

The results are shown as plots of several important pavement response parameters vs. tire pressure. Figure 5 shows
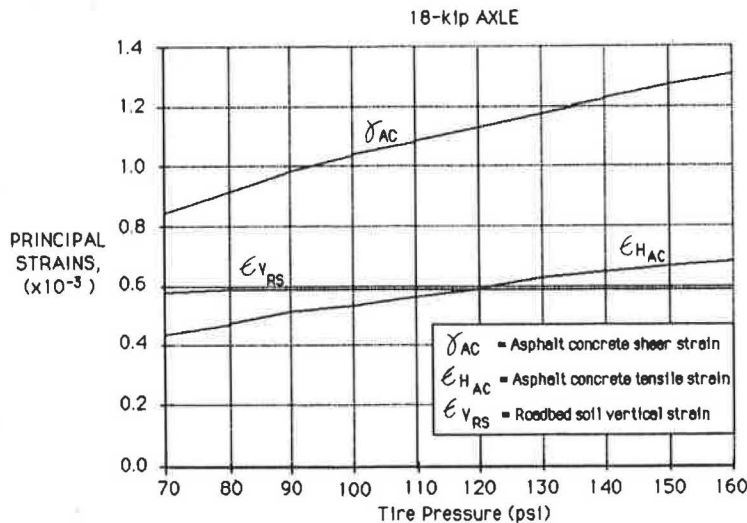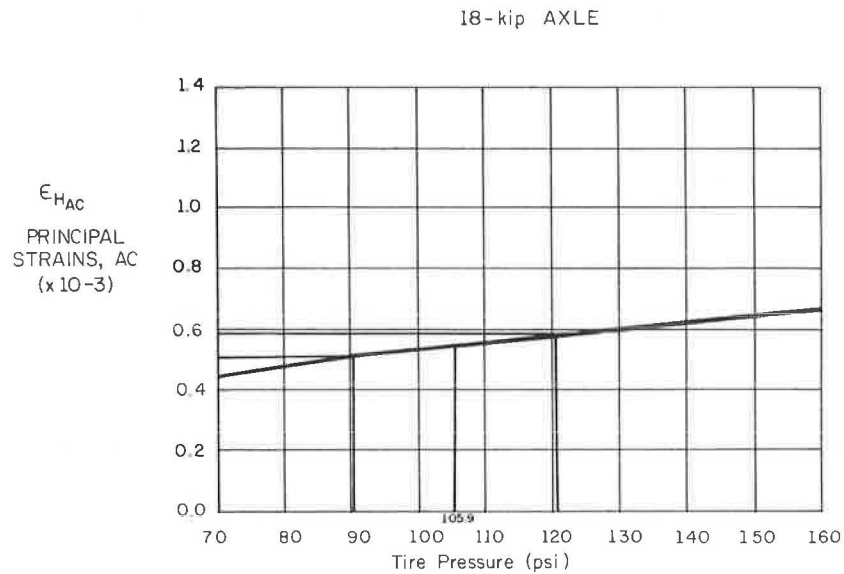

FIGURE 5 Plot of principal strain in the pavement structure vs. tire pressure from ARE Inc. study.

18-kip AXLE

$\epsilon_{H_{AC}}$

PRINCIPAL
STRAINS, AC
(x 10-3)

FIGURE 6 **Plot of principal strain versus tire pressure.**

a plot of the principal horizontal tensile and shear strains at the bottom of the asphalt layer and vertical compressive strain at the subgrade level vs. tire pressure for the 18-kip axle load. This plot indicates that horizontal tensile strain and shear strain increase as tire pressure increases whereas vertical strain on the roadbed soil remains fairly constant. The implication is that tire pressure increases may affect the surface layer in terms of reduced fatigue life, increased surface rutting, or increased roughness but that there is very little effect in terms of pavement damage attributable to vertical strain on the roadbed soil.

By superimposing the range that contains 90 percent of the field-measured tire pressures for radial steering-axle tires on the principal strain vs. tire pressure plot as shown in Figure 6, about a 12 percent increase in principal strain is observed.

From field measurements discussed in the previous section:

Mean Radial Tire Pressure (steering axle) = 105.9 psi;
Interval containing 90 percent of all observations = 90.2 to 121.6 psi corresponding to strains of 0.51×10^{-3} in./in. to 0.59×10^{-3} in./in.

To examine the effect of these strain differences on pavement life, a fatigue or damage model can be used. The fatigue equation for less than 10 percent cracking developed by Finn et al. (*16*) produces the following results:

$$\log N_f (\leq 10\%) = 15.947 - 3.291 \log(strain/10^{-6})$$

$$- 0.854 \log(E/103)$$

therefore, at 90.2 psi, strain = 0.51×10-3 in./in., $E = 300,000$ psi;

$N_f = 83,350$ applications

and at 121.6 psi, strain = 0.59×10-3 in./in., so

$N_f = 51,601$ applications

These remaining life analyses show that for a 35 percent increase in tire pressure from 90 to 121 psi, pavement life is reduced by 38 percent according to the Finn equation. The

resulting effects on pavement life must certainly be considered significant. The results on a stronger (thicker) pavement would probably not be as significant although it seems clear that tire pressure should be considered in any new pavement design methodology.

IMPROVED DAMAGE MODEL AND EQUIVALENCE FACTOR DEVELOPMENT

A damage model (as it will be referred to in this context) is an equation that can be used to predict the number of load applications that can be sustained by a given pavement structure in a given environment before it reaches some preestablished failure criterion. For example, a damage model developed in NCHRP 1-10B (*16*) was used in the previous section to show effects of increased tire pressure on pavement life. The primary and most obvious application of a damage model is in the pavement structural design process where it provides a means for selection of pavement layer thicknesses and, depending on the nature of the model, also provides a basis for determining the relative effects of different wheel loads, tire pressures, and load configurations on a pavement's load-carrying capacity. The latter provision translates further into a means for converting mixed-axle-load traffic into an equivalent *design* number of axle load repetitions of a uniform magnitude.

The following criteria were selected for the development of improved mechanistic damage models for ADOT.

• Consider seasonal variation of roadbed soil support. To develop a mechanistic damage model with a potentially higher degree of accuracy than that of previous research efforts, it was considered essential that the seasonal variation of roadbed soil support at the AASHO Road Test be evaluated. To accomplish this, it was necessary to translate seasonal deflections and laboratory test results into pavement material properties so that the resulting variation of critical pavement stresses and strains could be considered. Miner's linear damage

hypothesis (*17*) was assumed to be valid, thus allowing the individual seasonal damages for each AASHO Road Test section to be accumulated and used in the analysis process.

• Consider effects of steering axles independently from load axles. Since steering-axle loads ranged as high as 12,000 lb at the Road Test, it was decided that their effects should be considered separately from the trailing axles. This was accomplished within the same linear damage framework used for considering seasonal effects.

• Use serviceability as performance criterion. Traffic repetitions corresponding to a serviceability index of 2.5 were used in developing the damage models.

• Develop separate damage models for single-axle and tandem-axle loads. This was included in the criteria for model development in order to maximize precision and to provide a better basis for evaluating the relative difference between single- and tandem-axle loads.

• Use ELSYM5 as the mechanistic model.

Although 25 years old, the data base of information from the AASHO Road Test experiment is still the best organized, most extensive, thorough, and accurately collected set of roadway performance data. Consequently, these data were selected for detailed analysis to develop the damage models.

A new set of 18-kip single-axle equivalence factors was then developed using the mechanistic damage models. The new factors were mechanistically derived and are intended to eventually replace the AASHTO load equivalence factors currently used by ADOT. One significant improvement in this new set of equivalence factors is that they were developed considering tire pressure. The resulting factors should, therefore, allow more accurate estimates of equivalent loads accounting for the higher tire pressures that have been observed on Arizona highways as previously described.

The equivalence factors are dependent on a number of different parameters. These include the thicknesses and moduli of all pavement layers, tire pressure, axle type, and load. Several of the parameters have more influence than others. The parameters that have relatively little effect on the equivalence factors were fixed in the development. The minimum performance level was fixed at a terminal serviceability of 2.5. The parameters that were varied in the analysis include load, tire pressure, modulus of roadbed soil, thickness of subbase and base, thickness of asphalt concrete layer, and axle type.

Given the damage models developed in the project, the technique for generating 18-kip single-axle equivalence factors for a variety of conditions is relatively simple. An equivalence factor is a ratio of the relative damage between a given loading condition (*x/c/p*), and a standard 18-kip single-axle load. (Note: *x* refers to the load magnitude, *c* to the load configuration, and *p* to the tire pressure.) The equivalence factor for load (*x/c/p*), therefore, can be calculated as the ratio of the allowable 18-kip single-axle load applications to the allowable applications for load (*x/c/p*):

$$e_{x/c/p} = (N_f)_{18/1/75}/(N_f)_{x/c/p}$$

$(N_f)_{18/1/75}$ is calculated for the selected structural and soil support conditions using the single-axle damage model with a standard 75-psi tire pressure, and 18-kip single-axle load. $(N_f)_{x/c/p}$ is calculated (for the same structural and soil support conditions) using the appropriate single- or tandem-axle damage model along with the load magnitude (*x*) and tire pressure (*p*) corresponding to load (*x/c/p*). Two sets of damage models were used in the development. For 3- and 6-in. surface thicknesses, the set of models with tensile strain at the bottom of the asphalt layer as the response parameter was used. For thin surface treatments, the models with vertical strain at the subgrade as response parameter were used.

COMPUTER PROGRAM DEVELOPMENT

One of the major objectives of this research project was to develop computer programs to predict 18-kip equivalent single-axle loadings (18KESALs) for Arizona highways. Two such programs were developed as a result of the research.

The first program is called FEDESAL. This program uses Arizona loadometer data to predict an average number of equivalent loads per 1,000 vehicles based on the FHWA method. The other program, WIMESAL, reads WIM data and converts them to an estimate of the number of equivalent loads applied on a particular section of highway. Both programs have the option of using the AASHTO equivalence factors or the new ARE Inc. equivalence factors which account for tire pressure. Table 5 provides comparisons of the two equivalence factors at selected loads.

The results of the FEDESAL program are 18-kip vehicle equivalence factors that are the average number of 18KESALs

TABLE 5 COMPARISON OF AASHTO AND ARE INC. EQUIVALENCE FACTORS FOR SINGLE AXLES

Axle Load (kips)	AASHTO Equiv. Factor (75 psi)	ARE Equiv. Factor (75 psi)	ARE Equiv. Factor (110 psi)	ARE Equiv. Factor (145 psi)
4	.003	.0026	.0060	.0096
10	.102	.1446	.5555	1.2790
18	1.0	1.0	5.295	15.517
30	6.8	6.97	25.3	90.1
50	60	60.5	236.9	427.7

$P_t = 2.5$, and SN = 4.

```
                                                            DATE 05/01/86
                                                            PAGE 3
                        AVERAGE 18 KIP EQUIVALENT SINGLE
                          AXLE LOADS PER 1000 VEHICLES
                          USING FHWA TRUCK WEIGHT DATA


        COMMENTS:   ARE Inc Equivalence Factors Used
                    Rigid Factors not Calculated
                    Example Run for Final Report

    Station Location:   Urban

    Road Characteristics Used to Compute ARE Inc Factors

              Surface Thickness:  Medium  = 1 - 5 in.
         Base/Subbase Thickness:  Medium  = 10 - 17 in. overall
            Roadbed Soil Modulus:       12000.0 psi
                   Tire Pressure:         105.0 psi
```

| | | CURRENT 18 KIP ESAL PER 1000 VEHICLES | | FIVE-YEAR AVERAGE 18 KIP ESAL PER 1000 VEHICLES | |
VEHICLE CLASS	TOTAL VEHICLE COUNTS	RIGID	FLEXIBLE	RIGID	FLEXIBLE
LT	5	.0	73.8	.0	72.6
MT	4	.0	1679.4	.0	986.0
TS	8	.0	17865.0	.0	12880.7
TT	0	.0	.0	.0	.0
TST	4	.0	4007.6	.0	6021.8

FIGURE 7   Output from FEDESAL using ARE, Inc. equivalence factors.

per 1,000 vehicles. These averages are calculated across two pavement surface types, three highway functional classes, and an option of either five or nine vehicle classifications. There is an option to use either AASHTO equivalence factors, or the choice of a factorial of the new ARE Inc. equivalence factors. Another option allows the use of an axle-load-distribution shifting algorithm to predict the effect on equivalent load estimates of changing the legal axle load limits. There is also an option to obtain the 18KESAL estimates on only the current year's data or to determine a 5-year moving average using 5 years of historical 18KESAL data. One additional option allows a check on the FHWA loadometer data to assist in locating input errors. An example output using ARE Inc. equivalence factors is shown in Figure 7.

The other main program developed on the project is called WIMESAL. This is a project level 18KESAL prediction program for weigh-in-motion (WIM) data. The program reads WIM data on an individual highway section and produces estimates of base-year, 10-year, and 20-year accumulated equivalent loads. This will allow much more accurate estimates of the number of equivalent loads applied to a particular highway section.

Program WIMESAL has the option to use AASHTO equivalence factors or ARE Inc. equivalence factors accounting for tire pressure and for the specific structure of the highway section under consideration. The output is an estimate of the total accumulated number of 18KESALs on individual highway sections. These total 18KESAL estimates are presented for the base-year and as 10-year and 20-year predictions, given a growth factor for the section. An example of the output from program WIMESAL is shown in Figure 8.

SUMMARY

This investigation has resulted in the development of new computer programs to

● analyze loadometer data from permanent weigh stations in Arizona,
● analyze weigh-in-motion data to provide information similar to that obtained from fixed weigh stations,
● analyze the effect of increased legal load limits on truck equivalence values, and
● use mechanistic relationships to calculate load equivalence factors as a function of tire pressure, structure, truck classifications, single-axle–single wheel, single-axle–dual-wheel, tandem-axle–dual-wheel, and tridem axle–dual wheels, year, and even location in the case of the WIM program.

This study also provided the following information:

● field data to show that current summer operating tire pressures on trucks operating in Arizona are approaching 120 psi, and
● tire data from a number of sources which show footprint size and shape, current truck tire operating pressures, and tire pressure distribution on the pavement surface.

PREDICTED ACCUMULATED LOADS AND
AVERAGE 18 KIP EQUIVALENT SINGLE
AXLE LOADS PER 1000 VEHICLES
USING WIM TRUCK WEIGHT DATA

```
LOCATION:   Test Section
TRAFFIC
  GROWTH:   1.50% per year
COMMENTS:   ARE Inc Equivalence Factors Used
            Rigid Factors not Calculated
            Example Run for Final Report

     Road Characteristics Used to Compute ARE Inc factors

          Surface Thickness:   Medium  = 1 - 5 in.
     Base/Subbase Thickness:   Thick   > 17 in. overall
        Roadbed Soil Modulus:  15000.0 psi
              Tire Pressure:      90.0 psi
```

PREDICTED TOTAL ACCUMULATED EQUIVALENT LOADS

VEHICLE CLASS	FLEXIBLE 1-YEAR	10-YEAR	20-YEAR
5	4824.	51622.	110725.
6	12730.	136222.	292188.
7	0.	0.	0.
8	11239.	119688.	255644.
9	652832.	6963483.	14894410.
10	0.	0.	0.
11	0.	0.	0.
12	70469.	751874.	1608661.
13	0.	0.	0.
TOTAL	752095.	8022889.	17161630.

FIGURE 8   Output from WIM program using ARE, Inc. factors.

ACKNOWLEDGMENTS

REFERENCES

1. S. W. Hudson, S. B. Seeds, F. N. Finn, and R. F. Carmichael. *Evaluation of Increased Pavement Loading,* Vol. I, Research Results and Findings. Draft Final Report prepared for Arizona Department of Transportation, 1986.
2. R. High and S. W. Hudson. *Evaluation of Increased Pavement Loading,* Vol. II, ESAL Program Documentation. Draft Final Report prepared for Arizona Department of Transportation, 1986.
3. *Special Report 61E: The AASHO Road Test—Report 5, Pavement Research.* HRB, National Research Council, Washington, D.C., 1962.
4. D. R. Middleton, F. L. Roberts, and T. Chira-Chavala. Measurement and Analysis of Truck Tire Pressures on Texas Highways. Presented at 65th Annual Meeting of the Transportation Research Board, 1986.
5. *Relationships Between Vehicle Configurations and Highway Design.* (The Turner Proposal). Draft Proposal, TRB, National Research Council, Washington, D.C., 1986.
6. F. L. Roberts and B. T. Rosson. Effects of Higher Tire Pressures on Strain in Thin ACP. Presented at 65th Annual Meeting of the Transportation Research Board, Washington, D.C., 1985.
7. K. M. Marshek, W. R. Hudson, R. B. Connell, H. H. Chen, and C. L. Saraf. *Experimental Investigation of Truck Tire Inflation Pressure on Pavement-Tire Contact Area and Pressure Distribution.* Report No. 386-1. Center for Transportation Research, University of Texas, Austin, 1985.
8. K. M. Marshek, W. R. Hudson, H. H. Chen, C. L. Saraf, and R. B. Connell. *Effect of Truck Tire Inflation Pressure and Axle Load on Pavement Performance.* Report No. 386-2F. Center for Transportation Research, University of Texas, Austin, 1985.
9. R. B. Connell. *Experimental Determination of Truck Tire Contact Pressures and Their Effect on Flexible and Rigid Pavement Performance.* M.S. thesis, University of Texas, Austin, 1985.
10. K. M. Marshek, H. H. Chen, R. B. Connell, and W. R. Hudson. Experimental Determination of Truck Tire-Pavement Contact Pressure Distribution. Presented at 65th Annual Meeting of Transportation Research Board, Washington, D.C., 1986.
11. H. H. Chen, K. M. Marshek, and C. L. Saraf, The Effects of Truck Tire Contact Pressure Distribution on the Design of Flex-

ible Pavements—A 3D Finite Element Approach. Presented at 65th Annual Meeting of Transportation Research Board, Washington, D.C., 1986.

12. K. M. Marshek, H. H. Chen, R. B. Connell, and C. L. Saraf. The Effects of Truck Tire Inflation Pressure and Axle Load on Flexible and Rigid Pavement Performance. Presented at 65th Annual Meeting of Transportation Research Board, Washington, D.C., 1986.

13. *1985 Year Book.* Tire and Rim Association Inc., Akron, Ohio.

14. *Special Report 61C: The AASHO Road Test—Report 3, Traffic Operations and Pavement Maintenance.* HRB, National Research Council, Washington, D.C., 1962.

15. G. Ahlborn. *Elastic Layered System with Normal Loads.* Institute of Transportation and Traffic Engineering, University of California, Berkeley, 1972.

16. F. Finn, C. L. Saraf, R. Kulkarni, K. Nair, W. Smith, and A. Abdullah. *Development of Pavement Structural Subsystems,* Vol. 1. Final Report, NCHRP Project 1-10B. TRB, National Research Council, Washington, D.C., 1977.

17. M. A. Miner. Cumulative Damage in Fatigue. *Journal of Applied Mechanics, ASME,* September 1945.

Effect of Load, Tire Pressure, and Tire Type on Flexible Pavement Response

Ramon F. Bonaquist, Charles J. Churilla, and Deborah M. Freund

In recent years, decreased fatigue life, increased rutting, and accelerated serviceability loss in flexible pavements have been attributed to the effects of increased tire pressure. This study used the Federal Highway Administration Accelerated Loading Facility to measure the effects of load, tire pressure, and tire type on the response of a flexible pavement. Surface deflection, surface strain, and strain at the bottom of the asphalt layer were measured. Each of these responses was affected more by load than by tire pressure. Fatigue equivalency factors were developed using an exponential relationship between the number of cycles to failure and the magnitude of the tensile strain at the bottom of the asphalt layer. Since this strain was affected more by load than by tire pressure, the equivalency factors are influenced more by load. Doubling the wheel load (from 9,400 to 19,000 lb) increased predicted damage 1,000 percent whereas doubling the tire pressure (from 76 to 140 psi) increased predicted damage only 20 percent. On the basis of these fatigue equivalency factors, it was concluded that for the pavement section studied, the effect of increasing tire pressure from 76 to 140 psi is equivalent to an axle load increase of approximately 2,000 lb. This equivalency is valid for both radial and bias ply tires.

In recent years, the effect of increased truck tire pressures on flexible pavement performance has become a subject of great concern. Various researchers have used analytical methods to attribute decreased fatigue life, increased rutting, and accelerated serviceability loss to the effects of increased tire pressure (1–3). The purpose of this study was to investigate these concerns by measuring the effects of load, tire pressure, and tire type on the response of an asphalt concrete pavement. This experiment was conducted on Lane 2, Section 2 of the Federal Highway Administration (FHWA) Pavement Testing Facility (PTF).

BACKGROUND

The Pavement Testing Facility is an outdoor, full-scale pavement testing laboratory located at the Turner-Fairbank Highway Research Center in McLean, Virginia. The purpose of the PTF is to quantify the performance of full-scale test pavements trafficked with an accelerated rate of loading. The facility consists of two 200-ft-long instrumented bituminous concrete test pavements, the Accelerated Loading Facility (ALF) test machine, and a computer-controlled data acquisition system.

The test pavements represent typical in-service flexible

FIGURE 1 Accelerated Loading Facility machine at the FHWA Pavement Testing Facility.

pavements. Lane 1 consists of a 2-in. asphalt concrete wearing course, a 3-in. asphalt concrete binder course, and a 5-in. crushed aggregate base course. Lane 2 consists of a 2-in. wearing course, a 5-in. binder course, and a 12-in. base course.

Both pavements were constructed on a uniform AASHTO classification A-4(0) subgrade soil. Details concerning the design and construction of the test pavements were presented in a previous report (4).

The ALF test machine is shown in Figure 1. It simulates one-half of a dual-tire single axle with loads ranging from 9,400 lb to 22,500 lb. The test wheel assembly travels at 12.5 mph over 40 ft of pavement. To simulate highway traffic, the loads are applied in one direction and are normally distributed about a 48-in. wheelpath. The ALF requires very little power to operate because gravity is used to accelerate and decelerate the test wheel assembly. Other features include all-weather, computer-controlled operation, and transportability for field testing.

The pavement instrumentation and data acquisition system form an integral part of the PTF. The pavement instrumentation includes thermocouples and moisture cells at various depths in the pavement, strain gauges at the bottom of the asphalt concrete binder, and a device for measuring surface deflection. In addition, rut depth and slope variance are obtained with an automatic profiling device. Signals from the various pavement instruments and the automatic profiling device are directed through

signal-conditioning equipment to analog-to-digital converters mounted in a personal computer. Software was developed to collect environmental data and pavement response and performance data as part of the routine operation of the PTF. The pavement instrumentation and data acquisition system were described in detail in a previous report (*4*).

RESEARCH APPROACH

Experimental Design

The objective of this study was to measure pavement response for various combinations of load and tire pressure for two types of tires. The experiment was designed as a complete factorial with load, tire pressure, and tire type as the controlled variables. Three load levels, three tire pressures, and two tire types were used in the experiment. Table 1 summarizes the experimental design. For each experimental cell, the following data were collected:

1. Tire contact area,
2. Surface deflection,
3. Surface strain,
4. Strain at the bottom of the asphalt layer, and
5. Pavement temperature.

Details concerning each of these measurements are presented in the Data Collection section of this paper.

Test Sequence

Ideally, the experimental combinations should be tested randomly with temperature and moisture conditions constant. The amount of work and down time required to change tires and loads, however, prohibited complete randomization. Since tire pressure is easy to vary, and loads can be changed quicker than tires, the test sequence outlined in Table 1 was used. On the basis of AASHTO equivalency factors, approximately 280,000 18-kip equivalent single-axle loads (ESALs) were applied to the pavement during this study as part of the normal research program at the PTF. The tests using radial tires and the 19,000-lb load were repeated at the end of the experiment to assess the effect of accumulated damage during the experiment.

TABLE 1   EXPERIMENTAL DESIGN AND TEST SEQUENCE

Load (lb)	Radial			Bias Ply		
	76 (psi)	108 (psi)	140 (psi)	76 (psi)	108 (psi)	140 (psi)
9,400	1	3	2	18	17	16
14,100	4	6	5	13	15	14
19,000	9	7	8	11	12	10
19,000	21	19	20			

Numbers represent test sequence.

Temperature and Moisture

Pavement temperature and moisture conditions cannot be controlled at the PTF. To minimize the effects of temperature changes, all tests were conducted between 10:00 p.m. and 9:00 a.m. For the test sequence used in this study, temperature variations between tire pressures at a given load level were much smaller than temperature variations between load levels. Pavement temperatures were measured with each test to provide data for temperature adjustments. Moisture cell measurements taken during the study indicated that moisture conditions were constant.

Pavement Condition

The pavement was subjected to approximately 39,000 ESALs before this study was conducted. An additional 280,000 ESALs were applied during the study. Pavement condition monitoring before and after this study indicated little change in pavement condition during the study. Cracking of the test pavement was first observed at approximately 5 million ESALs.

DATA COLLECTION

Tire Contact Area

Two types of tires, radial and bias ply, were used in this study. The radial tires were Michelin 11 R 22.5. As purchased, the diameter of these tires was too large for use on the ALF. The tire supplier reduced the diameter by grinding, which removed most of the tread rubber. These tires have been used in normal operation of the ALF since October 1986. The bias ply tires were Kelly Springfield 10-22.5. These tires were purchased in a size compatible with the ground Michelins and were new at the time the experiment was conducted.

The tire contact areas were obtained by placing a sheet of posterboard on the pavement surface. The dual wheel assembly of the ALF was either lowered vertically or slowly rolled onto the posterboard. Paint was then sprayed around the tires to outline the contact areas. Finally, the dual wheel assembly was either raised vertically or slowly rolled off the posterboard. Rolling was used with the 19,000-lb load because this load exceeded the capacity of the lifting device used to raise and lower the wheel assembly vertically.

The contact areas were obtained from the posterboard outlines using a Talos digitizing board connected to an IBM-PC-compatible microcomputer. Each print was digitized at least three, and up to five, times to minimize deviation due to operator error. The contact areas were computed by algorithm for the individual tires in each pair. No correction was made for tread area. Figure 2 shows typical digitized traces for radial and bias ply tires.

Pavement Response Measurements

The pavement responses measured during this study were surface deflection, surface strain, and strain at the bottom of the asphalt layer. Response curves were obtained for each of the measurements by using the computer data acquisition

RADIAL

SIZE: 11R-22.5
LOAD: 9400 LB
PRESSURE: 76 PSI

BIAS PLY

SIZE: 10-22.5
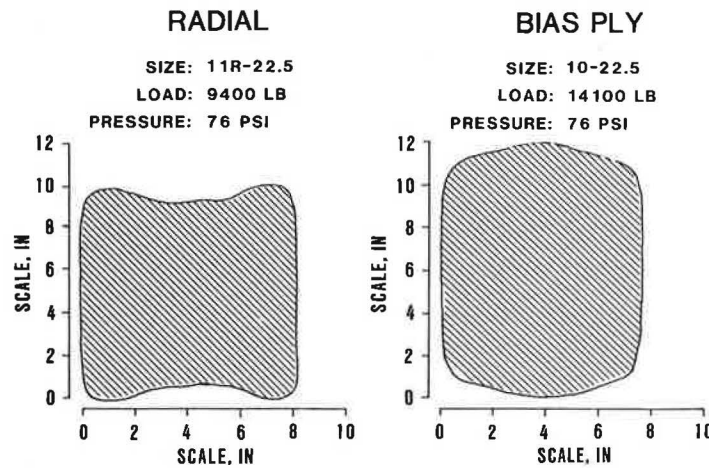LOAD: 14100 LB
PRESSURE: 76 PSI

FIGURE 2   Typical tire contact areas.

system to monitor pavement instruments as the ALF wheel assembly traversed the pavement. The distance between successive measurements of any response instrument was 3.9 in.

Figure 3 shows the location of the pavement instrumentation relative to the centerline of the test section. Pavement response measurements were made with the centerline of the ALF dual-wheel assembly at three locations relative to the centerline of the test section. These three locations correspond to offsets of 0, +14.75, and −14.75 in.

Surface Deflections

Surface deflections were measured with a linear variable differential transformer (LVDT) mounted at the midpoint of a 15-ft-long rigid reference beam. The beam was placed adjacent to the ALF wheels approximately 27 in. from the cen-

terline of the dual wheels. As shown in Figure 3, surface deflections were measured at two locations with the wheel at +14.75-in. offset and two locations with the wheel at −14.75-in. offset. The measurements at each location were repeated three times for a total of 12 measurements for each experimental cell.

Surface Strain

Surface strains were measured with 2-in. gauge-length bonded-foil-resistance strain gauges. The gauges were installed in accordance with the manufacturer's recommendations at the locations shown in Figure 3. Each strain gauge was connected in a quarter bridge configuration with one of the channels of the computer data acquisition system. No temperature-compensating gauges were installed because the strains were measured under moving wheel loads where temperature changes between unstrained and strained conditions are negligible. Although coverings were applied to protect the gauges and leadwires from moisture and mechanical damage, some of the gauges became inoperative. The failures were usually caused by broken lead wires or loose aggregate tearing the foil grid. Failed gauges were repaired or reinstalled only when the ALF was shut down for tire changes or mechanical repairs.

The surface strain gauge locations were selected to provide strain measurements outside the contact area as well as under the sidewall and center of the tire. As shown in Figure 3, surface strains were measured at five locations for each offset position. For the −14.75-in. offset position, all gauges were outside the contact area. The measurements at each location were repeated six times for a total of 18 measurements per gauge for each experimental cell.
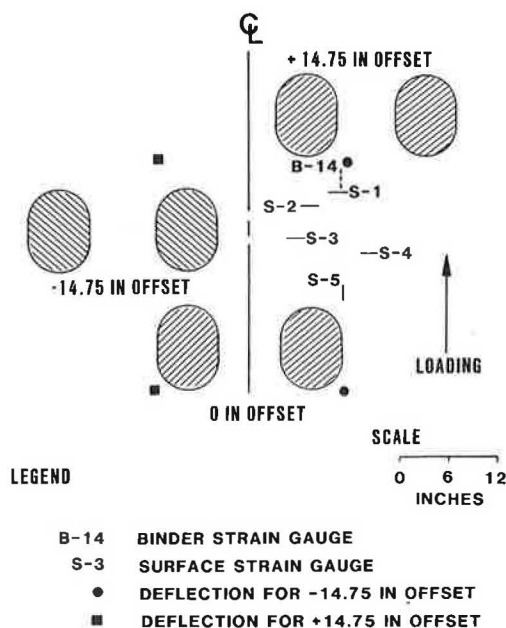
Strain at the Bottom of the Asphalt Layer

During construction, strain gauges were installed at the interface between the asphalt binder and the crushed aggregate base. These gauges were used to measure the strain at the bottom of the asphalt layer. Details concerning the installation and operation of these gauges were presented in a previous

LEGEND

B-14   BINDER STRAIN GAUGE
S-3   SURFACE STRAIN GAUGE
●   DEFLECTION FOR -14.75 IN OFFSET
■   DEFLECTION FOR +14.75 IN OFFSET

FIGURE 3   Location of pavement instrumentation.

report (*4*). Only one of these gauges was operational during this study. Figure 3 shows the location of this gauge relative to the dual wheel for each offset position. Measurements were repeated six times for a total of 18 measurements for each experimental cell.

Pavement Temperatures

For each pavement response measurement, the temperature of the asphalt layers was measured with thermocouples installed at the pavement surface and at 2-in. increments in the pavement adjacent to the response instrumentation. These temperature measurements provide a thermal profile for the asphalt layer which can be used for temperature adjustment of the pavement response measurements.

LAYER THEORY SENSITIVITY ANALYSIS

Critical Responses

For conventional flexible pavements, various researchers have identified the following critical pavement responses:

1. Surface deflection,
2. Vertical compressive stress at the pavement surface,
3. Vertical compressive stress at the top of the granular base layer,
4. Vertical compressive stress at the top of the subgrade layer, and
5. Radial tensile strain at the bottom of the asphalt layer.

The first four responses have been related to rutting whereas the fifth response has been related to fatigue cracking.

Layered-Elastic Analysis

Elastic-layer theory was used to conduct a sensitivity analysis of the critical responses of Lane 2, Section 2, to the effects of load and tire pressure. The ELSYM5 computer program was used to calculate the critical stresses and strains for each combination of load and tire pressure used in this study. Pavement responses at the locations of the field instrumentation were also calculated and will be presented with the field data in subsequent sections.

The pavement was characterized as a three-layer elastic system as outlined in Table 2. The layer thicknesses represent average values measured by differential leveling during construction of the pavement sections (*4*). The elastic moduli were selected to represent average conditions during this study and were obtained from the results of laboratory tests (*4*). The Poisson's ratios are typical assumed values. Table 3 presents the results of the sensitivity analysis for critical pavement responses at the center of one of the dual wheels. Figure 4 presents the effect of load and tire pressure on the vertical compressive stress within the pavement structure. The sensitivity analysis indicates the following concerning the effect of load and tire pressure on the pavement section for Lane 2, Section 2:

1. Between the dual wheels, contact stress has little effect on the critical pavement responses whereas load affects all critical responses.
2. Under one of the dual wheels, contact stress as well as load affects all critical responses except the vertical compressive stress at the top of the subgrade, which is affected only by load.
3. Under one of the dual wheels, the vertical compressive stresses within the asphalt layer are influenced more by contact stress than by load. This is in contrast with all other critical responses, which are affected more by load than by contact stress.

PTF TEST RESULTS

Tire Contact Areas

Most pavement response models assume a uniform circular tire, with the contact area computed as the ratio of load to inflation pressure. Figure 5 presents a comparison of measured and calculated contact areas. Differences in measured vs. computed areas varied from 12 to 58 in.[2]. Measured areas were larger than calculated areas except at the 19,000-lb load, 76-psi tire pressure. Differences increased with increasing tire pressures across all load ranges for radial as well as bias ply tires. The measured areas were not equal for the two tires. Except at the 19,000-lb load, 140-psi tire pressure, the area for the left tire was smaller than that for the right tire. This difference ranged 1 to 7 in.[2] and can be attributed to the pavement cross slope.

TABLE 2   LAYERED ELASTIC REPRESENTATION OF LANE 2, SECTION 2

Layer	Thickness (in)	Modulus (psi)	Poisson's ratio
Asphalt Concrete	6.8	180,000	0.35
Crushed Aggregate Base	11.2	20,000	0.37
Subgrade	120.0	8,000	0.45

Rigid layer assumed 138 in below pavement surface.

TABLE 3 CRITICAL PAVEMENT RESPONSES AT THE CENTER OF A WHEEL

Critical Response	9,400 lb			14,100 lb			19,000 lb		
	76 (psi)	108 (psi)	140 (psi)	76 (psi)	108 (psi)	140 (psi)	76 (psi)	108 (psi)	140 (psi)
Surface Deflection (0.001 in)	20.8	21.9	22.9	29.2	30.6	32.0	38.1	39.6	41.1
Contact Stress (psi)	-76	-108	-140	-76	-108	-140	-76	-108	-140
Vertical Stress at Top of Base (psi)	-14	-15	-16	-19	-21	-22	-24	-27	-28
Vertical Stress at Top of Subgrade (psi)	-4	-4	-4	-6	-6	-6	-8	-8	-8
Strain at the Bottom of the Asphalt Layer (Microstrain)	+299	+324	+340	+397	+440	+469	+482	+544	+588

− Denotes Compression.

+ Denotes Tension.
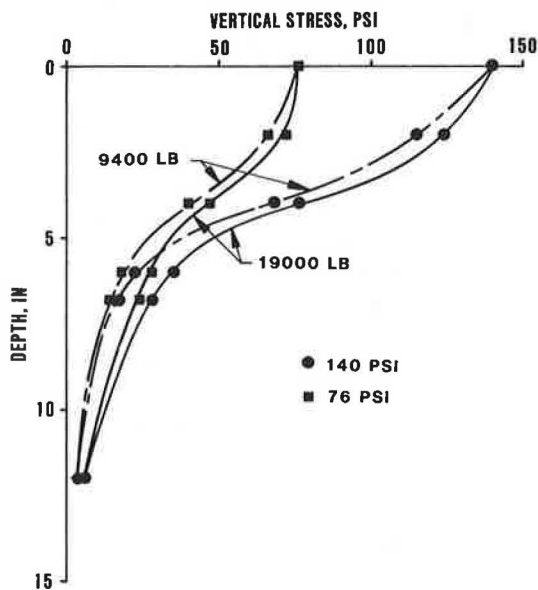
FIGURE 4 Effect of load and contact pressure on vertical stress based on ELSYM5.
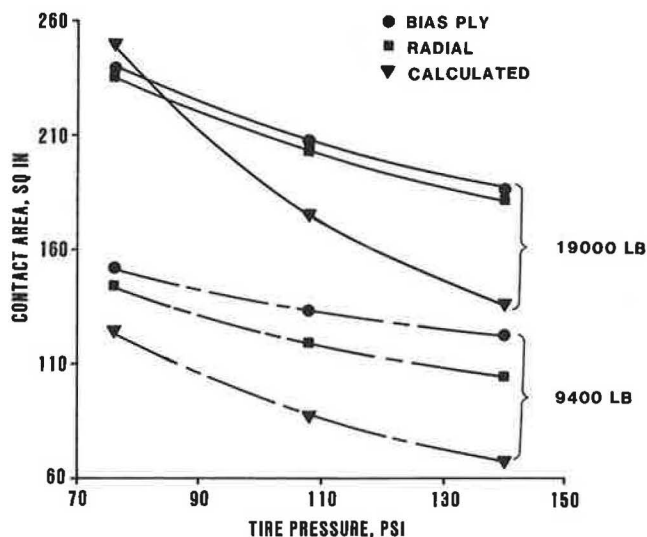
FIGURE 5 Comparison of measured and calculated tire contact areas.

ALF Loading

Figure 6 shows the ALF dual-tire trolley assembly. The load on the test wheels is applied by the addition or subtraction of the ballast weights. Each weight is approximately 2,200 lb, and the minimum weight of 9,400 lb is obtained by removing all the weights. At the minimum weight, the entire mass of the trolley is unsprung. With the addition of the first ballast weight, an air bag and shock absorber assembly is incorporated into the trolley assembly. Thus, at 19,000 lb, approximately 50 percent of the load is sprung.

The loading characteristics of ALF changed as the sprung load increased from approximately 0 to 9,000 lb. Figure 7 shows the variation of load with longitudinal distance for the three load levels used in this study. The loads were measured with load cells mounted in the trolley assembly. As can be seen in Figure 7, the ALF applied a significant dynamic load component. This dynamic load is largest at the lighter loads when most of the load is unsprung. The pavement instrumentation was located at a wheel position of approximately 160 in. At this location, the dynamic component represents approximately 10 to 20 percent of the total load.
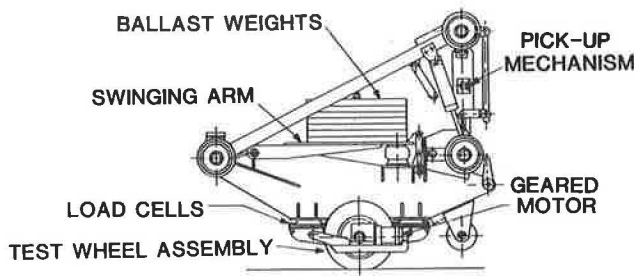
FIGURE 6 Schematic of ALF dual-wheel trolley assembly.

Pavement Response

Surface Deflection

Figure 8 presents the effect of load and tire pressure on surface deflection for radial and bias ply tires. Each data point represents the average of six tests. Theoretical pavement surface deflections from the sensitivity analysis are also shown in Figure 8.

The effects of load and tire pressure on surface deflection agree well with those predicted by layer theory. Both show the surface deflection 27 in. from the center of the dual wheels to be highly sensitive to load and insensitive to tire pressure. At 19,000 lb, the surface deflections for the radial tires are somewhat higher than those for the bias ply tires. This may be the result of differences in load or temperature that have not been accounted for in the analysis.

Surface Strain

The only surface strain gauge operational throughout this study was Gauge 4. This gauge was mounted in the transverse direction and was located between the dual wheels when the assembly was at the +14.75-in. offset. Figure 9 shows the effect of load and tire pressure on the surface strain measured by Gauge 4 for radial and bias ply tires. Each data point in that figure represents the average of six tests which have not
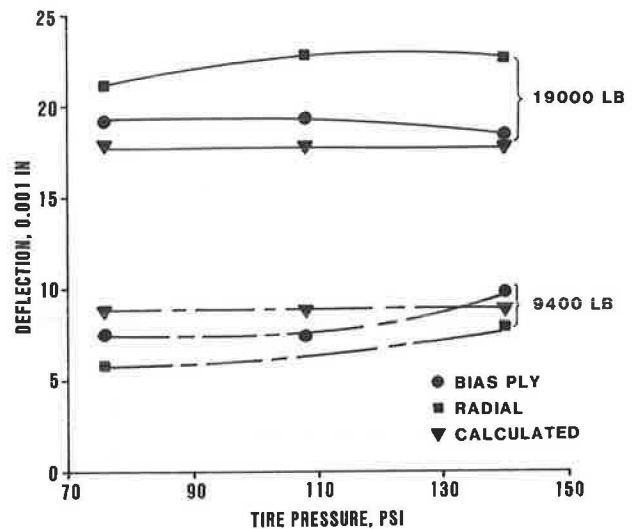
FIGURE 8 Effect of load, tire pressure, and tire type on surface deflection.

been corrected for temperature or load variations. Theoretical surface strains from the sensitivity analysis are also shown. Figure 9 presents data for the +14.75-in. offset position. Similar effects were obtained for the other offset positions.

At the instrumentation locations, the theoretical surface strains are insensitive to tire pressure and are affected only slightly by load. The measured surface strains, however, show a different pattern. They are relatively insensitive to tire pressure but highly sensitive to load. At the 19,000-lb level, the bias ply tires produce much higher surface strains than the radial tires. This effect is probably due to temperature, not tire type. The average pavement temperatures during these tests were 6°F to 10°F higher than those during the corresponding tests for radial tires. On the basis of laboratory resilient modulus data, this temperature difference would result in a 100,000-psi decrease in modulus for the asphalt layer.

At all loads and tire pressures, the measured surface strains were significantly higher than those predicted by layer theory.
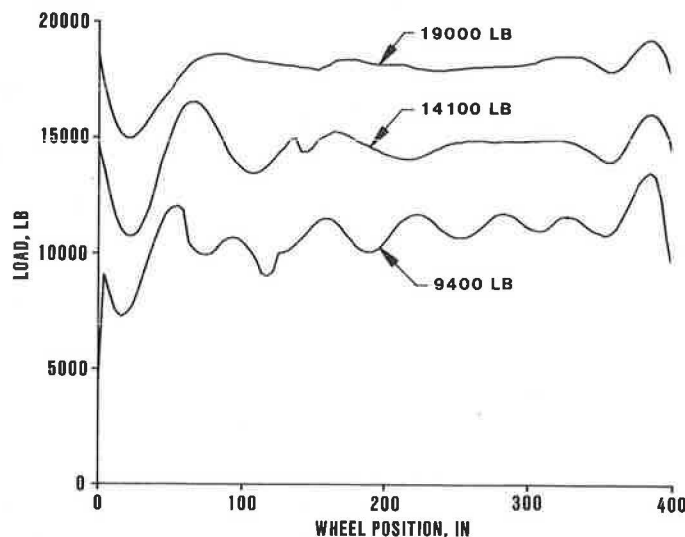

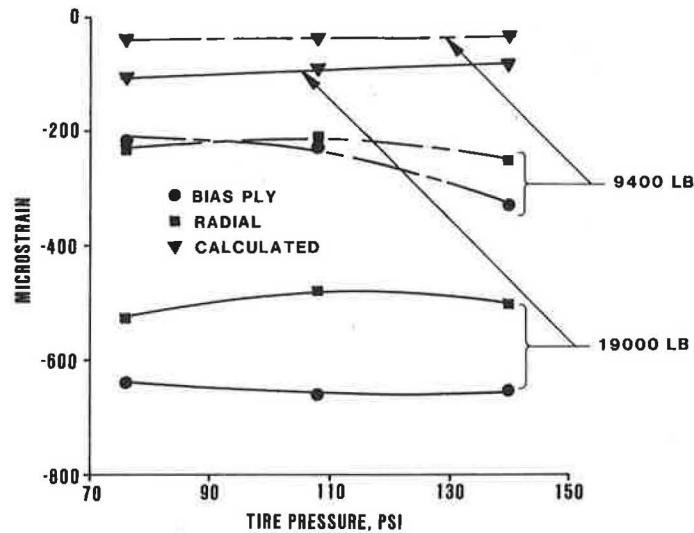FIGURE 7 Typical ALF loading at 9,400, 14,100, and 19,000 lb.

FIGURE 9 Effect of load, tire pressure, and tire type on transverse surface strain.

This may be the result of horizontal tire forces induced at the surface of the pavement which are not accounted for in the layered-elastic analysis.

Strain at the Bottom of the Asphalt Layer

Figure 10 shows the effect of load and tire pressure on the strain at the bottom of the asphalt layer for radial and bias ply tires. Each data point in this figure represents the average of six tests which have not been corrected for temperature or load variations. Theoretical strains from the sensitivity analysis are also shown. The tests for the radial tires at 19,000 lb were repeated to assess the effect of accumulated damage during the study. The repeat test showed good agreement with the original tests, indicating that significant pavement damage did not occur during this study. Figure 10 presents

data for the +14.75-in. offset position. Similar effects were obtained for the other offset positions.

The effects of load and tire pressure agree well with those predicted by layer theory. Both show the strain at the bottom of the asphalt layer to be highly sensitive to load and slightly sensitive to tire pressure. At 19,000 lb, the bias ply tires produce much higher strains at the bottom of the asphalt layer than the radial tires. Again, this effect is probably due to temperature as described in the previous section for surface strains.

ANALYSIS

Fatigue Life

The strains at the bottom of the asphalt layer can be used to assess the relative effects of load, tire pressure, and tire type
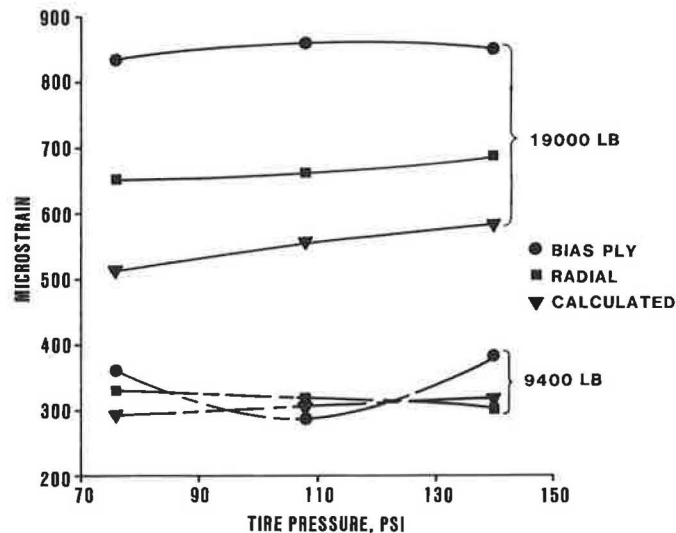

FIGURE 10 Effect of load, tire pressure, and tire type on longitudinal strain at the bottom of the asphalt layer.

on fatigue cracking for Lane 2, Section 2. Fatigue equivalency factors may be developed for each combination used in this study. By definition, an equivalency factor is the damage produced by one pass of any load configuration divided by the damage produced by one pass of a standard load configuration. Using Miner's law, the damage caused by one pass is the reciprocal of the fatigue life. Equation 1 is a mathematical expression for the fatigue equivalency factor:

$$F = N_f(\text{Std})/N_f(\text{Any}) \qquad (1)$$

where

$$\begin{aligned}
F &= \text{fatigue equivalency factor,} \\
N_f(\text{Any}) &= \text{fatigue life for any load configuration, and} \\
N_f(\text{Std}) &= \text{fatigue life for the standard load configuration.}
\end{aligned}$$

Finn et al. (5) presented the following distress prediction model for fatigue cracking:

$$N_f = K_1(1/e_t)^{3.291} (1/E^*)^{0.854} \qquad (2)$$

where

$$\begin{aligned}
N_f &= \text{fatigue life,} \\
e_t &= \text{tensile strain at the bottom of the asphalt layer, and} \\
E^* &= \text{dynamic modulus, and} \\
K_1 &= \text{constant.}
\end{aligned}$$

This model is based on laboratory fatigue curves and may be adjusted to correlate with field observations by changing K_1. Using the above model, the fatigue equivalency factor may be expressed as

$$F = \left[\frac{e_t(\text{Any})}{e_t(\text{Std})}\right]^{3.291} \left[\frac{E^*(\text{Any})}{E^*(\text{Std})}\right]^{0.854} \qquad (3)$$

where

$$\begin{aligned}
e_t(\text{Any}) &= \text{tensile strain at the bottom of the asphalt layer} \\
&\quad \text{for any load configuration,} \\
e_t(\text{Std}) &= \text{tensile strain at the bottom of the asphalt layer} \\
&\quad \text{for the standard load configuration,} \\
E^*(\text{Any}) &= \text{dynamic modulus at the temperature for} \\
&\quad e_t(\text{Any}), \text{ and} \\
E^*(\text{Std}) &= \text{dynamic modulus at the temperature for } e_t(\text{Std}).
\end{aligned}$$

The second term in Equation 3 may be used to adjust for temperature differences.

Table 4 presents the fatigue equivalency factors for each load-tire pressure combination using bias ply tires with 9,400-lb load and 76-psi tire pressure as the standard configuration,

TABLE 5 FATIGUE EQUIVALENCY FACTORS FROM THEORETICAL STRAINS USING 9,400 lb, 76 psi AS STANDARD

Load (lb)	76 (psi)	108 (psi)	140 (psi)
9,000	1.0	1.2	1.2
9,400	1.1	1.3	1.4
10,000	1.4	1.6	1.7
11,000	1.8	2.1	2.3
14,100	3.4	4.2	4.7
19,000	7.2	9.4	10.9

and 82°F as the standard temperature. Similar fatigue equivalency factors were developed from the theoretical strains and are presented in Tables 5 and 6. Although the fatigue equivalency factors developed from measured strain data exhibit some inconsistencies, the overall trends show a large effect due to load and a smaller effect due to tire pressure. In addition, the factors based on measured strains agree well with those based on theoretical strains.

The fatigue equivalency factors presented here are specific to the ALF loading, the pavement section studied, the environmental conditions during the field testing, and the assumed fatigue model. More general factors, however, could be developed and used to assess the effects of changing truck characteristics on pavement fatigue life.

Rutting

A similar analysis for rutting could not be conducted because the pavement responses measured in this study are not direct inputs to current rutting models. In addition, the rutting phenomenon is much more complex and may occur in any layer of the pavement structure. The trends shown in the sensitivity analysis, however, may be used to qualitatively discuss the effects of load and tire pressure on rutting for Lane 2, Section 2.

The location in the pavement structure where rutting will occur is a function of the vertical compressive stress and the resistance of each layer to permanent deformation. The sen-

TABLE 4 FATIGUE EQUIVALENCY FACTORS FROM MEASURED STRAINS USING BIAS PLY TIRES AT 9,400 lb, 76 psi AS STANDARD

Load (lb)	76 psi		108 psi		140 psi	
	Radial	Bias Ply	Radial	Bias Ply	Radial	Bias Ply
9,400	0.8	1.0	0.6	0.5	0.6	1.2
14,100	4.3	5.0	4.3	6.1	6.2	7.3
19,000	10.3	11.1	10.8	12.3	12.2	11.9

TABLE 6 FATIGUE EQUIVALENCY FACTORS FROM THEORETICAL STRAINS USING 9,000 lb, 76 psi AS STANDARD

Load (lb)	76 (psi)	108 (psi)	140 (psi)
9,400	1.0	1.2	1.3
10,000	1.2	1.4	1.5
11,000	1.5	1.8	2.0
14,100	3.1	3.7	4.1
19,000	6.4	8.3	9.6

sitivity analysis of Lane 2, Section 2, indicated that load influences the vertical compressive stress in the base and subgrade layers more than tire pressure. Conversely, in the asphalt layer, tire pressure has the greatest effect on vertical compressive stress. Therefore, for Lane 2, Section 2, rutting that occurs in the asphalt layer would be accelerated by high tire pressures.

Lane 2, Section 3, at the PTF has the same cross-section as Lane 2, Section 2, and was trafficked to failure with a 19,000-lb load and 100-psi tire pressure. This section was tested from January to June 1987 when the pavement temperature was low. Rutting was the major form of distress observed, with rut depths averaging 0.75 in. at failure. A post mortem evaluation was conducted to assess the amount of rutting attributable to each layer. This evaluation concluded that the majority of the rutting occurred in the crushed aggregate base layer (*6*).

Thus, the crushed aggregate base layer appears to have the critical combination of stress and rutting resistance for Lane 2 at the PTF. On the basis of the sensitivity analysis, tire pressure has little effect on rutting in this layer.

FINDINGS AND CONCLUSIONS

In recent years, the effect of increased truck tire pressures on flexible pavement performance has become a subject of great concern. Decreased fatigue life, increased rutting, and accelerated serviceability loss have been attributed to the effects of increased tire pressure.

This study investigated these concerns by using the Federal Highway Administration Accelerated Loading Facility to measure the effects of load, tire pressure, and tire type on the response of a flexible pavement. Although the findings and conclusions presented below are specific to the ALF loading, the pavement section studied and the environmental conditions during the testing, they provide valuable information concerning the combined effects of load and tire pressure.

Findings

The following is a summary of the findings of this study:

1. The measured tire contact areas were significantly larger than contact areas calculated as the ratio of load to tire pressure, except at high loads and low tire pressure.

2. The measured pavement responses—surface deflection, surface strain, and strain at the bottom of the asphalt layer—were affected by load as well as tire pressure. For the loads and tire pressures used in this study, load had a greater effect than tire pressure.

3. Although layer theory underestimated many of the measured pavement responses, the measured effects of load and tire pressure were in general agreement with those predicted by layer theory.

4. For tests conducted at approximately the same temperature, the measured pavement responses were similar for radial and bias ply tires.

Conclusions

Specific conclusions concerning the relative effects of load, tire pressure, and tire type on rutting and serviceability loss could not be drawn from the data presented in this paper. The measured pavement responses were not indicators of rutting potential, and an evaluation of serviceability loss requires performance data under each combination of load, tire pressure, and tire type.

The relative effects of load and tire pressure on pavement fatigue can be investigated using fatigue equivalency factors which account for load as well as tire pressure. Such factors were developed in this study using an exponential relationship between the number of cycles to failure and the magnitude of the tensile strain at the bottom of the asphalt layer. Since this strain was affected more by load than by tire pressure, the equivalency factors are influenced more by load. Doubling the load (from 9,400 to 19,000 lb) increased predicted damage 1,000 percent, whereas doubling the tire pressure from 76 to 140 psi increased predicted damage only 20 percent. From these fatigue factors, it is concluded that for the pavement section studied, the effect of increasing tire pressure from 76 to 140 psi is equivalent to an axle load increase of approximately 2,000 lbs. This equivalency is valid for radial and bias ply tires.

REFERENCES

1. K. M. Marshek, H. H. Chen, R. B. Connell, and C. L. Saraf. Effects of Truck Tire Inflation Pressure and Axle Load on Flexible and Rigid Pavement Performance. *Transportation Research Record 1070.* TRB, National Research Council, Washington, D.C., 1986, pp. 14–21.
2. H. F. Southgate and R. L. Dean. *Effects of Load Distributions and Axle and Tire Configurations on Pavement Fatigue.* Research Report UKTRP-85-13. Kentucky Transportation Research Program, University of Kentucky, Lexington, 1985.

3. F. L. Roberts, J. T. Tielking, D. Middleton, R. L. Lytton, and K. Tseng. *Effects of Tire Pressure on Flexible Pavements*. Research Report 372-1F, Texas Transportation Institute, Texas A&M University, College Station, 1986.
4. D. A. Anderson, W. P. Kilareski, and Z. Suddiqui. *Pavement Testing Facility—Design and Construction*. Report FHWA/RD-88/059. FHWA, U.S. Department of Transportation, Washington, D.C., 1987.
5. F. Finn, C. L. Saraf, R. Kulkarni, K. Nair, W. Smith, and A. Abdullah. *NCHRP Report 291: Development of Pavement Structural Subsystems*. TRB, National Research Council, Washington, D.C., 1986.
6. D. A. Anderson, P. Sebally, and N. Tabatae. *Pavement Testing Facility—Performance of Initial Two Test Sections*. Report FHWA/RD-88/060. FHWA, U.S. Department of Transportation, Washington, D.C., 1987.

Field Evaluation of Thermal Deformations in Undoweled PCC Pavement Slabs

M. Poblete, R. Salsilli, R. Valenzuela, A. Bull, and P. Spratz

This paper presents some of the results obtained in extensive research of the Chilean in-service network of PCC paved roads, in which measurements have been conducted in 21 test sections covering various conditions of climate, pavement structure, and age. In test slabs, simultaneous measurements were made of internal temperatures and absolute vertical displacements of slabs, as well as openings of transverse joints and faultings. The results show a "permanent" upward curling of slabs in all pavements sections included in the study, as modified by daily temperature variations. The curling is demonstrated in the field by the perceptible rocking of the slabs under the early morning traffic and by the systematic transverse cracking and corner breaks of some rather new pavements with no signs of pumping. Cracking seems to start from the surface downward and from the edges inward. Detailed evaluation of the internal stresses with the superimposed nonlinear effects of environmental and wheel loads, calibrated with these results, is under way.

About one-third of Chile's 6,700-km network of paved roads are Portland cement concrete, located mainly in the central and southern regions and carrying the heaviest traffic, especially along the Pan-American Highway.

Toward the end of the 1970s, an extensive reconstruction program of the most deteriorated sections of the network was started by the Highway Division of the Chilean Ministry of Public Works, and it is now almost complete. In order to define maintenance policies for these sections, a Maintenance Management System is being implemented (*1*). To this end, the Highway Division assigned the Universidad de Chile to model the structural deterioration of concrete pavements, which had been designed and constructed under general AASHTO guides and specifications. Therefore, monitoring the pavement for the effects of climate, traffic, and subgrade support was considered (*2*). Development and calibration of the predictive analytical model required implementation of survey and measurement methodologies which are now performed periodically at 21 locations along the concrete pavement network. In addition, these local surveys and measurements are expected to facilitate the calibration of mechanized equipment, such as a Lacroix-type deflectometer and a profilometer, which are used extensively by the Highway Division.

Ambient temperatures in the concrete paved roads are mild, with no big differences along the instrumented sections, and are free of frost conditions affecting the soil. Figure 1 shows

M. Poblete, R. Salsilli, and R. Valenzuela, Instituto de Investigaciones y Ensayes de Materiales (IDIEM), Universidad de Chile, Casilla 1420, Santiago, Chile. A. Bull and P. Spratz, Direccion de Vialidad, Ministerio de Obras Publicas, Casilla 72, Santiago, Chile

the number of days with heavy rains (>5 mm/24 hr) increasing southward (*3*), from an average of less than 15 days in test section 1 to more than 120 in test section 21, mostly during the winter. Consequently, ambient humidity is far from saturation during the rest of the year, with strong hydro-evaporation conditions predominating.

After 3 years of periodic monitoring, local surveys and measurements have shown that an upward curling of the slabs prevails during most of the daily thermal cycle; part of this deformation is permanent, but the remainder varies daily in accordance with changes in the thermal condition. Identical effects have been reported from California by Hveem (*4*), Tremper and Spellman (*5*), and others. This condition of partial support exhibited by deformed slabs accelerates concrete fatigue, thus reducing the number of theoretically allowed loading cycles. Cracking occurring before the third year of service in some pavements subjected to heavy traffic could be explained by these findings.

In order to consider these effects in predictive deterioration models, calculations are in progress to evaluate internal stresses through finite-element techniques, fitting the measured deformations with those computed under equivalent conditions of edge restraints, support, and loading. This work constitutes the follow-up step of the research program and will be the subject of future research.

FIELD MEASUREMENTS AND RESULTS

Along the heavily trafficked central-south regions of Chile (shown in Figure 1), 21 test sections (TS) were selected to be monitored for the effects of weather conditions, pavement aging, and slab support stiffnesses. In Table 1, location and pavement structural characteristics for the 21 test sections are shown. The instrumentation designed and installed in each of the 21 test sections (*6*) allows the measurement of internal temperatures and absolute vertical displacements of slabs, as well as openings of transverse joints and faultings, using the elements shown in Figure 2. For deep reference bases (DRB), drilling was performed using percussion-rotation and compressed air, to cause the least alteration to subgrade soils; likewise, borehole reconstruction was performed to reproduce pavement conditions as closely as possible.

The diagram shown in Figure 3 illustrates the analog-digital data acquisition system used for the simultaneous measurement of temperatures, thermal displacements, and load deflections; values are processed in-situ by a portable PC. Signal monitoring allows qualification of the results, recording of results for further analysis, or repeating of measurements.
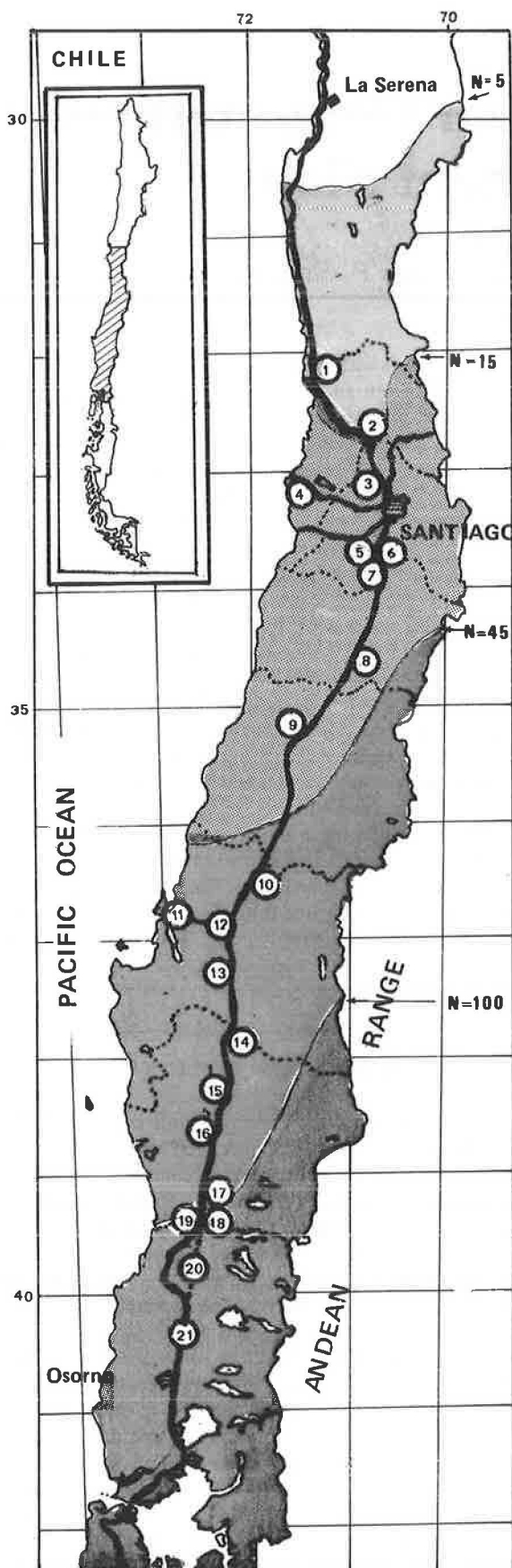
FIGURE 1 Map of test sections and days per year (N) of heavy rainfall.

Once a measurement cycle has been completed, instruments, cables, and connectors are taken to the next test section, leaving only the reference bases in place with the LVDT housings enclosed by lids mounted flush with the pavement.

The data presented herein were gathered during summer 1986, winter 1986, and summer 1987, over a continuous 24-hr cycle. Accuracy of the measurements by their frequency is shown in Table 2.

Typical internal slab temperatures, recorded during 24 hr on a sunny summer day, are plotted in Figure 4 by depth of measurement. Minimum mean temperature occurs early in the morning, whereas maximum mean temperature occurs typically between 3 p.m. and 5 p.m. The temperature range on the slab surface becomes 4 times higher than the temperature range at the slab bottom, and the temperature distribution never becomes linear with depth or constant in slab thickness.

Therefore, thermal gradients exist within the slab during the 24-hr period. Negative gradients—when the slab surface is cooler than the bottom—tend to predominate from late afternoon to late morning through the night (Fig. 4) and during the whole year. Accumulated hours at various thermal gradients are presented in Figure 5; the histogram is the result of semiempirical modeling calibrated through actual field measurements (7). Positive gradients, though higher in absolute value, exist for only a few hours on a sunny summer day.

As a consequence of daily variations in thermal gradients, pavement slabs undergo continuous deformations, as may be derived from the isograms in Figure 6, which were obtained on a summer day in 1985 by precise measurements (to ±0.01 mm) of nine topographical reference bases installed in a slab. These isograms show the upward concave shape of the slab for the early morning negative gradient (Figure 7a), and a nearly cylindrical shape of longitudinal axis during the afternoon hours with positive gradient and high mean temperature, when the rotation of the slab's transverse edges is prevented by the locked joints (Figure 7c). Such behavior is typical and was observed in all instances of high mean temperatures. Rotation is not prevented at the longitudinal joint where two slabs belonging to adjacent lanes and paved at different dates are linked together through steel tie bars.

Horizontal slab movements measured at transverse joints near the slab outer edge are shown in Figure 8, for five moments of a complete cycle during a sunny summer day. Sections remain plane at all times, but rotate with the gradient. With negative gradients the joint can be completely open if the mean temperature is low enough, whereas the bottom edges can be compressed if the mean temperature is high. For positive gradients and high enough mean temperatures, the joint can close, thus preventing any rotation (locked joints).

On cloudy winter days the temperatures are low and very stable, as are the gradients, and hence the edges do not rotate significantly. However, the joints stay open and there is little or no compression at the lower edges. Note that the absolute value of joint openings at given temperatures is not equal for all pavements, but depends on conditions such as the level of maximum temperature in the fresh concrete, drying shrinkage (5), or swelling due to seasonal moisture absorption (8).

Figure 9 illustrates joint opening variation in the mean plane, divided by the mean length of the slabs adjacent to the instrumented joint. A linear relationship with the mean temperature for winter and summer was obtained. On sunny summer

TABLE 1 LOCATION AND STRUCTURAL CHARACTERISTICS OF TEST SECTIONS

Number	Latitude South		Longitude West		Slab construction Season 'Year	Pavement Thickness (m)	Joint Spacing (m)	Edge Drain	Base	Infrastructure Sub Base	Sub Grade (USCS)	Water T. Depth (m)
01	32°	22'	71°	21'	Spr'83	0.23	3.7 - 4.6	Y	CTB	AC*	ML	---
02	32°	52'	70°	49'	Spr'81	0.23	4.5 - 5.4	N	CTB	PCC*	CL	---
03	33°	13'	70°	44'	Win'84	0.24	3.4 - 3.6	Y	CSB	PCC	CH	3.4
04	33°	15'	71°	23'	Sum'85	0.26	3.4 - 3.6	Y	CSB	GRM	SM	3.0
05	33°	40'	70°	55'	Spr'75	0.22	3.4 - 5.4	N	GRB	GRM	GC	---
06	33°	48'	70°	45'	Aut'83	0.24	4.2 - 4.6	N	GRB	AC	SP	---
07	34°	04'	70°	42'	Aut'83	0.25	3.6 - 4.6	N	GRB	PCC	GP	---
08	34°	34'	70°	58'	Sum'83	0.23	3.7 - 4.3	N	CTB	PCC	SM	---
09	35°	21'	71°	31'	Aut'83	0.23	3.7 - 4.6	Y	CTB	AC	SM	---
10	36°	32'	72°	04'	Aut'82	0.21	4.5 - 4.6	N	GRB	PCC	GP	2.0
11	36°	49'	73°	01'	Spr'84	0.23	3.5	Y	CTB	AC	ML	---
12	37°	02'	72°	26'	Aut'84	0.22	3.5 - 3.6	Y	CSB	PCC	SC	2.6
13	37°	10'	72°	24'	Win'82	0.21	4.4 - 4.6	N	CTB	PCC	SP	2.5
14	37°	50'	72°	02'	Aut'79	0.21	4.3 - 4.8	N	CTB	PCC	SM	---
15	38°	14'	72°	22'	Aut'84	0.23	4.0	Y	CSB	PCC	ML	---
16	38°	46'	72°	34'	Aut'81	0.21	4.4 - 4.6	N	CTB	PCC	CL	---
17	39°	07'	72°	41'	Aut'83	0.22	4.5	Y	GRB	GRM	GM	3.0
18	39°	22'	72°	38'	Spr'84	0.22	3.8 - 4.3	Y	CTB	GRM	CL	---
19	39°	33'	72°	56'	Aut'83	0.23	4.4 - 5.0	N	CTB	PCC	ML	---
20	39°	40'	72°	56'	Spr'83	0.23	4.3 - 4.6	N	GRB	GRM	GM	2.0
21	40°	02'	72°	58'	Sum'83	0.22	4.5	N	CTB	PCC	ML	1.5

*Old "AC" or "PCC" pavements overlayed with "PCC".

days, when slab temperature increases sufficiently and the lower edges of the slabs come into contact, compression builds up, and the openings decrease nonlinearly until the joints are completely locked. The experimental straight lines obtained for a given test section with mean temperatures below the locking temperature have equal slopes of

$$\alpha = 1.14 \times 10^{-5} \ (°C)^{-1}$$

This value is very close to the thermal expansion coefficient of concrete, determined in the laboratory under free-expansion conditions, and is among the largest values reported in the literature (9) for siliceous high-hardness aggregates, which are predominant in Chile. Hence, the eventual restrictions of slab expansion in the field, due to friction between the base and the contact area whose magnitude depends on the degree of upward curling, appear to be of minor significance in this case. When comparing the data obtained at different dates and therefore under different pavement moisture conditions, the vertical distance between the winter line and the summer line, considered as a dry reference state, would represent the swelling of concrete. This behavior was observed in all 21 test sections (10).

The vertical movements of two typical pavement slabs, obtained from points DRB 2, 3, 4, and 5, are shown in the upper part of each graph illustrated in Figures 10 and 11, with ordinates that are increasing upward and refer to the smallest value for the corresponding day. The curves represented in the lower part of each graph, with ordinates that are increasing downward, correspond to the maximum deflection under the slow-moving load of an 81-kN axle, measured at the same four points of the slab. To better assess the evolution of thermal conditions throughout the day, the gradient and the mean temperature have been superimposed in graphs DRB 4 and DRB 5, respectively. This allows observation of the following details:

• Vertical movements of slab corners and edges (DRB points 2, 5, and 3) oscillating all day following thermal gradient variation become minimal when this gradient becomes maximum or positive. When the gradient is negative, the corners and edges stay uplifted and the slab then presents a perceptible upward curling that matches the previous results obtained from topographical levelings.

• The slab remains curled upward when the thermal gradient becomes null, as was observed at 10 a.m. (warming) of the summer day cycle (Figure 10).

• Behavior of the central point, DRB 4, is always contrary to the behavior of the corners and the edges. Therefore, when
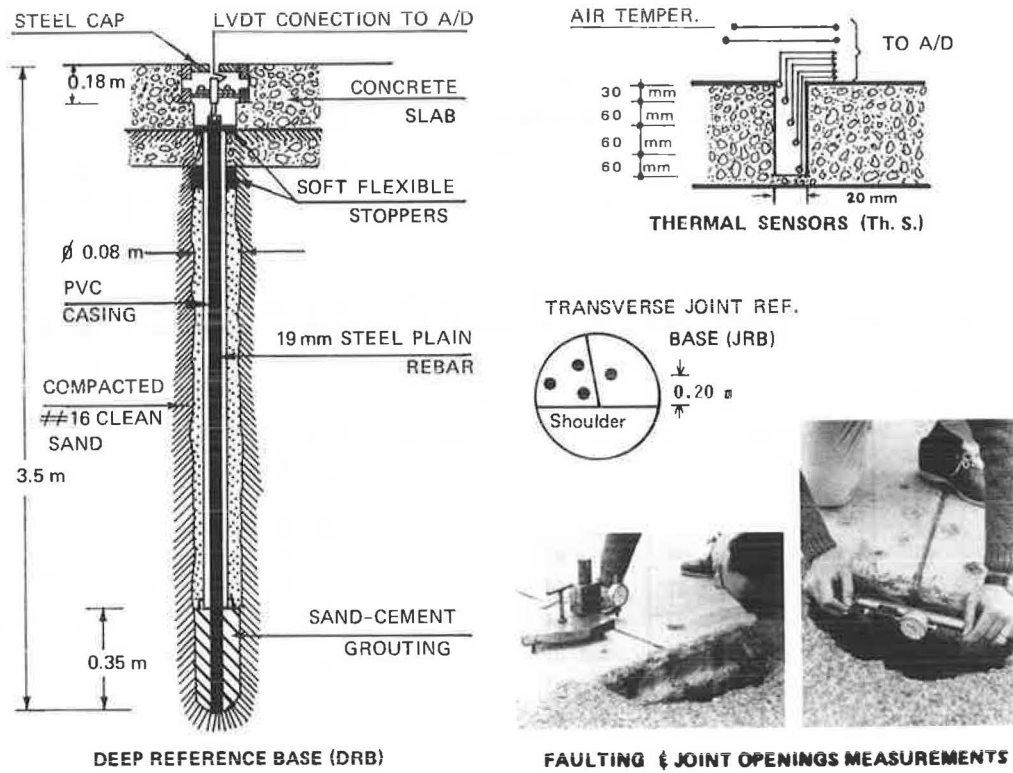
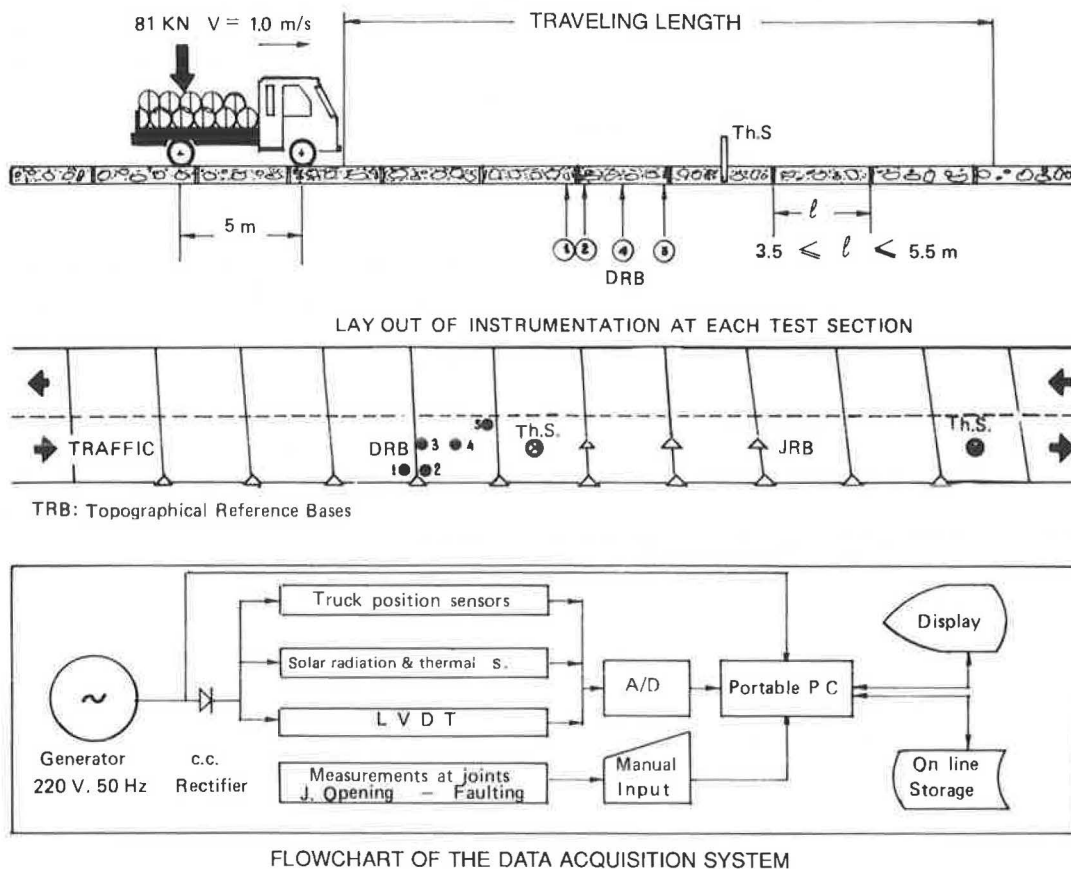**FIGURE 2** Instrumentation devices in the test sections.

FIGURE 3 Schematic layout of instrumentation used.

TABLE 2 LIST OF MEASUREMENTS CARRIED OUT IN ALL TEST SECTIONS

Measure	Accuracy	Frecuency
Temperatures	± 0.20 °C	every 5 min
Displacements	± 0.01 mm	every 5 min
Deflections	± 0.01 mm	every 1 hour
J. Openings	± 0.05 mm	every 2 hour
Faultings	± 0.10 mm	once a day

FIGURE 5 Histogram of modeled thermal gradients for typical test sections.

corners and edges are supported, due to some strong positive gradient, the slab center rises; so does DRB point 3 in some cases, causing the nearly cylindrical shape illustrated in Figure 7c.

• Maximum deflections under load, determined at DRB points 2, 5, and 3, show a behavior that is very similar to that due to thermal gradient, and there is a proportionality between the magnitudes of deflection and edge lifting.

• Deflections in winter may not at any time during the day reach such low values as may be derived from Figure 11. This would indicate that the condition of partial support at the center of the slab may last the whole day, as it occurred in the case presented here.

The deformation at the corner point DRB 1 of the adjoining slab is similar to the behavior at point DRB 2, though generally of different magnitude, as it appears from Table 3, which summarizes all data obtained for the 21 test sections. To analyze this apparent anomaly in homogeneous pavement sections, deformations were normalized by using a standard orthogonal 3.50-m × 4.50-m slab as a reference. In Figure

12, all pairs of points DRB 1 to DRB 2 of normalized maximum deformations are plotted against each other. Having eliminated the geometric difference for every deformation, the discrepancy that still persists has to be explained by the interlock created in the joint crack with some preferential inclination to one side.

A different behavior is observed at the opposite corner in the same slab. Figure 13 shows the marked symmetry that exists in the upliftings of points DRB 2 and 5 in opposite corners, thus illustrating the reduced restriction imposed by the tie bars built in the longitudinal construction joints between two-lane pavements. In the special case of four-lane dual-carriage ways represented by test sections 2 and 11, some rocking of the instrumented outer lane would be produced by the central lane during intense cooling after a hot summer day.
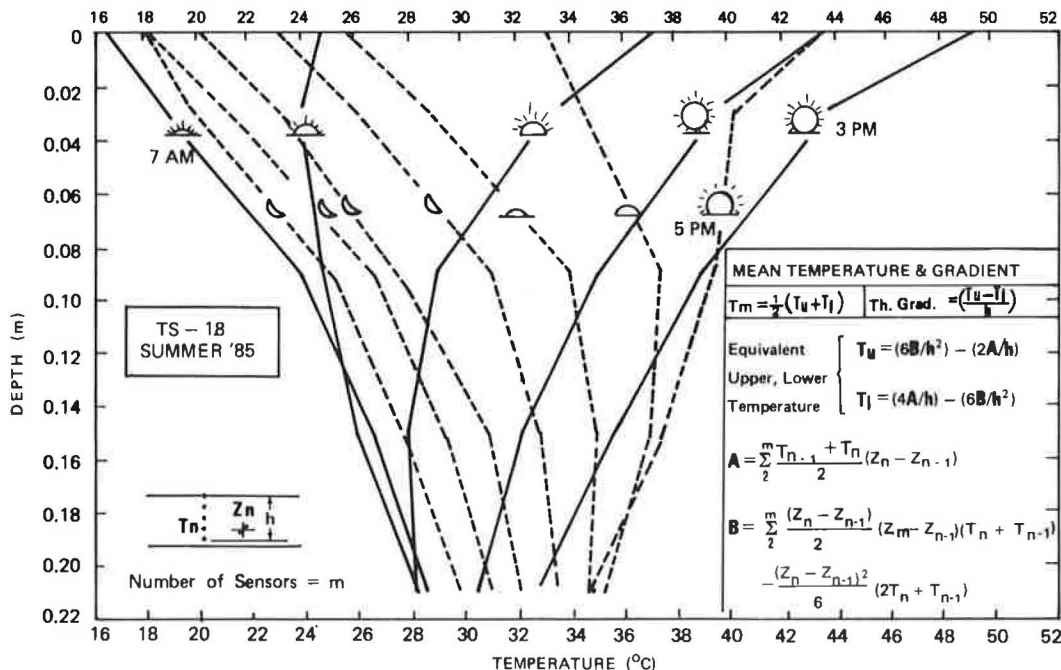

FIGURE 4 Internal temperature distribution every 2 hr during a measurement cycle.
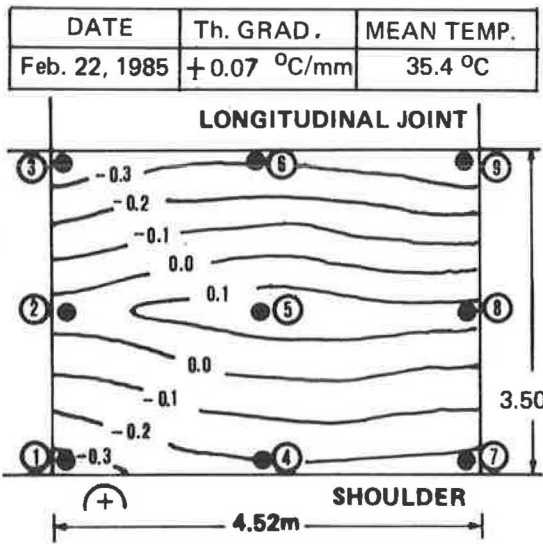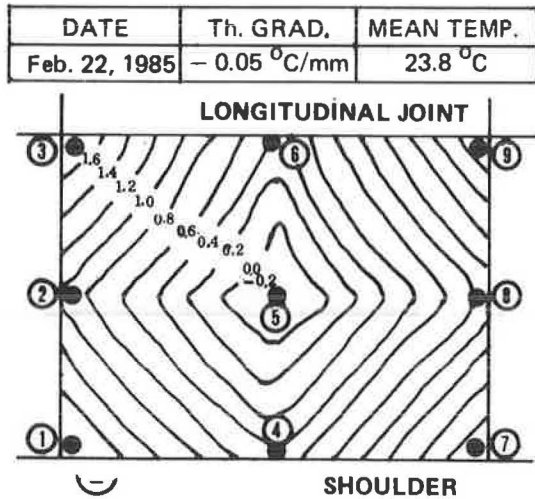
DATE	Th. GRAD.	MEAN TEMP.
Feb. 22, 1985	− 0.05 °C/mm	23.8 °C

FIGURE 6 Isograms of a typical slab deformed by temperature (°C/mm).

DATE	Th. GRAD.	MEAN TEMP.
Feb. 22, 1985	+ 0.07 °C/mm	35.4 °C

FIGURE 7 Typical shapes of slabs deformed by temperature.

From Table 3 it can also be seen that the upward-curling deformation occurs with greater or less significance in all pavements, and it occurs in the south at magnitudes similar to those in the north, in spite of climatic differences. Furthermore, the duration of this phenomenon covers the main part of the day, at least 14 hr in summer and the whole day during winter.

Figures 14, 15, and 16 show the relationships between slab deformation and thermal gradients for different geographical locations, as well as relationships with pavement age and base types. The behavior of the corners and of the whole transverse edge during the morning warming is different than the behavior during the evening cooling. This is due to the lower rotation restriction existing at joints when they stay more open (low mean temperature in the early morning). As surface temperature increases, the slab edges go down, and the joints get compressed and tend to lock up. In the afternoon, surface cooling reverses the process, but in a different way because
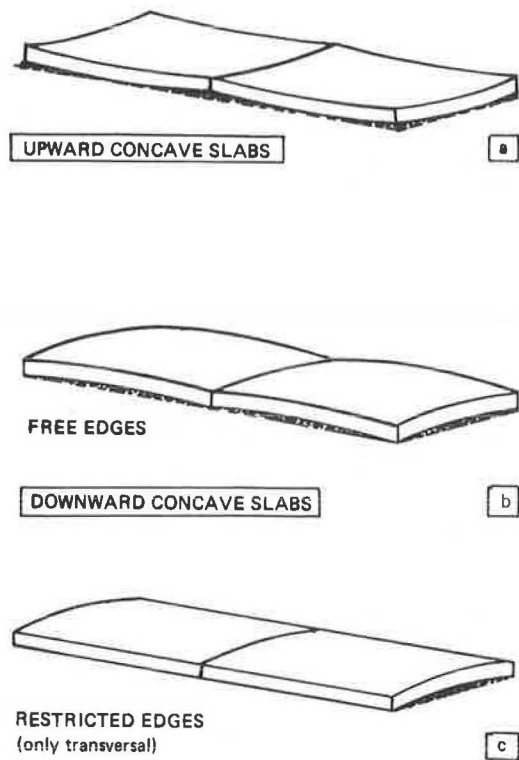
the thermal inertia of concrete causes a very slow decompression in the slabs. In this case, the upward curling remains restricted while the gradient is decreasing. This phenomenon occurs in the three cases with respect to summer and is representative of all 21 test sections (10). In winter, owing to low mean temperatures, the open joints do not restrict the deformation; therefore both branches tend to coincide on a single straight line.

Furthermore, from Figures 14 and 15, it may be seen that the slabs require a certain positive gradient in order to reach the condition of full support. This would prove the existence of a thermal-independent cause of upward curling. Its origin could be the moisture differential through the slab thickness, since the upper portion is nearly always drier than the bottom. On the other hand, excessively high fresh concrete temperatures that are frequent on hot summer days undoubtedly contribute to a larger shrinkage and to more open joints. Consequently there is less restriction on the slabs' transverse edges and greater freedom to rotate and to uplift, regardless of the thermal gradients. Similar effects are clearly experienced early each autumn when the pavement reaches its maximum dryness.

This upward curling was also found in an older pavement, but as shown in Figure 16, it is almost negligible when compared to the other ones. The difference is assumed to be related in some way to the modern use of membrane-forming curing compounds under prevailing environmental conditions of high evaporation, as compared with the old practice of polyethylene film coverings or dikes for pond curing wherein temperature can be regulated (9).
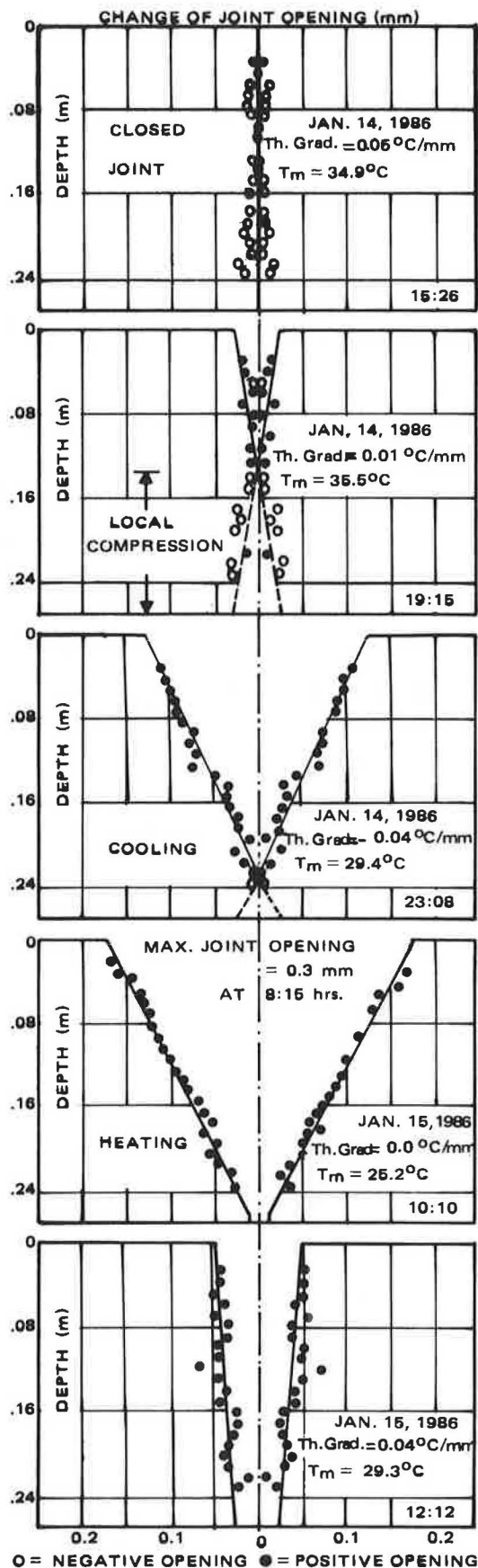
FIGURE 8 Movement pattern of a joint during a
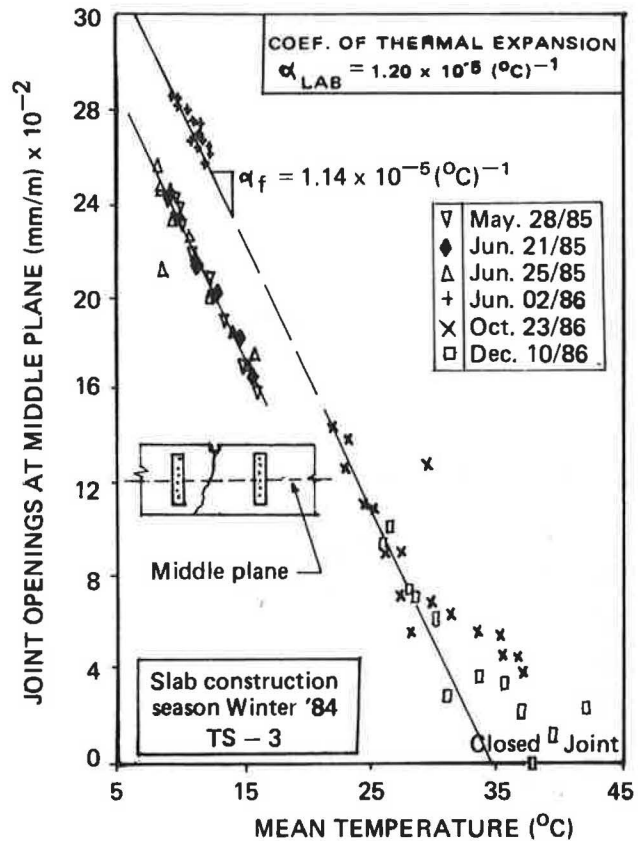24-hr cycle, measured by outer edge.

FIGURE 9 Longitudinal thermal deformation of a typical
PCC pavement measured at joints.

CONCLUSIONS

The instrumentation as well as the measurement methodology presented herein have proven to be efficient for quantifying, with a high degree of accuracy and repeatability, the absolute movements and deformations that can occur in concrete pavement slabs.

In all the pavement sections included in this study, the generalized prevailing upward curling of the slabs, causing considerable lack of support at slab edges, has been verified. This condition is reversed only during the hours of high solar radiation.

In order to obtain the effective support of slab edges, a significant positive thermal gradient has to be generated in the concrete slab to overcome a "permanent" upward curling that occurs independently of the thermal one.

Under conditions where positive gradients are higher than the "support initiation gradient," the slabs normally are expanded and rotation at their transverse edges is restricted (Figure 7c); thus a cylindrical shape is imposed on the slab with its longitudinal edges supported. The traditional downward curling may appear only if the transverse edges are free to rotate (Figure 7b), something that seldom occurs when the mean temperatures in the pavement remain low enough during a sunny day.

In view of the foregoing, upward curling with partial support localized in the central zone of the slab, and minimum collaboration of contiguous slabs owing to a relatively more
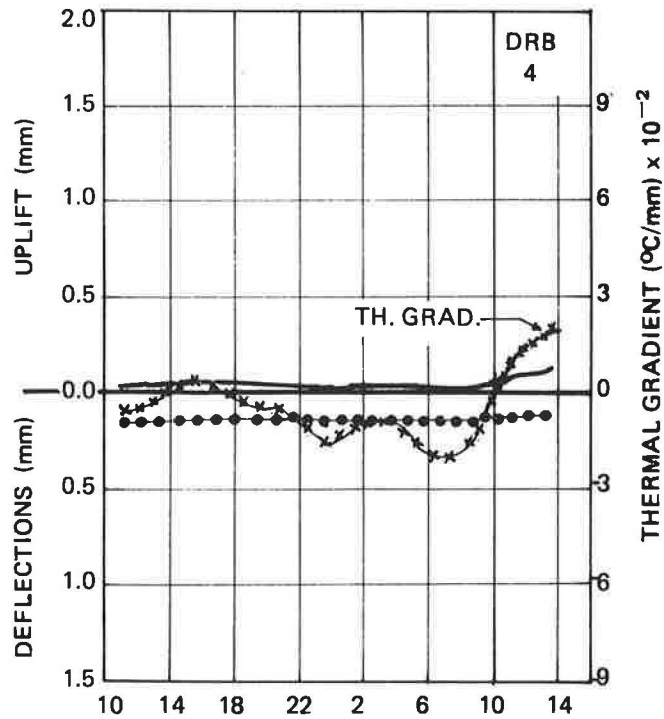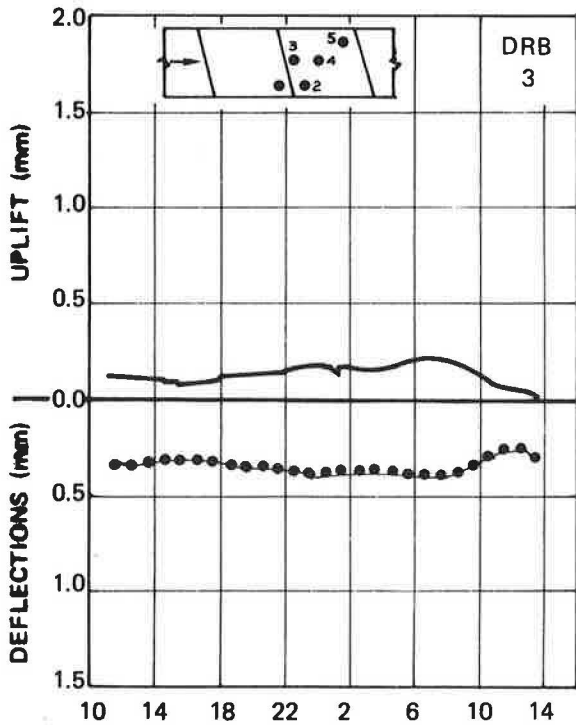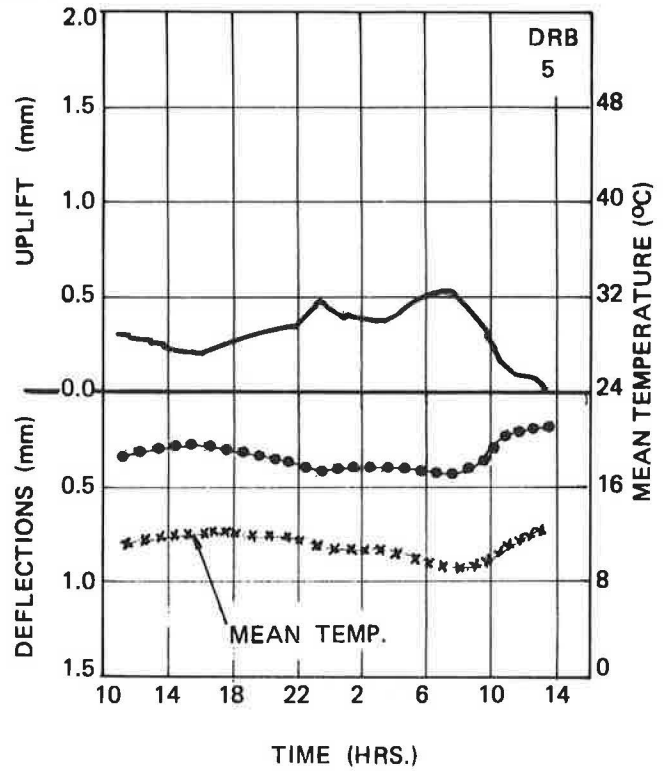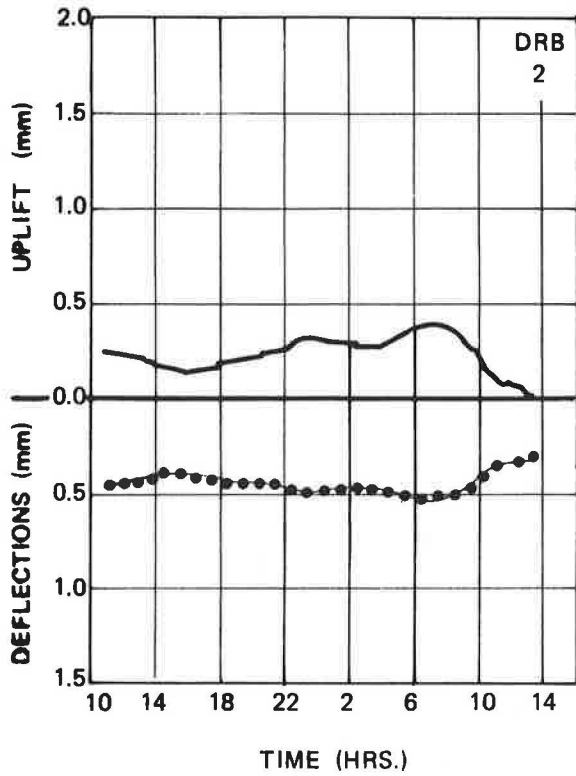
SUNNY
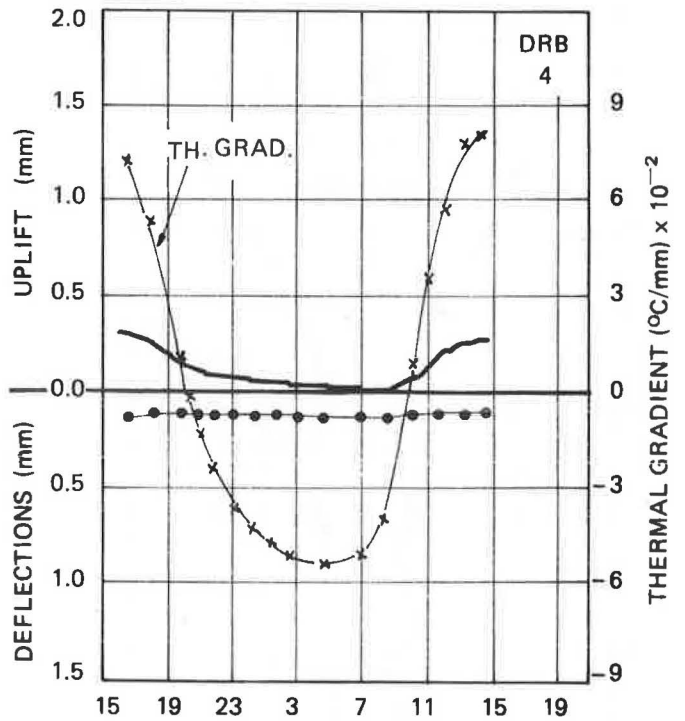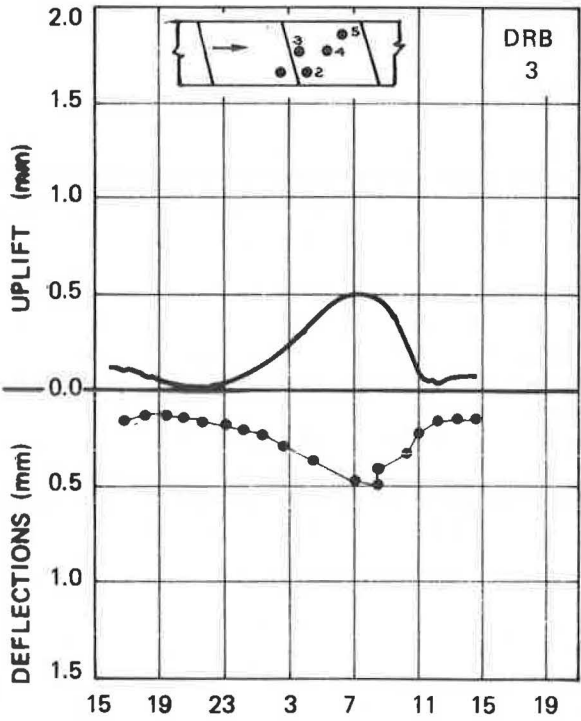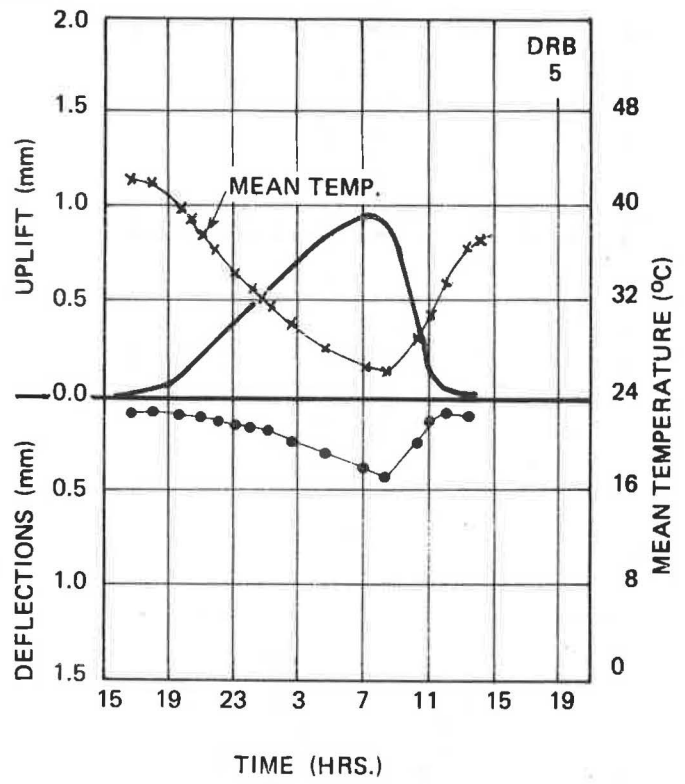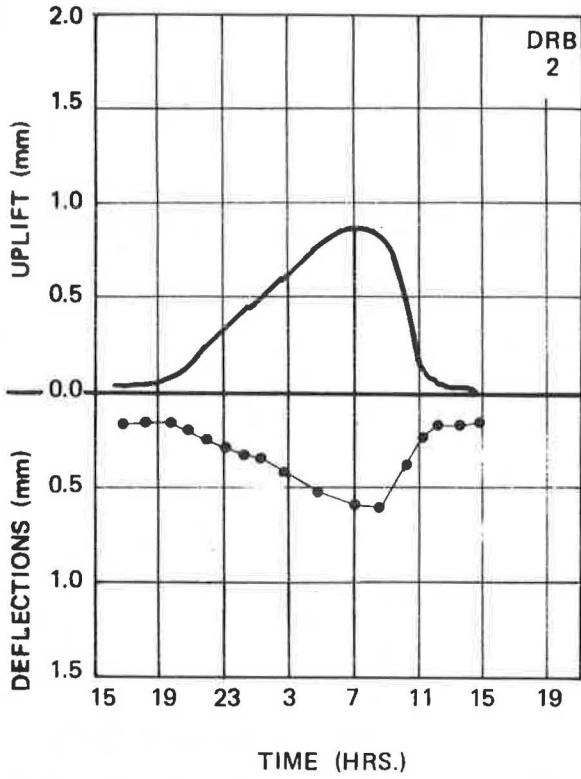
FIGURE 10 Continuous slab displacements and load deflections during a summer day cycle, for an 81-kN moving load.

CLOUDY

FIGURE 11   Continuous slab displacements and load deflections during a winter day cycle, for an 81-kN moving load.

TABLE 3 MAXIMUM UPLIFT OF CORNERS

Test Section		Slab Length (m)		Slab Construc. Season	Measure Season	Thermal Cond.		Max. Uplift of Corners* (mm)			Accumulated hours
		L₁	L₂			Mean T. °C	Grad. °C/mm	DRB 1	DRB 2	DRB 5	
Longotoma	1	4.56	4.06	Spr. '83	Sum. '86	22.5	-0.03	1.98	1.13	1.00	21
					Aut. '86	11.5	-0.02	0.95	0.60	0.57	18
					Sum. '87	24.5	-0.03	1.55	0.91	0.90	19
Las Chilcas	2	4.54	5.15	Spr. '81	Win. '86	12.0	-0.04	0.73	0.63	0.82	24
					Sum. '87	28.5	-0.05	0.90	0.88	1.70	16
Lampa	3	3.50	3.49	Win. '84	Aut. '86	9.0	-0.02	0.70	0.42	0.52	24
					Sum. '87	26.5	-0.05	1.05	0.92	0.95	15
Lo Vásquez	4	3.44	3.53	Sum. '85	Sum. '86	23.0	-0.05	1.65	1.30	1.42	19
					Win. '86	6.5	-0.03	0.60	0.45	0.50	24
					Sum. '87	23.7	-0.05	1.25	1.05	1.20	16
Talagante	5	5.00	4.55	Win. '75	Aut. '86	12.0	0.00	0.15	0.45	0.25	24
					Sum. '86	25.5	-0.06	0.64	0.70	0.65	10.5
Paine	6	4.64	4.57	Aut. '83	Aut. '86	7.0	-0.03	0.59	0.52	0.30	24
					Sum. '86	25.5	-0.04	0.63	0.65	0.57	14
Graneros	7	4.50	4.48	Aut. '83	Sum. '86	23.5	-0.06	1.25	1.25	1.35	14.5
					Win. '86	8.5	-0.04	0.75	0.63	0.70	18
					Sum. '87	25.0	-0.05	1.52	1.52	1.63	18
San Fernando	8	3.97	3.92	Sum. '83	Sum. '86	25.0	-0.04	1.20	1.28	1.57	19
					Aut. '86	9.0	0.00	0.08	0.45	0.27	20
					Sum. '87	22.5	-0.05	1.70	1.86	2.00	20
San Rafael	9	4.23	3.77	Aut. '83	Sum. '86	25.5	-0.06	1.05	0.95	0.85	18
					Aut. '86	12.5	0.00	0.25	0.30	0.25	24
					Sum. '87	23.0	-0.05	1.62	1.60	1.55	20
Cocharcas	10	4.56	4.52	Aut. '82	Win. '86	11.7	-0.03	0.35	0.65	0.40	20
Concepción	11	3.42	3.39	Win. '84	Win. '86	13.0	-0.01	0.20	0.20	0.11	16
					Sum. '87	23.5	-0.04	0.44	0.44	1.12	18
Cabrero	12	3.50	3.52	Aut. '84	Win. '86	11.0	-0.02	0.27	0.50	0.50	20
					Sum. '87	28.0	-0.04	0.68	0.70	0.76	20
Laja	13	4.52	4.62	Win. '82	Win. '86	9.3	-0.02	0.18	0.36	0.25	20
					Sum. '87	26.0	-0.06	1.12	1.22	1.12	16
C. Esperanza	14	4.42	4.70	Aut. '79	Win. '86	10.0	-0.01	0.10	0.58	0.49	21
					Sum. '87	26.5	-0.06	1.44	1.57	1.82	14
Victoria	15	4.00	4.02	Aut. '84	Win. '86	9.5	-0.01	0.12	0.12	0.12	24
					Sum. '87	23.0	-0.03	0.52	0.50	0.56	16
Temuco	16	4.55	4.47	Aut. '81	Win. '86	11.5	0.00	0.06	0.13	0.07	20
					Sum. '87	23.0	-0.03	0.61	0.66	0.38	16
Gorbea	17	4.47	4.49	Aut. '83	Win. '86	9.0	-0.02	0.38	0.40	0.34	24
					Sum. '87	23.0	-0.04	0.62	0.62	0.72	16
Loncoche	18	4.03	3.84	Spr. '84	Win. '86	4.5	-0.02	0.30	0.22	0.20	20
					Sum. '87	17.2	-0.05	0.53	0.49	0.68	15
Mariquina	19	4.55	4.44	Aut. '83	Win. '86	2.8	-0.03	0.50	0.42	0.40	20
					Sum. '87	23.0	-0.04	0.96	0.96		15
Mafil	20	4.48	4.55	Spr. '83	Win. '86	5.1	-0.02	0.15	0.25	0.17	19
					Sum. '87	23.1	-0.04	1.30	1.38	1.29	16
Rio Bueno	21	4.50	4.48	Sum. '83	Win. '86	3.2	-0.04	0.19	0.19	0.25	16
					Sum. '87	24.0	-0.03	0.80	1.21	1.09	14

*Winter data are relative to the day minimum and do not represent the total corner uplift
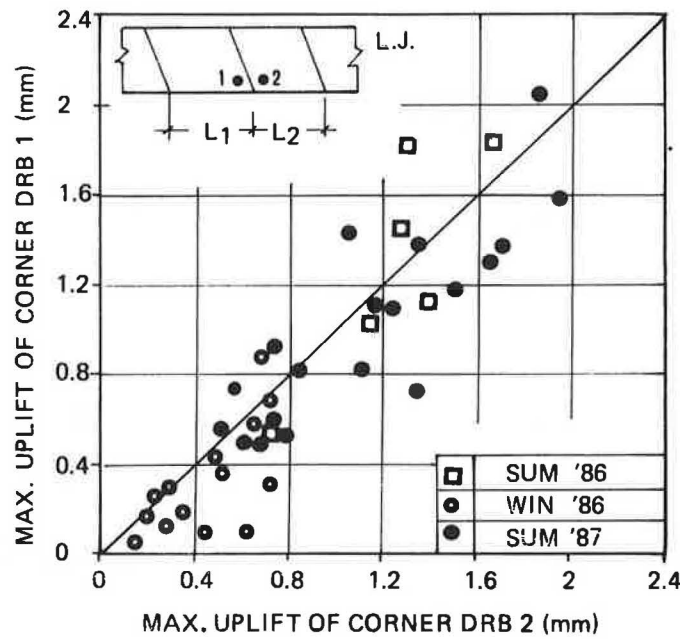
FIGURE 12 Comparison between maximum uplifts of adjoining corners (data from 21 test sections).
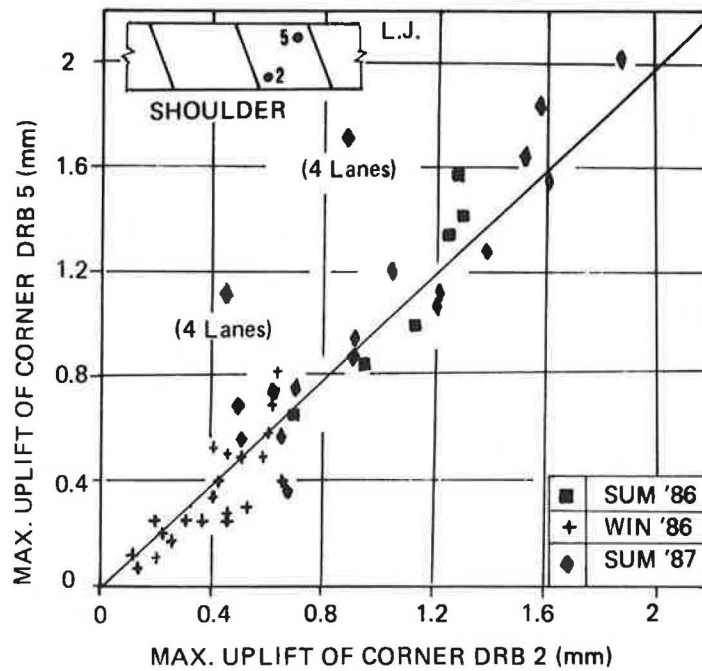

FIGURE 13 Comparison between maximum uplifts of opposite corners (data from 21 test sections).

pronounced opening of the joints, appear to be the prevailing unfavorable boundary conditions of the pavement slabs, which differs from the full support assumption usually considered in the engineering design of concrete pavements (*11, 12*). Conversely, the situation represented by the downward "cylindrical" shape is considered comparatively less detrimental.

These findings satisfactorily explain the distress that is being observed in some newer pavements where there are no signs of pumping, and whose cracking usually develops transversely at the middle of the slab, starting from the longitudinal edge. In addition, it has been verified through boreholes at the test section slabs that cracks start from the surface and move downward.

Detailed evaluation of the internal stresses with the superimposed nonlinear effects of environmental and wheel loads, calibrated with these results, is under way.
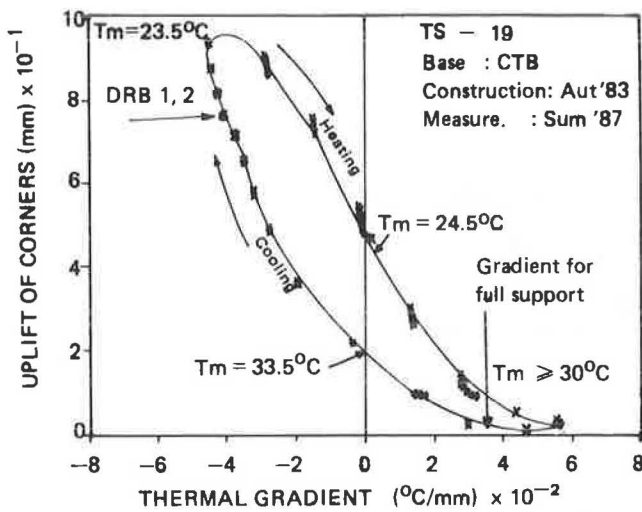
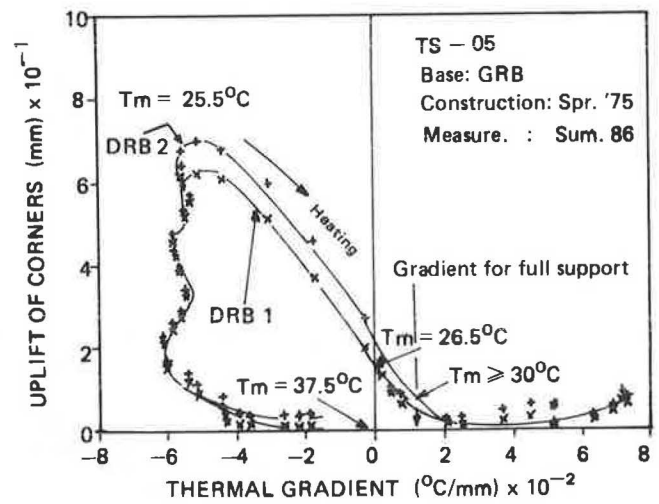**FIGURE 14** Slab corner displacements due to thermal gradient changes for new pavement in south region.

FIGURE 16 Slab corner displacements due to thermal gradient changes for old pavement in central region.
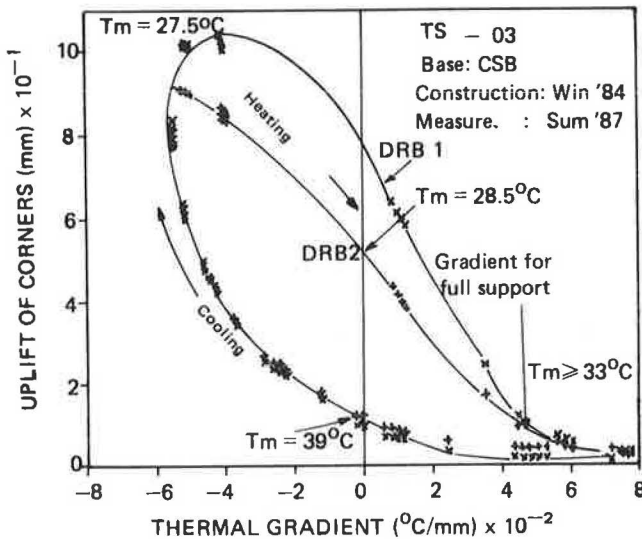

FIGURE 15 Slab corner displacements due to thermal gradient changes for new pavement in central region.

ACKNOWLEDGMENTS

The authors thank the Highway Division of the Ministry of Public Works for its permission to publish the results presented here. Special acknowledgments are given to the Concrete Pavement Group at the Institute of Research and Testing of Materials, IDIEM, for their constant assistance and support.

REFERENCES

1. Chilean Ministry of Public Works. Highway Maintenance and Rehabilitation Program in Chile. Presented at 2nd North American Conference on Managing Pavements, Toronto, Canada, 1987.
2. L. Ortega and P. Spratz. Performance Measures on Plain Concrete Pavements Without Dowels. *Proc., International Conference on Roads and Developments,* Paris, 1984, pp. 199–204.
3. A. Garcia. *Study of Rainfall Infiltration in a Concrete Pavement Structure,* Master's thesis, University of Chile, 1986 (in Spanish).
4. F. N. Hveem. Slab Warping Affects Pavement Performance. *Proc. ACI,* Vol. 47, 1951, pp. 797–808.
5. B. Tremper and D. L. Spellman. Shrinkage of Concrete—Comparison of Laboratory and Field Performance. In *Highway Research Record 3,* HRB, National Research Council, Washington, D.C., 1963, pp. 30–61.
6. IDIEM, University of Chile. *Field Instrumentation, Equipment and Measurement Methodology.* Highway Division, Chilean Ministry of Public Works. 1986 (in Spanish).
7. P. Ceza. *Study of the Temperature Distribution in a Concrete Pavement Structure.* Master's thesis, University of Chile, 1986 (in Spanish).
8. A. Neville. *Properties of Concrete.* Pitman Publishing Ltd., 1975.
9. "Curing Concrete" and "Volume Changes of Concrete." In *Design and Control of Concrete Mixtures.* PCA, 1984.
10. IDIEM, University of Chile. Concrete Pavements Research Project. *Annual Report 1986,* Vol. II. Highway Division, Chilean Ministry of Public Works. (in Spanish).
11. R. Packard. *Thickness Design for Concrete Highway and Street Pavements.* Portland Cement Association, 1984.
12. *AASHTO Interim Guide for Design of Pavement Structures, 1972.* American Association of State Highway and Transportation Officials, Chapter III, rev. 1981, pp. 25–36.